ERK1/2 signalling and protein ubiquitylation in the control of apoptosis

Kate Ann Stuart

Girton College, University of Cambridge

The Babraham Institute

This dissertation is submitted for the degree of Doctor of Philosophy

September 2018

Summary

Title: ERK1/2 signalling and protein ubiquitylation in the control of apoptosis.

Name: Kate Stuart

Programmed cell death, or apoptosis, is critical for normal developmental processes that involve cell turnover including embryogenesis and development and function of the immune system. It is preceded by classical changes in cell morphology, driven by biochemical changes including caspase activation. Apoptosis is deregulated in multiple human diseases, with suppression of apoptosis being critical for carcinogenesis. As such, proteins that regulate apoptosis are tightly regulated by cell fate signalling pathways.

The ERK1/2 signalling pathway is a key regulator of cell intrinsic apoptosis, in part through regulation of the pro-apoptotic protein 'BCL2-interacting mediator of cell death' (BIM). BIM is phosphorylated by ERK1/2 and this serves to drive its K48-linked polyubiquitylation and proteasome-dependent degradation, thereby promoting cell survival. βTrCP, an F-box protein that acts in a larger SCF complex, is one of several E3 ligases that have been proposed to polyubiquitinate BIM. This study demonstrated that of the major isoforms of BIM only BIM_{EL} interacts with βTrCP. ERK1/2-driven phosphorylation of BIM_{EL} is essential for this interaction, leading to BIM_{EL} destabilisation and degradation. As a consequence, tumour cells that are addicted to ERK1/2 signalling undergo BIM-dependent cell death in response to MEK1/2 inhibitors when combined with BH3-mimetics such as ABT263, small molecules that inhibit pro-survival proteins of the apoptotic pathway.

The RSK1/2 protein kinases, immediate downstream targets of ERK1/2, have also been implicated in the destabilisation of BIM_{EL}. Specifically phosphorylation of BIM_{EL} by RSK1/2 is proposed to be required for βTrCP binding. This study revealed that whilst the putative RSK1/2 phosphorylation sites in BIM_{EL} may be required for βTrCP binding, inhibition of RSK activity by three distinct RSK inhibitors does not block BIM_{EL}:βTrCP binding or BIM_{EL} turnover. Furthermore, tumour cells that are addicted to ERK1/2 signalling for survival are not addicted to RSK activity, arguing against a role for RSK in the regulation of BIM_{EL}. This suggests that ERK1/2 and an as yet unidentified kinase cooperate to drive BIM_{EL} degradation.

Deubiquitylating enzymes (DUBs) remove ubiquitin from target proteins. In the context of BIM_{EL}, DUB activity might oppose E3 ligases and thus cause its accumulation. Until recently the DUB for BIM was unknown however, USP27x has now been suggested. Follow-up validation of the reported interaction

between BIM_{EL} and USP27x was challenging but loss of BIM_{EL} polyubiquitination was observed following overexpression of USP27x, suggesting that USP27x may serve as a DUB for BIM.

Numerous DUBs control cellular processes that are dysregulated in cancer, including proliferation and apoptosis, making them attractive therapeutic targets. Recent interest in the DUB USP30 has increased as it has been shown to inhibit parkin-mediated mitophagy, with defective mitophagy being linked to Parkinson's disease. USP30 has also been suggested to play a role in apoptosis and its depletion was shown to sensitise cells to BH3 mimetics. These findings suggest that USP30 depletion or inhibition could provide a means for inducing tumour cell death. Indeed, combining a novel USP30 inhibitor (MTX32), provided by Mission Therapeutics, with the BH3 mimetic, ABT-263, induced apoptotic tumour cell death that required BAX and caspase activation. However, this was not replicated by a more selective USP30 inhibitor (MTX48), suggesting that the observed apoptotic cell death reflected the off-target effects of MTX32 rather than specific inhibition of USP 30.

Finally, an RNAi screen, targeting 94 DUBs, and 8 sentrin/SUMO-specific proteases (SENPs), in the human genome, was performed to identify DUBs that modulate cell death induced by MEK1/2 or mTOR inhibition. As such, inhibitors of identified 'hit' DUBs might be suitable as a combinatorial therapy with MEK1/2 or mTOR inhibitors in the treatment of cancer. The RNAi screen identified several DUBs, including USP10, YOD1, and VCIP135, that, when knocked down, sensitised HCT116 cells to MEK1/2 inhibitor treatment and enhanced MEK1/2 inhibitor induced cell death in a BAX-dependent fashion.

This work is discussed in the context of the role of ERK1/2 signalling as a pro-survival pathway, its specific role in BIM regulation, the potential for co-targeting DUBs and the ERK1/2 pathway to inhibit the growth of ERK1/2 addicted tumour cells and suggestions for future work are outlined.

Declaration

This thesis contains original work that has not previously been submitted for a degree or diploma or other qualifications at the University of Cambridge or any other University or similar institution. It is the result of my own work and contains nothing which is the outcome of work done in collaboration with others, except as specified in the text and acknowledgements. The length does not exceed the limit as stated in the Memorandum to Graduate Students. The dissertation does not exceed the limit of 60 000 words imposed by the Cambridge University Faculty of Biology Degree Committee.

Kate Stuart

Acknowledgements

I would first like to thank my supervisor Simon Cook for giving me the opportunity to work in his laboratory. Without his guidance, patience (I know I worry a lot) and support my PhD would not have been possible. A big thank you to my co-supervisor at Mission Therapeutics, Yaara Ofir-Rosenfeld, for supporting me and providing me with practical advice whilst performing the RNAi screens. In addition, I would like to thank Jeanine Harrigan at Mission Therapeutics mostly for her time and for the helpful comments/revisions during the final stages of my thesis writing.

Thank you to everyone in the Cook lab, it has been a privilege to work with you all over the last four years. I am particularly grateful to my mentor Becky, without her reassurance and guidance I would not be the scientist I am today. Kathy (Bob), thank you so all of your support, endless knowledge and for helping me out on numerous occasions.

I have made many friends at Babraham who have kept me sane over the last four years, in particular Katherine and Ine thank you for all of the chats, lunchtime walks and for generally knowing how to make me laugh. I would like thank Victoria, who has seen me at my worst and best during this process and who has provided me with unwavering support. Thank you for making me believe that I can do this even when I thought could not. I could not wish for a better person to share my future with. Finally, I would like to thank my family, Peter, Sally and Sarah for their endless love and support.

Acknowledgement of assistance received during the course of this thesis

1. Initial Training in techniques and laboratory practice and subsequent mentoring

Flow cytometry training – Rachel Walker

General laboratory practice – Kathy Balmanno and Rebecca Gilley

Immunoprecipitation training – Anne Ashford

Molecular biology training – Anne Ashford and Rebecca Gilley

RNAi screening – Yaara Ofir-Rosenfield

Tissue culture training - Rebecca Gilley

Western blotting training – Rebecca Gilley

2. Data obtained from a technical service provider

None

3. Data produced jointly

Chapter 5 was performed at Mission Therapeutics particularly with help of Nadia Arnaudo, Aurelie Le Feuvre Yaara Ofir-Rosenfeld and Aleksandra Zemia.

4. Data/materials provided by someone else

For materials provided by others, see Materials and Methods.

Figure 3.5F was performed by Ceri Wiggins, a previous member of the Cook Lab.

Publications associated with this thesis

COOK, S. J., STUART, K., GILLEY, R. & SALE, M. J. 2017. Control of cell death and mitochondrial fission by ERK1/2 MAP kinase signalling. *Febs j,* 284**,** 4177-4195.

Abbreviations

4E-BP	eIF (eukaryotic initiation factor) 4E-binding protein
A1/BFL	BCL2-related protein A1
A	Alanine
aa	Amino acid
ADP	Adenosine diphosphate
AIF	Apoptosis-inducing factor
AKT	v-akt murine thymoma viral oncogene homologue 1
ANOVA	Analysis of variance
AML	Acute myeloid leukaemia
AMSH	Associated molecule with the SH3 domain
AMSH-LP	AMSH-like protease
AP1	Activator protein 1
APC/C	Anaphase promoting complex or cyclosome
APAF1	Apoptotic protease activating factor1
ARAF	v-raf murine sarcoma 3611 viral oncogene homolog
ARTS	Sept4_i2
ATM	Ataxia-telangiectasia mutated
ATP	Adenosine triphosphate
ATR	Ataxia telangiectasia and Rad3 related
βTrCP	Beta-transducin repeat-containing protein
BAD	BCL2/BCL-$_{XL}$ associated death promoter
BAK	BCL2 homologous antagonist killer
BAP1	BRCA1 Associated Protein 1
BAX	BCL2-associated X protein
BC (groove)	BH3 and C-terminus-binding groove
BCL2	B-cell leukaemia/lymphoma 3
BCL-X$_L$	B-cell leukaemia/lymphoma extra large
BCL-w	B-cell leukaemia/lymphoma-like protein 2
BH	BCL2-homology
BH3	BCL2-homology 3
BI-1	BAX inhibitor 1
BID	BH3-interacting domain death agonist
BIK	BCL2-interacting killer
BIM	BCL2-interacting mediator
BIM$_{EL}$	BIM-extra long
BIM$_L$	BIM-long
BIM$_S$	BIM-short
BMF	BCL2- modifying factor
BOK	BCL2-related ovarian killer
BOP	BH3-only protein
BRAF	v-raf murine sarcoma viral oncogene homologue B1
BRAFi	BRAF inhibitor
BRCA	Breast cancer type 1
BRcat	Benign-catalytic
BRUCE/Apollon	BIRC6 – baculoviral IAP repeat containing 6
BSA	Bovine serum albumin
C	Cysteine
cAMP	Cyclic adenosine monophosphate
CARD	Caspase activation and recruitment domain
Cas9	CRISPR associated protein 9
CbI	Casitas B-lineage Lymphoma
CCNA	Cyclin A
CCNB	Cyclin B
CCND	Cyclin D
CCNE	Cyclin E
CDC	Cell division cycle
CDH1	Cadherin 1, E-cadherin

CDH2	Cadherin 2, N-cadherin
CDK	Cyclin-dependent kinase
Chk1	Checkpoint kinase 1
CHOP	CCAAT/enhancer-binding protein homologous protein
cIAP1	cellular inhibitor of apoptosis protein-1
cIAP2	cellular inhibitor of apoptosis protein-2
CIP/KIP	CDK interacting protein/Kinase inhibitory protein
CIS	Cytokine-inducible Src homology 2-domain-containing protein
CK	Casein kinase
CKI	CDK Inhibitor
CLL	Chronic lymphocytic leukaemia
CNS	Central nervous system
COXIV	Mitochondrial cytochrome c oxidase subunit IV
CRAF	v-raf 1 murine leukaemia viral oncogene homolog 1
CRC	Colorectal carcinoma
CREB	cAMP-response element-binding
CRISPR	Clustered regularly interspaced short palindromic repeats
CRL	Cullin-RING
CTG	CellTiter-Glo®
CTKD	C-terminal kinase domain
CV	Coefficient of variance
DD	Death domain
DDR	DNA damage response
DED	Death effector domain
DEF	Docking site for ERK, FXFP
DeSIs	deSUMOylating isopeptidases
DIABLO	Direct IAP-Binding Protein with Low pI
DISC	Death induced signalling complex
DKO	Double knockout
DLC-1	Dynein light chain 1
DMSO	Dimethyl sulphoxide
DNA	Deoxyribonucleic acid
DSB	Double strand break
DUB	Deubiquitylating enzyme
DUSP	Dual-specificity phosphatase
E2F	E2 factor
EBP	Enhancer-binding protein
ECM	Extracellular matrix
EGF	Epidermal growth factor
EGFR	Epidermal growth factor receptor
EGFR-TKIs	EGFR-tyrosine kinase inhibitors
eIF4E	Eukaryotic translation initiation factor 4E
EMT	Epithelial-mesenchymal transition
ER	Endoplasmic reticulum
ERAD	ER-associated degradation
ERBB	Erythroblastic leukemia viral oncogene homologue
ERK	Extracellular signal–regulated kinase
ERKi	ERK inhibitor
ETS	E26 transformation-specific or E-twenty-six
EV	Empty vector
FACS	Fluorescence activated cell sorting
FAS	Fatty acid synthetase
FADD	FAS associated death domain protein
FBS	Fetal bovine serum
FGF	Fibroblast growth factor
FL	Follicular lymphoma
FOXO	Forkhead box
FT	Farnesyltransferase
G	Glycine

G1	Growth or gap phase 1
G2	Growth or gap phase 2
GAP	GTPase-activating proteins or GTPase-acceletaing proteins
GEF	Guanine nucleotide exchange factor
GRB2	Growth factor receptor-bound protein 2
GSH	Glutathionine
GSK	Glycogen synthase kinase
GST	Glutathione S-transferase
GTP	Guanosine triphosphate
GTPase	Guanosine triphosphatase
HA	Human influenze hemagglutinin
HECT	homologous to E6 associated protein C terminus
HM	Heavy membrane
HOIL-1	Haem-oxidised IRP2 ubiquitin ligase-1
HOIP	Haem-oxidised IRP2 ubiquitin liase-1 interacting protein
HR1	HEK293 cells stably expressing conditional kinase ΔCRAF-1:ER*
HRK	Harakiri, BCL2 Interacting Protein
hr(s)	Hour(s)
4HT	4-hydroxytamoxifen
IAP	Inhibitor of apoptosis
IDP	Intrinsically disordered protein
IκB	Inhibitor of NF-κB
IMS	Intermembrane space
ITCH	Itchy E3 Ubiquitin Protein Ligase
IU1	1-[1-(4-fluorophenyl)-2,5-dimethylpyrrol-3-yl]-2-pyrrolidin-1-ylethanone
JAMM	JAB1/MPN/Mov34 metalloenzyme
JNK	c-Jun N-terminal kinase
K	Lysine
KIF11	Kinesin family member 11
KO	Knockout
KD	Kinase dead, Kinase domain
kDa	Kilodalton
KRAS	Kirsten rat sarcoma
LATS	Large Tumour Suppressor
LB	Luria broth
LKB1	Liver kinase B1
MAPK	Mitogen activated protein kinase
MCL1	Myeloid cell leukemia 1
MCM	Minichromosome maintenance protein complex
MCPIP	Monocyte chemotactic protein-induced protein
MEF	Mouse embryonic fibroblast
MEK	MAP kinase/ERK kinase
MEKi	MEK inhibitor
Met	Methionine
MINDYs	(MIU)-containing DUB family
miRNA	Micro-RNA
MIU	Motif interacing with ubiquitin
MJD	Machado-Joseph disease domain
MKP	MAP kinase phosphatase
MNK	MAP kinase signal-integrating kinase
MOAP	modulator of apoptosis
MOM	Mitochondrial outer membrane
MOMP	Mitochondrial outer membrane permeabilisation
mRNA	Messenger RNA
MSK	Mitogen- and stress- activated kinase
mTOR	Mammalian target of rapamycin
mTORC	Mammalian target of rapamycin complex

Myc	Cellular homologue of myelocytomatosis viral oncogene (v-Myc)/ myecytomatosis cancer (c-Myc)
NEDD8	Neural precursor cell expressed, developmentally down-regulated 8
NEMO	NF-κB essential modulator
NF1	Neurofibromatosis type 1
NF-κB	Nuclear factor kappa B
NGF	Nerve growth factor
NMR	Nuclear magnetic resonance
NPM	Nucleophosmin
NSCLC	Non-small cell lung cancer
NTKD	N-terminal kinase domain
OMM	Outer mitochondrial membrane
OTU	Ovarian tumour proteases
P	Proline
p-	phospho-
PAGE	Polyacrylamide gel electrophoresis
PARP	Poly (ADP-ribose) polymerase
PBS	Phosphate buffered saline
PCD	Programmed cell death
PCR	Polymerase chain reaction
PDK1	Phosphoinositide-dependent kinase-1
PEST	Rich in proline [P], glutamic acid [E], serine [S], and threonine [T]
PI	Propidium iodide
PIKK	PI3K-related kinase
PINK	PTEN-induced kinase
PI3K	Phosphatidylinositol-3 kinase
PIP_2	Phosphatidylinositol-3,4-bisphosphate
PIP_3	Phosphatidylinositol-3,4,5-trisphosphate
PKA	Protein kinase A
PKB	Protein kinase B
PLCε	Phospholipase C
PP2A	Protein phosphatase 2A
PTEN	Phosphatase and tensin homologue
PTM	Post-translation modification
PUMA	p53-upregulated modulator of apoptosis
Q-Vd-OPh	Quinoline-Val-Asp-Difluorophenoxymethyl Ketone
RACK	Receptor for activated C kinase
RALGDS	Ral guanine nucleotide dissociation stimulator
RAS	Rat sarcoma oncogene
RASGAPs	Ras GTPase activating protein
RB	Retinoblastoma
RBD	RAS-binding domain
RBR	Ring-between-ring
Rcat	Required for catalysis
RCD	Regulated cell death
RING	really interesting new gene
RIP1	Receptor interacting serine/threonine-protein kinase 1
RNA	Ribonucleic acid
ROS	Reactive oxygen species
RSK	Ribosomal S6 kinase
RTK	Receptor tyrosine kinase
RUNX3	Runt-related transcription factor 3
S/Ser	Serine
SCF	Skp, Cullin, F-box
SD	Standard deviation
SDS	Sodium dodecyl sulphate
SDS-PAGE	SDS polyacrylamide gel electrophoresis
SENPs	SUMO-specific proteases

SH3	Src-homology 3a
SHC	Src Homology 2 Domain Containing Transforming Protein
siRNA	Small interfering RNA
SLL	Small lymphocytic lymphoma
SMAC	Second mitochondria-derived activator of caspase
SMAD	Mothers against DPP homolog
SMURF	SMAD specific E3 ubiquitin protein ligase
SNAI1	Snail family zinc finger 1
SNAI2	Snail family zinc finger 2
SOS	Son of sevenless homolog
SPRED	Sprouty-related EVH1 domain containing protein
SPRY	Sprouty
SRC	Rous sarcoma oncogene
STAM	Signal transducing adaptor molecule
STAMBPL1	Signal transducing adaptor molecule binding protein like 1
SUMO	Small ubiquitin-like modifier
T	Threonine
TBS	Tris-buffered saline
TBST	Tris-buffered saline with Tween
TCA	Trichloroacetic acid
TDP	TAR DNA-binding protein
TG	Tris-glycine
TGF	Transforming-growth factor
TNF	Tumour necrosis factor
TNFAIP3	Tumour necrosis factor alpha-induced protein 3
TOM	Translocase of outer membrane
TRADD	TNFR associated death domain protein
TRAF	TNF receptor-associated factor 1
TRAIL	TNF-related apoptosis-inducing ligand
TRIM	Tripartite motif-containing 33
TSC1/2	Tuberculosis sclerosis 1 and 2 heterodimer
TWIST1	Twist Family BHLH Transcription Factor 1
Ub	Ubiquitin
UBA	Ubiquitin-associated
UBB	Ubiquitin B
UBC	Ubiquitin C
UBD	Ubiquitin-binding domain
UBL	Ubiquitin-like domain
UBZ	Ubiquitin-binding zinc finger
UCH	ubiquitin carboxy-terminal hydrolases
UbVME	Ubiquitin vinyl methyl ester
UIM	Ubiquitin-interacting motif
ULK	Unc-51-like kinase 1
ULP	ubiquitin-like proteases
UPS	ubiquitin-proteasome system
USP	Ubiquitin specific protease
UTR	Untranslated region
VIM	Vimentin
VCIP135	Valosin-containing protein p97/p47 complex-interacting protein p135
WEE1	WEE1 G2 Checkpoint Kinase
WT	Wild-type
XIAP	X-linked inhibitor of apoptosis
Y	Tyrosine
YAP	Yes-associated protein
YB1	Y-box binding protein 1
ZEB1	Zinc finger E-box binding homeobox 1

ZEB2	Zinc finger E-box binding homeobox 2
ZHA	ZUFSP helical arm
ZNF	Zinc-finger
ZNF-UBP	Zinc-finger ubiquitin binding domain
ZUFSP	Zinc finger UFM1-specific peptidase domain protein

Contents

List of figures

Chapter 1

Chapter 2

Chapter 3

Chapter 4

Chapter 5

Chapter 6

List of tables

Chapter 2

Chapter 1: Introduction

1. Chapter 1

1.1. Cancer

Cancer is the second leading cause of mortality worldwide, and was estimated to be responsible for 9.6 million deaths in 2018 (WHO). In general, it is the name given to a group of over 200 related diseases characterised by dysregulated cell division and the enhanced invasive potential of cells. Tumourigenesis, the process of tumour development, is coupled with the acquisition of certain key competencies that enable cells to proliferate and disseminate. In 2000, Hanahan and Weinberg., described "the six hallmarks of cancer" attained during the neoplastic transformation of cells; sustained proliferation, evasion of cell death, development of replicative immortality, the induction of angiogenesis, insensitivity to growth-suppressing signals and the activation of invasion and metastasis (Hanahan and Weinberg, 2000). A decade later additional hallmarks were proposed; the evasion of immune surveillance and the reprogramming of energy metabolism (Hanahan and Weinberg, 2011, Kroemer and Pouyssegur, 2008, Luo *et al.*, 2009), as well as two characteristics that enable tumour progression; genomic instability and tumour-promoting inflammation (Colotta *et al.*, 2009, Hanahan and Weinberg, 2011, Negrini *et al.*, 2010).

During tumourigenesis cells acquire numerous genetic alterations, including mutational and epigenetic changes, that enable cells to attain and maintain the described characteristics. 'Driver' mutations can promote tumour initiation and progression, whilst 'passenger' mutations occur as a consequence of the genomic instability of cancer cell (Haber and Settleman, 2007). Some cancers can be dependent upon one or more 'driver' mutation for growth and metastasis, also known as "oncogene addiction" (Weinstein and Joe, 2008). Despite the numerous mutations that cancer cells acquire during tumourigenesis, studies have revealed that they are often dependent upon a single or a few oncogenes for their continued growth. Identification of the oncogene(s) and/or mutations driving cell proliferation is therefore fundamental for our understanding of cancer pathologies and development of targeted cancer therapies.

The deregulation of cell cycle control, promotion of metastasis by epithelial to mesenchymal transition (EMT) and the evasion of apoptosis in cancer cells are of particular interest for this study and are discussed in more detail.

1.1.1. Cell cycle control and cancer

The cell-division cycle or cell cycle consists of a series of events, which enable a cell to replicate its DNA and divide. It is a tightly regulated process, which can be divided into four phases; G1 (growth or gap

phase), S (DNA synthesis), G2 (growth or gap phase 2) and M (mitosis) phase (Figure 1.1). Cell cycle controls are required to ensure only one DNA replication event occurs per cell cycle and that this is restricted to S phase.

As cells move through the cell cycle there are numerous 'checkpoints' at which cell cycle progression can be halted until favourable conditions for cell division are restored. Passage through these checkpoints and into each phase of the cell cycle requires cyclin-dependent kinases (CDKs), activated by their cognate cyclin partners. The expression and degradation of cyclins fluctuates throughout the cell cycle and this correlates with activation of their respective CDKs (Jeffrey *et al.*, 1995, Russo *et al.*, 1996). Active CDKs then phosphorylate their substrates allowing cell cycle progression. CDK activity is also regulated through the action of endogenous CDK inhibitors (CKIs), the INK4 family ($p15^{INK4B}$, $p16^{INK4A}$, $p18^{INK4C}$ and $p19^{INK4D}$), which inhibit CDK4/6, and the CIP/KIP family ($p21^{CIP1}$, $p27^{KIP1}$ and $p57^{KIP2}$), which inhibit CDK2 and CDK1 (Sherr and Roberts, 1999).

In early G1, cells respond to extracellular signals, including mitogens, either resulting in progression towards cell division or withdrawal from the cell cycle into the quiescent G0 state (Malumbres and Barbacid, 2001). Once the cell progresses past the restriction point, in late G1, cell cycle progression is independent of growth factors (Planas-Silva and Weinberg, 1997). Committed entry into S phase and passage through the G1/S checkpoint requires active E2F, which is reliant on the sequential activity of CDK4/6-cyclin D and CDK2-cyclin E complexes. Expression of the D-type cyclins (cyclin D1, cyclin D2 and cyclin D3) stimulates activation of CDK4/6 in mid-G1, which hyperphosphorylate the retinoblastoma protein (RB) family of proteins (RB, p107 and p130). Phosphorylation of RB disrupts its interaction with E2F, enabling E2F-mediated S-phase gene transcription, such as the induction of expression of cyclin E/A, along with components required for DNA replication such as minichromosome maintenance protein complex (MCM) 2/3/5/7 (Sherr and McCormick, 2002, Stevaux and Dyson, 2002). In late G1, cyclin E binds to CDK2, which, via a positive feedback loop, further promotes the phosphorylation of RB and helps to accelerate S phase entry, once sufficient CDK2 is active.

During the G1 phase of the cell cycle, CIP/KIP family proteins can bind to and promote the assembly of CDK4/6-cyclin D complexes, thereby inducing the activation of CDK4/6 (Sherr and Roberts, 1999). Additionally, the binding of CIP/KIP family proteins to CDK4/6 alleviates their inhibitory effect on CDK2, facilitating activation of CDK2 late in G1. Furthermore, CDK2 can phosphorylate $p27^{KIP1}$, targeting it for degradation, thereby promoting its own activity. Together this acts to promote cell cycle progression. In contrast, INK4 family proteins can bind to and inhibit CDK4/6, displacing CIP/KIP family proteins, thus enabling them to bind to and inhibit CDK2, leading to cell cycle arrest at the G1/S checkpoint (Sherr and Roberts, 1999).

Once in S phase, cyclin A, binds to and activates CDK2. Activated CDK2 then phosphorylates numerous substrates, in addition to RB and $p27^{KIP1}$, including replication factors A and C, required for DNA replication, and nucleophosmin (NPM), required for centrosome duplication (Asghar *et al.*, 2015, Okuda *et al.*, 2000). CDK1-cyclin A and CDK1-cyclin B complexes then regulate progression through G2 and into M phase (Nurse, 1990), and abrupt degradation of cyclin A and cyclin B during mitosis is required for mitotic exit.

DNA damage can activate cell cycle arrest at the majority of the cell cycle checkpoints. At the G2/M checkpoint damage can induce the activation of WEE1 which phosphorylates CDK1 inhibiting its function and causes cell cycle arrest. Arrest at this checkpoint requires the inhibition of CDC25 phosphatases which, under normal conditions, dephosphorylate P-loop residues of CDK1 enabling ATP binding and activation of CDK1 (Kumagai and Dunphy, 1991, Lundgren *et al.*, 1991, Strausfeld *et al.*, 1991). Of note, DNA damage can induce the nuclear accumulation of the deubiquitylating enzyme (DUB), USP50, which stabilises WEE1, counteracting CDC25B to promote cell cycle arrest (Aressy *et al.*, 2010). DNA damage can also induce longer-term cell cycle arrest mediated by the effects of p53 on gene expression. Through the activation of ATM and ATR kinases, and subsequent activation Chk1/2, p53 is stabilised. p53 can then repress the expression of multiple genes required for progression, including cyclin B1 and CDC25C and induce the expression of $p21^{CIP1}$, which inhibits CDK1-cyclin B1 (Taylor and Stark, 2001, Vousden and Lu, 2002).

A hallmark of cancer is the sustained proliferation of tumour cells (Hanahan and Weinberg, 2000). One way in which cancer cells have evolved to evade cell cycle controls, acquire pro-proliferative signals and go through tumourigenesis is through the inactivation of RB. This can occur through homozygous mutation, or deletion or silencing of RB, which ultimately precludes RB from inhibiting E2F (Sherr and McCormick, 2002). Dysregulation of the CDK4/6-RB axis can also occur through oncogenic activation of CDK4/6 activity (Sherr and McCormick, 2002). Amplification of *CCND1* (cyclin D1) and *CDK4* as well as activating mutations within *CDK4* have been observed to drive proliferation of cancer cells (Buckley *et al.*, 1993, Ormandy *et al.*, 2003, Sherr and McCormick, 2002, Wolfel *et al.*, 1995). Genetic or epigenetic mutations of additional negative regulators of cell cycle progression have been observed, including members of the INK4 family and p53, which promote tumourigenesis. Despite this, the most common mechanism by which tumour cells attain constitutive pro-proliferative signals is through activating mutations of key mitogenic signalling pathways, including the RAF-MEK1/2-ERK1/2 signalling pathway.

Figure 1.1 Overview of cell cycle control by cyclin-dependent kinases (CDKs), cyclins and CDK inhibitors (CKIs) at cell cycle checkpoints

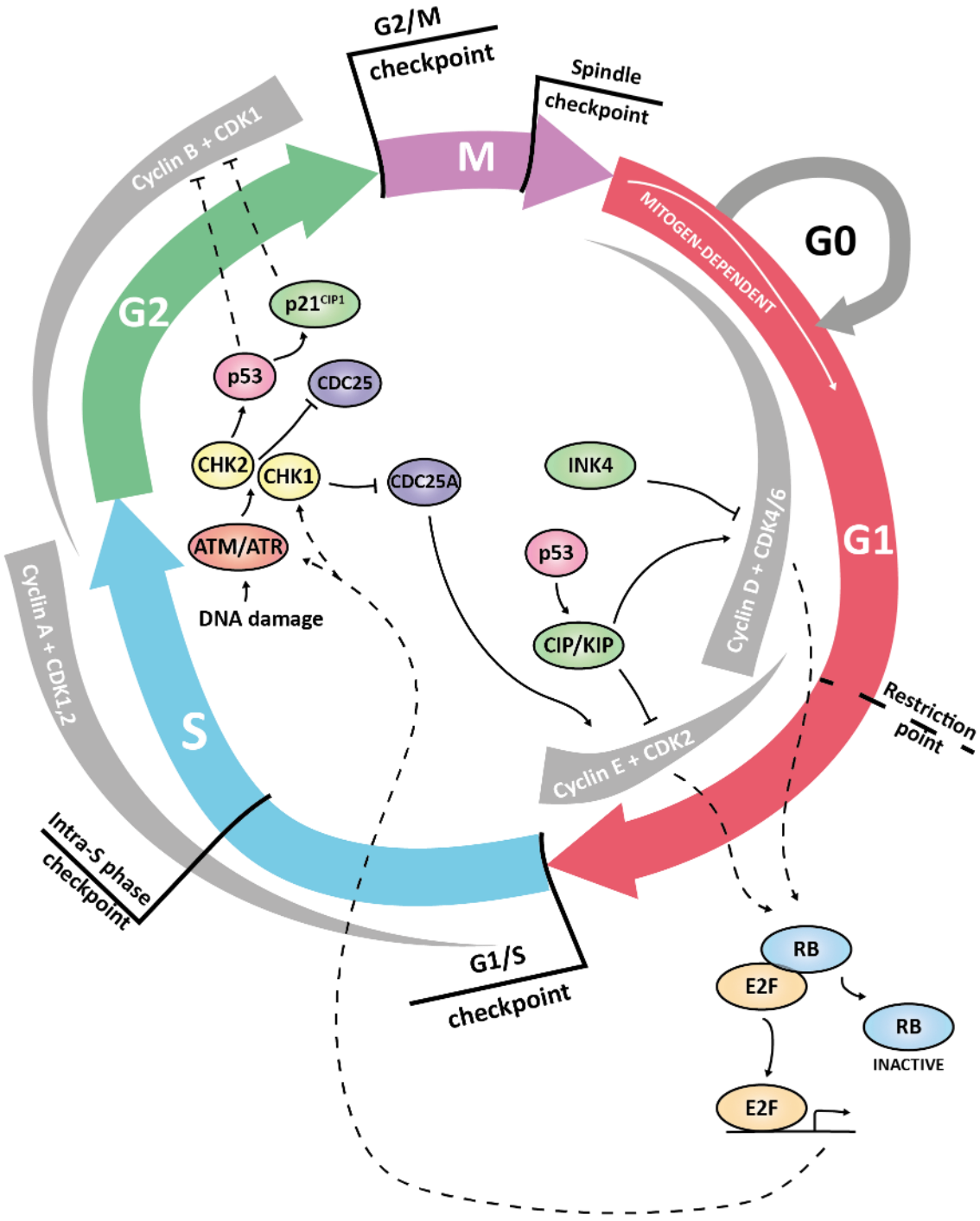

Figure 1.1 Overview of cell cycle control by cyclin-dependent kinases (CDKs), cyclins and CDK inhibitors (CKIs) at cell cycle checkpoints. In general, the cell cycle is made up of four phases, G1, S, G2 and M, separated by checkpoints at which the cell can arrest until favourable conditions for progression are met. Activation of CDK4/6, by interaction with cyclin D enables the cell to move through G1 phase. The activity of CDK4/6 are opposed by INK4 family proteins including $p16^{INK4}$. In contrast, CIP/KIP CDK inhibitors enable the assembly of CDK4/6-cyclin D complexes, thereby simultaneously relieving inhibition on CDK2-cyclin E. Critically, activation of CDK4/6-cyclin D and CDK2-cyclin E is requried for hypophosphorlyation and inhibition of RB, alleviating its inhibItion on E2F, therefore, enabling the transcription of genes required for entry into S phase and DNA replication. Transition through S phase is driven by CDK2-cyclinA, which is then taken over by CDK1-cycin A and later CDK1-cyclin B during G2 and M phase of the cell cycle. DNA damage, as well as E2F activation, can cause the activation of Chk1/Chk2, which can induce the stability of p53 and inhibit CDC25 phosphatases. This acts to inhibit CDK1 activity as well as interaction between CDK1 and cyclin B, thereby arresting the cell cycle, preventing progression through into mitosis. Following mitosis, cells can re-enter G1 phase of the cell cycle or reversibly exit the cell cycle into the G0 phase or quiescent state (adapted from Orford and Scadden, 2008).

1.1.2. Epithelial-mesenchymal transition and cancer

Epithelial-mesenchymal transition (EMT) is the process by which epithelial cells stably or transiently acquire invasive and migratory traits characteristic of mesenchymal cells (Polyak and Weinberg, 2009, Yilmaz and Christofori, 2009). Epithelial cells typically exhibit tight cell-cell contacts and an apico-basal polarity, which enables them to form a semi-permeable barrier against the environment. In contrast, mesenchymal cells lack cellular polarisation, exhibit a spindly fibroblastic morphology and only interact with each other through focal points, thereby enabling them to have enhanced motility and invasive potential. At the molecular level, loss of E-cadherin (CDH1) and the presence of N-cadherin (CDH2) and vimentin (VIM) are hallmarks of EMT (Kalluri and Weinberg, 2009, Yang and Weinberg, 2008).

Key transcription factors including SNAI1, SNAI2, TWIST1, ZEB1 and ZEB2 contribute to the repression of CDH1 and therefore facilitate the enhanced migratory phenotype associated with EMT. In addition, these transcription factors regulate numerous genes required for the mesenchymal phenotype, including claudins and desmosomes (Huang *et al.*, 2012b, Lamouille *et al.*, 2014).

EMT is a critical process required during embryogenesis, wound healing, organ fibrosis and tissue regeneration (Hay, 1995, Kalluri, 2009, Thiery *et al.*, 2009). However, it additionally contributes to tumour metastasis (Kalluri and Weinberg, 2009). Several signalling pathways (PI3K-PKB, ERK1/2, and TGFβ pathways) can contribute to the induction of EMT during tumourigenesis (Katsuno *et al.*, 2013, Larue and Bellacosa, 2005, Tripathi and Garg, 2018, Weiss *et al.*, 2012).

1.2. Cell Death

Regulated cell death (RCD) is an intracellular event that has evolved to play a central role in a diverse range of cellular developmental processes including embryogenesis, neuronal development, tissue homeostasis and immunity. This term has now evolved to include all forms of cell death that utilise a predestined molecular mechanism, including necrosis, necroptosis, pyroptosis, autophagy and apoptosis.

1.2.1. Apoptosis

The most prominent and well-studied form of RCD is apoptosis. In contrast to other mechanisms of RCD, apoptosis is characterised by distinct morphological changes including nuclear condensation, cell shrinkage, membrane blebbing and DNA fragmentation (Kerr *et al.*, 1972). Apoptotic cells retain plasma membrane integrity and, to some extent, metabolic activity during the end of apoptosis, which enables their rapid clearance by phagocytosis, commonly termed efferocytosis (Green *et al.*, 2016). There are two distinct apoptotic pathways, the cell-intrinsic and cell-extrinsic, which both converge to activate

effector caspases. Importantly, contrary to previous opinions, apoptosis and consequent efferocytosis has been demonstrated to induce an immunological response (Green *et al.*, 2009, Yatim *et al.*, 2017)

The first insight into the mechanism underlying apoptosis came from the discovery that the *BCL2* gene acts as an oncogene (Tsujimoto *et al.*, 1984); BCL2 was later found to prevent haemopoietic cell death when overexpressed in the absence of cytokines (Vaux *et al.*, 1988). This led to the current understanding that defects in apoptotic pathways can contribute to many human diseases, including cancer and degenerative disorders (Cory and Adams, 2002, Hotchkiss *et al.*, 2009).

1.2.1.1. Caspases

Initially identified in *C.elegans* (Ellis and Horvitz, 1986), cysteine aspartic acid-specific proteases, or caspases, are the key effector molecules of apoptosis. They cleave numerous intracellular substrates to initiate and execute apoptosis (Parrish *et al.*, 2013). Due to their destructive potential, caspases originate as inactive zymogens that are activated in response to an apoptotic signal. Caspases can be broadly categorised based on their role in apoptosis (caspase-2, -3, -6, -7, -8, -9 and 10) or the inflammation response (caspase-1, -4, -5, and -12). The caspases involved in the apoptotic response can be further sub-divided into two groups: the initiator caspases and the effector or executioner caspases (McIlwain *et al.*, 2013, Riedl and Shi, 2004, Shalini *et al.*, 2015).

The initiator caspases (caspase-2, -8, -9, -10) have a long N-terminal pro-domain that contains either a death effector domain (DED) or a caspase-recruitment domain (CARD), depending upon the apoptotic pathway they are involved in. This pro-domain interacts with adaptor proteins providing a scaffold for the dimerisation and autocatalytic cleavage at aspartic acid residues in their linker regions leading to the formation of an active heterotetramer. This is termed activation by 'induced proximity' (Boatright *et al.*, 2003, Oberst *et al.*, 2010). Effector caspases (caspase-3, -6, -7) are expressed as inactive homodimers. Cleavage by activated initiator caspases results in a conformational change that generates a mature protease (McIlwain *et al.*, 2013).

1.2.1.2. Extrinsic Pathway of Apoptosis

The extrinsic or 'death receptor' apoptotic pathway is initiated when 'death ligands' or cytokines such as tumour necrosis factor (TNF), FAS ligand or TRAIL (TNF-related apoptosis-inducing ligand) bind to their cognate 'death receptors' (TNF-R1, FAS or TRAIL-R1/2) at the plasma membrane. The resulting active death receptor oligomers recruit adaptor proteins, including FAS-associated protein with death domain (FADD) and TNF receptor-associated protein with death domain (TRADD/RIP1), via a death domain (DD)-DD interaction (Boldin *et al.*, 1996, Guicciardi and Gores, 2009). Adaptor proteins possess an additional interacting domain, the death effector domain (DED), which provides a platform for the

activation of the initiator caspases, -8 and -10, via the formation of a death inducing signalling complex (DISC) (Boatright *et al.*, 2003, Boldin *et al.*, 1996, Strasser *et al.*, 2009).The active initiator caspases can then cleave and activate the downstream effector caspases.

1.2.1.3. Intrinsic Pathway of Apoptosis

The cell intrinsic or mitochondrial apoptotic pathway is initiated by a variety of microenvironmental perturbations including DNA damage, endoplasmic reticulum (ER) stress, reactive oxygen species (ROS) and mitotic defects (Czabotar *et al.*, 2014, Pihan *et al.*, 2017, Vitale *et al.*, 2017). In this pathway, apoptosis is regulated by the collaborative action of the BCL2 protein family (Youle and Strasser, 2008), which can be functionally divided into pro-survival and pro-apoptotic proteins (Figure 1.2). Collectively these proteins act to initiate mitochondrial outer membrane permeabilisation (MOMP) in response to pro-apoptotic signals (Figure 1.3).

BCL2 protein family

In mammals, all BCL2 family members contain at least one of four conserved BCL2-homology (BH) domains. The pro-survival BCL2 family members include BCL2, BCL-w, BCL-X_L, MCL1 and A1. They all possess four BH domains (BH1-4) and harbour a C-terminal domain that targets them to intracellular membranes including the outer mitochondrial membrane (OMM), where they act to prevent apoptosis by binding to and inhibiting pro-apoptotic BH3-only proteins (BOPs) and the effector proteins BAK and BAX (Chipuk *et al.*, 2010). In addition to those described, BCL-B (Nrh) has also been suggested to be a pro-survival BCL2 protein that selectively binds to BAX to suppress apoptosis (Ke *et al.*, 2001, Zhai *et al.*, 2003). Interestingly, some pro-survival proteins can promote cellular survival through regulation of Ca^{2+} homeostasis at the ER membrane (Rong and Distelhorst, 2008, Scorrano *et al.*, 2003) or by promoting metabolism by interacting with the F_1F_0 ATP synthase (Chen *et al.*, 2011b, Green *et al.*, 2014). However, these roles have been controversial and as such their principal role is to inhibit apoptosis through their interaction with 'activator' BH3-only and effector pro-apoptotic proteins (O'Neill *et al.*, 2016).

The effector proteins, BAK and BAX, as well as the lesser known BOK, possess structural components of all four BH regions, where an α-helix at their N-terminus structurally resembles the BH4 domain (Kvansakul and Hinds, 2015). BOK (BCL2-related ovarian killer) only appears to drive apoptosis under a specific set of circumstances, distinct from BAK and BAX, including disruption of the ER-associated degradation (ERAD) pathway (Llambi *et al.*, 2016). However, its exact role as an effector protein remains unclear (Kalkavan and Green, 2017). Inactivation of either BAK or BAX can impair apoptosis by

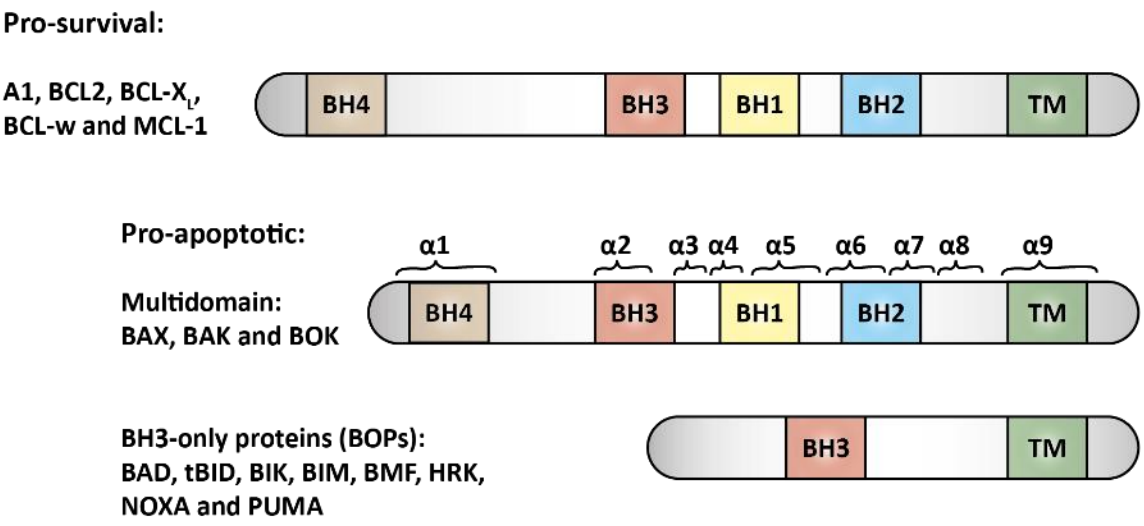

Figure 1.2 Structure of the BCL2 family of proteins. Pro-survival and pro-apoptotic proteins including BAK and BAX all share at least one of the conserved BH domains and most possess a hydrophobic transmembrane (TM) domain at their C-terminus that is required for targeting and orientation within a membrane (adapted from Czabotar et al., 2014).

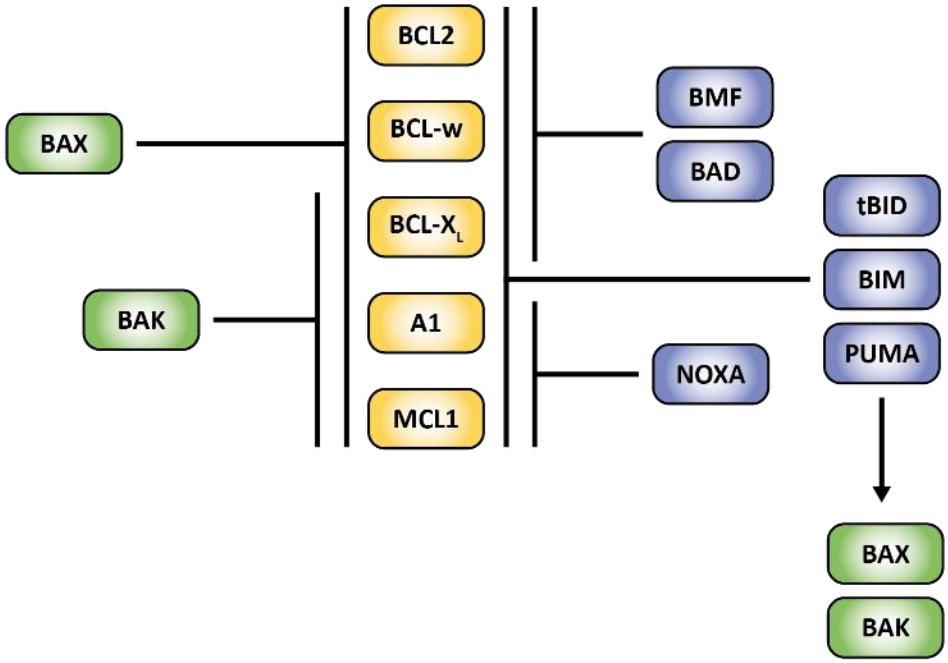

Figure 1.4 Selective binding between pro-survival and BH3-only BCL2 and effector pro-apoptotic family members. BCL2 pro-survival proteins are shown in yellow, whilst pro-apoptotic BH3-only proteins (BOPs) are depicted in blue and effector proteins shown in green.

Figure 1.3 The mitochondrial-mediated pathway for apoptosis.

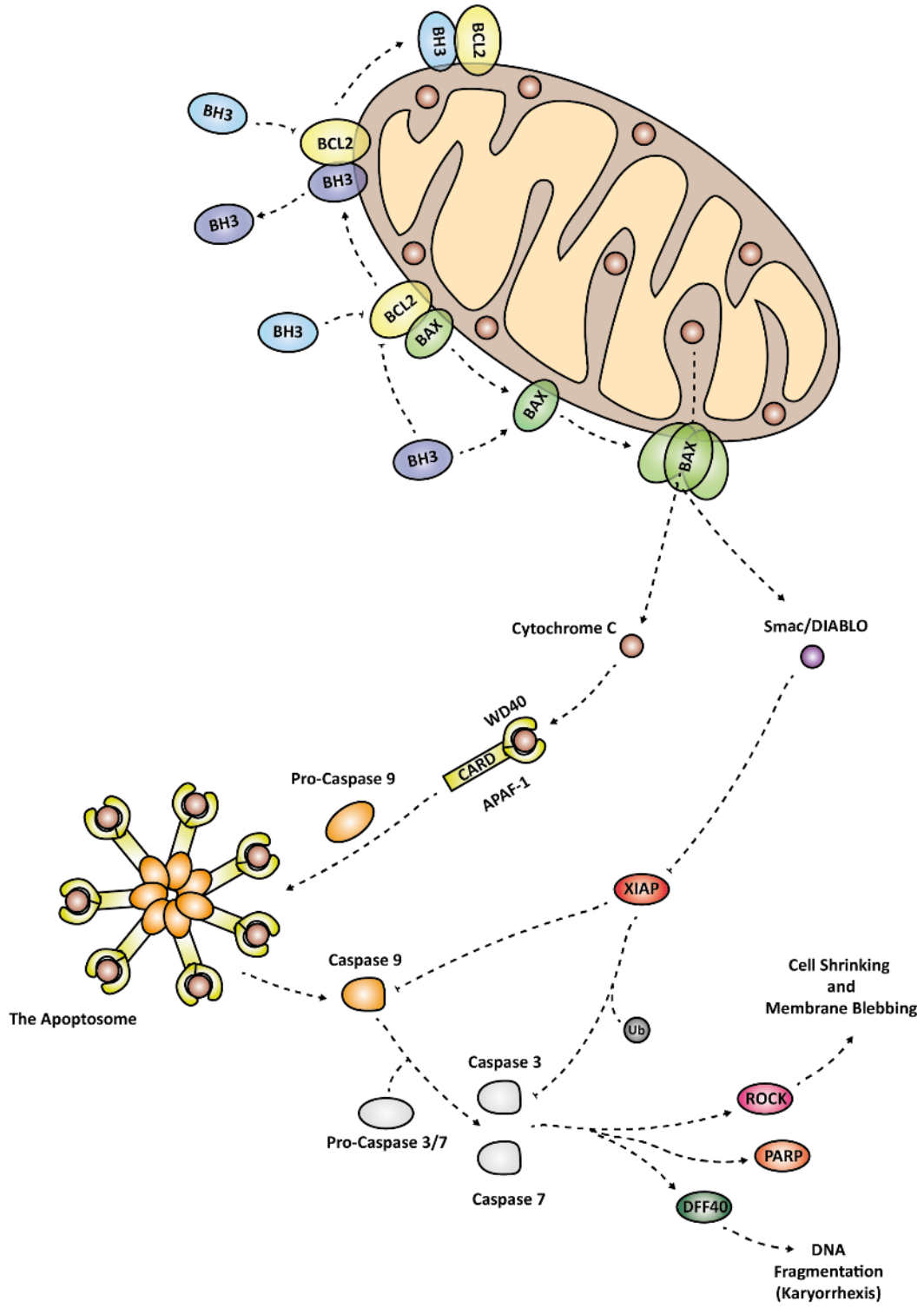

Figure 1.3 The mitochondrial-mediated pathway for apoptosis. This pathway is regulated by pro-apoptotic and pro-survival BCL2 family proteins. Pro-survival proteins (yellow) interact with pro-apoptotic family members (blue and green) via an interaction between their BC hydrophobic groove and a BH3 domain. BOPs can interact with BCL2 proteins releasing BAX and BAK from pro-survival proteins. 'Sensitiser' BOPs (light blue) are required to release 'activator' BOPs from pro-survival proteins. 'Activator' BOPs (dark blue) can then bind to and directly activate BAK/BAX, inducing conformational changes that result in their dimerisation and oligomerisation. BAK/BAX oligomers are thought to form a pore in the outer mitochondriaml membrane (OMM) resulting in mitochondrial outer membrane permeabilisation (MOMP) and release of effector molecules that initiate the caspase cascade and enabling the cellular changes required for cell death. Cytochrome c interacts with APAF1 inducing the formation of the apoptosome which recruits and activates procaspase-9. Active caspase-9 then activates executioner caspase-3 and -7. In addition to cytochrome c, SMAC/DIABLO is released and inhibits XIAP, enabling activation of the caspase cascade. Effectors of late stage apoptosis include ROCK (Rho-associated protein kinase) and DFF40 (caspase activated DNase (CAD)). Caspase-3 and -7 activate caspase activated DNAses (CADs) including DFF40, which results in DNA fragmentation, and ROCK which causes cell shrinkage and membrane blebbing. PARP (poly(ADP-ribose)polymerase) is cleaved by caspase-3 and -7 which prevents recruitment of DNA repair proteins. Its cleavage is considered a hallmark of apoptosis.

select stimuli but inactivation of both abolishes apoptosis by the mitochondrial pathway, indicating some unique roles for each and underlining their importance in initiating MOMP and apoptosis (Wei *et al.*, 2001).

There are at least eight BH3-only proteins (BOPs) including BAD, BID, BIK, PUMA, BMF, HRK, NOXA and BIM. As their name suggests, the only region they share in common with other BCL2 family members is the BH3 domain. Similar to BAK and BAX, they can bind to and selectively inhibit pro-survival BCL2 proteins. In addition, several have been shown to directly interact with the effector pro-apoptotic proteins, promoting their activation and enabling the initiation of intrinsic apoptosis (Kuwana *et al.*, 2005). Differences between the interaction profiles of these BOPs (Figure 1.3) is due to variations in their BH3 domain sequences (Certo *et al.*, 2006).

Activation of BAX, BAK and MOMP

When the concentrations of BOPs reaches a critical level, sufficient to both neutralise pro-survival proteins and activate effector pro-apoptotic proteins, apoptosis is triggered. All BOPs and BAK/BAX can interact with at least one pro-survival BCL2 protein (Figure 1.3). However, different BOPs and BAX/BAK bind to the pro-survival proteins with differing affinities (Kuwana *et al.*, 2005).

The BH1, BH2 and BH3 domains of the pro-survival proteins combine to form a hydrophobic groove (BC groove) that can interact with the BH3 domain amphipathic α-helix of the pro-apoptotic proteins (Czabotar *et al.*, 2007, Sattler *et al.*, 1997). This interaction is thought to neutralise the pro-apoptotic proteins and inhibit apoptosis. In contrast, if an apoptotic signal is detected, BOPs can compete for binding to pro-survival proteins, initiating the release and activation of the pro-apoptotic proteins BAK and BAX.

Two models have been proposed to explain how BAK and BAX are activated. The direct activation model suggests that BOPs can be grouped into 'sensitiser' BOPs; BAD, NOXA, BMF and HRK, and 'activator' BOPs; BIM, tBID and PUMA. Interaction between 'sensitiser' BOPs and BCL2 pro-survival proteins results in the displacement of 'activator' BOPs, which can then activate BAK/BAX. Contrary to this, BMF and NOXA have also been shown to activate BAK (Du *et al.*, 2011, Hockings *et al.*, 2015), suggesting that this division may be more fluid than first thought.

'Activator' BOPs bind to and induce conformational changes in BAK and BAX that lead to their activation and oligomerisation in the OMM (Brouwer *et al.*, 2014, Czabotar *et al.*, 2013, Kuwana *et al.*, 2005, Letai *et al.*, 2002, Lovell *et al.*, 2008, Moldoveanu *et al.*, 2013, Robin *et al.*, 2015) (Figure 1.4). The BH3 domain of 'activator' BOPs has been proposed to bind to a 'rear' or distal site (α1 and α6) on BAX (Gavathiotis *et al.*, 2010, Gavathiotis *et al.*, 2008, Kim *et al.*, 2009) activating BAX and leading to MOMP. There is also evidence that 'activator' BOPs can interact with a 'front' or surface hydrophobic groove,

similar in structure to the BC groove found in BCL2 pro-survival proteins, in BAK and BAX (Czabotar *et al.*, 2013, Dai *et al.*, 2011, Moldoveanu *et al.*, 2013) and that it is this site that is solely required for their activation (Czabotar *et al.*, 2014, Okamoto *et al.*, 2013, Peng *et al.*, 2013).

The second, indirect activation, model for the activation of BAK/BAX suggests BAK and BAX are 'primed' and bound to BCL2 pro-survival proteins, prior to induction of apoptosis (Willis *et al.*, 2007). BOPs compete for binding to BCL2 pro-survival proteins via their BH3 domain, leading to the release of BAK and BAX. A combination of the 'direct' and 'indirect' model has been suggested to be the definitive mechanism for the activation of BAK and BAX. One suggested mechanism is a `priming-capture-displacement' model where BAK and BAX are primed and immediately captured by the BCL2 pro-survival proteins. BAK and BAX are then displaced by BOPs, including BIM, allowing for their activation and oligomerisation (Strasser *et al.*, 2011).

BAK and BAX have globular structures in which an α5-helix is surrounded by 8 additional amphipathic helices. All studies and models have indicated that BAK and BAX must undergo a large conformational rearrangement to become active and initiate apoptosis. In healthy cells, monomeric BAX shuttles between the cytosol and the OMM. However, upon exposure of cells to apoptotic stimuli, BAX transiently engages with an 'activator' BOP at the distal site (α1 and α6), which enables the release of the transmembrane α9 helix of BAX from its 'front' hydrophobic groove, targeting it to and anchoring it in the outer mitochondrial membrane (OMM) (Adams and Cory, 2017, Gavathiotis *et al.*, 2010, Gavathiotis *et al.*, 2008, Suzuki *et al.*, 2000). Interestingly, mitochondrial outer membrane (MOM)-bound BAX has also been demonstrated to be 'retro-transposed' back into the cytosol via pro-survival proteins, including BCL-X_L, which is crucial for preventing unwanted death (Edlich *et al.*, 2011). Unlike BAX, the majority of BAK is found constitutively inserted in the OMM via its α9 helix .

Further rearrangements in BAK and BAX are predicted to require 'activator' BOPs to engage with their 'front' hydrophobic groove. Several structural rearrangements have been suggested including: the release of the N-terminal segment (including the α1 helix), exposure of their BH3 α2 helices, core (α2-α5)/latch (α6-α8) dissociation and insertion of α5-α6 helices into the OMM (Alsop *et al.*, 2015, Annis *et al.*, 2005, Brouwer *et al.*, 2014, Czabotar *et al.*, 2013, Oh *et al.*, 2010, Westphal *et al.*, 2014b). Ultimately, this results in the release of 'activator' BOPs and the transient exposure of the BH3 domain of BAK or BAX. The BH3 domain can compete for binding to the groove of a neighbouring BAX, or BAK, monomer, enabling hetero- and homo- dimerisation and oligomerisation (Czabotar *et al.*, 2013, Dewson *et al.*, 2012, Ma *et al.*, 2013, Zhang *et al.*, 2010). 'Symmetric' (Dewson *et al.*, 2008) and 'asymmetric' dimers have been found (Gavathiotis *et al.*, 2010, Kim *et al.*, 2009), however the former is the more accepted mode for dimerisation.

How BAK and BAX oligomers interact with the OMM to form a pore to drive MOMP is not completely understood. Recent structural observations have suggested that the long established hairpin insertion or 'umbrella' model for pore formation (Annis *et al.*, 2005) may not be correct. Instead of inserting into the membrane the α4 and α5 helices lie in-plane with the OMM and may insert shallowly into the membrane, in addition to the α6, α7 and α8 helices, to drive lipid rearrangements and pore formation (Uren *et al.*, 2017, Westphal *et al.*, 2014a, Westphal *et al.*, 2014b). Preliminary high resolution images of the pore structures are beginning to emerge; however they fail to distinguish between structures in which BAX α-helices have shallowing inserted in the MOM generating a 'lipid rim' and 'BAX-lined' pores within the MOM (Adams and Cory, 2017, Grosse *et al.*, 2016, Kuwana *et al.*, 2016, Salvador-Gallego *et al.*, 2016).

The permeabilisation of the OMM by BAK/BAX releases components from the intra-mitochondrial space (IMS) including cytochrome c, which binds to the WD domains of APAF-1 triggering the activation of caspase-9 and the activation of downstream effector caspases (Riedl and Salvesen, 2007, Tait and Green, 2010). During MOMP, release of additional IMS proteins, including SMAC (Second mitochondria-derived activator of apoptosis)/DIABLO (Direct IAP-Binding Protein with Low pI) results in the disruption of the caspase-XIAP (inhibitor of apoptosis) interaction, thus relieving the inhibitory effect of XIAP to further promote caspase activation (Liu *et al.*, 2000) (Figure 1.4).

BH3 Profiling

BH3 profiling utilises peptides derived from the BH3 domains of BOPs to predict cellular responses to stimuli including inhibitors. It measures changes in pro-apoptotic signalling, mitochondrial depolarisation and the induction of MOMP in response to exposure of mitochondria or cells to different BH3 peptides (Del Gaizo Moore and Letai, 2013).

This approach can be used to determine the dependency of cells on different pro-survival proteins by exploiting the fact that different BOPs are capable of interacting with different pro-survival proteins, as depicted in Figure 1.4, with differing affinities. As shown here activator peptides BIM and BID would bind to all pre-survival proteins. However, NOXA is more selective and binds to MCL1 and A1 with high affinity and therefore if a response is observed with this peptide it suggests that these cells have a dependency on MCL1 and/or A1 for survival. This technique has been used to assess the dependency of tumour cells on different pro-survival proteins which can be used to predict the chemosensitivity of these cells and therefore could be used to guide treatment of patients (Butterworth *et al.*, 2016, Touzeau *et al.*, 2016).

1.2.1.4. Targeting apoptosis as a cancer therapy

Aberrant or impaired apoptosis is considered a hallmark of cancer (Hanahan and Weinberg, 2000); as such the balance of pro-apoptotic and pro-survival BCL2 proteins is shifted in favour of survival in cancer cells. For example, the tumour suppressor p53 normally drives the expression of the pro-apoptotic proteins, NOXA and PUMA, in response to DNA damage but is frequently inactivated by mutations in cancer (Nakajima and Tanaka, 2007). Cancer cells can also develop a dependency on elevated levels of pro-survival proteins to evade apoptosis whilst oncogenic signalling pathways can repress the expression of pro-death BOPs such as BIM, PUMA and BMF (Balmanno and Cook, 2009, Cook *et al.*, 2017, Duronio, 2008). Several small drug-like molecules have been developed that aim to target the BCL2 pro-survival proteins and shift the balance from pro-survival towards pro-apoptotic, thereby providing a novel means to enhance tumour cell death (Letai, 2017, Montero and Letai, 2017). These compounds include the antisense oligonucleotide oblimersen that targets BCL2 pro-survival proteins (Klasa *et al.*, 2002), BH3 peptides and BH3 mimetics that mimic the BH3 domain of the pro-apoptotic proteins (Adams and Cory, 2017).

BH3 mimetics

Despite promising preclinical results oblimersen performed poorly *in vivo* as it was unable to reduce expression of pro-survival BCL2 proteins (O'Brien *et al.*, 2009). As a result, BH3 mimetics have become a more favourable therapeutic approach and several are in clinical trials or clinically approved for the treatment of specific cancer lineages. The BH3 mimetics ABT-737 and ABT-263 (Navitoclax) have nanomolar affinity for BCL2, BCL-X_L, and BCL-w, but negligible affinity for MCL1 or A1 (Anderson *et al.*, 2014, Oltersdorf *et al.*, 2005, Tse *et al.*, 2008). They are therefore most effective against tumours expressing high levels of BCL2, BCL-X_L, and BCL-w and act by displacing BAK and BAX from pro-survival proteins to induce apoptosis (Del Gaizo Moore *et al.*, 2007, Konopleva *et al.*, 2006, van Delft *et al.*, 2006). Crystal structures of ABT-737, bound to BCL-X_L (Lee *et al.*, 2007), and ABT-263, bound to BCL2 (Souers *et al.*, 2013), revealed that the interaction between BH3 mimetics and pro-survival proteins differs from that between the BH3 domain of BIM and BCL-X_L (Liu *et al.*, 2003). Interestingly, it revealed that BH3 mimetics are able to penetrate the p2 hydrophobic pocket, of the pro-survival protein, much deeper than the BH3 domain of BIM.

In early clinical trials, ABT-263 was shown to be effective in tumours with high levels of BCL2 including chronic lymphocytic leukaemia (CLL) and follicular lymphoma (FL) (Roberts *et al.*, 2012); in contrast more modest effects were observed against solid tumours, which may require combinations of ABT-263 with other cancer therapies to drive tumour cell death (Rudin *et al.*, 2012, Sale and Cook, 2013). Unfortunately, patients treated with ABT-263 developed thrombocytopenia due to on-target BCL-X_L

inhibition, therefore ABT-263 was re-engineered to generate ABT-199 (Venetoclax), a mimetic that selectively targets BCL2. ABT-199 exploits a difference between the p4 hydrophobic pocket of pro-survival proteins, thereby preventing it from inhibiting BCL-X_L, and thus protects patients from developing thrombocytopenia (Souers *et al.*, 2013, Vandenberg and Cory, 2013). ABT-199 showed promising results in patients with CLL, small lymphocytic lymphoma (SLL) and acute myeloid leukaemia (AML) (Souers *et al.*, 2013), and in 2016 was approved for the treatment of CLL.

BH3 mimetics are not as effective against tumours that predominantly express the pro-survival protein MCL1, which is implicated in resistance to ABT-263 and ABT-199 (Leverson *et al.*, 2015, van Delft *et al.*, 2006, Xiao *et al.*, 2015, Yecies *et al.*, 2010, Zhang *et al.*, 2011). Pan *et al.* have shown that the pan-BCL2 family inhibitor, (-)BI97D6, can overcome resistance to the BH3 mimetic ABT-737 in tumours that express MCL1 and induce apoptosis (Pan *et al.*, 2015). In addition, preclinical trials with the MCL1 inhibitor, S63845, have been promising (Kotschy *et al.*, 2016, Merino *et al.*, 2017). Ashkenazi *et al.* have described additional BH3 mimetics in development (Ashkenazi *et al.*, 2017), including the BCL-X_L specific mimetic WEHI-539 (Lessene *et al.*, 2013, Leverson *et al.*, 2015) as well as A-1155463 and A1331852, which may be of therapeutic benefit in the treatment of solid tumours, including colorectal cancers that have elevated BCL-X_L expression (Zhang *et al.*, 2015).

Targeting BAK/BAX

Recent modelling of the activation of BAK/BAX has meant that these pro-apoptotic proteins could potentially be targeted by small molecules to directly activate them, increasing intrinsic apoptosis and cell death. Small molecules could potentially target the distal site (α1 and α6) of BAX, the 'front' hydrophobic groove and the region that controls activation of BAX by release of the 'latch' domain from the 'core' domain (Gavathiotis *et al.*, 2012, Zhao *et al.*, 2014). Interestingly, Niu *et al.* have described small-molecule inhibitors of BAK/BAX, MSN-125 and MSN-50, which prevent BAK/BAX oligomerisation, inhibiting apoptosis and promoting neuroprotection (Niu *et al.*, 2017). In addition, BAX inhibitor 1 (BI-1), an endogenous anti-apoptotic protein, could be a potential therapeutic target as it was demonstrated to inhibit BAX-dependent apoptosis, promote chemoresistance and tumour cell survival (Grzmil *et al.*, 2006, Krajewski *et al.*, 1999, Robinson *et al.*, 2011, Xu and Reed, 1998).

IAP antagonists

There are eight known inhibitors of apoptosis (IAPs) including cellular IAPs (cIAPs); cIAP-1, cIAP-2, XIAP and SURVIVIN (Oberoi-Khanuja *et al.*, 2013). In general they act to antagonise effector caspases, thereby inhibiting apoptosis. Protein levels of IAPs are elevated in many cancers and, as a result, small molecules are in pre-clinical trials that act to mimic SMAC/DIABLO, thereby antagonising IAPs and

relieving their inhibitory effect on effector caspases (Fulda and Vucic, 2012, Straub, 2011). Key small-molecule IAP antagonists or 'SMAC mimetics' include Birinapant (TL32711), which is a bivalent small molecule SMAC mimetic that targets cellular cIAPs resulting in the inactivation of the the NF-κB pathway (Benetatos *et al.*, 2014, Gyrd-Hansen and Meier, 2010). Recent data also suggests that Birinapant, and an additional 'SMAC mimetic' AT-406, could be used in combination with the BH3 mimetic ABT-199 to drive apoptosis of tumour cells with high BCL2 expression (Perimenis *et al.*, 2016).

1.3. Ras-RAF-MEK1/2-ERK1/2 signalling

Rat sarcoma (Ras) proteins were first identified to be encoded by retroviral oncogenes commandeered by Kirsten and Harvey rat sarcoma viruses from the host genome. Additional studies established *ras* genes to be transfectable oncogenes in human tumours. From these findings *ras* was demonstrated to be mutated in tumour cells and retroviruses and had the ability to regulate cell growth (Barbacid, 1987, Downward, 2003).

There are multiple downstream effectors of Ras, the majority of which promote cell survival, cell cycle progression and cell motility. The main effectors of Ras are RAF, PI3K, RALGDS and PLCε, which contain a Ras-binding domain (RBD) that enables them to interact with the effector loop of Ras (Downward, 2003).

Ras can directly bind to class IA phosphoinositide 3'-kinases (PI3K) which phosphorylate phosphatidylinositol-4,5-bisphosphate (PIP_2) at the plasma membrane to generate the second messenger phosphatidylinositol-3,4,5-trisphosphate (PIP_3). This process is opposed by the lipid phosphatase PTEN, which dephosphorylates PIP_3 to PIP_2 (Maehama and Dixon, 1998). PIP_3 can then recruit and activate downstream effector proteins including PDK1 and AKT/PKB. Of note, AKT phosphorylates and negatively regulates or inhibits numerous factors implicated in cell proliferation and apoptosis such as $p21^{CIP1}$, $p27^{KIP1}$, FOXO1/3/4, BAD, BAX and caspase-9. Similar to that described for PI3K, the RAL guanine nucleotide dissociation stimulator (RALGDS) pathway contributes to the inhibition of FOXO transcription factors known to regulate the expression cell cycle regulatory proteins ($p27^{KIP1}$) and apoptotic proteins (BIM and FAS ligand) (De Ruiter *et al.*, 2001). Therefore, both pathways predominantly act to promote cell-cycle progression and inhibit apoptosis.

The Ras regulated RAF-MEK1/2-ERK1/2 (ERK1/2) signalling pathway has also been shown to be important in promoting cell survival, particularly tumour cell survival (Balmanno and Cook, 2009). Furthermore, since the ERK1/2 signalling pathway is hyperactivated in a wide variety of cancers it has attracted significant interest as a therapeutic target. Indeed, BRAF and MEK inhibitors have now been approved for clinical use in certain cancers whilst ERK inhibitors are entering clinical trials (Caunt *et al.*, 2015, Downward, 2003, Holderfield *et al.*, 2014, Kidger *et al.*, 2018).

1.3.1. Overview of Ras-RAF-MEK1/2-ERK1/2 signalling pathway

Depending upon the stimulus transmitted to Ras, at the plasma membrane, activation of the downstream Ras-dependent RAF-MEK1/2-ERK1/2 (ERK1/2) signalling cascade can result in cell survival, proliferation, differentiation or apoptosis (Figure 1.5). Ligand engagement of receptor tyrosine kinases (RTKs) at the plasma membrane results in the autophosphorylation of RTKs and recruitment of adaptor proteins, including GRB2 (growth factor receptor-bound protein) and SHC (src homolgy 2 domain containing transforming protein). Together these adaptor proteins recruit SOS (son of sevenless), a GEF (guanine nucleotide exchange factor), that promotes an active 'on' GTP-bound form of Ras (HRas, KRas and NRas), via the dissociation of GDP (Cherfils and Zeghouf, 2013, Takai *et al.*, 2001). Both GEFs and GAPs (GTPase-activating proteins) regulate the activity of Ras where GAPs oppose GEF activity and inactivate Ras by promoting GTP hydrolysis (Bos *et al.*, 2007, Cherfils and Zeghouf, 2013). Examples of GAPs include NF1, p120GAP (RasGAP) and SynGAP (Bos *et al.*, 2007, Cherfils and Zeghouf, 2013). Scheffzek et al, demonstrated that RasGAP positions its 'arginine finger' within the phosphate-binding site of Ras, thereby neutralising the charge developed as a consequence of transition and enhancing GTP hydrolysis (Scheffzek *et al.*, 1997). RasGAP is also important to stabilise the position of Q61 within Ras, which is frequently mutated in cancer. Additionally, Ras requires post-translational modification for its association with the plasma membrane. Farnesylation of Ras at its C-terminus, by farnesyltransferase (FT), results in the attachment of a hydrophobic farnesyl group to Ras that allows for its membrane-association (Chang *et al.*, 2003).

In its GTP-bound form Ras is in its active conformation, due to structural rearrangements in switches I and II; this enables it to bind to and activate downstream effector proteins. Ras-GTP binds to RAF (ARAF, CRAF and BRAF) and disrupts its interaction with 14-3-3 proteins. This generates a more 'open' form of RAF, which allows for additional activation events including phosphorylation of RAF by SRC (Leicht *et al.*, 2007) and its homo- and hetero-dimerisation (Rushworth *et al.*, 2006, Weber *et al.*, 2001).

The kinases downstream of RAF, MEK1/2 and ERK1/2, require phosphorylation for activation. Active RAF phosphorylates MEK1/2 at conserved serine (Ser or S) residues within their activation loops. This enables these active dual specificity kinases MEK1/2 to phosphorylate the threonine (Thr or T) and tyrosine (Y) residues, consecutively, within the activation loop T-E-Y sequences of ERK1/2, thereby enabling conformational changes required for its activation (Aoki *et al.*, 2011, Roskoski, 2012). ERK1/2 binds to its substrates via the docking domains D-domain and F-domain (DEF domain), and catalyses the phosphorylation of proline (P) directed Ser/Thr residues (Bardwell *et al.*, 2003, Burkhard *et al.*, 2011, Jacobs *et al.*, 1999). Translocation of active ERK1/2 to the nucleus results in the phosphorylation of ETS and AP-1 transcription factors that drive immediate-early and delayed-early gene expression (Yoon and Seger, 2006), ultimately leading to cell proliferation and survival.

Figure 1.5 Overview of the Ras-RAF-MEK1/2-ERK1/2 (ERK1/2) signalling pathway.

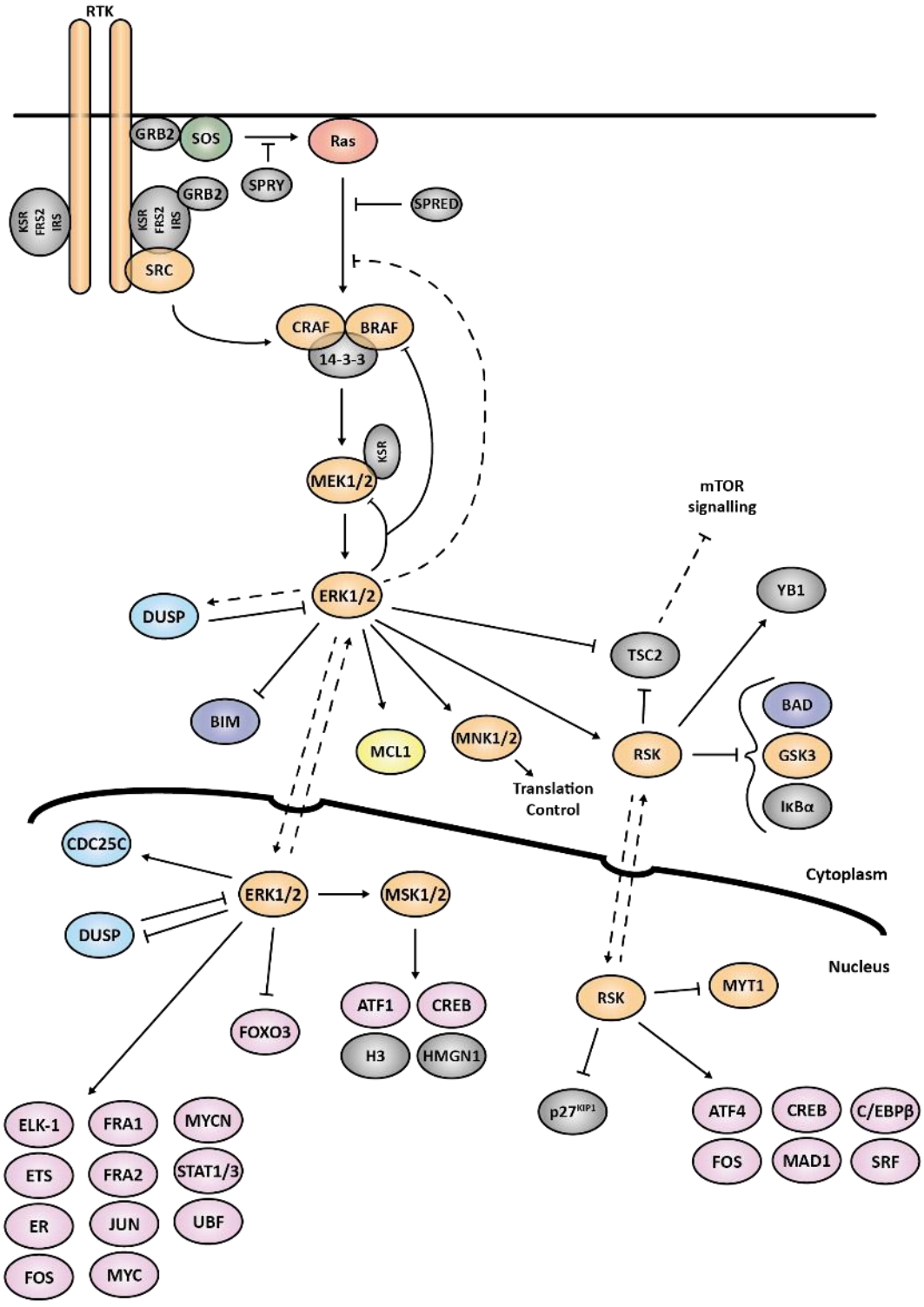

Figure 1.5 Overview of the Ras-RAF-MEK1/2-ERK1/2 (ERK1/2) signalling pathway. Ligand binding at the RTK (receptor tyrosine kinase) enabling its autophosphorylation and recruitment of SOS (son of sevenless) which activates Ras at the plasma membrane. Active GTP-bound Ras binds to and activates RAF, which then phosphorlyates and activates MEK1/2, which in turn phosphorylates and activates ERK1/2. Scaffold proteins including KSR are required to accommodate activation of downstream kinases and therefore complete activation of the signalling cascade. In the cytoplasm, active ERK1/2 can phosphorylate and activate numerous downstream kinases including RSK, MSK and MNK. In addition, phosphorylated ERK1/2 can translocate to the nucleus and activate multiple transcription factors, including ETS and AP-1 families, some of which are depicted in pink, that in turn induce the expression of genes required for, and to regulate, cell proliferation and survival. The ERK1/2 signalling pathway is regulated by multiple feedback mechanisms. Rapid feedback mechanisms can occur directly as a consequence of inhibitory phosphorylation by ERK1/2 and downstream kinases including RSK. Slower feedback mechanisms rely upon the *de novo* expression of DUSPs, SPRED and SPRY proteins. Together these act to dampen down the signalling output to fine-tune the ERK1/2 signalling cascade response.

ERK1/2 signalling is regulated by negative, and to a lesser extent, positive feedback. Rapid negative feedback can occur via inhibitory phosphorylation of upstream components by ERK1/2, including RAF (Dougherty *et al.*, 2005, Ritt *et al.*, 2010) and MEK (Eblen *et al.*, 2004). Thus, active ERK1/2 regulates its own activation indicative of a negative feedback loop.

On a longer timescale, sprouty (SPRY), SPRED and the dual-specificity phosphatases (DUSPs) act to inhibit ERK1/2 signalling. Interestingly, ERK1/2 signalling has been proposed to induce the expression of *SPRY* and *DUSP5/6* mRNA, thus resulting in a negative feedback loop regulating its own activity (Ekerot *et al.*, 2008, Kucharska *et al.*, 2009, Ozaki *et al.*, 2001). SPRY inhibits ERK1/2 signalling at the level of RTKs, SOS and RAF (Masoumi-Moghaddam *et al.*, 2014), whilst DUSPs, notably the MAP kinase phosphatases (MKPs), oppose MEK1/2 and dephosphorylate ERK1/2 at the T-E-Y motif, thereby terminating activation of ERK1/2 (Caunt and Keyse, 2013, Kidger and Keyse, 2016). As DUSPs are localised to different cellular compartments it enables the spatial regulation of ERK1/2 activation (Caunt *et al.*, 2008). SPRED has been shown to block RAF activation by inhibiting the phosphorylation and therefore activation of RAF, potentially through the disruption of the Ras-RAF interaction (Cabrita and Christofori, 2008, Wakioka *et al.*, 2001).

Interestingly, DUSP1 (MKP-1), SPRY proteins and SPRED proteins have been demonstrated to be regulated through ubiquitylation. DUSP1 (MKP-1) has been shown to be phosphorylated by ERK, thereby driving its ubiquitylation, by the SKP2 (S-phase kinase-associated protein 2)/CKS1 (CD28 protein kinase b1) E3 ligase complex, resulting in its degradation (Calvisi *et al.*, 2008, Lin *et al.*, 2003, Lin and Yang, 2006). In addition, the degradation of SPRY proteins, including SPRY2, was observed to occur as a consequence of interaction with the E3 ligases c-Cbl and Siah2 (Egan *et al.*, 2002, Hall *et al.*, 2003, Nadeau *et al.*, 2007, Rubin *et al.*, 2003). SPRED proteins (SPRED-2) have been demonstrated to be ubiquitylated in response to cellular stimulation with EGF (Lock *et al.*, 2006).

1.3.1.1. p90 RSK

As depicted in Figure 1.5, one of the downstream targets of ERK1/2 is RSK. p90 ribosomal S6 kinases (RSK1/2/3/4) are a family of Ser/Thr kinases that regulate multiple cellular processes including cell proliferation and cell cycle progression.

All RSK isoforms are comprised of two kinase domains, an N-terminal kinase domain (NTKD) and a C-terminal kinase domain (CTKD), which are connected via a linker region (Anjum and Blenis, 2008, Carriere *et al.*, 2008, Romeo *et al.*, 2012). Unlike the other RSK isoforms, RSK4, is constitutively active, predominantly found in the cytosol and acts independently of growth factors (Dummier *et al.*, 2005). ERK1/2 can interact with the ERK1/2-docking D-domain in the C terminus of RSK (Roux *et al.*, 2003). Once activated, ERK1/2 phosphorylates T573 in the activation loop of the CTKD of RSK (described amino

acids (aa) are for RSK1), and additionally may phosphorylate S363 and T359 within the linker domain. Phosphorylation of T573 activates the CTKD and results in the autophosphorylation of S380. This provides a platform for the recruitment of PDK1 to the linker region, which additionally phosphorylates S221 in the NTKD, resulting in the full activation of RSK and subsequent phosphorylation of a diverse set of cytoplasmic and nuclear substrates. Differences in the N-terminal sequence of the RSK isoforms could account for their varied substrates. In addition to ERK1/2, RSK can be activated by alternative kinases including p38 MAPK and ERK5 (Ranganathan *et al.*, 2006, Zaru *et al.*, 2007) and specifically RSK2 can be phosphorylated by FGFR3 at Y529.

Interestingly, the RSK isoforms are functionally different in the context of cancer. RSK1 and/or RSK2 have been demonstrated to promote tumour cell growth and survival, whilst RSK3 and RSK4 have been reported to act as tumour suppressors; notably RSK4 has been demonstrated to contribute to p53-dependent cell cycle arrest and oncogene-induced senescence (Berns *et al.*, 2004, Bignone *et al.*, 2007, Lopez-Vicente *et al.*, 2009). Given this, inhibitors have been developed to target specific RSK isoforms which could be used as anti-cancer therapies (Casalvieri *et al.*, 2017).

1.3.1.2. ERK1/2-mediated regulation of pro-survival BCL2 proteins.

Survival factors can activate the ERK1/2 signalling pathway to increase expression of pro-survival proteins including BCL2, BCL-X_L and MCL1 (Figure 1.6). For example, activation of ERK1/2 and the downstream kinases RSK1/2 and MSK1/2 leads to the phosphorylation and activation of the transcription factor CREB (cAMP-response element-binding protein), which promotes the transcription of several pro-survival BCL2 proteins (Bonni *et al.*, 1999, Boucher *et al.*, 2000, Wilson *et al.*, 1996).

ERK1/2 signalling also regulates the stability of MCL1. ERK1/2 phosphorylates MCL1 at T163 within its N-terminal PEST (Proline (P), glutamic acid (E), serine (S) and threonine (T) rich sequence) domain, leading to increased protein stability (Domina *et al.*, 2004). This pro-survival signal is counteracted by GSK3β, which phosphorylates MCL1 on S159, promoting its polyubiquitylation and proteasomal degradation (Maurer *et al.*, 2006).

1.3.1.3. ERK1/2-mediated regulation of pro-apoptotic BH3-only proteins (BOPs).

At least six of the described BOPs have been proposed to be regulated by the ERK1/2 signalling pathway (Balmanno and Cook, 2009) (Figure 1.6). BAD, BIM, BMF, PUMA and BIK are all repressed or inhibited as a result of ERK1/2 signalling. Phosphorylation of BAD results in its sequestation by 14-3-3 proteins in the cytosol, which inhibits its pro-apoptotic activity at the mitochondria (Zha *et al.*, 1996). Specifically, BAD is phosphorylated on S112, in a MEK1/2-dependent manner (Fang *et al.*, 1999, Scheid *et al.*, 1999) by RSK and MSK downstream of ERK1/2 (Bonni *et al.*, 1999, She *et al.*, 2002, Shimamura

et al., 2000). Phosphorylation of BAD at S112, in addition to S136, enables the cAMP-dependent PKA-driven phosphorylation of BAD within its BH3 domain (S155) which prevents it interaction with BCL-X_L (Datta *et al.*, 2000). In addition to inactivation, ERK1/2 signalling has been suggested, in certain cell types, to promote the proteasomal degradation of BAD (Fueller *et al.*, 2008, Howie *et al.*, 2008). Phosphorylation of BIK by ERK1/2 has been demonstrated to induce its ubiquitin-dependent proteasomal degradation (Lopez *et al.*, 2012). However, this is controversial and recent studies have suggested that these observations may have been an artefact of its cell cycle-dependent regulation rather than ERK1/2 activity (Cook *et al.*, 2017, Sale and Cook, 2014).

Inhibition of the ERK1/2 pathway, by MEK1/2 inhibitors, has been shown to induce the expression of BIM, BMF and PUMA (Balmanno and Cook, 2009, Sale and Cook, 2013).The mechanism by which ERK1/2 signalling represses BMF is unclear. However, ERK2 has been shown to phosphorylate and inhibit BMF (Shao and Aplin, 2012) and the ERK1/2 pathway can regulate the expression and localisation of BMF (Shao and Aplin, 2012, VanBrocklin *et al.*, 2009). ERK1/2-dependent regulation of FOXO3 (Forkhead box O3) may block the expression of PUMA (Yang *et al.*, 2008), however the exact mechanism is unclear.

In contrast to the previously described BOPs, activation of the ERK1/2 signalling pathway induces *NOXA* mRNA and protein expression, which is thought to occur due to the CREB-driven transcription of *NOXA* (Liu *et al.*, 2014). As a consequence of induction, NOXA has been suggested to bind to MCL1, and displace Beclin-1, thereby inducing autophagy (Elgendy *et al.*, 2011, Liu *et al.*, 2014). Conversely, RAF and/or MEK1/2 inhibition, in cancers driven by ERK1/2 signalling ($BRAF^{V600E}$ melanoma), caused the downregulation NOXA (Basile and Aplin, 2012).

1.3.2. BIM

BIM (BCL2 interacting mediator of cell death) was identified by its binding to BCL2 in a cDNA expression cloning screen and as BOD (BCL2-related ovarian death gene) in a yeast two-hybrid screen (Hsu *et al.*, 1998, O'Connor *et al.*, 1998). BIM plays an important role in leukocyte homeostasis by promoting B and T cell apoptosis. It is also essential for preventing autoimmunity, by eliminating autoreactive lymphocytes.

As a consequence of BIM being an important regulator of apoptosis, its expression is tightly regulated. Expression of *BIM* is upregulated at the transcription level via the transcription factor FOXO (Dijkers *et al.*, 2000, Gilley *et al.*, 2003). Following cytokine withdrawal in lymphocytes, transcription of *BIM* is promoted by FOXO3A (Dijkers *et al.*, 2000). The activity of FOXO proteins is regulated through posttranslational modifications (PTMs) including phosphorylation and ubiquitylation. Phosphorylation

Figure 1.6 Regulation of apoptosis by ERK1/2 signalling.

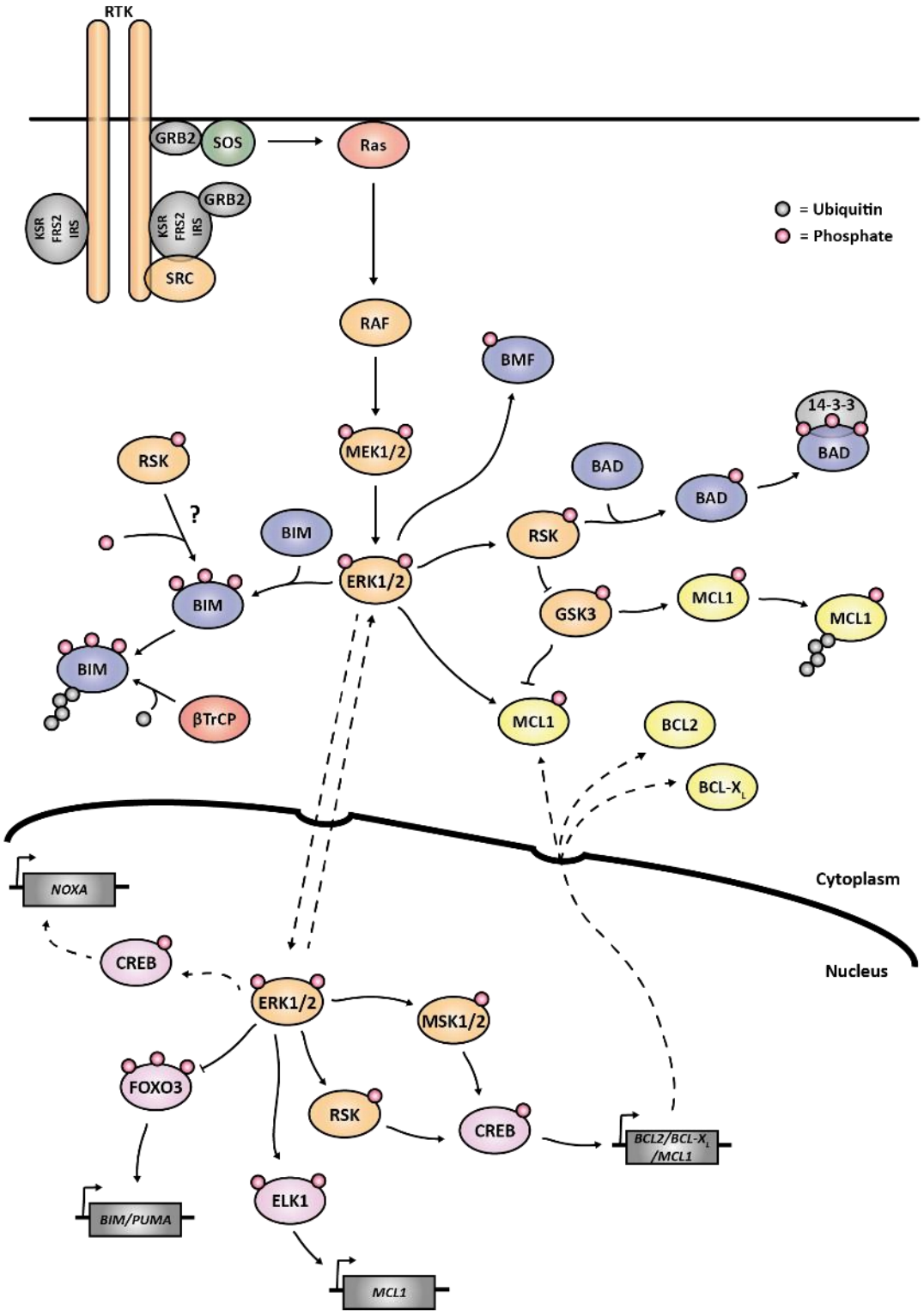

Figure 1.6 Regulation of apoptosis by ERK1/2 signalling. Activation of the ERK1/2 signalling pathway influences the expression and/or activity of several pro-apoptotic and pro-survival BCL2 proteins. Active ERK1/2 can in turn phosphorylate substrates directly, including the pro-apoptotic protein BIM, leading to its polyubiquitylation and degradation via the proteasome or activate downstream kinases including RSK, which can phosphorylate additional targets including BAD resulting in its sequestration by 14-3-3 proteins and inactivation. In the nucleus, ERK1/2, and downstream kinases, can activate transcription factors, including CREB and ELK1, which can induce the transcription of pro-survival proteins, *BCL2, BCL-X*$_L$ and *MCL1*. In addition ERK1/2 can phosphorylate FOXO3, initiating its degradation and abolishing FOXO3-driven transcription of pro-apoptoic proteins *BIM* and *PUMA*. In contrast, ERK1/2 activity can induce the transcription of *NOXA*. Despite this, in general, ERK1/2 signalling induces the expression of pro-survival proteins and represses the expression of pro-apoptotic proteins, thereby promoting cell survival (adapted from Balmanno and Cook, 2009, Sale and Cook, 2013, Cook et al., 2017).

of FOXO3A by active PKB has been shown to drive its nuclear export and therefore reduce the expression of BIM. PKB phosphorylation of FOXO3A has also been shown to promote its degradation by the proteasome (Huang *et al.*, 2005). The ERK1/2 pathway also inhibits FOXO3A by causing its phosphorylation, consequent polyubiquitylation and degradation by the 26S proteasome (Yang *et al.*, 2008). As such, the expression of *BIM* is induced in response to withdrawal of cytokines, and survival factors, as a consequence of inactivation of the PKB or ERK1/2 signalling pathways (Dijkers *et al.*, 2000, Weston *et al.*, 2003). In addition, in sympathetic neurons, withdrawal of nerve growth factor (NGF) results in an increase in *BIM* mRNA in response to overexpression of FOXO transcription factors and activation of the JNK-c-Jun pathway (Gilley *et al.*, 2003, Putcha *et al.*, 2003, Whitfield *et al.*, 2001).

Other transcriptional and post-translational regulators of BIM include CHOP-C/EBPα and protein phosphatase 2A (PP2A) (Puthalakath *et al.*, 2007). These both increase the expression and reduce the degradation (respectively) of BIM following ER stress. Recently CHOP-C/EBPα has been shown to cooperate with FOXO3A to induce expression of BIM in neuronal cells (Ghosh *et al.*, 2012). In addition, the transcription factor RUNX3 increases expression of BIM in gastric cancer cell lines following treatment with TGF-β (Yano *et al.*, 2006). BIM is also regulated at the post-transcriptional level by micro RNAs, including miR-17-92a and miR-494 (Guo *et al.*, 2013, Romano *et al.*, 2012).

BIM can be found as multiple protein isoforms generated by alternative splicing (Adachi *et al.*, 2005, Bouillet *et al.*, 2001). The most common of these are BIM_S, BIM_L and BIM_{EL}, which vary in pro-apoptotic potency and abundance (O'Connor *et al.*, 1998), with BIM_S being the most toxic and least abundant isoform. The difference in potency can be partially attributed to the presence or absence of a dynein light chain 1 (DLC-1) domain (Puthalakath *et al.*, 1999). The absence of a DLC-1 domain has been proposed to prevent the sequestration of BIM_S at microtubules making BIM_S a more cytotoxic isoform. In response to a pro-apoptotic signal BIM_L and/or BIM_{EL} are phosphorylated by JNK at T116, resulting in their dissociation from microtubules (Lei and Davis, 2003).

Structurally, BIM possesses a C-terminal sequence required for its targeting and anchorage in the OMM. Once attached to the membrane BIM is active and can recruit and activate pro-apoptotic BCL2 proteins. Localisation to the OMM is independent of its BH3 domain and the presence of BCL2 proteins, but requires the rest of the protein to be intact (Wilfling *et al.*, 2012).

BIM_{EL} is the largest (198 amino acids) and most abundant isoform and is proposed to have the lowest pro-apoptotic potency, although it is still a potent pro-death protein (O'Connor *et al.*, 1998). Unlike BIM_S and BIM_L, BIM_{EL} contains a DEF domain that enables it to bind to ERK1/2 (Ley *et al.*, 2005). BIM_{EL} possesses multiple phosphorylation sites as well as two sites for ubiquitylation (K3 and K108) and these sites provide a means for the post-translational control of BIM_{EL} abundance. ERK1/2 phosphorylates BIM_{EL} on at least three Ser-Pro sites, including S69, targeting BIM_{EL} for K48-linked polyubiquitylation

and subsequent degradation, via the 26S proteasome (Ewings *et al.*, 2007, Ley *et al.*, 2003, Ley *et al.*, 2004, Luciano *et al.*, 2003, Marani *et al.*, 2004, Wiggins *et al.*, 2011). Studies have also shown that a mutant form of BIM_{EL}, lacking both lysine residues required for K48-linked polyubiquitylation, can still be degraded upon activation of the ERK1/2 pathway independently of the canonical 26S proteasome (Wiggins *et al.*, 2011). Others have suggested that phosphorylation of BIM_{EL}, by ERK1/2, primes BIM_{EL} for additional phosphorylation by RSK1/2, generating a binding site required for its polyubiquitylation and proteasomal degradation (Dehan *et al.*, 2009). Interestingly, phosphorylation of BIM_{EL}, by ERK1/2, has been demonstrated to drive its dissociation from pro-survival BCL2 proteins, including BCL-X_L and MCL1, which enhanced its degradation (Ewings *et al.*, 2007). Tumour cells addicted to ERK1/2 signalling are reliant upon the phosphorylation-dependent repression of BIM (Wickenden *et al.*, 2008) and inhibitors of the ERK1/2 pathway induce the expression of BIM in multiple cancer cell lines (Faber *et al.*, 2011).

Many candidates have been suggested for the E3 ubiquitin ligase required for the polyubiquitylation of Bim_{EL}, however the majority of published data indicates that $SCF^{\beta\text{-}TrCP}$ is the E3 ligase for Bim_{EL}. In addition to βTrCP, as part of a larger SCF complex, c-Cbl, a RING finger protein, has also been proposed to act as an E3 ligase for BIM_{EL} in osteoclasts (Akiyama *et al.*, 2003). However, this is controversial as, unlike that observed for BIM_{EL}, the majority of c-Cbl substrates require phosphorylation of conserved tyrosine residues for substrate-E3 ligase interaction, polyubiquitination and degradation and, as such, there is no evidence of a direct interaction between BIM_{EL} and c-Cbl (El Chami *et al.*, 2005, Meng *et al.*, 1999, Wiggins *et al.*, 2007).

In response to paclitaxel treatment of cancer cells, RACK1 complexes with DLC1 and BIM_{EL} and results in the CIS-mediated degradation of BIM_{EL} by ElonginB/C-Cullin2-CIS (Zhang *et al.*, 2008). In contrast to this, in renal cell carcinoma cells, Guo *et al.* demonstrated that pVHL, part of the elongins B and C and Cul2 family, stabilised BIM_{EL}. This was predicted to be as a result of inhibition of ERK1/2-dependent phosphorylation of BIM_{EL} or as a consequence of the interference between BIM_{EL} and its E3 ligase (Guo *et al.*, 2009). These two studies suggest that the same E3 ligase core can have opposing effects on the same protein.

During mitosis $APC^{CDC\text{-}20}$ has been shown to interact with BIM_{EL} to promote its degradation. In this case, phosphorylation by ERK1/2 and RSK1/2 is not required for this interaction (Wan *et al.*, 2014). Moustafa-Kamal and colleagues demonstrated that during mitosis the degradation of BIM_{EL} is regulated by the Aurora A kinase and protein phosphatase 2A (PP2A) (Moustafa-Kamal *et al.*, 2013). Aurora A phosphorylates BIM_{EL} within the recognised βTrCP binding motif at S93, S94 and S98, enabling interaction with βTrCP1, thus promoting its polyubiquitination and degradation. Indeed, mutation of S94/S98 but not S69, a known ERK1/2 phosphorylation site, resulted in defective polyubiquitination and stabilisation of BIM_{EL} in mitosis. Similarly, inhibition of Aurora A by MLN8054, stabilised BIM_{EL}

(Moustafa-Kamal *et al.*, 2013). Mitotic phosphorylation of BIM_{EL} by CDK1 has also been found to drive the polyubiquitination and degradation of BIM_{EL} (Gilley *et al.*, 2012). More recently, Thompson *et al.* identified, by mass spectrometry, that TRIM2, a RING-containing E3 ligase, interacts with ERK1/2-driven phosphorylated BIM (Thompson *et al.*, 2011). However, it still needs to be determined if TRIM2 requires additional proteins to drive the ubiquitylation of BIM or acts alone. In murine B-ALL cells, the E3 ligase TRIM33 has been shown to prevent apoptosis by interfering with the activation of BIM (Wang *et al.*, 2015a). In addition, increased expression of E3 ligase SIAH1 resulted in the induction of apoptosis as a consequence of increased expression of BIM, via the JNK pathway (Wen *et al.*, 2010). Overall, given the various E3 ligases reported to ubiquitylate BIM, it suggests a level of redundancy in the E3 ligase-driven regulation of BIM. It also implies that specific E3 ligases may play a role in the regulation of BIM under a specific set of conditions, including different drug treatments, cell lines and the stage of the cell cycle.

The counteracting deubiquitylating enzyme (DUB) for BIM has recently been identified (Weber *et al.*, 2016). USP27x was shown to interact with BIM, dependent upon its ERK1/2-driven phosphorylation, resulting in its increased expression. Overexpression of USP27x also resulted in an increase in caspase-dependent apoptosis.

In addition to its role in apoptosis, BIM has been shown to inhibit autophagy by directly interacting with and mislocalising Beclin-1 (Luo *et al.*, 2012). BIM_{EL} is phosphorylated at S59 in response to activation of the ERK1/2 signalling pathway in inflammatory breast cancer which leads to BIM_{EL} being sequestered by LC8 and Beclin-1 which protects cells from extracellular matrix (ECM)-detachment-induced apoptosis (anoikis) (Buchheit *et al.*, 2014).

1.3.3. Ras-RAF-MEK1/2-ERK1/2 signalling in cancer

Aberrations in the ERK1/2 signalling pathway are frequently found in cancer. Ras is mutated in ~20-30% of all cancers (Bos, 1989, Karnoub and Weinberg, 2008). The most abundant mutations in KRas are at codon 12, 13 and 61, and mechanistically prevent GAPs from enhancing the GTPase activity of Ras, thereby rendering Ras constitutively active which drives inappropriate cell proliferation (Adari *et al.*, 1988, Trahey and McCormick, 1987).

More recently, mutations in RAF, MEK1/2 and ERK1/2 have also been identified in cancer (Caunt *et al.*, 2015, Davies *et al.*, 2002, Kidger *et al.*, 2018). BRAF mutations are found in ~66% of melanoma (Davies *et al.*, 2002). The most common mutation is V600E and this alters its conformation alleviating inhibition by its N-terminal regulatory region (Tran *et al.*, 2005, Wan *et al.*, 2004). The first described mutation of MEK was $MEK2^{P298L}$ in lung cancer and since then several activating mutations have been identified in ovarian cancer, melanoma and colorectal carcinoma (CRC) (Arcila *et al.*, 2015, Bansal *et al.*, 1997, Estep

et al., 2007, Marks *et al.*, 2008, Nikolaev *et al.*, 2011). Primary disease causing mutations in ERK1/2 appear to be rare, however some have been found including ERK2^{E322K} in cervical carcinoma and head and neck squamous cell carcinoma (Arvind *et al.*, 2005, Lawrence *et al.*, 2014, Ojesina *et al.*, 2013).

1.3.3.1. Inhibition of ERK1/2 signalling as a cancer therapy.

As a consequence of the dependence on ERK1/2 signalling for tumour proliferation there is significant interest in the development of potent small-molecule inhibitors of all components of the pathway.

The discovery of activating BRAF^{V600E} mutations (Davies *et al.*, 2002) led the development of vermurafenib (PLX4032), and soon after dabrafenib, which are potent and highly selective BRAF inhibitors (BRAFi), only effective in tumours containing BRAF^{V600E} driver mutations including melanoma and hairy cell leukaemia (Holderfield *et al.*, 2014, Joseph *et al.*, 2010, Tiacci *et al.*, 2015). Unfortunately, these inhibitors drive paradoxical activation of MEK1/2 and ERK1/2 in tumours with wild-type BRAF, including those with Ras mutations (Holderfield *et al.*, 2014, Poulikakos *et al.*, 2011). As a consequence, attention has refocused on the development of MEK inhibitors (MEKi) to treat Ras mutant tumours (Caunt *et al.*, 2015).

The first MEKi to be assessed *in vivo* was PD184352, which was shown to inhibit the growth of CRC xenografts (Sebolt-Leopold *et al.*, 1999). However due to low potency and poor bioavailability (Rinehart *et al.*, 2004), more selective MEKis have since been developed. The outcome of MEKi treatment on tumour cells largely depends on its mechanism of action, namely whether its action abrogates the phosphorylation of MEK1/2 or not. In cells with wild-type BRAF, including those with Ras mutations, loss of ERK1/2 activity with allosteric MEKis (PD0325901, selumetinib and cobimetinib) relieves negative feedback on the pathway. This typically results in the accumulation of phosphorylated MEK1/2, activation of ERK1/2 and restoration of pathway output. As a result, these MEKis have been used to treat BRAF^{V600E} tumour cells, as here BRAF acts as an active monomer independent of CRAF binding and is therefore insensitive to negative feedback (Caunt *et al.*, 2015). In contrast, MEKis that also inhibit MEK1/2 phosphorylation by disrupting the conformation of its activation loop (feedback buster' MEKis; trametinib and GDC-0623) suppress the rebound in ERK1/2 activation caused by the removal of negative feedback and therefore generate a more durable pathway inhibition (Hatzivassiliou *et al.*, 2013, Lito *et al.*, 2014). Both trametinib and cobimetinib are clinically approved for the treatment of BRAF^{V600E} mutant tumours. MEKi treatment of tumour cells typically causes a G1 arrest despite the induction of pro-apoptotic proteins including BIM, BMF and PUMA. This outcome is most likely due to the high expression of pro-survival proteins. This arrest provides an opportunity for tumour cells to adapt and develop acquired resistance to these drugs (Sale and Cook, 2013) (Figure 1.7).

Figure 1.7 Combined treatment of ERK1/2-addicted tumour cells with MEK1/2 inhibitors and BH3 mimetics overcomes cell cycle arrest, observed with MEK1/2 inhibitor monotherapy, to induce apoptosis.

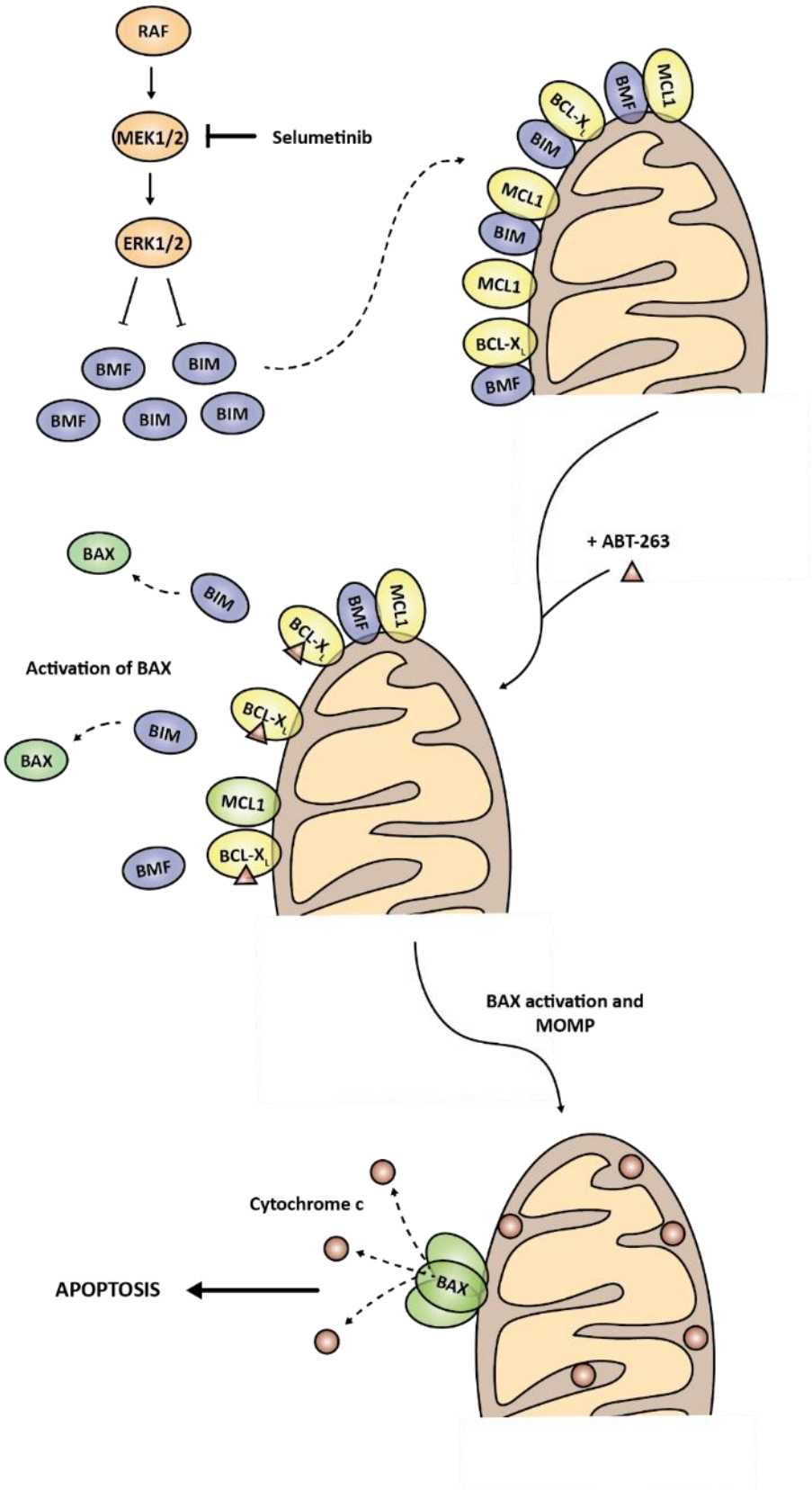

Figure 1.7 Combined treatment of ERK1/2-addicted tumour cells with MEK1/2 inhibitors and BH3 mimetics overcomes cell cycle arrest, observed with MEK1/2 inhibitor monotherapy, to induce apoptosis. Based on work from Sale and Cook, treatment of tumour cells with the MEK1/2 inhibitor Selumetinib resulted in a cytostatic G1 cell cycle arrest due, in part, to residual BCL2 pro-survival proteins masking the pro-apoptotic effect of induced BIM and BMF proteins. Addition of the BH3 mimetic, to cells treated with the MEK1/2 inhibitor, inhibited pro-survival proteins releasing pro-apoptotic proteins, induced as a consequence of MEK1/2 inhibition, which can then bind to and activate effector pro-apoptotic proteins, BAX. Thus, enabling MOMP, release of cytochrome c and activation of the caspase cascade (Sale and Cook, 2013).

Acquired resistance to BRAFis emerges due to multiple mechanisms including the generation of alternative splice variants of BRAF, using alternative pathways involving ARAF, CRAF or alternative activators of MEK1/2, emergence of mutations in KRas and MEK1 and an up-regulation of RTKs (Johannessen *et al.*, 2010, Montagut *et al.*, 2008, Nazarian *et al.*, 2010, Poulikakos *et al.*, 2011, Wagle *et al.*, 2011). Acquired resistance to MEKis arises due to amplification of the driving oncogene, KRas or BRAF (Little *et al.*, 2011) and mutations in MEK1 (Emery *et al.*, 2009). The common feature in most, if not all, of these studies is the re-activation or maintenance of ERK1/2 signalling in the presence of BRAFi or MEKi. Combining BH3 mimetics with BRAFi or MEKi is an effective way of harnessing ERK1/2 pathway addiction to drive apoptosis and these combinations have proved very effective in killing tumour cells and delaying the onset of acquired resistance to ERK1/2 pathway inhibitors (Sale and Cook, 2013) (Figure 1.7). In part due to toxicity in normal tissue with MEKi monotherapy, BRAFi and MEKi have been used in combination (Long *et al.*, 2014), however like that seen with BRAFi and MEKi monotherapy, cells with mutant BRAF quickly develop resistance and may require additional therapies to prolong responses including immunotherapies (Ahronian *et al.*, 2015, Hu-Lieskovan *et al.*, 2015).

ERK1/2 inhibitors (ERKis) have been developed over the last 15 years (Kidger *et al.*, 2018). The majority of the described ERKis are reversible and ATP-competitively target catalytic activity; however some inhibit the ability of ERK1/2 to be phosphorylated by MEK1/2 and are termed 'dual mechanism' inhibitors, including SCH772984 (Deng *et al.*, 2014, Lim *et al.*, 2016, Zhu *et al.*, 2015). Allosteric inhibitors are in-development and have been shown to prevent ERK1/2 from interacting with its described binding partners (Chen *et al.*, 2006, Hancock *et al.*, 2005). Like MEKis, ERKis do not discriminate between mutant and wild-type ERK1/2 and they therefore have the potential to be toxic outside of a narrow therapeutic window. As such, ERKis may have limited use as a monotherapy (Goetz *et al.*, 2014) and may be best used in combination with BH3 mimetics or to treat mutant BRAF tumour cells that have acquired resistance to BRAFi through reactivation of ERK1/2 signalling (Morris *et al.*, 2013).

1.3.4. mTOR signalling

mTOR (mechanistic target of rapamycin) is a Ser/Thr kinase in the PI3K-related kinase (PIKK) family. It is the catalytic subunit of two distinct protein complexes, mTOR Complex 1 (mTORC1) and mTOR complex 2 (mTORC2). mTORC1 is the better understood of the complexes and is in part activated through inhibition of the tuberous sclerosis 1 and 2 heterodimer (TSC1/2) by ERK1/2, PKB and RSK (Laplante and Sabatini, 2012). mTORC1 has been shown to repress autophagy, through phosphorylation of unc-51-like kinase 1 (ULK1), and promote protein synthesis, through phosphorylation of S6 kinase and 4E-BP (eIF (eukaryotic initiation factor) 4E-binding protein) 1 and 2 (Ben-Sahra *et al.*, 2013, De Benedetti and Graff, 2004, Kim *et al.*, 2011a). Phosphorylation of 4EBP

results in the initiation of cap-dependent translation through the release of eIF4E. Of note, ERK1/2 and mTOR signalling have been found to converge at the level of eIF4E (Cope *et al.*, 2014, Hou *et al.*, 2012). Ultimately, the mTOR pathway senses environmental conditions and regulates cell growth, proliferation and survival.

Deregulated mTOR signalling has been implicated in driving the progression of several diseases including cancer (Menon and Manning, 2008, Saxton and Sabatini, 2017). mTOR is hyperactivated in many cancers due to mutational activation of Ras, BRAF and PI3K and repression of LKB1, PTEN, and TSC1/2, in addition to mutations in mTOR itself (Gerlinger *et al.*, 2012, Laplante and Sabatini, 2012). As such, ATP-competitive mTOR inhibitors are in-development for the treatment of cancer. Similar to that observed for inhibitors of the ERK1/2 pathway, cells can develop resistance mechanisms to mTOR inhibition. Predominantly, this has been shown to be through the maintenance or activation of cap-dependent mRNA translation. Cope *et al.* observed that resistance to the mTOR inhibitor AZD8055 occurred through the amplification of *eIF4E* which resulted in an increase in eIF4E responsive mRNA products including MCL1 and cyclin D1 (Cope *et al.*, 2014). They also observed that these cells exhibit a cytostatic G1 arrest to acute mTOR inhibitor treatment.

Due to the suggested limitations of mTOR inhibitors as a single agent, combinatorial treatments have been suggested to hold more promise (Conciatori *et al.*, 2018). Treatment with mTOR inhibitors has also been demonstrated to activate autophagy and the UPS, both of which are required to degrade and recycle proteins. mTORC1 inhibition was shown to rapidly cause an increase in proteasome-dependent proteolysis, which Zhao *et al.* have suggested to be caused by an increase in protein ubiquitylation (Zhao *et al.*, 2015). Given this, combination studies that have been used include the use of mTOR inhibitors and Bortezomib, the proteasome inhibitor, to prevent the degradation of IκB and therefore activation of NF-κB signalling (Conciatori *et al.*, 2018, Wang *et al.*, 2012)

1.4. Ubiquitin as a post-translational modification.

Modification of a protein with functional groups, after translation, is a universal mechanism for altering its behaviour. Different types of PTM, including phosphorylation, acetylation, glycosylation and ubiquitylation, can alter the charge, hydrophobicity, conformation, stability and localisation of a given protein (Venne *et al.*, 2014). Given this, changes in such post-translational modifications (PTMs) are linked to numerous diseases.

Ubiquitylation of proteins is one of the most important regulatory PTMs and plays a central role in protein degradation as well as numerous non-degradative roles including protein trafficking, DNA damage response pathways and cell signalling (Chen and Sun, 2009, Hershko and Ciechanover, 1998, Komander and Rape, 2012, Swatek and Komander, 2016, Yau and Rape, 2016).

Ubiquitin (Ub) is conjugated to a protein in a series of catalytic reactions culminating in the E3 ligase-driven formation of an isopeptide bond. However, ubiquitylation is reversible and a family of approximately 100 enzymes, deubiquitinating enzymes (DUBs), oppose E3 ligases and remove Ub from a target protein (Komander *et al.*, 2009a, Nijman *et al.*, 2005).

1.4.1. Ubiquitylation.

Ub is a compact 76 aa protein that possesses a flexible six-residue carboxy-terminal tail. It is covalently attached to a protein in a three-step enzymatic cascade conducted sequentially by; ubiquitin-activating enzymes (E1), ubiquitin-conjugating enzymes (E2), and ubiquitin ligase enzymes (E3). These enzymes collectively act to covalently attach Ub, usually, via its carboxy terminus to lysine (K) residues within the target protein (Komander, 2009, Pickart, 2001) (Figure 1.8A). Interestingly, 'E4 enzymes' have also been described that collaborate with E1, E2 and E3 enzymes for multiubiquitylation of substrates (Hoppe, 2005). Examples of E4 enzymes include the yeast UFD2 (ubiquitin fusion degradation) and p300/CREB (Shi *et al.*, 2009).

Ubiquitin conjugation

E3 ligases are capable of catalysing the initial ubiquitylation of the substrate and consequent formation of polyubiquitin chains. To achieve this, E3 ligases must be capable of interacting with an E2 enzyme, the ubiquitylation signal of a substrate and also of targeting individual lysine residues within an acceptor Ub molecule (Berndsen and Wolberger, 2014, Kulathu and Komander, 2012).

Other post-translational modifications, including phosphorylation, may be required for the E3 ligase, or E2 enzyme, to recognise the target protein. This event provides additional regulation, particularly in signals that lead to protein degradation (Berndsen and Wolberger, 2014). E3 ligases can exist in an autoinhibited state predominantly as a consequence of intramolecular interactions. Release from inhibition can occur as consequence of post-translational modification, but also as a result of protein-interactions including, SMURF2 (E3):SMAD7 (Kavsak *et al.*, 2000) and HOIP (E3):HOIL-1L and/or SHARPIN (Ikeda *et al.*, 2011, Tokunaga *et al.*, 2011).

There are more than 600 E3 ligases encoded by the human genome, which can be sub-divided according to the motif that is responsible for the mechanism of Ub transfer (Metzger *et al.*, 2012) (Figure 1.8B). HECT (homologous to E6 associated protein C terminus) ligases attach Ub to the target protein in a two-step reaction, where Ub is transferred from an E2 enzyme to the active site cysteine within the C-lobe of the HECT domain, forming a thioester-linked HECT-Ub intermediate and from there to the substrate (Huang *et al.*, 1999, Metzger *et al.*, 2012). In contrast, RING (really interesting new gene) and U-box ligases act as scaffolds, binding the substrate and an E2 enzyme simultaneously which

Figure 1.8 Overview of ubiquitylation.

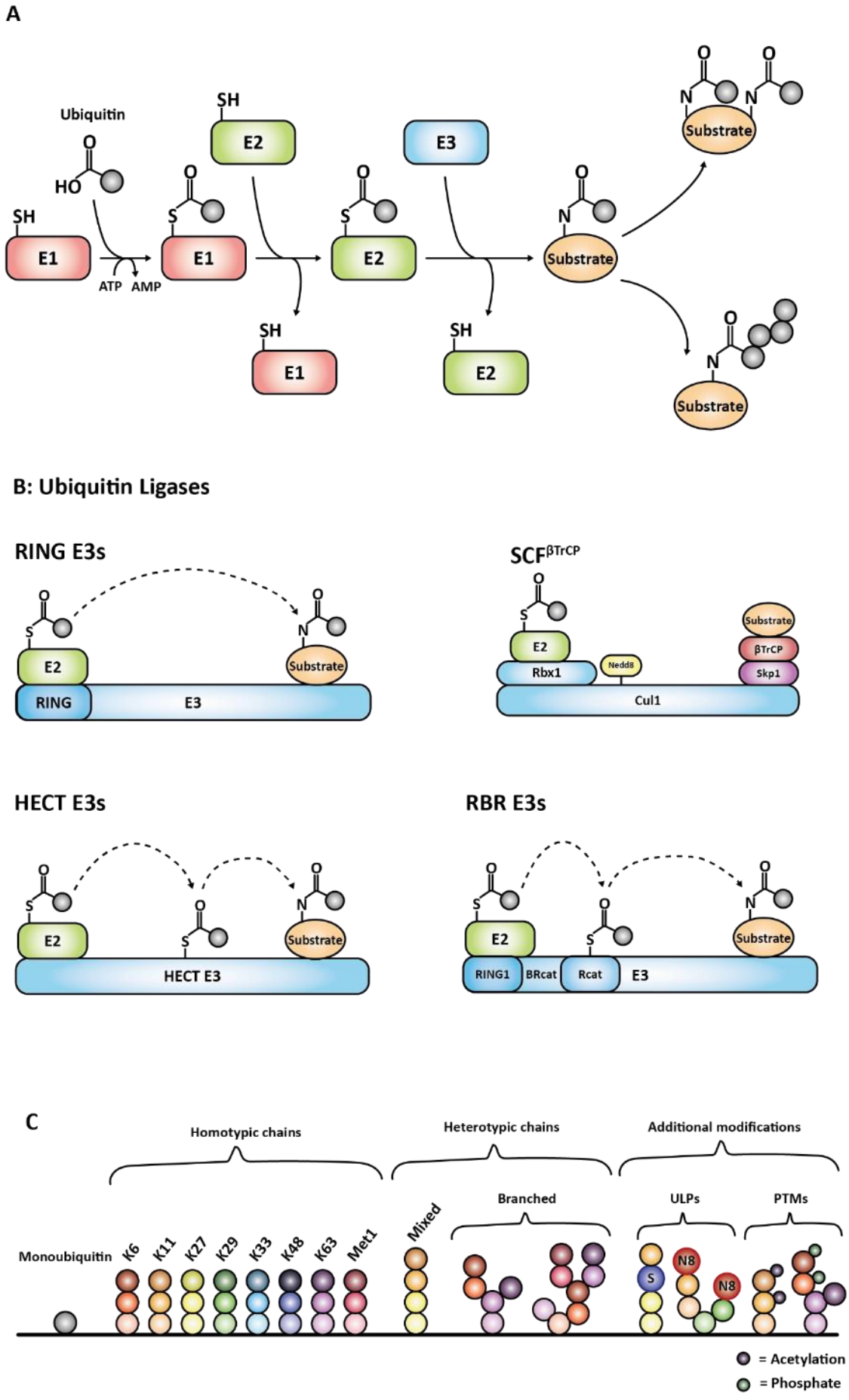

Figure 1.8 Overview of ubiquitylation. (A) Ubiquitin (Ub) is covalently attached to its substrate in a series of enzyme catalysed reactions. Initially the E1 (Ub-activating enzyme) catalyses the ATP-driven activation of Ub and its attachment to the E1 enzyme via the formation of an isopeptide bond between the C-terminus of Ub and the catalytic cysteine of the E1 ligase. Ub is then transferred from the E1 ligase to the E2 (Ub-conjugating enzmye) ligase and then, depending upon the E3 ligase (shown in Figure 1.8B), directly to the substrate or via the E3 ligase to the substrate. The subtrate specifying part of the reaction is through the E3 ligase which binds to both the E2 ligase and the substrate (adapted from Morreale and Walden, 2016). **(B)** In general, RING E3 ligases transfer Ub directly from the E2 ligase to its substrate. An example includes $SCF^{\beta TrCP}$ which is depicted. It is a Cullin-RING ligase and is composed of substrate receptor, βTrCP, an adaptor protein, Skp1, Cullin and a Ring-box protein, Rbx1. Cullin-RING E3 ligases are additionally regulated by neddylation (Nedd8). In contrast, HECT and RBR E3 ligases require a two-step mechanism for Ub transfer. Ub is first transferred from the E2 ligase to the E3 ligases itself and then from the E3 ligase to its substrate (adapted from Morreale and Walden, 2016). **(C)** A diagram depicting the complexity of ubiquitylation, with monoubiquitylation being the least complex Ub addition. Ub can be attached as polyubiquitin chains, comprised of one chain linkage type or are heterotypic, either mixed and/or branched chains. Additional complexity comes from the addition of ubiquitin-like proteins (ULPs) or post-translationl modifications (PTMs), including acetylation (shown in purple) and phosphorylation (shown in green) to the Ub molecules in the polyubiquitin chain (adapted from Mevissen and Komander, 2017).

orientates the E2-Ub thioester complex allowing for the direct transfer of Ub from the E2 enzyme to the substrate without the formation of covalent Ub-ligase intermediates (Budhidarmo *et al.*, 2012, Deshaies and Joazeiro, 2009).

RING domains act by coordinating two zinc ions between a series of cysteine and histidine residues. Several RING E3 ligases contain multiple proteins, these include the CRL ligases (Cullin-RING ligases), of which the SCF (Skp1-Cullin-F-box) family is the best characterised (Skowyra *et al.*, 1997).

A family of RBR (RING1-BRcat-Rcat or RING-betweenRING-RING) E3 ligases has also been described that contain a single canonical RING domain (RING1) and two further domains, one being the catalytic domain (Rcat) and a second that is structurally similar to Rcat but lacks ubiquitylation activity (BRcat) (Eisenhaber *et al.*, 2007, Spratt *et al.*, 2014). Interestingly, given their structural similarity to the RING E3 ligases, they behave mechanistically as a RING-HECT hybrid as they attach Ub to a substrate independently of an E2 ligase via a catalytic cysteine within its C terminus, but also recruit thioester-bound E2 enzymes via their RING domain. An important example of this sub-class of RING E3 ligases is Parkin, the E3 ligase that mediates the clearance of defective mitochondria and whose mutation has been linked to Parkinson's disease (Narendra and Youle, 2011).

Forms of Protein Ubiquitylation

Ub can be attached to a target protein as monomers, multi-monomers and as a polyubiquitin chain. For the latter one of eight internal residues (K6-, K11-, K27-, K29- K33-, K38-, K63- or Met1) can be used to form polyubiquitin chains (Komander, 2009, Peng *et al.*, 2003) (Figure 1.8C). The type of chain linkage formed dictates the fate of the target protein. The most widely studied forms of polyubiquitin chains are K48-linked, which marks the protein for degradation by the proteasome, and K63-linked which plays a non-degradative role important in protein trafficking and cell signalling. Ub polymers can be heterotypic and contain a mixture of linkages within the same chain, or one Ub molecule can be modified on multiple sites to form a branched (forked) polyubiquitin chain (Komander and Rape, 2012, Swatek and Komander, 2016, Yau and Rape, 2016) (Figure 1.8C). Greater complexity is achieved by adding ubiquitin-like proteins and/or post-translational modifications (acetylation and phosphorylation) to Ub chains (Figure 1.8C) (Swatek and Komander, 2016).

The different polyubiquitin chain types form contrasting structural conformations; 'compact' or 'open' (linear). K48-, K6- and K11-linked polyubiquitin chains adopt a compact conformation, whilst Met1- and K63- linked chains form a more 'open' or 'linear' conformation. Structural studies have revealed that K48-, K6- and K11-linked polyubiquitin chains rely upon interactions between surface hydrophobic patches (Ile44 and Ile36) on the Ub molecule to generate their compact structures. Overall, these conformations generate differing degrees of structural flexibility and positioning of functional surfaces.

This provides a means for binding partners to distinguish between the different types of polyubiquitin chain (Komander and Rape, 2012).

1.4.1.1. Ubiquitin-mediated regulation of apoptosis.

As previously described, ubiquitylation modulates a diverse range of cellular processes including apoptosis (Broemer and Meier, 2009). The ubiquitin-proteasome system (UPS) is comprised of the 26S proteasome and Ub-conjugation machinery and is the major extra-lysosomal pathway required for the degradation of proteins. The tagging of proteins with K48-, K11- and K29-linked chains, and more recently K48/K63 branched Ub chains (Ohtake *et al.*, 2018), can direct proteins to the 26S proteasome (Swatek and Komander, 2016, Yau and Rape, 2016). Coordinated degradation of proteins, via the UPS, is important for appropriate apoptosis and has been demonstrated to be required for the degradation of key cell death proteins, including BCL2 proteins, IAPs and caspases (Jesenberger and Jentsch, 2002) and as such, failure of the UPS is linked to tumourigenesis and metastasis.

Ubiquitin attachment can have an anti-apoptotic role and the classic example of this is in the regulation of p53. p53 is a tumour suppressor protein and, upon activation of various stresses, downregulates pro-survival proteins including BCL2 and upregulates pro-apoptotic proteins including APAF-1, BAX, PUMA, NOXA and Fas (Ryan *et al.*, 2001). p53 has also been demonstrated to localise to the mitochondria, promoting BAK/BAX oligomerisation and inducing MOMP (Schuler *et al.*, 2000). As such, p53 is tightly regulated and is often downregulated or mutated in tumour cells. Ubiquitylation of p53, by the E3 ligase MDM2, results in its nuclear export and degradation by the proteasome (Boyd *et al.*, 2000, Geyer *et al.*, 2000, Haupt *et al.*, 1997, Kubbutat *et al.*, 1997). Given this, MDM2 is itself regulated through interactions with E3 ligases and $p14^{ARF}$, which predominantly cause the degradation of MDM2, thereby stabilising p53 (Bernardi *et al.*, 2004, Joo *et al.*, 2011, Zhang *et al.*, 1998). Additional E3 ligases have been suggested for p53 including PIRH, COP1, TRAF7 and Cullin4B which have all been demonstrated to drive the degradation of p53 (Gupta *et al.*, 2018).

Ubiquitylation is required to drive the activation of the NF-κB pathway. Unlike p53, activation of NF-kB predominantly results in the expression of several genes required for survival, including IAPs, BCL2 and A1, and inhibitors of extrinsic apoptosis. As such it is considered to play a pro-survival role (Kreuz *et al.*, 2001, Wang *et al.*, 1998, Zong *et al.*, 1999). Several components of the TNF-activated NF-kB pathway need to be ubiquitylated for activation of NF-kB; including components of the IκB kinase (IKK) complex (IKKα, IKKβ and NEMO), inhibitors of NF-kB (IkBα) and RIP1 (Karin and Ben-Neriah, 2000). In contrast to that previously described, RIP1 and NEMO have been found to be polyubiquitylated with K63-linked and/or Met1-linked chains, which aids in recruiting downstream signalling components to activate NF-κB (Ea *et al.*, 2006, Rahighi *et al.*, 2009, Tokunaga *et al.*, 2009, Wertz *et al.*, 2004). To add complexity,

NEMO has also been demonstrated to be polyubiquitylated with K29-linked chains, which has been shown to drive its degradation and leads to cell death (Zotti *et al.*, 2011). Additionally, under certain circumstances, activation of NF-kB can induce apoptosis including in T cells where activation results in the expression of Fas ligand and TRAIL, required for extrinsic apoptosis.

As described, members of the IAP family have been demonstrated to inhibit caspase activity. XIAP, cIAP1 and cIAP2 all bind to and block the activity of both initiator and effector caspases. However, IAP proteins have also been shown to act as E3 ligases (Vaux and Silke, 2005). XIAP, cIAP1 and cIAP2 all possess a RING domain at their carboxy-terminus and, in response to apoptotic stimuli, both XIAP and cIAP1 have been found to autoubiquitylate themselves, driving their degradation, and enabling cells to commit to apoptosis (Yang *et al.*, 2000). In addition, XIAP has been shown to ubiquitylate caspase-3. However, the functional outcome of this modification has not been fully determined (Morizane *et al.*, 2005, Schile *et al.*, 2008, Suzuki *et al.*, 2001, Vaux and Silke, 2005) and as there was no decrease in caspase-3 following ubiquitylation it suggests that ubiquitylation may have a non-degradative function (Suzuki *et al.*, 2001). Interestingly, cIAP1 and cIAP2 have also been demonstrated to catalyse the K63-linked ubiquitylation of RIP1, thereby activating NF-κB signalling (Bertrand *et al.*, 2008).

BRUCE/Apollon, an IAP that contains a C-terminal E2 motif (Hauser *et al.*, 1998), can inhibit SMAC-induced apoptosis by promoting the Ub-driven degradation of SMAC (Hao *et al.*, 2004) and also the cleavage of pro-caspase 9 (Qiu and Goldberg, 2005). Interestingly, BRUCE/Apollon is itself subject to Ub-dependent proteasomal degradation which results in the initiation of apoptosis (Qiu *et al.*, 2004, Qiu and Goldberg, 2002).

It is apparent that other BCL2 proteins are regulated via ubiquitylation and this can result in both the activation or inhibition of apoptosis. Following caspase cleavage and activation, tBID is polyubiquitylated at its N-terminus. This drives proteasomal degradation of the N-terminal fragment of tBID (tBID-N) enabling conformational changes freeing its C-terminal BH3 domain to interact with and inhibit pro-survival BCL2 proteins (Chou *et al.*, 1999, McDonnell *et al.*, 1999), thereby inducing apoptosis. Unusually, unconventional, non-lysine residues act as attachment points for K48-linked polyubiquitin attachment on tBID (Tait *et al.*, 2007).

In response to ubiquitylation the pro-survival protein BCL2 is degraded by the UPS (Dimmeler *et al.*, 1999, Kassi *et al.*, 2009, Wang *et al.*, 2008). Several proteins have been identified that regulate its degradation, including ARTS (Apoptosis-Related protein in the TGF-β Signalling pathway) (Edison *et al.*, 2017). ARTS has also been found to decrease XIAP protein levels (Gottfried *et al.*, 2004), and Edison *et al.* recently demonstrated that ARTS binds both XIAP and BCL2 enabling XIAP to ubiquitylate BCL2 and drive its proteasomal degradation.

To date five E3 ligases have been suggested to regulate MCL1, dependent upon the cell type. An example is the BH3-containing E3 ligase MULE/ARF-BP1, which polyubiquitylates MCL1 resulting in its proteasomal degradation and the induction of apoptosis (Zhong *et al.*, 2005). However, the interaction between MULE and MCL1 is weak and overexpression of BIM and PUMA has been demonstrated to displace MULE and stabilise MCL1 (Czabotar *et al.*, 2007, Mei *et al.*, 2005, Warr *et al.*, 2011). In contrast, others have shown the interaction between NOXA and MCL1 can enhance the interaction between MCL1 and MULE and drive its degradation (Czabotar *et al.*, 2007, Gomez-Bougie *et al.*, 2011, Willis *et al.*, 2005).

Many of the pro-apoptotic BCL2 family members are also subject to ubiquitylation, including BAD, BAX and BAK, resulting in the inhibition of apoptosis. UPS-dependent degradation of BAX results in cell survival and the degradation of its most abundant isoform, BAXα, has been linked to poor prognosis in leukemia patients (Agrawal *et al.*, 2008, Li and Dou, 2000). MOAP-1 (modulator of apoptosis-1), a binding partner of BAX, is also degraded as a consequence of ubiquitylation. Ub-driven degradation of MOAP-1 prevents the conformational changes required for activation of BAX, therefore its ubiquitylation is inhibited upon induction of apoptosis (Fu *et al.*, 2007, Huang *et al.*, 2012a, Matsuura *et al.*, 2016).

1.4.2. Deubiquitylation

DUBs oppose E3 ligases and hydrolyse the isopeptide bond between a 'distal' and 'proximal' Ub molecule or between Ub and a target protein. DUBs encoded by the human genome can be divided into two distinct groups, metalloproteases and the more numerous cysteine proteases, based on their mechanism of catalysis (Komander *et al.*, 2009a).

In general, DUBs are multi-domain proteins, which, along with distinct catalytic domains, possess Ub binding domains (UBDs) which include zinc-finger ubiquitin binding domains (ZnF-UBP), ubiquitin-like domains (UBL) and ubiquitin-associated domains (UBA) (Komander *et al.*, 2009a). There are approximately 20 different types of UBD, which employ diverse mechanisms to recognise Ub (Husnjak and Dikic, 2012). The majority of UBDs are α-helical and recognise the hydrophobic patch around Ile44 on Ub (Kulathu and Komander, 2012).

DUB Families

The metalloproteases, classified as the JAMM/MPN + (JAP1/MPN/MOV34) domain superfamily, posses a catalytic site, which contains an aspartate residue and water, coordinated by two zinc molecules. The catalytic mechanism of this family was elucidated from the structure of STAM (AMSH)-like protease (AMSH-LP/STAMBPLI) bound to a K63-linked diUb molecule. It revealed that a zinc ion activates water

molecules to form hydroxide ions that then attack the carboxyl carbon of the isopeptide (Sato *et al.*, 2008).

The cysteine proteases can be further subdivided into at least five families; the ubiquitin-specific proteases (USPs), the ubiquitin carboxy-terminal hydrolases (UCHs), the ovarian tumour proteases (OTUs), the Machado-Joseph disease domain (MJD) protein domain proteases (Clague *et al.*, 2013, Komander *et al.*, 2009a) and the motif interacting with ubiquitin (MIU)-containing DUB family (MINDYs) (Abdul Rehman *et al.*, 2016). An additional cysteine protease superfamily, the MCPIP (monocyte chemotactic protein-induced protein) superfamily has also been reported (Fraile *et al.*, 2012, Liang *et al.*, 2010), however, it is unclear if they have DUB activity. Similar to cysteine protein papains (Storer and Menard, 1994), cysteine proteases catalyse the hydrolysis of an isopeptide bond using a catalytic diad or triad. Within the triad a histidine residue lowers the pK_a of the catalytic cysteine, which enables the nucleophilic attack of the isopeptide bond. A potential third residue (Aspartate or Asparagine) is required for the polarisation and alignment of the histidine residue.

Kwasna *et al.* have recently identified an additional DUB family, ZUFSP/ZUP1, which shares no homology to those described above (Haahr *et al.*, 2018, Hermanns *et al.*, 2018, Hewings *et al.*, 2018, Kwasna *et al.*, 2018). A high-resolution crystal structure of ZUFSP revealed that it possesses a unique catalytic domain, which contains unique UBDs; ZHA and UBZ. These bind to distal Ub molecules and polyubiquitin, respectively, and selectively cleave K63-linked polyubiquitin chains. ZUFSP was demonstrated to interact with several proteins required for DNA replication and repair and this suggests that it plays an important role in the regulation of genome stability (Kwasna *et al.*, 2018).

Additional proteases can cleave ubiquitin-like modifiers/proteins from target proteins and are therefore termed ubiquitin-like proteases (ULPs). Examples of ubiquitin-like modifiers include small ubiquitin-related modifiers (SUMOs), cleaved by sentrin/SUMO-specific proteases (SENPs) and deSUMOylating isopeptidases (DeSIs) families, and NEDD8, cleaved by NEDP1 (Nedd8-specific protease 1) (Hickey *et al.*, 2012, Shin *et al.*, 2012).

Ubiquitin-specific proteases (USPs)

The USP family is the largest DUB family in mammalian cells, comprising ~56 members. The catalytic domain of USPs structurally resembles a hand and contains three sub-domains: the palm, the thumb and fingers (Hu *et al.*, 2002). Their large catalytic domain resides in between the palm and the thumb, where fingers 'grip' the 'distal' Ub molecule and position the C-terminus of Ub between the palm and the thumb. In most USPs the catalytic domain contains extensions and insertions that fold to form additional domains. These can influence enzymatic ability and localisation. In general, USPs show very little linkage preference, however some USPs have been described that preferentially cleave one

linkage type; an example is USP30, which has recently been demonstrated to prefentially cleave K6-linked polyubiquitin chains (Cunningham *et al.*, 2015, Gersch *et al.*, 2017).

USPs are localised throughout the cell including the nucleus (USP1 and USP7), the nucleolus (USP36 and USP39), endosomes (USP8), microtubules (USP21 and USP33) and the mitochondria (USP30) (Clague *et al.*, 2013, Clague and Urbe, 2017, Urbe *et al.*, 2012). To date USP19 and USP30 are the only known DUBs to contain transmembrane domains.

1.4.2.1. General roles of DUBs

Although there are around 100 human DUBs only a small number have been structurally and functionally characterised. Structural data, NMR and crystallography has increased our understanding of DUB activity, how they are regulated and what enables their specificity for a certain substrate/chain type.

How DUBs select which modifier to cleave, how they target this modifier and where they cleave ubiquitin chains has been extensively studied (Mevissen and Komander, 2017). In general, DUBs have been demonstrated to recognise their specific target based on Ub chain type and/or the substrate itself (Komander *et al.*, 2009b). The linkage specificity of DUBs can vary between families; for example, the majority of JAMM metalloproteases specifically cleave K63 chains (McCullough *et al.*, 2004, Ritorto *et al.*, 2014, Sato *et al.*, 2008), whilst MINDY DUBs are specific for K48 chains (Abdul Rehman *et al.*, 2016). The topological differences between the types of polyubiquitin chain and also the architecture of the DUB itself may explain how DUBs are capable of distinguishing between chain types and/or substrates.

The majority of DUBs possess a primary recognition site (S1 site) for Ub within their catalytic domain. This site binds to and guides the C-terminus of Ub and the scissile bond into the DUB active site, thus driving hydrolysis. In doing so, DUBs can completely remove or edit the Ub chain, via endo- or exo-cleavage (Komander *et al.*, 2009b). In the case of polyubiquitin chains, the distal Ub will occupy the S1 site, whilst the following Ub can occupy an additional S1' site. However, this is not always the case and may account for the general lack of chain specificity of USPs. The S1' site can also be occupied by the substrate, indicating the substrate specificity of select DUBs (Morgan *et al.*, 2016). To add complexity, the S1' site can be provided by UBDs within the DUB or from additional binding partners, an example includes the DUBs AMSH and AMSH-LP which require the UBD, UIM (ubiquitin-interacting motif), of STAM to activate the DUB and create a larger S1' site to enable the DUB to directly bind to K63-linked substrates (McCullough *et al.*, 2006). Outside of the described S1 and S1' Ub binding sites, additional UBDs within the DUB or accessory UBDs in *cis* have been described that are required to target DUBs specifically to select polyubiquitin chains (Abdul Rehman *et al.*, 2016, Clague *et al.*, 2013, Flierman *et al.*, 2016, Mevissen and Komander, 2017).

Ub is encoded by four genes; UBA52, RPS27A, UBB and UBC. The UBA52 and RPS27A genes generate Ub that is fused to ribosomal proteins whilst the remaining two genes produce polyubiquitin chains. DUBs function to process these linear polyubiquitin precursor proteins to generate a 'free' ubiquitin pool within the cell. There are specialised DUBs, including USP5, that are responsible for the precursor processing of Ub (Kimura and Tanaka, 2010, Redman and Rechsteiner, 1989).

USP14, UCHL5 (UCH37) and PSMD14 (RPN11/POH1) are three DUBs found within the proteasome. These can hydrolyse the isopeptide bond between the target protein and the Ub chain before the protein is degraded, thereby recycling Ub. USP14 reversibly binds to the RPN1 subunit within the 19S regulatory subunit of the proteasome through an N-terminal UBL domain; this binding event activates USP14. Unlike USP14, PSMD14 is a constituent component of the 26S proteasome and unlike USP14 and UCHL5 removes complete polyubiquitin chains from a target protein (Ristic *et al.*, 2014). Once the Ub chain is removed, different DUBs process the Ub chain into its monomeric state. Both of these roles of DUBs are essential for maintaining Ub homeostasis within the cell.

DUBs can regulate target activity and degradation of substrates by removing monoubiquitin or degradative or non-degradative polyubiquitin signals from the substrate. Removal of distal Ub molecules from a polyubiquitin chain can also result in chain editing leading to the target protein receiving a different Ub signal (Komander *et al.*, 2009a) (Figure 1.9).

Regulation of DUB abundance, localisation and catalytic activity.

The activity of DUBs is often cryptic and requires the binding of its substrate to enable structural rearrangements required for its activity (Reyes-Turcu *et al.*, 2009). To ensure that DUB activity is 'on-target' many mechanisms exist that temporally and spatially restrict their activity. These include post-translational modification of DUBs, alteration in their subcellular localisation, regulation of activity through association with E2/E3 enzymes or cofactors, as well as through their integration into larger protein complexes (Heideker and Wertz, 2015, Mevissen *et al.*, 2013, Reyes-Turcu *et al.*, 2009).

The catalytic activity of DUBs can be positively and negatively regulated through phosphorylation, ubiquitylation, SUMOylation and oxidation of catalytic cysteine residues by reactive oxygen species. Phosphorylation of USP8 results in its inhibition via association with 14-3-3 proteins (Mizuno *et al.*, 2007). However, phosphorylation events activate TNFAIP3 and USP37 (Huang *et al.*, 2011, Hutti *et al.*, 2007). Cezanne (OTUD7B) has been found to undergo post-translational control by reactive oxygen or nitrogen species, which inhibits Cezanne (OTUD7B) thereby relieving its negative regulation of the NF-κB pathway (Enesa *et al.*, 2008). Subcellular localisation of DUBs can also be regulated through phosphorylation. For example, USP10 localises to the nucleus upon ATM-driven phosphorylation (Yuan *et al.*, 2010).

Figure 1.9 General roles of deubiquitylating enzyme (DUBs).

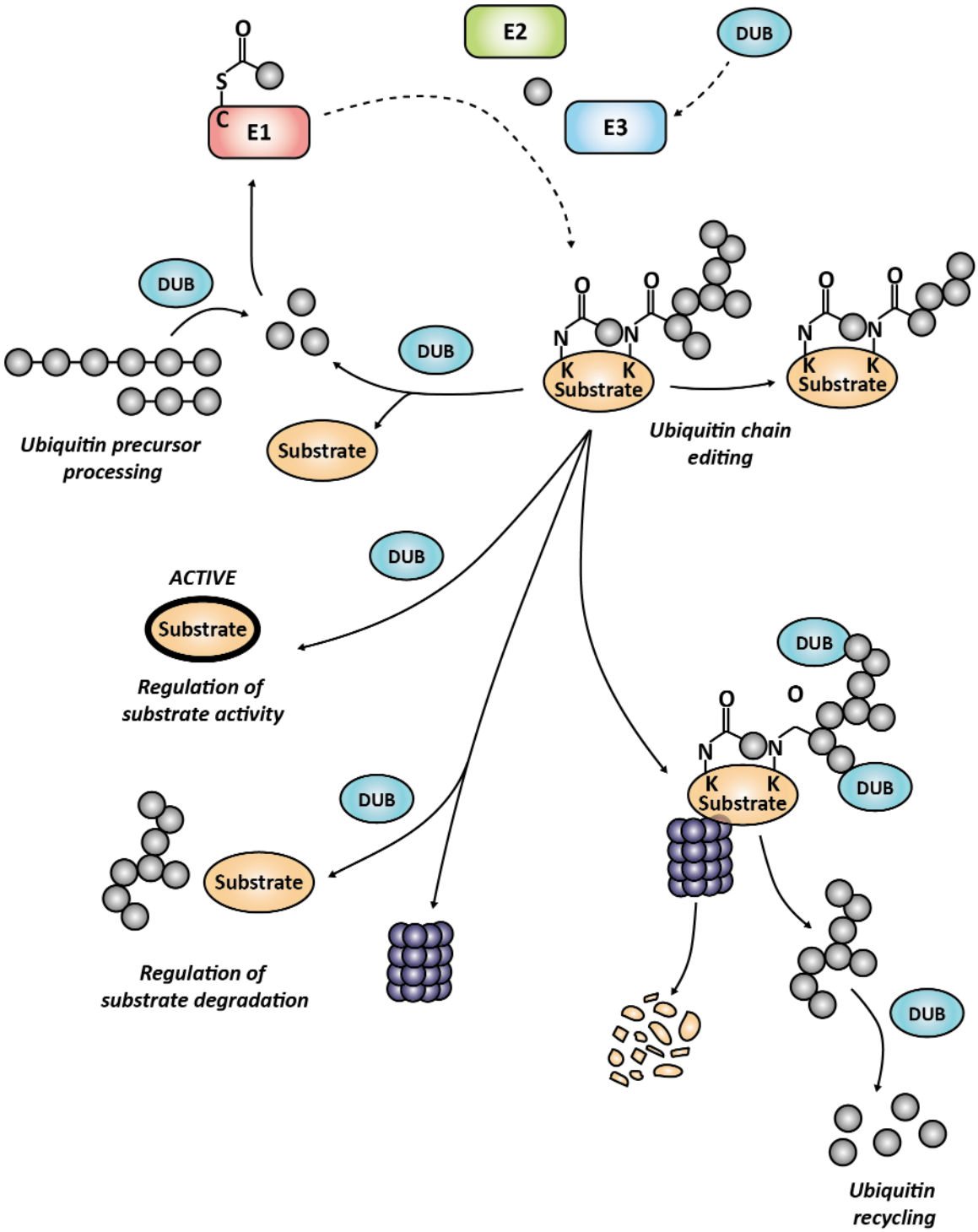

Figure 1.9 General roles of deubiquitylating enzyme (DUBs). DUBs regulate a wide variety of signalling pathways through the removal of ubiquitin (Ub) from a target substrate. Initially DUBs are required to process Ub from a linear polyprotein precursor into free Ub. One of the predominant roles of Ub attachment is regulation of the stability of the substrate. In general Ub attachment results in the degradation of the substrate by the proteasome. DUBs are required to remove Ub from the substrate prior to its degradation. This not only helps to prevent the degradation of Ub but also enables the recycling of free Ub back into the cell, thus maintaining the free Ub pool and Ub homeostasis. Given this, DUBs can also act to prevent the degradation of a substrate by removing or editing Ub chains prior to its targeting to the proteasome. Thus, they are thought to increase protein levels in the cell. DUBs can also remove non-degradative polyubiquitin chains as well as edit them. This can regulate the activity of the substrate. In addition DUBs can remove Ub from E3 ligases, thus stabilising them (adapted from Komander *et al.*, 2009, Bennett *et al.*, 2010, Clague *et al.*, 2012).

Some DUBs are incapable of binding to Ub with high affinity and rely upon binding partners or a complex of proteins to bind and catalyse the removal of Ub from their target protein (Sowa *et al.*, 2009). Several USPs, including USP1, USP12 and USP46, have been demonstrated to be activated through interaction with WD40 repeat-containing proteins (Cohn *et al.*, 2009, Cohn *et al.*, 2007). Interestingly, protein complexes often contain E3 ligases (Ventii and Wilkinson, 2008).

1.4.2.2. DUBs in disease.

DUBs have been demonstrated to play important roles in DNA repair, apoptosis, cell cycle control, growth factor signalling and immunity (Clague *et al.*, 2012, Jacq *et al.*, 2013). Given this, DUB deregulation, through overexpression and/or mutational defects, has been linked to numerous disease pathologies including neurological disorders, autoimmunity, inflammation, infectious diseases and cancer (Harrigan *et al.*, 2017).

Certain DUBs have been described to have intrinsic oncogenic or tumour suppressor characteristics, such as BRCA1-associated protein 1 (BAP1), whose mutation is linked to melanoma, mesothelioma and renal cell carcinoma (Murali *et al.*, 2013, Sacco *et al.*, 2010). DUBs can also act to regulate known oncogenes and tumour suppressors, including USP28, which stabilises c-Myc (MYC), a proto-oncogene, in colon and breast carcinoma (Cremona *et al.*, 2016, Popov *et al.*, 2007). DUBs can also regulate cellular pathways known to be therapeutically relevant in cancer, such as the DNA damage response and repair pathways, which, as described previously, are repressed as a hallmark of cancer (Jackson and Durocher, 2013). An example is USP11, which was identified in an overexpression screen to deubiquitylate H2AX (Yu *et al.*, 2016). Knockdown of USP11 resulted in an increase in 53BP1 and Ub formation at double strand breaks (DSBs) in addition to an increase in ubiquitylated H2AX, thereby suggesting a role for USP11 in DSB signalling and repair. In agreement with this, knockdown of USP11 sensitised cells to poly(ADP-ribose) polymerase (PARP) inhibition, via olaparib (Schoenfeld *et al.*, 2004b, Wiltshire *et al.*, 2010). At the molecular level, USP11 was shown to regulate the interaction between BRCA1 and BRCA2, required for DNA repair, by controlling the ubiquitylation of partner and localizer of BRCA2 (PALB2) (Orthwein *et al.*, 2015). Overall DUBs have been demonstrated to regulate all stages of metastasis, including resistance to apoptosis, discussed later (He *et al.*, 2017).

Mitochondria play a vital role in metabolism and energy production within the cell; as such mitochondrial dysregulation is associated with neurodegenerative disorders including Alzheimer's disease and Parkinson's disease. Removal of damaged or unnecessary mitochondria, also known as mitophagy, is regulated by ubiquitylation (Ross *et al.*, 2015). Mitophagy is regulated by the Ser/Thr kinase PTEN-induced kinase 1 (PINK1) and the E3 ligase Parkin. Under basal conditions, PINK1 is imported into the mitochondria and undergoes proteolytic cleavage, which targets it for proteasomal

degradation. Lack of PINK1 at the mitochondria is indicative of functioning import machinery and of healthy mitochondria. Failure in this import mechanism, often as a consequence of mitochondrial dysfunction, results in the accumulation of PINK1 at the OMM resulting in its autophosphorylation, dimerization and activation. In this state, PINK1 is capable of interacting with and recruiting Parkin to the mitochondria. Parkin is autoinhibited and requires activation by PINK1, demonstrated to be through the phosphorylation of both S65 in Ub and the UBL domain Parkin (Iguchi *et al.*, 2013, Kane *et al.*, 2014, Kondapalli *et al.*, 2012, Koyano *et al.*, 2014, Shiba-Fukushima *et al.*, 2012, Wauer *et al.*, 2015a, Wauer *et al.*, 2015b). The binding of phosphorylated Ub to Parkin results in conformational changes that enable its S65 phosphorylation by PINK1 (Kumar *et al.*, 2017, Wauer *et al.*, 2015a), which is required for full activation of Parkin (Gladkova *et al.*, 2018). Activated Parkin ubiquitylates OMM proteins including MIRO, mitofusion and TOM20/22, marking mitochondria for degradation (Chan *et al.*, 2011, Harper *et al.*, 2018, Narendra and Youle, 2011, Sarraf *et al.*, 2013).

USP30 antagonises the E3 ligase Parkin by removing Ub from mitochondrially bound proteins and thus opposes Parkin-mediated mitophagy (Figure 1.10) (Bingol *et al.*, 2014, Cunningham *et al.*, 2015, Durcan and Fon, 2015, Liang *et al.*, 2015). Under normal conditions, USP30 prevents inappropriate mitophagy; however, under conditions resulting in mitochondrial dysfunction, including as a result of defects in Parkin, USP30 can counteract the clearance of defective mitochondria through removal of Ub from MOM proteins. This would lead to the accumulation of metabolically and energetically-deficient cells (Bingol *et al.*, 2014). Knockdown of USP30 improved mitochondria integrity and rescued defective mitophagy (Bingol *et al.*, 2014, Nakamura and Hirose, 2008), suggesting that inhibiting USP30 should enhance mitophagy and drive the clearance of dysfunctional mitochondria. Therefore, USP30 could be a novel therapeutic target for treatment of Parkinson's disease. USP30 inhibitors are in-development (Jones *et al.*, 2016, Kemp and Jones, 2017, Yue *et al.,* 2014) and described in more detail in Chapter 4.

Further interrogation of the role in USP30 in mitophagy, in the absence of overexpression of Parkin and depolarising agents, has recently revealed that USP30 may play a more significant role upstream of PINK1, thereby predominantly acting to prevent the accidental activation of mitophagy under basal conditions (Ganley, 2018, Marcassa *et al.*, 2018).

USP30 has also been shown to play a role in BAX/BAK-dependent (Intrinsic) apoptosis, where its depletion sensitises cells to BH3 mimetics (Liang *et al.*, 2015). These findings suggest that USP30 depletion or inhibition could provide a means for inducing tumour cell death.

Figure 1.10 General diagram depicting the regulation of mitophagy by deubiquitylation via the deubiquitylating enzyme (DUB) USP30.

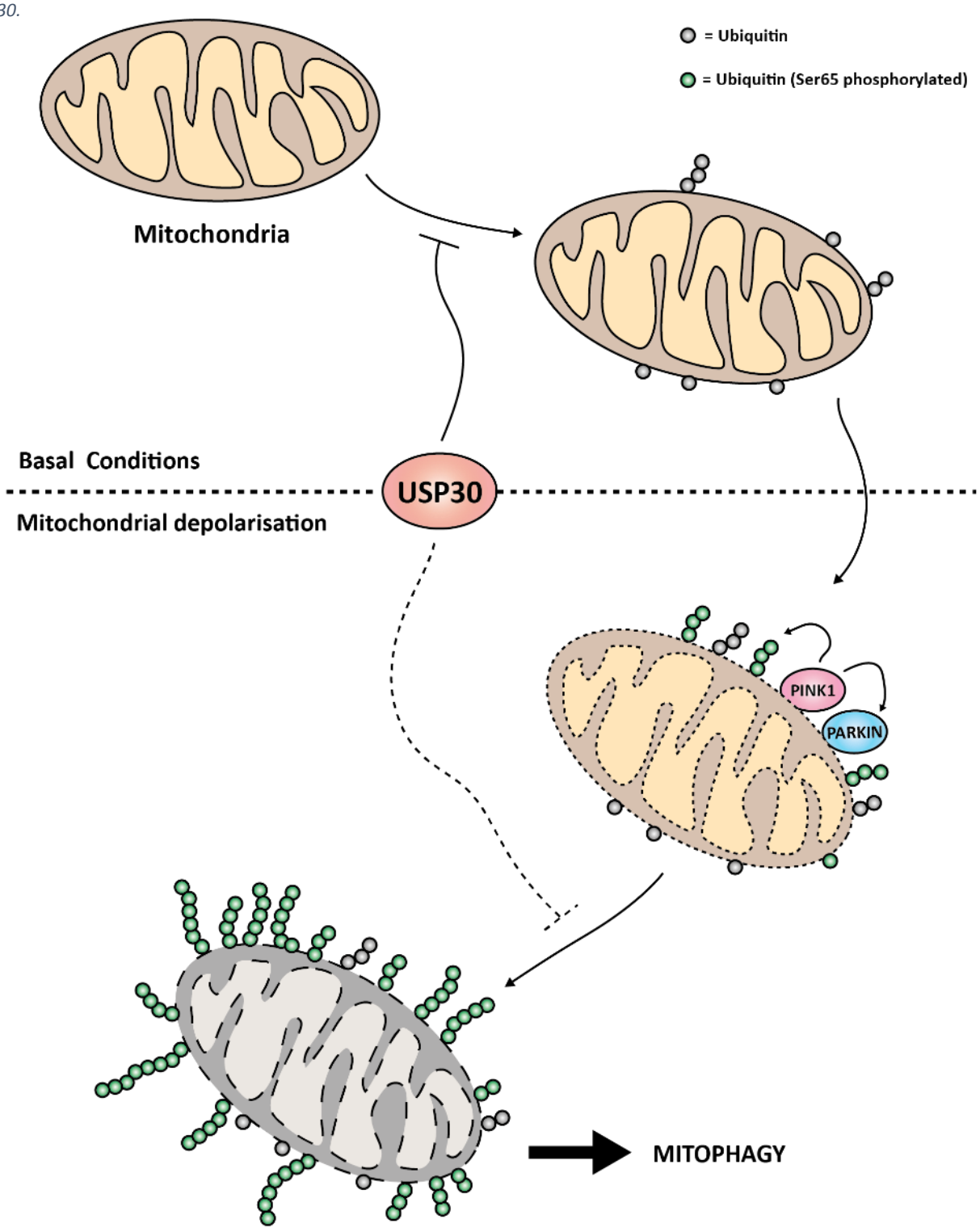

Figure 1.10 General diagram depicting the regulation of mitophagy by deubiquitylation via the deubiquitylating enzyme (DUB) USP30. Under basl conditions, PINK1 protein is maintained at a low level and PARKIN is autoinhibited within the cytoplasm. Under these conditions USP30 is active and prevents the accumulation of inappropriately ubiquitylated proteins. Given this, USP30 has been suggested to act as a 'safety catch' to prevent mitophagy from accidentally being induced. Upon mitochondrial depolarisation, PINK1 is stabilised at the mitochondrial outer membrane (MOM) and can activate PARKIN, through phosphorylation of PARKIN and Ub (Ser65). PARKIN is then able to ubiquitylate numerous MOM proteins, which in turn can recruit ubiquitin-binding autophagy receptors enabling mitophagy. USP30 has also been suggested to negatively regulate mitophagy at this stage, however is role under basal conditions maybe more dominant (adapted from Ganley, 2018).

1.4.2.3. Role of DUBs in apoptosis.

At least 14 DUBs have been found to play a role in multiple pathways involved in positively and negatively regulating apoptosis (Bhattacharya and Ghosh, 2014, Gupta *et al.*, 2018, Ramakrishna *et al.*, 2011). The role of DUBs in apoptosis is complex and a single DUB can have opposing roles both promoting apoptosis or aiding survival. For example, USP2 has been found to cause cell death by deubiquitinating tAIF (apoptosis-inducing factor) (Oh *et al.*, 2011), but has also been found to inhibit apoptosis by stabilising fatty acid synthase (FAS) (Graner *et al.*, 2004).

DUBs have been found that directly deubiquitylate pro-survival and pro-apoptotic proteins. In addition to that described for BIM_{EL}, it has been demonstrated that USP9x can deubiquitylate and stabilise MCL1 resulting in tumour cell survival (Schwickart *et al.*, 2010). USP15 has been shown to activate caspase-3 during Paclitaxel- (a microtubule-targeting cancer treatment) induced apoptosis (Xu *et al.*, 2009), by regulating the interaction between pro-caspase-3 and the E3 ligase SCF complex. A complete understanding of how DUBs regulate cell death could validate pharmacological approaches to treating diseases, including cancer, where ubiquitylation and cell death is dysregulated.

Inhibition of DUBs as a therapeutic strategy.

It is increasingly apparent how manipulating components of the ubiquitin system would be of great therapeutic benefit (Cohen and Tcherpakov, 2010). Treatment of refractory multiple myeloma and mantle cell myeloma with Bortezomib, a proteasome inhibitor, resulted in the blockage of targeted proteolysis leading to cell cycle arrest and apoptosis (Chen *et al.*, 2011a, Richardson *et al.*, 2003). This focused attention on the UPS as a suitable target for cancer treatment. Indeed, VLX1570, an inhibitor that targets the proteasome-associated DUBs, USP14 and UCHL5, is currently the most advanced DUB inhibitor (D'Arcy *et al.*, 2011, Wang *et al.*, 2015b). The development of DUB inhibitors is a rapidly expanding field due, in part, to our greater understanding of DUB biology and the development of technologies to assess DUB activity/inhibition. DUBs are also readily druggable targets, with a well-defined catalytic cleft. One such DUB of interest is USP7, several small molecule inhibitors of which have been described, including P22077 (P5091) and more recently FT671 and FT827 (Altun *et al.*, 2011, Chen *et al.*, 2017, Colland *et al.*, 2009, Gavory *et al.*, 2018, Kemp, 2016, Reverdy *et al.*, 2012, Tian *et al.*, 2011, Turnbull *et al.*, 2017, Weinstock *et al.*, 2012). At the molecular level, inhibition of USP7 stabilises and increases p53 levels, via the increased degradation of its negative regulator MDM2, resulting in an increase in the transcription of p53 target genes, including p21 (Turnbull *et al.*, 2017). Overall, inhibiting USP7 repressed tumour cell growth in mice (Turnbull *et al.*, 2017) and has also been shown to drive apoptosis of tumour cells; however whether this was due to off-target effects is unknown (Chauhan *et*

al., 2012, Colland *et al.*, 2009, Cummins and Vogelstein, 2004, Fan *et al.*, 2013, Li *et al.*, 2004, Li *et al.*, 2002).

Targeting signalling pathways required for cancer cell survival, from receptor tyrosine kinases (RTKs) to downstream kinases, has proven to be successful in the treatment of cancer. Ubiquitylation of RTKs, including EGFR (epidermal growth factor receptor), serves as a signal to drive their internalisation, via the early and late endosomes, to lysosomes for degradation. As such, mutations that permit evasion of RTK degradation can drive tumour cell growth (Peschard and Park, 2003). USP8 has been shown to deubiquitylate EGFR at early endosomes, thereby rescuing EGFR from degradation (Mizuno *et al.*, 2005, Niendorf *et al.*, 2007). As EGFR has been demonstrated to be both amplified and mutated in cancer, there is a rationale for the development of USP8 inhibitors in the treatment of cancers. In accordance with this, inhibition of USP8 activity or knockdown of USP8 overcame resistance to EGF receptor-tyrosine kinases inhibitors (EGFR-TKIs) in non-small cell lung cancer (NSCLC) in part through downregulation of EGFR, in addition to other RTKs, ERBB2 and MET (Byun *et al.*, 2013).

In addition to targeting DUBs as a cancer treatment, DUB inhibitors are being developed to treat neurodegenerative diseases. One of the hallmarks of neurodegenerative disorders is the accumulation or aggregation of ubiquitylated proteins within particular areas of the CNS (Ristic *et al.*, 2014). Targeting DUBs that prevent the degradation of ubiquitylated proteins could be of therapeutic benefit in the treatment of these diseases. IU1, and additional analogues, are reversible small-molecule inhibitors that target USP14 and enhance the degradation of ubiquitylated proteins (Lee *et al.*, 2010). In particular, an IU1 analogue enhanced the degradation of Tau and TAR DNA-binding protein 43 (TDP43), the accumulation of which is linked to neurodegenerative diseases in cultured cells (Lee *et al.*, 2010). However, this failed to enhance proteasomal degradation of Tau in neurons and therefore the clinical relevance of IU1 in the treatment of Alzheimer's disease is unclear (Kiprowska *et al.*, 2017). Despite this, selectively targeting DUBs has the potential to treat a multitude of diseases with high unmet clinical need.

1.5. Aims of this thesis

Apoptosis is an essential process required for cell death and a hallmark of tumourigenesis is its evasion. Therefore, understanding the regulation of apoptosis could be of therapeutic benefit in a wide range of diseases, including cancer. ERK1/2 has been shown to regulate apoptosis by activating/supressing components of the apoptotic signalling cascade, but also inhibition of ERK1/2 signalling components can induce apoptosis in certain cancer cell lines. BIM, a potent pro-apoptotic protein, has been proposed to be regulated, cooperatively, by ERK1/2 and RSK1/2, and crucially they act to induce its proteasomal degradation.

To this end, the aims of my thesis were to:

- Examine the role of ERK1/2 and RSK in the degradation of BIM.
- Characterise the requirement of these kinases for the interaction between BIM and βTrCP.
- Elucidate the role RSK plays in the regulation of BIM in tumour cells, particularly by observing if inhibition of RSK combines with BH3 mimetics to drive BIM-dependent cell death.
- Investigate the counteracting DUB for BIM and evaluate the role of the USP27x in the regulation of BIM in our system.

Ubiquitylation has also been demonstrated to regulate several signalling pathways linked to apoptosis, including ERK1/2 signalling, as well as apoptotic proteins themselves. Recently, Liang *et al.* demonstrated that the DUB USP30 may play an pro-survival role in cancer cells as knockdown of USP30 combined with BH3-mimetics to induce tumour cell death (Liang *et al.*, 2015). Thus, during this study an additional aim was to:

- Evaluate if novel USP30 inhibitors combine with BH3 mimetics to drive apoptosis.

There has been a recent effort to develop therapies that prolong tumour regression and/or delay acquired resistance to clinically available inhibitors, including MEKis. As the ERK1/2 pathway is closely integrated with Ub-regulated signalling processes, the final aims of my thesis were to:

- Elucidate if knockdown of a DUB, by siRNA, combined with chosen inhibitors to drive tumour cell death.
- If any 'hits' were identified to evaluate the role they play in regulating cell death

Chapter 2: Material and Methods

2. Chapter 2

2.1. Equipment and reagents

2.1.1. Laboratory suppliers

Equipment and reagents were procured from the following companies:

Sources of general laboratory equipment and reagents

BD Biosciences	
LSRII Flow Cytometry	
BioRad	
20% Sodium dodecyl sulphate (SDS) 30% v/v acrylamide/bis solution BioRad mini trans blot Bradford reagent (Protein assay reagent)	Gel electrophoresis apparatus N,N,N',N'-Tetramethylethylenediamine (TEMED) Precision Plus protein markers Protein G-horseradish peroxidase
BMG Labtech	
PHERAstar microplate reader	CLARIOstar microplate reader
Calibiochem	
Q-VD-OPh	
Fisher Scientific	
Glycine Potassium hydroxide	
GE Healthcare	
Enhanced chemilluminescence system	
Hoefer	
Gel casting apparatus Mighty small II gel apparatus	
LI-COR	
Odyssey Imaging System	
Life Technologies	
DH5α competent cells Dulbecco's Modified Eagles Medium Geneticin (G418) L-glutamine Lipofectamine 2000 Lipofectamine RNAiMAX	OptiMEM Penicillin/Streptomycin RPMI Secondary antibodies for immunofluorescence SYBR green PCR master mix

	Trypsin
Marvel	
Non-fat powder milk	
Melford	
4-(2-hydroxyethyl)-1-piperazineethanesulfonic acid (HEPES) 5-Bromo-4-chloro-3-indolyl-β-D-galactoside [X-gal]	Tris
Millipore	
Immobilon Western Chemiluminescent HRP substrate	Immobilon-P PVDF membrane
Panasonic	
CO_2 Incubator	
Promega	
CellTiter-Glo® (CTG) Luminescent Cell Viability Assay	Pfu DNA polymerase
QIAGEN	
Plasmid plus mini kit Plasmid plus maxi kit QIAquick Gel Extraction Kit	QIAquick PCR purification kit QuantiTect reverse transcriptase kit RNAeasy Minielute Cleanup kit
Sartorius	
IncuCyte® ZOOM live-cell imaging system	
Sigma-Aldrich	
4-hydroxytamoxifen (4HT) Aprotinin Bovine serum albumin (BSA) Coomassie brilliant blue Dimethyl sulphoxide (DMSO) Ethidium bromide Ethylene glycol bis(2-aminoethyl ether)-N,N,N'N'-tetraacetic acid (EGTA) Ethylenediaminetetraacetic acid (EDTA) Leupeptin	Magnesium chloride β-Mercaptoethanol Phenylmethylsulfonyl fluoride (PMSF) Propidium iodide Ribonuclease A Sodium fluoride Sodium orthovanadate Triton X-100 Tween-20
Thermo Scientific	
All tissue culture plasticware (Nunc) ND-1000 spectrophotometer (Nanodrop)	YOYO®-1 Iodide (491/509) (Y3601)
VWR BDH Prolabo	
Acetic acid	Propan-2-ol

Calcium chloride	Potassium chloride
Ethanol	Potassium dihydrogen phosphate
Glycerol	Sodium azide
Glucose	Sodium bicarbonate
Haemocytometer	Sodium chloride
Magnesium chloride	Sodium hydroxide
Methanol	Trichloroacetic acid
Orthoboric acid	
Zymogen Research	
Direct-zol™ RNA Miniprep kit	

Table 2.1

2.1.2. Pharmacological inhibitors

Source and target of pharmacological inhibitors used

Inhibitor	Target	Mechanism of action	Supplier	Catalogue number
ABT-263 (Navitoclax)	BCL2, BCL-X_L, BCL-w	BH3 mimetic	Selleckchem	S1001
Alisertib (MLN8237)	Aurora A	ATP competitive	Selleckchem	S1133
AZ4216	GSK-3β	ATP competitive	AstraZeneca	
AZD8055 (8055)	mTOR	ATP competitive	Selleckchem	S1555
BI-D1870	RSK1/2/3/4	ATP competitive inhibitor of the NTKD of RSK	Selleckchem	S2843
CHIR-99021	GSK-3αβ	ATP competitve	Selleckchem	S2924
D4476	CK1	ATP competitive	Tocris	2902/10
Emetine	Ribosome	Binds to 40S subunit to inhibit protein translation	Sigma-Aldrich	E2375
FMK	RSK1/2/4	Binds irreversibly to the ATP-binding site of the NTKD	Axon Mechem BV	1848
GDC-0623	MEK1/2	Non-ATP-competitive; analog of CI-1040; stabilises a RAF-MEK complex	Astex	
GDC-0994	ERK1/2	ATP competitive	AstraZeneca	
GSK2606414	PERK	Binds inactive ATP-binding region	MERCK	516535
LJH685	RSK1/2/3	ATP competitve	Selleckchem	S7870
MG132	Proteasome	Competitive inhibitor at the chymotrypsin-like site	Sigma-Aldrich	C2211

MTX086432 (MTX32)	USP30	Unknown	Mission Therapeutics	
MTX088748-001-001 (MTX48)	USP30	Unknown	Mission Therapeutics	
PF 670462	CK1δ/ε	ATP competitive	Tocris	3316/10
PD0325901 (PD901)	MEK1/2	Non ATP-competitive	Selleckchem	S1036
S63845	MCL1	Binds to the BH3-binding groove of MCL1	Selleckchem	S8383
SCH772984	ERK1/2	ATP competitive	Selleckchem	S7101
Selumetinib/ AZD6244	MEK1/2	ATP and substrate uncompetitive allosteric inhibitor	AstraZeneca	
Trametinib (GSK1120212)	MEK1/2	Allosteric non-ATP-competitive inhibitor	Selleckchem	S2673

Table 2.2

2.1.3. Solutions

All solutions were dissolved in MilliQ deionised water unless specified otherwise.

General laboratory solutions

Solution	Components
2 x Hepes buffered saline (HBS)	50mM HEPES 280mM NaCl 1.5mM Na_2HPO_4
Coomassie Brilliant Blue solution	50% v/v methanol 0.05% w/v Coomassie Brilliant Blue
Luria Broth (LB)	10g/L Tryptone 10g/L NaCl 5g/L Yeast extract
Phosphate-buffered saline (PBS)	137mM NaCl 2.7mM KCl 1.47mM KH_2PO_4 8.1mM Na_2HPO_4
siRNA buffer (GE Dharmacon)	60mM KCL 6 mM HEPES pH 7.5 0.2 mM $MgCl_2$
Tris-buffered saline with Tween (TBST)	50mM Tris-HCl, pH 7.6 150mM NaCl 0.1% v/v Tween 20

Western Blot Destain solution	7% v/v acetic acid 5% v/v methanol

Table 2.3

Solutions used for SDS-PAGE and Western blotting

Solution	Contents
SDS running buffer pH 8.3	192 mM glycine 25 mM Tris base 0.1% w/v SDS
Western blot transfer buffer	192 mM glycine 25 mM Tris base 20% w/v methanol
Blocking buffer (5% milk/TBST)	10 mM Tris-HCl, pH 8.0 150 mM NaCl 0.1% v/v Tween 20 5% w/v Marvel
Blocking buffer (5% BSA/TBST)	10 mM Tris-HCl, pH 8.0 150 mM NaCl 0.1% v/v Tween 20 5% w/v BSA
4 x Laemmli buffer	200 mM Tris-HCl, pH 6.8 8% w/v SDS 40% v/v Glycerol 4% v/v β-mercaptoethanol 0.04% w/v bromophenol blue
TG Lysis Buffer	20 mM Tris-HCl, pH 7.5 137 mM NaCl 1 mM EGTA 1% v/v Triton X-100 10% v/v glycerol 1.5 mM $MgCl_2$ 1 mM Na_3VO_4 1 mM PMSF 10 µg mL^{-1} aprotinin 10 µg mL^{-1} leupeptin 50 mM NaF

Table 2.4

Solutions used for Subcellular Fractionation

Solution	Components
Isotonic Fractionation Lysis Buffer	250 mM Sucrose 0.5 mM EDTA 20 mM HEPES 500 µM Na_3VO_4 10 µg mL^{-1} aprotinin 10 µg mL^{-1} leupeptin

Table 2.5

2.1.4. Antibodies

The following primary and secondary antibodies were used for Western blotting experiments and LI-COR experiments.

Primary antibodies, blocking solutions and dilutions used for Western blotting

Antibody	Blocking solution	Dilution	Species of origin	Company	Catalogue number
β-actin	5% milk/TBST	1:10000	Mouse	Sigma	A5441
BAK	5% milk/TBST	1:1000	Rabbit	Cell Signalling Technology	sc-832
BAX	5% milk/TBST	1:1000	Rabbit	Cell Signalling Technology	sc-493
BIM	5% milk/TBST	1:1000	Rabbit	Millipore	AB17003
p-BIM (S69)	5% milk/TBST	1:1000	Rabbit	Cell Signalling Technology	4581
BCL2	5% milk/TBST	1:500	Mouse	Santa Cruz Biotechnology	sc-492
BCL-X_L	5% milk/TBST	1:1000	Rabbit	Cell Signalling Technology	2762
BCL-w	5% milk/TBST	1:1000	Rabbit	Cell Signalling Technology	2724
β-Catenin	5% BSA/TBST	1:1000	Mouse	BD biosciences	610153
p-β-Catenin (S33/S37/T41)	5% BSA/TBST	1:1000	Rabbit	Cell Signalling Technology	9561
COXIV	5% milk/TBST	1:1000	Mouse	Abcam	ab33985
ERK1	5% milk/TBST	1:3000	Mouse	BD Biosciences	610031
ERK1/2	5% milk/TBST	1:1000	Rabbit	Cell Signalling Technology	9102

p-ERK1/2 (T202/Y204)	5% milk/TBST	1:1000	Mouse	Cell Signalling Technology	9106
FLAG M2	5% milk/TBST	1:1000	Mouse	Sigma	F3165
FOXO1A	5% milk/TBST	1:1000	Rabbit	Cell Signalling Technology	2880
p-FOXO1A (S322/S325)	5% milk/TBST	1:1000	Rabbit	Abcam	Ab60945
G3BP2	5% milk/TBST	1:1000	Rabbit	Abcam	Ab86135
HA-probe	5% milk/TBST	1:500	Mouse	Santa Cruz Biotechnology	sc-7392
HA-probe	5% milk/TBST	1:500	Rabbit	Santa Cruz Biotechnology	sc-805
MCL1	5% milk/TBST	1:1000	Rabbit	Santa Cruz Biotechnology	sc-819
PARP	5% milk/TBST	1:1000	Rabbit	Cell Signalling Technology	9542
PLK1	5% milk/TBST	1:1000	Rabbit	Cell Signalling Technology	4513
p-PLK1 (T210)	5% milk/TBST	1:1000	Rabbit	Cell Signalling Technology	9062
RSK1/2/3	5% BSA/TBST	1:1000	Rabbit	Cell Signalling Technology	9355
p-RSK (T380)	5% BSA/TBST	1:1000	Rabbit	Cell Signalling Technology	9341
p-RSK (T359/S363)	5% BSA/TBST	1:1000	Rabbit	Cell Signalling Technology	9344
S6K	5% BSA/TBST	1:1000	Rabbit	Cell Signalling Technology	9202
p-S6K (T389)	5% BSA/TBST	1:1000	Rabbit	Cell Signalling Technology	9205
β-TrCP	5% milk/TBST	1:1000	Rabbit	Cell Signalling Technology	4394
UCHL3	5% milk/TBST	1:1000	Mouse	Provided by *MISSION* Therapeutics Ltd	N/A
USP2	5% milk/TBST	1:1000	Rabbit		N/A
USP5	5% milk/TBST	1:1000	Rabbit		N/A
USP10	5% milk/TBST	1:2000	Rabbit	Abcam	Ab70895
USP11	5% milk/TBST	1:4000	Rabbit	Bethyl	A301-613A
USP16	5% milk/TBST	1:1000	Rabbit	Proteintech	14055-1-AP
USP30	5% BSA/TBST	1:250	Rabbit	Atlas Antibodies	HPA016952
TNFAIP3 (A20)	5% milk/TBST	1:1000	Rabbit	Cell Signalling Technology	5630

TNFAIP3 (A20)	5% milk/TBST	1:1000	Rabbit	Novus	NBP1-77533
VCIP135 (VCPIP1)	5% milk/TBST	1:1000	Rabbit	Cell Signalling Technology	88153
YAP	5% milk/TBST	1:1000	Rabbit	Cell Signalling Technology	4912
p-YAP (S127)	5% milk/TBST	1:1000	Rabbit	Cell Signalling Technology	13008
YB-1	5% milk/TBST	1:1000	Rabbit	Cell Signalling Technology	4202
p-YB-1 (S102)	5% milk/TBST	1:1000	Rabbit	Cell Signalling Technology	2900
YOD1	5% milk/TBST	1:1000	Rabbit	Sigma	HPA028400
p53	5% milk/TBST	1:1000	Mouse	Calbiochem	OP43

Table 2.6

Secondary antibodies used for Western blotting

Antibody	Blocking solution	Dilution	Company	Catalogue number
Goat anti-mouse IgG-HRP conjugate	5% milk/TBST	1:3000	BioRad	170-6516
Goat anti-rabbit IgG-HRP conjugate	5% milk/TBST	1:3000	BioRad	170-6515

Table 2.7

Secondary antibodies used for LI-COR experiments

Antibody	Blocking solution	Dilution	Company	Catalogue number
Goat anti-mouse IgG--(H+L) Cross-Adsorbed Secondary Antibody, Alexa Fluor 568	5% milk/TBST	1:50000	ThermoFisher Scientific	A-11029
Goat anti-rabbit IgG-(H+L) Cross-Adsorbed Secondary Antibody, Alexa Fluor 568	5% milk/TBST	1:50000	ThermoFisher Scientific	A-11011

Table 2.8

2.1.5. siRNA oligonucleotides

The following siRNA oligonucleotide sequences were used for RNA interference.

Sequences of oligonucleotides used for siRNA

Target RNA	Supplier	Catalogue number	Sense oligonucleotide sequence (5'-3') Antisense oligonucleotide sequence (3'-5')
BCL-X_L	Dharmacon (GE LifeSciences)	siGenome Human SMARTpool: M-003458-06-0005	- (Purchased prior to start of PhD)
BTRC	Dharmacon (GE LifeSciences)	ON-TARGETplus SMARTpool: L-0033463-00-0005	5'-UGACAACACUAUCAGAUUA-3' 3'-ACUGUUGUGAUAGUCUAAU-5' 5'-CACAUAAACUCGUAUCUUA-3' 3'-GUGUAUUUGAGCAUAGAAU-5' 5'-GACCUUAAAUGGACACAAA-3' 3'-CUGGAAUUUACCUGUGUUU-5' 5'-ACACCGAGCUGCUGUCAAU-3' 3'-UGUGGCUCGACGACAGUUA-5'
Non-targeting	Dharmacon	-	5'-UAAGGCUAUGAAGAGAUAC(rUrU)-3' 3'-(rUrU)AUUCCGAUACUUCUCUAUG-5'
Non-targeting	Dharmacon (GE LifeSciences)	siGENOME Non-targeting siRNA pool (D-001206-13-20)	5'-UAGCGACUAAACACAUCAA-3' 3'-AUCGCUGAUUUGUGUAGUU-5' 5'-UAAGGCUAUGAAGAGAUAC-3' 3'-AUUCCGAUACUUCUCUAUG-5' 5'-AUGUAUUGGCCUGUAUUAG-3' 3'-UACAUAACCGGACAUAAUC-5' 5'-AUGAACGUGAAUUGCUCAA-3' 3'-UACUUGCACUUAACGAGUU-5'
Luciferase (siLUC)	Eurofins MWG/Operon	N/A, custom synthesis	5'-CGUACGCGGAAUACUUCGA(dTdT)-3' 3'-(dTdT)GCAUGCGCCUUAUGAAGCU-5'
USP10 (USP10_1)	QIAGEN	S100072989	5'-TCGCTTTGGATGGAAGTTCTA-3'
USP10 (USP10_5)	QIAGEN	S100302113	5'-AACACAGCTTCTGTTGACTCT-3'
USP10 (USP10_69)	Ambion	4427038/s17369	5'-CAGUCAAGGUGAUCAACCA-3'
USP11 (HS-USP11_3)	Eurofins MWG/Operon	N/A, custom synthesis	5'-AAGGUCGAAGUGUACCCAGUA(dTdT)-3' 3'-(dTdT)UUCCAGCUUCACAUGGGUCAU-5'
USP11 (HS_USP11_5)	Eurofins MWG/Operon	N/A, custom synthesis	5'-CUGCGUCGGGUACGUGAUGAA(dTdT)-3' 3'-(dTdT)GACGCAGCCCAUGCACUACUU-5'
USP11 (HS_USP11_6)	Eurofins MWG/Operon	N/A, custom synthesis	5'-ACCGAUUCUAUUGGCCUAGUA(dTdT)-3' 3'-(dTdT)UGGCUAAGAUAACCGGAUCAU-5'

USP16 (USP16_02D)	Dharmacon (GE LifeSciences)	D-0060667-02	5'-GGAACAAGGUAAUUUGAAA-3' 3'-CCUUGUUCCAUUAAACUUU-5'
USP16 (USP16_03D)	Dharmacon (GE LifeSciences)	D-006067-03	5'-GAACACAGUGGUACUAUGA-3' 3'-CUUGUGUCACCAUGAUACU-5'
USP16 (HS_USP16_ 11)	QIAGEN	S105021191	5'-AAUGGCUGAAAUAACGAUAAA-3' 3'-UUACCGACUUUAUUGCUAUUU-5'
TNFAIP3	Dharmacon (GE LifeSciences)	ON-TARGETplus SMARTpool: L-027369-00-0005	5'-CUGCAGUACUUGCUUCAAA-3' 3'-GACGUCAUGAACGAAGUUU-5' 5'-CAACUCAUCUCAUCAAUGC-3' 3'-GUUGAGUAGAGUAGUUACG-5' 5'-UCUGGUAGAUGAUUACUUU-3' 3'-AGACCAUCUACUAAUGAAA-5' 5'-CAACGAAUGCUUUCAGUUC-3' 3'-GUUGCUUACGAAAGUCAAG-5'
VCIP135	Dharmacon (GE LifeSciences)	ON-TARGETplus SMARTpool: L-019137-00-0005	5'-GAGAAGCUCUGGUGAUUAU-3' 3'-CUCUUCGAGACCACUAAUA-5' 5'-GGGACAGACUUUAGUAAUA-3' 3'-CCCUGUCUGAAAUCAUUAU-5' 5'-GGAGAUGGGUCUAUUGUGU-3' 3'-CCUCUACCCAGAUAACACA-5' 5'-CGACAGAAUUACAAUAGAA-3' 3'-GCUGUCUUAAUGUUAUCUU-5'
YOD1	Dharmacon	ON-TARGETplus SMARTpool: L-009919-00-0005	5'-GCAAUAGAGAUAUCGAUUU-3' 3'-CGUUAUCUCUAUAGCUAAA-5' 5'-CAUCCAAUCUGGUGACAUG-3' 3'-GUAGGUUAGACCACUGUAC-5' 5'-GAUCCAGACUUCUAUAGUG-3' 3'-CUAGGUCUGAAGAUAUCAC-5' 5'-GACAGGCCAUACCAACUUU-3' 3'-CUGUCCGGUAUGGUUGAAA-5'

Table 2.9

2.1.6. Plasmids

pcDNA3.1 HA–BIM_{EL} (rat sequence) provided by Paul Coffer (University Medical Center, Utrecht, The Netherlands). All variants of this and the βTrCP overexpression vector were kindly provided by Rebecca Gilley (The Babraham Institute, Cambridge, UK) and Ceri Wiggins (previous PhD student, The Babraham Institute, Cambridge, UK). pFLAG_CMV_6c_USP30, pFLAG_CMV_6c_USP30 C77A, pFLAG_CMV_6c_USP2, pFLAG_CMV_6c_USP2 C267A, pFLAG_CMV_6c_Cezanne, pFLAG_CMV_6c_Cezanne C194S, pFLAG_CMV_6c_USP8, pFLAG_CMV_6c_USP8 C748A, pFLAG_CMV_6c_USP15 and pFLAG_CMV_6c_USP15 C269A provided by *MISSION* Therapeutics Ltd. (Babraham Research Campus, Moneta (Building 280),

Cambridge, UK). GST-Dsk2 UBA, wild-type and inactive M342R and F344A mutant (Ohno *et al.*, 2005), were provided by Nia Bryant (Institute of Molecular, Cell and Systems Biology, University of Glasgow).

2.2. Cell lines and culture

2.2.1. Colorectal cancer cell lines

COLO205

COLO205 cells are an epithelial-like colorectal adenocarcinoma cell line that was established in 1978 from an ascites metastasis in a 70 year old male Caucasian patient. These cells harbour an activating BRAF mutation (V600E) and were purchased from ATCC.

HCT116

HCT116 cells are an epithelial-like colorectal carcinoma cell line that harbours an activating KRas mutation (G13D) and an activating PI3KCA mutation (H1047R). They were a gift from Prof Bert Vogelstein (Johns Hopkins University, Baltimore, USA).

2.2.2. Melanoma cell lines

A375

A375 cells are an epithelial-like malignant melanoma established from a 54 year old female. These cells habour an activating BRAF mutation (V600E).

BIM-/- A375 cells

BIM-/- A375 cells are derivatives of A375 cells (above) which have been edited, using CRISPR-cas9 technology, to generate a double knockout of BIM. Cells were kindly provided by Rebecca Gilley (The Babraham Institute, Cambridge, UK).

gRNA sequences designed to target BIM

Guide RNA (gRNA) to *BCL2L11* (encoding BIM) were designed using the Zhang lab gRNA designing tool (http://crispr.mit.edu/) and cloned into a pSpCas9(BB)-2A-GFP genome editing vector, kindly provided from Feng Zhang (Addgene plasmid #48138). Validation of the clones

used in this thesis (data not shown) confirmed that all three major isoforms of BIM (BIM_{EL}, BIM_L and BIM_S) had been knocked-out. CRIPSR-cas9 performed by Rebecca Gilley (The Babraham Institute, Cambridge, UK).

Target	gRNA identifier	gRNA sequence (5'-3')	Exon targeted
BIM	BIMg2	5'-caccGCAACCACTATCTCAGTGCAA-3' 5'-aaacTTGTCACAACTCATGGGTGC-3'	2

Table 2.10

2.2.3. Additional cell lines

HR1

HR1 cells are a clonal derivative of HEK293 cells that have been engineered to stably express the pCMVneomycΔRAF-1:ER* construct (described Bougham et al 2006). This cell line was provided by Kathryn Balmanno (The Babraham Institute, Cambridge, UK).

2.2.4. Cell culture medium

The following medium was used for routine cell culture:

Cell culture medium and medium supplements for each cell line

Cell line	Medium	Supplementation
A375 (BIM-/- A375 cells) **HCT116**	DMEM (Life Technologies 41966)	10% (v/v) foetal bovine serum 2 mM L-glutamine 100 U/mL penicillin 100 µg/mL streptomycin
COLO205	RPMI 1640 (Life Technologies 21875)	10% (v/v) foetal bovine serum 2 mM L-glutamine 100 U/mL penicillin 100 µg/mL streptomycin
HR1	DMEM (Life Technologies 41966)	10% (v/v) foetal bovine serum 2 mM L-glutamine 100 U/mL penicillin 100 µg/mL streptomycin 400 µg/mL G418

Table 2.11

2.2.5. Routine cell culture

Cells were cultured at 37 ^{o}C in a humidified incubator with 5% CO_2 and split 2-3 times a week once they had reached 80% confluency. For passaging, growth medium was aspirated, cells were washed with PBS, treated with pre-warmed trypsin/EDTA solution and then incubated at 37 ^{o}C for 2-5 minutes, depending on the cell line. Detached cells were resuspended in fresh pre-warmed media and diluted to the desired dilution in a new tissue culture flask.

2.2.6. Cell line storage

Cells were trypsinised as above, resuspended in fresh medium and cell pellets collected by centrifugation. The medium was then aspirated and cells were resuspended in 10% v/v FBS/DMSO to yield a cell density of ~1-2 × 10^6 cells/mL. The resulting suspension was then aliquoted (1 mL per cryovial) and frozen slowly in an insulating box at -80 °C. For longer term storage of cells, cryovials were transferred to liquid nitrogen. As required, cells were rapidly thawed at 37 °C and placed into a fresh 25 cm^3 culture flask containing 9 ml pre-warmed medium. The following day, this medium was replaced to remove traces of DMSO and fresh put back in its place.

The cell lines were reanimated by thawing rapidly at 37 °C and resuspending in 9 mL fresh media. The cells were spun at 1500 x g for 3 minutes to pellet cells. The cell pellet was resuspended gently in 8 mL fresh media and placed into a T25 flask to grow until 80% confluent.

2.3. Cell Treatments

2.3.1. Drug Treatments

Stock solutions of drugs were diluted in cell culture medium to yield the desired final drug concentrations. Vehicle-only containing medium was used as control samples. Treated cells were incubated at 37 ^{o}C for the length of time stated in the figure legend.

2.3.2. Calcium Phosphate Transfection of HR1 cells

Cells were seeded at an appropriate density and allowed to settle overnight. After 24 hours plasmid DNA was diluted in sterile H_2O and 2 M $CaCl_2$ to a final concentration of 250 mM (1:8 dilution). This solution was mixed and an equivalent volume of 2 x HBS was added dropwise. The complete solution was vortexed and left at room temperature for 10 minutes and then added drop wise to plated cells, at an approximate cell density of 50%.

2.3.3. Lipofectamine 2000® Transfection of HCT116 cells

Cells were seeded in antibiotic free media and allowed to settle overnight to reach an approximate density of 50%. After 18 hours plasmid DNA was mixed with pre-warmed Opti-MEM® medium (1 mL for a 10 cm^3 dish). In a separate tube an equivalent volume of Opti-MEM® medium was mixed with Lipofectamine® 2000 reagent (1:100 dilution). Both tubes were allowed left for 5 minutes and then combined and left for 20 minutes. The transfection mix was added drop wise to the dish and left at 37 ^oC with 5% CO_2 for 6 hours. After 6 hours, the medium was changed to fresh pre-warmed antibiotic free media and the cells were incubated for the required time at 37 ^oC with 5% CO_2 prior to further treatment or analysis.

2.3.4. RNA interference

siRNA oligonucleotides were resuspended in 1 x siRNA buffer or sterile H_2O to generate a 20 µM stock solution. Any further lower dilutions were made on the day of transfection and discarded after use. siRNA oligonucleotides were mixed with an optimised ratio of Opti-MEM® medium to Lipofectamine® RNAiMAX (for a single well of a 6-well plate 2.2 µL of Lipofectamine® RNAiMAX to 500 µL of Opti-MEM®) and incubated for 20 minutes at room temperature. Cells were trypsinised and resuspended in antibiotic free media (2 mL for a single well of a 6-well plate) to an optimised cell density and then plated, together with siRNA-lipid complexes, to achieve a final siRNA concentration of 10-20 nM, or that stated in figure legends. Cells were incubated for the required time at 37 ^oC with 5% CO_2 prior to further treatment or analysis.

2.4. DNA and RNA manipulation

2.4.1. Plasmid preparation

DH5α bacterial cells were transformed with plasmid DNA (10-100 ng of DNA), plated onto LB plates containing antibiotics (100 µg/mL ampicillin or 30 µg/mL kanamycin) and incubated overnight at 37 ^{o}C. Subsequent colonies were picked and used to inoculate LB solution plus antibiotics, and were left in a shaking (225 rpm) incubator at 37 ^{o}C overnight. Plasmid DNA was extracted using a QIAGEN Plasmid Plus Mini/Maxi kit, following manufacturer's instructions. DNA concentration and A260/A280 ratio were subsequently determined using a NanoDrop spectrophotometer, sequenced and stored at -20 ^{o}C.

2.4.2. Genomic RNA isolation

Cells were lysed with 1 ml of TRI reagent per 10 cm^3 of culture dish and homogenised by pipetting and vortexing. Samples were incubated for 5 minutes at room temperature to permit complete dissociation of nucleoprotein complexes. Lysates were transferred to sterile RNase free tubes, genomic RNA was isolated using Direct-zol RNA MiniPrep kit according to manufacturer's instructions. Genomic DNA was removed from samples through and in-column DNase I digestion. RNA eluted with DNase/RNase-free water and stored at -80^{o}C for short-term storage.

2.4.3. cDNA preparation

cDNA was synthesised from 1 µg of purified RNA using the QuantiTect Reverse Transcription kit (QIAGEN), according to manufacturer's instructions. cDNA was diluted 1:20 in RNase-free water and stored at -20^{o}C.

2.4.4. PCR reactions

cDNA was used as the starting material for the PCR amplification of USP27x. For the amplification of DNA, PCR was performed using Pfu DNA polymerase, according to manufacturer's instructions. The PCR primers used for this reactions were purchased from SIGMA and are shown below:

Sequences of USP27x primers

Mutant	Primer sequence (5'-3')
USP27x	Fwd - CGATCGGATCCATGTGTAAGGACTATGTATATG Rev - CGATCGAATTCTCAGTAGGCTTGTGTGTTC

Table 2.12

2.4.5. Restriction endonuclease digestion and ligation reactions

Restriction digests were performed on 1-2 µg of plasmid DNA in a 50 µL reaction containing 1 x Restriction buffer and 1 µL of restriction enzyme. Reactions were incubated at 37 ^{o}C for 2 hours. All digested products were analysed by gel electrophoresis (1% agarose prepared in 1 x TBE containing 0.01% Ethidium bromide).

2.4.6. Gel electrophoresis

DNA was analysed or separated by gel electrophoresis on 1% agarose gel prepared in 1 x TBE containing 0.01% Ethidium bromide. DNA samples were mixed with 5 x DNA loading buffer prior to loading onto the gels. Gels were visualised by UV transilluminator at 254 nM. Bands were excised using a clean scalpel blade and the DNA was purified using QIAquick Gel Extraction kit (QIAGEN) according to the manufacturer's instructions.

2.4.7. DNA ligation

Consequent ligation reactions were carried out on digested DNA products, in a 1:3 (vector:insert) ratio, using a T4 DNA ligase (Promega) at 16 ^{o}C overnight. Reactions were consequently transformed into DH5α bacterial cells. DNA extracted was reanalysed by DNA digestion and gel electrophoresis to confirm insertion of the required DNA sequence.

2.4.8. Site-directed mutagenesis

The mutated pFLAG-CMV-6c-USP27x (C87A) was generated using the QuikChange II XL site-directed mutagenesis kit according to manufacturer's instructions. The following primers were purchased and used in site-directed mutagenesis:

Sequences of USP27x mutagenesis primers

Mutant	Primer sequence (5'-3')
C87A	Fwd - CAATCTTGGCAACACGGCCTTTATGAACTGCATTGTCC Rev - GGACAATGCAGTTCATAAAGGCCGTGTTGCCAAGATTG

Table 2.13

2.5. Preparation of whole cell lysates

The cell culture medium is discarded or collected depending upon the cell line used. Cells were washed with ice cold PBS and harvested using TG lysis buffer (20 mM Tris-Cl pH 7.5, 137 mM NaCl, 1 mM EGTA, 1% v/v Triton X-100, 10% v/v glycerol, 1.5 mM $MgCl_2$, 1 mM Na_3VO_4, 1 mM PMSF, 10 µg mL^{-1} leupeptin, 10 µg mL^{-1} aprotinin, 50 mM NaF). Collected lysates were cleared by centrifugation at 12,000 x g at 4 ^oC for 10 minutes and the supernatant protein concentration was measured using the Bradford protein assay. Samples were prepared for Western blotting by boiling for 5 minutes in 1 x Laemmli sample buffer and stored at -20 ^oC.

2.5.1. Bradford Assay

For each sample, 40 µL Bradford reagent was mixed with 158 µL water and 2 µL of cell lysate. The absorbance was read at 595 nm and the volume of protein lysate loaded to each well of the SDS-PAGE gel was adjusted accordingly to achieve equal protein loading.

2.6. SDS-PAGE and Western blotting

Resolving and stacking SDS-PAGE gels were assembled as described in the tables below:

Resolving gel composition

Component	Resolving gel percentage (%)			
	8	**10**	**12**	**14**
30% Acrylamine/Bis (mL)	16.2	19.8	24	27.6
1.5 M Tris pH 8.8 (mL)	15	15	15	15
ddH_2O (mL)	27.6	24	19.8	16.2
20% SDS (mL)	0.6	0.6	0.6	0.6
10% APS (mL)	0.6	0.6	0.6	0.6

TEMED (µL)	60	60	60	60

Table 2.14

Stacking gel composition

Component	Stacking gel percentage (%)		
	4	**5**	**6**
30% Acrylamine/Bis (mL)	2.67	3.33	4
1.5 M Tris pH 6.8 (mL)	5	5	5
ddH_2O (mL)	11.93	11.27	10.6
20% SDS (mL)	0.2	0.2	0.2
10% APS (mL)	0.2	0.2	0.2
TEMED (µL)	50	50	50

Table 2.15

Equivalent amounts of protein were resolved by SDS-PAGE at a constant voltage of 100 V for 2-3 hours. At least one lane contains 8 µL of protein standard (Precision Plus Dual Colour Standard). Proteins were transferred to methanol-activated PVDF membrane at 300 mA for 90-120 minutes. Membranes were blocked for 1 hour in 5% (w/v) milk/TBST or BSA/TBST at room temperature and then probed with primary antibodies at 4 ^{o}C overnight, with gentle agitation. After incubation the membranes were washed three times in TBST and then probed with the appropriate secondary antibodies diluted in TBST/5% (w/v) milk for 1 hour at room temperature. Following incubation membranes were washed three times in TBST and antibody-antigen complexes detected using the GE Healthcare enhanced chemiluminescent (ECL) system. For LI-COR Odyssey analysis, washed membranes were incubated for 1 hour at room temperature with a fluorophore conjugated secondary antibody diluted 1:50000 in 5% (w/v) milk/TBST. The blots were washed three times in TBST for 5 minutes and a final wash in water prior to detection on the LI-COR Odyssey imaging machine. The resulting bands were quantified using LI-COR Odyssey software.

2.7. Crude subcellular fractionation analysis

Cells were seeded and allowed to settle overnight. Media was aspirated and cells were washed in 1 x PBS. 500 µL of Isotonic Fractionation Lysis Buffer was added per 10 cm^3 dish and cells were scraped and transferred into an 1.5 mL eppendorf tube. Cells were lysed by drawing

them through a 25-gauge needle 10 times. Cells were spun at 900 x g for 1 minute at 4 ^{o}C and the subsequent supernatant was spun at the maximum speed of the table-top refrigerated microcentrifuge (approximately 20,000 x g) at 4 ^{o}C for 20 minutes. The supernatant was removed and labelled as the cytosolic fraction and the pellet was resuspended in an equivalent volume of Isotonic lysis buffer plus 1% Triton X-100 and labelled the heavy membrane fraction. Concentrations of protein were measured using the Bradford assay and lysates were stored as previously described.

2.8. Immunoprecipitation

Cells were lysed in TG lysis buffer and precleared with Protein A-sepharose beads for 1 hour at 4 ^{o}C. A fraction of this lysate was retained for input blots. Mouse anti-HA monoclonal IgG_{2a} (Kappa light chain) (sc-7392) was subsequently added to the remaining lysate. Each sample contained equivalent quantities of protein and were made to the same volume with additional TG lysis buffer. Antibody-antigen complexes were allowed to form at 4 ^{o}C for 1 hour, with end-over-end rotation. Protein A-sepharose beads were then added to the lysates and were incubated for a further 3 hours at 4 ^{o}C, turning end-over-end. Following centrifugation, the beads were washed three times in ice cold TG lysis buffer, before eluting the beads in 4 x SB, followed by boiling for 5 minutes. Eluents and input fractions were then subjected to SDS-PAGE and Western blotting.

2.9. Polyubiquitination assay

pGEX GST-Dsk2 UBA, wild type and inactive M34R and F344A mutant, were expressed in DH5α cells, purified and immobilised onto glutathione-sepharose beads and stored in storage buffer at 4 ^{o}C. A 20 mL overnight culture was used to inoculate 300 mL LB broth and grown at 37 °C with shaking at 225 rpm until the optical density of the cell suspension was 0.5-0.6 at 595 nm. Cells were then treated with 0.2 mM IPTG and grown for a further 3-4 hours at 30 °C. Cells were pelleted by centrifugation at 4,000 x g for 10 minutes and lysed in 30 mL bacterial lysis buffer for 30 minutes on ice. The cell lysate was spun at 15,000 x g for 20 minutes at 4 °C and 1-2 mL washed glutathione-s-transferase (GST) beads were added to the resulting supernatant. The lysate/bead suspension was incubated end-over-end for 2 hour at 4 °C. The

beads were washed once in lysis buffer and twice in PBS and then spun down before being resuspended in 3 mL of storage buffer. Beads were then pipetted into 500 µL aliquots and stored at 4 ^{o}C.

To assess BIM_{EL} polyubiquitination, HR1 cells were transfected and treated as indicated in figure legends. Post treatment cells were washed in ice-cold PBS and lysed using ice-cold TG lysis buffer. Lysates were cleared by centrifugation (12,000 x g for 10 minutes at 4 ^{o}C) and protein levels determined by Bradford assay. Lysates were divided and either stored as input sample in 1 x Laemmli buffer or pre-incubated under rotation at 4 ^{o}C with GST-only beads for 30 minutes. Following pre-incubation, the GST-only beads were pelleted at 2000 x g for 1 minute at 4 ^{o}C and the lysate was removed, normalised for protein content and incubated under rotation with 20 µL of GST-Dsk2 (or mutant Dsk2 (ΔDsk2)) bound sepharose beads at 4 ^{o}C for 90 minutes. The beads were washed three times with 1 mL ice-cold TG lysis buffer and resuspended in 40 µL 1 x Laemmli buffer and stored at -20 ^{o}C.

2.10. DUB activity probe assay

Cells were lysed in ice-cold TG lysis buffer, which was supplemented with 5 mM β-mercaptoethanol (BME), or the lysis buffer described in Table 2.15 and shown in Figure 4.1. Lysates were cleared by centrifugation (12,000 x g for 10 minutes at 4 ^{o}C) and protein concentrations determined using a standard protein concentration curve, utilising a Bradford assay. Following this, 20 µg of cell lysates were incubated with 0.5 µg of HA-UbVME probe for one hour at room temperature. The remaining lysate and the lysate incubated with the DUB activity probe were then prepared for Western blotting by boiling for 5 minutes in 1 x Laemmli sample buffer and stored at -20 ^{o}C.

Components of Mission Therapeutics Lysis buffer

Mission Therapeutics Lysis Buffer	50 mM Tris-HCl, pH 7.5 150 mM NaCl 0.1% NP-40 0.5% CHAPS 5 mM $MgCl_2$ 5 mM BME 1 Roche mini-protease table (per 10 mL)

1 Roche mini-phosphatase tablet (per 10 mL)

Table 2.16

2.11. Propidium iodide staining and flow cytometry

Following harvest, cells were pelleted by centrifugation at 1,500 rpm, at 4 ^{o}C, for 5 minutes, washed in PBS, and then resuspended in 0.2 mL PBS. Cells were vortexed and fixed in 2 mL ice-cold 70% (v/v) ethanol/PBS, and stored at 4 ^{o}C for at least 1 hour. On the day of analysis, samples were centrifuged, washed with PBS and resuspended in 0.25 mL PBS containing 25 µg RNase and 12.5 µg of propidium iodide (PI) and incubated at 37 ^{o}C for 30 minutes. Prior to analysis, the cell suspension was passed through a 25-gauge needle to generate a single cell suspension. PI fluorescence was analysed with a FACS Calibur machine (BD Biosciences), using a 488 nm excitation laser line and a 670 nm long pass filter to measure binding of PI to DNA, and counting 10,000 cells per sample. Data was analysed using FlowJo X.

2.12. Deubiquitylating enzyme (DUB) RNAi Screen

Figures 2.1 and 2.2 depict how the RNAi screens were performed. Of note, all steps where possible were performed in a tissue-culture grade hood. The siRNA used in the screen were purchased by Mission Therapeutics prior to the start of my project from QIAGEN. In general, on the day the screen was performed, 8, 96-well plates were removed from the freezer, containing at least twice the required volume of pre-aliquoted DUB siRNA, one volume of siRNA required for inhibitor treated plates and the other for control non-treated plates. These were labelled L1a-d and L2a-d, where plates L1a-d were spotted with 4 different siRNA for the same DUB, one on each plate, for a set of DUBs and plates L2a-d were spotted with 4 different siRNA for the same DUB, one on each plate, for a different set of DUBs (Figure 2.2). These plates were spun down and the positive (siBCL-X_L) and negative (siLUC, 4 per plate) controls were aliquoted onto these plates.

The optimised concentration of RNAiMAX and pre-warmed Opti-MEM®, required for transfection of both treated and non-treated plates, were mixed. The RNAiMAX:OptiMEM mix was aliquoted into each well of the 8, 96-well plates and placed to mix on a shaker for 5

minutes and then then removed from the shaker and placed on the side, unstacked, for 20 minutes. Whilst lipid:siRNA complexes were forming, HCT116 cells were trypsinised, counted and diluted to the optimised concentration with antibiotic free media. YOYO-1® dye was added, at a dilution factor of 1:20000, to the HCT116 cells. The RNAiMAX/OptiMEM/siRNA mix in each of the 8, 96 well plates was split into two plates, one to be treated and the other left untreated to give a total of 16, 96-well plates. The optimised concentration of cells were then plated into these wells to give a total volume of 135 µL per well.

Cells were left to settle for ~24 hours. Following this, all plates were removed from the incubator. One set of plates (8, 96-well plates) were left untreated, but treated with DMSO, and the other set of plates (8, 96-well plates) were treated with the optimised concentration of the inhibitor, diluted to this concentration in antibiotic-free media. In addition, positive drug controls were pipetted onto plates, for example ABT-263 + inhibitor (Figure 2.2).

At the end of the screen all plates were removed from the incubator and placed in the IncuCyte® ZOOM. This captured images of each well, which could then be analysed for confluency, 'phase' and cell death (fluorescent YOYO®-1 dye). Cells were then lysed and CTG viability assay was performed, according to manufacturer's instructions, and illuminescence was measured on the CLARIOstar microplate reader.

Further analysis of the data was performed using sensitivity index (SI) analysis. Prior to performing SI analysis, all end-point assay measurements were normalised to the average siLUC value for the plate the DUB of interest was spotted on.

The following calculation was used to determine SI values:

$$\mathbf{SI = (Rc/Cc*Cd/Cc)-(Rd/Cc)}$$

Rc is the average 'value' in drug-untreated wells transfected with active siRNA against a select DUB, Rd is the average 'value' in drug-treated wells with active siRNA against a select DUB, Cc is the average 'value' in drug-untreated wells with control siRNA (siLUC averaged across all plates), and Cd is the average 'value' in drug-treated wells with control siRNA (siLUC averaged across all plates). As three end-point assays were performed on the RNAi screen, the 'value' would be representative of the end-point analysis used for SI analysis. Once SI values for each DUB are determined, a 'hit' was identified if 3 more siRNA for that DUB generated an SI value

above or below the set threshold (determined by the end-point assay used). The 'threshold' was determined using this calculation:

Threshold = SI mean for siLUC (across all plates) + (std*z value)

For the work performed here the z value was set at a constant of 3, recommended on conversation with Mission Therapeutics.

Further siRNA work validating 'hits' described in Chapter 6 was performed according to section 2.3.4.

Figure 2.1 Schematic representation of how the deubiquitylating enzyme (DUB) RNAi screen was performed.

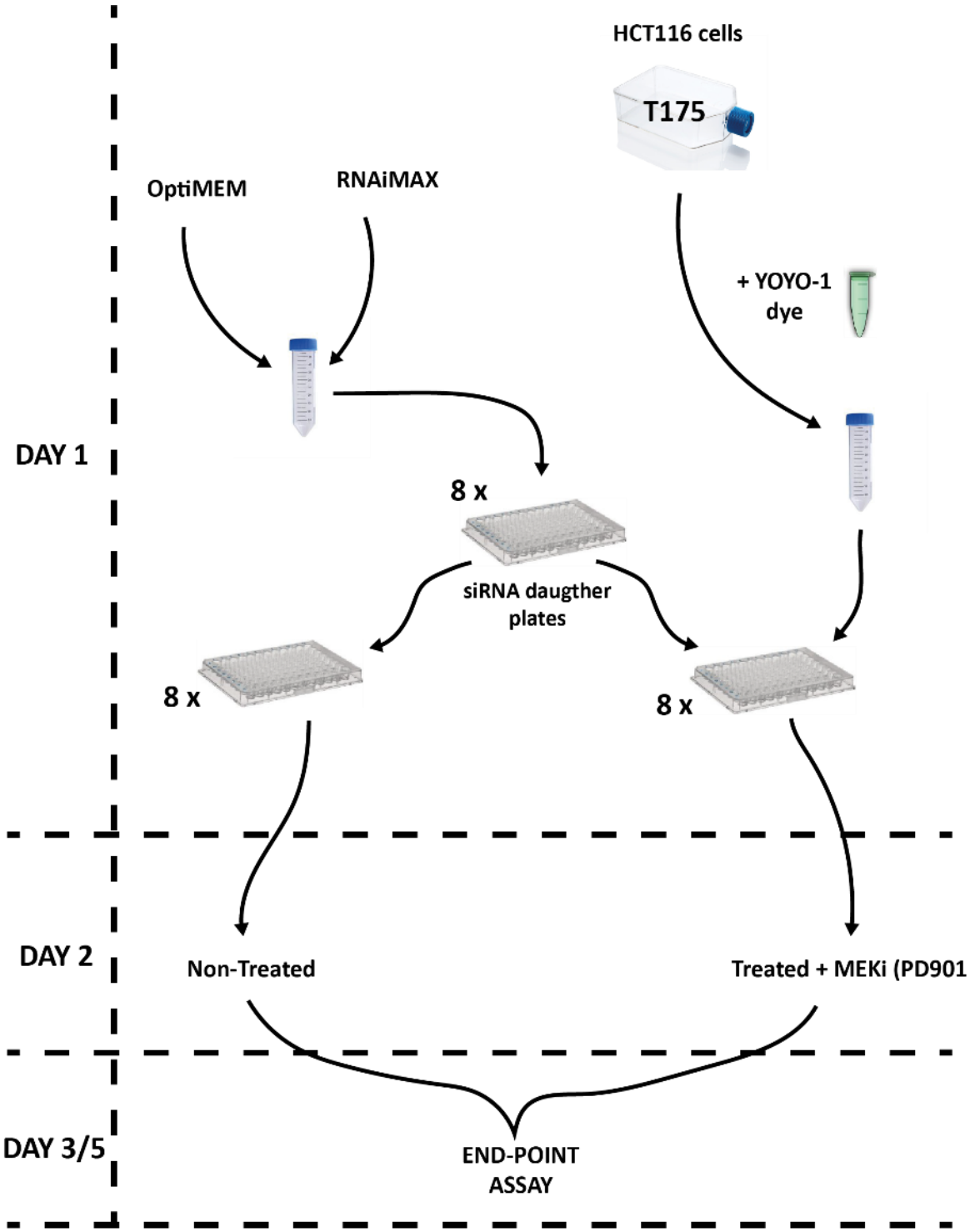

Figure 2.1 Schematic representation of how the deubiquitylating enzyme (DUB) RNAi screen was performed. On day 1 HCT116 cells are reverse transfected with DUB siRNA using RNAiMAX and OptiMEM. Initially 8 siRNA daughther plates (L1a-d and L2a-d) are removed from the freezer and spun down. To these plates optimised concentrations of RNAiMAX and OptiMEM were added. These plates were left for 25 minutes for lipid:siRNA complexes to form and then split in two, into 2 sets of 8 plates. Whilst complexes were forming HCT1116 cells were trypsinised and counted and resuspended in antibiotic free media to the optimised concentration. YOYO-1 dye was added to these cells. Cells were added to the 2 sets of 8 plates and placed in an incubator at 37°C. After ~24 hours (day 2) plates were removed from the incubator and 1 set of 8 plates were treated with the optimised concentration of inhibitor. Plates were then placed back into the incubator until the end of the screen when end-point assays were performed, either on day 3 or day 6.

Figure 2.2 Overview of the siRNA plate plans used during the deubiquitylating enzyme (DUB) RNAi screens.

Plates L1a-d

	1	2	3	4	5	6	7	8	9	10	11	12
A												
B		Luc	USP5	USP9Y	USP15	USP20	USP27X	USP33	USP39	USP45	Luc	
C		USP1	USP6	USP10	USP16	USP21	USP28	USP34	USP40	USP46	KIF11	
D		USP2	USP32P2	USP11	USP17	USP22	USP29	USP35	USP41	USP47	NT	
E		USP3	USP7	USP12	DUB3	USP24	USP30	USP36	USP42	USP48	BCL-X_L	
F		USP4	USP8	USP13	USP18	USP25	USP31	USP37	USP43	USP49	+ve	
G		Luc	USP9x	USP14	USP19	USP26	USP32	USP38	USP44	Eg5	Luc	
H												

Plates L2a-d

	1	2	3	4	5	6	7	8	9	10	11	12
A												
B		Luc	SENP7	SENP1	BRCC3	FLJ14981	JOSD1	YOD1	OTUD7B	USP51	Luc	
C		UCHL1	FAM105A	SENP3	COPS5	DESI1	JOSD2	OTUD4	DESI2	USP52	KIF11	
D		UCHL3	FAM105B	SENP5	COPS6	PSMD14	JOSD3	OTUD5	TNFAIP3	USP53	NT	
E		BAP1	USPL1	SENP6	EIF3H	PSMD7	OTUB1	OTUD6A	ZRANB1	USP54	BCL-X_L	
F		SENP2	CYLD	STAMBP	EIF3F	ATXN3	OTUB2	OTUD6B	VCIP135	SENP8	+ve	
G		Luc	UCHL5	AMSH-LP	MYSM1	ATXN3L	OTUD1	OTUD7A	USP50	Eg5	Luc	
H												

Figure 2.2 Overview of the siRNA plate plans used during the deubiquitylating enzyme (DUB) RNAi screens. The siRNA targeting DUBs in the human genome are depicted above. Each DUB is targeted by 4 different siRNA, spotted in the same well on plates L1a-d or L2a-d. Those siRNA depicted in red were spotted onto the plates on the day the screen was performed. For +ve = positive inhibitor control; untreated plates (L1a-d and L2a-d) treated with ABT-263 and treated plates L1a-d with ABT-263 + inhibitor at concentration used for screen, and treated plates L2a-d with ABT-263 + high concentration of inhibitor. For BCL-X_L, untreated plates (L1a-d and L2a-d) treated with DMSO and treated plates L1a-d with inhibitor at concentration used for screen, and treated plates L2a-d with high concentration of inhibitor.

Chapter 3: Characterising the ubiquitylation and deubiquitylation of BIM

3. Chapter 3

3.1. Introduction

BIM is a pro-apoptotic BH3-only protein that is a major determinant, along with other BCL2 proteins, for the initiation of cell-intrinsic apoptosis. As a consequence of its importance in the initiation of cell death, the transcription, expression and activity of BIM are tightly regulated and alterations in its expression are associated with disease.

Tumour cells that possess RTK, Ras or BRAF oncogenes are addicted to ERK1/2 signalling for survival, and this in part reflects suppression of BIM expression. As a consequence, BIM has been shown, in multiple settings, to induce tumour cell death in response to drugs targeting the ERK1/2 pathway (Sale and Cook, 2013). Therefore, detailed information regarding the regulation of BIM may guide the use of oncogene-targeted cancer therapies (Gillings *et al.*, 2009).

Alternative splicing of BIM results in at least 18 different isoforms, of which three, BIM_S, BIM_L and BIM_{EL}, are the major variants. BIM_{EL}, the least potent but most abundant isoform, undergoes ERK1/2-driven phosphorylation, on at least three Ser-Pro sites, including S69 (S65 in Rat), targeting it for K48-linked polyubiquitylation and subsequent degradation via the 26S proteasome (Ewings *et al.*, 2007, Ley *et al.*, 2003, Ley *et al.*, 2004, Luciano *et al.*, 2003, Marani *et al.*, 2004, Wiggins *et al.*, 2011).

In addition to regulation by ERK1/2, Dehan *et al.* demonstrated that RSK1/2 co-operates with ERK1/2 to phosphorylate BIM_{EL}. They showed that activation of RSK1/2, by ERK1/2, resulted in the phosphorylation of BIM_{EL} on S93, S94 and S98, providing a binding site for the F-box protein βTrCP1/2, as part of a larger E3 ligase SCF complex, allowing for the polyubiquitylation and degradation of BIM_{EL}. This study suggested a significant role for RSK1/2 in the post-translational regulation of BIM_{EL}. If RSK1/2 is a regulator of BIM_{EL} turnover one could reason that this would validate the use of RSK inhibitors in the treatment of cancer. Since RSK is just one of >200 described substrates of ERK1/2, RSK inhibition might result in an increase in BIM_{EL} protein with fewer side effects than direct inhibition of ERK1/2 activity. As such, it could provide a means to drive BIM-dependent tumour cell death in a more selective manner (Dehan *et al.*, 2009).

In most cases, βTrCP specifically recognises a conserved phosphodegron within its substrates, DpSGX(n)pS, or variants on this, where pS represents phospho-serine and X represents any amino acid. Indeed, phosphorylation of serine residues, within this motif, is the major regulatory mechanism controlling substrate-βTrCP interaction (Fuchs *et al.*, 2004). The described sequence has been found in a large number of proteins, summarised in Coyaud *et al.*, which have all been shown to be regulated

in response to βTrCP binding (Coyaud *et al.*, 2015). These include β-catenin (Hart *et al.*, 1999, Latres *et al.*, 1999, Liu *et al.*, 2002), yes-associated protein (YAP) (Zhao *et al.*, 2010b), NF-κB1 p105 (Lang *et al.*, 2003, Orian *et al.*, 2000), and cell division cycle 25 homologue (CDC25A) (Busino *et al.*, 2003, Jin *et al.*, 2003). Thus, βTrCP regulates a diverse set of signalling pathways. Recently Shimizu and colleagues have described a novel technique using the described phosphodegron as a means for isolating novel substrates of βTrCP, using βTrCP-phosphodegron-motif specific antibodies for immunoprecipitation of phospho-peptides, followed by mass spectrometry (Shimizu *et al.*, 2017), thus, demonstrating that this degron in sufficient for substrate recognition.

As previously described, alternative E3 ligases have been suggested for BIM_{EL}. However to date the most convincing candidate is $SCF^{\beta TrCP}$. As seen by Dehan *et al.*, Moustafa-Kamal *et al.* confirmed the requirement for phosphorylation of BIM_{EL} at S93, S94 and S98 for interaction with βTrCP1 during mitosis (Moustafa-Kamal *et al.*, 2013). They showed that, in mitosis, Aurora A was required for the phosphorylation and consequential degradation of BIM_{EL} and that mutation of S94/S98 but not S69, a known ERK1/2 phosphorylation site, resulted in defective polyubiquitylation and stabilisation of BIM_{EL}.

Until recently, the DUB responsible for the deubiquitylation of BIM_{EL} was unknown. Weber *et al.* used mass spectrometry to identify BIM_{EL} interacting proteins and found that the DUB, USP27x, bound to BIM_{EL} resulting in its deubiquitylation, stabilisation and accumulation. Like βTrCP, the binding of USP27x to BIM_{EL} was reliant upon the ERK1/2-driven phosphorylation of BIM_{EL} (Weber *et al.*, 2016).

Work in this chapter sets out to examine the role of ERK1/2 and RSK in the degradation of BIM and to fully characterise the described interaction between βTrCP and BIM. In addition, work was performed to investigate the DUB for BIM including studying the involvement of USP27x in our system.

3.2. Results

3.2.1. Regulation of BIM_{EL} by the ERK1/2 pathway.

Preliminary experiments aimed to confirm that BIM_{EL} was dynamically regulated by the ERK1/2 pathway (Figure 3.1A). The HR1 cell line used for the following experiments is a model system for studying the effects of ERK1/2 signalling on a given protein as the cells stably express the conditional protein kinase ΔRAF-1:ER* so that treatment with 4-hydroxytamoxifen (4HT) selectively activates the ERK1/2 signalling pathway.

Figure 3.1 Regulation of BIMEL by the ERK1/2 pathway

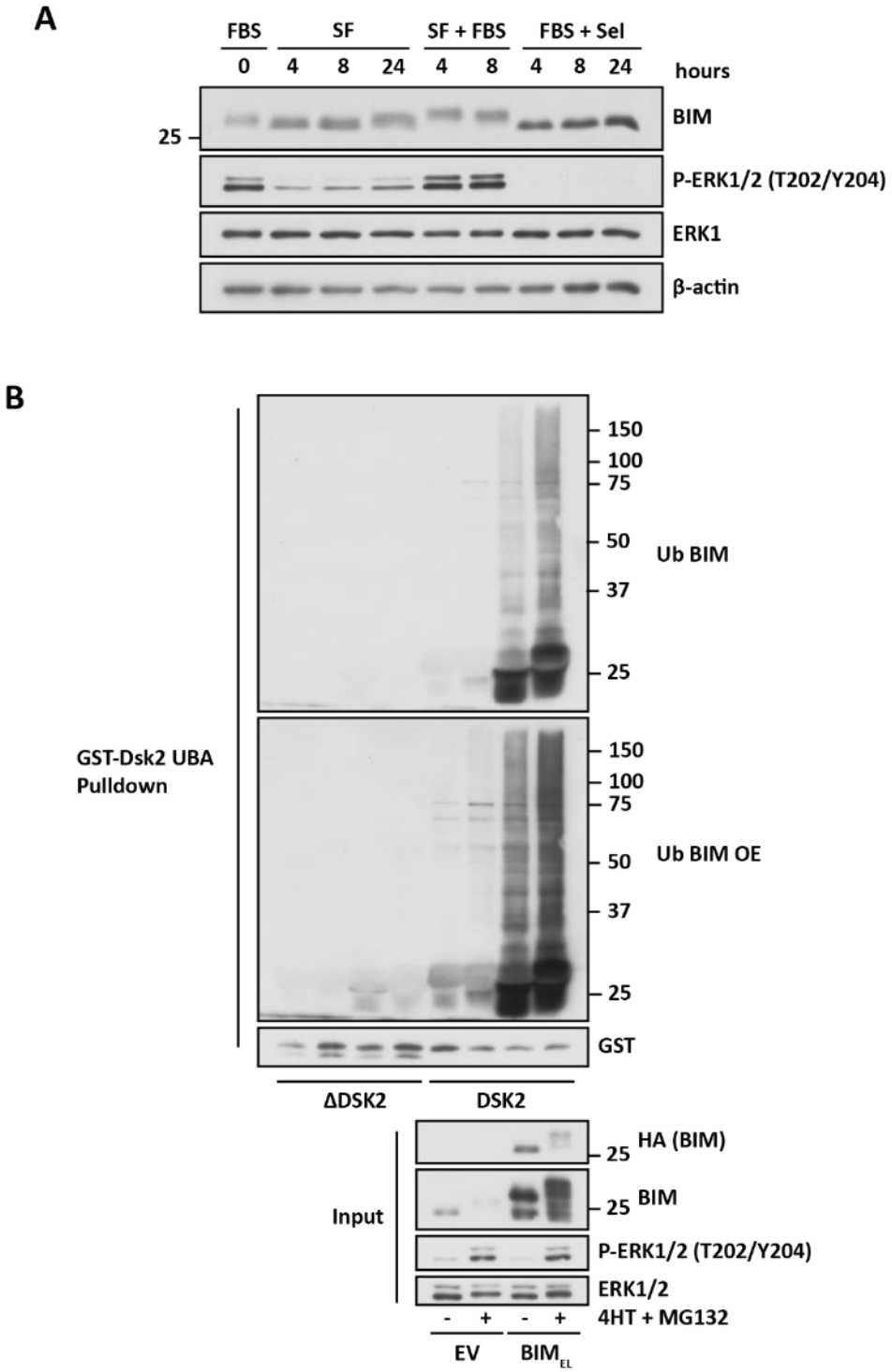

Figure 3.1 Regulation of BIM_{EL} by the ERK1/2 pathway (A) Subconfluent HCT116 cells were treated with 10% FBS or switched to serum free (SF) media. For a select set of samples maintined in SF media, FBS was reintroduced for increasing amounts of time (SF + FBS). For a select set of samples maintained in 10% FBS 1 μM of selumetinib (Sel) was introduced for increasing amounts of time (FBS + Sel). Cells were lysed, fractionated by SDS-PAGE and subjected to western blotting with the antibodies indicated in the figure. This data is representative of one experiment. **(B)** Cycling HR1 cells were transfected with empty vector (EV) or pcDNA3-HA-BIM_{EL} (BIM_{EL}). After 16 hours cells were switched to SF media and incubated with or without 10 μM MG132 and 100 nM 4HT for 90 minutes. Cell lysates were incubated with GST Dsk2 beads or GST ΔDsk2 beads and pulldowns were analysed by western blotting using described antibodies. Results shown here are from one experiment.
OE = overexposed.

Serum starvation of HR1 cells led to the inactivation of the ERK1/2 signalling pathway as shown by a reduction in the phosphorylated, active form of ERK1/2. As a consequence of this, BIM_{EL} was dephosphorylated, as shown by the increased mobility of BIM_{EL} on SDS-PAGE. Re-introduction of FBS to serum starved cells resulted in the reactivation of the ERK1/2 pathway, retarding the mobility of BIM_{EL} on SDS-PAGE, indicative of the re-phosphorylation of BIM_{EL}. Finally complete inhibition of ERK1/2 signalling, using the MEK1/2 inhibitor selumetinib, led to the dephosphorylation of ERK1/2 and BIM_{EL} and a corresponding increase in BIM_{EL} protein levels, presumably due to a reduction in its proteasomal degradation (Ley *et al.*, 2003).

As previously described by Wiggins *et al.*, data presented here confirmed that K48-linked polyubiquitylated BIM_{EL} could be detected using the immobilised UBA domain Dsk2 as an affinity capture resin (Figure 3.1B) (Wiggins *et al.*, 2011). Here, following incubation of cell lysates with GST-Dsk2, GSH-agarose pull-downs were able to isolate polyubiquitylated BIM_{EL}; the amount of polyubiquitylated BIM_{EL} was enhanced upon activation of the ERK1/2 signalling pathway (Figure 3.1B).

3.2.2. Tumour cells addicted to ERK1/2 signalling for survival are not addicted to RSK activity.

The Cook Lab previously demonstrated that tumour cells addicted to ERK1/2 signalling undergo BIM-dependent cell death in response to combined treatment with MEK1/2 inhibitors and BH3 mimetics, such as ABT-263 (Sale and Cook, 2013). As it has been previously suggested that RSK1/2 is required downstream of ERK1/2 to regulate the stability of BIM_{EL}, an aim of this study was to investigate if the same trend was observed when RSK inhibitors and ABT-263 were used in combination.

COLO205 and A375 cells were chosen for these experiments. Both cell lines harbour a $BRAF^{V600E}$ oncogene and are addicted to ERK1/2 signalling. Previous reports have demonstrated that combined treatment of these cell lines with the MEK1/2 inhibitor, selumetinib, and ABT-263 showed a significant increase in cell death, which, at least in the case of COLO205 cells, was found to be dependent on BIM (Sale and Cook, 2013). As well as this, several tools within the Cook lab could be used to further dissect the cell death response induced as a result of inhibitor treatment, including CRISPR-Cas9 BIM knockout A375 cells.

Treatment of COLO205 cells with the MEK1/2 inhibitor selumetinib blocked ERK1/2 phosphorylation and inhibited RSK activity as judged by the dephosphorylation of YB1, a transcription factor and recognised RSK substrate (Figure 3.2A). Selumetinib treatment in turn increased BIM expression, with this BIM protein being the hypophosphorylated stabilised form. Despite this increase in BIM, selumetinib treatment failed to drive apoptosis as judged by modest levels of PARP cleavage (Figure

3.2A) and the accumulation of cells in G1 of the cell cycle with no evidence of dead cells with sub-G1 DNA content (Figure 3.2B). However, combination of selumetinib with ABT-263 resulted in a striking apoptotic cell death (Figure 3.2B), whereas treatment with ABT-263 alone was ineffective, confirming previous observations (Sale and Cook., 2013). In contrast to this, the selective RSK inhibitor LJH685, used at two different doses, completely blocked YB1 phosphorylation, so was active against RSK, but failed to increase BIM protein levels and failed to combine with ABT-263 to drive COLO205 cell death, arguing against a role for RSK in the regulation of BIM.

To investigate this further the A375 melanoma cell line was studied using three different RSK inhibitors, LJH685, FMK and BI-D1870. Pan-RSK inhibitors, BI-D1870 and LJH685 are competitive inhibitors of the ATP-binding site of the NTKD of RSK. Fluoromethylketone (FMK) irreversibly binds to the active cysteine in the ATP-binding site of the CTKD of RSK1/2/4, so is unable to target RSK3 due to it lacking the key cysteine within the CTKD required for inhibition (Aronchik *et al.*, 2014, Casalvieri *et al.*, 2017, Cohen *et al.*, 2005). However, despite target engagement, BI-D1870 has been described to have a large number of off-target interactions (Edgar *et al.*, 2014, Roffe *et al.*, 2015, Sapkota *et al.*, 2007).

As previously seen in COLO205 cells, treatment of A375 cells with selumetinib alone resulted in an increase in BIM protein but minimal induction of cell death, as judged by sub-G1 DNA (Figure 3.2C and Figure 3.2D). Similarly, combined treatment with selumetinib and ABT-263 resulted in the accumulation of hypophosphorylated BIM but instead of an increase in the percentage of cells in G1 phase of the cell cycle seen with selumetinib treatment alone, the combined treatment led to an increase in sub-G1 DNA indicative of an increase in cell death (Figure 3.2C and Figure 3.2D). In contrast, treatment with any of the given RSK inhibitors resulted in the on-target loss of phosphorylated YB1, but failed to prevent the phosphorylation and degradation of BIM (Figure 3.2C). As observed in COLO205 cells, treatment of A375 cells with the RSK inhibitors, LJH685 and FMK, in combination with ABT-263, failed to drive an increase in the percentage of cells with sub-G1 DNA (Figure 3.2D). Treatment of A375 cells with BI-D1870, alone, as well as in combination with ABT-263, induced a comparable increase in sub-G1 DNA to that seen with combined selumetinib and ABT-263 treatment, which could be due to the known off-target effects of this inhibitor (Figure 3.2D). However, it was certainly unrelated to changes in BIM_{EL} abundance. Indeed, none of the RSK inhibitors increased BIM_{EL} abundance in either COLO205 or A375 cells, whereas selumetinib consistently did.

Figure 3.2 Dynamic regulation of BIMEL in tumour cells by ERK1/2 but not RSK.

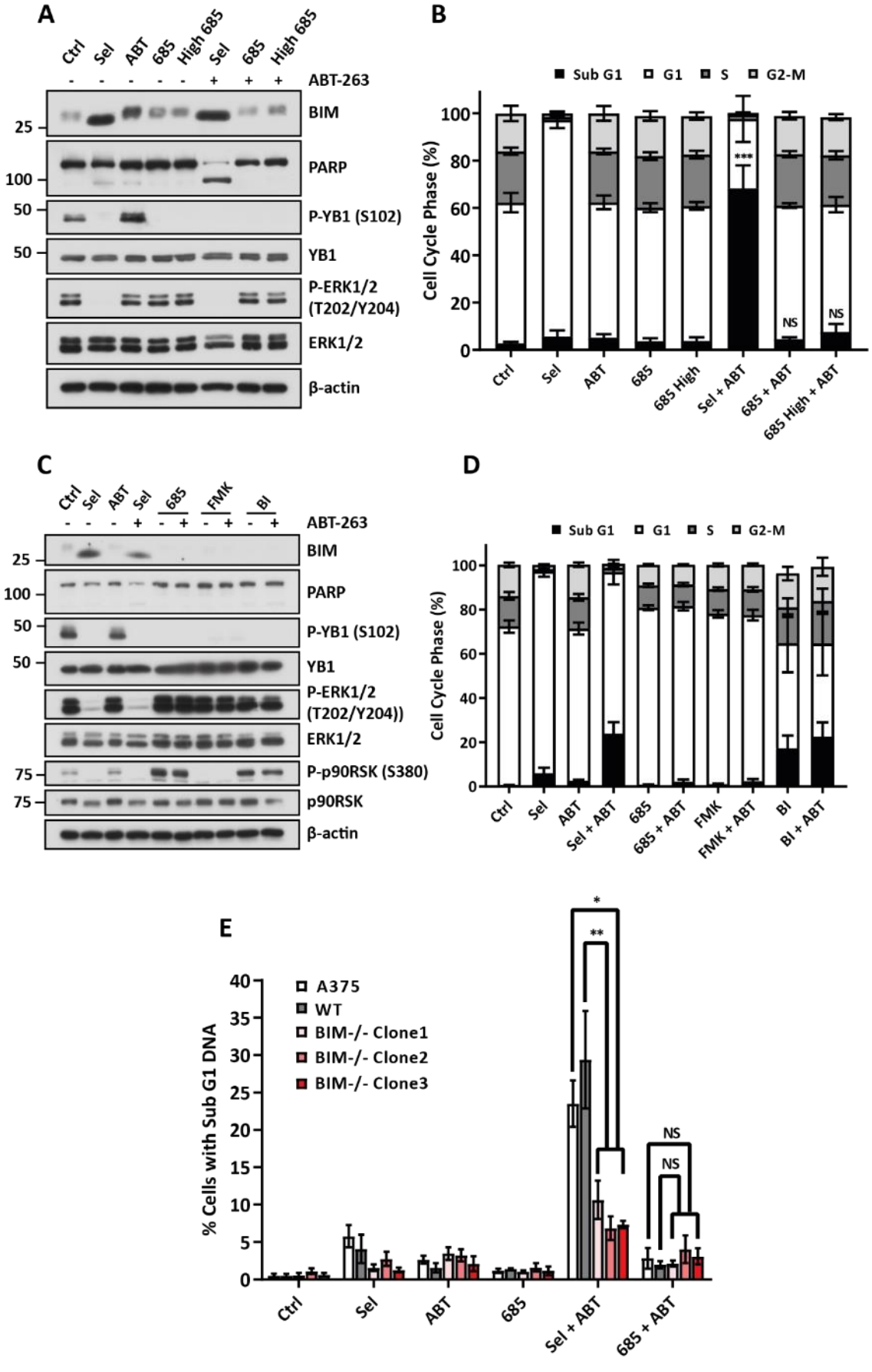

F

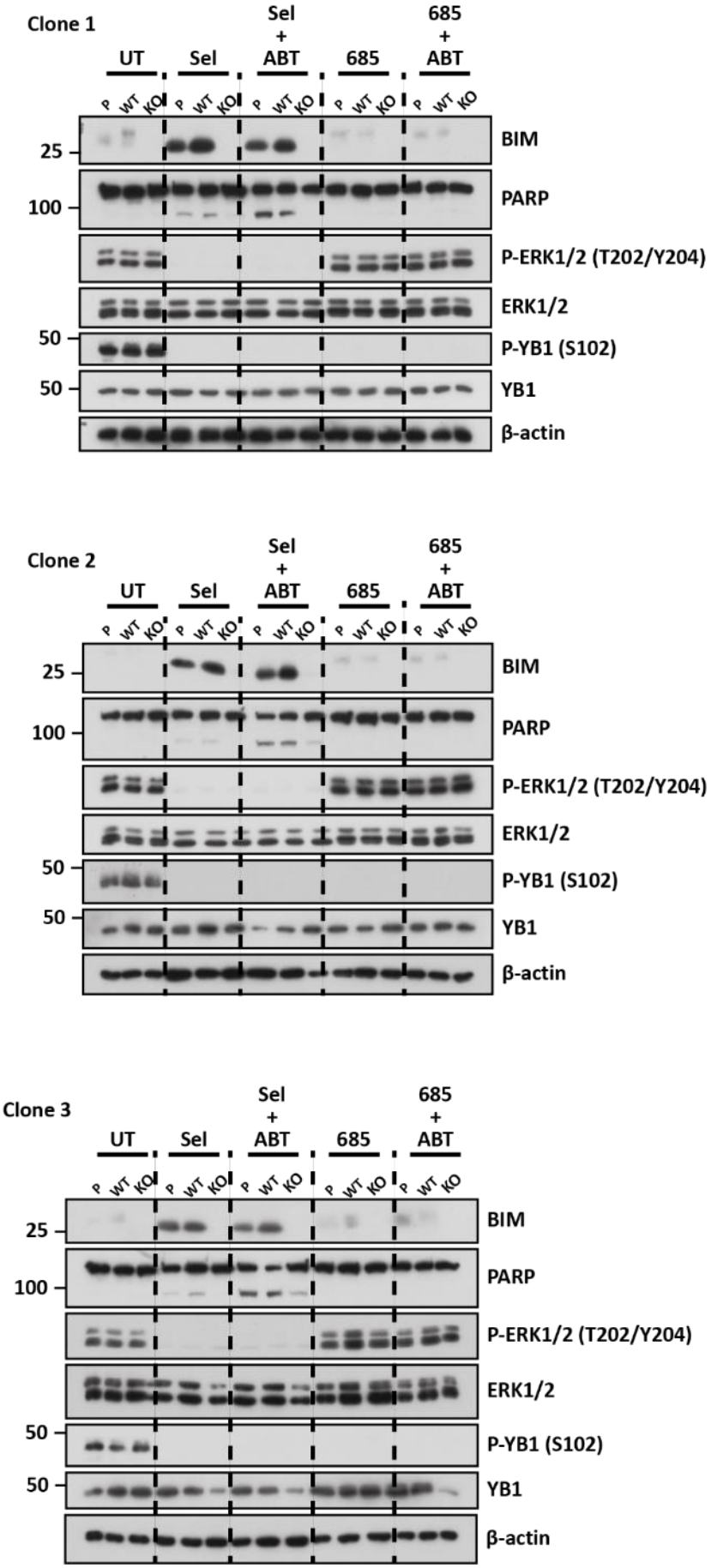
Clone 1
UT
Sel
Sel + ABT
685
685 + ABT
P WT KO
25
100
50
50
BIM
PARP
P-ERK1/2 (T202/Y204)
ERK1/2
P-YB1 (S102)
YB1
β-actin
Clone 2
UT
Sel
Sel + ABT
685
685 + ABT
P WT KO
25
100
50
50
BIM
PARP
P-ERK1/2 (T202/Y204)
ERK1/2
P-YB1 (S102)
YB1
β-actin
Clone 3
UT
Sel
Sel + ABT
685
685 + ABT
P WT KO
25
100
50
50
BIM
PARP
P-ERK1/2 (T202/Y204)
ERK1/2
P-YB1 (S102)
YB1
β-actin

Figure 3.2 Dynamic regulation of BIM_{EL} in tumour cells by ERK1/2 but not RSK. (A + B) COLO205 cells were treated with DMSO (Ctrl) or treated with 1 μM Selumentinib (Sel), 5 μM or 20 μM LJH685 (685 or 685 High) with or without 0.2 μM ABT-263 (ABT) for 48 hours after which **(A)** cells were lysed, fractionated by SDS-PAGE and subjected to western blotting with the antibodies indicated in the figure. This data is representative of one experiment, of which at least two have been performed giving similar results. Or **(B)** fixed and stained with propidium iodide and cell death (sub-G1 DNA) determined by flow cytometry. Results shown here are representative of the mean ± SD of three independent experiments, where each biological replicate is performed in technical triplicate. $P < 0.0001$ (***) or not significant (ns) for Sel vs Sel + ABT-263, 685 vs 685 + ABT or 685 High vs 685 High + ABT, as determined by one-way ANOVA with Tukey post-hoc test. **(C + D)** A375 cells were treated with DMSO (Ctrl) or treated with 1 μM Selumentinib (Sel), 6 μM FMK, 6 μM BI-D1870 (BI) or 10 μM LJH685 (685) with or without 1 μM ABT-263 (ABT) for 48 hours after which **(C)** cells were lysed, fractionated by SDS-PAGE and subjected to western blotting with the antibodies indicated in the figure. This data is representative of one experiment, of which at least two have been performed giving similar results. Or **(D)** fixed and stained with propidium iodide and cell death (sub-G1 DNA) determined by flow cytometry. Results shown here are representative of the mean ± SD of three independent experiments, where each biological replicate is performed in technical triplicate. **(E)** Parental A375 cells (A375), wild-type control cells (WT) and three individual BIM -/- clones, generated by CRISPR/Cas9, were treated with DMSO (Ctrl), with 1 μM selumetinib (Sel) or 10 μM LJH685 (685) with or without 1 μM ABT-263. After 48 hrs cells were fixed and stained with propidium iodide and cell death (sub-G1 DNA) determined by flow cytometry. Results shown here are representative of the mean ± SD of three independent experiments, where each biological replicate is performed in technical triplicate. $P < 0.001$ (**), $P < 0.01$ (*) or not significant (ns) for A375 vs BIM-/- Clone1/2/3 or WT vs Clone1/2/3 for Sel + ABT or 685 + ABT, as determined by one-way ANOVA with Tukey post-hoc test. **(F)** Parental A375 cells (P), wild-type control cells (WT) and three individual BIM -/- clones, generated by CRISPR/Cas9, (KO) were treated with DMSO (UT), with 1 μM selumetinib (Sel) or 10 μM LJH685 (685) with or without 1 μM ABT-263. After 48 hours cells were lysed, fractionated by SDS-PAGE and subjected to western blotting with the antibodies indicated in the figure. This data is representative of one experiment, of which two have been performed giving similar results.

Finally to confirm that cell death in this system was dependent on BIM, A375 cells were used in which BIM had been knocked out by CRISPR-Cas9. Deletion of BIM in three different clones led to a reduction in cell death in response to treatment with selumetinib and ABT-263. However, there was no observed difference in cell death between parental and BIM-/- A375 cells treated with a combination of LJH685 and ABT-263 (Figure 3.2E). Western blot analysis of the three CRIPSR/cas9 clones confirmed that BIM had been successfully knocked-out in all clones, and that inhibition of MEK1/2 and RSK, with or with ABT-263, resulted in the corresponding inhibition of phosphorylation of target proteins (Figure 3.2F).

Overall, data in Figure 3.2 demonstrated that inhibitors of MEK1/2 but not RSK increased the abundance of BIM and combined with a BH3 mimetic to kill cancer cells in a BIM-dependent manner. More than this, the data began to suggest that RSK might not regulate the stability of BIM.

3.2.3. A domain unique to BIM_{EL} is required for interaction with βTrCP.

For this study a reliable βTrCP antibody was required and as a consequence initial experiments, in which HR1 cells were transfect with siRNA against βTrCP or a vector over-expressing βTrCP, were performed to validate the chosen antibody. (Figure 3.3). βTrCP is expressed as two paralogs, βTrCP1 (FBXW1) and βTrCP2 (FBXW11), related by duplication within the genome. These two proteins share ~80% sequence homology, particularly within their WD40 domains (Butticaz *et al.*, 2007, Frescas and Pagano, 2008). The siRNA used here targets βTrCP1 and the antibody used here specifically recognises βTrCP1 at ~60 kDa. Herein the term βTrCP will refer to βTrCP1 unless stated otherwise.

As described, there are three major isoforms of BIM, shown in Figure 3.4A, with BIM_{EL} being the largest, most abundant and least potent isoform. Overexpression of HA-tagged versions of these isoforms in HR1 cells, followed by HA-immunoprecipitation, confirmed that of the major isoforms only BIM_{EL} interacted with βTrCP, suggesting a domain unique to this isoform was required for the observed interaction (Figure 3.4B). As well as this, a control BIM_{EL} construct with mutations within the known BH3 domain did not prevent the interaction between BIM_{EL} and βTrCP.

3.2.4. Phosphorylation of BIM_{EL} is required for interaction with βTrCP.

Exon 3, unique to BIM_{EL}, contains phosphorylation sites for ERK1/2 as well as those proposed for RSK1/2. Potential phosphorylation sites for ERK1/2 also exist within exon 4 of BIM_{EL}. A schematic

Figure 3.3 Validation of the βTrCP antibody.

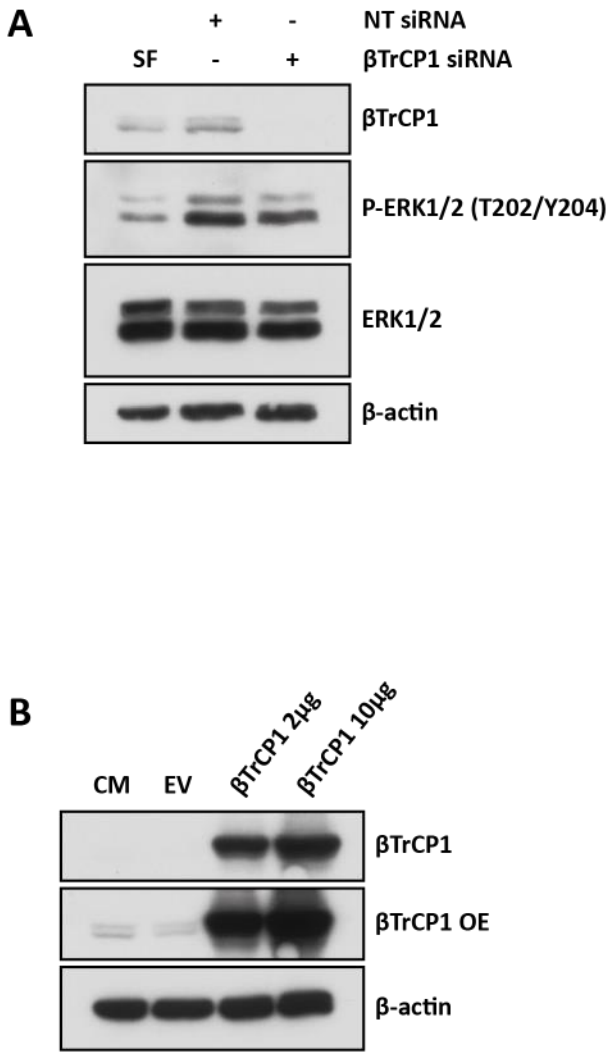

Figure 3.3 Validation of the βTrCP antibody. (A) HR1 cells were left untransfected in serum-free media (SF), transfected with 20 nM of non-targeting (NT) or βTrCP siRNA for 48 hours. Post-transfection cells were lysed, fractionated by SDS-PAGE and subjected to immunoblotting using indicated antibodies. This data is representative of a single experiment. **(B)** HR1 cells were left untransfected in complete media (CM) or tranfected with 10 μg of empty vector (EV), 2 μg or 10 μg of a vector expressing βTrCP. This data is representative of a single experiment.

Figure 3.4 A 'unique' domain to BIM_{EL} is required for interaction with βTrCP

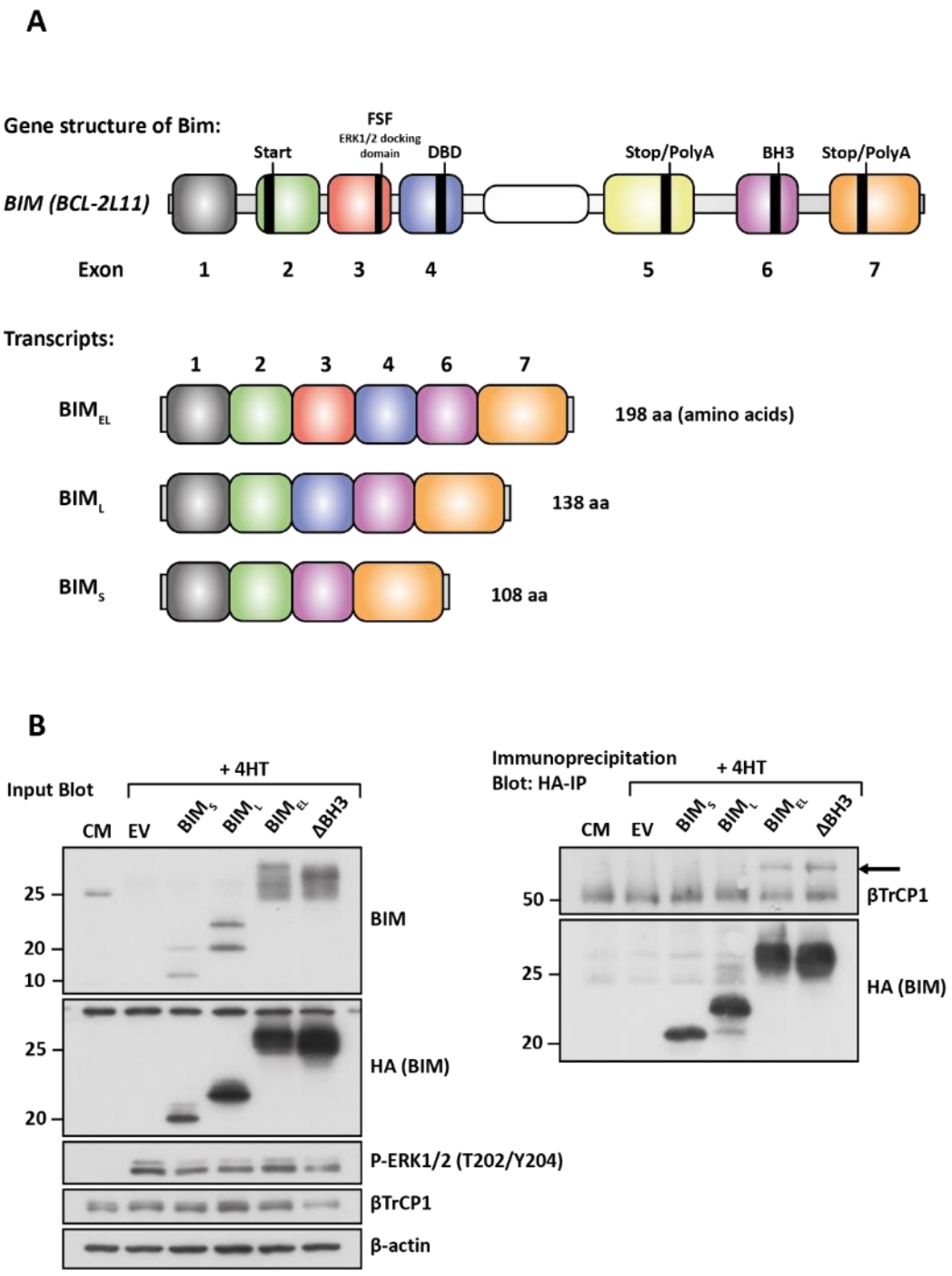

Figure 3.4 A 'unique' domain to BIM_{EL} is required for interaction with βTrCP. (A) Schemtatic representation of the gene structure and major isoforms transcripts of BIM. FSF represent the known ERK1/2 docking domain and DBD represents the Dynein-bindin domain. **(B)** HR1 cells were left untransfected in complete media (CM), transfected with empty vector (EV) or with HA-BIM_S, HA-BIM_L, HA-BIM_{EL} or HA-BIM_{EL}ΔBH3 (ΔBH3) for 16 hours post transfection, media was switched to serum free media, except CM, containing 10 μM MG132 for 30 minutes prior to stimulation with 100 nM 4HT for 90 minutes. Whole cell extracts were usd for immunoprecipitation (IP) of HA. Input and IP samples were then fractionated by SDS-PAGE and immunoblotted with indicated antibodies. Arrow indicates the band representative of βTrCP. This data is representative of one experiment, of which at least two have been performed giving similar results.

of exons 1-4 of BIM_{EL} is shown in Figure 3.5A, with the ERK1/2 and putative RSK1/2 phosphorylation sites mapped to exons 3 and 4. Mutation of these sites enabled the requirement for phosphorylation at these residues for the interaction between BIM_{EL} and βTrCP to be assessed. Thus, this data would help deduce if RSK was required for the regulation of BIM_{EL}.

Mutation of the three ERK1/2 phosphorylation sites in exon 3 reversed the ERK1/2-induced mobility shift in BIM_{EL} and abolished βTrCP binding (E1-3 mutant, Figure 3.5B). Additional mutation of three other ERK1/2 phosphorylation sites caused a further enhancement in mobility of BIM_{EL} in SDS-PAGE but no additional reduction in βTrCP binding (E1-6 mutant, Figure 3.5B). Thus, the ERK1/2 phosphorylation sites in exon 3 were absolutely required for βTrCP binding.

In contrast, mutation of the proposed RSK1/2 phosphorylation sites minimally reduced the mobility shift of BIM_{EL} but abolished the interaction between βTrCP and BIM_{EL} (R1-3 mutant, Figure 3.5C). As expected, the combination of mutating the ERK1/2 and RSK1/2 phosphorylation sites yielded the same outcome as that seen with mutating the ERK1/2 phosphorylation sites alone, complete dephosphorylation and accumulation of BIM_{EL} and loss of interaction with βTrCP (E1-6 and R1-3 mutant, Figure 3.5C). Overall immunoprecipitation of overexpressed HA-BIM_{EL} revealed that both ERK1/2 and RSK1/2 phosphorylation sites were required for the interaction between BIM_{EL} and βTrCP, but only mutation of ERK1/2 phosphorylation sites resulted in the accumulation of de-phosphorylated BIM_{EL} (Figure 3.5B and Figure 3.5C).

In accordance with Figure 3.5B and Figure 3.5C, mutation of ERK1/2 phosphorylation sites resulted in a reduction in BIM_{EL} polyubiquitylation (E1-6 mutant, Figure 3.5D). A similar polyubiquitylation pattern was observed following mutation of putative RSK1/2 phosphorylation sites, with or without mutated ERK1/2 phosphorylation sites, despite minimal enhancement of mobility of BIM_{EL} following the mutation of putative RSK1/2 phosphorylation sites alone (R1-3 mutant, Figure 3.5D). This suggested that both ERK1/2 and RSK1/2 phosphorylation sites were required for the polyubiquitylation of BIM_{EL}.

R3, S94 (S98 in Human), mutated in the HA-BIM_{EL} R1-3 expression vector, is located within the ERK1/2 docking domain on BIM_{EL} (Ley *et al.*, 2005). Binding of ERK1/2 to this domain is required for BIM_{EL} phosphorylation and degradation. Therefore, evaluating the effect of mutating the putative RSK1/2 sites on the ERK1/2-driven phosphorylation of BIM_{EL} was warranted. Addition of 4HT to HR1 cells, transfected with wild-type BIM_{EL}, resulted in the phosphorylation of BIM_{EL} on S65 (S69 in Human) and the binding of βTrCP (Figure 3.5E). Following mutation of putative RSK1/2 phosphorylation sites, a modest reduction in the phosphorylation of BIM_{EL} at S65 was observed. However, BIM_{EL} was no longer able to interact with βTrCP (Figure 3.5E). Thus suggesting that mutating the R1-3 sites might influence the docking of ERK1/2 to BIM_{EL}. Indeed, a previous PhD student in the Cook lab demonstrated that

mutating suggested RSK1/2 phosphorylation sites substantially reduced the ability of BIM_{EL} to interact with ERK1 (C. Wiggins, PhD Thesis). GST pulldown using wild-type and mutant BIM_{EL} revealed that GST-BIM_{EL} precipitated far more ERK1, from 4HT-treated lysates, than GST-BIM_{EL} R1-3. Prior treatment with the MEK1/2 inhibitor, U0126, prevented either construct from interacting with ERK1, probably due to the inhibition of ERK1/2 activity (Figure 3.5F). To further elucidate whether mutating residues R1-3 impacted the ability of ERK1/2 to interact with BIM_{EL}, BIM_{EL} phosphorylation was examined over a range of phosphorylated ERK1/2 levels by titrating in increasing concentrations of the MEK1/2 inhibitor selumetinib (Figure 3.5G and Figure 3.5H). Quantitative LI-COR analysis revealed that whilst phosphorylated S69 on wild-type and BIM_{EL} R1-3 was equally inhibited at maximal doses of selumetinib, at intermediate or 'limiting' levels of phosphorylated ERK1/2, the BIM_{EL} R1-3 phospho-mutant exhibited a strong reduction in phosphorylated BIM_{EL} at S69. This suggests that the R1-3 RSK1/2 phosphorylation site mutant does indeed impact ERK1/2 binding in cells making it challenging to draw conclusions, using the R1-3 mutant, regarding the necessity of RSK1/2 phosphorylation sites in the regulation of the degradation of BIM_{EL}. As an alternative approach, selective RSK inhibitors were again used to assess the role of RSK activity in the regulation of BIM_{EL}.

3.2.5. RSK activity is not required for BIM_{EL} polyubiquitylation and turnover.

To investigate the role of ERK1/2 and RSK phosphorylation in the degradation of BIM_{EL} several pharmacological inhibitors of the ERK/RSK signalling cascade were used. Throughout these experiments HR1 cells were used which express a ΔRAF-1:ER* construct to drive the activation of ERK1/2 and therefore RSK1/2, a downstream target of ERK1/2, following the addition of 4HT.

Activation of ERK1/2 signalling resulted in a shift in mobility of BIM_{EL}, indicative that ERK1/2 signalling drives the phosphorylation of BIM_{EL}. Following treatment with the MEK1/2 inhibitor, trametinib, or the ERK1/2 inhibitors, GDC-0994 and SCH772984, BIM_{EL} protein accumulated in its hypophosphorylated form (Figure 3.6A). This correlated with the inability of BIM_{EL} to interact with βTrCP (Figure 3.6A). In contrast, treatment with any of the given RSK inhibitors, FMK, BI-D1870 or LJH685, had no effect on the phosphorylation and degradation of BIM_{EL}, but successfully blocked the phosphorylation of a known substrate, YB1 (Figure 3.6A and Figure 3.6B). In accordance with this, inhibition of RSK did not prevent the interaction between βTrCP and BIM_{EL} (Figure 3.6A and Figure 3.6B).

Figure 3.5 Investigating the requirement of ERK1/2 and RSK phosphorylation sites in the regulation of BIM_{EL}.

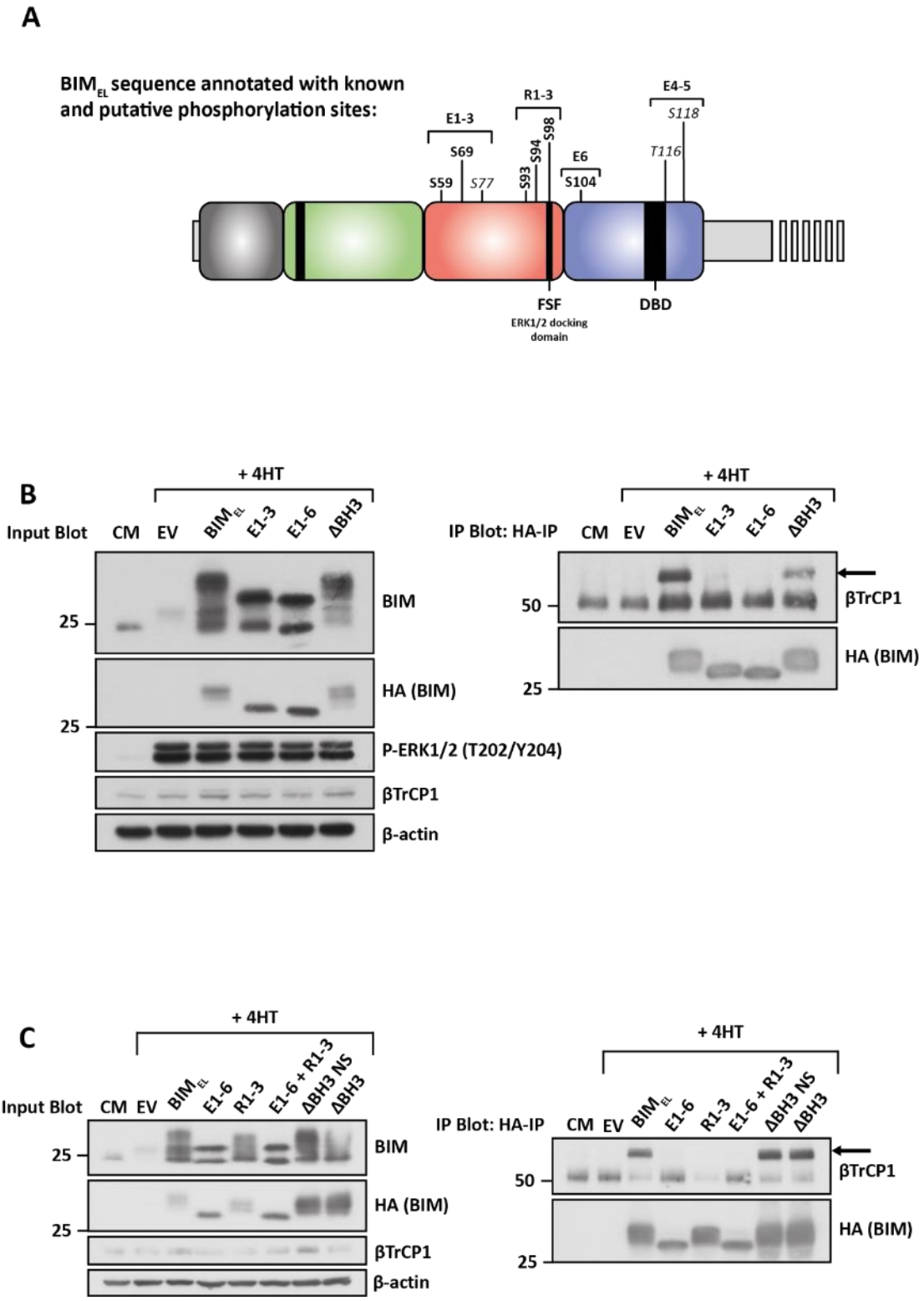

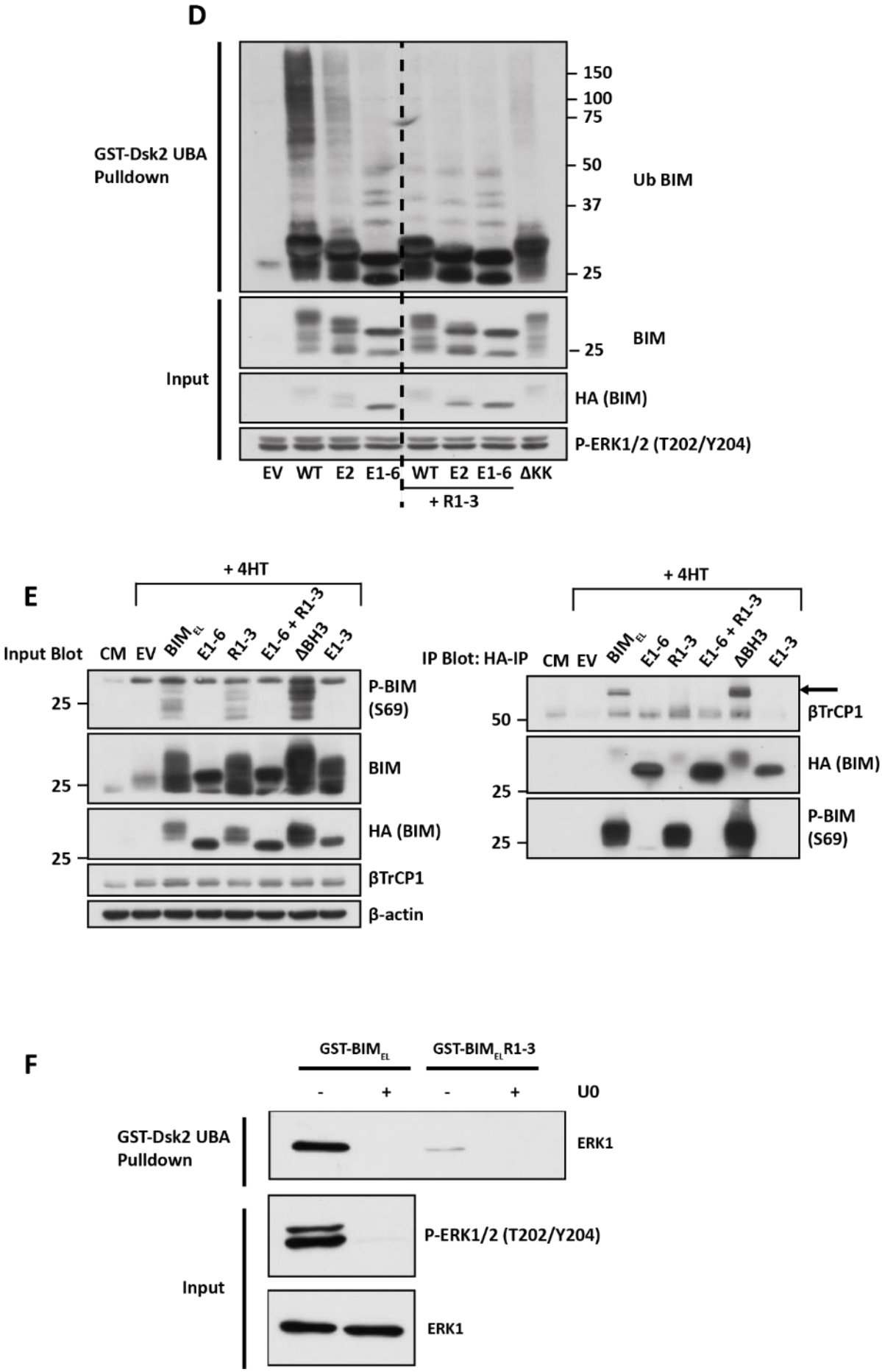
D
GST-Dsk2 UBA Pulldown
Input
150
100
75
50
37
25
Ub BIM
BIM
HA (BIM)
P-ERK1/2 (T202/Y204)
EV WT E2 E1-6 WT E2 E1-6 ΔKK
+ R1-3
E
+ 4HT
Input Blot CM EV BIMEL E1-6 R1-3 E1-6 + R1-3 ΔBH3 E1-3
P-BIM (S69)
BIM
HA (BIM)
βTrCP1
β-actin
IP Blot: HA-IP
50
F
GST-BIMEL
GST-BIMEL R1-3
- + - +
U0
GST-Dsk2 UBA Pulldown
ERK1
P-ERK1/2 (T202/Y204)
Input

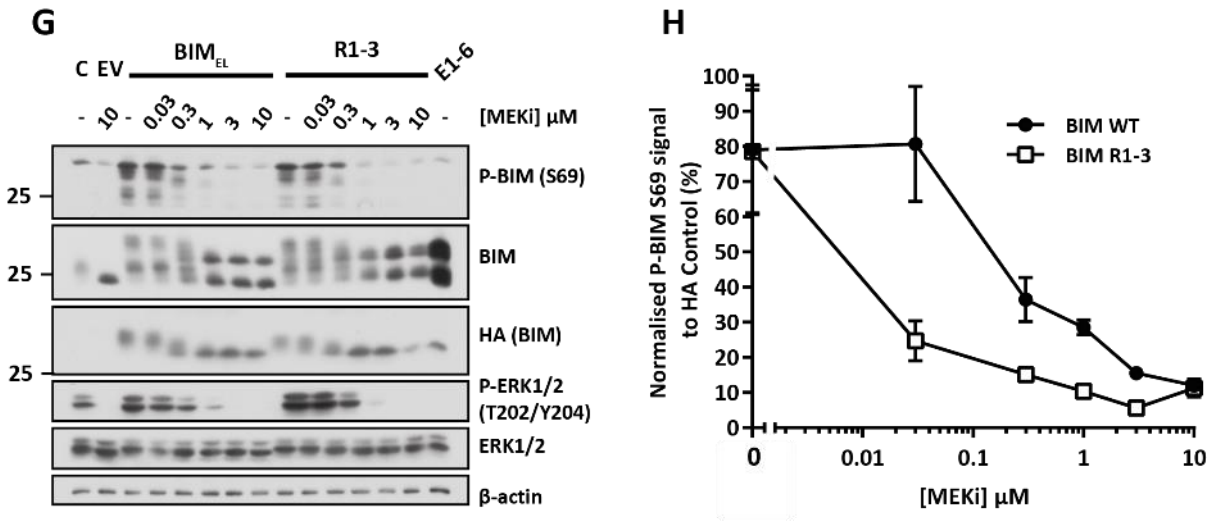

Figure 3.5 Investigating the requirement of ERK1/2 and RSK phosphorylation sites in the regulation of BIM$_{EL}$. (A) Schematic of BIM$_{EL}$ showing all known and suggested phosphorylation sites. E1-3 (known ERK1/2 phosphorylation sites) and R1-3 (putative RSK1/2 phosphorylation sites) are within Exon 3, whilst E4-6 (putative and known ERK1/2 phosphorylation sites) are within Exon 4. HR1 cells were left untransfected (CM/C), transfected with empty vector (EV) or with HA-BIM$_{EL}$(BIM$_{EL}$), HA-BIM$_{EL}$E1-3 (E1-3), HA-BIM$_{EL}$E1-6 (E1-6), HA-BIM$_{EL}$R1-3 (R1-3), HA-BIM$_{EL}$E1-6 + R1-3 (E1-6 + R1-3), HA-BIM$_{EL}$ΔBH3 (ΔBH3) or a no-splice variant HA-BIM$_{EL}$ΔBH3 (ΔBH3 NS), as indicated in the above figure. **(B + C + E)** 16 hours post transfection, media was switched to serum free media, except CM samples, containing 10 µM MG132 for 30 minutes prior to stimulation with 100 nM 4HT for 90 minutes. Whole cell extracts were used for immunoprecipitation (IP) of HA. Input and IP samples were then fractionated by SDS-PAGE and immunoblotted with indicated antibodies. Arrow indicates the band representative of β TrCP. This data is representative of one experiment, of which at least two have been performed giving similar results. **(D)** 16 hours post transfection, media was switched to serum free media, except CM samples, containing 10 µM MG132 for 30 minutes prior to stimulation with 100 nM 4HT for 90 minutes. Whole cell lysates were used for precipitation of ubiquitinated proteins using GST-Dsk2 UBA beads. Input and pulldown samples were then fracionated by SDS-PAGE and immunoblotted with indicated antibodies. This data is representative of one experiment, of which at least two have been performed giving similar results. **(F)** Representative figure taken from Ceri Wiggins thesis, Cook lab 2009; HR1 cells were switched to serum free media in the presence or absence of 10 µM U0126 for 30 mins prior to stimulation with 4HT for 1 hr. Whole cell lysates were generated, normalised for protein content and used for precipitation of ERK1 using GST-BIM$_{EL}$ or GST-BIM$_{EL}$R1-3. Input and pulldown samples were then fracionated by SDS-PAGE and immunoblotted with indicated antibodies. This data is representative of one experiment, of which at least two have been performed giving similar results. **(G + H)** 16 hours post transfection, media was switched to serum free media containing 10 µM MG132 with increasing concentrations of the MEK1/2 inhibitor, selumetinib, for 30 minutes prior to stimulation with 100 nM 4HT for 3 hours. **(G)** Whole cell extracts were fractionated by SDS-PAGE and immunoblotted with indicated antibodies. This data is representative of one experiment, of which at least two have been performed giving similar results. **(H)** Whole cell extracts were fractionated by SDS-PAGE, immunoblotted and analysed quantitatively by Licor. Results shown here are representative of the mean ± SD of three independent experiments.

Activation of the ERK1/2 signalling pathway resulted in the polyubiquitylation of BIM_{EL}, as judged using the previously described GST-Dsk2 pulldown shown in Figure 3.1B (figure 3.6C). Treatment with the MEK1/2 inhibitor, trametinib, but not the RSK inhibitor, LJH685, abolished the polyubiquitylation of BIM_{EL} (Figure 3.6C), indicating that RSK activity was not required for the K48-linked polyubiquitylation of BIM_{EL}. Together the data suggests that phosphorylation by ERK1/2 but not RSK is required for the interaction between BIM_{EL} and βTrCP and therefore for the polyubiquitylation and turnover of BIM_{EL}.

3.2.6. Investigating the ability of alternative kinases to regulate the stability of BIM_{EL}.

The preceding results suggested whilst the putative RSK1/2 phosphorylation sites might be required for the interaction between BIM_{EL} and βTrCP, RSK activity was not required for this interaction and therefore the turnover of BIM_{EL}. This suggested that an alternative kinase could cooperate with ERK1/2 to drive the polyubiquitylation and degradation of BIM_{EL}, by phosphorylating BIM_{EL} at S89, S90 and S94 (S93, S94 and S98 in Human), within the βTrCP binding motif or BIM_{EL} degron.

Aurora A has been proposed to phosphorylate BIM_{EL} during mitosis at the putative RSK1/2 phosphorylation sites (Moustafa-Kamal *et al.*, 2013). Therefore experiments were performed to evaluate if Aurora A activity was responsible for regulating BIM_{EL} under these conditions. Treatment with Aurora A inhibitors impedes the phosphorylation of the well-characterised Aurora A phosphorylation site, T210, on Polo-like kinase-1 (PLK1) (Macurek *et al.*, 2008, Seki *et al.*, 2008). HR1 cells, overexpressing HA-BIM_{EL}, were treated with the Aurora A inhibitor, alisertinib (MLN8237), at increasing concentrations, which led to the loss of phosphorylated PLK specifically at T210. As with inhibition of RSK, treatment with alisertinib did not prevent the phosphorylation of BIM_{EL}, abrogate the interaction between BIM_{EL} and βTrCP and as such did not protect BIM_{EL} from degradation (Figure 3.7A). Thus, suggesting that under these conditions Aurora A did not regulate the stability of BIM_{EL}.

Given this, the ability of alternative Ser/Thr protein kinases to target BIM_{EL} for phosphorylation-driven degradation was assessed. The Phospho-(Ser/Thr) Kinase Substrate Antibody kit, purchased from Cell Signalling Technology, can be used to evaluate whether specific phospho-motifs for a given kinase are present within a chosen substrate. Comparing lysates from HR1 cells transfected with BIM_{EL} or the BIM_{EL} R1-3 mutant should reveal if any of these kinases could phosphorylate wild-type BIM_{EL} but not mutant BIM_{EL}. Unfortunately, analysis using this kit did not suggest any kinases

Figure 3.6 Phosphorylation by ERK1/2 but not RSK promotes the ubiquitination and turnover of BIM_{EL}.

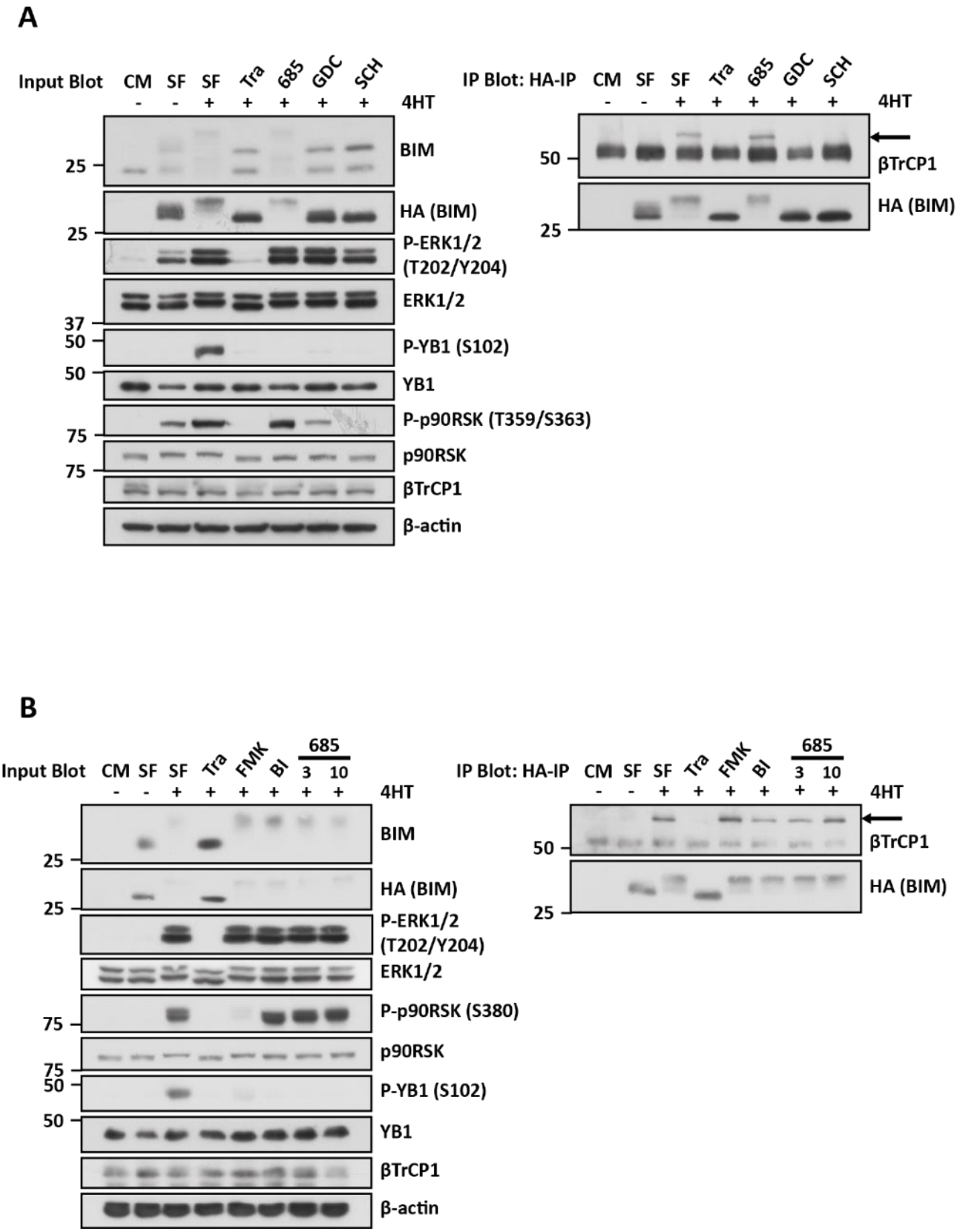

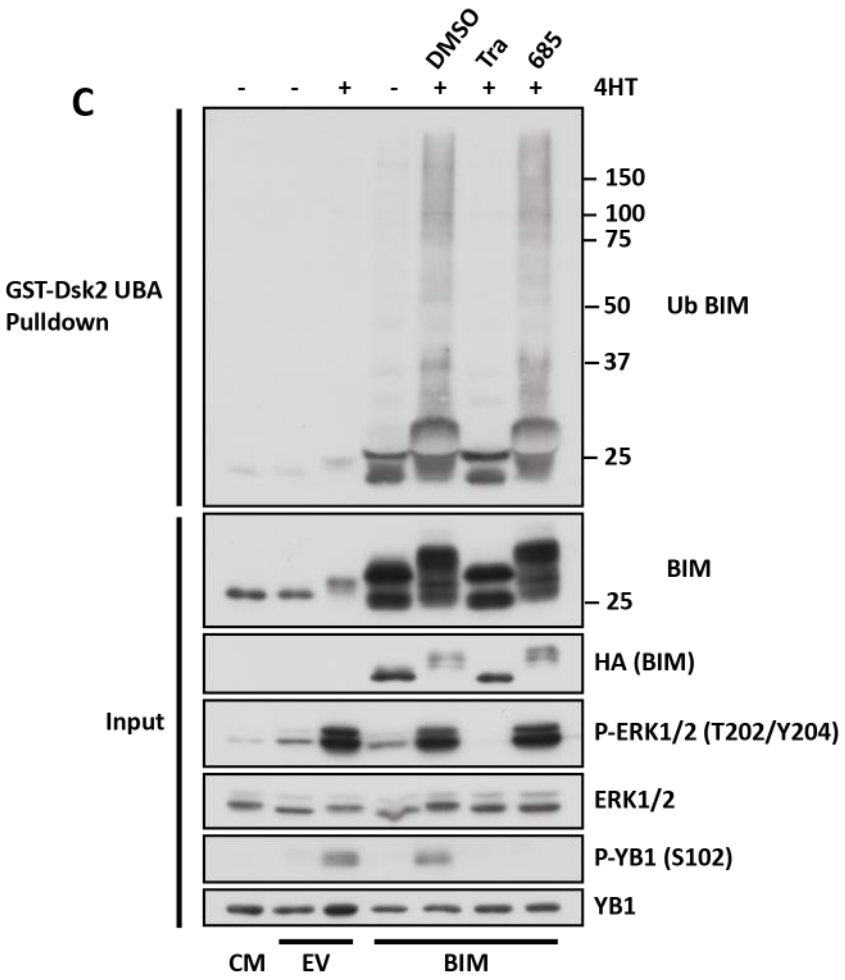

Figure 3.6 Phosphorylation by ERK1/2 but not RSK promotes the ubiquitination and turnover of BIM_{EL} (A + B) HR1 cells were transfected with HA-BIM_{EL} for 16 hours. Cells were maintained in complete media (CM) or switched to serum free (SF) medium containing ementine for 30 minutes with or without **(A)** 1 µM Trametinib (Tra), 10 µM LJH685 (685), 3 µM GDC-0994 (GDC) or 0.3 µM SCH772984 (SCH), **(B)** 1 µM Trametinib (Tra), 6 µM FMK, 10 µM BI-D1870 (BI), 3 µM or 10 µM LJH685 (685) prior to stimulation with 4HT for 3 hours. Whole cell lysates were generated and used for immunoprecipitation (IP) of HA. Input and IP samples were then fractionated by SDS-PAGE and immunoblotted with indicated antibodies. Arrow indicates the band representative of βTrCP. This data is representative of one experiment, of which at least two have been performed giving similar results. **(C)** HR1 cells were transfected with empty vector (EV) or HA-BIM_{EL}. 16 hours post transfection, media was switched to serum free media, except CM samples, containing 10 µM MG132 for 30 minutes with or without DMSO, 1 µM Trametinib (Tra) or 10 µM LJH685 (685), prior to stimulation with 100 nM 4HT for 90 minutes. Whole cell lysates were used for precipitation of ubiquitinated proteins using GST-Dsk2 UBA beads. Input and pulldown samples were then fracionated by SDS-PAGE and immunoblotted with indicated antibodies. This data is representative of one experiment, of which at least two have been performed giving similar results.

that were only capable of phosphorylating wild-type BIM_{EL} alone. Interrogation of immunoprecipitated lysates, with the PKA consensus motif recognition antibody, showed an increase in the presence of phosphorylated PKA consensus motifs in wild-type compared to mutant BIM_{EL} suggesting that mutation of putative RSK1/2 phosphorylation sites reduced the 'amount' of potential PKA phosphorylation sites (Figure 3.7B). However, there was no complete loss of phosphorylated PKA consensus motif following R1-3 mutation. Interestingly interrogation with AMPK and CDK consensus motif recognition antibodies revealed that unlike wild-type BIM_{EL}, mutant BIM_{EL} possessed phosphorylated consensus motifs for these kinases. Thus, implying potential conformational changes in this mutant allowing for AMPK and CDK to phosphorylate BIM_{EL} (Figure 3.7B).

Using data generated from proximity-based biotinylation or BioID, multiple substrates have been confirmed and identified for $SCF^{\beta TrCP1/2}$ (Coyaud *et al.*, 2015). Numerous βTrCP substrates harbour the sequence DSGX(n)S, or variants on this, where, as stated previously, phosphorylation of serine residues is required for interaction with $SCF^{\beta TrCP1/2}$, ultimately regulating the stability of these proteins (Frescas and Pagano, 2008, Winston *et al.*, 1999).

Comparing the sequence of BIM_{EL}, with known substrates, confirmed that BIM_{EL} possesses the described βTrCP binding motif and is therefore capable of undergoing polyubiquitylation under the control of βTrCP (Figure 3.7C) consistent with the interaction that was observed herein. Similar to that described by Dehan *et al.*, where cooperative phosphorylation of BIM_{EL} by ERK1/2 and RSK1/2 is required for interaction with βTrCP, both YAP and β-catenin are reliant upon 'priming' phosphorylation events for interaction with βTrCP. Degradation of β-catenin, in response to interaction with βTrCP, is reliant upon phosphorylation by CK1α at S45, which allows for protein phosphorylation by GSK3 within its βTrCP binding motif (Liu *et al.*, 2002). In the case of YAP, phosphorylation of key serine residues, including S381, by Lats primes the protein for additional phosphorylation by CK1δ/ε within the βTrCP binding motif (Zhao *et al.*, 2010b). Similarities to β-catenin led to the discovery of the cooperative phosphorylation of Snail (SNAI1), by CK1ε and GSK3β leading to its interaction with βTrCP1 and subsequent degradation (Xu *et al.*, 2010).

Using a PhosphoMotif database, based on Amanchy *et al.*, several kinases were identified that might have the potential to phosphorylate BIM_{EL} within the βTrCP binding motif in the BIM_{EL} degron (Amanchy *et al.*, 2007) (Figure 3.7D). Both CK1 and GSK3 are conserved Ser/Thr protein kinases and, from the described consensus motifs, might be capable of phosphorylating BIM_{EL} at conserved serine residues within the described BIM_{EL} degron, in a similar manner to that described above for YAP and β-catenin. To this end, inhibitors active against GSK3α/β (CHIR 99021 and AZ4216) and CK1 ((D4476 (CK1α/δ/ε) and PF 670462 (CK1δε)) were used to see if inhibition of these kinases prevented the

phosphorylation of BIM_{EL}, abolished the interaction between BIM_{EL} and βTrCP and therefore rescued BIM_{EL} from degradation (Figure 3.7E and Figure 3.7F).

Previously, GSK3 inhibitors, CHIR 99021 and AZ4216, have been shown to regulate the stability of β-catenin, with increasing concentrations of inhibitor resulting in a decrease in the phosphorylation of β-catenin at S33, S37 and T41 and an increase in protein stability (Ashford *et al.*, 2014, Yost *et al.*, 1996). Treatment of HEK293 cells with CK1 inhibitor, D4476, was found to inhibit the phosphorylation of FOXO1a on S322 and S325, thereby retarding its nuclear exclusion (Rena *et al.*, 2004, Rena *et al.*, 2002). These were used as markers of successful GSK3 or CK1 inhibition.

Activation of the ERK1/2 pathway resulted in the phosphorylation of BIM_{EL}, as judged from its decreased electrophoretic mobility on SDS-PAGE. As previously described, treatment with the MEK1/2 inhibitor, trametinib, resulted in the inhibition of BIM_{EL} phosphorylation, the loss of interaction between BIM_{EL} and βTrCP, resulting in the increased stability of BIM_{EL}. Treatment with the RSK inhibitor LJH685, did not affect the phosphorylation of BIM_{EL}, the interaction between BIM_{EL} and βTrCP and therefore the degradation of BIM_{EL}, despite strong inhibition of RSK (Figure 3.7E and Figure 3.7F).

CHIR 99021 and AZ4216 treatment of HR1 cells led to the inhibition of phosphorylation and resultant accumulation of β-catenin, indicating target inhibition. At the chosen concentrations of CHIR99021 and AZ4216, there was no effect on the phosphorylation or degradation of BIM_{EL} or on the interaction between BIM_{EL} and βTrCP (Figure 3.7E).

Similarly, treatment with the CK1 inhibitors, PF 670462 and D4476, did not prevent the phosphorylation or degradation of BIM_{EL}, and did not abolish the interaction between βTrCP and BIM_{EL} (Figure 3.7F). Addition of CK1 inhibitors did not visibly reduce phosphorylation of FOXO1A at S322/S325, however there was a reduction in phosphorylation and a slight accumulation of FOXO1A following treatment, indicative that these inhibitors were working at the chosen concentrations (Figure 3.7F). These experiments suggest that more work needs to be done to identify an alternative kinase that is responsible for regulating the degradation of BIM_{EL}, via phosphorylation of the βTrCP binding site in the BIM_{EL} degron.

To investigate if βTrCP is required to regulate the polyubiquitylation of BIM_{EL} in our system, the effect of knockdown of βTrCP on the polyubiquitylation pattern of BIM_{EL} was investigated. Interestingly targeted knockdown of βTrCP did not alter the polyubiquitylation of BIM_{EL} (Figure 3.7G), which could indicate that additional E3 ligases can interact with BIM_{EL} and drive its polyubiquitylation. Additionally activation of ERK1/2 signalling resulted in the induction of βTrCP protein levels (Figure 3.7G).

Figure 3.7 Investigating alternative kinases responsible for the interaction with βTrCP and degradation of BIM_{EL}.

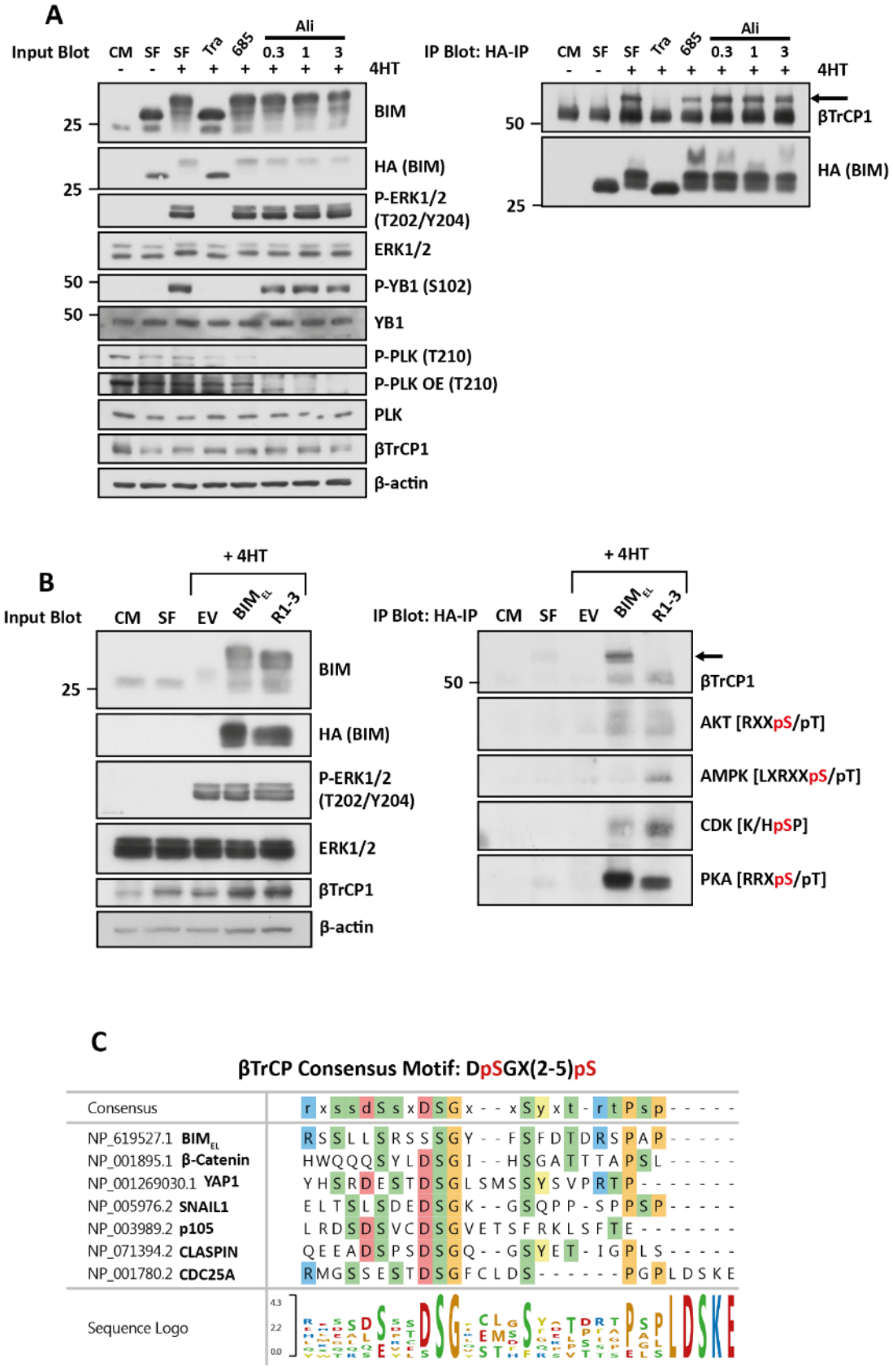

D

82 89 90 94 101
Rat BIM_{EL} : SSLLSRS-S-S-G-Y-F-S-FDTDRSP

86 93 94 98 105
Human BIM_{EL} : SSLLSRS-S-S-G-Y-F-S-FDTDRSP

Kinase	Consensus motif	Corresponding motif in BIM_{EL}	PubMed Reference
GSK3	pSxxxpS	SGYFS	Pearson and Kemp., 1998
CK1	[pS/pT]XXX[S/T/M/L/V/I/F]/ [pS/pT]XX[S/T]	SGYFSF/SFDT	Marin et al., 2003
CK2	pSXX[E/pS/pT]/pSXX[E/pS/pT]	SFDT/SSGY	Roach., 1991
PKA	RXpS/[R/K]X[pS/pT]/RXXpS	RSSS	Kreegipuu et al., 1998, Kastan and Lim., 2000, Shabb., 2001
PKC	[R/K]X[pS/pT]/[R/K]XX[pS/pT]	RSSS	Kreegipuu et al., 1998, Nishikawa et al., 1997, Pearson and Kemp., 1998, Kastan and Lim., 2000
Chk1 kinase	[M/I/L/V]X[R/K]XX[pS/pT]	LSRSSS	Hutchins et al., 2000
MAPKAPK1 (RSK1)	X[R/K]XRXX[pS/pT]X/ XRRXX[pS/pT]X and in general RXRXXS	RSSS	Leighton et al., 1995, Romeo et al., 2012

E

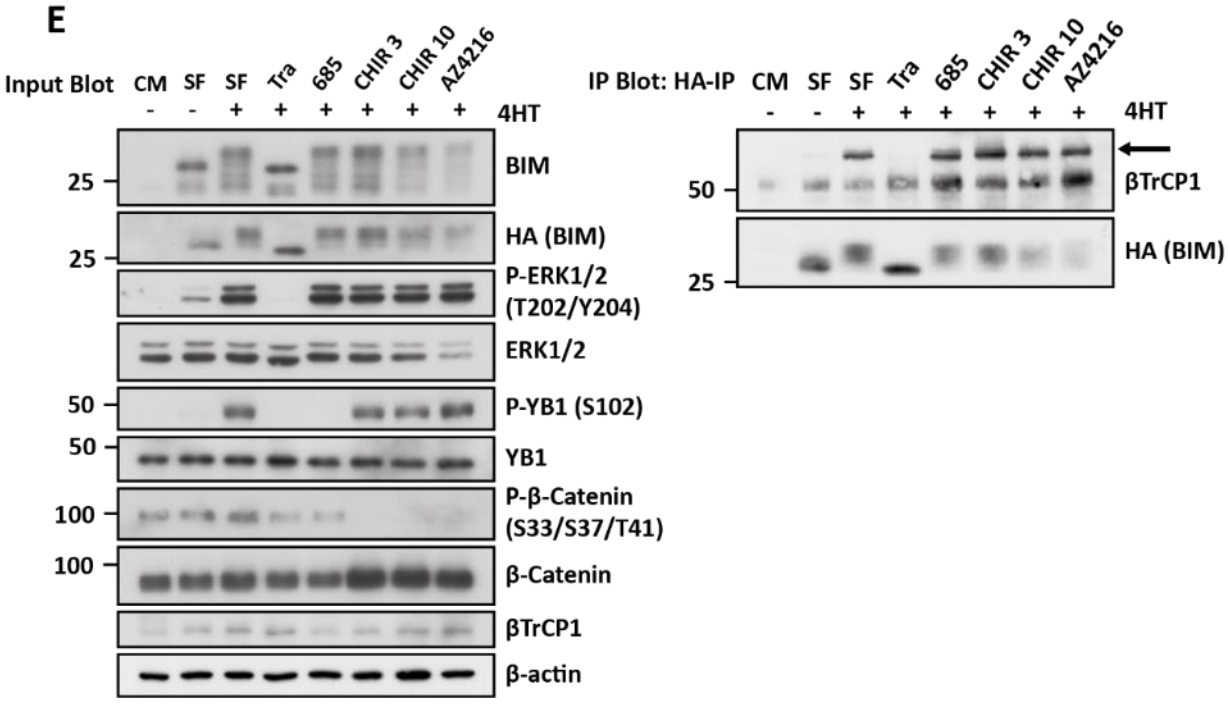

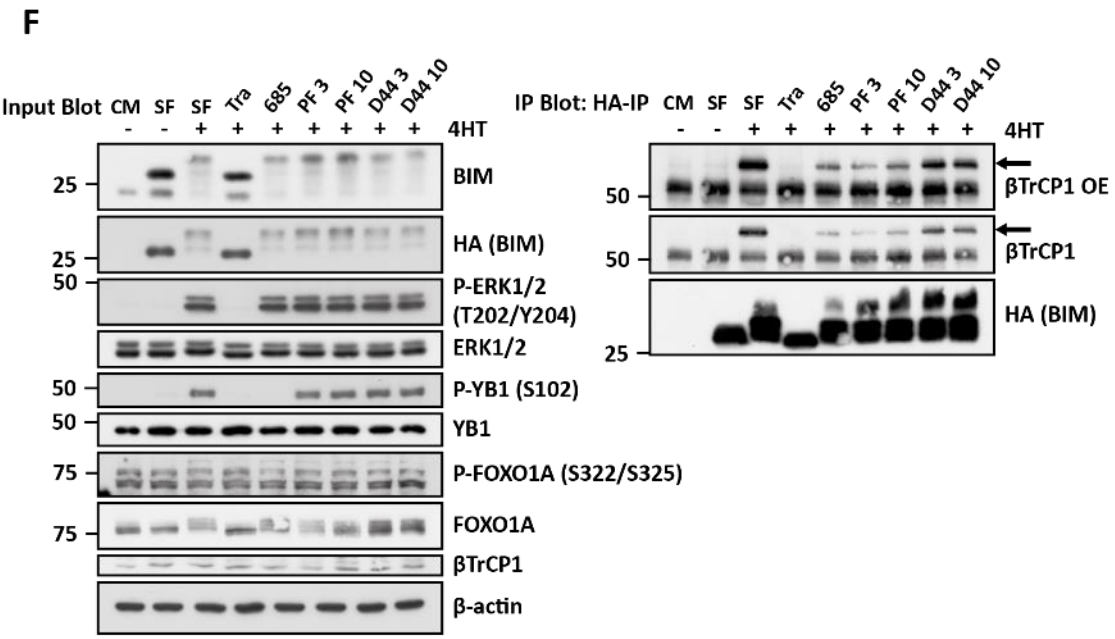
F
Input Blot
CM
SF
SF
Tra
685
PF 3
PF 10
D44 3
D44 10
4HT
BIM
HA (BIM)
P-ERK1/2 (T202/Y204)
ERK1/2
P-YB1 (S102)
YB1
P-FOXO1A (S322/S325)
FOXO1A
βTrCP1
β-actin
IP Blot: HA-IP
βTrCP1 OE
βTrCP1
HA (BIM)

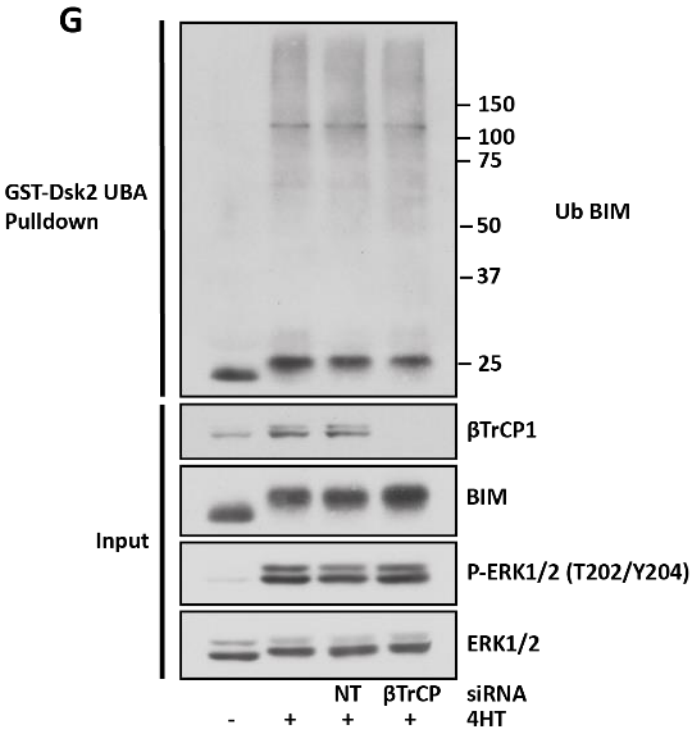
G
GST-Dsk2 UBA Pulldown
Ub BIM
Input
βTrCP1
BIM
P-ERK1/2 (T202/Y204)
ERK1/2
NT
βTrCP
siRNA
4HT

Figure 3.7 Investigating alternative kinases responsible for the interaction with βTrCP and degradation of BIM_{EL} (A) HR1 cells were transfected with HA-BIM_{EL} for 16 hours. Cells were maintained in complete media (CM) or switched to serum free (SF) medium containing ementine for 30 minutes with or without 1 μM Trametinib (Tra), 10 μM LJH685 (685) or 0.3/1/3 μM Alisertinib (Ali) prior to stimulation with 4HT for 3 hours. Whole cell lysates were generated and used for immunoprecipitation (IP) of HA. Input and IP samples were then fractionated by SDS-PAGE and immunoblotted with indicated antibodies. Arrow indicates the band representative of βTrCP. This data is representative of one experiment, of which at least two have been performed giving similar results. **(B)** HR1 cells were transfected with empty vector (EV), HA-BIM_{EL} or HA-BIM_{EL}R1-3 (R1-3) for 16 hours. Post transfection, media was switched to serum free media, except the complete media (CM) sample, containing 10 μM MG132 for 30 minutes prior to stimulation with 100 nM 4HT for 90 minutes. Whole cell extracts were used for immunoprecipitation (IP) of HA. Input and IP samples were then fractionated by SDS-PAGE and immunoblotted with indicated antibodies. Arrow indicates the band representative of βTrCP. This data is representative of one experiment, of which at least two have been performed giving similar results. **(C)** Schematic comparing sequences of known βTrCP substrates with that of BIM_{EL}, generated using MegAlign Pro®. Version 13.0. DNASTAR. Madison, WI., using MAFFT multiple sequence alignment tool. All sequences for the described proteins were taken from Pubmed. **(D)** Select Serine/Threonine Protein Kinases and their consensus sequences that have the capability of phosphorylating BIM_{EL} (Human and Rat) within the described βTrCP phosphodegron. **(E)** HR1 cells were transfected with HA-BIM_{EL} for 16 hours. Cells were maintained in complete media (CM) or switched to serum free (SF) medium containing ementine for 30 minutes with or without 1 μM Trametinib (Tra), 10 μM LJH685 (685), 3/10 μM CHIR99021 (CHIR) or 10 μM AZ4216 prior to stimulation with 4HT for 3 hours. Whole cell lysates were generated and used for immunoprecipitation (IP) of HA. Input and IP samples were then fractionated by SDS-PAGE and immunoblotted with indicated antibodies. Arrow indicates the band representative of βTrCP. This data is representative of one experiment, of which at least two have been performed giving similar results. **(F)** HR1 cells were transfected with HA-BIM_{EL} for 16 hours. Cells were maintained in complete media (CM) or switched to serum free (SF) medium containing ementine for 30 minutes with or without 1 μM Trametinib (Tra), 10 μM LJH685 (685), 3/10 μM PF 670462 (PF) or 3/10 μM D4476 (D44) prior to stimulation with 4HT for 3 hours. Whole cell lysates were generated and used for immunoprecipitation (IP) of HA. Input and IP samples were then fractionated by SDS-PAGE and immunoblotted with indicated antibodies. Arrow indicates the band representative of βTrCP. This data is representative of one experiment, of which at least two have been performed giving similar results. **(G)** Cycling HR1 cells were transfected with non-targeting siRNA (NT) or βTrCP siRNA (βTrCP). 48 hrs post-transfection media was switched to serum free media, containing 10 μM MG132 for 30 minutes prior to stimulation with 100 nM 4HT for 90 minutes. Whole cell lysates were used for precipitation of ubiquitinated proteins using GST-Dsk2 UBA beads. Input and pulldown samples were then fracionated by SDS-PAGE and immunoblotted with indicated antibodies. This data is representative of one experiment, of which at least two have been performed giving similar results.

3.2.7. Despite residing at the mitochondria, USP30 is not the DUB for BIM_{EL}.

As shown by previous results presented in this chapter, and those of others, BIM is degraded in response to activation of the Ras-RAF-MEK1/2-ERK1/2 pathway, indicating that both the polyubiquitylation and deubiquitylation of BIM will affect survival and therefore tumour development. As previously described multiple E3 ubiquitin ligases for BIM_{EL} have been suggested, however until recently the DUB for BIM_{EL} has not been found. Therefore, a candidate approach was employed in an attempt to find the DUB for BIM_{EL}.

BIM contains a hydrophobic tail that results in its localisation to the OMM (O'Connor *et al.*, 1998, Wilfling *et al.*, 2012). This OMM localisation is independent of its BH3 domain suggesting that it does not need to be bound to BCL2 proteins for OMM localisation. The following fractionation experiments were designed to determine if BIM_{EL} translocates from the mitochondria to the cytosol upon phosphorylation and polyubiquitylation. This might indicate if potential DUBs for BIM_{EL} would need to reside at or have the ability to translocate to the mitochondria. Of note, to date, USP30 is the only known DUB to contain a transmembrane domain targeting it to the OMM (Nakamura and Hirose, 2008).

Crude sub-cellular fractionation analysis of HR1 cells revealed endogenous BIM_{EL} was localised to the heavy membrane (HM) fraction (Figure 3.8A), which contained mitochondrial membranes, with COXIV used as a mitochondrial marker. Serum withdrawal resulted in an increase in the amount BIM_{EL} protein found in the HM fraction, which correlates with an increase in the total BIM protein. Activation of ERK1/2 resulted in the phosphorylation of BIM_{EL} and a decrease in total levels of BIM_{EL}. Addition of the proteasome inhibitor MG132 led to a small accumulation of phosphorylated BIM_{EL} at the mitochondria. Very little BIM_{EL} could be detected in the cytosolic fraction, shown by the cytosolic marker ERK1, from serum starved cells. However, overexposure of blots did reveal a small amount of phosphorylated BIM_{EL} in the cytosolic fraction from cells in which the ERK1/2 pathway had been activated (Figure 3.8A). These findings mimic that already seen by Putcha *et al.* and Weston *et al.* and further suggest the post-translational modification of BIM_{EL} occurs at the mitochondrial membrane. Based on these findings a candidate approach was adopted to investigate the DUB for BIM_{EL} beginning with USP30 and other DUBs that are known to regulate mitochondrial proteins (Putcha *et al.*, 2001, Weston *et al.*, 2003).

In common with previous reports, endogenous and overexpressed USP30 was primarily located in the HM fraction (Nakamura and Hirose, 2008). However, in contrast to this report, data presented here suggested that in complete media USP30 localised to the cytosolic fraction, and upon serum starvation either translocated to the HM fraction and/or was modified, within the cytosol, resulting in an increase in its molecular weight (shown by asterix in Figure 3.8B). This raises the interesting possibility that

USP30 may be regulated by nutrient conditions. Overexpressed BIM_{EL} and USP30 localised to both fractions but the majority of both proteins were localised to the HM fraction (Figure 3.8B). Given this colocalisation, USP30 had the potential to deubiquitylate BIM_{EL}.

During this study, USP2 was used as a positive control as it is a known 'promiscuous' DUB, which, when overexpressed, should cleave polyubiquitin chains irrespective of their chain linkage (Komander *et al.*, 2009b). The catalytic domain of Cezanne specifically cleaves K11 chains, which BIM_{EL} is not known to possess, thus overexpression of Cezanne should have no effect on the polyubiquitylation of BIM_{EL} and therefore acts a negative control (Mevissen *et al.*, 2013). From probed lysates, USP2 and USP30 exhibited DUB activity *in vitro*. Addition of the HA-UbVME probe (described in more detail in Chapter 4) resulted in a band shift of catalytically active DUBs as compared to catalytically inactive DUBs, indicative of the probe irreversibly binding to the cysteine residue present within the catalytic triad of the DUB (Figure 3.8C and Figure 3.8D). It was more challenging to observe whether overexpressed Cezanne was catalytically active as there was no obvious band shift, however both catalytically active and inactive Cezanne were shown to be overexpressed by a large increase in Cezanne protein compared to all other sample lanes (Figure 3.8D). Using the described Dsk2 pulldown (Figure 3.1B), the effect of USP2, Cezanne or USP30 overexpression on the polyubiquitylation pattern of BIM_{EL} could be assessed. Overexpression of USP30 did not affect the polyubiquitylation of overexpressed or endogenous BIM_{EL}, despite the overexpression of USP2 greatly reducing its polyubiquitylation and the overexpression of Cezanne having no affect. This indicated that this assay could not only detect DUB activity against BIM_{EL} but that USP30 was unable to deubiquitylate BIM_{EL} (Figure 3.8C and Figure 3.8D).

3.2.8. Neither USP8 nor USP15 is the DUB for BIM_{EL}.

USP8 and USP15 both regulate mitochondrial-associated proteins. Like USP30, USP15 overexpression resulted in impaired mitophagy by deubiquitinating known PARKIN substrates, whereas USP15 knockdown led to the enhanced clearance of defective mitochondria (Cornelissen *et al.*, 2014). In contrast to this, USP8 directly deubiquitylates PARKIN, thus delaying recruitment of PARKIN to the mitochondrial membrane thereby also preventing mitophagy (Durcan *et al.*, 2014).

Figure 3.8 USP30, located at the mitochondria, is not the DUB for BIM_{EL}.

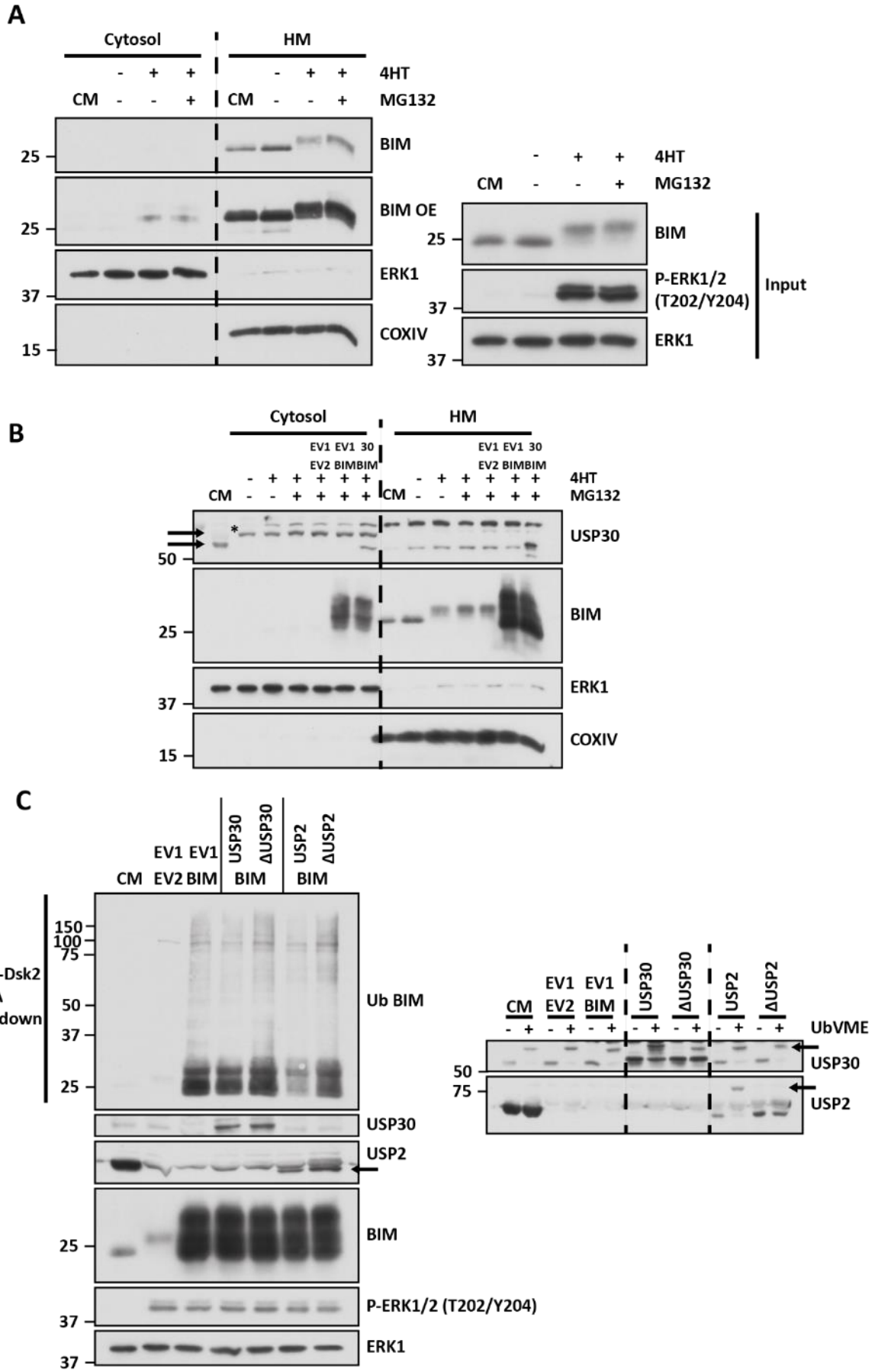

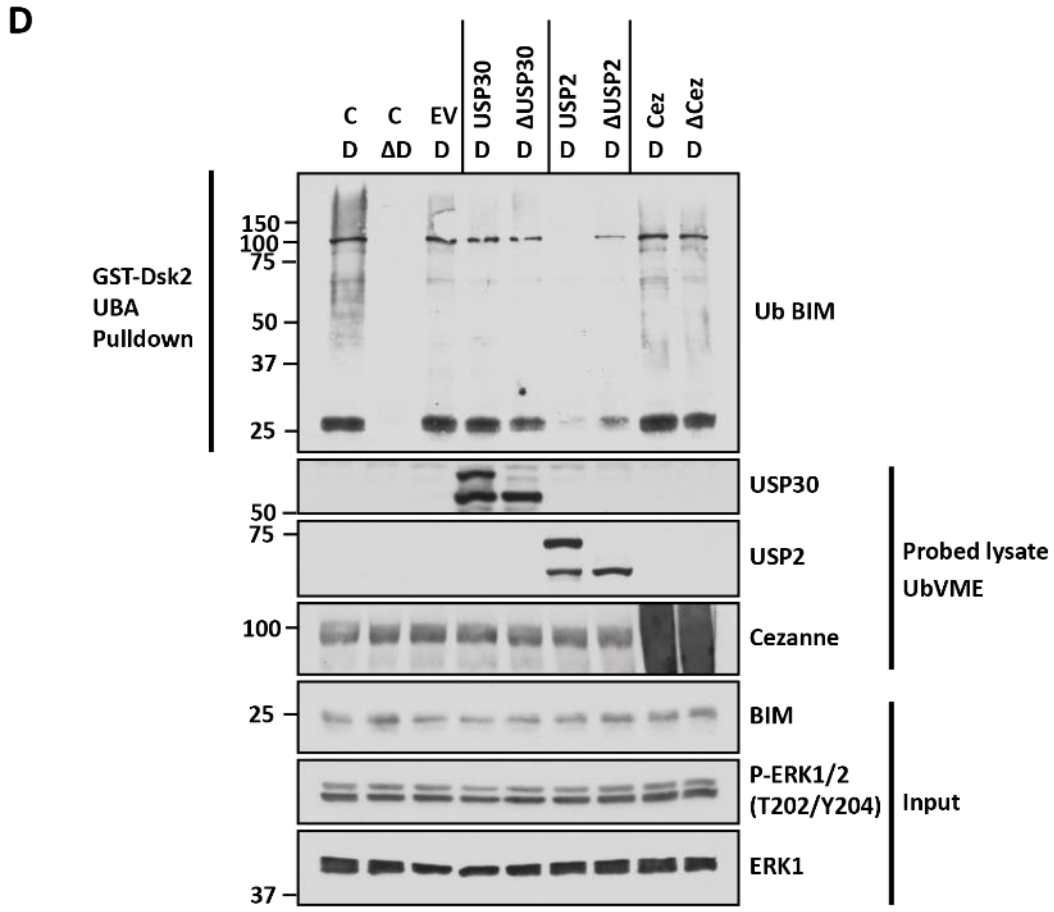

Figure 3.8 USP30, located at the mitochondria, is not the DUB for BIM$_{EL}$ (A) Cycling HR1 cells were left overnight to settle (~18 hrs). Cells were maintained in complete media (CM) or switched to serum free medium in the presence or absence of 10 μM MG132 and 100 nM 4HT. Cells were lysed in fractionation buffer and fractionated into cytosolic and heavy membrane (HM) fractions, input and fractionated samples were further fractionated by SDS-PAGE and immunoblotted with indicated antibodies. This data is representative of one experiment, of which at least two have been performed giving similar results. **(B)** HR1 cells were left untransfected (CM), transfected with empty vector (pFLAG-CMV-6c (EV1) or pcDNA3 (EV2)), pcDNA3-HA-BIM$_{EL}$ (BIM) or pFLAG-CMV-6c-USP30 (30). 16 hours post transfection, media was switched to serum free media, except CM samples, containing 10 μM MG132 for 30 minutes prior to stimulation with 100 nM 4HT for 90 minutes. Cells were lysed in fractionation buffer and fractionated into cytosolic and heavy membrane (HM) fractions, input and fractionated samples were further fractionated by SDS-PAGE and immunoblotted with indicated antibodies. This data is representative of one experiment, of which at least two have been performed giving similar results. **(C)** Cycling HR1 cells were left overnight to settle (~18 hrs), then left untransfected (CM) or transfected with empty vector (pFLAG-CMV-6c (EV1) or pcDNA3 (EV2)), pcDNA3-HA-BIM$_{EL}$ (BIM), pFLAG-CMV-6c-USP30 (USP30), pFLAG-CMV-6c-ΔUSP30 (ΔUSP30) (C77A), pFLAG-CMV-6c-USP2 (USP2) or pFLAG-CMV-6c-ΔUSP2 (ΔUSP2) (C267A), or combinations of these vectors. 16 hours post transfection, media was switched to serum free media, except CM samples, containing 10 μM MG132 for 30 minutes prior to stimulation with 100 nM 4HT for 90 minutes. Whole cell lysates were used for precipitation of ubiquitinated proteins using GST-Dsk2 UBA beads. Along with this, post-lysis, 0.5 μg of UbVME probe was added to 20 μg of lysate for one hour at room temperature. Pulldown lysates, probed lysates and input lysates were fractionated by SDS-PAGE and subjected to western blotting with the antibodies indicated in the figure. This data is representative of one experiment, of which at least two have been performed giving similar results. **(D)** Cycling HR1 cells were left O/N to settle (~18 hrs), then left untransfected (C) or transfected with empty vector (pFLAG-CMV-6c (EV)), pFLAG-CMV-6c-USP30 (USP30), pFLAG-CMV-6c-ΔUSP30 (ΔUSP30), pFLAG-CMV-6c-USP2 (USP2), pFLAG-CMV-6c-ΔUSP2 (ΔUSP2) , pFLAG-CMV-6c-Cezanne (Cez), pFLAG-CMV-6c-ΔCezanne (ΔCez) (C194S), or combinations of these vectors. 16 hours post transfection, media was switched to serum free media, containing 10 μM MG132 for 30 minutes prior to stimulation with 100 nM 4HT for 90 minutes. Whole cell lysates were used for precipitation of ubiquitinated proteins using GST-Dsk2 UBA beads (D) or a mutant form of GST-Dsk2 UBA beads (ΔD) . Along with this, post-lysis, 0.5 μg of UbVME probe was added to 20 μg of lysate for one hour at room temperature. Pulldown lysates, probed lysates and input lysates were fractionated by SDS-PAGE and subjected to western blotting with the antibodies indicated in the figure. This data is representative of one experiment, of which at two have been performed giving similar results.

Therefore, experiments were performed to assess if overexpressing these DUBs altered the ability of Dsk2 to pulldown polyubiquitylated BIM_{EL}.

The HA-UbVME probe was used to confirm that USP8, USP15 and USP2 were all active when expressed in cells and assayed *in vitro*. Overexpression of USP8 and USP15 did not result in any significant alteration in the polyubiquitylation of BIM_{EL}, compared to the lane in which catalytically active USP2 was overexpressed (Figure 3.9). However, this data was less convincing than that presented in Figure 3.8.

3.2.9. Investigating the regulation of BIM_{EL} by USP27x.

Whilst attempting to find the DUB for BIM_{EL} Weber *et al.* proposed that USP27x interacts with BIM_{EL}, resulting in its deubiquitylation (Weber *et al.*, 2016). Despite numerous attempts, of which only one is shown, immunoprecipitation of HA-BIM_{EL} failed to detect an interaction with FLAG-tagged USP27x. Regardless of this, an interaction between BIM_{EL} and βTrCP was still observed (Figure 3.10A).

Despite this, transfection of HR1 cells with increasing amounts of USP27x resulted in a decrease in the polyubiquitylation of BIM_{EL} which was not observed with catalytically inactive USP27x (Figure 3.10B). Thus, despite not being able to observe a direct interaction between BIM_{EL} and USP27x, the catalytic activity of USP27x was capable of removing polyubiquitin chains from BIM_{EL}. Therefore, in agreement with Weber *et al.* USP27x is able to deubiquitylate BIM_{EL}. Interestingly, overexpression of catalytically inactive USP27x resulted in the accumulation of polyubiquitylated BIM_{EL} (Figure 3.10B).

3.3. Discussion

3.3.1. ERK1/2, but not RSK, is required for BIM_{EL} polyubiquitylation and degradation.

Tumour cells that possess $BRAF^{V600E}$ mutations are addicted to ERK1/2 for survival and undergo BIM-dependent apoptosis when MEK1/2 or ERK1/2 are inhibited in combinaton with ABT-263 treatment. In contrast, data presented in this chapter demonstrated that they are not addicted to RSK activity and thus inhibition of RSK, in combination with ABT-263 did not drive cell death. CRISPR-Cas9 knockout of BIM was revealed to rescue cells from cell death driven by ERK1/2 but not RSK inhibition. This suggests that RSK activity was not required to suppress BIM expression to drive tumour cell survival. Given this, the role of RSK, in the regulation of BIM, was investigated further and compared to regulation by ERK1/2.

Figure 3.9 Neither USP8 nor USP15 are the DUB for BIM_{EL}.

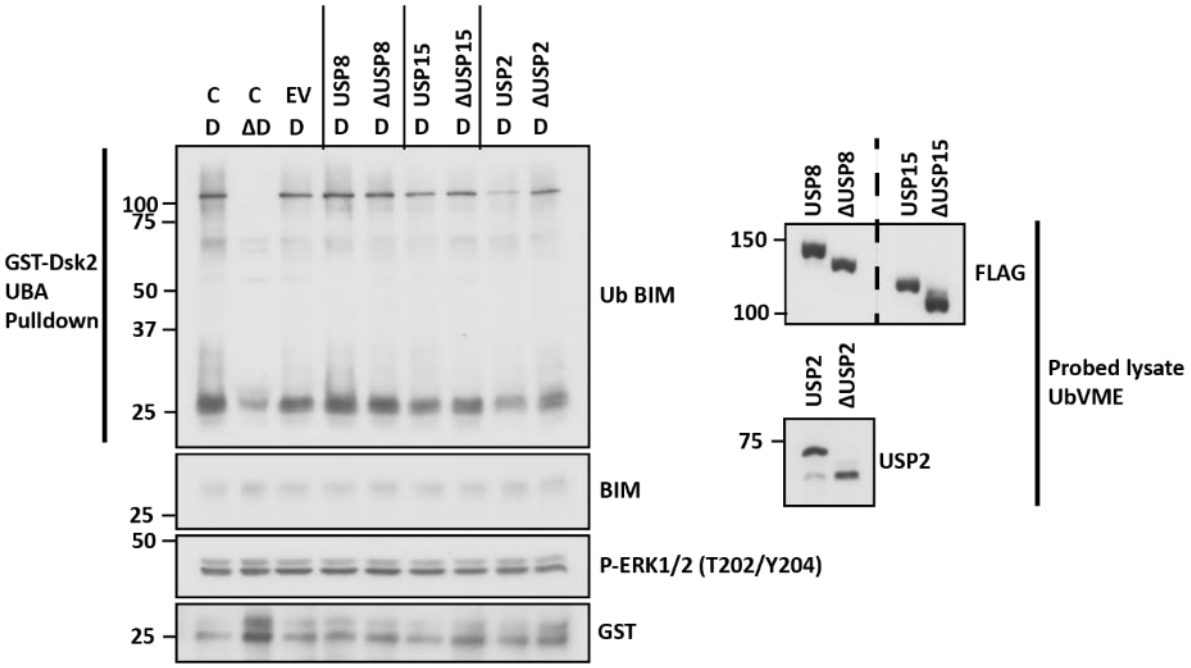

Figure 3.9 Neither USP8 nor USP15 are the DUB for BIM_{EL} Cycling HR1 cells were left O/N to settle (~18 hrs), then left untransfected (CM) or transfected with empty vector (pFLAG-CMV-6c (EV1) or pcDNA3 (EV2)), pcDNA3-HA-BIM_{EL} (BIM), pFLAG-CMV-6c-USP8 (USP8), pFLAG-CMV-6c-ΔUSP8 (ΔUSP8) (C748A), pFLAG-CMV-6c-USP15 (USP15), pFLAG-CMV-6c-Δ USP15 (ΔUSP15) (C269A), pFLAG-CMV-6c-USP2 (USP2) or pFLAG-CMV-6c-ΔUSP2 (ΔUSP2), or combinations of these vectors. 16 hours post transfection, media was switched to serum free media, except CM samples, containing 10 μM MG132 for 30 minutes prior to stimulation with 100 nM 4HT for 90 minutes. Whole cell lysates were used for precipitation of ubiquitinated proteins using GST-Dsk2 UBA beads or a mutant form of GST-Dsk2 UBA beads (GST-ΔDsk2 UBA) . Along with this, post-lysis, 0.5 μg of UbVME probe was added to 20 μg of lysate for one hour at room temperature. Pulldown lysates, probed lysates and input lysates were fractionated by SDS-PAGE and subjected to western blotting with the antibodies indicated in the figure. This data is representative of one experiment, of which two have been performed giving similar results.

Figure 3.10 Despite reduction in polyubiquitylation of BIM_{EL} following overexpression of USP27x, no interaction between the two can be detected.

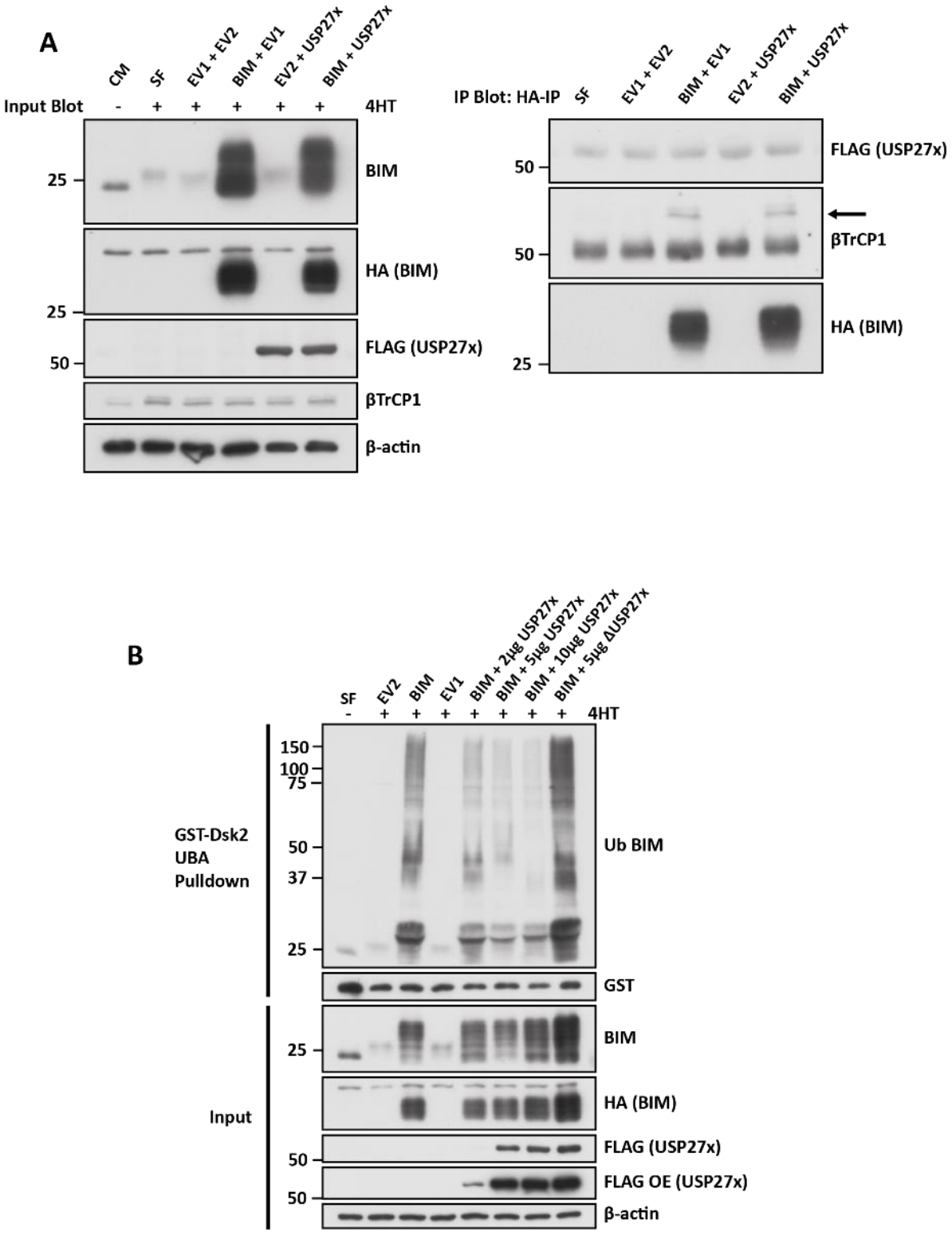

Figure 3.10 Despite reduction in polyubquitination of BIM_{EL} following overexpression of USP27x, no interaction between the two can be detected. (A) Cycling HR1 cells were left O/N to settle (~18 hrs), then left untransfected (CM/SF) or transfected with empty vector (pFLAG-CMV-6c (EV1) or pcDNA3 (EV2)), pcDNA3-HA-BIM_{EL} (BIM) or pFLAG-CMV-6c-USP27x (USP27x) or combinations of these vectors at varying concentrations. 16 hours post transfection, media was switched to serum free (SF) media, except CM sample, with or without 10 µM MG132 for 30 minutes prior to stimulation with 100 nM 4HT for 90 minutes. Whole cell lysates were generated and used for immunoprecipitation (IP) of HA. Input and IP lysates were fractionated by SDS-PAGE and subjected to western blotting with the antibodies indicated in the figure. This data is representative of one experiment, of which at least two have been performed giving similar results. **(B)** Cycling HR1 cells were left O/N to settle (~18 hrs), then left untransfected (SF) or transfected with empty vector (pFLAG-CMV-6c (EV1) or pcDNA3 (EV2)), pcDNA3-HA-BIM_{EL} (BIM), pFLAG-CMV-6c-USP27x (USP27x) or pFLAG-CMV-6c-ΔUSP27x (ΔUSP27x) (C87A), or combinations of these vectors at varying concentrations. 16 hours post transfection, media was switched to serum free (SF) media with or without 10 µM MG132 for 30 minutes prior to stimulation with 100 nM 4HT for 90 minutes. Whole cell lysates were used for precipitation of ubiquitinated proteins using GST-Dsk2 UBA beads. Pulldown lysates and input lysates were fractionated by SDS-PAGE and subjected to western blotting with the antibodies indicated in th e figure. This data is representative of one experiment, of which at least two have been performed giving similar results.

BIM is a potent pro-apoptotic BH3-only protein and its deregulated expression has been linked to numerous diseases, in particular cancer. As such, a complete understanding of the regulatory mechanisms driving/opposing the degradation of BIM_{EL} are vital. It is well established that ERK1/2 phosphorylates BIM_{EL} leading to its polyubiquitylation and degradation (Ley *et al.*, 2003, Ley *et al.*, 2004). Dehan *et al.* demonstrated that the F-box protein βTrCP1/2, as part of an SCF ubiquitin ligase complex, could act as an E3 ligase for BIM_{EL} (Dehan *et al.*, 2009). Results presented in this chapter confirmed and extended aspects of the Dehan *et al.* study by showing that βTrCP interacted with BIM_{EL}, that this was dependent on ERK1/2 activity and ERK1/2 phosphorylation sites, identified previously in the Cook lab.

Dehan *et al.* also proposed that phosphorylation of S93, S94 and S98, by RSK1/2 was prerequisite for binding of the $SCF^{\beta TrCP1/2}$ (Dehan *et al.*, 2009). They observed that mutating S69 inhibited phosphorylation of the βTrCP binding motif within the BIM_{EL} degron, and suggested that this indicates that ERK1/2-driven phosphorylation of S69 was required for phosphorylation at S93, S94 and S98 by RSK1/2 and βTrCP binding. To look into the role of RSK phosphorylation, the previously described RSK1/2 phosphorylation sites within the suggested BIM_{EL} degron were mutated. As suggested by Dehan *et al.*, mutating these sites abrogated the interaction between BIM_{EL} and βTrCP. However, further examination of these phosphorylation sites revealed that all three residues lie around or within the ERK1/2 docking domain, with S94 (S90 in Rat) lying directly within this FSF domain (Ley *et al.*, 2005). As a consequence of this, mutating this site could disrupt the ability of ERK1/2 to interact with BIM_{EL}, and would thus prevent ERK1/2 from phosphorylating BIM_{EL}. As shown in multiple experiments, this would, by itself, prevent βTrCP from interacting with BIM_{EL} and this could provide an explanation as to why the loss of the putative RSK1/2 phosphorylation sites resulted in the inability of βTrCP to interact with BIM_{EL}. Indeed, mutating the three putative RSK1/2 phosphorylation sites resulted in a decrease in the phosphorylation of BIM_{EL} at the critical ERK1/2 phosphorylation site (S65 in Rat and S69 in Human); this was most apparent at intermediate or limiting levels of phosphorylated ERK1/2 imposed by low concentrations of a MEK1/2 inhibitor. Overall, it can be assumed that mutating the R1-3 sites is likely to reduce ERK1/2 docking and phosphorylation of BIM_{EL} and, as a consequence, will artificially reduce the interaction between BIM_{EL} and βTrCP. This could also imply that conclusions drawn using the R1-3 mutant (Dehan *et al.*, 2009) could be misleading and that the BIM_{EL}-βTrCP interaction is not lost due to the inability of RSK1/2 to phosphorylate BIM_{EL}.

Mutation of the putative RSK1/2 phosphorylation sites led to a reduction in the polyubiquitylation of BIM_{EL} to a similar level seen with loss of all ERK1/2 phosphorylation sites. Indeed, the observed reduction in the ability of ERK1/2 bind to and phosphorylate BIM_{EL} could explain the reduced polyubiquitylation of BIM_{EL}. However, it is also known that βTrCP binds to its substrate via

phosphorylated serine residues within their phosphodegron, where a crystal structure revealed that both the serine residues within the described phosphodegron are required to form hydrogen bonds and electrostatic interactions with the WD40 domains of βTrCP (Wu *et al.*, 2003). Therefore, a simpler explanation could be that mutating these residues will prevent βTrCP from binding to BIM_{EL} and therefore would reduce the polyubiquitylation of BIM_{EL} regardless of the kinase responsible for phosphorylating these residues.

As a consequence of reduced confidence in the phosphorylation site mutants of RSK1/2, the role of RSK activity in the regulation of BIM_{EL} was investigated using pharmacological inhibitors. Inhibition of RSK with three different inhibitors did not affect the turnover BIM_{EL}, despite loss of YB1 phosphorylation. Indeed, no evidence was found to support a role for RSK activity in the interaction between BIM_{EL} and βTrCP, and inhibition of RSK did not affect the polyubiquitylation of BIM_{EL}. As phosphorylation at the described BIM_{EL} degron is suggested to be prerequisite for βTrCP binding, an alternative Ser/Thr kinase downstream of ERK1/2 could be responsible for phosphorylating BIM_{EL} resulting in its reduced stability. Using PhosphoMotif databases, as well as examples of known βTrCP substrates, several kinases were predicted to be capable of phosphorylating BIM_{EL} within its degron at the suggested βTrCP binding motif, including GSK3 and CK1. These kinases have previously been shown to require prior 'priming' phosphorylation to phosphorylate their substrates enabling the binding of βTrCP. Unfortunately, inhibitors of GSK3 and CK1 did not yield any alteration in the phosphorylation or degradation of BIM_{EL}.

Interestingly, MSK1/2 shares a similar substrate specificity to RSK1/2, where its general substrate consensus has been suggested to be RXXpS/pT (Deak *et al.*, 1998). Indeed, both require phosphorylation by ERK1/2 for activation and function (Deak *et al.*, 1998). However, unlike RSK1/2, the majority of identified MSK1/2 substrates are nuclear (Arthur, 2008, Reyskens and Arthur, 2016). Interestingly, both RSK1/2 and MSK1/2 can phosphorylate the transcription factor CREB, however a lower K_m value was observed for MSK1 suggesting that despite both kinases being capable of phosphorylating CREB, MSK rather than RSK is responsible (Cargnello and Roux, 2011). This suggests that MSK1/2 could function, downstream of ERK1/2, as kinase for BIM_{EL} and phosphorylated BIM_{EL} within its described degron.

To identify additional kinases required to phosphorylate BIM_{EL} within its degron, a less targeted, more global approach may be required, treating HR1 cells with broad spectrum inhibitors at high concentrations to look for changes in the degradation of BIM_{EL}, alterations in its interaction with βTrCP and reduction in the polyubiquitylation of BIM_{EL}.

Alternatively ERK1/2 may act alone to promote the binding of BIM_{EL} to βTrCP, despite the inability of ERK1/2 to phosphorylate the given serine residues within the βTrCP binding motif. Interestingly, Kanemori and colleagues have described a non-phosphorylated motif, DDGϕXD, where ϕ represents a hydrophobic amino acid, for βTrCP binding in Xenopus Cdc25A; this was also found to act as a functional binding site for βTrCP in humans (Kanemori *et al.*, 2005). Despite BIM_{EL} not containing the described sequence it does present the possibility that βTrCP could interact with BIM_{EL} independently of phosphorylation at the conventional degron and solely rely upon ERK1/2 activity for interaction with βTrCP and degradation. Under these conditions the role of ERK1/2 phosphorylation could be to drive the dissociation of BIM_{EL} from the pro-survival proteins, MCL1 and BCL-X_L, previously demonstrated by Ewings *et al.*, rather than to provide a platform for βTrCP binding. This idea was further supported by the observation that phosphorylation of S69 is not only required for the degradation of BIM_{EL} but is prerequisite for the dissociation of BIM_{EL} from pro-survival proteins (Ewings *et al.*, 2007, Ley *et al.*, 2004, Luciano *et al.*, 2003). Here dissociation from MCL1 and BCL-X_L could unmask the binding site for βTrCP, enabling βTrCP to interact with BIM_{EL} resulting in its polyubiquitylation and degradation. In keeping with findings presented in this chapter, Ewings and colleagues went on to show that mutating the BH3 domain of BIM_{EL}, thus preventing BIM_{EL} from interacting with MCL1 and BCL-X_L, resulted in accelerated turnover of BIM_{EL} (Ewings *et al.*, 2007). Thus, indicating that dissociation from pro-survival proteins is sufficient to promote the degradation of BIM_{EL}, perhaps by revealing an E3 ligase binding site.

Interestingly, in accordance with that previously shown by Wiggins *et al.*, targeted knockdown of βTrCP did not affect the polyubiquitylation and turnover of BIM_{EL} (Wiggins *et al.*, 2011). This suggests that there could be a redundancy in the E3 ligase responsible for the polyubiquitylation of BIM_{EL}. Validated βTrCP siRNA used in these experiments specifically targets βTrCP1, therefore the lack of reduction in the polyubiquitylation of BIM_{EL} could be as a consequence of βTrCP2 binding to and targeting BIM_{EL} for polyubiquitylation. In the literature there are conflicting opinions with regards to the redundancy of these two paralogs. Some studies identified that both paralogs can perform the same function, and that loss of both is required to supress down modulation of a protein (Butticaz *et al.*, 2007), whilst others have identified unique roles for βTrCP2 suggesting that they are functionally different (Nakagawa *et al.*, 2015). Dehan *et al.* did not look into the functional redundancy of these two proteins in the context polyubiquitylation of BIM_{EL}, they only demonstrated that BIM_{EL} interacts, *in vitro* with FLAG-tagged βTrCP2 (Dehan *et al.*, 2009).

An additional theory could be that an alternative F-box protein, in complex with SCF, could interact with BIM_{EL}, driving its polyubiquitylation in the absence of βTrCP. Indeed, this has been shown by Vinas-Castells *et al.* where, under conditions were SNAIL1 is unable to bind βTrCP, it is still

polyubiquitylated and degraded (Vinas-Castells *et al.*, 2010). Under these conditions the F-box protein FBXl14 interacts with SNAIL1 (SNAIL/SNAI1) regulating its degradation. However, Wiggins *et al.* demonstrated that targeted knockdown of Cul1, a key component of the larger SCF complex, and overexpression of interfering mutants of Cul1 or interfering mutants of Ubc12, a protein required for the conjugation of NEDD8 to all cullin proteins, did not alter the turnover of BIM_{EL} (Wiggins *et al.*, 2011). They went on to suggest that an alternative E3 ligase is responsible for the polyubiquitylation of BIM_{EL}, when $SCF^{\beta TrCP1/2}$ is unable to do so. An example of E3 ligase redundancy is shown in the regulation of the substrates of Hsp70 and Hsp90. Under 'normal' conditions CHIP, an RING E3 ligase, is responsible for the regulation of Hsp70/Hsp90 substrates (Morishima *et al.*, 2008). However, in mouse embryonic fibroblasts (MEFs) lacking CHIP, neuronal nitric oxide (nNOS), an established CHIP substrate, is still ubiquitylated. Further examination revealed that the RBR E3 ligase Parkin was able to modify nNOS, establishing a redundancy of CHIP in these cells. Not only this, it suggests that two types of ubiquitin ligases were able to act on the same substrate. Therefore, it presents the possibility that BIM_{EL} could be regulated by multiples families of E3 ligases. Given that BIM is one of the most potent BOPs it perhaps makes sense to have redundant mechanisms to ensure its degradation.

3.3.2. Overexpression of USP27x resulted in the reduction in the polyubiquitylation of BIM_{EL}.

Initial attempts, to identify a DUB for BIM_{EL}, using a candidate approach, were unsuccessful. Despite USP30, USP8 and USP15 being located within or having the ability to translocate to the mitochondria overexpression of these DUBs did not reduce the polyubiquitylation of BIM_{EL}. Whilst investigating the DUB for BIM_{EL}, Weber and colleagues demonstrated that USP27x was capable of interacting with BIM_{EL}, thereby reducing its polyubiquitylation and increasing its stability (Weber *et al.*, 2016).

The interaction between a DUB and its substrate is transient and/or weak, and therefore, despite multiple attempts and overexpression of proteins, this could be the underlying reason why the described interaction between BIM_{EL} and USP27x was not observed. As previously described, overexpression of catalytically active USP27x resulted in the reduction in the polyubiquitylation of BIM_{EL}. Interestingly overexpression of catalytically inactive USP27x resulted in the accumulation of polyubiquitylated BIM_{EL}. McCullough *et al.* have previously demonstrated that the catalytically inactive mutant of the DUB AMSH induced the accumulation of the ubiquitylated form of its substrate STAM (McCullough *et al.*, 2004) One explanation for the observed increase in polyubiquitylated BIM_{EL} is that catalytically inactive USP27x exerts a dominant negative effect on BIM_{EL}. Thus, the interaction of catalytically inactive USP27x with BIM_{EL} would prevent endogenous USP27x from interacting with BIM_{EL}, thereby protecting polyubiquitylated BIM_{EL}. This is analogous to catalytically inactive mutants

of tyrosine phosphatases (Flint *et al.*, 1997) in that catalytically inactive USP27x would displace endogenous USP27x that would share the same binding site on BIM_{EL}. Several DUBs have also been shown to interact with E3 ligases, indeed, Weber *et al.* indicated that βTrCP forms a complex with USP27x and BIM_{EL} (Weber *et al.*, 2016). Therefore, one could speculate that USP27x could recruit βTrCP, to polyubiquitylated BIM_{EL}, aiding its ubiquitylation and that this ubiquitylated form of BIM_{EL} is stabilised by catalytically inactive USP27x.

As with the E3 ligase for BIM_{EL}, the DUB for BIM_{EL} would play a vital role in the regulation of a key apoptotic protein and as BIM has been shown to induce tumour cell death, in response to targeted treatment, information regarding the DUB for BIM_{EL} may play a role in oncogene-targeted cancer therapies. Despite a reduction in the polyubiquitylation of BIM_{EL}, following overexpression of USP27x, it is possible that USP27x is not the only DUB for BIM_{EL}. Indeed multiple DUBs have been found to regulate the same cellular process, suggesting a level of redundancy in the DUB protein families (Vlasschaert *et al.*, 2017). Functional redundancy is likely related to their sequence homology. Indeed, USP4, USP15 and USP11 are known paralogous DUBs in that they are related by duplication within the genome and have been shown to play redundant roles based on their substrates and interacting partners, including TGFBR1 and SMAD7 (Vlasschaert *et al.*, 2015). An alternative example is that numerous DUBs have been found to target histones, with BAP1 and USP16 both deubiquitylating H2A-Ub, under different DNA damaging conditions (Joo *et al.*, 2007, Sahtoe *et al.*, 2016).

In summary, using pharmacological inhibitors, the data presented in this chapter has established that RSK is not required for the regulation of the BIM_{EL}. Thus suggesting that an alternative kinase or indeed ERK1/2 alone is sufficient to drive the degradation of BIM_{EL}. Additionally data here has suggested that there is a redundancy in the E3 ligase and DUB for BIM_{EL}, thus emphasising the importance for the regulation of this potent pro-apoptotic protein.

Chapter 4: Investigating the potential for combining USP30 inhibitors and the BH3 mimetic, ABT-263, to drive apoptosis

4. Chapter 4

4.1. Introduction

Mitochondria are highly dynamic organelles that play an essential role in cellular energy production, metabolism and cell death (Nunnari and Suomalainen, 2012). Ubiquitylation of key mitochondrial proteins is required for the maintenance of mitochondrial morphology and for the maintenance of a healthy mitochondrial network (Chan, 2012). Damaged or dysfunctional mitochondria are degraded by mitophagy, a discrete form of autophagy, regulated by the concerted action of PINK1, a ubiquitin kinase, Parkin, an E3 ligase, and the DUB, USP30 (Bingol *et al.*, 2014, Cunningham *et al.*, 2015, Kane *et al.*, 2014, Kazlauskaite *et al.*, 2014, Kondapalli *et al.*, 2012, Koyano *et al.*, 2014, Narendra *et al.*, 2008, Narendra and Youle, 2011, Sarraf *et al.*, 2013, Vives-Bauza *et al.*, 2010, Wauer *et al.*, 2015b). Mutation of both the PINK1 and Parkin genes, and therefore mitochondrial dysfunction, is associated with early-onset recessive Parkinson's disease, a neurodegenerative disorder characterised by a loss of dopaminergic neurons in the substantia nigra (Corti *et al.*, 2011, Hauser and Hastings, 2013, Kitada *et al.*, 1998, Valente *et al.*, 2004). Here, mutation of PINK1 or Parkin results in impaired Parkin recruitment, ubiquitylation of mitochondria targets and/or mitophagy. This could account for the synaptic dysfunction, associated with reduction in dopamine release and synaptic plasticity, observed in Parkinson's disease (Gispert *et al.*, 2009, Goldberg *et al.*, 2003, Matsuda *et al.*, 2010, Narendra and Youle, 2011, Rakovic *et al.*, 2011, Reeve *et al.*, 2018, Vives-Bauza *et al.*, 2010, Winklhofer and Haass, 2010).

Indeed, promoting mitophagy could provide a therapeutic basis for the treatment of Parkinson's disease. Inhibition of USP30 provides a novel means for improving the rate of mitophagy, due to the removal of an enzymatic activity that opposes Parkin-mediated mitophagy, resulting in an increase in the lysosomal clearance of dysfunctional mitochondria. Thus, USP30 has become an attractive target for the treatment of diseases driven by the accumulation of defective mitochondria.

Several MEK1/2 inhibitors have been approved for the treatment of cancer cells harbouring mutations within BRAF and KRas oncogenes. The use of MEK1/2 inhibitors typically results in the rapid emergence of acquired resistance and disease progression (Little *et al.*, 2011). Despite an increase in the expression of pro-apoptotic proteins, including BIM, tumour cells typically exhibit a G1 cell cycle arrest providing an opportunity for cells to develop acquired resistance (Sale and Cook, 2013). Combination therapies have shown promising results in transforming the observed cytostatic response into a cytotoxic response. An example is the synergistic combination of the MEK1/2 inhibitor, selumetinib, and BH3 mimetics, including ABT-263, leading to the induction of a BAK/BAX-dependent cell death

response (Sale and Cook, 2013). BAK/BAX-dependent apoptosis or mitochondrion-mediated apoptotic cell death is regulated by pro-apoptotic and pro-survival BCL2 proteins. Oligomerisation of the activated pro-apoptotic effector proteins BAK and BAX within the OMM generates a pore allowing for the release of apoptotic factors, notably cytochrome c, ultimately initiating a series of events leading to caspase-dependent cell death (Adams and Cory, 2007, Tait, 2010). BH3 mimetics act to initiate the described apoptotic response by mimicking pro-apoptotic BH3-only proteins and inserting their BH3 domain into the corresponding groove of pro-survival BCL2 protein, releasing pro-apoptotic factors to drive the activation of BAK and BAX resulting in apoptosis (Baell and Huang, 2002, Lessene *et al.*, 2008).

A recent study proposed that knocking down the mitochondrial-associated DUB, USP30, sensitises cancer cells to BH3 mimetics, where this combination resulted in the induction of BAK/BAX-dependent cell death. This suggested an anti-apoptotic role for USP30, making it a potential target in combinatorial anti-cancer therapies (Liang *et al.*, 2015).

Dodecapeptides and aptamers have previously been described as inhibitors of USP30 (Bingol, Corn and Zhang 2014, Yue *et al.*, 2014). As well as this, 15-oxospiramilactone (S3) is in preclinical trials as a USP30 inhibitor in the treatment for neurodegenerative diseases (Harrigan *et al.*, 2017, Yue *et al.*, 2014). Administration of S3 in cells lacking one of the key mitochondrial fusion proteins (MFN1-/- and MFN2-/- MEFs) significantly increased the percentage of cells containing elongated mitochondria, suggesting S3 has the potential to restore mitochondrial function to cells defective in mitochondrial fusion (Yue *et al.*, 2014). Kluge and colleagues have recently compared two structurally similar USP30 compounds, MF-094 and MF-095, as a means of assessing the implications of selective USP30 inhibition (Kluge *et al.*, 2018). The compounds developed by Kluge and colleagues were based on racemic phenylalanine derivatives found to inhibit USP30 through a high-throughput screen. Inhibition of USP30, using the more selective and potent compound, MF-094, resulted in an increased rate of mitophagy, when compared to treatment with MF-095 the less potent USP30 inhibitor (Kluge *et al.*, 2018).

Mission Therapeutics have also published several patents detailing USP30 inhibitors in-development for the treatment of mitochondrial disorders including Parkinson's disease (Jones *et al.*, 2016, Kemp and Jones, 2017). Here, in collaboration with Mission Therapeutics, KRas G13D mutant HCT116 cells were treated with novel USP30 inhibitors, MTX32 and MTX48, and the BH3 mimetic ABT-263 to investigate whether these agents could combine to drive apoptosis.

4.2. Results

4.2.1. MTX32 rapidly enters cells and inhibits USP30.

The use of a USP30 inhibitor required an appropriate cell based assay to confirm that USP30 was successfully inhibited. Activity-based probes (ABPs) mimic their substrate, covalently interacting with the active site of the enzyme in an enzyme-catalysed reaction. To this end, ubiquitin-based activity probes have aided in the discovery of novel DUBs and also in the development of DUB inhibitors, due to their ability to monitor the potency and selectivity of a given inhibitor (Balakirev *et al.*, 2003, Borodovsky *et al.*, 2001, Borodovsky *et al.*, 2002, Kramer *et al.*, 2012, McGouran *et al.*, 2012, Niphakis and Cravatt, 2014). The HA-tagged UbVME probe, HA-Ahx-Ahx-Ub-VME, possesses a C-terminal VME warhead designed to react with the active site cysteine present in the majority of DUBs, including the USP and UCH DUB families (Borodovsky *et al.*, 2002). A schematic of this is shown in Figure 4.1A. Specifically, the UbVME ABP can be an effective tool for confirming and profiling target engagement of DUB inhibitors (Figure 4.1B) and has been shown to target a wide range of DUBs with very little cross-reactivity to other proteases (Altun *et al.*, 2011, Ward *et al.*, 2016).

To test the ability of the HA-UbVME probe to interact irreversibly with USP30, in our chosen lysis conditions, HCT116 cells were treated post-lysis with the ABP and fractionated by SDS-PAGE gel electrophoresis. Addition of the probe resulted in a visible band shift in USP30, as well as two other highly expressed DUBs, USP5 and UCHL3, in HCT116 cells, indicative of a DUB-probe interaction (Figure 4.1C).

Target engagement of the USP30 inhibitor, MTX32, was analysed using the UbVME probe. MTX32 rapidly entered HCT116 cells and inhibited USP30. ~10 minutes post-treatment with MTX32, USP30 was maximally inhibited, as indicated by the shift of the 'active' USP30 band to a lower molecular weight. Inhibition of USP30 was maintained throughout the 48 hr time course. However, at longer time points, the abundance of 'probed' USP30 decreased whilst unprobed USP30 protein levels remained constant, suggesting probed USP30 was being degraded (Figure 4.2). To investigate the specificity of MTX32 in HCT116 cells, probed lysates were also interrogated for the inhibition of two alternative DUBs, USP5 and UCHL3, chosen based on their molecular weight, their endogenous protein levels in HCT116 cells as well as their known ability to interact with the UbVME probe.

Figure 4.1 Competitive ubiquitin probe labelling for DUB inhibitor profiling.

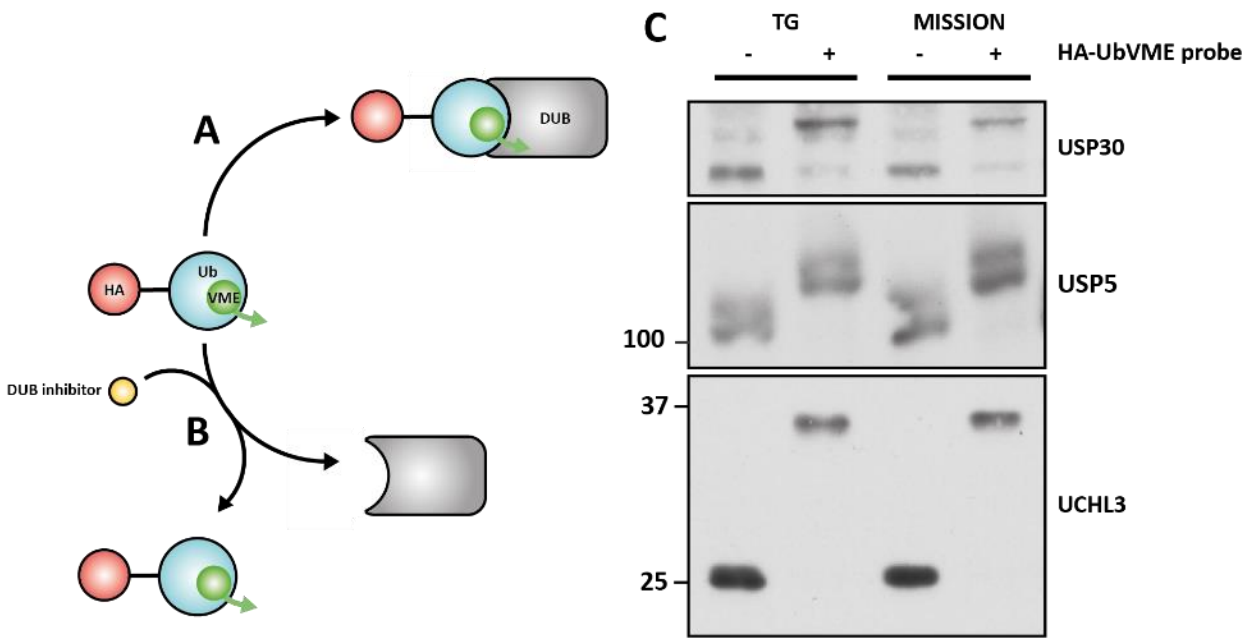

Figure 4.1 Competitive ubiquitin probe labelling for DUB inhibitor profiling. (A) Ub-based probe reacts with the active-site cysteine residue present in several families of active DUBs. Within the ABP, ubiquitin is targeted to the S1 pocket. The C-terminal G76 of ubiquitin is chemically modified with an electrophilic warhead VME, designed to irreversibly reactive with the active site cysteine. Whilst the N-terminal HA tag allows for target engagement analysis using affinity tag pulldown and detection by western blot. **(B)** Addition of a DUB inhibitor capable of occupying/altering the structure of the active site of a DUB results in the inability of the UbVME ABP to interact with the DUB. Allowing for analysis of inhibitor specificity. **(C)** SDS-PAGE anaylsis of the ability of the UbVME probe to interact with chosen DUBs in the given lysis buffer, TG or MISSION lysis buffers, see Materials and Methods. Post-lysis 0.5 µg of HA-UbVME probe was incubated with 20 µg of lysate for one hour at room temperature. Probed lysates were fractionated by SDS-PAGE and subjected to western blotting with the antibodies indicated in the figure. This data is representative of a single experiment.

Figure 4.2 Rapid inhibition of USP30 and UCHL3 by MTX32

.

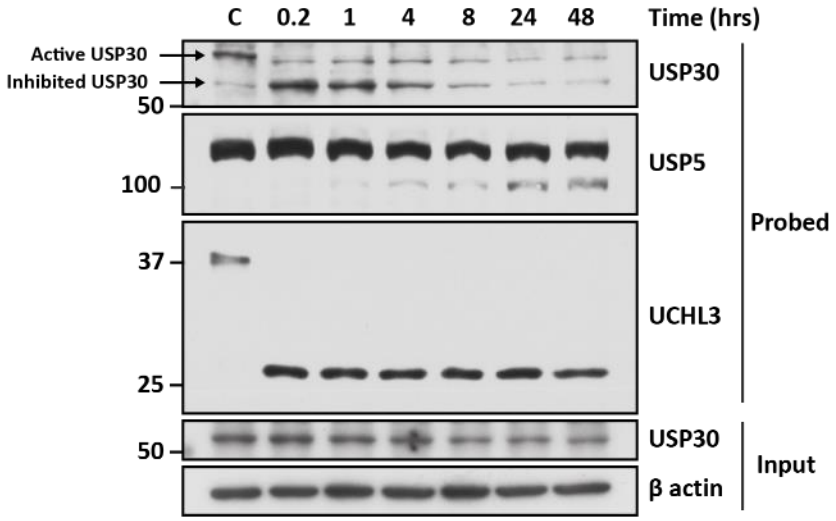

Figure 4.2 Rapid inhibition of USP30 and UCHL3 by MTX32. HCT116 cells were treated with DMSO (C) or 10 μM of MTX32 for increasing lengths of time. All samples were lysed at the same time and 20 μg of lysates was treated with 0.5 μg of HA-Ub-VME probe for one hour at room temperature. Whole cell lysates and probed lysates were fractionated by SDS-PAGE and subjected to western blotting with select antibodies. Arrows indicate bands representing active and inhibited USP30. A non-specific band is present, at a molecular weight between that of the active and inhibited USP30, which is not always present in all SDS-PAGE gels run. This data is representative of one experiment, of which at least two have been performed giving similar results.

MTX32 treatment rapidly inhibited UCHL3 and partially inhibited USP5, at longer time-points, suggesting that MTX32, at this chosen concentration, inhibits additional DUBs (Figure 4.2).

4.2.2. Combining MTX32 and ABT-263 treatment induces cell death in KRas mutant HCT116 cells.

MTX32 inhibited USP30 in a dose-dependent manner with maximal inhibition of USP30 at 10 μM (Figure 4.3A). MTX32 inhibited UCHL3 over a similar concentration range to USP30, but higher concentrations of MTX32 were required to inhibit USP5 (50 μM) (Figure 4.3A).

MTX32 and the BH3 mimetic, ABT-263, combined to induce cell death (Figure 4.3B and Figure 4.3C). The control of DMSO, as well as single inhibitor treatments showed minimal increase in the percentage of cells with sub-G1 DNA. However, combining the two inhibitors led to a significant increase in cell death (Figure 4.3C). The observed synergistic increase in cell death was only apparent over a narrow concentration range, with the greatest synergy observed at 10 μM MTX32 (Figure 4.3B). At this concentration MTX32 as a single agent resulted in ~10% of cells with sub-G1 DNA, which was increased to ~30% following introduction of 1 μM ABT-263. Western blot analysis confirmed that ABT-263 had no effect on the ability of MTX32 to inhibit USP30 (Figure 4.3A).

4.2.3. MTX32 and ABT-263 combine to induce BAX-dependent apoptosis.

Caspase inhibition using the pantropic caspase inhibitor Q-VD-OPh abolished the cell death response previously seen in Figure 4.3B and Figure 4.3C, demonstrating that MTX32 and ABT-263 combine to induce a caspase-dependent cell death (Figure 4.4A). Compared to the combination of MTX32 and ABT-263, the addition of Q-VD-OPh reduced cleaved PARP confirming a reduction in the cell death response following caspase inhibition. Western blot analysis confirmed that the addition of Q-VD-OPh and ABT-263 did not interfere with the inhibition of USP30 (Figure 4.4B).

To further investigate the mechanism by which MTX32 and ABT-263 induced caspase-dependent cell death, genetically engineered isogenic HCT116 cells lacking the effector pro-apoptotic proteins BAK, BAX or BAK/BAX were utilised (Figure 4.4C). HCT116 cells lacking BAK showed no defect in the apoptotic response to MTX32, ABT-263 or the combination. In contrast, HCT116 cells lacking BAX, and BAK-/- BAX-/- HCT116 cells, showed a significant reduction in the percentage of cells with sub-G1 DNA and were, as a consequence, resistant to cell death (Figure 4.4D), demonstrating that MTX32 and ABT-263 combined to induce BAX-dependent apoptosis. Similar to that shown in Figure 4.4B, knockout of BAX-/- did not interfere with the inhibition of USP30 following treatment with MTX32 (Figure 4.4E).

Figure 4.3 MTX32 and ABT-263 combine synergistically to induce cell death in HCT116 cells.

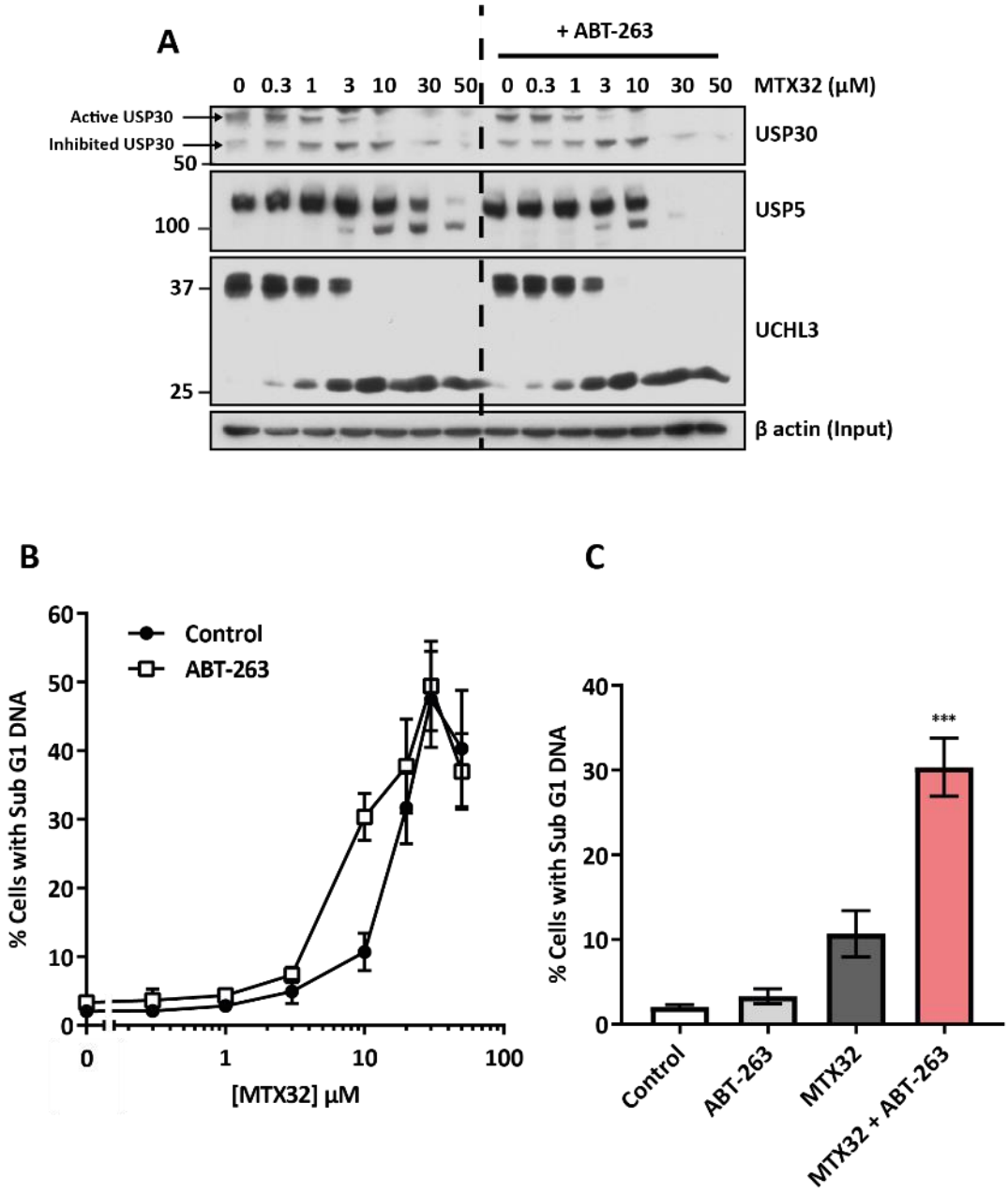

Figure 4.3 MTX32 and ABT-263 combine synergistically to induce cell death in HCT116 cells. (A + B) HCT116 cells were treated with increasing concentrations of MTX32 with or without 1μM ABT-263 for 48 hours. **(A)** Cells were lysed and post-lysis 0.5 μg of UbVME probe was added to 20 μg of lysate for one hour at room temperature. Probed lysates were fractionated by SDS-PAGE and subjected to western blotting with the antibodies indicated in the figure. Arrows indicate bands representing active and inhibited USP30. This data is representative of one experiment, of which at least two have been performed giving similar results. **(B)** Cells were fixed and stained with propidium iodide and cell death (sub-G1 DNA) determined by flow cytometry. Results shown here are representative of the mean ± SD of three independent experiments, where each biological replicate is performed in technical triplicate. **(C)** HCT116 cells were treated with DMSO (Control), 1 μM ABT-263, 10 μM MTX32 and the combination of 10 μM MTX32 and 1 μM ABT-263 for 48 hours. Cells were fixed, stained with propidium iodide and the sub-G1 fraction determined by flow cytometry. Results shown here are representative of the mean ± SD of three independent experiments, where each biological replicate is performed in technical triplicate. $P < 0.0001$ (***) for MTX32 + ABT versus all other groups determined by one-way ANOVA with Tukey test.

Figure 4.4 MTX32 and ABT-263 combine synergistically to induce BAX-dependent apoptosis in HCT116 cells.

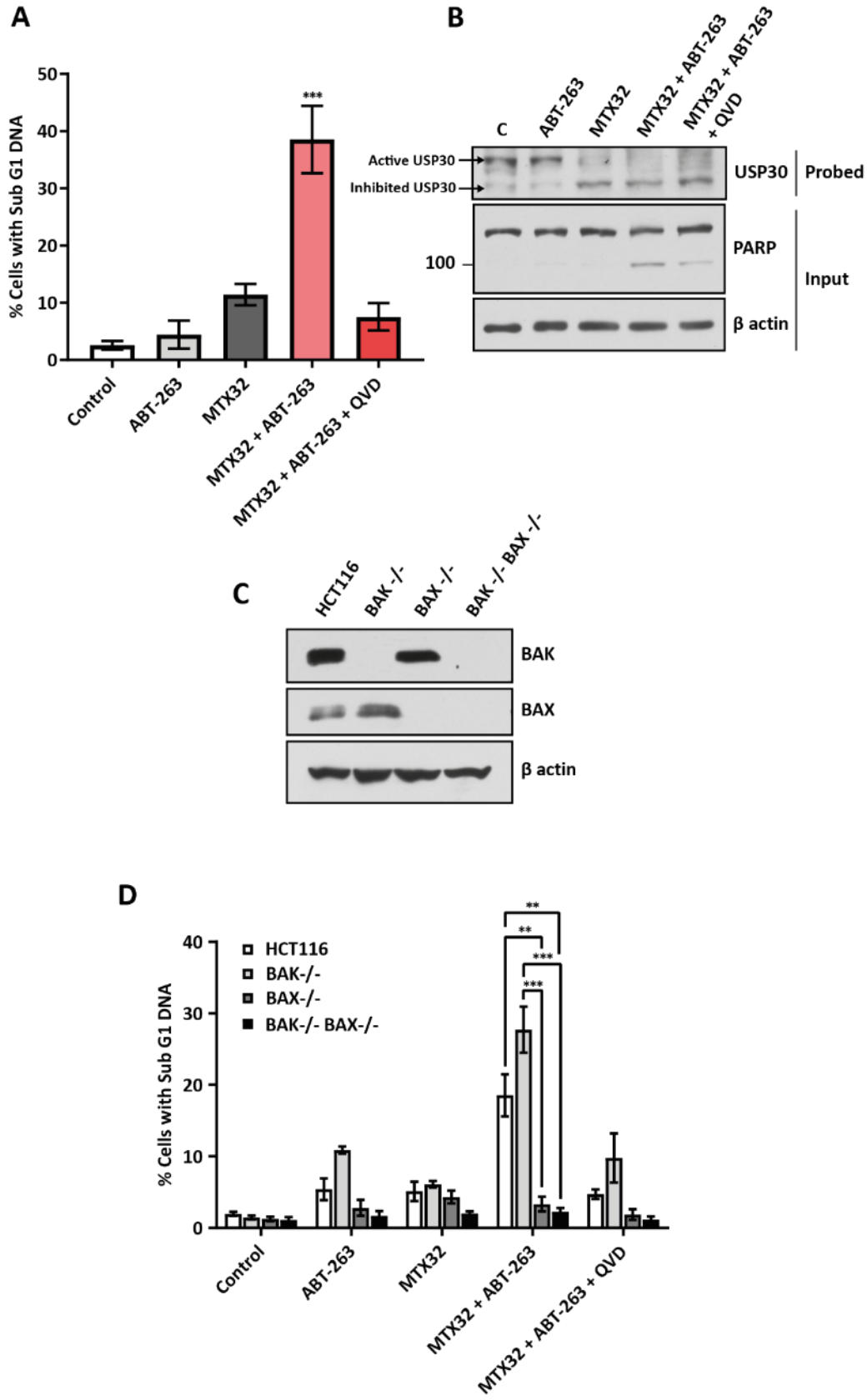

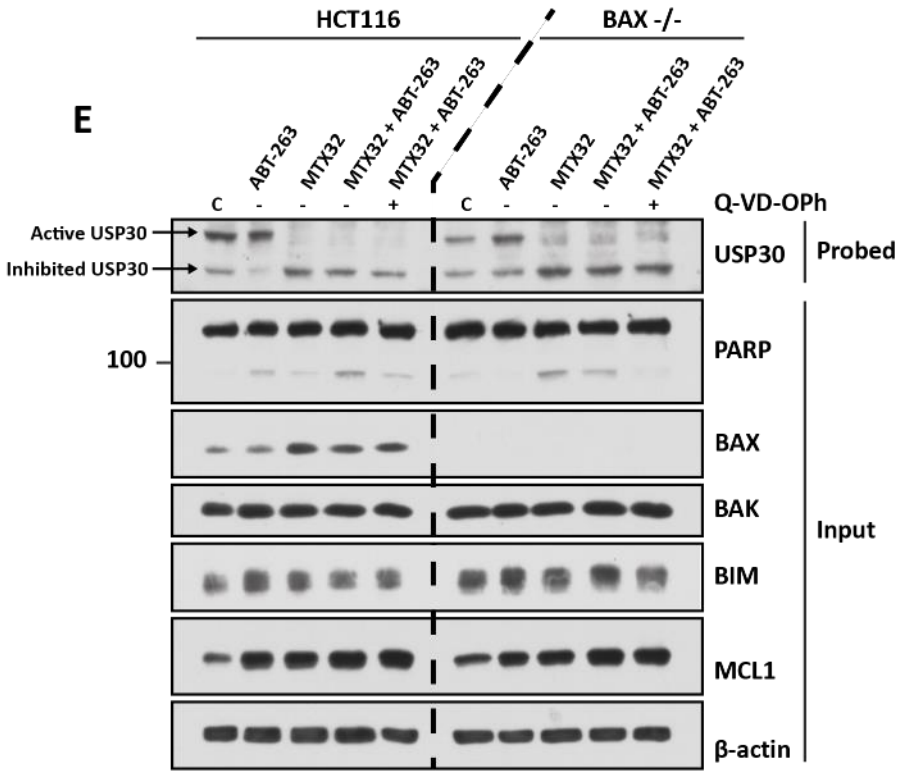

Figure 4.4 MTX32 and ABT-263 combine synergistically to induce BAX-dependent apoptosis in HCT116 cells. (A + B) HCT116 cells were treated with of DMSO control (C), 1 µM ABT-263, 10 µM MTX32 or the combination with or without 10 µM Q-VD-OPh for 48 hours. **(A)** Cells were fixed, stained with propidium iodide and cell death anaylsed by flow cytometry. Results representative of the mean ± SD of three independent experiments, where each biological replicate is performed in technical triplicate. $P < 0.0001$ (***) for MTX32 + ABT-263 versus all other groups determined by one-way ANOVA with Tukey test. **(B)** Cells were lysed and post-lysis 0.5 µg of UbVME probe was added to 20 µg of lysate, the remaining lysate was used as an input. Lysates were interograted by SDS-PAGE and immunoblotting using the described antibodies. Arrows indicate bands representing active and inhibited USP30. This data is representative of one experiment, of which at least two have been performed giving similar results. **(C)** HCT116 and genetically engineered isogenic BAK-/-, BAK-/- and BAK-/- BAX-/- cell lines were lysed and fractionated by SDS-PAGE and subjected to western blotting with the antibodies indicated in the figure. This data is representative of a single experiment. **(D)** HCT116, HCT116 BAK -/-, HCT116 BAX -/- and HCT116 BAK-/- BAX-/- cells were treated with DMSO (Control), 1 µM ABT-263, 10 µM MTX32, a combination of the two with or without 10 µM Q-VD-OPh for 48 hours. Cells fixed, stained with propidium iodide and cell death analysed by flow cytometry. Results representative of the mean ± SD of three independent experiments, where each biological replicate is performed in technical triplicate. $P < 0.001$ (**) or $P < 0.0001$ (***) for BAX -/- or BAK -/- BAX -/- versus HCT116 or BAK -/- within the MTX32 + ABT-263 treament group, determined by one-way ANOVA with Tukey test. **(E)** HCT116 and HCT116 BAX -/- cells were treated wiht DMSO (Control), 1 µM ABT-263, 10 µM MTX32, a combination of the two with or without 10 µM Q-VD-OPh for 48 hours. Cells were lysed and post-lysis 0.5 µg of UbVME probe was added to 20 µg of lysate, the remaining lysate was used as an input. Lysates were fractionated by SDS-PAGE and subjected to western blotting with the described antibodies. Arrows indicate bands representing active and inhibited USP30. This data is representative of one experiment, of which at least two have been performed giving similar results.

In accordance with others, treatment with ABT-263 resulted in an increase in MCL1 protein levels, most likely due to the enhanced protein stability of the MCL1 driven by phosphorylation of MCL1 by ERK and JNK, and Akt-mediated inhibition of GSK3β (Wang *et al.*, 2014). Elevated MCL1 protein levels were maintained in all conditions tested. Compared to control and single treatment ABT-263 samples, treatment with MTX32 with or without ABT-263 and Q-VD-OPh resulted in an increase in BAX expression (Figure 4.4E).

4.2.4. RNAi-mediated knockdown of USP30, in combination with ABT-263, does not yield a consistent increase in cell death.

To confirm if the genetic ablation of USP30 phenocopies the synergy observed between USP30 inhibition, with MTX32, and ABT-263, siRNA knockdown of USP30 was combined with 1 µM of ABT-263 (Figure 4.5A and Figure 4.5B). Treatment of HCT116 cells with MTX32, in combination with ABT-263, led to an increase in PARP cleavage and a corresponding increase in the percentage of cells with sub-G1 DNA (Figure 4.5B and Figure 4.5C). In accordance with published data, USP30 knockdown led to an increase in PARP cleavage, which was not due to transfection as shown from the non-targeting control (siLUC). However, knockdown of USP30, with all four siRNA, led to minimal cell death, which, when compared to the synergy observed with MTX32 and ABT-263, did not yield a significant, consistent increase in cell death (Figure 4.5C). This suggests that the synergy previously observed between MTX32 and ABT-263 could be due to off-target effects of MTX32.

4.2.5. MTX48 is a more selective inhibitor than MTX32.

HCT116 cells were treated with a related derivative of MTX32, MTX48, to test its ability to selectively inhibit USP30 and combine with ABT-263 to induce a cell death response (Figure 4.6. and Figure 4.7.). Increasing concentrations of MTX48 were added to HCT116 cells and treated, post-lysis, with the HA-UbVME probe. MTX48 maximally inhibited USP30 at 3 µM, initially indicating an increased potency of MTX48, compared to MTX32. As seen with MTX32, MTX48 rapidly entered HCT116 cells and inhibited USP30 over a 48 hr time course (Figure 4.6A). However, unlike MTX32, MTX48 was unable to completely inhibit UCHL3 activity and did not affect the activity of USP5 (Figure 4.6A and Figure 4.6B). Maximal inhibition of UCHL3 was observed after 4 hrs of treatment; however, this inhibitory effect was not sustained and after 48 hrs UCHL3 was inhibited to a similar level seen after one hr of MTX48 treatment.

Figure 4.5 siRNA targeting USP30 did not combine with ABT-263 to induce an increase in cell death.

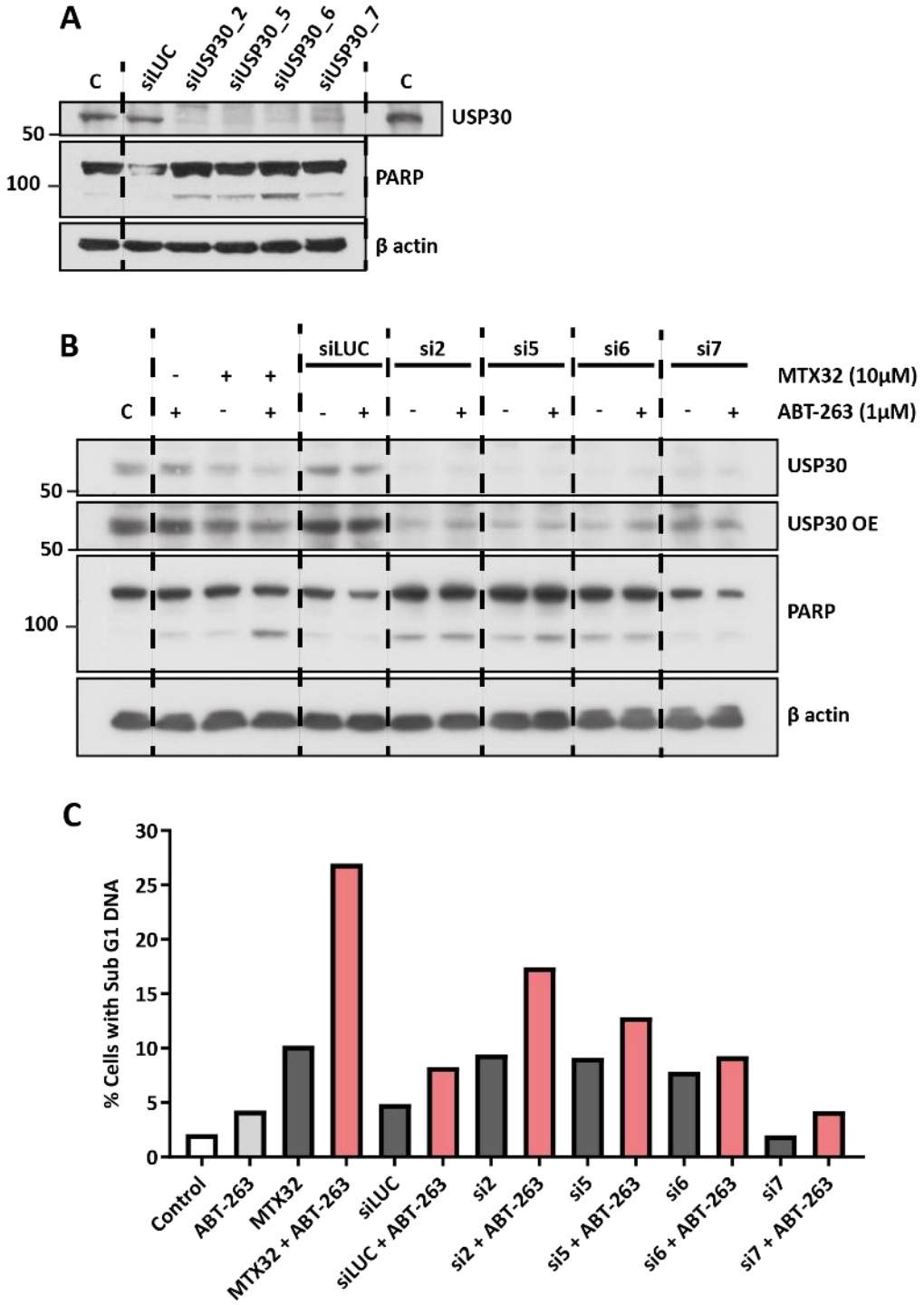

Figure 4.5 siRNA targeting USP30 did not combine with ABT-263 to induce an increase in cell death. (A) HCT116 cells were left untransfected (Control), transfected with siRNA targeting a non-human protein, luciferase (siLUC) or transfected with USP30 siRNA. 48 hours after transfection whole cell lysates wre prepared and western blotted with the indicated antibodies. This data is representative of a single experiment. **(B + C)** HCT116 cells were left untransfected/untreated (Control), treated with 1 μM ABT-263, with 10 μM MTX32, treated with a combination with 10 μM MTX32 and 1 μM ABT-263, transfected with siRNA targeting a non-human protein, luciferase (siLUC) or transfected with USP30 siRNA with or without 1 μM ABT-263. 48 hours after transfection whole cell lysates wre prepared and western blotted with the indicated antibodies **(B)** and cell death was determined by flow cytometry **(C)**. Results shown here are representative of a single experiment, where each biological replicate is performed in technical triplicate.

Figure 4.6 MTX48 rapidly inhibits USP30 from a concentration of 1 µM.

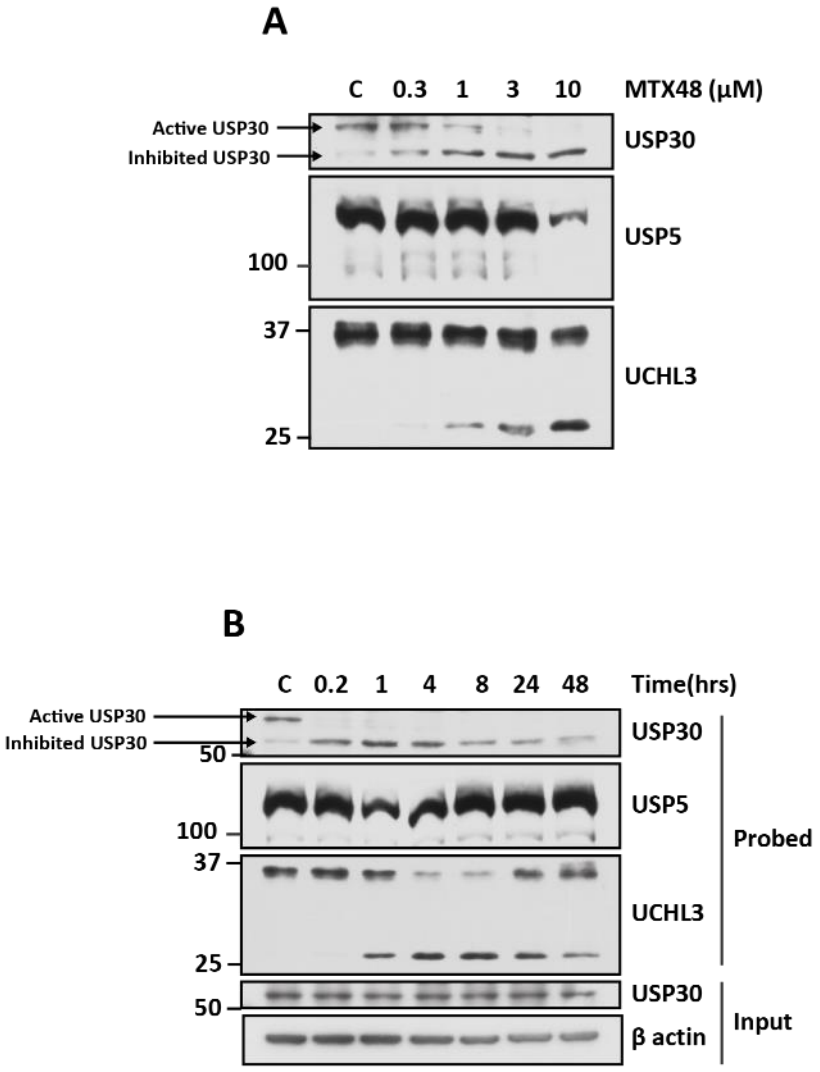

Figure 4.6 MTX48 rapidly inhibits USP30 from a concentration of 1 µM. (A) HCT116 cells were treated with DMSO (C) or increasing concentrations of MTX48 for 48 hours or **(B)** with DMSO (C) or 3 µM of MTX48 for increasing lengths of time. All samples were lysed at the same time and 20 µg of lysates was treated with 0.5 µg of HA-UbVME probe for one hour at room temperature. Whole cell lysates and probed lysates were fractionated by SDS-PAGE and subjected to western blotting with select antibodies. Arrows indicate bands representing active and inhibited USP30. This data is representative of one experiment, of which at least two have been performed giving similar results.

Combined treatment of MTX48 and ABT-263 did not result in a synergistic cell death (Figure 4.7). Despite inhibition of USP30 (Figure 4.7A), combining MTX48 and ABT-263 did not lead to an increase in the percentage of cells with sub-G1 DNA, compared to single drug treatment controls (Figure 4.7B), except at doses > 30 µM at which UCHL3 was inhibited. Comparing inhibition of MTX32 to MTX48 confirmed that the two USP30 inhibitors combined with ABT-263 to cause differing cell death responses. Whilst MTX32 combined with ABT-263 to promote cell death, MTX48 was unable to cause a similar response under any conditions tested (Figure 4.7C and Figure 4.7D).

To compare the selectivity of MTX32 and MTX48, HCT116 cells were treated with the USP30 inhibitors at increasing concentrations, lysed, probed with the ubiquitin activity-based probe, fractionated by SDS-PAGE electrophoresis and subjected to anti-HA immunoblotting. By interrogating lysates with an HA antibody, which will interact specifically with the N-terminus of the UbVME probe, a global view of the number of DUBs inhibited by MTX32 and MTX48 can be determined. The more selective the inhibitor, the fewer DUBs the inhibitor will bind to, and the more active DUBs the probe will irreversible interact with. Thus, a greater number of high molecular weight bands, representing active DUBs, will be present in the probed lysate HA blots. In contrast less selective inhibitors will have fewer representative active DUB bands in the probed lysates interrogated with the HA antibody (Schematic shown in Figure 4.8A). From Figure 4.8B, as the concentration of MTX32 was increased above 3 µM the number of HA reactive bands decreased, where the number of bands began to decrease at 3 µM of MTX32, specifically at ~37 KDa or above. At 30 µM MTX32 there were very few bands present indicating the non-specific binding of MTX32 to other active DUBs. In contrast, there are no obvious differences in the number of bands present in the HA blots of probed lysates from cells treated with increasing concentrations of MTX48. These results suggest that MTX48 is a much more selective DUB inhibitor than MTX32.

4.3. Discussion

4.3.1. Synergy between MTX32 and ABT-263 results in a BAX-dependent apoptotic response.

Results presented here indicate that MTX32 and ABT-263 combine synergistically to induce cell death (Figure 4.3). This confirms data previously shown by Liang *et al.*, using USP30 siRNA in combination with BH3 mimetics in U2-OS and MCF7 cells (Liang *et al.*, 2015).

BH3 mimetics prime tumour cells for apoptosis by targeting BCL2 pro-survival proteins, however they have been shown to have minimal effects as single agents. Thus, if inhibitors combine with BH3 mimetics to shift the balance from pro-survival towards pro-apoptotic BCL2 proteins, thereby

Figure 4.7 Despite inhibition of USP30, MTX48 does not combine with ABT-263 to induce cell death in HCT116 cells.

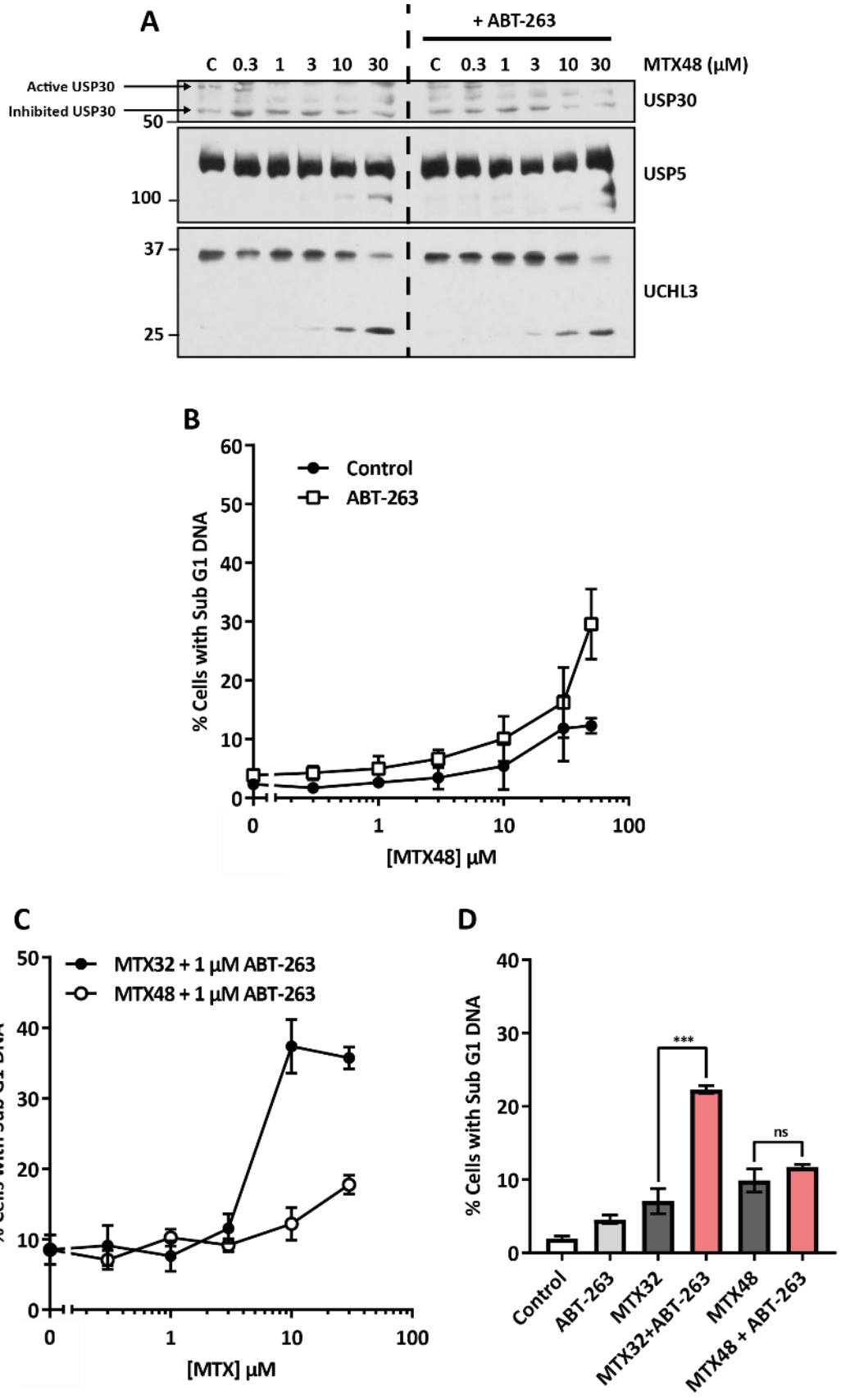

Figure 4.7 Despite inhibition of USP30, MTX48 does not combine with ABT-263 to induce cell death in HCT116 cells. (A + B) HCT116 cells were treated with increasing concentrations of MTX48 with or without 1μM ABT-263 for 48 hours. **(A)** Cells were lysed and post-lysis 0.5 μg of UbVME probe was added to 20 μg of lysate for one hour at room temperature. Probed lysates were fractionated by SDS-PAGE and subjected to western blotting with the antibodies indicated in the figure. Arrows indicate bands representing active and inhibited USP30. This data is representative of one experiment, of which at least two have been performed giving similar results. **(B)** Cells were fixed and stained with propidium iodide and cell death (sub-G1 DNA) determined by flow cytometry. Results shown here are representative of the mean ± SD of three independent experiments, where each biological replicate is performed in technical triplicate. **(C)** HCT116 cells were treated with increasing concentrations of MTX32 or increasing concentration of MTX48 with ABT-263 for 48 hours. Cells were fixed, stained with propidium iodide and the sub-G1 fraction determined by flow cytometry. Results shown here are representative of the mean ± SD of three independent experiments, where each biological replicate is performed in technical triplicate. **(D)** HCT116 cells were treated with DMSO (C), 1 μM ABT-263, 10μM MTX32/3 μM MXT48 with or without 1 μM ABT-263 for 48 hrs. Cells were fixed and stained with propidium iodide and cell death (sub-G1 DNA) determined by flow cytometry. Results shown here are representative of the mean ± SD of three independent experiments, where each biological replicate is performed in technical triplicate. $P < 0.0001$ (***) for MTX32 + ABT-263 versus MXT32 and ns for MTX48 + ABT-263 versus MTX48 determined by one-way ANOVA with Tukey test.

Figure 4.8 MTX48 is a more selective DUB inhibitor with fewer off-target effects at high concentrations.

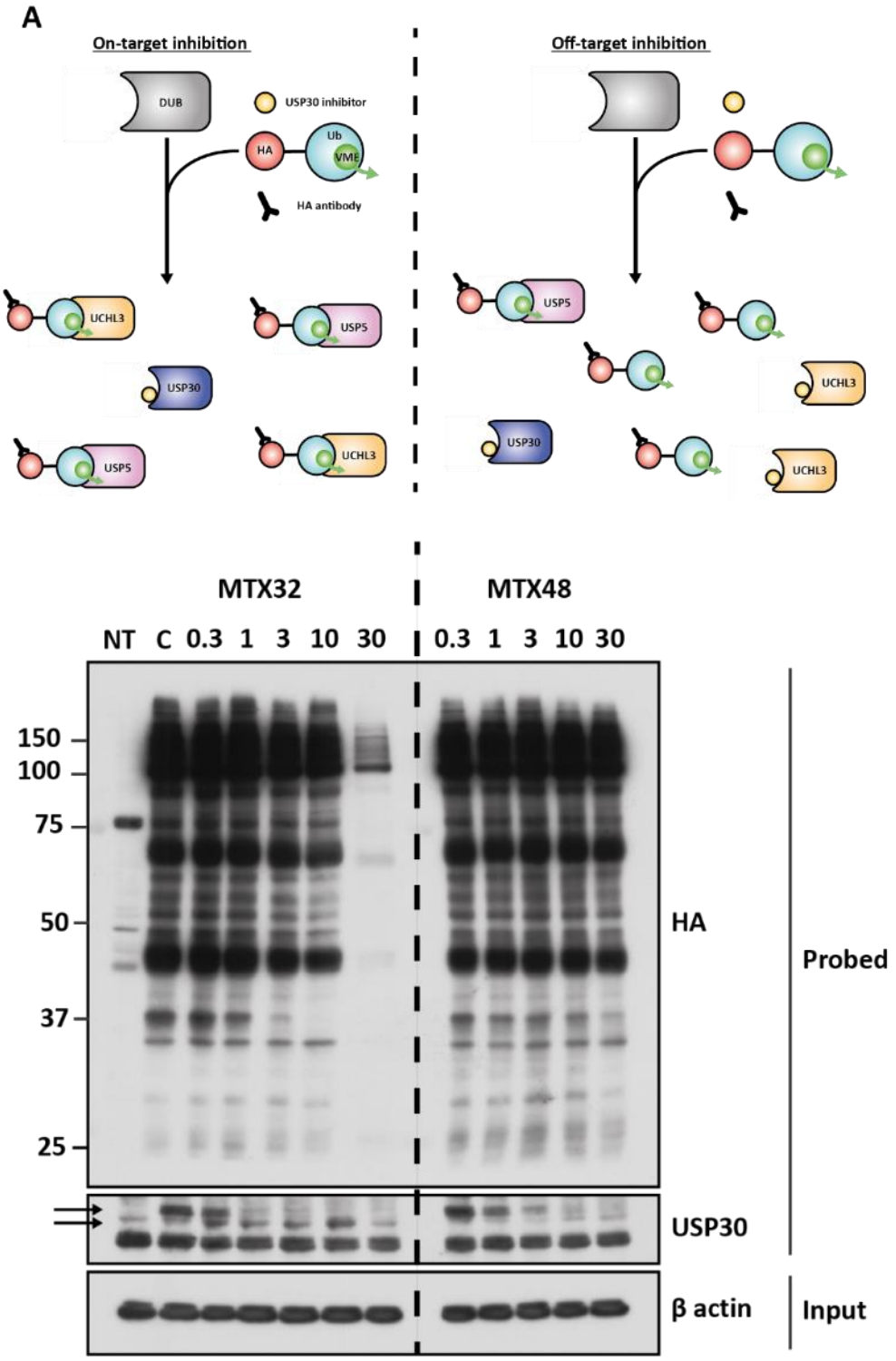

Figure 4.8 MTX48 is a more selective DUB inhibitor with fewer off-target effects at high concentrations. (A) A schematic representation of using the HA-UbVME as a means of analysing the specificity of chosen DUB inhibitors. **(B)** HCT116 cells were treated with DMSO (C) or increasing concentrations of MTX32 or MTX48 for 48 hours. 20 µg of lysates, except NT, was treated with 0.5 µg of HA-UbVME probe for one hour at room temperature. Whole cell lysates and probed lysates were fractionated by SDS-PAGE and subjected to western blotting with select antibodies. Arrows indicate bands representing active and inhibited USP30. This data is representative of one experiment, of which two have been performed giving similar results.

lowering the apoptotic threshold, a synergistic cell death response is observed. This effect has been extensively seen using a variety of inhibitors, including MEK1/2, ERK1/2 and BRAF inhibitors, in combination with BH3 mimetics, in several cell types (Corcoran *et al.*, 2013, Sale and Cook, 2013, Wroblewski *et al.*, 2013). More recently Faber and colleagues have investigated the effect of ABT-263 across >500 cancer cell lines, where they found in general that cell death was observed in cell lines that possessed high expression of the pro-apoptotic protein BIM and lower expression of pro-survival protein MCL1 (Faber *et al.*, 2015). This theory was realised in small-cell lung cancer cells, which require the addition of a mTORC1/2 inhibitor to reduce MCL1 expression, to sensitise cells to ABT-263. Further to this, cervical cancer cell lines, overexpressing MCL1, treated with a combination of an MCL1 inhibitor and the BH3 mimetic ABT-263, led to synergistic cell death response (Lian *et al.*, 2018).

In HCT116 cells, Sale and Cook observed that the underlying mechanism responsible for the synergy between the MEK1/2 inhibitor, selumetinib, and ABT-263 was reliant upon the upregulation of the pro-apoptotic protein BIM, as well as BMF and PUMA, and the activation and expression of BAX (Sale and Cook, 2013). As a comparison to this, Liang and colleagues observed that combining knockdown of USP30 with the BH3 mimetic, ABT-737, in U2-OS cells, resulted in a significant increase in BAK protein levels (Liang *et al.*, 2015). Consistent with the data presented in Figure 4.4D, where loss of BAX protected HCT116 cells from cell death, they observed a cell death response that was partially rescued by BAX knockdown but was significantly reduced by the dual knockdown of BAK and BAX. The rescue effect observed during this study was more significant with BAX-/- HCT116 cells than that observed by Liang *et al.* and this could be due to incomplete knockdown of BAX or the different cell types used in these two studies (Liang *et al.*, 2015). Unlike Liang and colleagues, an increase in BAX expression following combination treatment was observed, which could explain the dependency these cells have on BAX for the observed death response and would further explain why the loss of BAX protects HCT116 cells from cell death (Liang *et al.*, 2015).

4.3.2. MTX32 and MTX48 have different activity-based probe profiles.

During this study, the HA-UbVME probe was used to isolate active DUBs following inhibitor treatment of cells. Probed lysates were interrogated for specific inhibition of USP30 and used to provide a "competition profile" of MTX32 and MTX48. Activity-based probe profiling (ABPP) has been used successfully in the development of the DUB inhibitor VLX1570, which until recently was in clinical trials for the treatment of multiple myeloma (Wang *et al.*, 2016). In this study, combining the use of HA-UbVS, an alternative warhead to VME, with SDS-PAGE analysis revealed that VLX1570 inhibits proteasomal DUBs, more specifically, USP14.

The novel USP30 inhibitor, MTX32, and siRNA-mediated knockdown of USP30, in combination with ABT-263, resulted in vastly different sub-G1 DNA profiles (Figure 4.3 and Figure 4.5). Whilst the use of MTX32 in combination with ABT-263 resulted in an increase in cell death, knockdown of USP30 in combination with ABT-263 did not. Further to this, western blot interrogation of probed lysates showed that alternative highly expressed DUBs in HCT116 cells were rapidly inhibited post-treatment with MTX32, with or without ABT-263 (Figure 4.2 and Figure 4.3A). Together this indicates that the cell death response seen in HCT116 cells, with MTX32 and ABT-263, was not due to inhibition of USP30 but due to off-target inhibition of alternative DUBs.

Combining the use of the ABP, HA-UbVME, with HA immunoblotting enables ABPP of a chosen inhibitor. From Figure 4.8B higher concentrations of MTX32 resulted in the reduced ability of the probe to react with active DUBs due to increased levels of general DUB inhibition. This implies that MTX32 is a less selective USP30 inhibitor than MTX48, with more off-target inhibition of active DUBs. Given this, it should be noted that there are caveats associated with the use of ABPP experiments to assess the specificity of a given DUB inhibitor. The mode of action of a chosen inhibitor can influence the outcome of the ABPP assay, in particular the reversibility of the inhibitor. In general, irreversible DUB inhibitors will be affected by the time between inhibitor treatment of cells and post-lysis probe labelling, whilst reversible inhibitors will be affected by changes in inhibitor concentrations between inhibitor treatment and post-lysis probe labelling (Farshi *et al.*, 2015).

As there is a lack of structural information of the chosen inhibitors, they could have different reversibility profiles that could account for the different HA banding patterns (Figure 4.8B). Indeed, cells treated with MTX48 over 48 hrs and probed post-lysis with the ABP revealed that, unlike USP30, the inhibition of UCHL3 was not sustained (Figure 4.6B). This could be because the binding of MTX48 to UCHL3 is reversible, or newly synthesised UCHL3 may not be inhibited by MTX48. Results suggest that MTX32 irreversibly binds to UCHL3 in cells over the same time course (Figure 4.2), suggesting that the two inhibitors bind to given DUBs with differing modes of action and/or different binding affinities. In addition, the HA-UbVME probe may preferentially label certain families of DUBs which may bias the HA immunoblot read-out towards a small subset of DUBs, ultimately leading to incorrect conclusions being made about the specificity of a chosen inhibitor. Indeed, others have shown the HA-UbVME probe preferentially labels UCHL3, USP5/16 and USP9/24 over short periods of time (Altun *et al.*, 2011).

Overall, HA profiling was unable to identify the active DUBs targeted by MXT32 and MTX48, as many are of a similar molecular weight. Quantitative analysis of the DUBs inhibited by MTX32 and MTX48 could be performed using mass spectrometry (Altun *et al.*, 2011), and would ultimately confirm the

specificity of the chosen USP30 inhibitors. This would reveal how these DUBs differ in their off-target effects and may confirm that MTX32 is a less specific inhibitor than MTX48.

Based on the data presented here, and given the suggested off-target nature of MTX32, the synergy observed with the combined treatment of MTX32 and ABT-263 in HCT116 cells is not due to MTX32-driven inhibition of USP30. Instead, the increase in cell death is most likely due to the inhibition of additional DUBs that are vital for HCT116 cell survival. Candidates for this might include UCHL3, which, from our data, was rapidly and irreversibly inhibited by MTX32. Previous reports have demonstrated that UCHL3 is upregulated in a number of cancer cell types including breast and cervical cancers (Miyoshi *et al.*, 2006, Rolen *et al.*, 2006), where its expression has been linked to oncogenesis (Fang *et al.*, 2010). Inhibition of UCHL3, as well as other select DUBs, notably USP5, with chalcone-based small molecules resulted in cellular changes, including downregulation of cyclin D1 and upregulation of $p27^{KIP1}$, associated with the onset of apoptosis in several cancer cell lines (Issaenko and Amerik, 2012); suggesting here that UCHL3 could be a potential therapeutic target to drive tumour cell death. Other essential DUBs, in HCT116, have been summarised in Hart *et al.*, where CRISPR-Cas9 knockout of numerous DUBs alone resulted in a decrease in 'fitness' of these cells (Hart *et al.*, 2015). Interestingly examples from this study include USP5 and UCHL3, with USP5 having a consistently high Bayer factor value over several cell lines, including HCT116, indicative of a high confidence that USP5 is an important 'fitness' gene for cell survival. Therefore, inhibition of USP5 and UCHL3 alone could result in cell death of HCT116 cells and could explain the induction of apoptosis observed with MTX32 treatment of HCT116 cells.

Chapter 5: siRNA screens to identify deubiquitylating enzymes that regulate cell death driven by inhibitors of MEK1/2 or mTOR

5. Chapter 5

5.1. Introduction

Tumour cells with $BRAF^{V600E}$ mutations are now treated with a combination of BRAF inhibitors (vemurafenib and debrafenib) and MEK inhibitors (trametinib) and future development of this therapeutic regimen will involve intermittent dosing schedules, as well as combination with immune checkpoint blockade (CTLA-4 and PD-1/PD-L1), to prolong response times. However, BRAF inhibitors cannot be employed against tumours with wild-type BRAF, including those with Ras mutations, as BRAF inhibitors cause paradoxical activation of wild type RAF dimers and activation of ERK1/2 (Poulikakos *et al.*, 2011). This has refocused attention on the use of MEK inhibitors to treat Ras mutant tumour (Caunt *et al.*, 2015). Unfortunately, MEK inhibitors as a monotherapy have had limited success due to the collapse of feedback inhibition loops, pathway re-activation and adaptive pathway re-modelling through the *de novo* expression of ERK phosphatases (DUSPs) and inhibitors of ERK signalling (SPRY/SPRED proteins). In addition, monotherapy causes a cytostatic cell cycle arrest rather than a cell death response (Sale and Cook, 2013), allowing cells to adapt and acquire resistance (Little *et al.*, 2011). Notably, the majority of these limiting factors are regulated by protein ubiquitylation. DUSPs and SPRY/SPRED, regulated by *de novo* expression, have also been shown to be regulated by phosphorylation and ubiquitylation (Caunt and Keyse, 2013, Edwin *et al.*, 2010, Lin *et al.*, 2003, Lin and Yang, 2006). Additionally, the ability of MEK inhibitors to elicit cell death is arbitrated by expression of members of the BCL2 family, including BIM, PUMA, BMF, MCL1, BCL2 and BCL-X_L, all of which have been demonstrated to be regulated by ubiquitylation.

mTOR activity is de-regulated in up to 70% of cancers due to a variety of genetic lesions including Ras^{MUT}, $PIK3CA^{MUT}$ and loss of PTEN. As a result of this, ATP-competitive mTOR kinase inhibitors are undergoing clinical evaluation for the treatment of cancer. mTOR inhibitors face some of the same challenges as MEK inhibitors, including adaptation and the emergence of acquired resistance, demonstrated by the amplification of the *eIF4E* gene (Cope *et al.*, 2014). Additionally mTOR inhibitors typically promote cell cycle arrest rather than cell death (Cope *et al.*, 2014). Notably, one of the most prominent responses to mTOR inhibition is the induction of autophagy, as well as the ubiquitin proteasome system (UPS), which both act to degrade and re-cycle proteins within the cell. Indeed, Zhao and colleagues demonstrated that inhibition of mTOR rapidly resulted in an increase in K48-linked ubiquitylated proteins, known to be degraded by the UPS (Zhao *et al.*, 2015). In addition, many of the mRNAs translated in an mTOR-dependent manner encode cancer-relevant proteins that are also

regulated by the UPS, namely Cyclin D1 (CCND1), MCL1 and MYC (Dowling *et al.*, 2010, Farrell and Sears, 2014, Mojsa *et al.*, 2014, O *et al.*, 2009, Rosenwald *et al.*, 1995).

As demonstrated above, the ubiquitin system is involved in the regulation of almost every cellular signalling pathway, either through the UPS or non-proteolytic events. Deubiquitylating enzymes (DUBs) hydrolyse ubiquitin from a target protein and in doing so can rescue target proteins from various fates including degradation. Numerous studies have identified DUBs that regulate cellular processes required for cell proliferation, genome stability and cell survival and mutation and/or dysfunction of DUBs is often linked to disease. Of note, DUBs have been identified that regulate pathways frequently altered in tumourigenesis including those that regulate DNA damage responses and cell cycle checkpoints. Therefore, a subset of DUBs have become attractive drug targets for the treatment of cancer (Kemp., 2016, Tsukamoto., 2016), aided by the fact that proteases are readily druggable.

The emergence of resistance to new cancer therapeutics, including MEK1/2 or mTOR inhibitors, demands the development of novel drug combinations to prevent or delay its onset. Since both the ERK1/2 and mTOR pathways are so closely integrated with ubiquitin-regulated signalling processes it speculated that inhibition of one or more DUBs might uncover key vulnerabilities in tumour cells treated with MEK1/2 or mTOR inhibitors, a situation analogous to synthetic lethality (Hartwell *et al.*, 1997). To investigate this a DUB focused RNAi screen was performed to identify DUBs which, when knocked down, transformed MEK1/2 or mTOR inhibition from a cytostatic to a cytotoxic response.

5.2. Results

5.2.1. Optimisation of DUB RNAi screens.

All screens were chosen based on the knowledge and ongoing projects in the Cook Lab with the aim to identify DUBs that, when knocked down, combined with MEK1/2 or mTOR inhibitors to drive apoptosis. Therefore, several aspects of the screen needed to be optimised to maximise the difference between cell death observed following knockdown of the DUB/inhibitor treatment alone and combined knockdown with inhibitor treatment. Screens were performed over 3- and 5-days, (detailed in Chapter 2 and Figure 2.1). A 5-day screen was chosen over longer screens based on the limits of the longevity of the effects of siRNA transfection.

Technical considerations required to perform the DUB RNAi screens included, choice of cell line, the method of siRNA-delivery, the choice and concentration of inhibitor, the selection of appropriate

positive and negative controls, the choice of 'end-point' assay and the method to define the initial 'hits' from the screen.

5.2.1.1. Choice of cell line for RNAi screen.

The colorectal carcinoma cell line HCT116 was chosen for the DUB RNAi screens. These cells were chosen based on the knowledge that they were readily transfectable and based on prior data, generated by the Cook Lab, showing that they were sensitive to MEK1/2 inhibitors and mTOR inhibitors. Additionally, the Cook Lab possessed genetically engineered, isogenic HCT116 cells lines lacking the BCL2 effector proteins, BAK and BAX, which would be used as a secondary triage assay to assess the biological mechanisms underlying the cell death response observed with key 'hit' DUBs.

5.2.1.2. Confirmation that inhibitors have on-target effects in HCT116 cells.

Preliminary experiments were undertaken to confirm the relevant drugs were acting on-target (Figure 5.1). It was also important to define doses at which these inhibitors alone did not cause a significant increase in cell death, as judged by the sub-G1 DNA fraction from cell cycle analysis, compared to DMSO controls (Figure 5.1). For these experiments the MEK1/2 inhibitor PD0325901 (PD901) and the mTOR inhibitor AZD8055 (8055) were chosen to treat transfected HCT116 cells.

Active MEK1/2 has been demonstrated to phosphorylate ERK1/2 at T202/T204 leading to its activation (Butch and Guan, 1996). Subsequently ERK1/2 phosphorylates RSK at T573, within the activation loop of the CTKD of RSK. It is also believed to phosphorylate RSK at T359/S363 within its linker region. Phosphorylation within the activation loop results in the autophosphorylation at S380 of RSK (Dalby *et al.*, 1998, Kidger *et al.*, 2018). HCT116 cells were treated with increasing concentrations of the MEK1/2 inhibitor, PD901, for 48 hours. The efficacy of PD901 was then confirmed by western blot analysis, demonstrating that PD901 inhibited the phosphorylation of ERK1/2 (T202/T204) and RSK (S380) and that inhibition correlated with an accumulation of BIM_{EL} (Figure 5.1A). Flow cytometry data demonstrated that MEK1/2 inhibition by PD901 alone, resulted in a minimal increase in cell death over the concentration range tested. However, as previously shown (Sale and Cook, 2013), when combined with the BH3 mimetic ABT-263, this resulted in a considerable increase in cell death (Figure 5.1B).

Figure 5.1A and Figure 5.1B depict inhibition of MEK1/2 over 48 hrs, required for the 3-day RNAi screens, whilst Figure 5.1C and Figure 5.1D depict inhibition of MEK1/2 over 4-days, required for the 5-day RNAi screen. As previously seen, low concentrations of PD901 resulted in loss of phosphorylated ERK1/2 and RSK and an accumulation of BIM_{EL} protein (Figure 5.1C). Treatment of HCT116 cells with

increasing concentrations of PD901, over 4-days, resulted in an increase in sub-G1 DNA, with low concentrations of PD901 generating the required low sub-G1 populations (<30 %). Additionally PD901 combined with ABT-263 to cause a substantial increase in cell death (Figure 5.1D). Thus, treatment of HCT116 cells with PD901, for the two different time points, resulted in on-target loss of phosphorylation of downstream targets, but low concentrations of the inhibitor were required to prevent high levels of cell death when used alone.

Comparing cell cycle profiles of cells treated with PD901 for two days and four days revealed that treatment of cells with PD901 for four days induced a greater fraction of cells with sub-G1 DNA (Figure 5.1B and Figure 5.1D). This could be because of the toxic nature of this inhibitor at longer time points or that inhibition of ERK1/2 activity for an increased amount of time is required to observe death of HCT116 cells. This could be because it takes longer for pro-apoptotic proteins, including BIM, to accumulate.

Treatment of HCT116 cells with 8055, an ATP-competitive inhibitor of mTOR, resulted in the loss of T389 phosphorylated p70 ribosomal S6 kinase and phosphorylated T37 and T46 on 4EBP1, as previously described (Chresta *et al.*, 2010) (Figure 5.1E). Interestingly flow cytometry cell cycle analysis revealed that treatment with 8055 alone did not cause an increase in sub-G1 DNA with any of the inhibitor concentrations tested. However, combined treatment with 8055 and PD901 resulted in a substantial increase in cell death (Figure 5.1F). Thus, in theory, for the 3-day RNAi screen any of the tested concentrations of 8055 could be used as they inhibited downstream mTOR targets without causing a substantial increase in cell death.

5.2.1.3. Selection of appropriate controls for the RNAi screens.

Appropriate and robust controls were required to determine the quality and validity of the DUB RNAi screens. All output values were also normalised to selected controls and as such were used to determine the 'hit' DUBs from the screens. Positive and negative siRNA controls were also used to optimise the primary screens to determine the RNAiMAX volumes and also further assess optimal inhibitor concentrations to be used for the 3-day and 5-day screens.

For the DUB RNAi screens, positive and negative controls were added to all plates along with experimental DUB siRNA (Figure 2.2) and the consistency of these controls over each plate and

Figure 5.1 Optimisation of inhibitor concentrations of the chosen MEK1/2 and mTOR inhibitors in HCT116 cells.

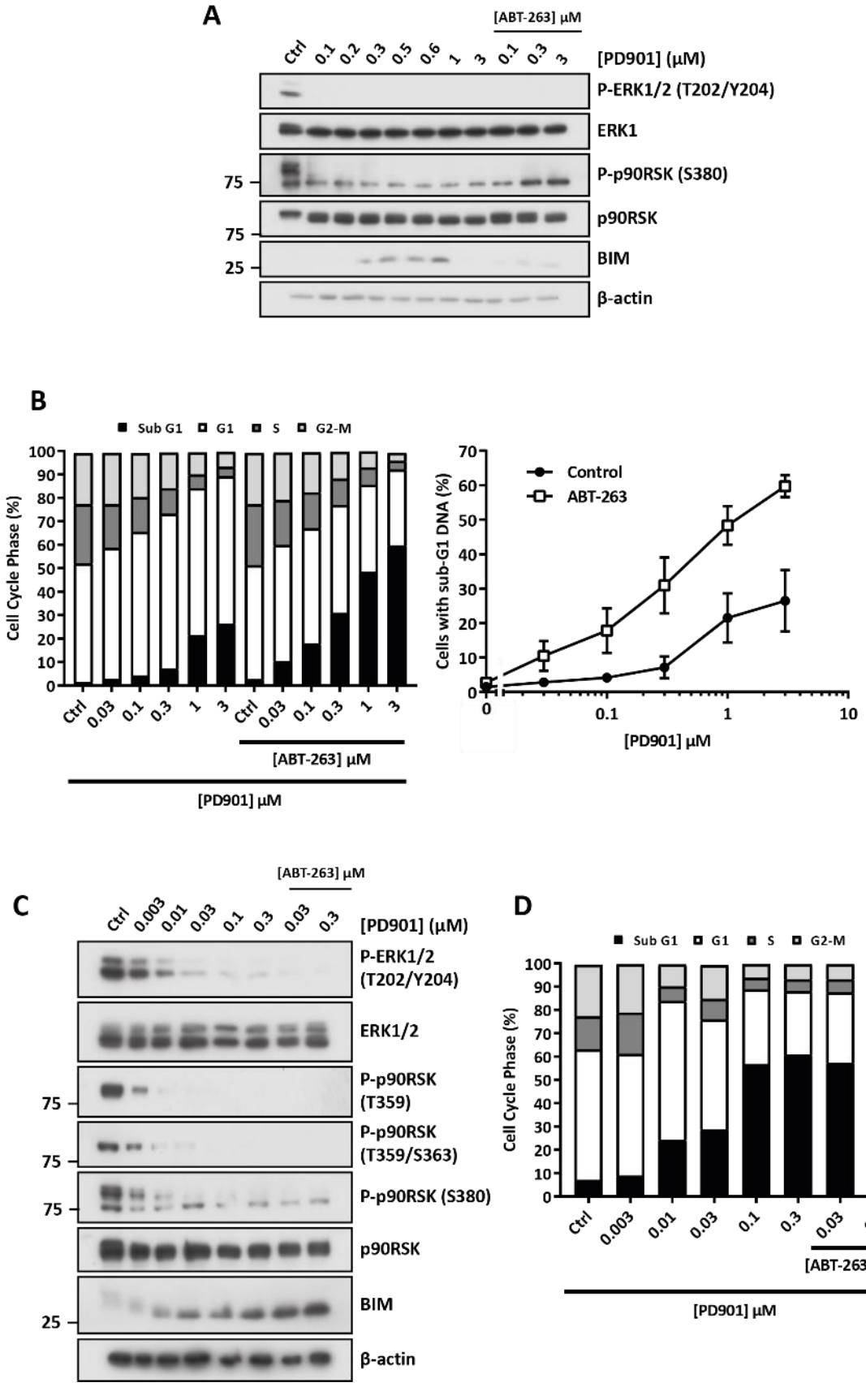

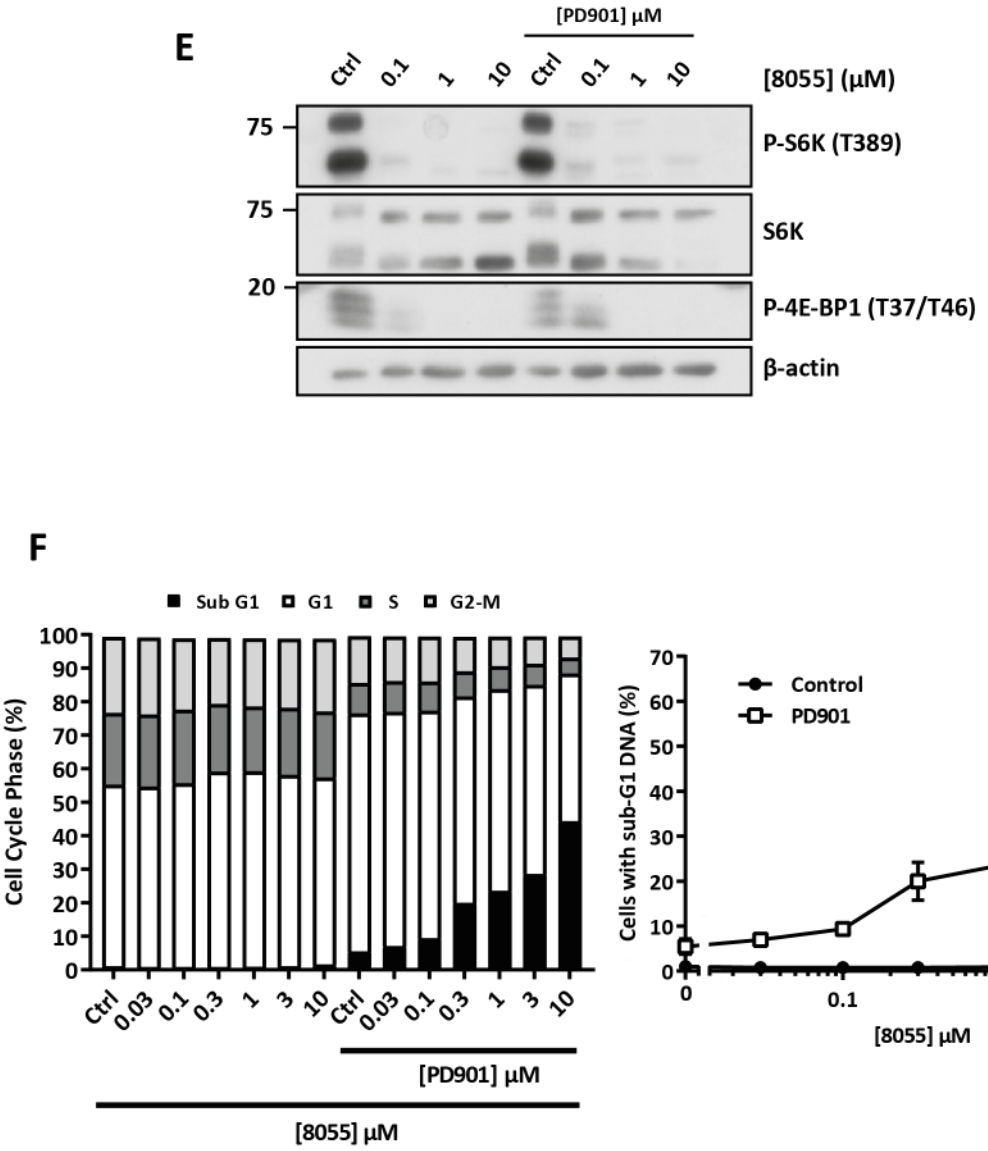

Figure 5.1 Optimisation of inhibitor concentrations of the chosen MEK1/2 and mTOR inhibitors in HCT116 cells. HCT116 cells were treated with **(A + B)** increasing concentrations of the MEK1/2 inhibitor, PD0325901 (PD901), for 2 days or **(C + D)** 4 days, with or without 1 µM ABT-263 or the **(E + F)** mTOR inhibitor, AZD8055 (8055), for 2 days, with or without 0.3 µM PD901. **(A + C + E)** Cells were lysed, fractionated by SDS-PAGE and subjected to western blotting with the antibodies indicated in the figure. This data is from a single experiment or **(B + D + F)** fixed and stained with propidium iodide and cell death (sub-G1 DNA) determined by flow cytometry. Results shown here are from a single experiment, where each biological replicate is performed in technical triplicate.

across all plates was examined. siLUC was used as a negative siRNA control, designed to target the Photinus pyralis (firefly) luciferase gene and as such was used to look at the effect of transfection on HCT116 cells alone. siEg5/siKIF11 and siBCL-X_L were used as positive siRNA controls, as knockdown of these genes should result in cell death. Kinesin family member 11 (KIF11, also known as Eg5) is an essential motor protein in mitosis and is essential for centromere segregation. Knockdown of KIF11 or inhibition of KIF11 resulted in an early accumulation of mitotic cells in G2 phase of the cell cycle and induced cell death (Martens-de Kemp *et al.*, 2013, Pau *et al.*, 2013). B-cell lymphoma-extra large (BCL-X_L) is a key pro-survival BCL2 protein which, as previously described, acts to prevent MOMP and cell death. Knockdown of BCL-X_L alone was found to inhibit cell proliferation and combine with other therapies to induce cell death (Bai *et al.*, 2005, Lee *et al.*, 2014, Takahashi *et al.*, 2013). Negative and positive inhibitor controls for cell death, DMSO and combined inhibitor treatments, respectively, were also added to each plate as Figure 5.1B demonstrated that treatment of HCT116 cells with PD901 and ABT-263 resulted in the induction of cell death (Figure 2.2).

5.2.1.4. Selection of experimental read-out for the RNAi screens.

For the DUB RNAi screens, the CellTiter-Glo® (CTG) luminescent cell viability assay was used as an end-point assay. The CTG assay quantifies intracellular ATP, which is an indicator of metabolically active cells. As such the higher the CTG value the more viable, active cells present in a select well, and the loss of CTG value is indicative of a reduction in metabolic activity and loss of viable cells. Additional end-point analysis was performed using the fluorescent dye YOYO®-1. YOYO®-1 is a cell impermeant cyanine dimer nucleic acid fluorescent stain that binds to double-stranded (ds) DNA and therefore enables evaluation of membrane integrity. High YOYO®-1 values, compared to controls, are indicative of a cytotoxic response or an induction of cell death. As a consequence of the YOYO®-1 dye being cell impermeant, it was added to cells at the same time as cell seeding and enabled the multiplexing of the two described end-point assays. Additionally YOYO®-1, unlike the CTG assay, did not require cell lysis to measure changes in fluorescence. As the output of the CTG viability assay is luminescence, CTG values were measured on a CLARIOstar® microplate reader. In contrast YOYO®-1 values were measured, prior to performing the CTG viability assay, on live cells using the IncuCyte® ZOOM live-cell imaging system. Additionally, this instrument measured 'phase' values, an estimate of total cell number, from all wells of plates that YOYO®-1 measurements were taken from. As an additional measure, cell death, measured from YOYO®-1 values, was divided by the confluency, either using CTG or phase values, to assess the cytotoxic effect of the knockdown of a DUB in combination with the chosen inhibitor, normalised to cell number. This would help to eliminate low confluency values that occurred as a consequence of a cytostatic effect rather than as a consequence of induced cell death

and in addition removes false negative data generated as a consequence of cells rapidly dying without having a chance to grow (for example seen with siEg5 data). Overall, these assays were chosen based on their availability and cost to Mission Therapeutics.

5.2.1.5. Optimising cell seeding.

Whilst at Mission Therapeutics, prior to the beginning of the complete DUB RNAi screens, pilot experiments were performed to optimise the concentration of HCT116 cells and the RNAiMAX volume added to the 96-well plates. Cells were seeded at increasing concentrations, from 500 cells/well to 30000 cells/well in triplicate (Figure 5.2A). These were then loaded into the IncuCyte® ZOOM and left to grow for 3 days. Live cell images of each well were taken every four hours and, using phase values, a growth curve for each well was compiled and additionally shown in Figure 5.2A. At the end of the 3-day time course, an estimation of cell growth was made using the CTG assay values. From the raw data generated, a density of cells that would give a final cell density of ~75 %, at the end of the 3-day screen, was chosen. Using the equation of the line, generated from the log growth phase, this was approximately 7000 cells/well for the 3-day screen (Figure 5.2B). The above method was repeated for the 5-day screen and determined that approximately 1000 cells/well should be seeded to give a final cell density of ~75 %.

5.2.1.6. Optimising RNAiMAX volume and inhibitor concentrations.

Lipofectamine™ RNAiMAX (RNAiMAX) was used to transiently transfect siRNA molecules into HCT116 cells. The volume of RNAiMAX was optimised, as high volumes of RNAiMAX alone can result in cell death. All siRNA were reverse transfected into HCT116 cells, as cells were seeded at the same time as siRNA and transfection reagents were added to wells.

Primary screening with three different volumes of RNAiMAX was performed, based on those suggested for a 96-well plate. These three volumes of RNAiMAX were tested with three different cell densities, around the optimised cell density determined above, as transfection can affect cell growth and/or result in cell death. Each of the cell density/RNAiMAX concentration combinations were tested with the non-targeting siRNA control, siLUC, and one of the positive siRNA controls, siEg5.

Figure 5.2 Optimisation of cell seeding for the 3-day DUB RNAi screens.

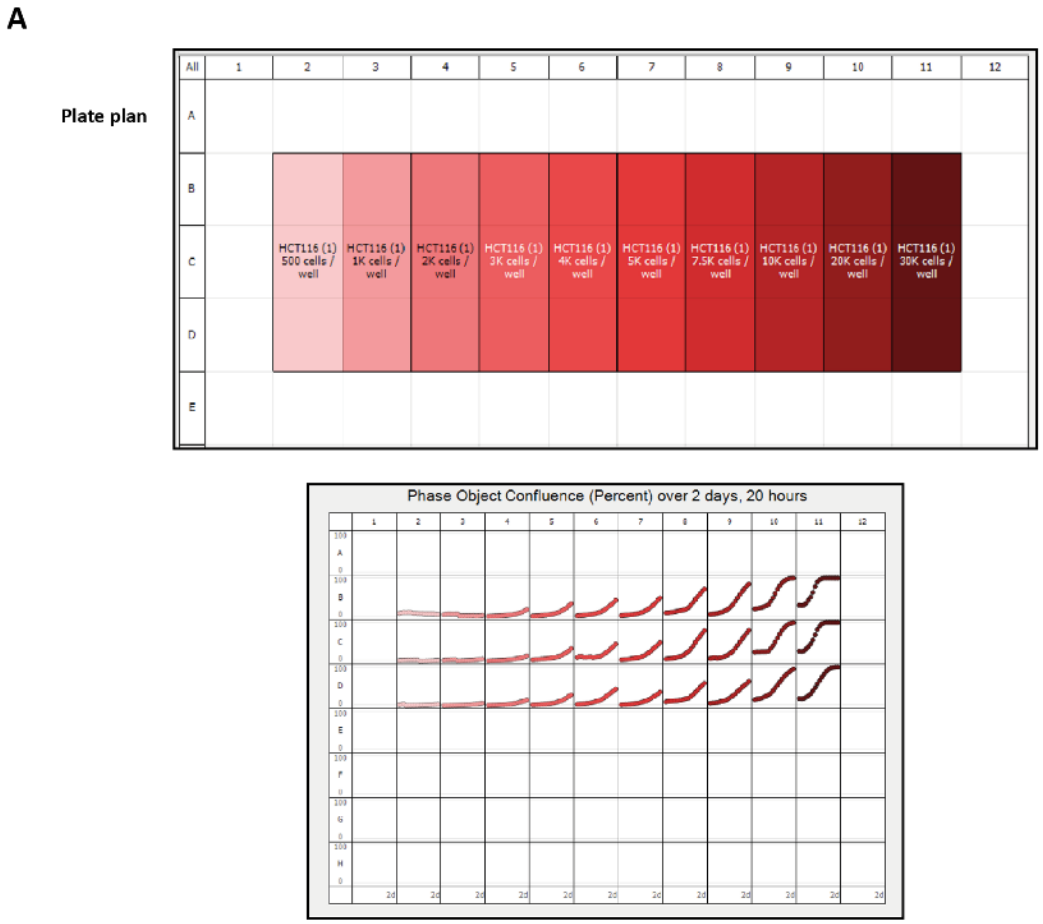

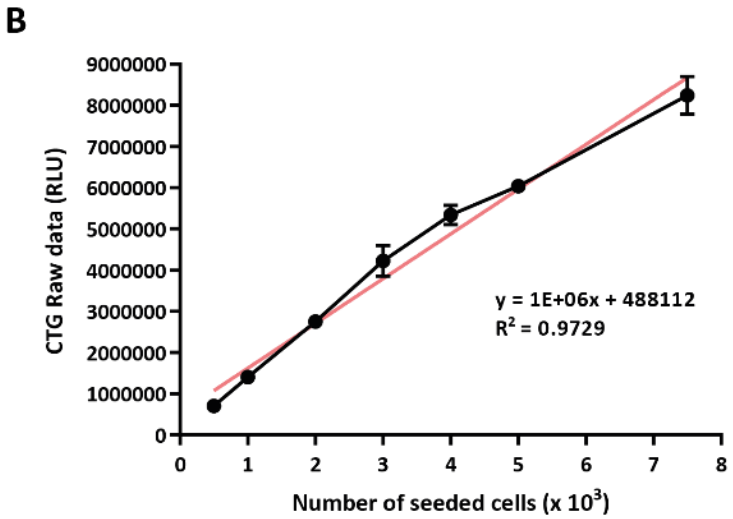

Figure 5.2 Optimisation of cell seeding for the 3-day DUB RNAi screens. (A) A plate plan and overall picture of results for each corresponding well for the optimisation of seeding of HCT116 cells for 3-days in a 96-well plate. The seeding density for HCT116 was determined using the equation of the line generated from steepest part of the growth curve, shown in **(B)**, using 75 % of the maximum growth observed in 3 days as the Y value.

For optimisation of the 3-day screens, HCT116 cells were reverse transfected with the control siRNA and left for 3 days in the IncuCyte® ZOOM (Figure 5.3A). As previously described live-cell images of each well were taken every four hours and, based on phase data, growth curves were compiled for each well and shown in Figure 5.3A. At the end of the 3-day time course, cell viability was assessed using CTG analysis. Comparing all data sets, 7000 cells/well remained the best cell density, as again ~75 % of maximal cell density was reached after 3 days. All of the RNAiMAX volumes successfully transfected HCT116 cells, at a cell density of 7000 cells/well, as judged by the reduction in cell viability following knockdown of Eg5 (Figure 5.3B). Based on this, 0.15 µL of RNAiMAX was chosen for further 3-day experiments. Transfection of HCT116 cells with this volume of RNAiMAX at this cell density resulted in ~20 % loss of cellular viability, comparing average raw untransfected CTG values and siLUC CTG values, which is below the 30 % cell death limit set for these screens. Figure 5.3C depicts representative images of total cell number or phase values at the end of the 3-day time course for the transfection controls using 0.15 µL RNAiMAX. These images revealed that knockdown of Eg5 in HCT116 cells resulted in a visible loss of cell number compared to transfection of siLUC, as judged by the 'phase mask' mapped onto IncuCyte® ZOOM images. Post optimisation of the 5-day screen, using the above method, resulted in a volume of 0.075 µL RNAiMAX being chosen for a cell density of 1000 cells/well.

Further optimisation of the concentration of the chosen inhibitors was required to confirm that the chosen concentration, previously found to cause on-target inhibition and minimal cell death, had the same affect at Mission Therapeutics in a 96-well plate format. For the 3-day DUB RNAi screen , HCT116 cells were seeded at a cell density of 7000 cells/well and reverse transfected with siLUC and left to settle for ~24 hours, then treated with increasing concentrations of PD901, as shown in Figure 5.3D. All plates were kept in the IncuCyte® ZOOM for the 3-day time course, and live-cell images were taken every four hours and at the end of the time course a composite growth curve was drawn using phase values (Figure 5.3D). Along with siLUC transfection controls, HCT116 were transfected with siEg5 and treated with the inhibitor controls of DMSO and PD901 and ABT-263. Analysing phase data, generated by the IncuCyte® ZOOM, revealed that as predicted transfection of siEg5 resulted in a reduction in confluency, whilst transfection of siLUC alone had very little effect and was comparable to the untransfected control (NT) (Figure 5.3E). The addition of PD901, in combination with transfection of siLUC, resulted in a moderate loss of confluency across all concentrations tested, compared to transfection of siLUC alone (Figure 5.3E).

Additionally, changes in cell death that occurred as a consequence of transfection and/or PD901 treatment, were examined using the YOYO®-1 dye. Figure 5.3F depicts images generated by the IncuCyte® ZOOM, at the end of the 3-day time course, demonstrating that transfection, as well as

Figure 5.3 Optimisation of RNAiMAX volumes and PD0325901 concentrations for the 3-day DUB RNAi screens.

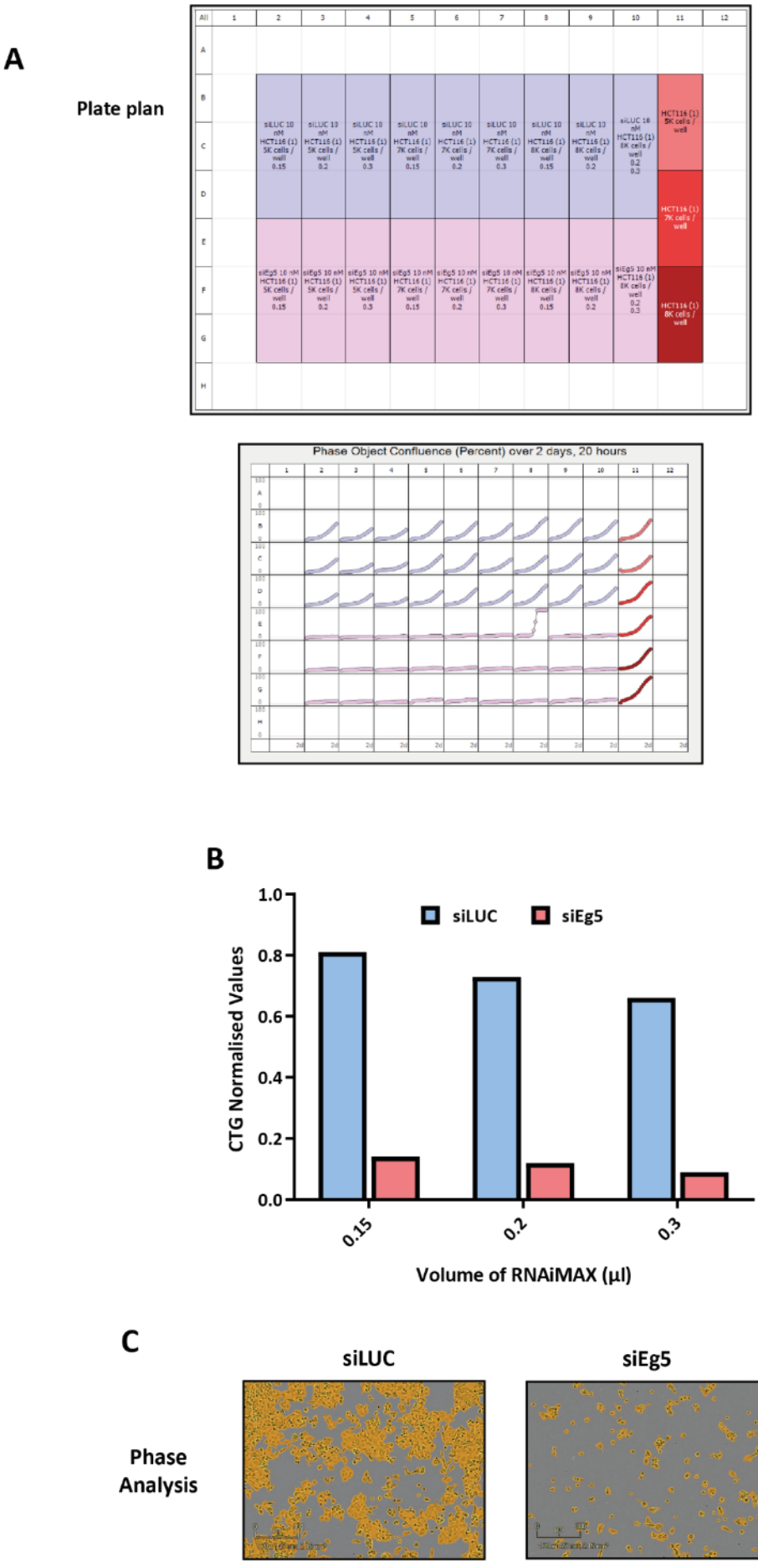

D **Plate plan**

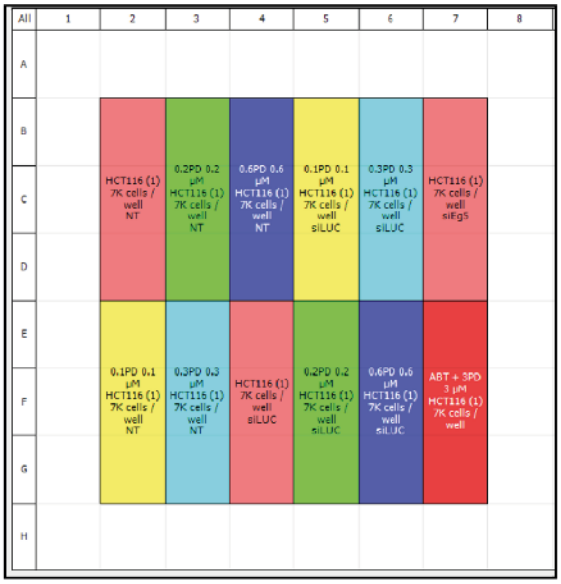

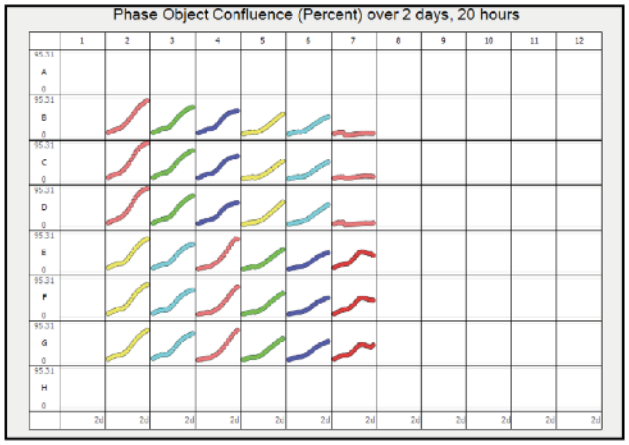

E

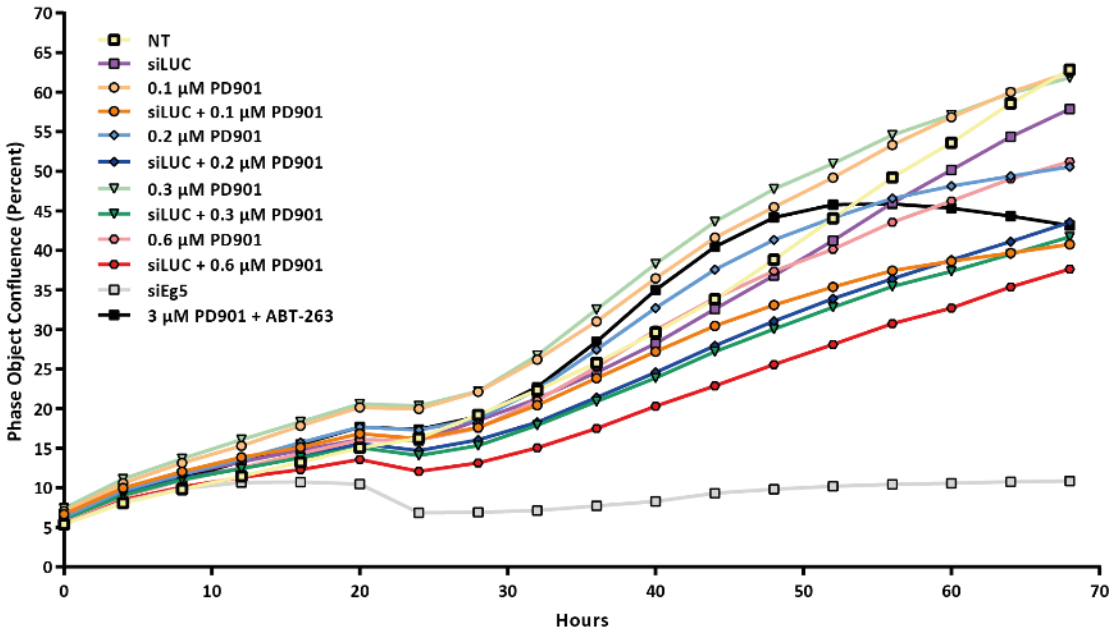

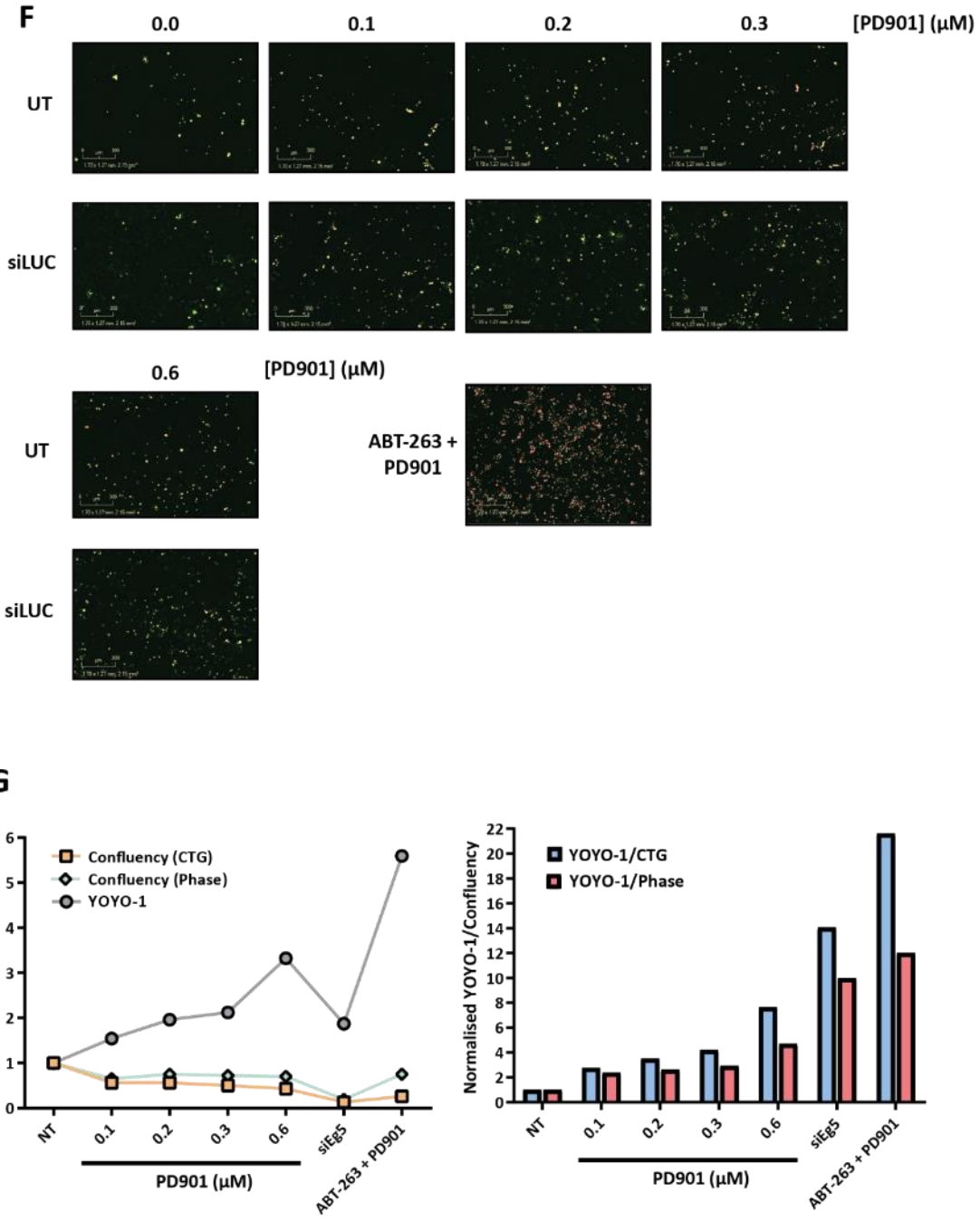

Figure 5.3 Optimisation of RNAiMAX volumes and PD0325901 concentrations for the 3-day DUB RNAi screens. (A) A plate plan and overall picture of results for each corresponding well for the optimisation of the RNAiMAX volume required for transfection of HCT116 cells for 3-days in a 96-well plate. The negative and positive transfection controls used in the RNAi screen were used to test transfection of HCT116, siLUC and siEg5, respectively. **(B)** Bar graphs depicting changes in cell viability following transfection of siLUC and siEg5 with varying volumes of RNAiMAX. All values were normalised to untransfected controls. As shown in **(C)** transfection of HCT116 cells with 0.15 μl of RNAiMAX was successful, as judged by the reduction in cell number or phase following knockdown of Eg5. These images were taken by the IncuCyte ZOOM, using the IncuCyte data analysis programme, Basic Analyser, with an optimised 'Confluence Mask' to count all cells from live cell images. **(D)** A plate plan and overall picture of results for each corresponding well for the optimisation of PD0325901 (PD901) concentrations for the treatment of HCT116 cells, post-transfection, in a 96 well plate. An overview of the raw phase data, or total cell count, obtained from inhibitor optimisation, using IncuCyte images, is shown in **(E)**. Images of YOYO-1 data obtained from the same optimisation experiment are shown in **(F)**. **(G)** Graphs depicting changes in confluency following treatment with increasing concentrations of PD901, both from phase data obtained from analysis of IncuCyte ZOOM images and from CTG viability assay analysis, as well as information about cell death following treatment with increasing concentrations of PD901, from YOYO-1 data measured from IncuCyte ZOOM images (Counts per image) as well as normalised cell death values.

increasing concentrations of PD901 resulted in small increases in cell death, as shown by the number of fluorescent cells compared to the positive inhibitor control, ABT-263 and PD901. Comparing YOYO®-1 data, CTG data, as well as 'normalised cell death', measured by dividing YOYO®-1 by 'confluency', concentrations of the inhibitor were selected that caused minimal increases in cell death (<30 %) over the time course of the DUB RNAi screen (Figure 5.3G). As such, based on the data presented here 0.2 µM of PD901 was chosen for the 3-day RNAi screen. The above experiments were repeated to optimise the concentration of PD901 required for the 5-day screen and the concentration of 8055 required for the 3-day screen (Data not shown). Given this, 0.03 µM of PD901 was chosen for the 5-day RNAi screen and 0.2 µM of 8055 was chosen for the 3-day screen.

5.2.1.7. Selection of siRNA for the DUB RNAi screens.

A graph depicting the classification of the DUBs used in the screen is shown in Figure 5.4. The DUB RNAi screening panel was purchased from QIAGEN and aliquoted into 96-well plates in-house. Additional siRNA targeting USP1, UCHL1, UCHL3, BAP1, SENP2, SENP7, FAM105A, FAM105B, as well as the additional control siRNA, siLUC, Eg5/KIF11 and siBCL-X_L were spotted onto the 96-well plates. All siRNA were aliquoted to give a final concentration of 10 nM. Four individual siRNA were used to target each DUB, giving a total of eight 96-well daughter plates, labelled L1a-d and L2a-d, depending upon the DUB targeted by the select siRNA (Figure 2.2)

5.2.1.8. Selection of method to define the initial 'hit' DUBs from the RNAi screens.

'Hits' from the screen were determined using Sensitivity Index (SI) values, generated from normalised CTG viability, phase or YOYO-1/confluency values for treated and untreated siRNA transfected cells compared to mean siLUC values, normalised to all siLUC values, treated or untreated, across all plates (more detailed description in Chapter 2).

In general, for SI values generated from CTG or phase values, positive SI values, above a set threshold, indicated that knockdown of that particular DUB, in combination with the chosen inhibitor resulted in a significant reduction in cell viability or cell number, and had a sensitisation effect, compared to siLUC controls and knockdown of the DUB alone. In contrast, for SI values generated from YOYO-1/confluency values, negative SI values, below a set threshold, indicated that knockdown of that particular DUB in combination with the chosen inhibitor resulted in a significant increase in cell death.

Figure 5.4 Deubiquitylating enzyme (DUB) RNAi screen overview.

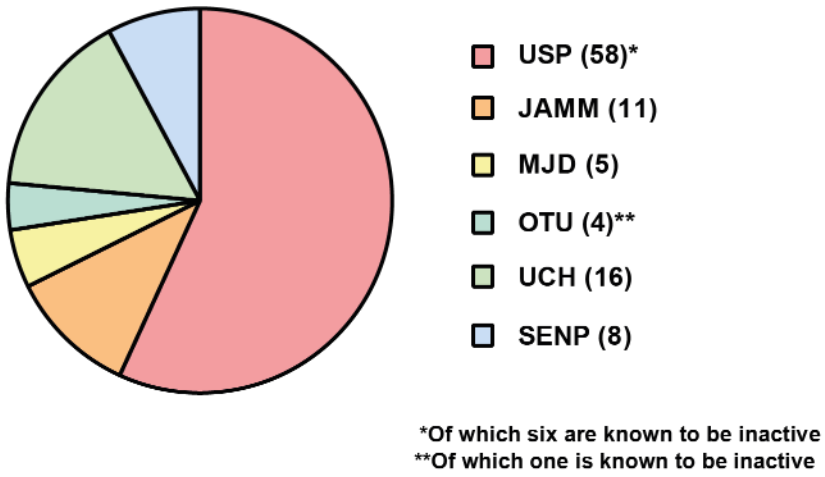

Figure 5.4 Deubiquitylating enzyme (DUB) RNAi screen overview. Overview of all DUBs targeted by siRNA in the RNAi 3-day and 5-day screens. In total 102 proteases were targeted, 94 DUBs and 8 SENP (sentrin/SUMO-specific protease) proteins. USP; Ubiquitin-specific proteases; JAMM; JAB1/MPN/Mov34 metalloenzymes; MJD; Machado-Josephin domain proteases; OTU; Ovarian tumour proteases; UCH; Ubiquitin carboxy-terminal hydrolases.

Therefore combined knockdown of that DUB and inhibitor treatment resulted in a cytotoxic effect, compared to siLUC controls or knockdown of the DUB alone. A DUB was defined as a 'hit' when three or more of the siRNA targeting that DUB combined with the inhibitor to give a significant SI value, above or below the set threshold.

The validity of the screen was assessed by confirming that all CTG and phase values for all siLUC controls were comparable both within the plates and across all plates. In addition, for a valid screen, knockdown of siLUC should not result in a >30 % reduction in cell viability or cell number. Along with analysis of negative controls, positive controls should cause a substantial decrease in normalised CTG and phase values and, from SI values, should be classed as 'hits' from the screen and cause a significant cytotoxic response following knockdown.

5.2.2. RNAi screen to identify DUBs that cooperate with the MEK1/2 inhibitor, PD0325901, to induce a cell death response.

5.2.2.1. Analysis of data generated from the 3-day combined DUB RNAi and PD0325901 screen.

Two 3-day DUB RNAi screens were performed in combination with MEK1/2 inhibition. To assess the validity of the two 3-day DUB RNAi screens, CTG values from HCT116 cells transfected with the negative control, siLUC, with or without PD901, were compared across all plates (Figure 5.5A). As previously demonstrated (Figure 2.2), four siLUC controls were spotted into the four corners of each plate. Analysis of these CTG values revealed that across all plates CTG values for siLUC controls were comparable and that treatment with PD901 resulted in ~35% reduction in cell viability across both screens

Transfection of HCT116 cells with the positive siRNA controls, siEg5 and siBCL-X_L, resulted in 80-85% loss of cell viability, across both screens performed, with or without treatment with PD901 (Figure 5.5B). In addition, combined treatment of HCT116 cells with PD901 and ABT-263, the positive inhibitor control, resulted in a loss of cell viability across both screens, with ABT-263 treatment alone not substantially reducing CTG values (Figure 5.5B). Despite a greater decrease in cell viability following treatment with PD901 than expected, the screens were deemed valid and, based on CTG data, further analysed to look for 'hit' DUBs.

Comparative analysis of all SI values generated from CTG data from the two 3-day RNAi screens, revealed that SI values were evenly distributed over a range of both positive and negative SI values with positive and negative inhibitor controls generating SI values at the extremes of the scale (Figure 5.6A). As previously described, positive SI values were associated with a sensitisation effect

Figure 5.5 Analysis of RNAi screen controls using CTG viability assay values generated from two, 3-day DUB RNAi screens combined with PD0325901 treatment.

Figure 5.5 MEK1/2 inhibitor, 3-day DUB RNAi Screen

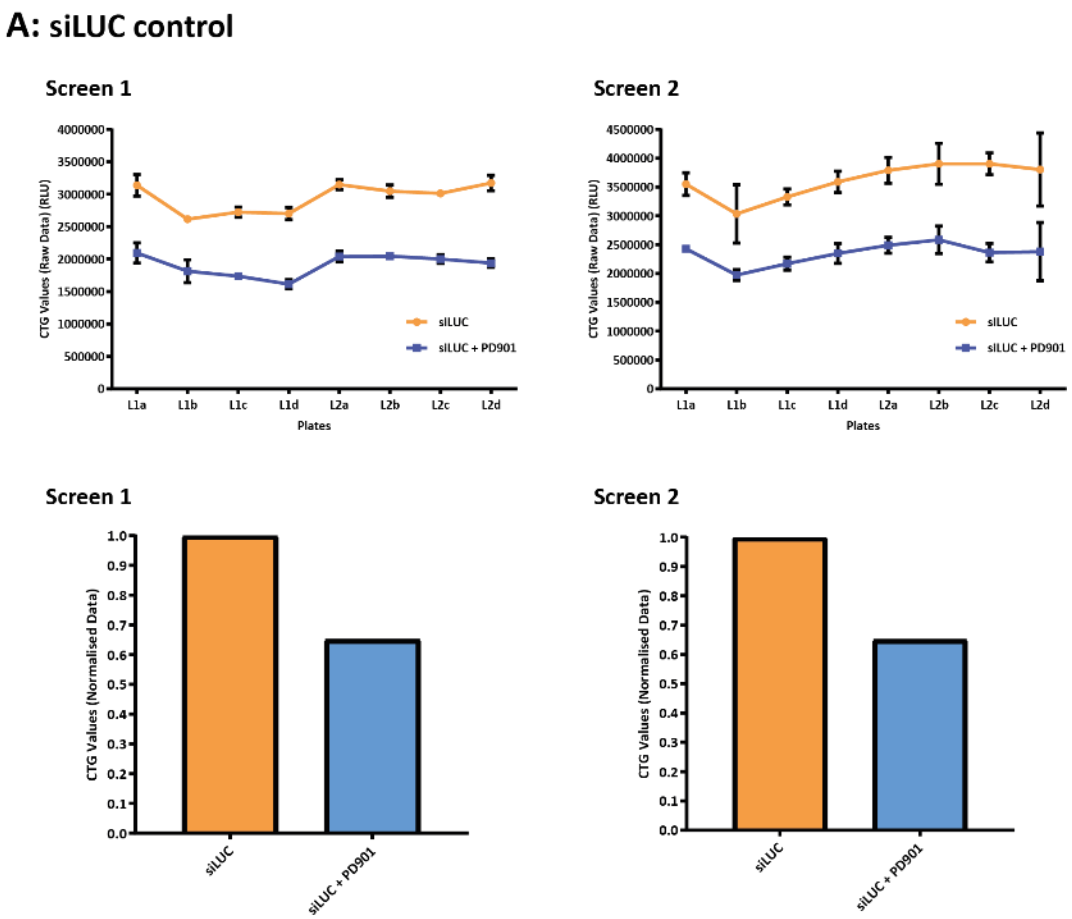

	Average CTG Raw values (RLU) (Screen 1/ Screen 2)	Normalised (Screen 1/ Screen 2)
siLUC	2945558/3613223	1.00
siLUC + PD901	1910867/2342393	0.65/0.65

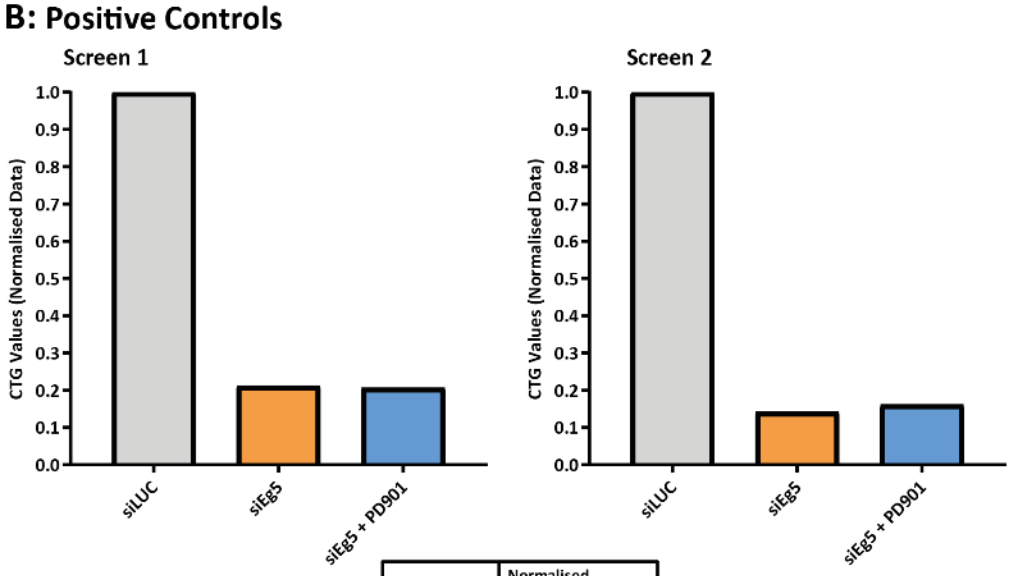

	Normalised (Screen 1/ Screen 2)
siLUC	1.00
siEg5	0.21/0.14
siEg5 + PD901	0.21/0.16

B: Positive Controls

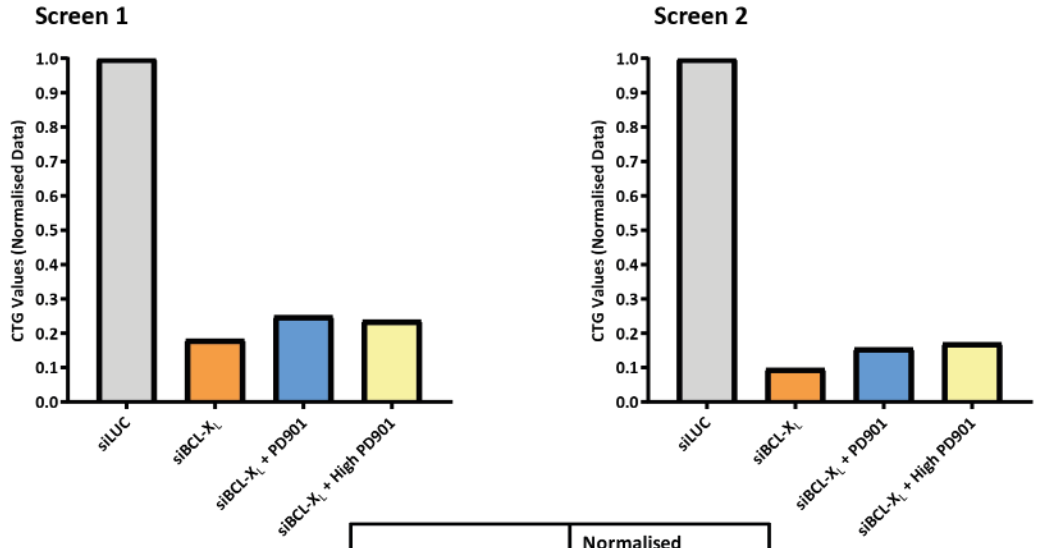

	Normalised (Screen 1/ Screen 2)
siLUC	1.00
siBCL-X_L	0.18/0.10
siBCL-X_L + PD901	0.25/0.16
siBCL-X_L + High PD901	0.24/0.17

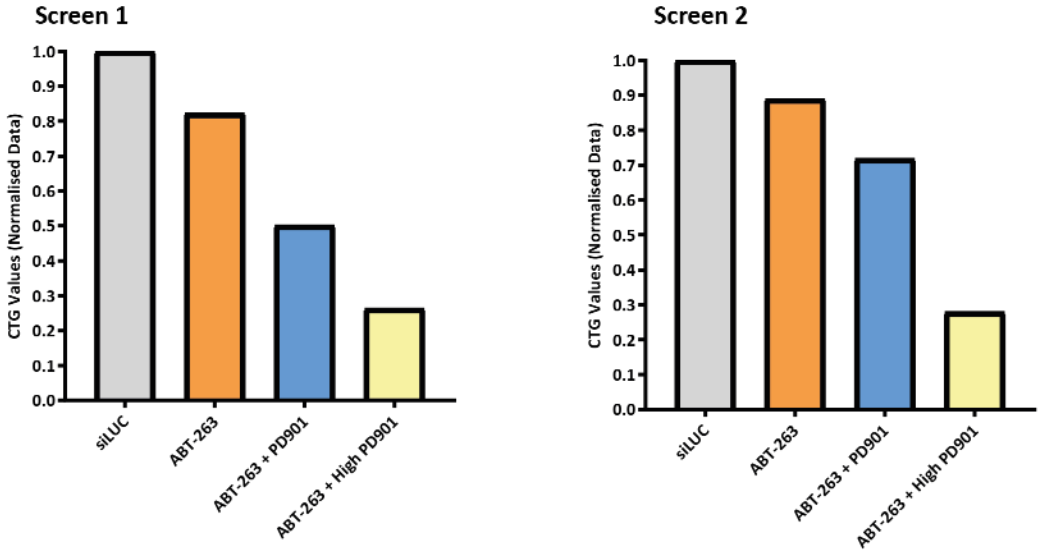

	Normalised (Screen 1/ Screen 2)
siLUC	1.00
ABT-263	0.82/0.89
ABT-263 + PD901	0.50/0.72
ABT-263 + High PD901	0.26/0.28

Figure 5.5 Analysis of RNAi screen controls using CTG viability assay values generated from two, 3-day DUB RNAi screens combined with PD0325901 treatment. Analysis of CTG viability assay values for RNAi controls, including **(A)** the negative siRNA control, siLUC, and **(B)** the positive siRNA controls, siEg5 and siBCL-$_{xL}$, and positive inhibitor controls of ABT-263 (1 µM), with or without PD901 (0.2 µM) or High PD901 (2 µM). All graphs are representative of data generated from a single screen, where all controls were plated at least once on all 8 plates, 8 treated and 8 untreated, tested, and all data was normalised to the siLUC controls across all plates, either treated or untreated for that screen. Collection of CTG viability assay values was performed using the CLARIOstar microplate reader.

as knockdown of that select DUB resulted in a significant reduction in cell viability following treatment with PD901.

A 'hit' DUB was denoted as one in which three or more targeting siRNA caused an increase in SI value, above a set threshold, as a consequence of treatment with PD901. Unfortunately very few 'hit' DUBs were identified from either screen (Figure 5.6B). Comparing both screens only USP29 could be described as 'hit' DUB. However, two out of the four siRNA targeting seven DUBs combined with PD901 to reduce cell viability and generate SI values that were above a set threshold in both screens (Figure 5.6C). Further analysis of normalised CTG values revealed that there was minimal reduction in cell viability following treatment with PD901 compared to knockdown of USP29 alone (Figure 5.6D). Knockdown of USP37 (siRNA1 and siRNA2) and YOD1 (siRNA2 and siRNA3) generated an increase in SI value, when knocked down with two targeting siRNA, in both screens (Figure 5.6D). These are not 'hits' as defined by the original definition however these DUBs are important as they appeared in additional screens described later in this chapter and YOD1 is described in more detail in Chapter 6.

In addition to analysis of the 3-day screens using CTG assay values, the screens were assessed using phase or confluency values, using live cell images generated by the IncuCyte® ZOOM. As previously seen with CTG values, phase values for siLUC were comparable across all plates and combined transfection of HCT116 cells with siLUC and treatment with PD901 resulted in ~34 % reduction in cell density (Figure 5.7A). Transfection of HCT116 cells with the positive siRNA control, siEg5, resulted in a reduction in normalised phase values, with or without PD901 treatment (Figure 5.7B). Additional positive controls, both siBCL-X_L and inhibitor treatment of PD901 and ABT-263, did not cause a significant reduction in confluency (Figure 5.7B). This could be because phase values did not take into account dead cells and as such, data was further analysed as a measure of 'normalised death' or YOYO®-1 value normalised to phase data (Figure 5.7C and Figure 5.7D). As a consequence of YOYO®-1 measuring 'dead' cells it was expected that treatment of transfected HCT116 cells with PD901 would result in an increase in YOYO®-1/Phase value. Indeed controls revealed that treatment of siLUC transfection HCT116 cells with PD901, resulted in an increase in YOYO-1/Phase value for both screens, over all plates (Figure 5.7C). Additionally, transfection of HCT116 with positive siRNA controls, siEg5 and siBCL-X_L, resulted in a substantial increase in YOYO®-1/Phase value indicative of an induction of cell death. Interestingly, a decrease in YOYO®-1/Phase value was observed following treatment with PD901 suggesting that MEK1/2 inhibition rescued HCT116 cells from siEg5-induced cell death. This could be because PD901 treatment induced a G1 cell cycle arrest, stalling cells and preventing them from going through mitosis, thus protecting them from the deleterious effect of Eg5 knockdown

Figure 5.6 Overview of 'hit' DUBs from the 3-day DUB RNAi screens, combined with MEK1/2 inhibitor treatment, generated from SI values from CTG data.

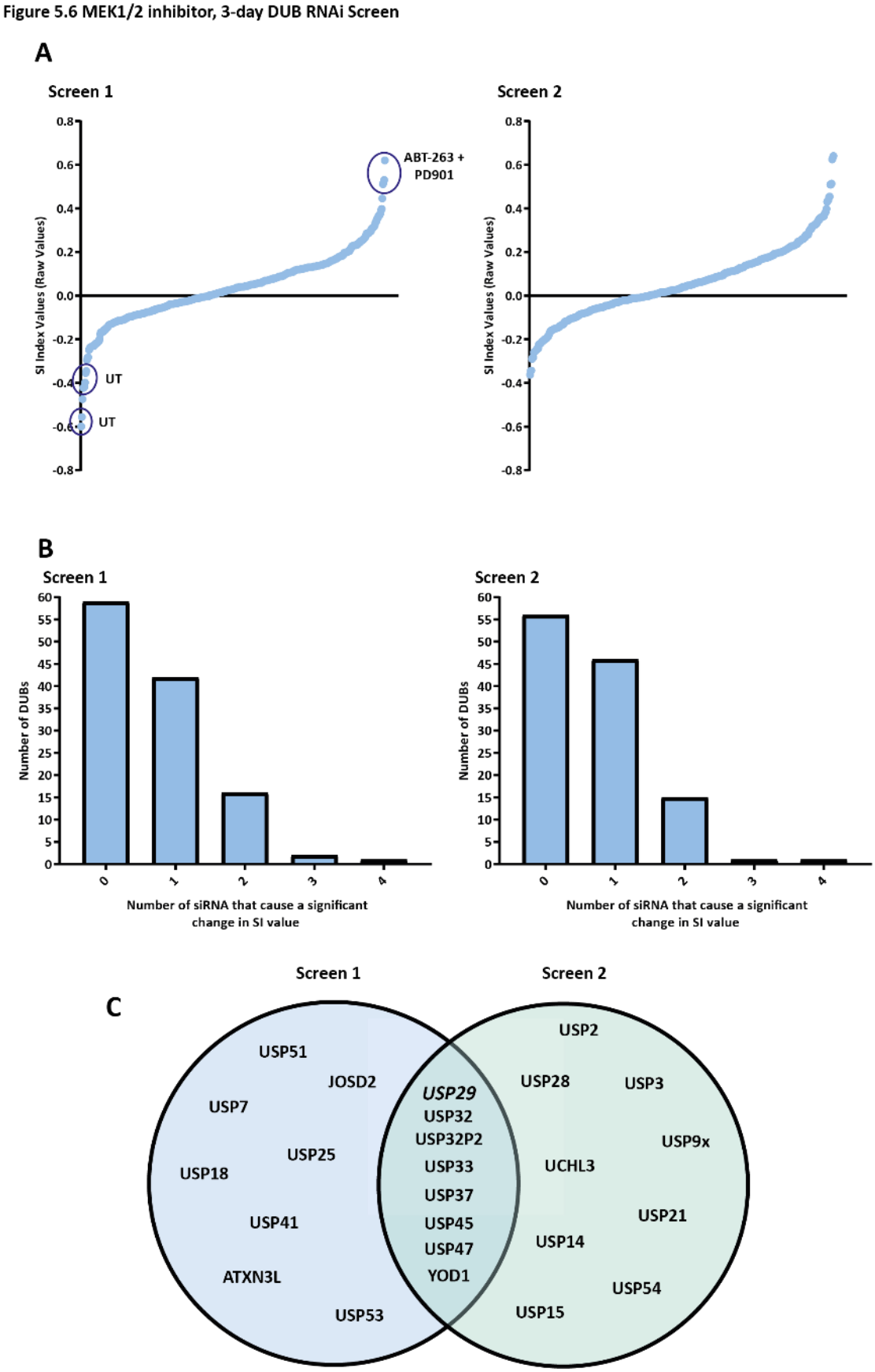

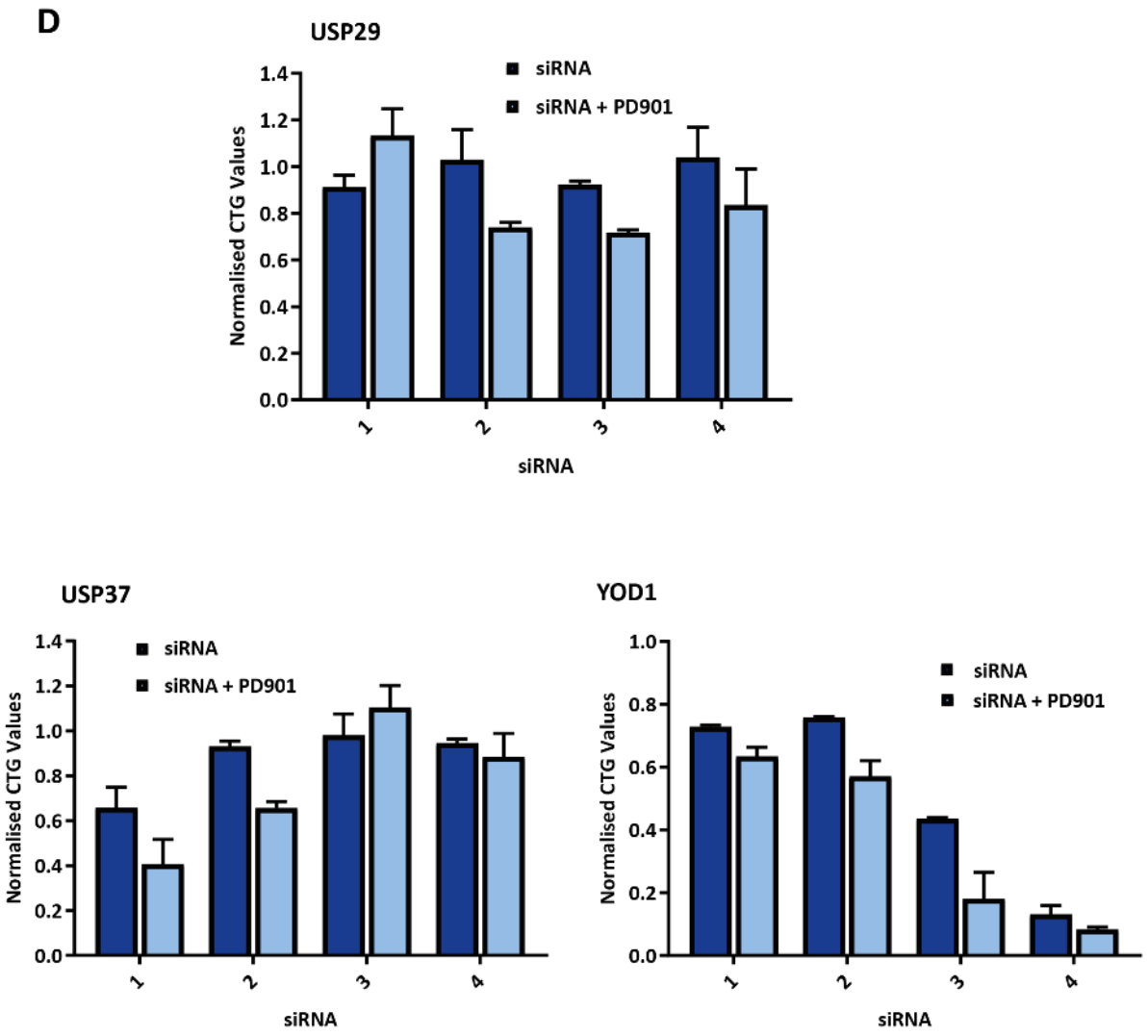

Figure 5.6 Overview of 'hit' DUBs from the 3-day DUB RNAi screens, combined with MEK1/2 inhibitor treatment, generated from SI values from CTG data. (A) Distribution of SI values across two complete screen. Highlighted in the circles are positive and negative inhibitor controls. **(B)** Data representative of the distribution of the number of siRNA for a particular DUB that generated an SI value, above a set threshold, indicative that knockdown of that DUB resulted in sensitisation to PD0325901 (PD901) and resulted in a decrease in cell viability. For example for Screen 1 and Screen 2, two, out of a potential four, siRNA targeting 15 DUBs generated an SI value above the set threshold, indicative that these DUBs combine wih PD901 to cause a decrease in cell viability. **(C)** A venn diagram comparing DUBs in which two or more siRNA for a particular DUB combined with PD901 to reduce cell viability for both 3-day PD901 RNAi screens. **(D)** Bar graphs representative of normalised CTG data for select DUBs. All data was represented as the mean ± SD of the two data sets generated from two 3-day DUB RNAi screen.

Figure 5.7 Analysis of RNAi screen controls using phase and YOYO-1/Phase values generated from the 3-day DUB RNAi screens, combined with MEK1/2 inhibitor treatment.

Figure 5.7 MEK1/2 inhibitor, 3-day DUB RNAi Screen

A: siLUC control

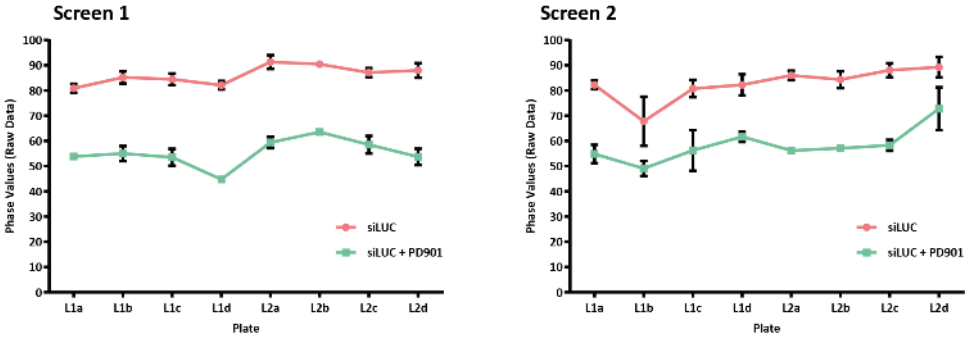

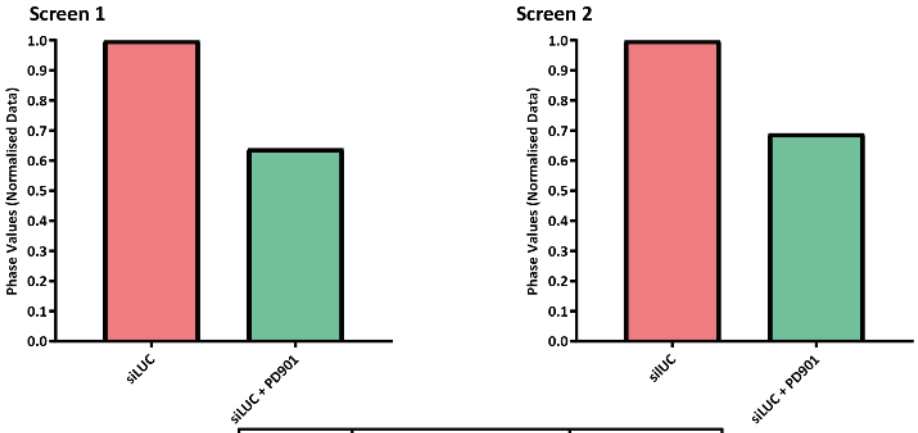

	Average Phase Raw values (Screen 1/ Screen 2)	Normalised (Screen 1/ Screen 2)
siLUC	86.2/82.6	1.00
siLUC + PD901	55.3/56.8	0.64/0.69

B: Positive Controls

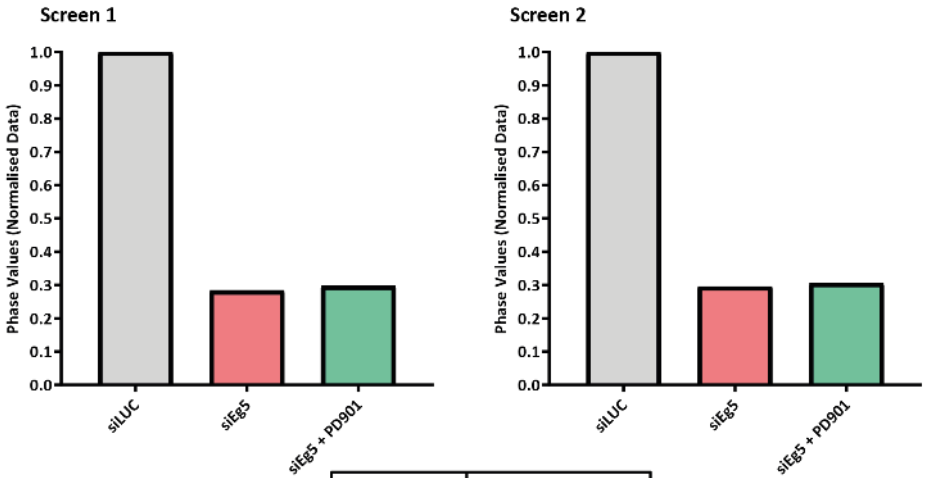

	Normalised (Screen 1/ Screen 2)
siLUC	1.00
siEg5	0.29/0.28
siEg5 + PD901	0.31/0.30

Figure 5.7 MEK1/2 inhibitor, 3-day DUB RNAi Screen

B: Positive Controls

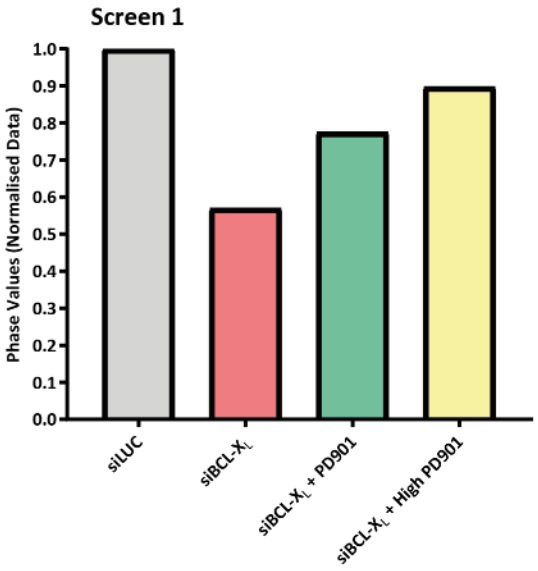

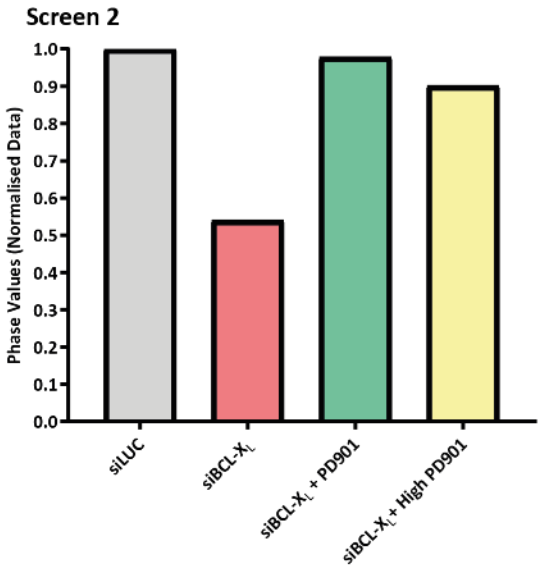

	Normalised (Screen 1/ Screen 2)
siLUC	1.00
siBCL-X_L	0.57/0.54
siBCL-X_L + PD901	0.77/0.98
siBCL-X_L + High PD901	0.90/0.90

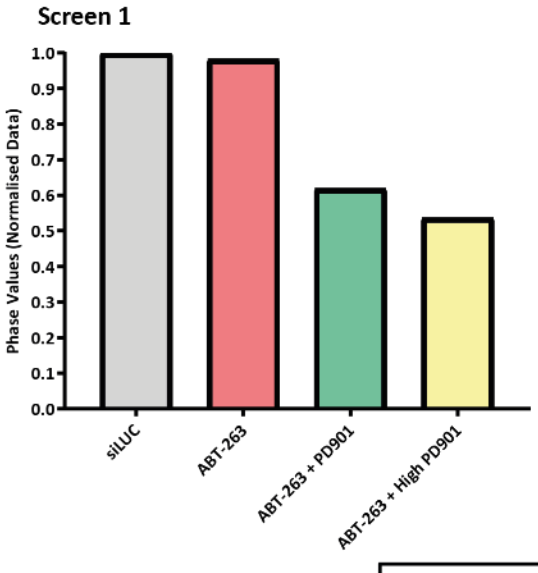

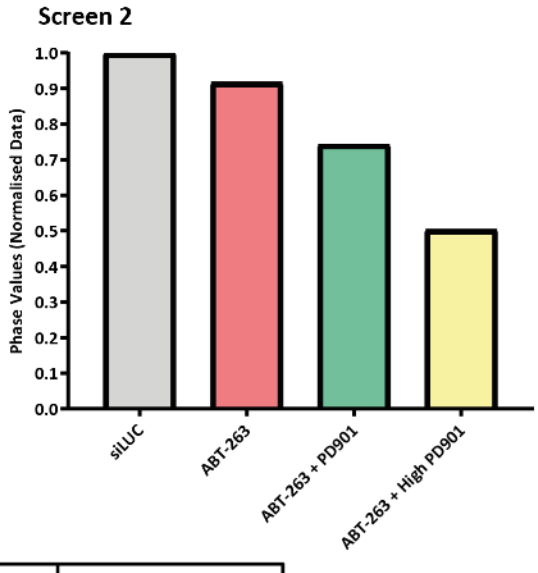

	Normalised (Screen 1/ Screen 2)
siLUC	1.00
ABT-263	0.98/0.91
ABT-263 + PD901	0.62/0.74
ABT-263 + High PD901	0.54/0.50

Figure 5.7 MEK1/2 inhibitor, 3-day DUB RNAi Screen

C: siLUC control

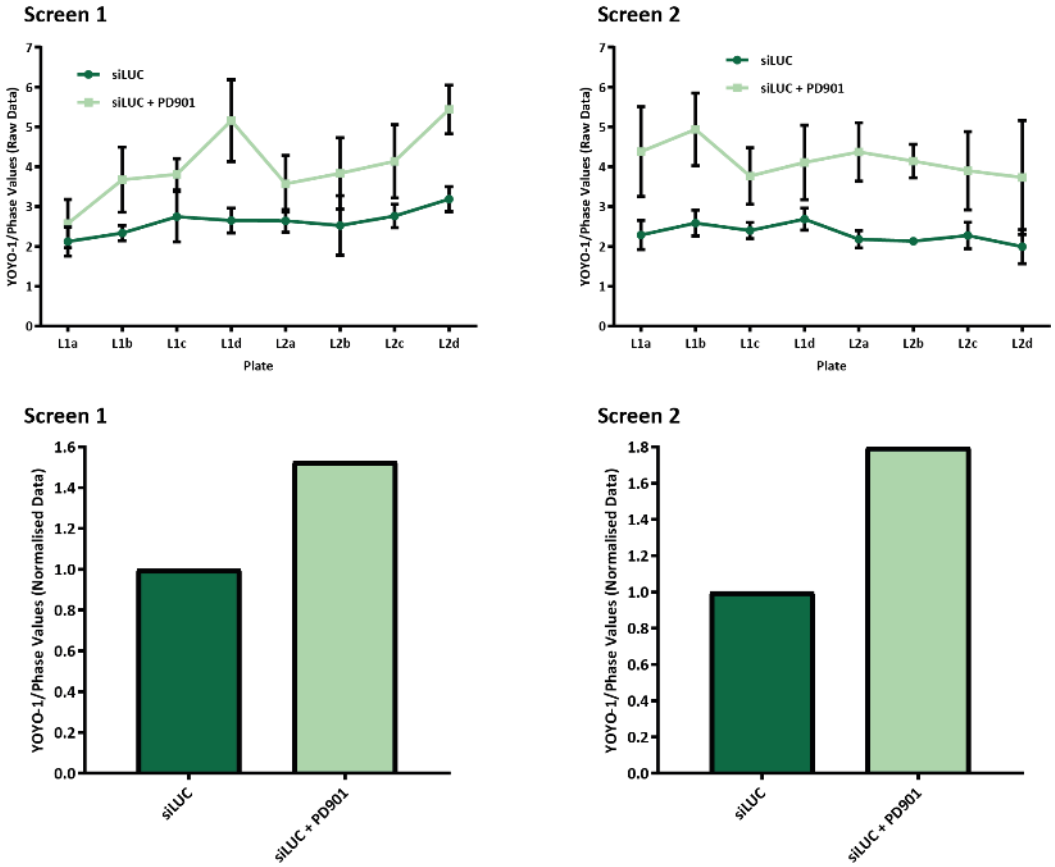

	Average YOYO-1/Phase Raw values (Screen 1/ Screen 2)	Normalised (Screen 1/ Screen 2)
siLUC	2.62/2.32	1.00
siLUC + PD901	4.04/4.17	1.53/1.80

D: Positive Controls

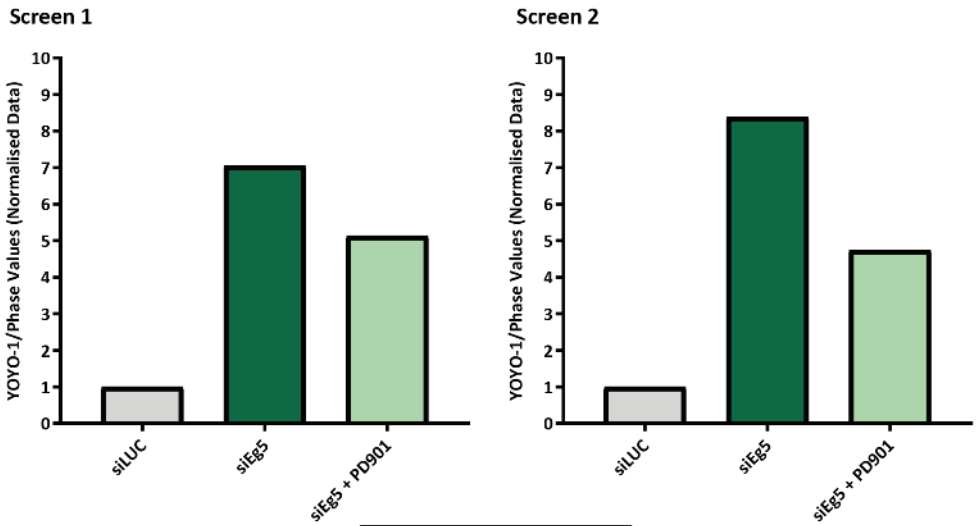

	Normalised (Screen 1/ Screen 2)
siLUC	1.00
siEg5	7.06/8.38
siEg5 + PD901	5.13/4.74

Figure 5.7 MEK1/2 inhibitor, 3-day DUB RNAi Screen

D: Positive Controls

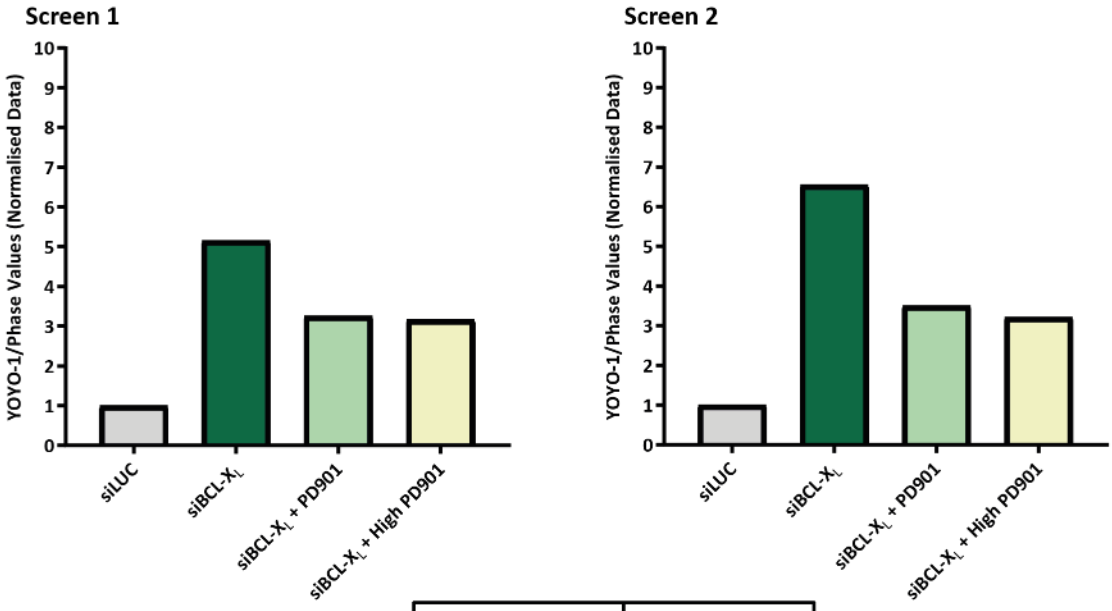

	Normalised (Screen 1/ Screen 2)
siLUC	1.00
siBCL-X_L	5.15/6.55
siBCL-X_L + PD901	3.26/3.50
siBCL-X_L + High PD901	3.16/3.21

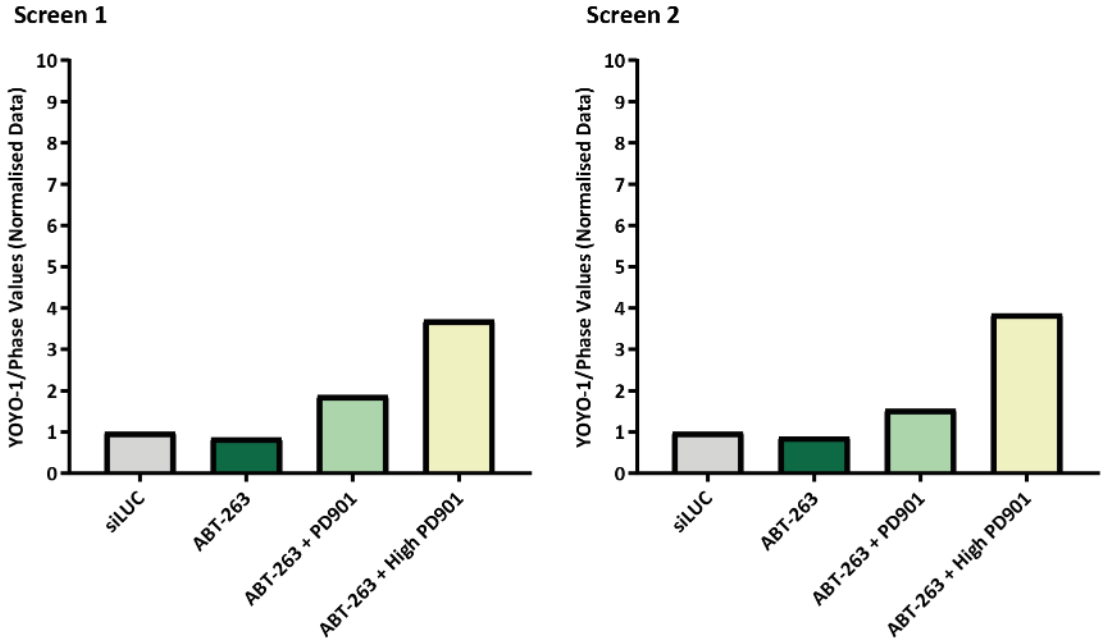

	Normalised (Screen 1/ Screen 2)
siLUC	1.00
ABT-263	0.86/0.88
ABT-263 + PD901	1.89/1.55
ABT-263 + High PD901	3.71/3.86

Figure 5.7 Analysis of RNAi screen controls using phase and YOYO-1/Phase values generated from the 3-day DUB RNAi screens, combined with MEK1/2 inhibitor treatment. Analysis of phase values for RNAi controls, including **(A)** the negative siRNA control, siLUC and **(B)** the positive siRNA controls, siEg5 and siBCL-$_{xL}$, and positive inhibitior controls of ABT-263 (1 μM), with or withour PD0325901 (PD901) (0.2 μM) or High PD901 (2 μM). All graphs are representative of data generated from a single screen, where all controls were plated at least once on all 8 plates, 8 treated and 8 untreated, tested, and all data was normalised to the siLUC controls across all plates, either treated or untreated for that screen. Phase values were generated as a percentage confluency (Phase Object Confluence), using the IncuCyte data analysis programme, Basic Analyser, with and an optimised 'Confluence Mask' to count all cells from live cell images taken by the IncuCyte ZOOM. Four images were taken for each well and phase values were an average percentage confluency from these four images. Analysis of YOYO-1/Phase values for RNAi controls, including **(C)** the negative siRNA control, siLUC and **(D)** the positive siRNA controls, siEg5 and siBCL-$_{xL}$, and positive inhibitior controls of ABT-263 (1 μM), with or withour PD901 (0.2 μM) or High PD901 (2 μM). All graphs are representative of data generated from a single screen, where all controls were plated at least once on all 8 plates, 8 treated and 8 untreated, tested, and all data was normalised to the siLUC controls across all plates, either treated or untreated for that screen. YOYO-1 data was measured as counts/images using the IncuCyte data analysis programme, Basic Analyser, with and optimised cell mask to count all fluorscent cells from live cell images taken by the IncuCyte ZOOM, where four images were taken for each well and YOYO-1 values were an average cell count from these four images. Phase values were generated as a percentage confluency (Phase Object Confluence), using the IncuCyte data analysis programme, Basic Analyser, with an optimised 'Confluence Mask' to count all cells from live cell images taken by the IncuCyte ZOOM. Four images were taken for each well and phase values were an average percentage confluency from these four images.

which, under normal circumstances, is required for centrosome separation and spindle assembly during mitosis.

Treatment of HCT116 cells with PD901 and ABT-263 resulted in an increase in cell death compared to treatment with ABT-263 alone or transfection with siLUC (Figure 5.7D). Despite an increase in YOYO®-1/Phase following treatment with PD901 the screens were deemed valid and based on YOYO®-1/Phase, was further analysed to look for 'hit' DUBs.

The distribution of all SI values generated from YOYO®-1/Phase data for the two 3-day screens were comparable to that seen from SI values generated from CTG values (Figure 5.8A). For SI values generated from YOYO®-1/Phase data, negative SI values, below a set threshold, indicated that targeted knockdown of the DUB resulted in sensitisation of HCT116 cells to PD901 treatment and resulted in significant induction in cell death. As previously seen from CTG data, very few 'hit' DUBs were identified from the two 3-day screens (Figure 5.8B). Comparing 'hit' DUBs, from screen 1, to DUBs, from screen 2, in which two out of four siRNA resulted in a significant reduction in SI value, revealed that USP37 and USP43 were found to cause a cell death response following knockdown and PD901 treatment in both screens (Figure 5.8C). Further analysis of USP37 and USP43 normalised phase and YOYO®-1/Phase values revealed that it matched that seen from SI analysis, as knockdown of USP37 and USP43 with at least two siRNA combined with PD901 to cause a marginal increase in YOYO®-1/Phase value or an induction of cell death(Figure 5.8D).

To complete the analysis of this screen changes in 'normalised cell death' were analysed using SI values generated from YOYO®-1/CTG values (Figure 5.9). As previously seen, very few 'hit' DUBs were observed using YOYO®-1/CTG data (Figure 5.9B). Several DUBs were found to be 'hit' DUBs in both 3-day screens (Figure 5.9C). However, comparing 'hit' DUBs from YOYO®-1/CTG data to DUBs in which at least 2 siRNA combined with MEK1/2 inhibition to cause a significant decrease SI value revealed that knockdown of USP37 was the only DUB to sensitise HCT116 to PD901 treatment (Figure 5.9D). Further analysis of normalised CTG and YOYO®-1/CTG data for knockdown of USP37, with or without PD901 treatment is shown in Figure 5.9E.

Unfortunately very few and no consistent 'hit' DUBs were identified from the 3-day DUB RNAi screens, in combination with MEK1/2 inhibition. There were several DUBs in which two siRNA for a select DUB combined with PD901 to induce a cell death response, however ideally for further experiments at least three siRNA, in combination with PD901, were required to cause a significant increase in cell death. Thus, a longer screen was performed to assess if an extended period of siRNA knockdown and inhibitor treatment was required to induce a cytotoxic effect in HCT116 cells.

Figure 5.8 Overview of 'hit' DUBs from the 3-day DUB RNAi screen, combined with MEK1/2 inhibitor treatment, generated from SI values from YOYO-1/Phase data.

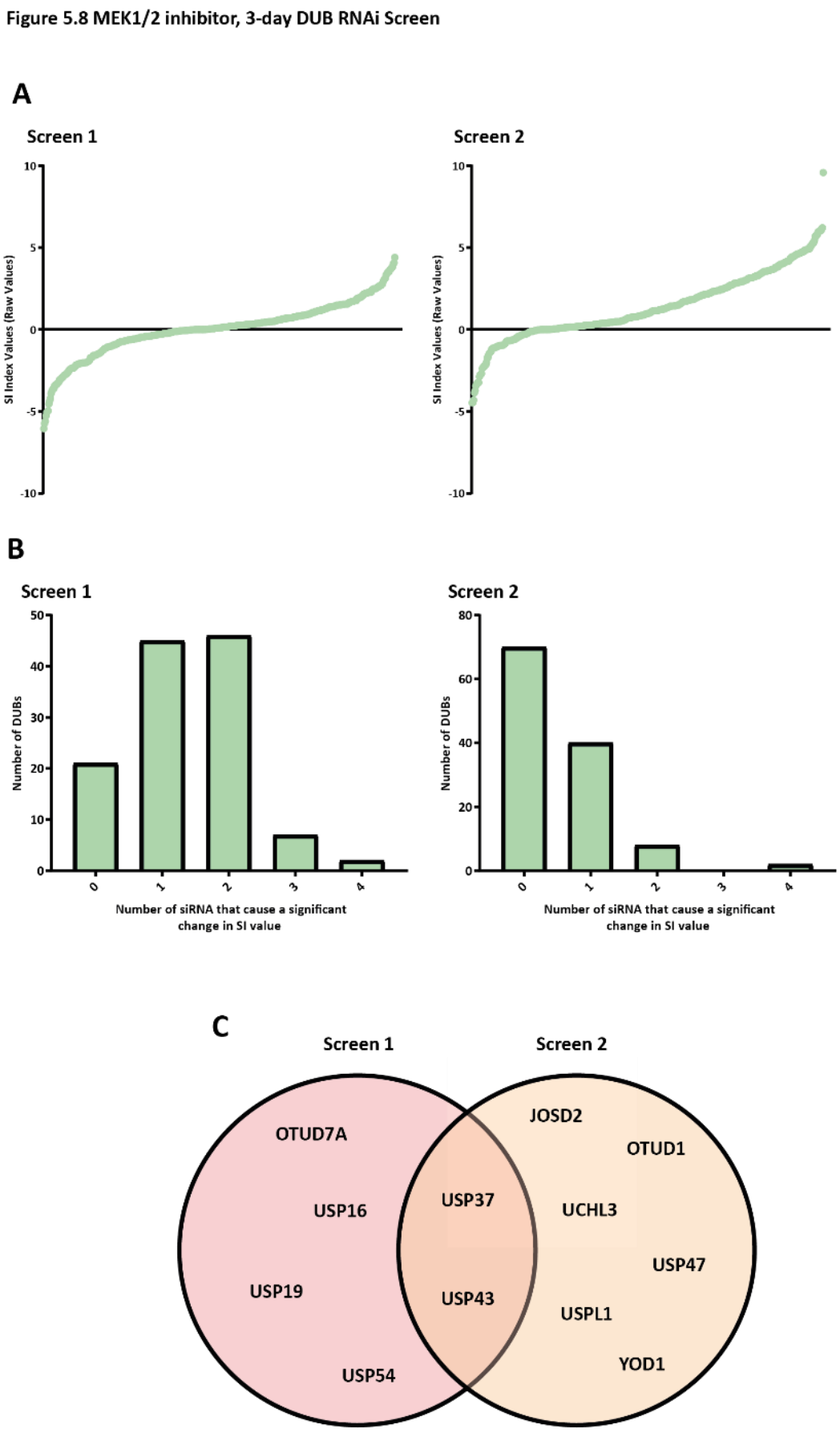

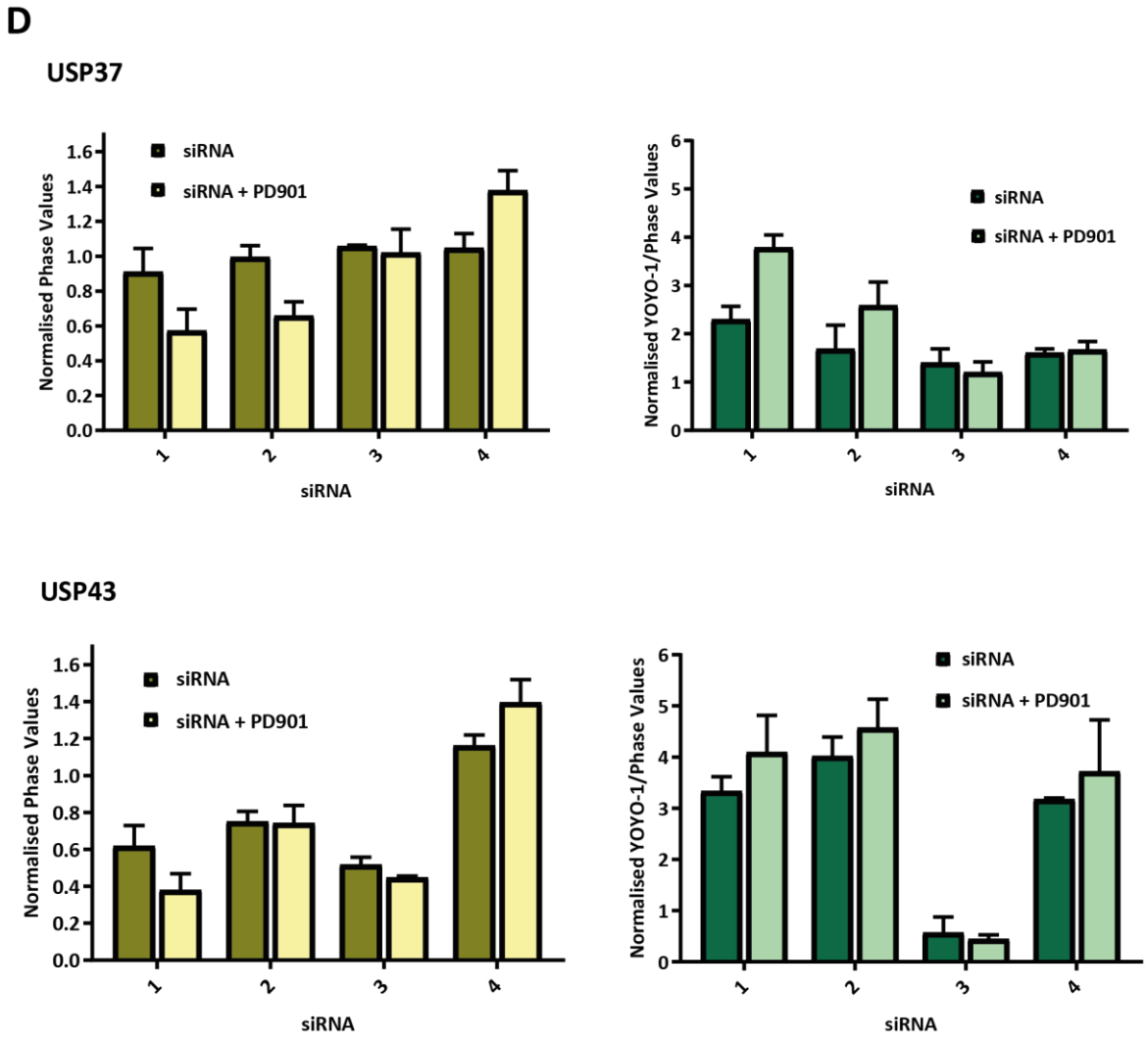

Figure 5.8 Overview of 'hit' DUBs from the 3-day DUB RNAi screen, combined with MEK1/2 inhibitor treatment, generated from SI values from YOYO-1/Phase data. (A) Distribution of SI values across complete screen. **(B)** Data representative of the distribution of the number of siRNA for a particular DUB that generated an SI value, below a set threshold, indicative that knockdown of that DUB resulted in sensitisation to PD901 and resulted in a cytoxic effect. For example for Screen 1 and Screen 2, two, out of a potential four, siRNA targeting 46 and eight DUBs, respectively, generated an SI value below the set threshold, indicative that these DUBs combine wih PD901 to cause a cell death response. **(C)** A venn diagram comparing 'hit' DUBs from the 3-day DUB RNAi screens. As no 3 siRNA 'hits' were observed from Screen 2, the DUBs identified, when knocked down with two siRNA, to combine with MEK1/2 inhibition from Screen 2 were compared to the 3 siRNA 'hits' obtained from Screen 1. **(D)** Bar graphs representative of normalised Phase data and YOYO-1/Phase data for each 'hit' DUB. All data was represented as the mean ± SD of the two data sets generated from two 3-day DUB RNAi screens.

Figure 5.9 Overview of 'hit' DUBs from the 3-day DUB RNAi screen, combined with MEK1/2 inhibitor treatment, generated from SI values from YOYO-1/CTG data.

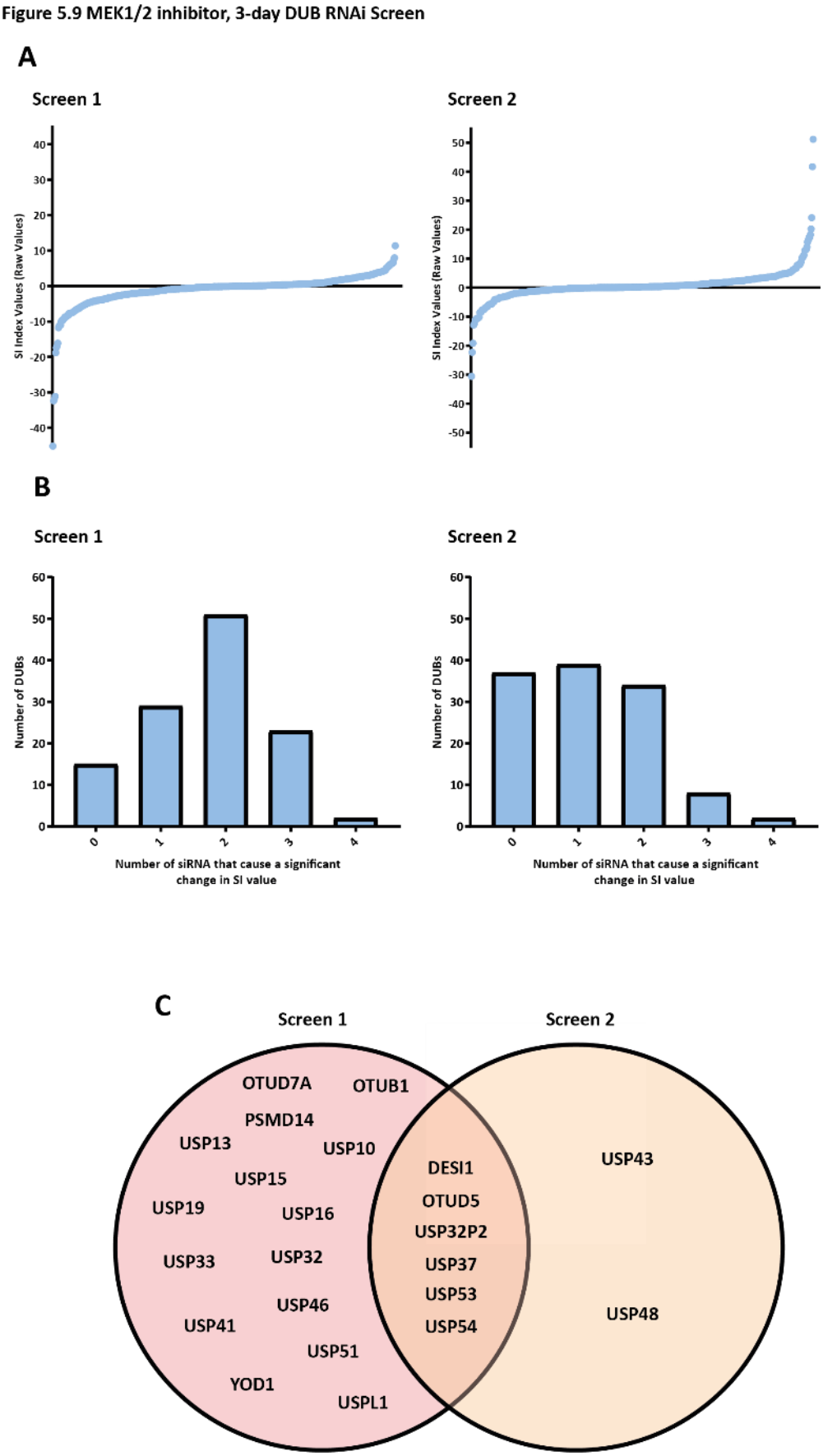

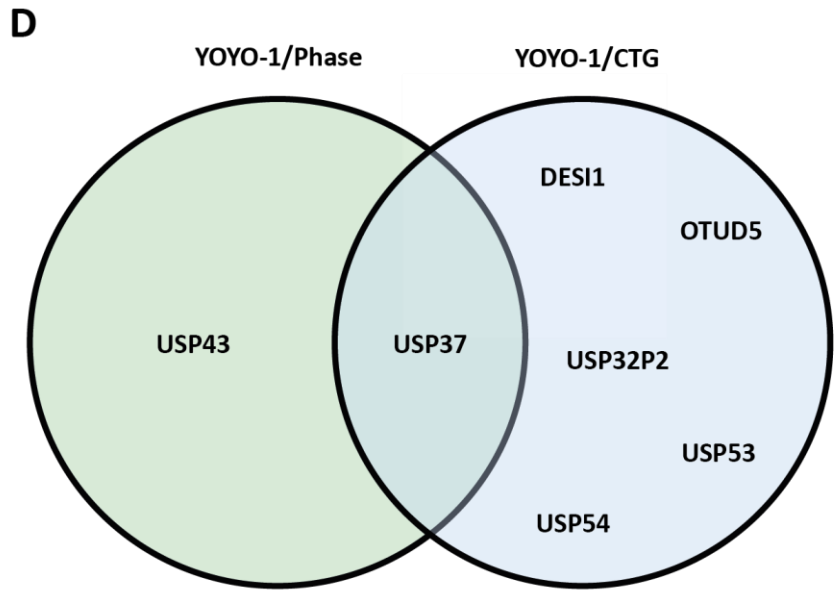

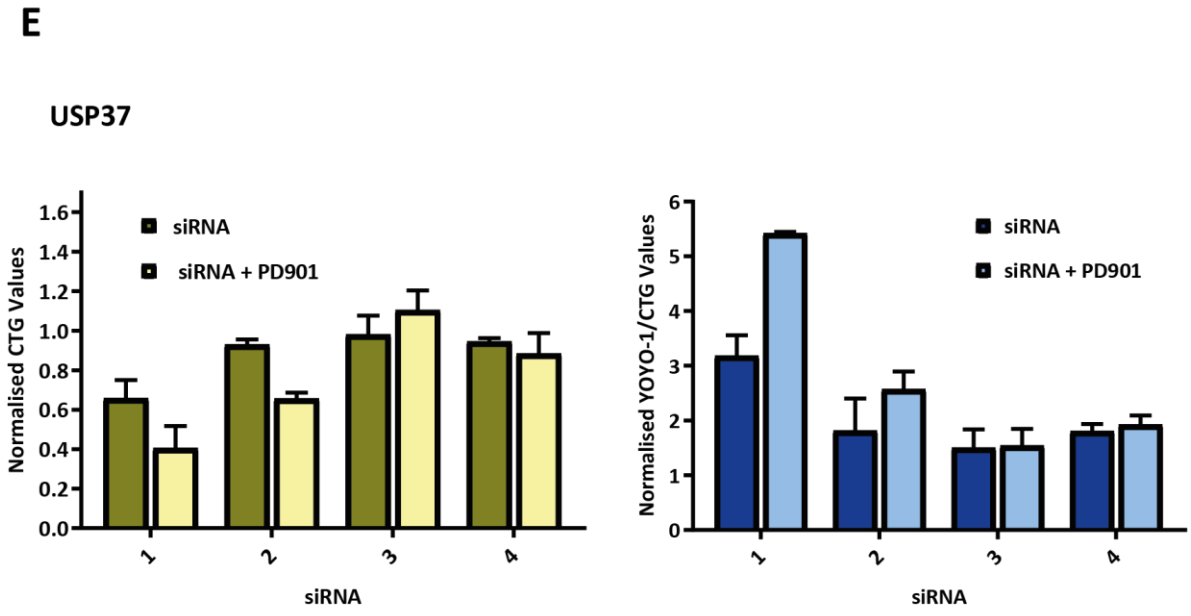

Figure 5.9 Overview of 'hit' DUBs from the 3-day DUB RNAi screen, combined with MEK1/2 inhibitor treatment, generated from SI values from YOYO-1/CTG data. (A) Distribution of SI values across complete screen. **(B)** Data representative of the distribution of the number of siRNA for a particular DUB that generated an SI value, below a set threshold, indicative that knockdown of that DUB resulted in sensitisation to PD0325901 (PD901) and resulted in a cytoxic effect. For example for Screen 1 and Screen 2, two, out of a potential four, siRNA targeting 51 and 34 DUBs, respectively, generated an SI value below the set threshold, indicative that these DUBs combine wih PD901 to cause a cell death response. **(C)** A venn diagram comparing 'hit' DUBs from the 2, 3-day DUB RNAi screens, generated using normalised YOYO-1/CTG data. **(D)** A venn diagram comparing 'hit' DUBs generated from YOYO-1/CTG data to YOYO-1/Phase data representative of DUBs in which, when knocked down with at least 2 siRNA, combined with MEK1/2 inhibition to cause a substantial cell death response, from the 3-day DUB RNAi screens. **(E)** A bar graph representative of normalised Phase data and YOYO-1/CTG data for USP37, the 'hit' DUB from both normalised YOYO-1/Phase and YOYO-1/CTG data from both PD901 DUB RNAi screens. All data was represented as the mean ± SD of the two data sets generated from the two 3-day DUB RNAi screens.

5.2.2.2. Analysis of data generated from the 5-day combined DUB RNAi and PD0325901 screen.

Analysis of the CTG assay values, from one 5-day DUB RNAi screen, revealed that the CTG values for the transfection control, siLUC, were consistent across all plates and that knockdown of siLUC in combination with PD901 resulted in a 36 % reduction in cell viability (Figure 5.10A). Similar to this, analysis of confluency, using phase values, were consistent for knockdown of siLUC across all plates and that combined knockdown of siLUC and inhibition of MEK1/2 resulted in a 30 % reduction in confluency (Figure 5.10C). All positive controls, including the siRNA controls, siEg5 and siBCL-X_L, with or without PD901 treatment, and the inhibitor control, PD901 and ABT-263, showed a reduction in CTG value (Figure 5.10B) as well as phase value (Figure 5.10D), compared to siLUC controls. Given all of this, this screen was considered reliable and as such 'hits' generated from this screen could be used for further analysis.

YOYO®-1 data, normalised to phase values, was analysed to see if knockdown of a DUB, in combination with PD901, induced a cell death response. For a 'hit' DUB, knockdown of a DUB should result in low YOYO®-1/Phase values and be comparable to transfection controls, however, following treatment with PD901 there should be a substantial increase in YOYO®-1/Phase values. Reanalysis of controls using YOYO®-1/Phase values revealed similar trends to that seen in the 3-day DUB RNAi screens (Figure 5.10E and Figure 5.10F). As expected transfection or treatment of HCT116 cells with positive controls, both siRNA and inhibitor controls, resulted in an increase in YOYO®-1/Phase values, compared to siLUC controls, indicative of a cytotoxic effect (Figure 5.10E). As a result of this 'hit' DUBs were evaluated using this SI values generated from YOYO®-1/Phase values.

An overview of all SI values, generated from YOYO®-1/Phase values, from the 5-day DUB RNAi screen revealed that SI values were evenly distributed, with the positive controls possessing the most negative SI values and conversely the negative controls possessing the most positive SI values (Figure 5.11A). Consolidating all SI values from all four siRNA against a select DUB, in combination with PD901, a 'hit' was classed as one in which three or more siRNA combined with PD901 to generate a significant decrease in SI value, below a set threshold, compared to siLUC controls as well as knockdown of the DUB alone. For the 5-day DUB RNAi screen, 20 DUBs were classed as 'hit' DUBs and knockdown of these DUBs combined with PD901 to induce cell death (Figure 5.11B and Figure 5.11C).

Further analysis of these 20 'hit' DUBs, revealed that several hits induced a substantial reduction in phase value following knockdown of that DUB alone. Therefore, these DUBs could be described as 'essential' for the survival of HCT116 cells and that combined knockdown of the DUB and MEK1/2

Figure 5.10 Analysis of RNAi screen controls using CTG viability assay, phase and YOYO-1/Phase values generated from the 5-day DUB RNAi screen, combined with MEK1/2 inhibitor treatment.

Figure 5.10 MEK1/2 inhibitor, 5-day DUB RNAi Screen

A: siLUC control

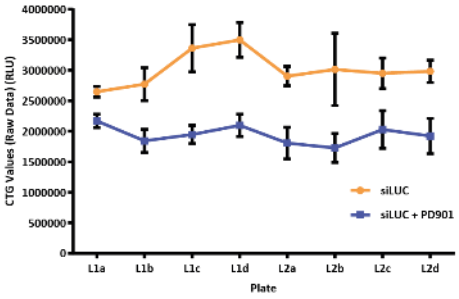

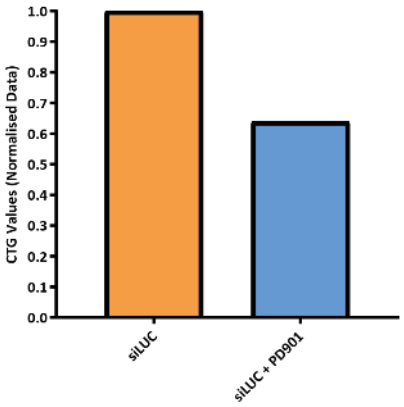

	Average CTG Raw values (RLU)	Normalised
siLUC	3015609	1.00
siLUC + PD901	1942510	0.64

B: Positive Controls

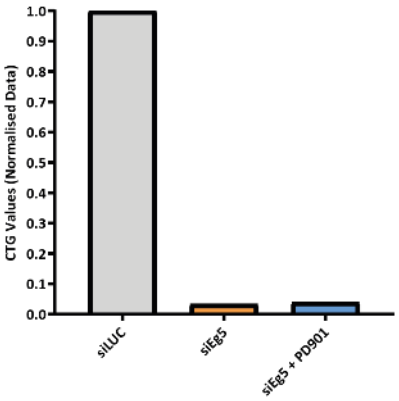

	Normalised
siLUC	1.00
siEg5	0.03
siEg5 + PD901	0.04

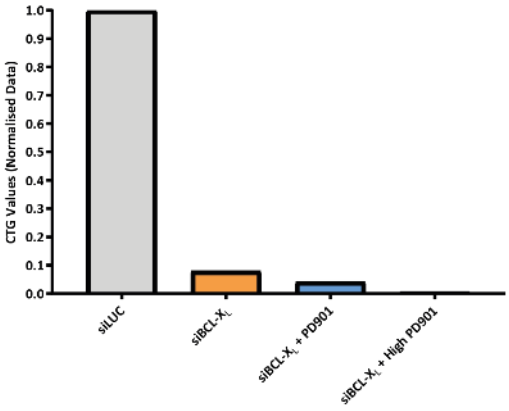

	Normalised
siLUC	1.00
siBCL-X_L	0.08
siBCL-X_L + PD901	0.04
siBCL-X_L + High PD901	0.01

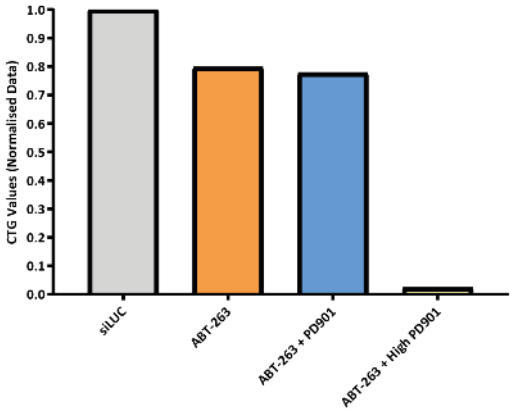

	Normalised
siLUC	1.00
ABT-263	0.80
ABT-263 + PD901	0.78
ABT-263 + High PD901	0.02

Figure 5.10 MEK1/2 inhibitor, 5-day DUB RNAi Screen

C: siLUC control

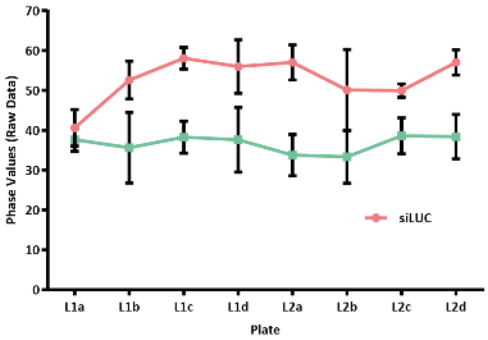

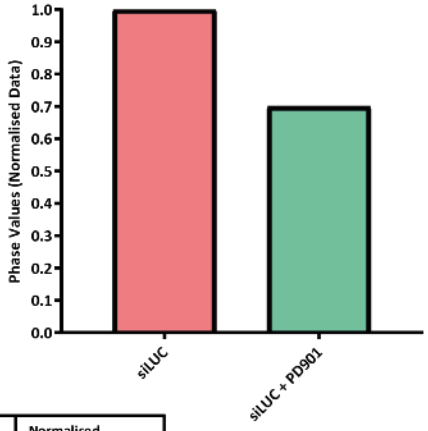

	Average Phase Raw values	Normalised
siLUC	52.7	1.00
siLUC + PD901	36.7	0.70

D: Positive Controls

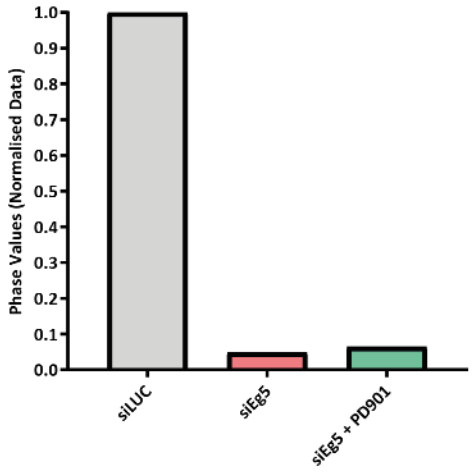

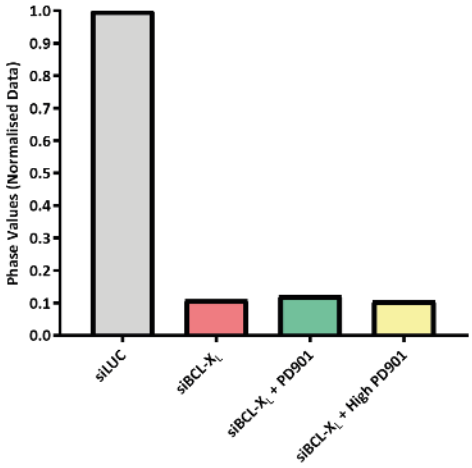

	Normalised
siLUC	1.00
siEg5	0.05
siEg5 + PD901	0.06

	Normalised
siLUC	1.00
siBCL-X_L	0.11
siBCL-X_L + PD901	0.12
siBCL-X_L + High PD901	0.11

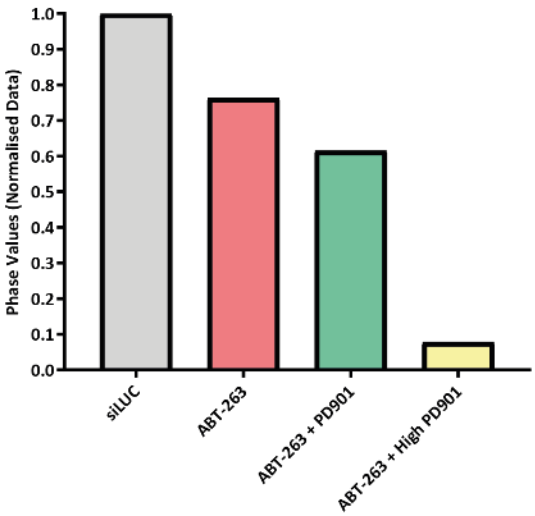

	Normalised
siLUC	1.00
ABT-263	0.76
ABT-263 + PD901	0.61
ABT-263 + High PD901	0.08

Figure 5.10 MEK1/2 inhibitor, 5-day DUB RNAi Screen

E: siLUC control

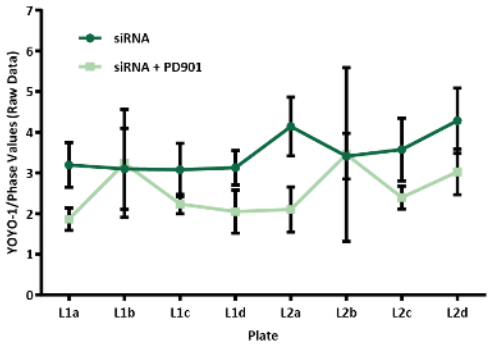

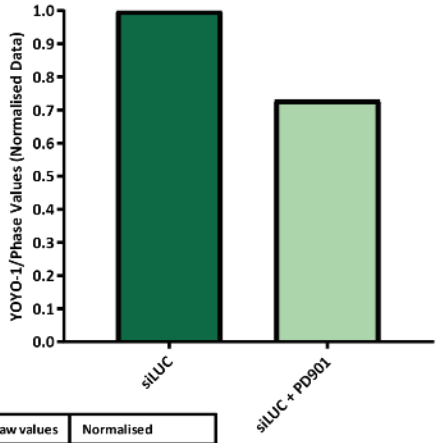

	Average YOYO-1/Phase Raw values	Normalised
siLUC	3.49	1.00
siLUC + PD901	2.54	0.73

F: Positive Controls

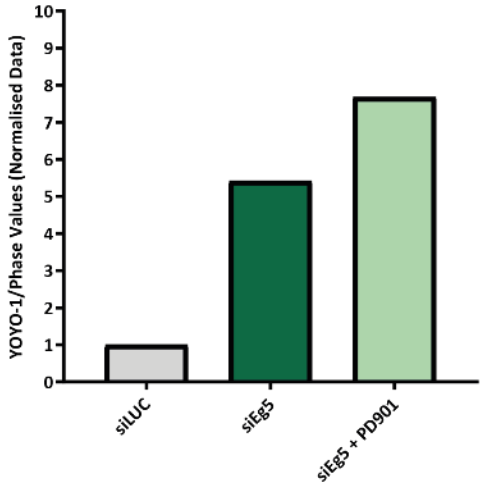

	Normalised
siLUC	1.00
siEg5	5.41
siEg5 + PD901	7.68

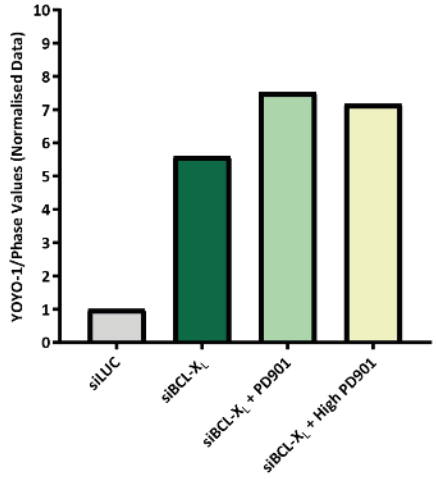

	Normalised
siLUC	1.00
siBCL-X_L	19.5
siBCL-X_L + PD901	19.1
siBCL-X_L + High PD901	18.2

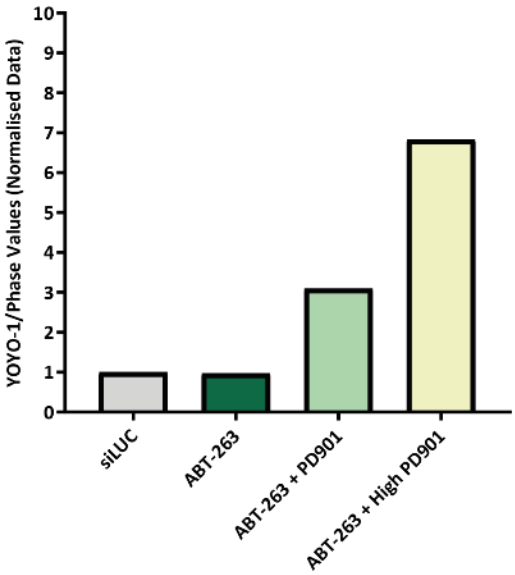

	Normalised
siLUC	1.00
ABT-263	0.97
ABT-263 + PD901	3.09
ABT-263 + High PD901	6.83

Figure 5.10 Analysis of RNAi screen controls using CTG viability assay, phase and YOYO-1/Phase values generated from the 5-day DUB RNAi screen, combined with MEK1/2 inhibitor treatment. Analysis of CTG viability assay values for RNAi controls, including **(A)** the negative siRNA control, siLUC and **(B)** the positive siRNA controls, siEg5 and siBCL-$_{xL}$, and positive inhibitior controls of ABT-263 (1 μM), with or without PD0325901 (PD901) (0.03 μM) or High PD901 (0.3 μM). All graphs are representative of data generated from one screen, where all controls were plated at least once on all 8 plates, 8 treated and 8 untreated, tested, and all data was normalised to the siLUC controls across all plates, either treated or untreated for that screen. Collection of CTG viability assay values was performed using the CLARIOstar microplate reader. Analysis of phase values for RNAi controls, including **(C)** the negative siRNA control, siLUC and **(D)** the positive siRNA controls, siEg5 and siBCL-$_{xL}$, and positive inhibitior controls of ABT-263 (1 μM), with or withour PD901 (0.03 μM) or High PD901 (0.3 μM). All graphs are representative of data generated from one screen, where all controls were plated at least once on all 8 plates, 8 treated and 8 untreated, tested, and all data was normalised to the siLUC controls across all plates, either treated or untreated for that screen. Phase values were generated as a percentage confluency (Phase Object Confluence), using the IncuCyte data analysis programme, Basic Analyser, with an optimised 'Confluence Mask' to count all cells from live cell images taken by the IncuCyte ZOOM. Four images were taken for each well and phase values were an average percentage confluency from these four images. Analysis of YOYO-1/Phase values for RNAi controls, including **(E)** the negative siRNA control, siLUC and **(F)** the positive siRNA controls, siEg5 and siBCL-$_{xL}$, and positive inhibitior controls of ABT-263 (1 μM), with or withour PD901 (0.03 μM) or High PD901 (0.3 μM). All graphs are representative of data generated from one screen, where all controls were plated at least once on all 8 plates, 8 treated and 8 untreated, tested, and all data was normalised to the siLUC controls across all plates, either treated or untreated for that screen. YOYO-1 data was measured as counts/images using the IncuCyte data analysis programme, Basic Analyser, with and optimised cell mask to count all fluorscent cells from live cell images taken by the IncuCyte ZOOM, where four images were taken for each well and YOYO-1 values were an average cell count from these four images. Phase values were generated as a percentage confluency (Phase Object Confluence), using the IncuCyte data analysis programme, Basic Analyser, with and an optimised 'Confluence Mask' to count all cells from live cell images taken by the IncuCyte ZOOM. Four images were taken for each well and phase values were an average percentage confluency from these four images.

inhibition induced cell death in already 'dying' cells. An example of this was seen with knockdown of PSMD14. Here, all siRNA targeting PSMD14 caused a considerable reduction in confluency, or phase, compared to siLUC controls. In accordance with this, knockdown of PSMD14 resulted in high YOYO®-1/Phase values and combining knockdown with PD901 only resulted in a marginal increase in cell death (Supplementary Information). Interestingly, results were inconsistent with different siRNA targeting the same DUB. For example, one siRNA targeting BRCC3 did not cause a reduction in cell number, whilst knockdown of BRCC3, alone, with the remaining three siRNA caused a substantial reduction in normalised phase values (Supplementary Information). Based on SI analysis several 'hit' DUBs, including USP10, USP16, TNFAIP3, VCIP135, and YOD1, were taken forward for further analysis, described in Chapter 6 (Figure 5.11D and Supplementary Information). For these 'hit' DUBs all siRNA targeting these DUBs should be consistent and ideally cause minimal reduction in phase value when transfected into HCT116 cells without inhibitor treatment.

Again, as a final analysis of 'normalised cell death', following knockdown of a DUB, in combination with PD901, SI values were generated and evaluated using YOYO®-1/CTG data (Figure 5.12A and Figure 5.12B). Comparing 'hit' DUBs generated from YOYO®-1/Phase SI values with 'hit' DUBs generated from YOYO®-1/CTG SI values revealed that several DUBs overlapped from both analysis approaches (Figure 5.12C). Further analysis of several overlapping 'hit' DUBs are shown in Figure 5.12D. For these 'hit' DUBs treatment of transfected HCT116 cells with PD901 resulted in a reduction in CTG value and an increase in YOYO®-1/CTG value, compared to values generated from knockdown of the DUB alone. This suggested that knockdown of these DUBs sensitised HCT116 cells to PD901 treatment. These DUBs were chosen and they are later described in more detail, and the effect of knockdown of these DUBs, in combination with PD901 is shown in Chapter 6. Due to the lack of 'hits' generated from the 3-day DUB RNAi screens it was challenging to compare 'hits' from the 3-day and 5-day DUB RNAi screen and define DUBs that sensitise HCT116 cells at 'early' and 'late' time points.

5.2.3. RNAi screen to identify DUBs that synergise with the mTOR inhibitor, AZD8055, to induce a cell death response.

Analysis of the phase values for controls generated, from one 3-day DUB RNAi screen with the mTOR inhibitor AZD8055 (8055), revealed that the phase values for the transfection control, siLUC, were consistent across all plates and that knockdown of siLUC, in combination 8055, resulted in a 33 % reduction in cell confluency (Figure 5.13A). Similar to that seen in the other DUB RNAi screens, knockdown of positive siRNA controls, either alone or in combination with 8055 resulted in a

Figure 5.11 Overview of 'hit' DUBs from the 5-day DUB RNAi screen, treated with a MEK1/2 inhibitor, generated from SI values from YOYO-1/Phase data.

Figure 5.11. MEK1/2 inhibitor, 5-day DUB RNAi Screen

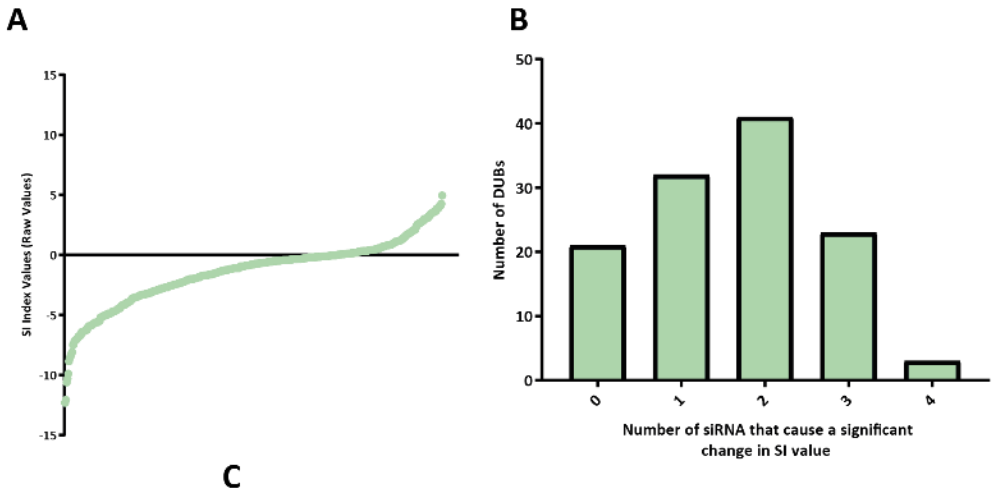

C

Number of siRNA that cause a significant change in SI value:	3	3	4
	BRCC3	USP20	USP31
	EIF3F	USP32P2	USPL1
	PSMD14	USP36	
	SENP5	USP39	
	TNFAIP3	USP41	
	UCHL1	USP44	
	USP10	USP51	
	USP11	YOD1	
	USP16	VCIP135	

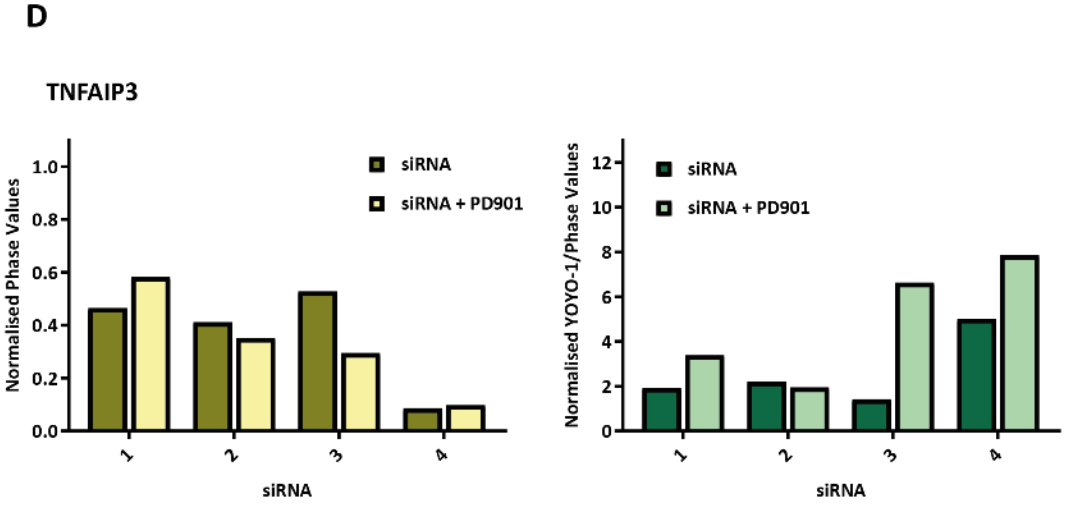

Figure 5.11 MEK1/2 inhibitor, 5-day DUB RNAi Screen

D

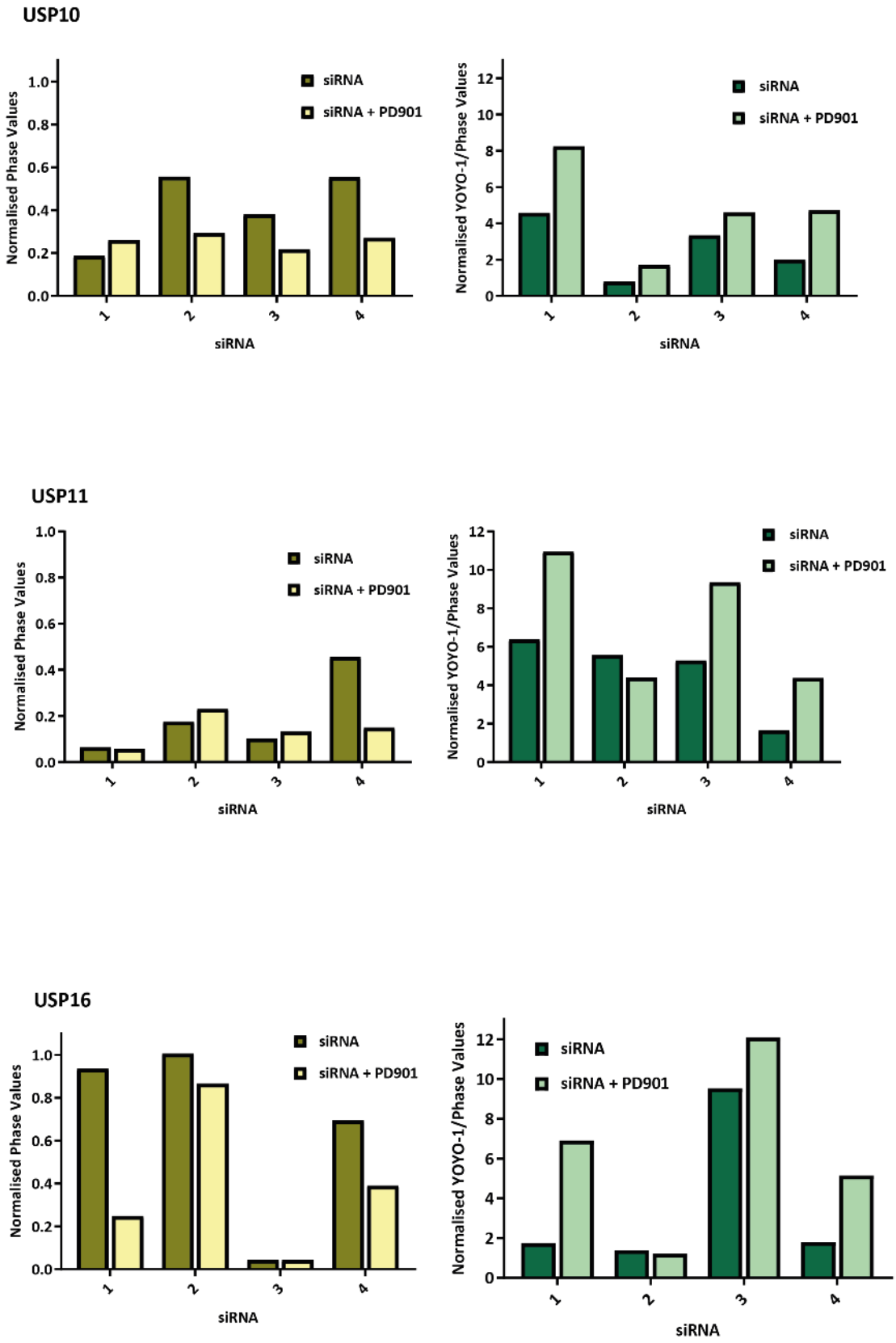

D

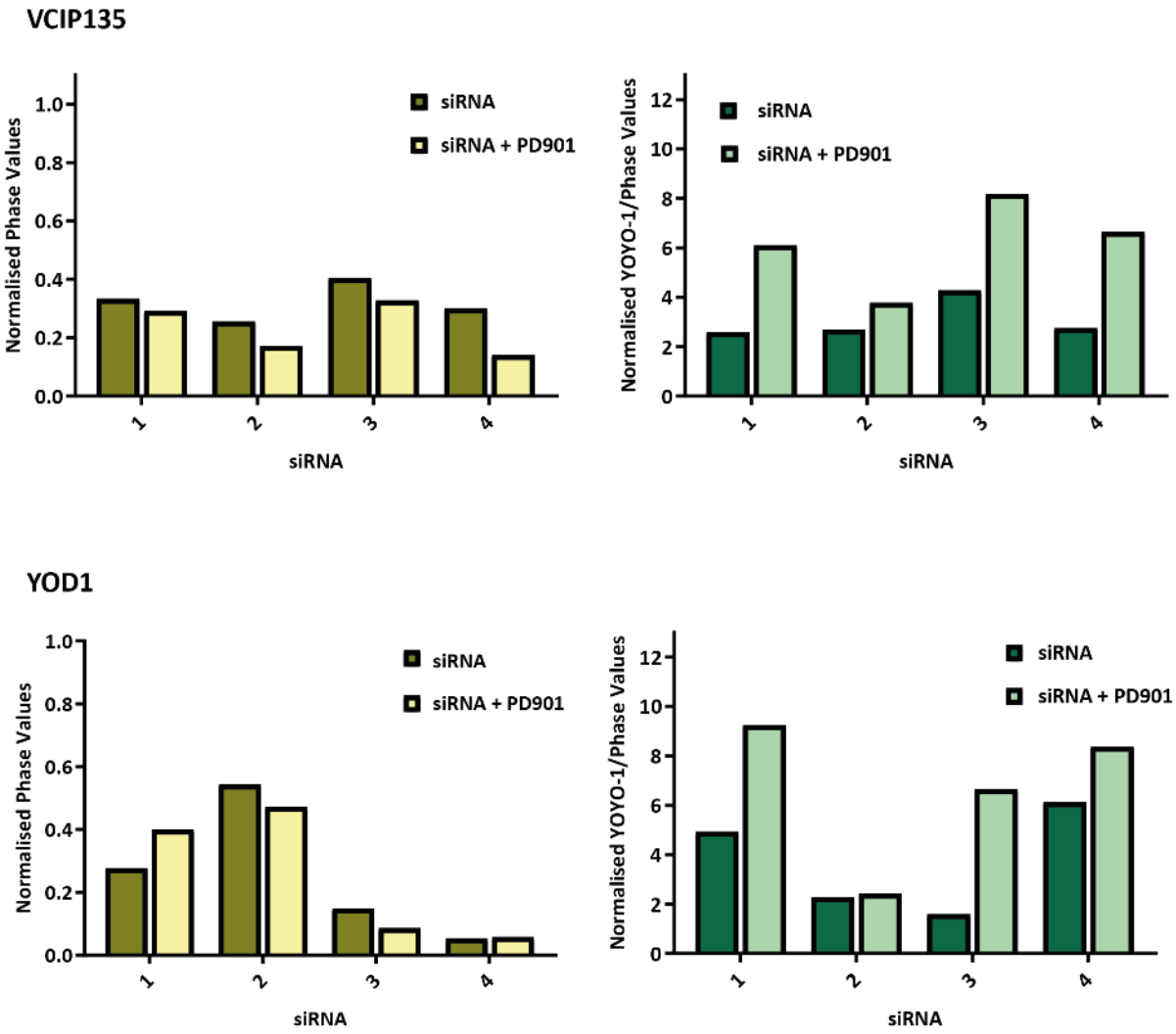

Figure 5.11 Overview of 'hit' DUBs from the 5-day DUB RNAi screen, treated with a MEK1/2 inhibitor, generated from SI values from YOYO-1/Phase data. (A) Distribution of SI values across complete screen. **(B)** Data representative of the distribution of the number of siRNA for a particular DUB that generated an SI value, below a set threshold, indicative that knockdown of that DUB resulted in sensitisation to PD0325901 (PD901) and resulted in a cytoxic effect. For example, 21 DUBs had no targeting siRNA that resulted in a significant change in SI value following treatment with PD901, in comparison three, out of a potential four, siRNA targeting 20 DUBs, and three positive controls, generated an SI value, below the set threshold, indicative that these DUBs combine wih PD901 to cause a cell death response. For our screens if three or more siRNA generated an SI value below the set threshold they were classed as 'hit' DUBs, a table of which is shown in **(C)**. **(D)** Bar graphs representative of normalised phase data and YOYO-1/Phase data for each 'hit' DUB. All data was taken from a single screen.

Figure 5.12 Overview of 'hit' DUBs from the 5-day DUB RNAi screen, treated with a MEK1/2 inhibitor, generated from SI values from YOYO-1/CTG data, and comparing these 'hits' to those generated from YOYO-1/Phase data.

Figure 5.12 MEK1/2 inhibitor, 5-day DUB RNAi Screen

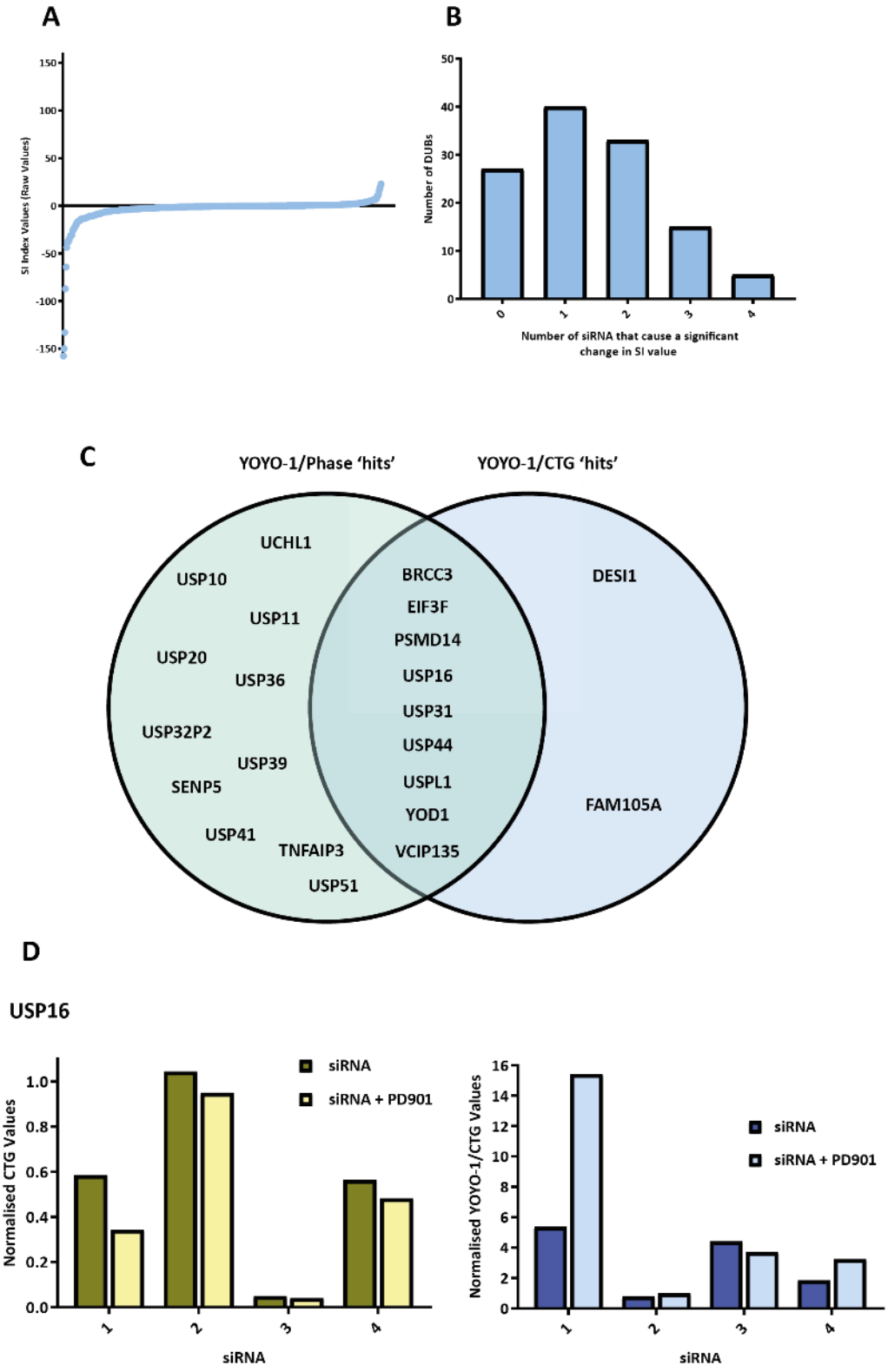

D

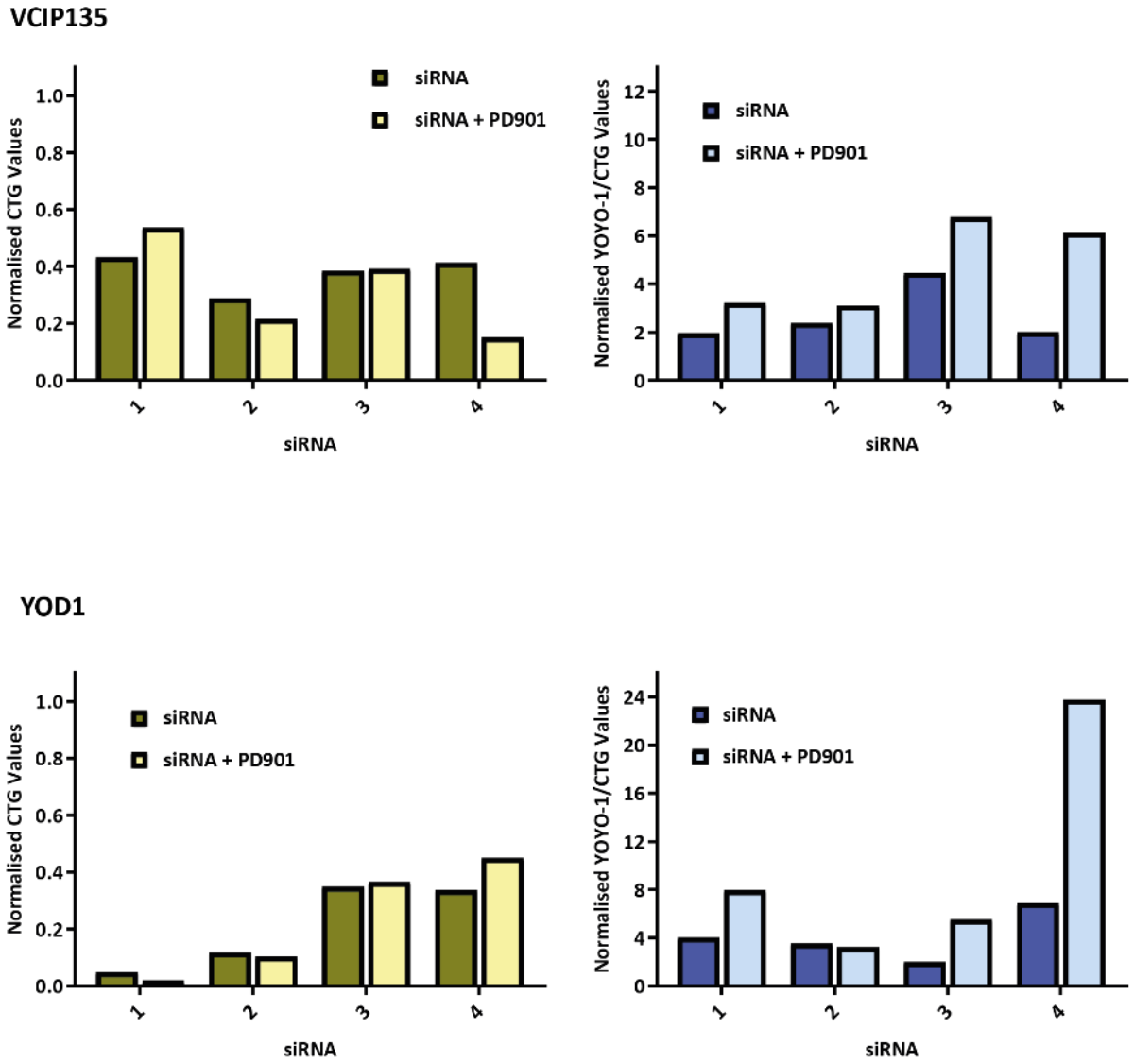

Figure 5.12 Overview of 'hit' DUBs from the 5-day DUB RNAi screen, treated with a MEK1/2 inhibitor, generated from SI values from YOYO-1/CTG data, and comparing these 'hits' to those generated from YOYO-1/Phase data. (A) Distribution of YOYO-1/CTG SI values across complete screen. **(B)** Data representative of the distribution of the number of siRNA for a particular DUB that generated an SI value, below a set threshold, indicative that knockdown of that DUB resulted in sensitisation to PD0325901 (PD901) and resulted in a cytoxic effect. For example, three, out of a potential four, siRNA targeting 11 DUBs, and four positive controls, generated an SI value, below the set threshold, indicative that these DUBs combine wih PD901 to cause a cell death response. For our screens if three or more siRNA generated an SI value below the set threshold they were classed as 'hit' DUBs. **(C)** A venn diagram comparing 'hit' DUBs generated from YOYO-1/Phase and YOYO-1/CTG data from the 5-day PD901 DUB RNAi screen. **(D)** Bar graphs representative of normalised CTG data and YOYO-1/CTG data for 'hit' DUBs that we chose to further investigate in Chapter 6. All data was taken from a single screen.

reduction in phase value. Treatment of HCT116 cells with 8055 and ABT-263 resulted in minimal decreases in confluency, that were only observed when treated with high concentrations of 8055 (Figure 5.13B). Additionally analysis of YOYO®-1/Phase controls revealed that transfection of siLUC, in HCT116 cells, resulted in minimal changes in YOYO®-1/Phase values and were consistent over all plates, with or without treatment with 8055 (Figure 5.13C). Interestingly combined knockdown of siLUC and treatment with 8055 resulted in a 10 % reduction in YOYO®-1/Phase value, indicative that treatment with 8055 reduced cell death in HCT116 cells, compared to transfection with siLUC alone. Transfection or inhibition, with high concentrations of ABT-263 and 8055, of HCT116 cells with positive controls resulted in an induction of cell death as shown by an increase in YOYO®-1/Phase values, compared to siLUC controls (Figure 5.13D).

Given the results from controls, this screen was considered reliable and further analysis of SI values, based on YOYO®-1/Phase values, was performed (Figure 5.14). Analysis of SI values across the complete screen revealed that SI values were evenly distributed (Figure 5.14A). Additionally knockdown of eight DUBs were revealed to sensitise HCT116 cells to 8055, resulting in the induction of cell death (Figure 5.14B and Figure 5.14C). Further analysis of these 'hit' DUBs revealed that, as predicted from SI values, knockdown of these DUBs combined with inhibition of mTOR to increase normalised YOYO®-1/Phase values with at least three targeting siRNA, compared to knockdown of the DUB alone. Several of these DUBs were also identified as 'hits' from the 5-day DUB RNAi screen in combination with MEK1/2 inhibition. This might suggest a shared common effector pathway of both signalling pathways.

Of note, analysis of SI values from the 3-day DUB RNAi screen, combined with mTOR inhibition, using CTG values was not shown as analysis did not generate any 'hit' DUBs, despite analysis of controls indicating that the screen was valid. This could suggest that knockdown of DUBs doesn't further sensitise cells to mTOR inhibition in HCT116 cells.

Figure 5.13 Analysis of RNAi screen controls using phase and YOYO-1/Phase values generated from the 3-day DUB RNAi screen, combined with mTOR inhibitor treatment.

Figure 5.13 mTOR inhibitor, DUB RNAi Screen

A: siLUC control

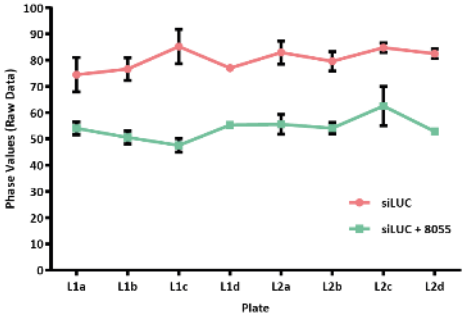

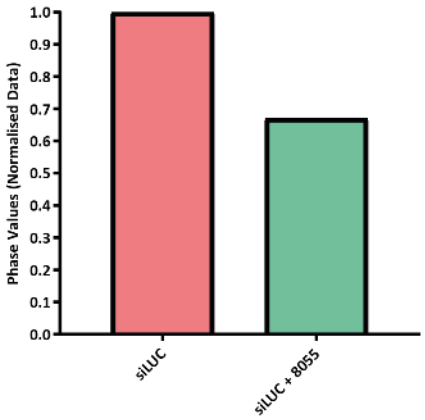

	Average Phase Raw values	Normalised
siLUC	80.4	1.00
siLUC + 8055	54.1	0.67

B: Positive Controls

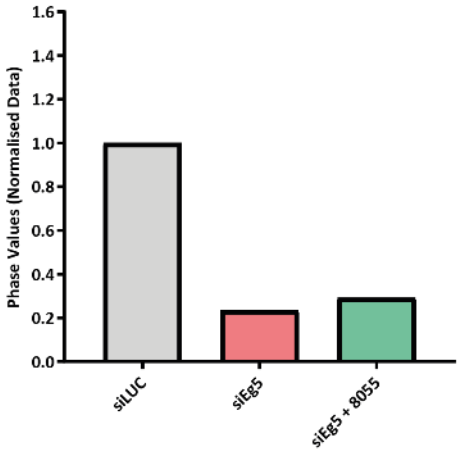

	Normalised
siLUC	1.00
siEg5	0.23
siEg5 + 8055	0.29

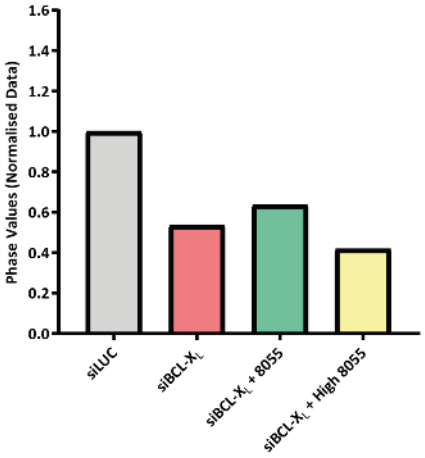

	Normalised
siLUC	1.00
siBCL-X_L	0.53
siBCL-X_L + 8055	0.64
siBCL-X_L + High 8055	0.42

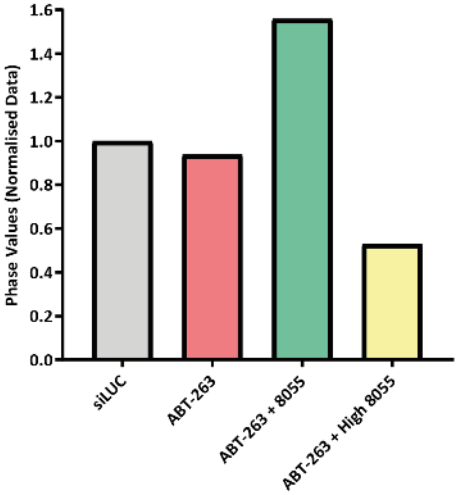

	Normalised
siLUC	1.00
ABT-263	0.94
ABT-263 + 8055	1.56
ABT-263 + High 8055	0.53

Figure 5.13 mTOR inhibitor, DUB RNAi Screen

C: siLUC control

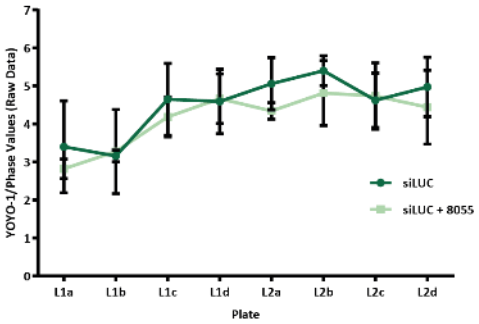

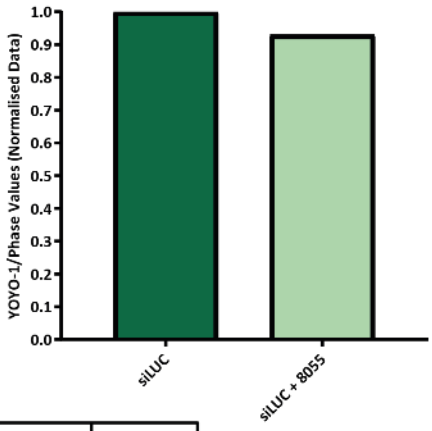

	Average YOYO-1/Phase Raw values	Normalised
siLUC	4.48	1.00
siLUC + 8055	4.16	0.93

D: Positive Controls

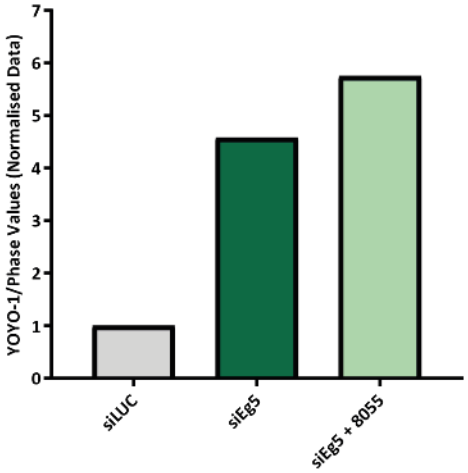

	Normalised
siLUC	1.00
siEg5	4.58
siEg5 + 8055	5.75

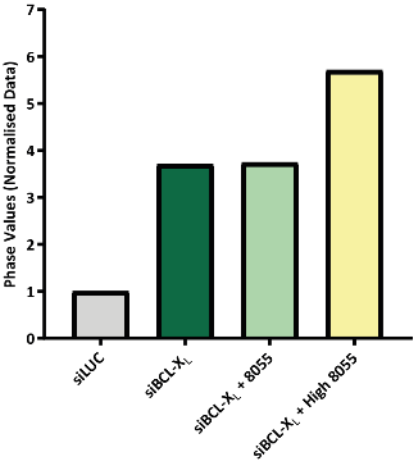

	Normalised
siLUC	1.00
siBCL-X$_L$	3.71
siBCL-X$_L$ + 8055	3.74
siBCL-X$_L$ + High 8055	5.71

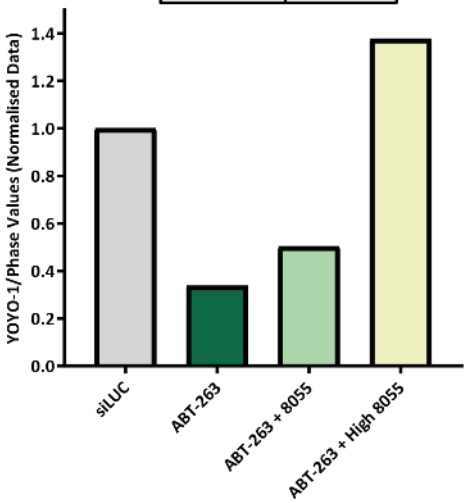

	Normalised
siLUC	1.00
ABT-263	0.34
ABT-263 + 8055	0.50
ABT-263 + High 8055	1.38

Figure 5.13 Analysis of RNAi screen controls using phase and YOYO-1/Phase values generated from the 3-day DUB RNAi screen, combined with mTOR inhibitor treatment. Analysis of phase values for RNAi controls, including **(A)** the negative siRNA control, siLUC and **(B)** positive siRNA controls, siEg5 and siBCL-$_{xL}$, and positive inhibitior controls of ABT-263 (1 μM), with or withour 8055 (0.2 μM) or High 8055 (2 μM). All graphs are representative of data generated from one screen, where all controls were plated at least once on all 8 plates, 8 treated and 8 untreated, tested, and all data was normalised to the siLUC controls across all plates, either treated or untreated for that screen. Phase values were generated as a percentage confluency (Phase Object Confluence), using the IncuCyte data analysis programme, Basic Analyser, with an optimised 'Confluence Mask' to count all cells from live cell images taken by the IncuCyte ZOOM. Four images were taken for each well and phase values were an average percentage confluency from these four images. Analysis of YOYO-1/Phase values for RNAi controls, including **(C)** the negative siRNA control, siLUC, and **(D)** the positive siRNA controls, siEg5 and siBCL-$_{xL}$, and positive inhibitior controls of ABT-263 (1 μM), with or withour 8055 (0.2 μM) or High 8055 (2 μM). All graphs are representative of data generated from one screen, where all controls were plated at least once on all 8 plates, 8 treated and 8 untreated, tested, and all data was normalised to the siLUC controls across all plates, either treated or untreated for that screen. YOYO-1 data was measured as counts/images using the IncuCyte data analysis programme, Basic Analyser, with and optimised cell mask to count all fluorscent cells from live cell images taken by the IncuCyte ZOOM, where four images were taken for each well and YOYO-1 values were an average cell count from these four images. Phase values were generated as a percentage confluency (Phase Object Confluence), using the IncuCyte data analysis programme, Basic Analyser, with and an optimised 'Confluence Mask' to count all cells from live cell images taken by the IncuCyte ZOOM. Four images were taken for each well and phase values were an average percentage confluency from these four images.

Figure 5.14 Overview of 'hit' DUBs from the 3-day DUB RNAi screen, treated with the mTOR inhibitor, AZD8055, generated from SI values from YOYO-1/Phase data.

Figure 5.14 mTOR inhibitor, DUB RNAi Screen

A

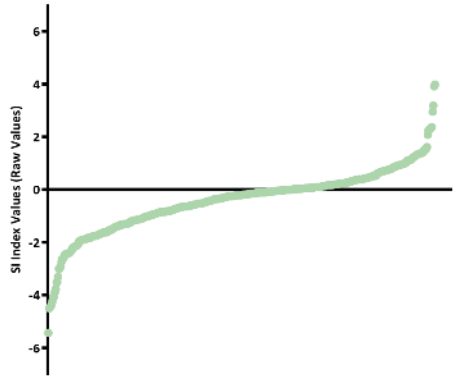

B

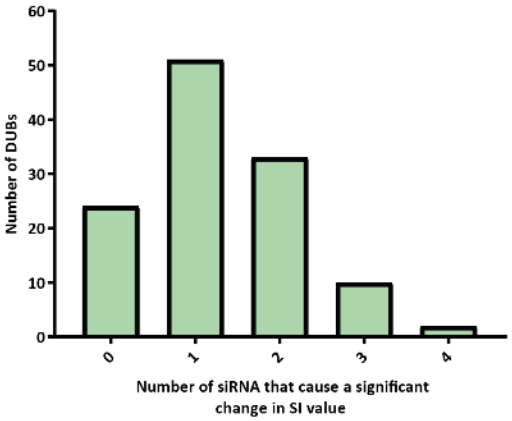

C

Number of siRNA that cause a significant change in SI value:	3	3
	BAP1	USP10
	EIF3F	USP53
	OTUD1	USPL1
	USP7	VCIP135

D

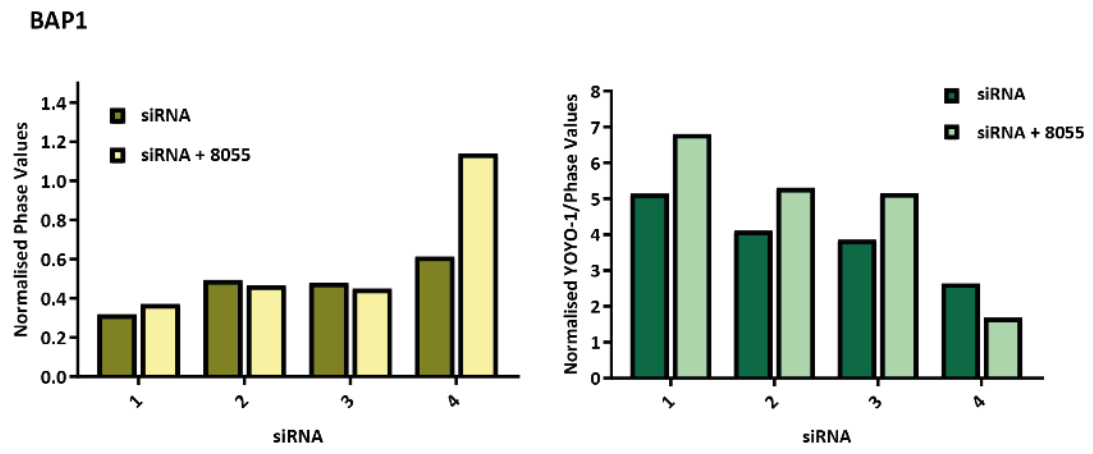

Figure 5.14 mTOR inhibitor, DUB RNAi Screen

D

EIF3F

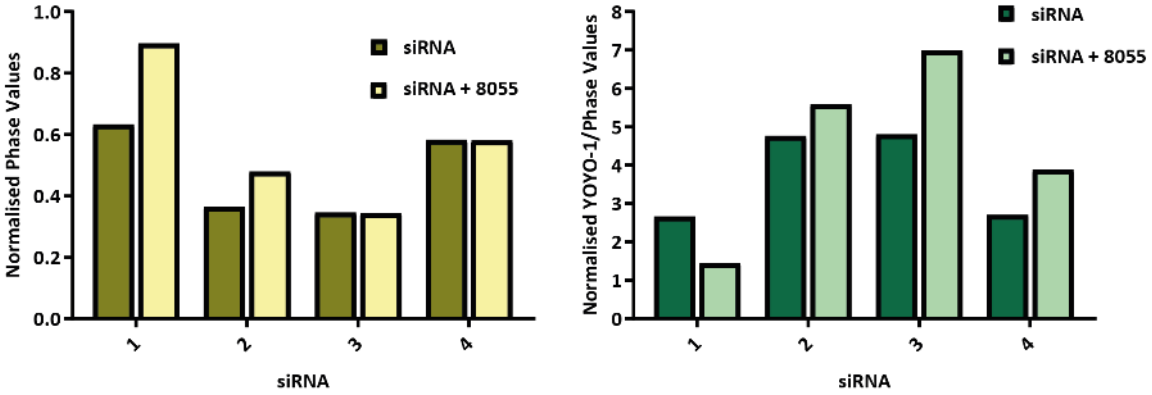

OTUD1

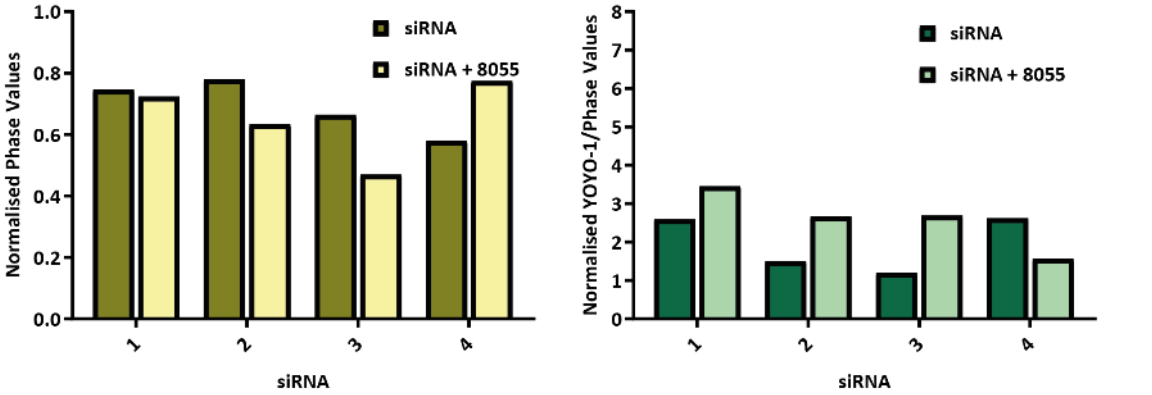

USP7

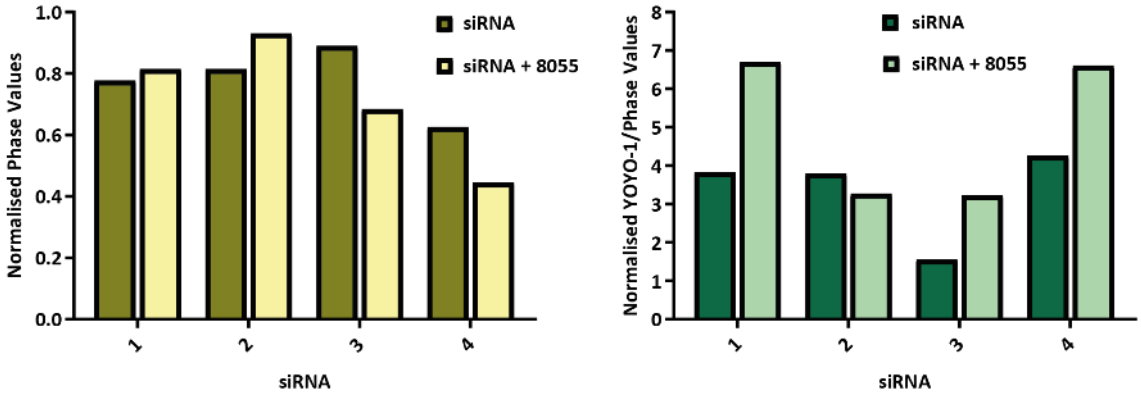

Figure 5.14 mTOR inhibitor, DUB RNAi Screen

D

USP10

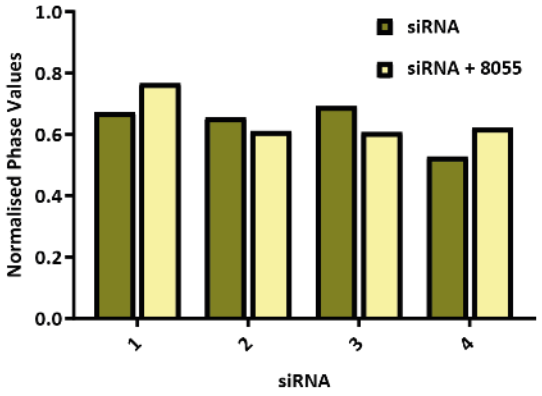

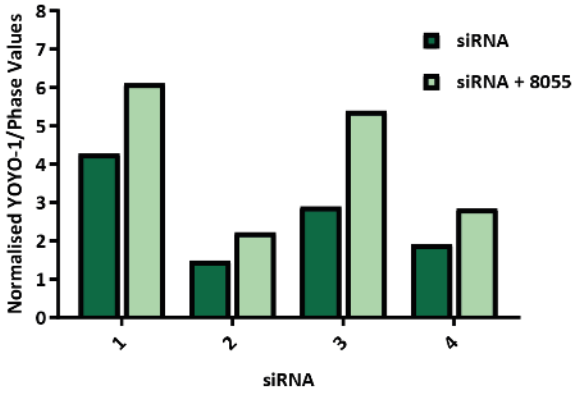

USP53

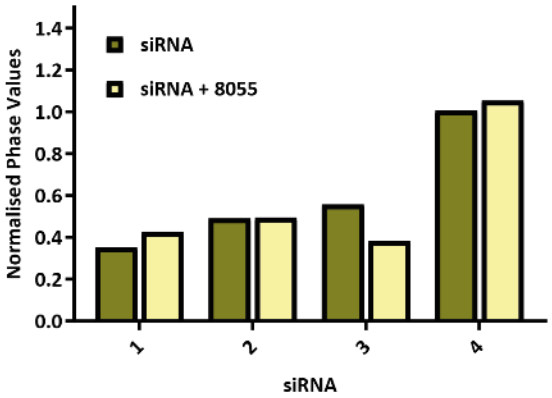

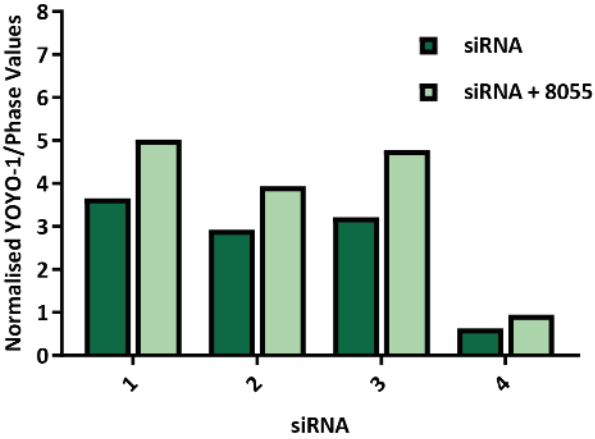

USPL1

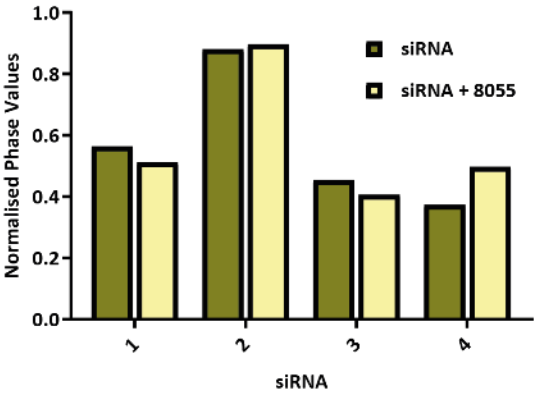

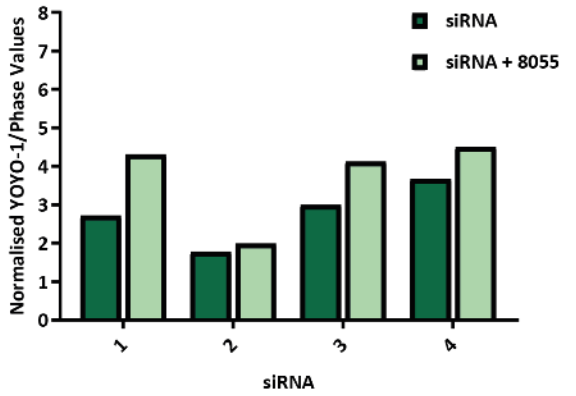

D

VCIP135

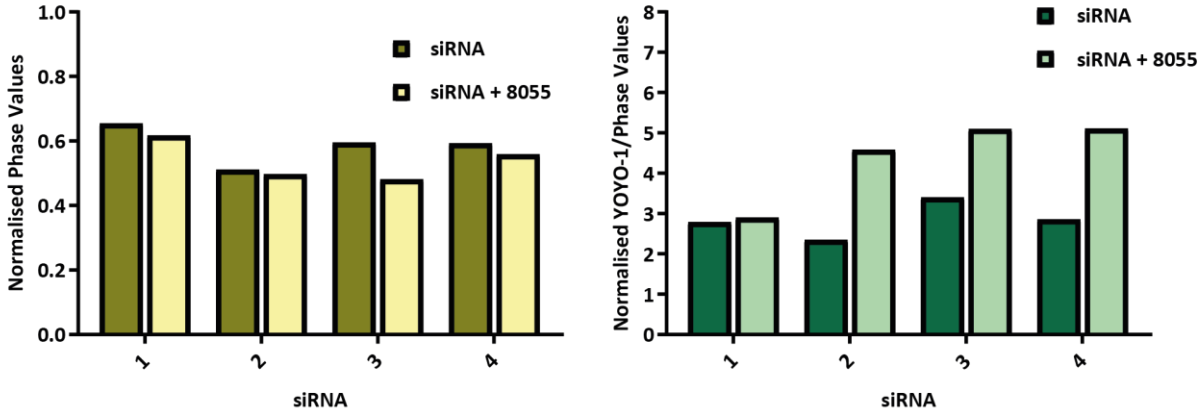

Figure 5.14 Overview of 'hit' DUBs from the 3-day DUB RNAi screen, treated with the mTOR inhibitor, AZD8055, generated from SI values from YOYO-1/Phase data. (A) Distribution of SI values across complete screen. **(B)** Data representative of the distribution of the number of siRNA for a particular DUB that generated a SI value, below a set threshold, indicative that knockdown of that DUB resulted in sensitisation to AZD8055 (8055) and resulted in a cytoxic effect. For example, 24 DUBs had no targeting siRNA that resulted in a significant change in SI value following treatment with 8055, in comparison eight DUBs, and two positive controls, have three, of a potential four, targeting siRNA that generate an SI value, below the set threshold, indicative that these DUBs combine wih 8055 to cause a cell death response. For our screens if three or more siRNA generated an SI value below the set threshold they were classed as 'hit' DUBs, a table of which is shown in **(C)**. **(D)** Bar graphs representative of normalised phase data and YOYO-1/Phase data for each 'hit' DUB. All data was taken from a single screen.

5.3. Discussion

5.3.1. Is RNAi the best screening method to assess the cytotoxic effect of inhibitor treatment sensitisation to DUB knockdown in HCT116 cells?

RNAi technologies have been invaluable in assessing the role that genes play in a multitude of biological processes as well as in disease (Falschlehner *et al.*, 2010). In cancer, RNAi can be used, along with inhibitor treatments, in synthetic lethality or synthetic sensitisation screens to assess genes required for cell viability or fitness.

One of the major challenges with RNAi is identifying siRNA which can completely ablate gene expression and therefore the downstream effects of target genes. In certain circumstances, residual expression of functional transcripts could be sufficient to disguise any loss-of-function phenotypes resulting in false negative results. This is especially true when the targeted RNA encodes an enzyme where 10% residual expression may be sufficient to maintain cellular functions (Lefloch *et al.*, 2008). In addition, one of the major issues associated with RNAi is off-target effects, which can generate false positive results and often leads to a lack of reproducibility of RNAi screen results (Brass *et al.*, 2008, Echeverri *et al.*, 2006, König *et al.*, 2008, Zhou *et al.*, 2008). As a consequence, several strategies have been developed to combat the 'off-target' nature of RNAi technologies, including chemical modification of siRNA.

The QIAGEN library of DUB siRNAs, used in the screen, were not validated at Mission Therapeutics prior to performing the screens, and thus there was no confirmation that gene expression of the DUBs had been abolished for the time periods examined. Secondary analysis of 'hit' DUBs, generated from the 5-day DUB RNAi screen, in combination with MEK1/2 inhibition, including western blot analysis is shown in Chapter 6. As siRNA only transiently ablate gene expression, and requires viral delivery platforms for stable and heritable knockdown of a gene, it was vital to confirm that 5-day siRNA transfection of HCT116 cells maintained the knockdown of gene expression of select DUBs. In addition to this, the sensitisation effects seen could not be confirmed to be due to on-target effects of the siRNA. During this study a pre-designed QIAGEN library was used to target all DUBs in the human genome and, as a consequence of this, the selected siRNA should have been assessed by QIAGEN and modified to minimalise 'off-target' effects therefore aiding in reducing the number of false-positive results generated from the screens. Moreover, the use of four individual siRNA and only describing a 'hit' DUB as one in which at least three of the siRNA combined with the inhibitor to cause an effect minimises the probability that an observed sensitisation effect was due to off-target effects of the chosen siRNA.

Advances in gene editing technologies, including CRISPR/Cas9 technologies, could overcome the majority of the described problems associated with RNAi technologies and could be a better means to assess the effect of genome-wide ablation of DUBs in combination with inhibitor treatments (Cong *et al.*, 2013, Mali *et al.*, 2013). Despite this, RNAi technologies are able to supress gene expression rapidly with high efficiency as it has been demonstrated that optimised siRNA can offer >70 % knockdown of intended mRNA upon delivery into target cells. In contrast, the ability of CRISPR/Cas9 to edit mammalian genes is variable and has an efficiency between 1 and 79 %, depending on the DNA damage response pathway that results from excision and as a consequence CRISPR/Cas9 treated cells need to be selected for gene modifications prior to use in screens and this increase in selection time may allow cells to adapt to gene loss (Unniyampurath *et al.*, 2016). Given this as well as time constraints and cost, RNAi screening was selected as was the best way to assess the cytotoxic effect of genome-wide knockdown of DUBs in combination with inhibition of select proteins.

5.3.2. Analysis of DUB RNAi screens using cell-based assays.

It is important to choose the right cell-based assay for the biological question that needs to be answered. Two analysis methods, the CellTiter-Glo® (CTG) Luminescent Cell Viability Assay and the YOYO®-1 fluorescent dye, were chosen to measure changes in cell fitness by observing changes in cellular viability and cell death following combined knockdown of a DUB and inhibitor treatment. These were chosen based on ease of use, cost and the ability of the two assays to be multiplexed.

Apoptosis and necrosis are associated with loss of specific markers related to cellular viability, including ATP, MTS and Resazurin, and an increase in apoptotic markers including an increase in LDH release and, in the case of apoptosis, an increase in activated caspases. These factors can be utilised by end-point assays to assess cellular viability and cytotoxicity. The first assay chosen for this study was the CTG assay, which measures changes in ATP levels. The amount of ATP present in cells is directly proportional to cellular viability and cell death is associated with loss of the ability of cells to produce ATP. The CTG reagent lyses cell membranes, releasing ATP, inhibits ATPases and provides luciferin and luciferase to measure the amount of ATP in a bioilluminescent reaction. The rapid nature of this assay should reduce artefacts that could occur as a consequence of interactions between inhibitors and assay components. Given this, problems associated with measuring intracellular ATP as an end-point assay have been well documented. das Neves and colleagues demonstrated that, within a genetically identical population of cells, there was significant cell-to-cell variability in mitochondrial mass as a consequence of uneven distribution of mitochondria during cell division (das Neves *et al.*, 2010). As a result of this, one could assume that intracellular ATP could vary between cells in the same well as well

as between wells seeded from the same cellular population. Different cell types have different amounts of ATP, and in tumour cells this has been linked to chemoresistance (Andreotti *et al.*, 1995, Kangas *et al.*, 1984, Zhou *et al.*, 2012). If HCT116 cells had a relatively low basal level of ATP it could be challenging to observe significant reduction in ATP levels following treatment. Additionally anchorage-dependent cells that undergo contact inhibition at high densities may show a difference in ATP content per cell at high densities and as a consequence there might be a non-linear relationship between cell number and luminescence. In addition, the cytoplasmic volume or cellular physiology of the cells can influence the intracellular ATP content. For example, oxygen depletion is liked to a rapid decrease in ATP (Crouch *et al.*, 1993).

Despite siRNA and inhibitor controls, from raw and normalised CTG data, generating graphs that match the expected trends, SI values generated from CTG analysis of the DUB RNAi screens, did not consistently show that positive controls were 'hits' from the screens and knockdown of very few or no DUBs sensitised HCT116 cells to inhibition using CTG analysis. This could suggest that DUB knockdown did not sensitise HCT116 cells to inhibition. In addition, it could suggest that the SI analysis method was not appropriate for the screen (discussed later). However, contrary to this, additional assessment of cell death, using the YOYO®-1 dye, did indicate that knockdown of a much larger set of DUBs in HCT116 cells combined with inhibitor treatment to induce a cytotoxic effect. HCT116 cells have been demonstrated to clump following seeding and have the potential to change morphology following inhibitor treatment and this could influence ATP content and cause the lack of 'hit' DUBs generated from CTG values from the screens. In general, intracellular ATP concentrations are a good estimate of cellular viability but the limitations of this measurement need to be taken into consideration when evaluating and interpreting data based on the CTG assay.

Additionally YOYO®-1, a cell impermeant stain that binds to dsDNA, was used to kinetically evaluate cytotoxicity from the screens, using the IncuCyte® ZOOM live-cell imaging system. A decrease in membrane integrity, associated with cell death, allows YOYO®-1 to enter cells and associate with dsDNA resulting in an increase in fluorescence. As previously described, the advantage of this dye was that it could be directly added to live cells and, as it did not require cell lysis to measure changes in fluorescence, it could be multiplexed with CTG data analysis.

Images taken by the IncuCyte® ZOOM capture cells at the centre of the well and, as HCT116 cells have been demonstrated to preferentially grow at the edges of the well, measurements using these images may not represent a complete picture of changes in phase or confluency, as well as cytotoxicity, YOYO®-1 fluorescent value, following inhibitor treatment. Additionally the IncuCyte® ZOOM camera was focused to capture images of adherent cells, therefore it would fail to image all non-

adherent/floating cells which could have 'died' as a consequence of combined DUB knockdown and inhibitor treatment. Therefore, again, IncuCyte® ZOOM images may not represent an accurate picture of the well and as a result of using these images may under representation of the cell death effect observed with combined treatment.

Alternative assays to assess the apoptotic or cytotoxic effect of combined knockdown of DUBs with inhibitor treatment include the Caspase-Glo™ 3/7 Assay as well as the MTS assay. The appearance of some apoptotic markers, including caspases, are transient and may only be detectable over a limited window of time. Therefore, assays that measure caspase activity including the Caspase-Glo™ 3/7 Assay would only be effective over a very select period of time and so would most likely not be appropriate for use as an end-point assay in a longer RNAi screen. Comparable to the CTG assay, the MTS cell viability assay measures the reduction of the tetrazolium salt, MTS, to a formazan compound. In viable cells, cell metabolism results in the production of NADH or NADPH, and these reducing products pass electrons to an intermediate electron transfer reagent that can reduce MTS into the formazan product. In contrast, cell death results in the inability of cells to generate formazan products. However compared to the CTG assay, which can detect a minimum of 15 cells, the MTS assay is less sensitive and requires approximately 1000 cells to detect changes in the formazan product.

Dyes and/or assays used to quantify cell fitness are inherently biased as they assess very specific yet different biological properties of a cell, which often only partially and indirectly reflect cellular viability. As such, the lack of reproducibility in 'hits' and the large number of false positive results generated from the different end-point assays reflects real biological differences observed during the screens.

Gilbert *et al.* evaluated the advantages of multiplexing end-point assays to analyse RNAi screens (Gilbert *et al.*, 2011). Using a biochemical approach, the CTG assay, with two fluorescence–based assay methods, Calcein and Hoeschst dyes, they assessed changes in cell fitness following knockdown of human kinome components. Specifically they observed that there was a ~50-58 % overlap between the observed genes required for fitness using two assay methods and that this was further reduced to 40-48 % following introduction of a third assay. Overall, they concluded that multiplexing, with at two or more fitness indicators, is vital to reduce false positive results and should increase the confidence of data required for 'hit' selection. Thus, the use of two 'fitness' measurements, as done for each of the screens, should increase the quality and robustness of hits generated from the screen. Alternative end-point assays could be considered and multiplexed with YOYO®-1 to evaluate if this reduced false positive results by comparing it to the end-point analyse methods used during this study.

5.3.3. Evaluation of 'hit' DUBs generated from 3-day and 5-day DUB RNAi screens.

From the analysis of data generated from the 3-day screens, very few DUBs were identified that robustly combined, when knocked down, with MEK1/2 inhibition to drive loss of cell viability and/or cell death. However, the two 3-day screens performed were valid as all controls, both negative and positive, for siRNA and inhibitors, generated raw data from multiple end-point analyses that matched the expected trend. Therefore, this could suggest that the original hypothesis may not be correct, and that despite the screen being valid, knockdown of DUBs do not combine with MEK1/2 inhibition to drive tumour cell death. Alternatively, it could suggest that the method used to analyse the screen, SI analysis, may not have been the best method to test the hypothesis. This method of analysis is used by Mission Therapeutics to assess the sensitivity of DUB RNAi screens to inhibitor treatments and values are based on the difference between the expected and observed combined effect of RNAi and drug treatment on cellular fitness. However, there are multiple alternative means for analysing RNAi screens which are often easier to perform and interpret including, those looking for fold-change, often combined with percentage cell viability, as well as additional parametric two-sample tests, including *t*-test and Z-factor. Ye *et al.*, has also described the use of a linear model, which is thought to overcome problems associated with SI analysis including cross-plate variation, which is averaged during SI calculations (Ye *et al.*, 2012). Alternative analysis should be performed to clarify if any of the DUBs observed by SI analysis to cause a significant effect on cell viability and cell death are identified by additional analysis and if SI analysis was limiting the number of 'hits' obtained from the screens.

USP29 was identified as a 'hit' from CTG data from both 3-day DUB RNAi screens, in combination with PD901. In addition, USP37 was identified to be a 'hit' from YOYO-1/CTG data from both 3-day screens and consistently two siRNA knocked down USP37 and combined to MEK1/2 inhibition to cause substantial decrease in cell viability or increase in cell death.

To date very little is known about USP29. Martin *et al.* demonstrated that USP29 regulates the stability of Claspin, an adaptor protein required to mediate cell cycle arrest at the ATR-Chk1 DNA damage checkpoint; thus, loss of USP29 resulted in defective S-phase progression (Martin *et al.*, 2015). The oncogenic transcription factor E2F1 induces the expression of USP37, which, following activation by CDK2, deubiquitylates and stabilises cyclin A and therefore regulates S-phase entry (Huang *et al.*, 2011). Delayed or defective entry into S-phase results in reduced cell progression and replication and could cause a cytostatic effect. How knockdown of USP29 or USP37 combines with MEK1/2 inhibition to induce a cytotoxic response rather than a cytostatic response is not presently known.

Kim *et al.*, demonstrated that USP37 expression contributed to cancer phenotypes by stabilising 14-3-3γ and conversely knockdown of USP37 resulted in loss of cell viability. Additionally they demonstrated

that levels of phosphorylated ERK gradually decreased as a consequence of USP37 depletion and suggested that this indicated that USP37 was involved in the MAPK signalling pathway (Kim *et al.*, 2015). As USP37 was identified as combining with MEK1/2 inhibition to induce cell death the concept that USP37 regulates the ERK1/2 pathway is plausible, however, further evaluation would be needed to confirm this.

The lack of reproducibility of 'hit' DUBs between the two 3-day DUB screens treated with the MEK1/2 inhibitor PD901, could have been caused by variations in cell seeding rather than changes in the assay chemistry. Variations in the plating of cells could have been amplified as HCT116 cells have a tendency to form clumps. In addition, it could suggest that in order to observe a 'hit' from this screen, irrespective of end-point assay analysis, statistical analysis and differences caused by experimental variability, the DUB must regulate, or be, the key gene driving tumour cell growth. Therefore, its knockdown would combine with MEK1/2 inhibition to drive a reproducible cell death phenotype. In addition, there might be functional redundancy between DUBs, therefore in order to observe a desired phenotype multiple DUBs may need to be targeted simultaneously.

USP29 and USP37 were not identified as 'hit' DUBs from the 5-day screen. It could therefore be suggested that USP29 and USP37 sensitise HCT116 cells to short PD901 treatments, whilst the DUBs identified during the 5-day screen require longer periods of transfection to sensitise HCT116 to inhibition of MEK1/2. However, the majority of these 'hits' were identified from a single screen and so additional screens need to be performed to reduce false-positive results and increase confidence in identified important DUBs.

Of the 'hits' identified in the mTOR inhibitor RNAi screen, USP7 and BAP1 have been well characterised for their roles in tumour progression. Previous reports have also demonstrated that knockdown of USP7 overcame resistance to bortezomib, by repressing NF-κB signalling in multiple myeloma (Yao *et al.*, 2018). In this case both bortezomib treatment and USP7 knockdown act to stabilise IκBα.

Recently USP7 has been demonstrated to be the DUB for c-Myc in neural stem cells (Nicklas *et al.*, 2018). As previously described Myc is regulated by mTOR signalling. mTORC1, one mTOR containing complex, regulates protein synthesis through the regulation of eIF4F assembly, where eIF4F has been demonstrated to stimulate the translation of Myc. The expression of Myc is frequently dysregulated in cancer and, as it regulates all characteristics associated with the hallmarks of cancer, over expression of Myc is linked to poor prognosis for patients. Targeting Myc stability could therefore result in tumour suppression. Pourdehnad *et al.* identified a link between Myc and mTOR, demonstrating that inhibiting mTOR-dependent 4EBP1 phosphorylation was required for tumour regression of Myc-driven cancers (Pourdehnad *et al.*, 2013). They demonstrated that Myc regulates the activity of 4EBP1 during tumour

initiation and enhances protein synthesis throughout tumour development through its regulation of 4EBP1. As shown in section 5.2.1.2., AZD8055 (8055) inhibits phosphorylation of 4EBP1 at the mTORC1 sites, indicative of inhibition of cap-dependent translation. Therefore, knockdown of USP7 and mTOR inhibition could combine to significantly reduce the phosphorylation of 4EBP1 and decrease the stability/protein synthesis of Myc resulting in tumour cell death where knockdown of USP7 or mTOR inhibition alone is not sufficient to cause such an effect.

The identified 'hit' DUBs from the DUB RNAi screen, in combination with 8055, would need to go through additional secondary analysis to assess if knockdown of these DUBs sensitise HCT116 cells to mTOR inhibition and to assess the downstream effects of combined knockdown and inhibition. However, in general, few 'hits' were identified from this screen. It could therefore be suggested again that knockdown of DUBs does not combine with mTOR inhibition to induce a cytotoxic response.

The 'hit' DUBs generated from the 5-day DUB RNAi screen, in combination with MEK1/2 inhibitor treatment, are further described in Chapter 6. In an ideal scenario the screen would have been performed twice and 'hits' would have been taken forward that overlapped between the two screens. However, as controls for the screen were convincing the screen was deemed valid and 'hits' from this screen were taken forward for further validation (Chapter 6).

Chapter 6: Validation of ‘hits’ from a deubiquitylating enzyme RNAi screen performed in combination with MEK1/2 inhibition

6. Chapter 6

6.1. Introduction

As previously described, the use of MEK1/2 inhibitors as a monotherapy for the treatment of Ras mutant tumour cells has had varying success, due in part to collapse of feedback loops or amplification of BRAF, KRas or activating mutations of MEK1/2 (Caunt *et al.*, 2015, Little *et al.*, 2011). Thus, the predominant mechanism of resistance to these inhibitors is re-activation of the ERK1/2 signalling pathway.

ERK1/2 signalling regulates multiple components of the apoptotic cell death pathway. Consequently, tumour cells with Ras, BRAF or MEK mutations are addicted to ERK1/2 signalling to promote cell survival through the repression/inactivation of pro-apoptotic proteins and the increased expression of pro-survival proteins (Balmanno and Cook, 2009). Inhibition of the ERK1/2 pathway, for example through MEK1/2 inhibition, results in the opposite effect causing an increase in pro-apoptotic proteins, such as BIM, BMF and PUMA (Sale and Cook, 2013). Despite this, monotherapy ERK1/2 pathway inhibition causes a cytostatic effect rather than a cytotoxic cell death response, allowing cells to adapt and acquire resistance to these inhibitors as described above (Little *et al.*, 2011, Sale and Cook, 2013). The observed cytostatic response is believed to be as a consequence of pro-survival proteins buffering the effect of the increased expression of pro-apoptotic proteins (Sale and Cook, 2013). Therefore, combining MEK1/2 inhibition with an inhibitor capable of reducing the expression of pro-survival proteins should induce apoptosis. Indeed, dual inhibition of MEK1/2 and BCL2/BCL-X_L, with BH3 mimetics, tips the balance towards a cytotoxic response leading to cell death (Sale and Cook, 2013).

The emergence of resistance to new cancer therapeutics, including MEK1/2 inhibitors, necessitates the need for the development of novel therapeutic combinations to drive the death of ERK1/2-addicted tumour cells. Notably, many of the limiting factors hindering cell death of these tumour cells are regulated through protein ubiquitylation, including DUSPs (Caunt and Keyse, 2013). Pro-survival proteins described to obstruct the cytotoxic effect of MEK1/2 inhibition are also regulated by ubiquitylation, including BCL2 and MCL1 (Edison *et al.*, 2017, Mojsa *et al.*, 2014). Additionally, as different thresholds of ERK1/2 signalling can promote cell survival or cell death it is possible that E3 ligases or DUBs regulating ERK1/2 components might push the magnitude of ERK1/2 signalling towards apoptosis (Hong *et al.*, 2018, Mebratu and Tesfaigzi, 2009). Therefore, it is likely that regulating ubiquitylation, via inhibition, in combination with MEK1/2 inhibition could drive tumour cell death, thereby transforming a cytostatic response observed with MEK1/2 inhibitor monotherapy to a cytotoxic response.

The aim of this study was to determine whether an induction in apoptosis, similar to that seen with combined treatment of a MEK1/2 inhibitor and a BH3 mimetic, would be achieved by combining knockdown of 'hit' DUBs, identified in Chapter 5, with MEK1/2 inhibition in HCT116 cells.

6.2. Results

6.2.1. Identification of key DUBs that combine with a MEK1/2 inhibitor (PD0325901) to induce a cell death response.

A 5-day DUB RNAi screen was performed to systematically identify DUBs that when knocked down combine with the MEK1/2 inhibitor PD0325901 (PD901) to induce cell death in HCT116 cells (Chapter 5). For follow up validation of the screen further experiments focused on six DUBs, which when knocked down, with three or more siRNA, showed, a significant increase in cell death following MEK1/2 inhibitor treatment.

Initially the 5-day RNAi screen identified 20 DUBs that when knocked down combined with PD901 to induce cell death using YOYO®-1/Phase analysis. From this list any DUBs that were found to be 'essential' for HCT116 cell 'fitness' or survival, using published data (Hart *et al.*, 2015) or from the 5-day screen itself were eliminated. Hart *et al.*performed a CRISPR-Cas9 screen to identify genes essential for 'fitness' in multiple tumour cell lines, including HCT116 cells, where a more positive log Bayes factor (BF) value is representative of increased confidence that knocking out that gene reduces 'fitness' of these cells. Of note, this screen did not investigate the corresponding phenotype associated with positive BF values. From the 5-day screen, an essential DUB was classified as one that when knocked down lowered the cell confluency below 30 % (phase). Using both BF values and information from the 5-day screen, this eliminated 11 DUBs from the generated list of 'hit' DUBs (Figure 6.1A and Figure 6.1B). In accordance with that found in the 5-day screen in HCT116 $KRas^{G13D}$ cells, Fraile and colleagues observed that USP39 was essential for KRas-driven cancer, where expression of USP39 in lung and colon carcinoma correlated with poor prognosis (Fraile *et al.*, 2017).

Further to this, an additional four DUBs, EIF3F, USP31, USP32P2 and USP51 and SENP5, a sentrin/SUMO-specific protease were excluded. These were eliminated because on further inspection, knockdown of these proteases alone with at least two siRNA, resulted in a large reduction in total cell number, as shown from normalised phase data, suggesting that these proteases may be essential for proliferation in HCT116 cells.

Figure 6.1 Elimination of essential DUBs leaves four key hit DUBs for further investigation.

A

Gene	BF_HCT116	BF_HCT116_ shRNA	BF_HELA	BF_GBM	BF_RPE1	BF_DLD1
PSMD14	321.42	29.163	156.175	78.893	76.515	37.632
USPL1	128.71	-16.897	112.573	79.479	68.006	16.157
USP39	117.74	51.862	134.672	82.596	24.325	28.78
USP36	31.587	-33.115	4.253	76.199	46.906	33.449
USP10	-1.058	-9.029	-24.201	-23.688	42.081	9.122
BRCC3	-14.06	-17.873	-37.007	2.51	-13.697	-7.292
USP16	-29.955	-14.128	-57.452	-24.238	-12.691	-7.431
EIF3F	-30.975	27.366	-22.461	-15.629	-0.876	-13.189
USP11	-38.125	-9.648	-19.319	-9.989	-39.693	-16.719
YOD1	-59.679	N/A	-33.95	-17.783	-39.995	-21.236
VCIP135	-49.252	-34.291	-40.16	30.142	-40.285	-17.693
UCHL1	-76.737	-30.36	-13.819	-26.547	-28.564	-20.706
USP41	-78.575	-0.546	-73.36	-35.41	-51.671	-10898
USP44	-93.194	-9.432	-55.97	-26.102	-34.936	-20.102
SENP5	-101.702	-29.858	-90.182	-19.41	-31.292	-17.955
USP51	-109.777	-9.631	-50.449	-14.542	-34.003	-13.148
USP20	-113.075	-15.835	-32.776	-9.266	0.72	-15.876
TNFAIP3 (A20)	-167.91	-12.26	-77.858	-28.024	-51.867	-23.325
LOC220594 (USP32P2)	N/A					
USP41	N/A					

B

Gene	Average % cell survival	BF_HCT116	BF_HCT116_ shRNA
PSMD14	6.1	321.42	29.163
PSMD7	6.9	58.496	46.78
BRCC3	7.3	-14.06	-17.873
COPS6	7.3	226.075	32.948
EIF3H	8.5	115.461	21.317
BAP1	9.6	60.565	-16.311
USPL1	9.9	128.71	-16.897
USP39	10.0	117.74	51.862
USP38	10.3	-93.617	-8.944
USP11	11.4	-38.125	-9.648
USP49	11.7	-161.313	-22.762
DESI1	12.1	-67.415	-9.897
USP28	12.1	-116.298	-28.311
OTUB1	12.4	-89.826	-17.836
USP53	13.1	-22.431	N/A
JOSD2	13.3	-63.382	N/A
UCHL1	13.3	-76.737	-30.36
USP36	14.5	31.587	-33.115
USP2	15.1	-127.657	-26.089
STAMBP	15.6	-95.167	-36.547
AMSH-LP	15.8	-145.77	-32.203
YOD1	16.0	-59.679	N/A
COPS5	17.0	81.51	0.213
USP7	17.0	133.534	1.721
USP20	17.1	-113.075	-15.835
USP41	18.7	N/A	N/A
JOSD1	19.4	-75.41	-28.667
USP44	20.7	-93.194	-9.432
USP8	26.2	-47.096	-18.46

C

Gene
EIF3F
LOC220594 (USP32P2)
SENP5
TNFAIP3 (A20)
USP10
USP16
USP31
USP51
VCIP135

Figure 6.1 Elimination of essential DUBs leaves four key hit DUBs for further investigation. (A) Table of all 20 hit DUBs from the 5-day DUB siRNA screen in combination with a MEKi. All log bayes factor (BF) values taken from Hart et al., 2015, where those highlighted in red are deemed 'essential' genes for fitness in HCT116 cells, thus eliminating them from the generated hit list. **(B)** Table of all essential DUBs in our screen, where knock down of these DUBs alone, with 3 or more independent siRNA, resulted in a lower than 30% phase value, when compared to transfection controls, indicative of poor cell survival. Those highlighted in red are DUBs that were identified as original hits and will be removed from the final hit list of DUBs. **(C)** Table of hit DUBs once all essential DUBs based on **(A)** and **(B)** have been removed. Those highlighted in orange are DUBs that were further eliminated based on thorough examination of phase data. Those highlighted in green are DUBs that were taken forward for further experiments.

Consistent with this, several studies have shown that SENP5 (sentrin/SUMO-specific protease 5) is essential for tumour cell growth. Ubiquitin-like proteases (ULPs), and a select set of DUBs, cleave ubiquitin-like molecules including small ubiquitin-like modifiers (SUMO1/2/3), neuronal precursor cell expressed, developmentally down-regulated 8 (NEDD8) and interferon-stimulated gene 15 (ISG15) from target proteins. SENP5 is an example of a ULP known to be essential for the processing of SUMO3 to generate its mature form, and is also involved in the removal of SUMO2 and SUMO3. Knockdown or inhibition of SENP5 resulted in cell cycle arrest at the G2/M checkpoint and apoptosis suggesting that it plays an important role in cell proliferation (Di Bacco *et al.*, 2006, Wang and Zhang, 2014, Zunino *et al.*, 2007). Wee *et al.*also identified SENP5 as a key prognosis-related gene in cancer, where it was upregulated in approximately 304 tumour samples (Wee *et al.*, 2018). Indeed, Cashman and colleagues demonstrated that low expression of SENP5 correlated with an improved prognosis in breast cancer (Cashman *et al.*, 2014).

Based on the phase data, as well as YOYO1/Phase data, and from discussions with colleagues at Mission Therapeutics, USP16, USP10, VCIP135 and TNFAIP3 were taken forward as 'hits' from this screen (Figure 6.1C).

6.2.2. Knockdown of USP11 with three independent siRNA confirms that USP11 is an essential gene in HCT116 cells.

To further validate and assess the reliability of the screen, experiments were performed to confirm that a DUB shown to be essential for survival of HCT116 cells did indeed induce cell death following its knockdown. Based on data generated from the 5-day screen, USP11 appeared to be an essential DUB and phase data revealed that knockdown of USP11 alone, with three siRNA, resulted in a dramatic loss of cell number. Data from the 5-day screen showed that 11.4 % of cells survived when USP11 was knocked down, using phase data normalised to the non-targeting control (siLUC) (Figure 6.1B).

USP11 has been found to modulate numerous signalling pathways including DNA damage response pathways, Notch and NF-κB signalling pathways (Schoenfeld *et al.*, 2004a, Sun *et al.*, 2010, Wu *et al.*, 2014) and multiple studies have identified a link between USP11 expression and tumorigenesis. For example, USP11 was required for TGFβ-induced EMT and metastasis in breast cancer (Garcia *et al.*, 2018). In addition, siRNA knockdown of USP11 resulted in reduced proliferation of several adherent cancer cell lines, including HCT116 cells (Saei *et al.*, 2018). In terms of mechanism, USP11 was found to deubiquitylate XIAP, resulting in its stabilisation, thereby inhibiting anoikis and apoptosis to promote cancer cell survival (Zhou *et al.*, 2017). Moreover, USP11 was found to promote the stability of p21, critical for the inhibition of cyclin-dependent kinases and control of cell cycle progression (Deng

et al., 2017). Additionally, upon DNA damage, USP11 interacts with BRCA2, resulting in the enhanced survival of breast cancer cells (Schoenfeld *et al.*, 2004b). Together, this suggests that USP11 could be a promising therapeutic target for treatment in several cancers and might be an essential DUB for HCT116 cell survival.

To investigate whether knockdown of USP11 had an effect on cell death, three USP11 siRNAs were transfected into HCT116 cells and the fraction of cells with sub-G1 DNA was analysed by flow cytometry. Western blot analysis revealed that the transfection was successful as all three siRNAs caused a loss of USP11 protein (Figure 6.2A). Knockdown of USP11 resulted in an increase in cell death in HCT116 cells (Figure 6.2B). An increase from ~10 % to ~50% of cells with sub-G1 DNA was observed following transfection of USP11 siRNAs (Figure 6.2B). The percentage of cells with sub-G1 DNA only marginally increased following treatment with PD901, thus not only confirming that indeed USP11 is an essential DUB in HCT116 cells but also increases confidence in the reliability of the 5-day screen. Loss of phosphorylated ERK1/2 following treatment with PD901 confirmed that PD901 successfully inhibited MEK1/2. In addition, it should be noted that knockdown of BCL-X_L was lethal confirming its use as a positive control in the screen.

6.2.3. USP16 is a partial hit with two independent siRNA showing a small increase in the fraction of cells with sub-G1 DNA following treatment with PD0325901.

The initial screen identified USP16 as a 'hit' DUB as knockdown of USP16 combined with the MEK1/2 inhibitor PD901 to induce cell death (Figure 5.11D). USP16 has been previously shown to regulate histone H2A, where knockdown of USP16 resulted in an increase in ubiquitinated H2A and a decrease in mature and progenitor cells without altering the number of hematopoietic stem cells (Cohen *et al.*, 2005, Gu *et al.*, 2016, Joo *et al.*, 2007, Yang *et al.*, 2014), thus, revealing a role for USP16 in the regulation of haematopoiesis. Interestingly, USP16 is found on chromosome 21 and is triplicated in Down's syndrome, which is characterised in part by haematopoietic disease (Adorno *et al.*, 2013). Multiple studies have implicated H2A deubiquitylation in the control of chromosomal condensation, consistent with the role of USP16 in this process (Joo *et al.*, 2007, Kouzarides, 2007). In addition, mass spectrometry data demonstrated that USP16 interacts with PLK1; this interaction resulted in the deubiquitylation of PLK1 and its recruitment to kinetochores allowing for correct chromosome alignment (Zhuo *et al.*, 2015).

Figure 6.2 USP11 is an essential gene for HCT116 survival.

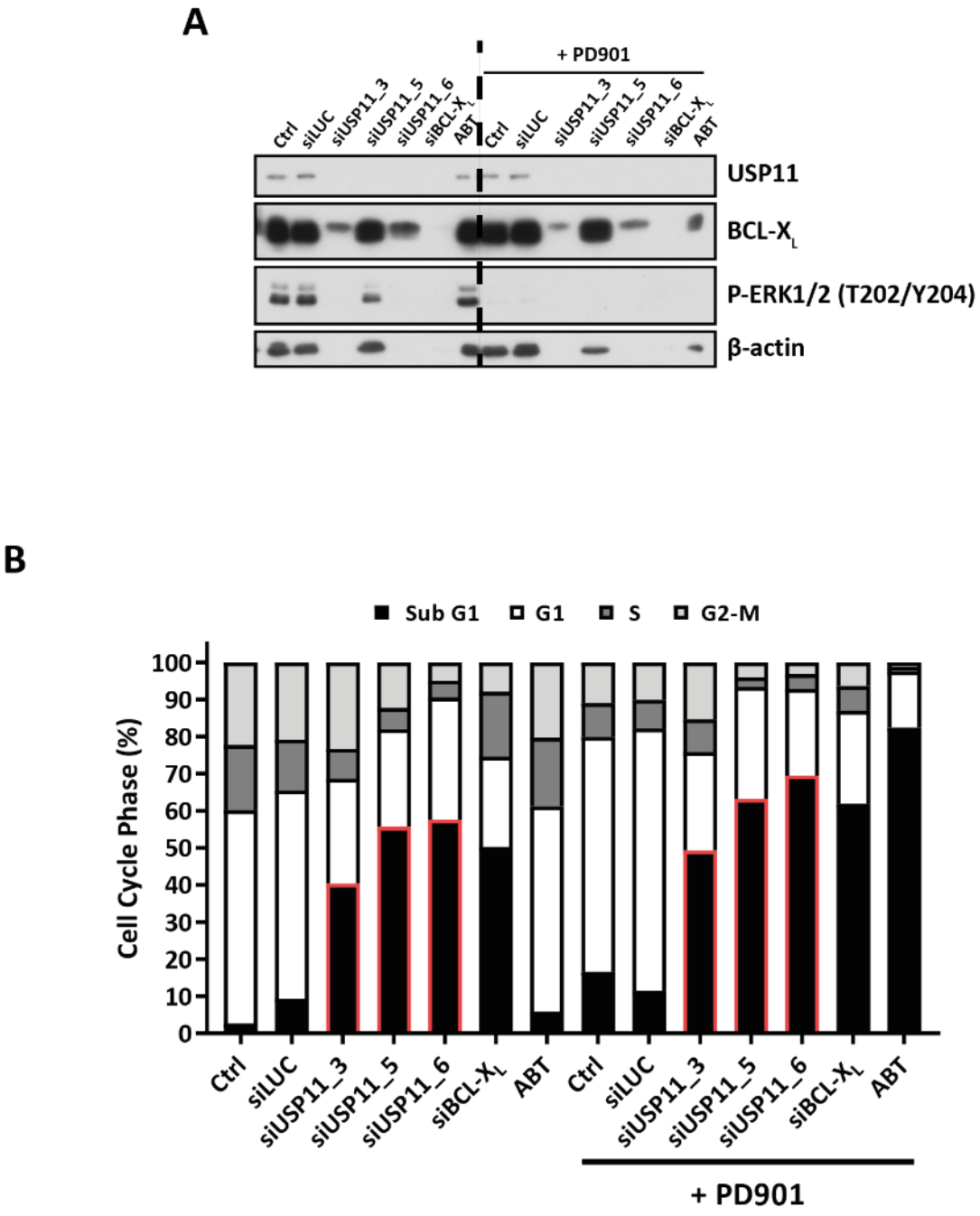

Figure 6.2 USP11 is an essential gene for HCT116 survival. (A + B) Cycling HCT116 cells were left untransfected (Ctrl) or transfected with 10 nM of indictated siRNA. 24 hrs post-transfection cells were treated with DMSO, 0.03 μM PD0325901 (PD901) or 1 μM ABT-263 (ABT) for a further 96 hrs after which **(A)** cells were lysed, fractionated by SDS-PAGE and subjected to western blotting with the antibodies indicated in the figure. This experiment was performed once, or **(B)** fixed and stained with propidium iodide and cell death (sub-G1 DNA) determined by flow cytometry. Results shown here are from one experiment, performed in technical triplicate.

Interestingly, USP16 is phosphorylated at the start of mitosis and dephosphorylated during the metaphase-anaphase transition (Clague *et al.*, 2008). Further work has shown that USP16 is required for cell-cycle progression. Deubiquitylation of H2A enables phosphorylation of Histone H3 at S10, by Aurora B, enabling G2/M transition. Therefore, in accordance with USP16 regulating H2A ubiquitylation, knockdown of USP16 resulted in the reduction of the percentage of cells in M phase and correlated with a delayed entry into mitosis (Clague *et al.*, 2008, Joo *et al.*, 2007). Thus, overall, USP16 regulates chromosomal condensation and progression through the G2/M checkpoint.

In HCT116 cells, despite all three siRNA knocking down USP16 with equal efficiency, knockdown of USP16 alone showed variable results (Figure 6.3A and Figure 6.3B). Knockdown of USP16 using siUSP16_03D resulted in a large increase in cell death, which only marginally increased further following MEK1/2 inhibition, shown by loss of ERK1/2 phosphorylation (Figure 6.3A and Figure 6.3B). In contrast, very little cell death was seen with transfection of the remaining two siRNA (Figure 6.3B). The large increase in the fraction of cells with sub-G1 DNA as a consequence of siUSP16_03D transfection could be due to off-target effects of this siRNA as compared to the other siRNAs used.

Following addition of PD901 to HCT116 cells transfected with siUSP16_O2D and siUSP16_11, a minor increase in the fraction of cells with sub-G1 DNA was seen. A maximum increase of ~25 % (siUSP16_11) was observed, compared to the positive control of PD901 and ABT-263, where ~80 % of the cells had sub-G1 DNA (Figure 6.3B), thus, USP16 is a weak hit. Data presented here demonstrated that USP16 knockdown failed to induce a consistent cytotoxic effect in combination with PD901. These experiments also emphasised the importance of choosing a variety of siRNA, targeting different regions of the gene, as although all three siRNAs successfully knocked down USP16, only two resulted in a comparable cell death response.

6.2.4. Knockdown of VCIP135 in combination MEK1/2 inhibition induces apoptosis.

VCIP135 was identified as a 'hit' from the 5-day DUB RNAi screen, described in Chapter 5, as three siRNAs against VCIP135 combined with MEK1/2 inhibition to induce cell death (Figure 5.11D).

Golgi membrane fusion is regulated, in part, by p97, an ATPase, that forms a complex with the cofactor p47 and the SNARE protein, syntaxin5, a receptor in the golgi membrane. Valosin-containing protein p97/p47 complex-interacting protein, p135 (VCIP135) acts as an additional cofactor for this complex; interaction of VCIP135 with this complex results in p97-driven ATP hydrolysis, dissociation of

Figure 6.3 Further analysis revealed that, in HCT116 cells, USP16 is not a 'hit' DUB.

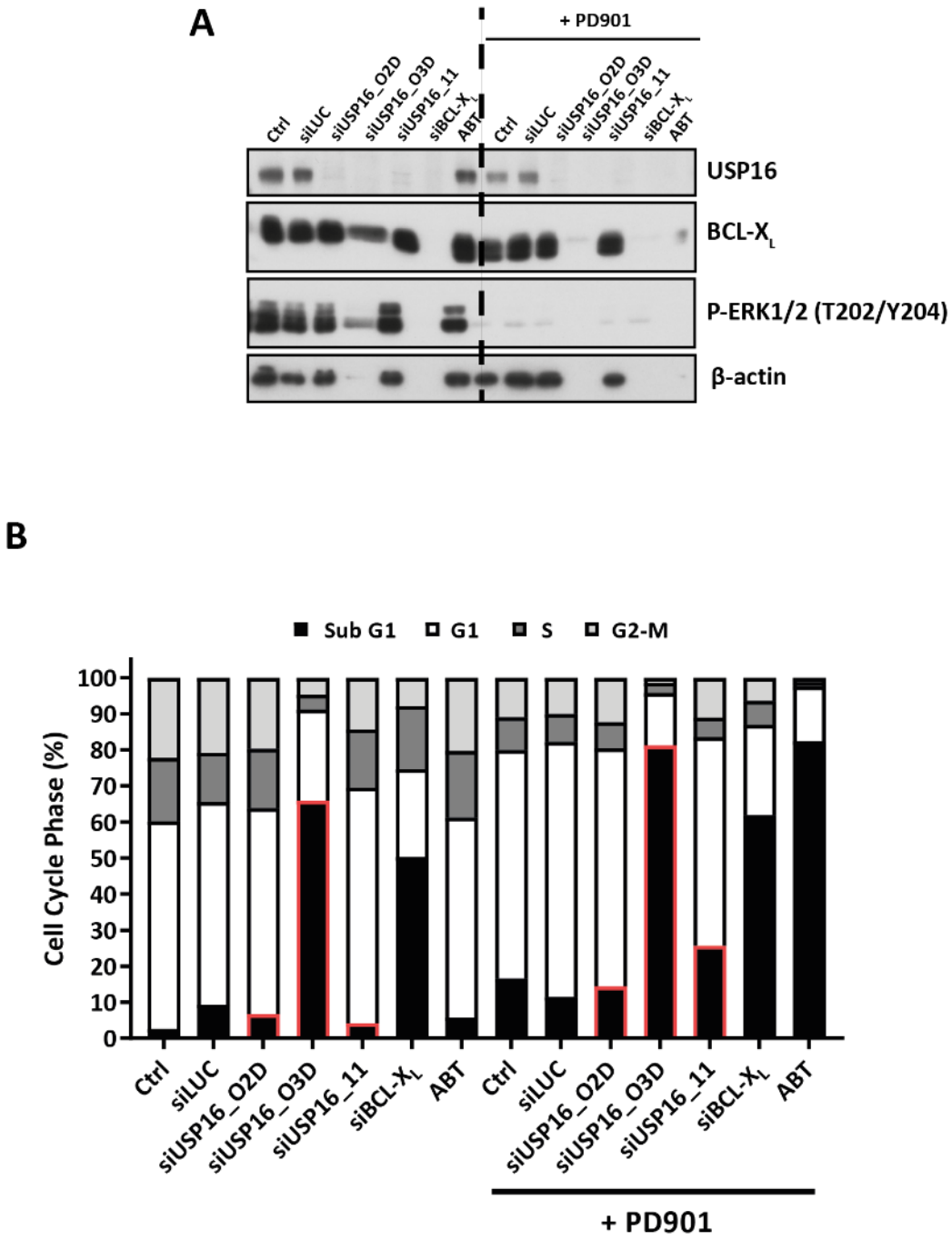

Figure 6.3 Further analysis revealed that, in HCT116 cells, USP16 is not a 'hit' DUB. (A + B) Cycling HCT116 cells were left untransfected (Ctrl) or transfected with 10 nM of indictated siRNA. 24 hrs post-transfection cells were treated with DMSO, 0.03 μM PD0325901 (PD901) or 1 μM ABT-263 (ABT) for a further 96 hrs after which **(A)** cells were lysed, fractionated by SDS-PAGE and subjected to western blotting with the antibodies indicated in the figure. This experiment was performed once, or **(B)** fixed and stained with propidium iodide and cell death (sub-G1 DNA) determined by flow cytometry. Results shown here are from one experiment, performed in technical triplicate.

the p97/p47/syntaxin5 complex and postmitotic membrane fusion (Uchiyama *et al.*, 2002). The deubiquitylating activity of VCIP135 is required for fusion events, although its exact target is unknown (Wang *et al.*, 2004). p37, like p47, can also form a complex with p97 and requires VCIP135 for Golgi and ER membrane fusion during interphase and at the end of mitosis (Uchiyama *et al.*, 2006). However, unlike p97/p47, p97/p37 does not rely upon the deubiquitylating activity of VCIP135 for membrane fusion and organelle maintenance during interphase (Totsukawa *et al.*, 2011, Uchiyama *et al.*, 2006). The activity of VCIP135 is tightly regulated throughout cell cycle progression. During mitosis, CDK1 phosphorylates VCIP135, thereby inhibiting its activity, preventing p97/p47-mediated Golgi reassembly (Zhang and Wang, 2015, Zhang *et al.*, 2014).

Like VCIP135, ERK1/2 signalling has been shown to regulate membrane fusion. The ERK1 isoform ERK1c translocates from the cytosol to the Golgi to regulate the fragmentation of the Golgi membrane during mitosis (Aebersold *et al.*, 2004). More importantly, ERK1/2 signalling plays a significant role in regulating mitochondrial morphology. Recently ERK1/2 have been shown to regulate mitochondrial fission machinery, DRP1, in cancer cells as well as induced pluripotent stem cells (Cook *et al.*, 2017, Kashatus *et al.*, 2015, Prieto *et al.*, 2016).

Further analysis of VCIP135 as a 'hit' revealed that siRNA knockdown of VCIP135, using a SMARTpool siRNA reagent, resulted in the successful loss of VCIP135 protein (Figure 6.4A). Additionally treatment of HCT116 cells with PD901, either in combination with VCIP135 knockdown or alone, resulted in loss of phosphorylated ERK1/2 indicative of MEK1/2 inhibition (Figure 6.4A). Knockdown of VCIP135, in combination with PD901 treatment, resulted in a significant increase in the fraction of cells with sub-G1 DNA, compared to knockdown of VCIP135 alone as well as knockdown of siLUC in combination with PD901 (Figure 6.4B). Results indicated that combining knockdown of VCIP135 with MEK1/2 inhibition led to a greater than additive effect, resulting in an induction of cell death.

To assess if cell death arising from VCIP135 knockdown in PD901 treated cells was indeed apoptosis, the cell death observed in response to knockdown and treatment was compared in WT and BAK/BAX DKO HCT116 cells. Knockout of BAK and BAX resulted in a substantial reduction in cell death (Figure 6.5A). Thus, combined VCIP135 siRNA transfection and PD901 treatment induced BAK/BAX-dependent apoptosis in HCT116 cells. Transfection of HCT116 cells with VCIP135 siRNA and treatment with PD901 did not cause any significant changes in the protein levels of pro-survival and pro-apoptotic BCL2 proteins, compared to control samples (Figure 6.5B). BIM and PUMA protein were observed to accumulate, but this was due only to treatment with the MEK1/2 inhibitor alone and not due to the combined knockdown of VCIP135 with PD901 treatment (Figure 6.5B).

Figure 6.4 Combination of VCIP135 knockdown with PD0325901 resulted in an increase in the fraction of cells with sub-G1 DNA.

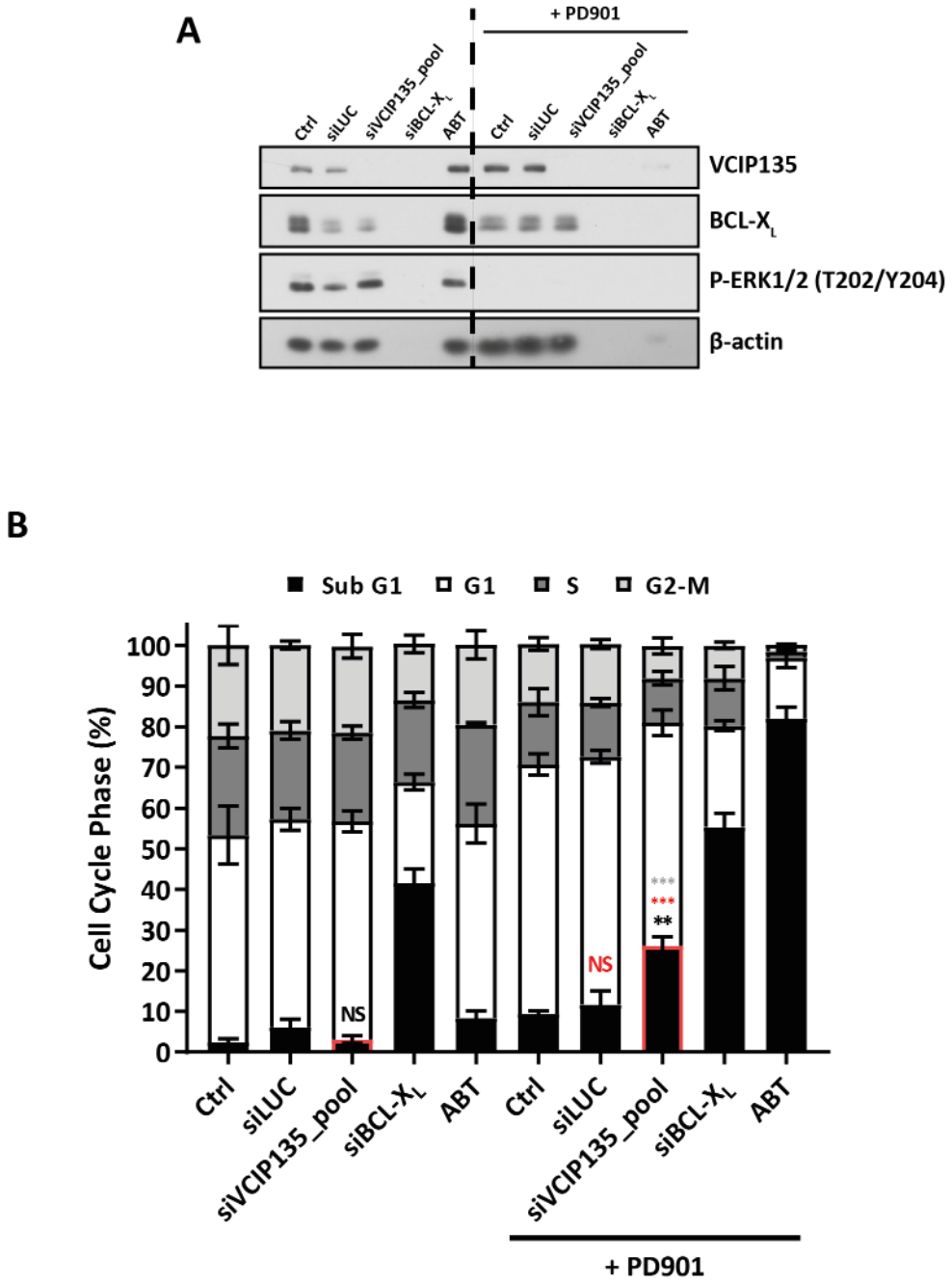

Figure 6.4 Combination of VCIP135 knockdown with PD0325901 resulted in an increase in the fraction of cells with sub-G1 DNA. (A + B) Cycling HCT116 cells were left untransfected (Ctrl) or transfected with 10 nM of indictated siRNA. 24 hrs post-transfection cells were treated with DMSO, 0.03 μM PD0325901 (PD901) or 1 μM ABT-263 (ABT) for a further 96 hrs after which **(A)** cells were lysed, fractionated by SDS-PAGE and subjected to western blotting with the antibodies indicated in the figure. This data is representative of one experiment, of which two have been performed giving similar results, or **(B)** fixed and stained with propidium iodide and cell death (sub-G1 DNA) determined by flow cytometry. Results shown here are representative of the mean ± SD of three independent experiments, where each biological replicate is performed in technical triplicate. $P < 0.0001$ (***), $P < 0.001$ (**), $P < 0.01$ (*) or not significant (ns) for siLUC vs siVCIP135 or siLUC + PD901 vs siVCIP135 + PD901 (Black), Ctrl + PD901 vs siVCIP135 + PD901 or siLUC + PD901 (Red), siVCIP135 vs siVCIP135 + PD901 (grey), as determined by one-way ANOVA with Tukey post-hoc test.

Figure 6.5 Cell death observed with the combination of VCIP135 knockdown and PD0325901 is BAK/BAX-dependent.

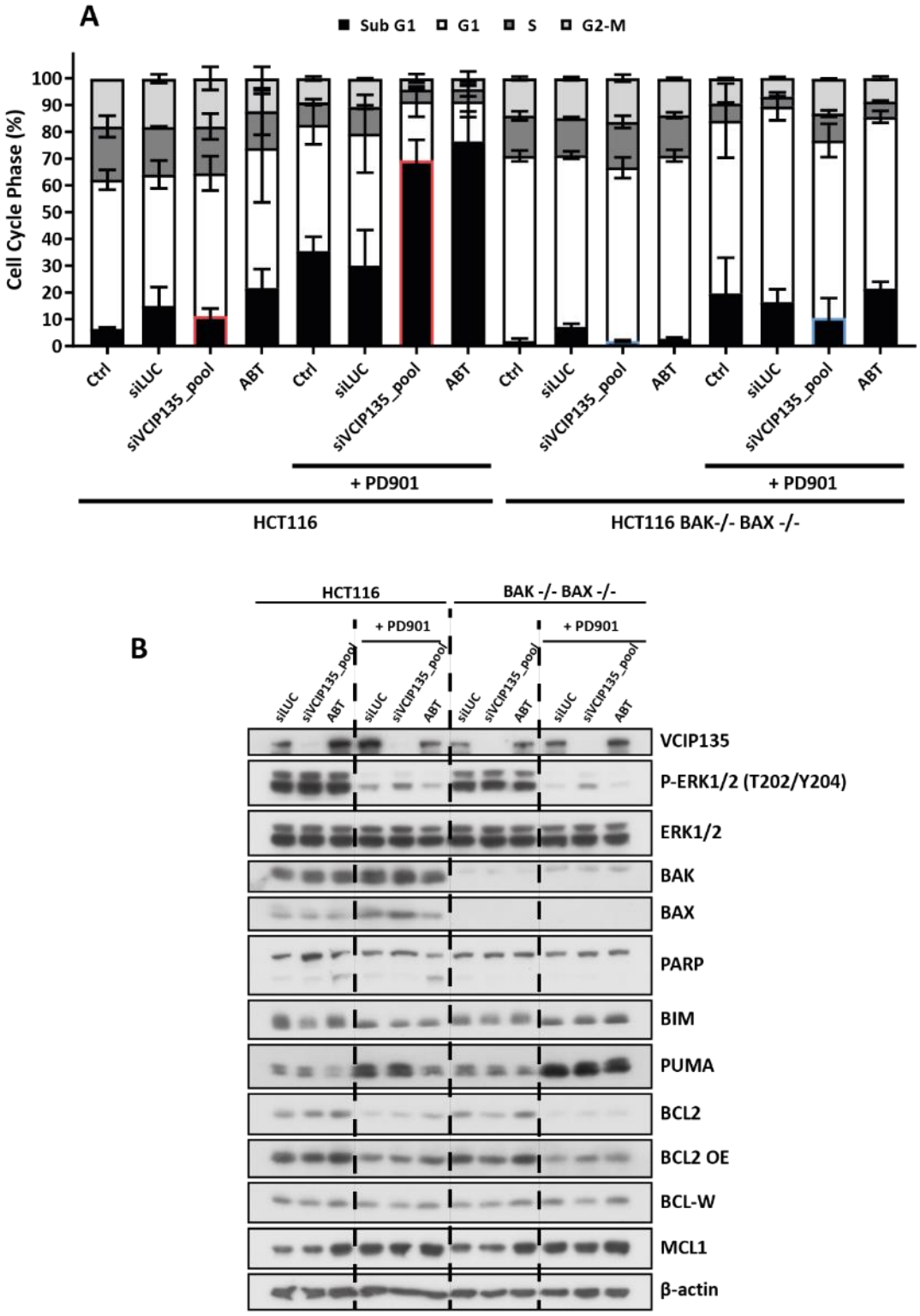

Figure 6.5 Cell death observed with the combination of VCIP135 knockdown and PD0325901 is BAK/BAX-dependent. (A + B) Cycling HCT116 and genetically engineered BAK-/- BAX-/- HCT116 cells were left untransfected (Ctrl) or transfected with 10 nM of indictated siRNA. 24 hrs post-transfection cells were treated with DMSO, 0.03 μM PD0325901 (PD901) or 1 μM ABT-263 (ABT) for a further 96 hrs after which cells were **(A)** fixed and stained with propidium iodide and cell death (sub-G1 DNA) determined by flow cytometry. Results shown here are representative of the mean ± SD of two independent experiments, where each biological replicate is performed in technical triplicate or **(B)** lysed, fractionated by SDS-PAGE and subjected to western blotting with the antibodies indicated in the figure. This data is representative of one experiment, of which two have been performed giving similar results.

6.2.5. Knockdown of TNFAIP3 in combination with MEK1/2 inhibition did not induce a cell death response.

TNFAIP3 was identified as a 'hit' from the 5-day DUB RNAi screen in combination with MEK1/2 inhibition (Figure 5.11D). The OTU deubiquitylating enzyme, tumour necrosis factor-alpha-induced protein 3 (TNFAIP3), also known as A20, has been shown to have numerous cellular functions, but primarily it plays a vital role in the regulation of inflammation. TNFAIP3 inhibits the canonical NF-κB signalling pathway, a pro-inflammatory signalling pathway, in which NF-κB transcription factors drive the effects of pro-inflammatory cytokines (Vucic *et al.*, 2011). Failure to regulate this pathway results in chronic inflammation and cell death (Lee *et al.*, 2000). Indeed, mice lacking TNFAIP3 have a severe defective inflammatory phenotype (Lee *et al.*, 2000). In humans, single nucleotide polymorphisms (SNPs) in TNFAIP3 are linked to numerous disease states including rheumatoid arthritis, Crohn's disease and systemic lupus erythematosus (SLE) (Graham *et al.*, 2008, Hammer *et al.*, 2011, Musone *et al.*, 2008, Plenge *et al.*, 2007, Shimane *et al.*, 2010, Thomson *et al.*, 2007).

TNFAIP3 can function as both an E3 ligase and a DUB in the NF-κB pathway. Specifically, TNFAIP3 cleaves K63 polyubiquitin chains from RIP1, a positive regulator of the pathway, and catalyses, via its ZnF4 (Zinc finger 4), the addition of K48-linked chains to RIP1, resulting in the proteasomal degradation of RIP1 (Wertz *et al.*, 2004). TNFAIP3 also inactivates several E2/E3 ligase complexes required for activation of canonical NF-κB signalling (Shembade *et al.*, 2010). However, there is additional evidence that TNFAIP3 can inhibit NF-κB signalling independently of its deubiquitylating activity (Skaug *et al.*, 2011). Interestingly, TNFAIP3 has also been shown to promote the stability of NIK, and in doing so activates non-canonical NF-κB signalling (Yamaguchi *et al.*, 2013). Consequently, Yamaguchi and colleagues concluded that TNFAIP3 activity can regulate the switch between canonical and non-canonical NF-κB signalling (Yamaguchi *et al.*, 2013).

NF-κB is constitutively activated in a variety of cancers, promoting the survival of these cells. This has been linked to the loss of negative regulators of NF-κB signalling, including TNFAIP3. Several studies have identified somatic mutations, deletions and alterations in the expression of TNFAIP3 in cancer (Fujii *et al.*, 2018). Interestingly re-expression of TNFAIP3 in tumour cells with mutated TNFAIP3 induced cell-cycle arrest and/or apoptosis, indicating a role for TNFAIP3 in promoting cell death (Compagno *et al.*, 2009, Kato *et al.*, 2009). In addition, down regulation of TNFAIP3 is also associated with metastasis, by regulating expression of E-cadherin and vimentin, and therefore EMT in nasopharyneal carcinoma cells (NPC) (Huang *et al.*, 2017b). Ultimately, one could predict that knockdown of TNFAIP3 could alleviate inhibition of canonical NF-κB signalling resulting in cell survival.

Knockdown of TNFAIP3, with or without PD901, in HCT116 cells, did not cause an increase in the fraction of cells with sub-G1 DNA, despite effective knockdown of TNFAIP3 protein (Figure 6.6A and Figure 6.6B). A small increase in the fraction of cells with G1 DNA was observed following treatment with PD901, indicative of cell cycle arrest, expected as a consequence of MEK1/2 inhibition in HCT116 cells (Figure 6.6B) (Sale and Cook, 2013). Therefore, TNFAIP3 was no longer considered a 'hit' since knockdown of TNFAIP3 did not combine with PD901 to induce cell death.

Interestingly, inhibition of MEK1/2, in general, was associated with a reduction of TNFAIP3 protein (Figure 6.6A), although the reason for this is unknown.

6.2.6. Knockdown of YOD1 in combination with MEK1/2 inhibition promotes cell death.

YOD1 was also identified as a 'hit' from the 5-day DUB RNAi screen, promoting cell death when combined with MEK1/2 inhibition (Figure 5.11D). Further analysis suggested that, at least from the 5-day DUB RNAi screen, it might be an essential DUB for survival of HCT116 cells. However, the effect of dual knockdown of YOD1 and MEK1/2 inhibition was investigated further, given that it had been identified as a 'hit' in the 3-day DUB RNAi screen and also when analysing data from the 5-day screen using different end-point assays.

First discovered in *Drosophilia*, the Hippo signalling pathway controls organ size by regulating cell proliferation, apoptosis and stem cell renewal. The biological relevance of the conserved Hippo signalling cascade was supported through studies of transgenic (Camargo *et al.*, 2007, Dong *et al.*, 2007) and knockout mice (Lu *et al.*, 2010, Song *et al.*, 2010, Zhou *et al.*, 2009) additionally indicating that activation of YAP/TAZ can induce tumourigenesis (Lei *et al.*, 2008, Zhao *et al.*, 2010a).

At the molecular level, activation of the Hippo kinase cascade results in the activation of LATS1/2, which phosphorylates YAP/TAZ, transcriptional coactivators that regulate gene expression through their interaction with TEAD1-4. This induces the cytoplasmic sequestration of YAP/TAZ and/or its ubiquitin-driven proteasomal degradation (Meng *et al.*, 2016, Pan, 2010, Zhao *et al.*, 2010a, Zhao *et al.*, 2007). In contrast to the above, inactivation of Hippo signalling results in the nuclear accumulation of unphosphorylated YAP/TAZ resulting in TEAD-mediated gene expression leading to cell proliferation and inhibition of apoptosis (Koontz *et al.*, 2013) (Figure 6.7).

Figure 6.6 Combination of YOD1 knockdown, but not TNFAIP3 with PD0325901 resulted in an increase in cell death.

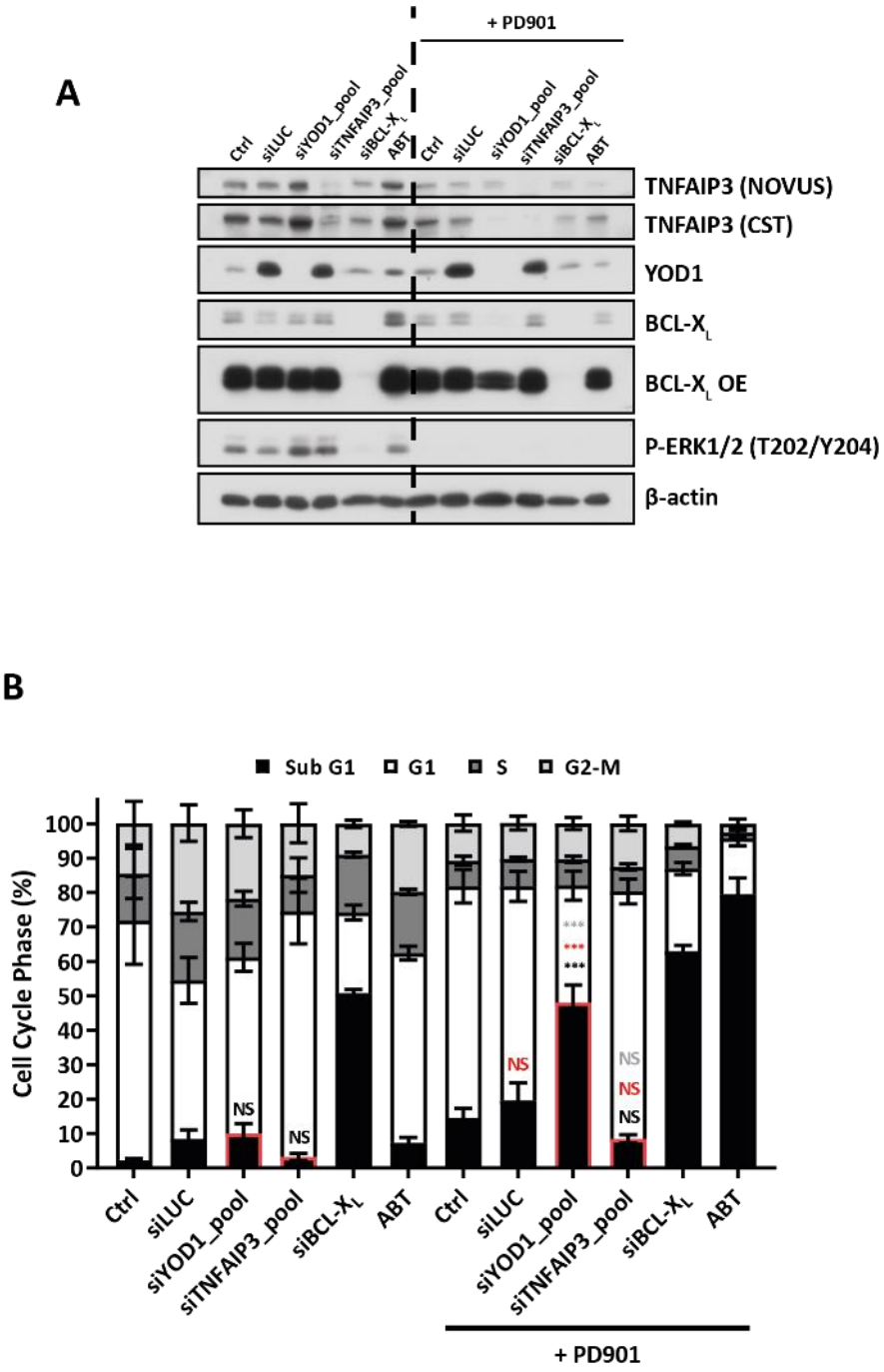

Figure 6.6 Combination of YOD1 knockdown, but not TNFAIP3 with PD0325901 resulted in an increase in cell death. (A + B) Cycling HCT116 cells were left untransfected (Ctrl) or transfected with 10 nM of indictated siRNA. 24 hrs post-transfection cells were treated with DMSO, 0.03 μM PD0325901 (PD901) or 1 μM ABT-263 (ABT) for a further 96 hrs after which **(A)** cells were lysed, fractionated by SDS-PAGE and subjected to western blotting with the antibodies indicated in the figure. This data is representative of one experiment, of which two have been performed giving similar results, or **(B)** fixed and stained with propidium iodide and cell death (sub-G1 DNA) determined by flow cytometry. Results shown here are representative of the mean ± SD of three independent experiments, where each biological replicate is performed in technical triplicate. $P < 0.0001$ (***), $P < 0.001$ (**), $P < 0.01$ (*) or not significant (ns) for siLUC vs siYOD1/siTNFAIP3 or siLUC + PD901 vs siYOD1/siTNFAIP3 + PD901 (Black), Ctrl + PD901 vs siYOD1/siTNFAIP3 + PD901 or siLUC + PD901 (Red), siYOD1/siTNFAIP3 vs siYOD1/siTNFAIP3 + PD901 (grey), as determined by one-way ANOVA with Tukey post-hoc test.

Figure 6.7 Schematic model for the role of YOD1 in the regulation of Hippo signalling.

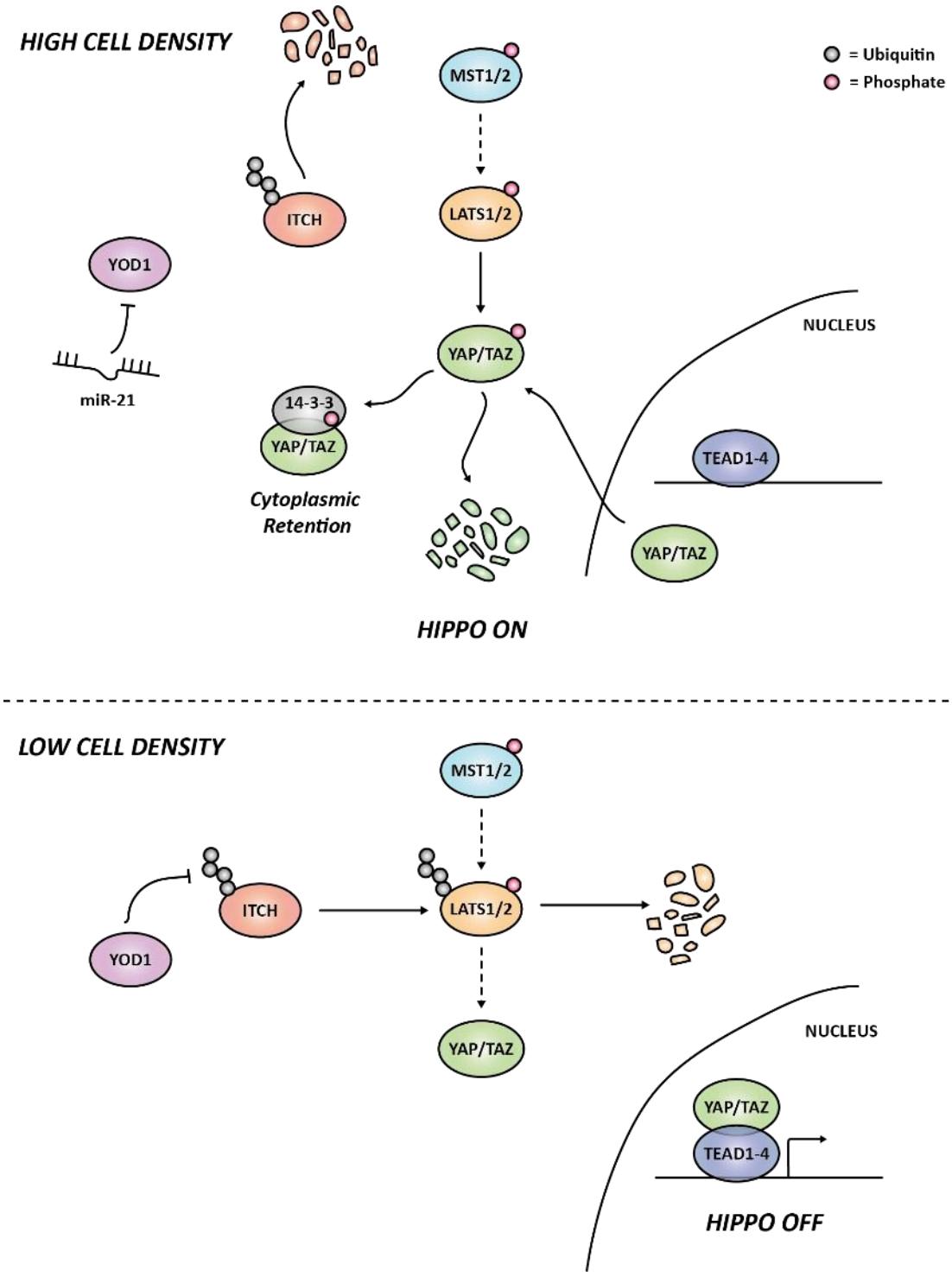

Figure 6.7 Schematic model for the role of YOD1 in the regulation of Hippo signalling. At high cell densities, miR-21 results in low levels of YOD1, enhanced phosphorylation of YAP/TAZ by LATS1/2 and reduction of YAP/TAZ-mediated target genes. At low cell densities, high YOD1 levels results in the increased stability of ITCH leading to the ubiquitylation and degradation of LATS1/2 alleviating inhibtion of YAP/TAZ signalling resulting in high expression of YAP/TAZ target genes and cell proliferation (Based on a schematic from Kim et al., 2017).

Several components of the Hippo signalling pathway are regulated through post-translational modification, including ubiquitylation. The E3 ligase ITCH was found to promote the ubiquitin-driven degradation of LATS1/2, activating YAP/TAZ and inducing the expression of YAP/TAZ target genes (Salah *et al.*, 2011). Recently YOD1 was identified to be the DUB for ITCH (Kim and Jho, 2017, Kim *et al.*, 2017). Deubiquitylation of ITCH, by YOD1, results in its increased stability again activating YAP/TAZ and inducing cell proliferation (Figure 6.7). Kim *et al.*, demonstrated that overexpression of YOD1 enhanced the migratory phenotype of HCT116 cells and that this was dependent on YAP (Kim *et al.*, 2017). By extrapolation, knockdown of YOD1 would induce the degradation of ITCH, preventing the ubiquitin-driven degradation of LATS1/2, resulting in the phosphorylation and degradation of YAP/TAZ and activation of the Hippo signalling pathway, restricting cell growth.

Hippo signalling is regulated by cell-cell contacts to link cell density to cell proliferation (Das Thakur *et al.*, 2010, Kim *et al.*, 2011b). The same seems to apply to YOD1. For example, miR-21 is regulated in a density-dependent manner and controls YOD1 expression. Cells grown to a high density have a high level of miR-21 which down regulates YOD1 and therefore activates the Hippo signalling pathway (Kim *et al.*, 2017) (Figure 6.7).

Interestingly, in the context of the DUB RNAi screen, ERK1/2 signalling can regulate the Hippo signalling pathway component YAP. Reduction in ERK1/2 activity by siRNA or small molecule inhibitors resulted in reduced YAP protein, due to increased rates of degradation, and a reduction in the mRNA levels of downstream Hippo signalling genes. Indeed, treatment of non-small cell lung cancer (NSLC) cells with the MEK1/2 inhibitor trametinib reduced YAP protein, which resulted in a reduction in the migration and invasion of these cells (You *et al.*, 2015). Additionally, Li et al, demonstrated that MEK1 and YAP directly interact and this is essential for tumourigenesis in liver cancer (Li *et al.*, 2013). Overall, this data supports the idea that knockdown of YOD1 in combination with ERK1/2 pathway inhibition has the potential to inhibit cell proliferation and induce apoptosis through the regulation of YAP. On this basis, YOD1 was followed up as a 'hit'.

Transfection of siYOD1 into HCT116 cells, using a SMARTpool siRNA reagent, resulted in the loss of YOD1 protein (Figure 6.6A). Treatment of HCT116 cells with PD901, either in combination with YOD1 knockdown or alone, resulted in loss of phosphorylated ERK1/2 indicative of MEK1/2 inhibition (Figure 6.6A). Interestingly, knockdown of YOD1 prevented the accumulation of BIM protein in PD901 treated cells; this was not seen with control siRNA (Figure 6.6A). Knockdown of YOD1 combined with PD901 to induce an increase in PARP cleavage indicative of an induction of apoptosis. The cell death response induced by combination treatment was confirmed from flow cytometry data. Knocking down YOD1 or treating HCT116 cells with PD901 alone resulted in little cell death; however, the combination resulted

in a statistically significant, synergistic increase in cell death (Figure 6.6B). To test whether, as predicted from western blot data in Figure 6.6A, the combination induced apoptosis, HCT116 cells lacking BAK and BAX were used. Knockout of BAK/BAX significantly reduced the fraction of cells with sub-G1 DNA therefore combined knockdown of YOD1 and PD901 treatment caused apoptosis of HCT116 cells (Figure 6.8A).

Of note, the significance of the increase in cell death observed with combined knockdown of YOD1 and inhibition of MEK1/2 in Figure 6.8 was different from that observed in Figure 6.6, which is discussed later on.

Knockdown of YOD1 did not result in the expected reduction in YAP protein. Interestingly, loss of YOD1 alone appeared to cause an increase in YAP protein and additionally resulted in a marginal increase in the phosphorylation of YAP at S127 (Figure 6.8B). Phosphorylation at this site, by LATS1/2 is known to drive the cytoplasmic localisation of YAP and is required for its interaction with 14-3-3 proteins, thereby inhibiting its biological function (Zhao *et al.*, 2007). This therefore suggests that knockdown of YOD1 could drive an increase in inactive phosphorylated YAP protein. In combination with PD901 treatment, YOD1 knockdown did result in a reduction in phosphorylated and total YAP compared to controls (Figure 6.8B). This could be due to an increase in the proteasomal degradation of YAP. However, additional analysis would have to be performed to confirm these findings.

6.2.7. Combining USP10 siRNA with PD0325901 treatment causes an increase in sub-G1 DNA.

In addition to the DUBs previously described, USP10 was also identified as a 'hit' from the 5-day DUB RNAi screen, promoting cell death when combined with MEK1/2 inhibition (Figure 5.11D).

In the literature, USP10 has been demonstrated to regulate p53 signalling, via G3BP2, in prostate cancer (Takayama *et al.*, 2018). p53 primarily acts as a tumour suppressor, and inactivation of the p53 pathway is linked to carcinogenesis (Kruse and Gu, 2009). G3BP2 (GTPase-activating protein-binding protein 2) is an androgen-responsive (AR) gene that regulates the localisation of p53, promoting its nuclear export and inhibiting p53 signalling (Ashikari *et al.*, 2017). Ashikari and colleagues have also demonstrated that knockdown of G3BP2 resulted in p53-mediated apoptosis (Ashikari *et al.*, 2017). USP10 interacts with G3BP2, in prostate cancer cells and in stress granules (SG), resulting in the increased stability of G3BP2, nuclear export of p53 and enhanced cell proliferation.

Figure 6.8 YOD1 siRNA in combination with PD0325901 induces a BAX/BAK-dependent cell death.

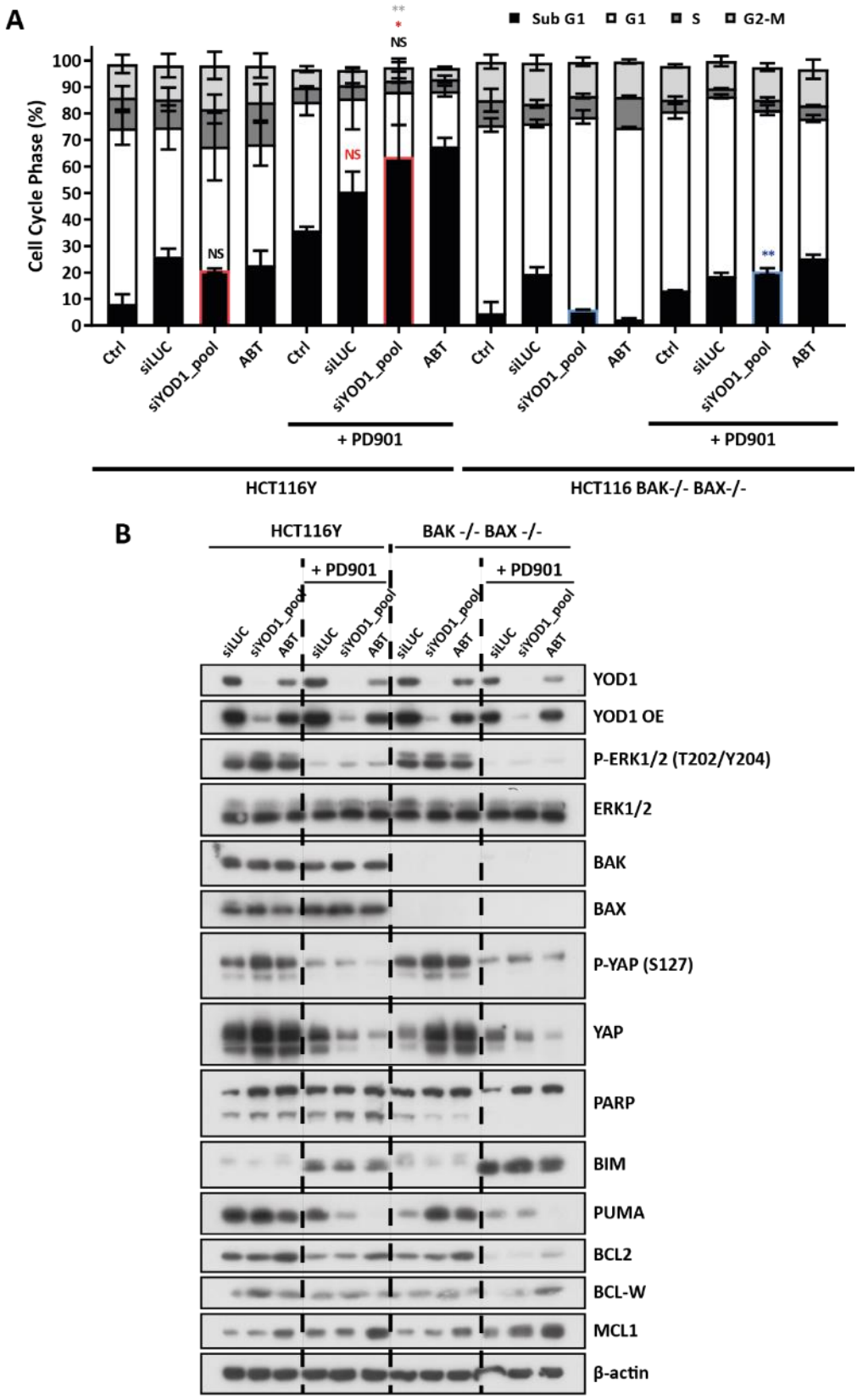

Figure 6.8 YOD1 siRNA in combination with PD0325901 induces a BAX/BAK-dependent cell death. (A + B) Cycling HCT116 and genetically engineered BAK-/- BAX-/- HCT116 cells were left untransfected (Ctrl) or transfected with 10 nM of indictated siRNA. 24 hrs post-transfection cells were treated with DMSO, 0.03 μM PD0325901 (PD901) or 1 μM ABT-263 (ABT) for a further 96 hrs after which cells were **(A)** fixed and stained with propidium iodide and cell death (sub-G1 DNA) determined by flow cytometry. Results shown here are representative of the mean ± SD of three independent experiments, where each biological replicate is performed in technical triplicate. $P < 0.0001$ (***), $P < 0.001$ (**), $P < 0.01$ (*) or not significant (ns) for siLUC vs siYOD1 or siLUC + PD901 vs siYOD1 + PD901 (Black), Ctrl + PD901 vs siYOD1 + PD901 or siLUC + PD901 (Red), siYOD1 vs siYOD1 + PD901 (grey), siYOD1 + PD901 vs siYOD1 + PD901 (BAK-/- BAX-/-) (Blue), as determined by one-way ANOVA with Tukey post-hoc test or **(B)** lysed, fractionated by SDS-PAGE and subjected to western blotting with the antibodies indicated in the figure. This data is representative of one experiment, of which two have been performed giving similar results,

Conversely, knockdown of USP10 resulted in the reduction of G3BP2 protein levels, relieving inhibition of p53 activity and resulting in impaired cell growth (Takayama *et al.*, 2018). Overall, data from these studies suggests an oncogenic role for USP10, in part by repressing p53 activity (Figure 6.9). In addition to prostate cancer, G3BP2 is associated with poor prognosis in breast cancer patients and is required for tumour initiation (French *et al.*, 2002, Gupta *et al.*, 2017). However, the role of USP10 may be context dependent as it has also been found to act as a tumour suppressor in cancer including lung cancer (Sun *et al.*, 2018).

Recently, Ouchida and colleagues demonstrated that USP10 was the DUB for the transcription factor SLUG/SNAI2 (Ouchida *et al.*, 2018). SLUG is a marker for cells undergoing epithelial-to-mesenchymal transition (EMT); SLUG represses E-cadherin expression and as result enhances EMT and metastasis in cancer (Puisieux *et al.*, 2014). Deubiquitylation of SLUG by USP10 stabilised SLUG protein in tumour cells, and, in contrast, knockdown of USP10 decreased expression of SLUG and Vimentin, consequently reducing the migratory phenotype of these cells (Ouchida *et al.*, 2018). Interestingly, EMT-transcription factors, including SLUG, have also been demonstrated to promote malignant transformation via the inhibition of p53 signalling (Puisieux *et al.*, 2014).

Further examination of USP10 as a 'hit', revealed that knockdown of USP10, resulted in loss of USP10 protein with three siRNAs (Figure 6.10A). Treatment of HCT116 cells with PD901, either in combination with USP10 knockdown or alone, resulted in loss of phosphorylated ERK1/2 indicative of MEK1/2 inhibition (Figure 6.10A). Knockdown of USP10, with siUSP10_1 resulted in a significant increase in the fraction of cells with sub-G1 DNA (Figure 6.10B). In contrast, knockdown of USP10 (siUSP10_5 and siUSP10_69) alone resulted in minimal cell death, which when combined with PD901 treatment resulted in a significant increase in cell death (Figure 6.10B). Interestingly, siUSP10_1 also combined with MEK1/2 inhibition to induce a significant increase in the fraction of cells with sub-G1 DNA, when compared with knockdown of USP10 alone or knockdown of siLUC, combined with PD901 treatment (Figure 6.10B). Synergy between knockdown of USP10 and PD901 treatment was only observed with siUSP10_5, whilst additional USP10 siRNA combined with MEK1/2 inhibition to cause an additive effect.

Combined treatment of siUSP10 and PD901 in HCT116 cells lacking BAK and BAX showed a significant reduction in the fraction of cells with sub-G1 DNA compared to WT cells. Thus, combined knockdown of USP10 and PD901 treatment induced BAK/BAX-dependent apoptosis of HCT116 cells. (Figure 6.11A).

The cooperative effect of siUSP10 and MEK1/2 inhibition was much less obvious in Figure 6.11 than in Figure 6.10. As a consequence, the significance of the increase in cell death observed following

Figure 6.9 Schematic model for the role of USP10 in the regulation of p53 signalling in prostate cancer

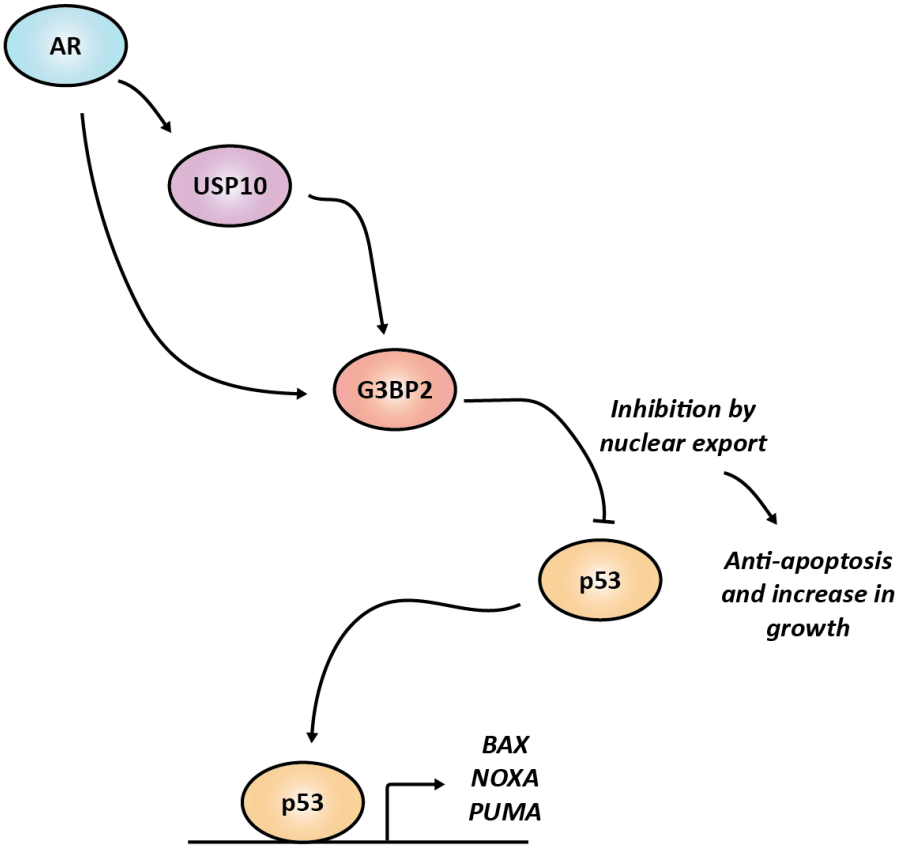

Figure 6.9 Schematic model for the role of USP10 in the regulation of p53 signalling in prostate cancer. Within the nucleus, p53 transcriptionally controls the expression of pro-apoptoic proteins including BAX, NOXA and PUMA. USP10 and G3BP2 are upregulated by androgen receptor activation. USP10 interacts with G3BP2 and enhances protein levels of G3BP2 by blocking its polyubiquitylation directed proteasomal degradation. This results in the inhibition of p53 signalling by promoting its nuclear export. (Based on a schematic from Takayama et al., 2018).

Figure 6.10 Knockdown of USP10 in combination with PD0325901, in HCT116 cells, resulted in an increase in cell death.

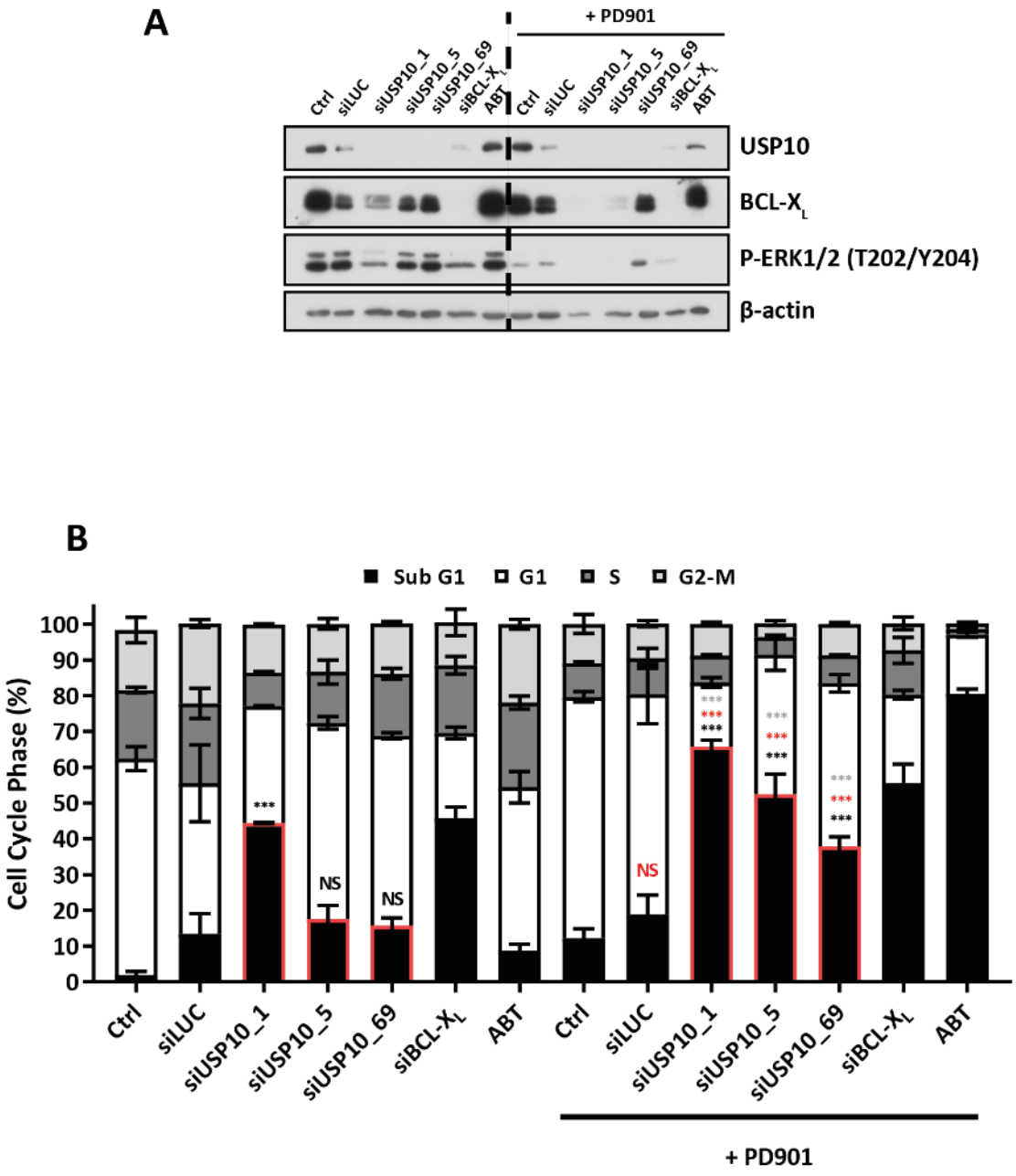

Figure 6.10 Knockdown of USP10 in combination with PD0325901, in HCT116 cells, resulted in an increase in cell death. (A + B) Cycling HCT116 cells were left untransfected (Ctrl) or transfected with 10 nM of indictated siRNA. 24 hrs post-transfection cells were treated with DMSO, 0.03 μM PD0325901 (PD901) or 1 μM ABT-263 (ABT) for a further 96 hours after which **(A)** cells were lysed, fractionated by SDS-PAGE and subjected to western blotting with the antibodies indicated in the figure. This data is representative of one experiment, of which two have been performed giving similar results, or **(B)** fixed and stained with propidium iodide and cell death (sub-G1 DNA) determined by flow cytometry. Results shown here are representative of the mean ± SD of three independent experiments, where each biological replicate is performed in technical triplicate. $P < 0.0001$ (***), $P < 0.001$ (**), $P < 0.01$ (*) or not significant (ns) for siLUC vs siUSP10 or siLUC + PD901 vs siUSP10 + PD901 (Black), Ctrl + PD901 vs siUSP10 + PD901 or siLUC + PD901 (Red), siUSP10 vs siUSP10 + PD901 (grey), as determined by one-way ANOVA with Tukey post-hoc test.

Figure 6.11 USP10 siRNA, with or without PD0325901, induces a BAK/BAX-dependent cell death.

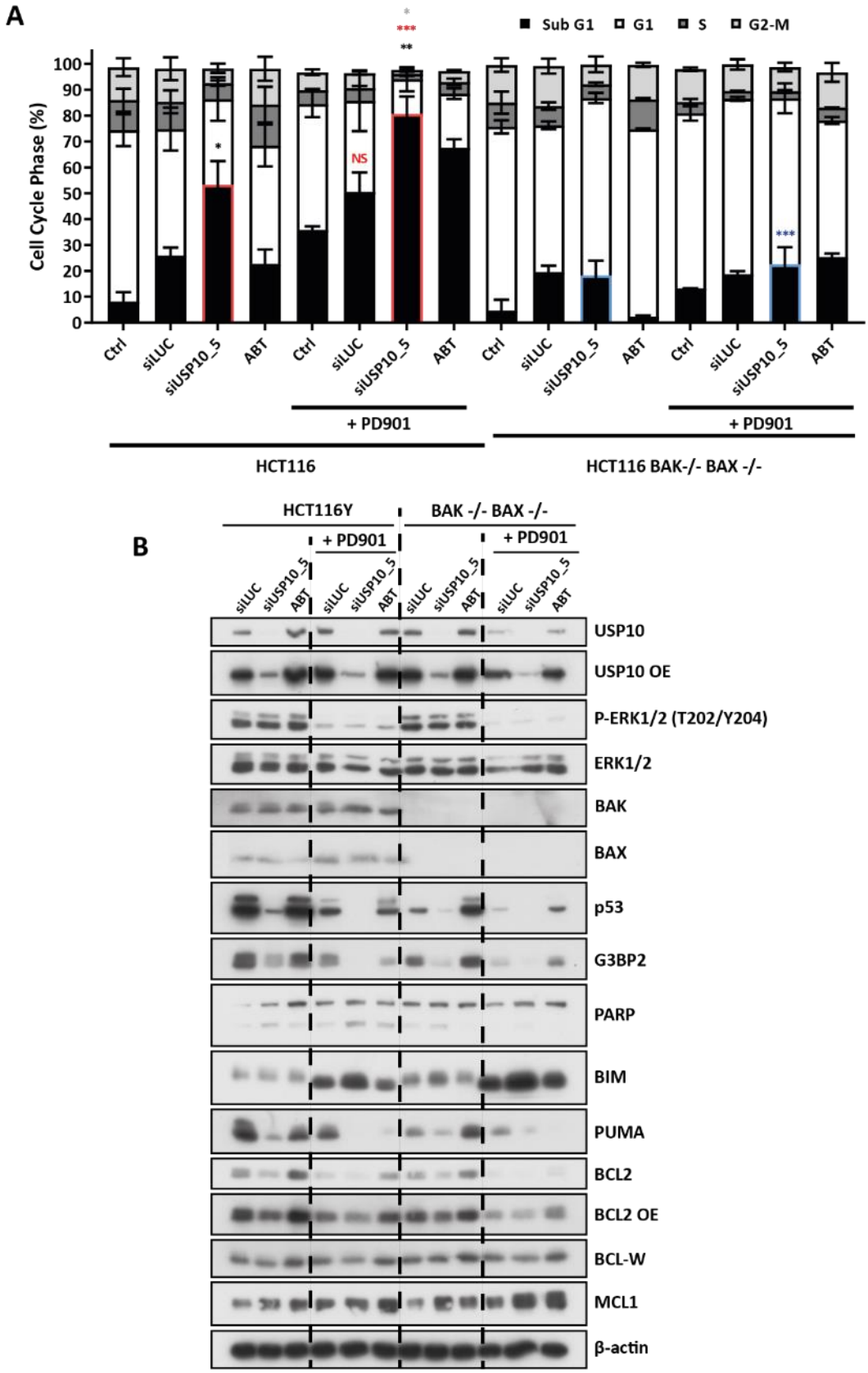

Figure 6.11 USP10 siRNA, with or without PD0325901, induces a BAK/BAX-dependent cell death. (A + B) Cycling HCT116 and genetically engineered BAK-/- BAX-/- HCT116 cells were left untransfected (Ctrl) or transfected with 10 nM of indictated siRNA. 24 hrs post-transfection cells were treated with DMSO, 0.03 μM PD0325901 (PD901) or 1 μM ABT-263 (ABT) for a further 96 hrs after which cells were **(A)** fixed and stained with propidium iodide and cell death (sub-G1 DNA) determined by flow cytometry. Results shown here are representative of the mean ± SD of three independent experiments, where each biological replicate is performed in technical triplicate. $P < 0.0001$ (***), $P < 0.001$ (**), $P < 0.01$ (*) or not significant (ns) for siLUC vs siUSP10 or siLUC + PD901 vs siUSP10 + PD901 (Black), Ctrl + PD901 vs siUSP10 + PD901 or siLUC + PD901 (Red), siUSP10 vs siUSP10 + PD901 (grey), siUSP10 + PD901 vs siUSP10 + PD901 (BAK-/- BAX-/-) (Blue), as determined by one-way ANOVA with Tukey post-hoc test, or **(B)** lysed, fractionated by SDS-PAGE and subjected to western blotting with the antibodies indicated in the figure. This data is representative of one experiment, of which two have been performed giving similar results.

combination in Figure 6.10 was different from that observed in Figure 6.11. This is discussed further in the Chapter.

As predicted from previous studies knockdown of USP10 resulted in a reduction in G3BP2 protein levels, as well as p53 protein levels (Figure 6.11B). It also resulted in the reduced expression of PUMA (p53 upregulated modulator of apoptosis), a pro-apoptotic BH3-only protein which is a known p53 target gene (Nakano and Vousden., 2001). Expression of these proteins was only examined for data generated in Figure 6.11 and should be evaluated in additional experiments to confirm these observations.

Additionally, the increase in cell death observed with all three USP10 siRNA, either alone, in the case with USP10_1, or in combination with PD901, was BAK/BAX-dependent (Figure 6.12A). Interestingly, the largest rescue from cell death, as a consequence of BAK/BAX knock out, was observed with USP10_1 siRNA, as shown by a dramatic reduction in the fraction of cells with sub-G1 DNA (Figure 6.12A). All three USP10 siRNA caused a comparable knockdown of USP10, however they caused varying effects on pro-survival and pro-apoptotic protein levels, discussed in 6.2.9. (Figure 6.12B). The difference in the effects on HCT116 cells, following transfection with siUSP10_1, compared to siUSP10_5 and siUSP10_69, could be because of off-target effects of siUSP10_1.

Overall of the five DUBs identified as 'hits' from the 5-day DUB RNAi screen, combined with PD901 treatment, only three DUBs, when knocked down, reproducibly combined with PD901 to induce apoptosis. These were VCIP135, YOD1 and USP10. The additional DUBs, USP16 and TNFAIP3, were excluded as they were only a partial 'hit' or did not combine, when knocked down, with PD901 to induce a cell death response, respectively.

6.2.8. Alternative MEK1/2 inhibitors phenocopy the cytotoxic effect observed with PD901 and YOD1 or USP10 knockdown.

As previously demonstrated, siUSP10 combined with the MEK1/2 inhibitor PD901 to induce apoptosis of HCT116 cells. To investigate if this response was robust HCT116 cells were treated with two alternative MEK1/2 inhibitors, post siUSP10_5 transfection, to see if they combined to reproduce the cell death response seen with PD901 treatment. GDC-0623 and trametinib are MEK1/2 inhibitors in clinical trials or clinically approved, respectively, for the treatment of cancer. Both these inhibitors have been demonstrated to block MEK1/2 phosphorylation and consequently prevent the feedback phosphorylation of MEK1/2 observed with alternative MEK1/2 inhibitors,

Figure 6.12 An increase in the fraction of cells with sub-G1 DNA was observed with all USP10 siRNA in combination with PD0325901.

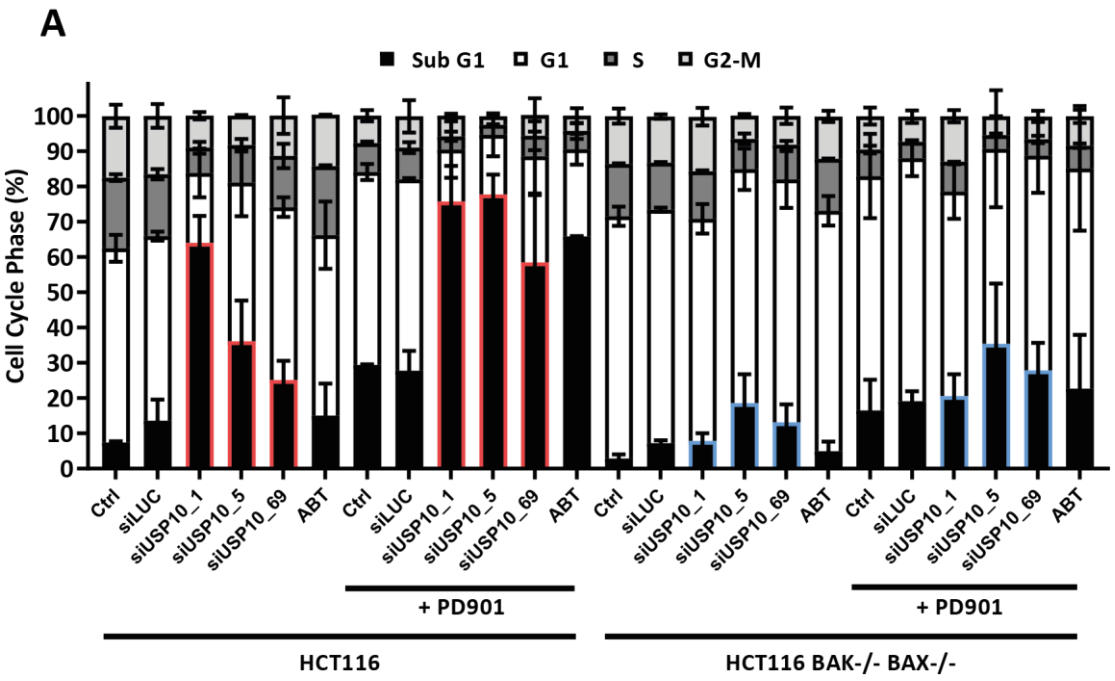

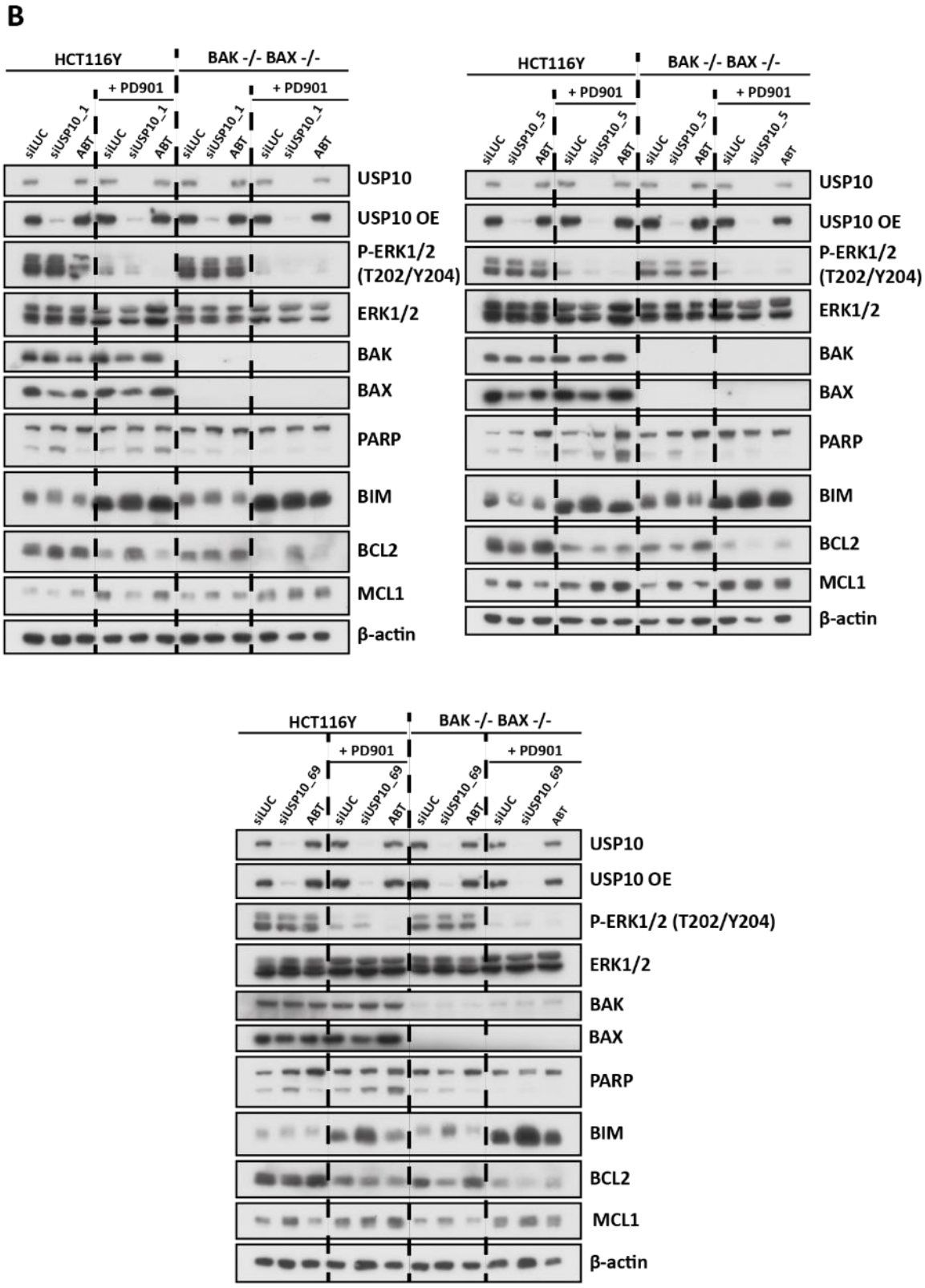

Figure 6.12 An increase in the fraction of cells with sub-G1 DNA was observed with all USP10 siRNA in combination with PD0325901. (A + B) Cycling HCT116 and genetically engineered BAK-/- BAX-/- HCT116 cells were left untransfected (Ctrl) or transfected with 10 nM of indictated siRNA. 24 hrs post-transfection cells were treated with DMSO, 0.03 μM PD0325901 (PD901) or 1 μM ABT-263 (ABT) for a further 96 hrs after which cells were **(A)** fixed and stained with propidium iodide and cell death (sub-G1 DNA) determined by flow cytometry. Results shown here are representative of the mean ± SD of two independent experiments, where each biological replicate is performed in technical triplicate, or **(B)** cells were lysed, fractionated by SDS-PAGE and subjected to western blotting with the antibodies indicated in the figure. This data is representative of one experiment, of which two have been performed giving similar results.

including selumetinib (Friday and Adjei, 2008, Gilmartin *et al.*, 2011, Hatzivassiliou *et al.*, 2013, Pratilas *et al.*, 2009).

Based on western blot and flow cytometry analysis, comparable concentrations of the MEK1/2 inhibitors trametinib and GDC-0623 were chosen, that alone, resulted in minimal cell death of HCT116 cells, ~20 %, but still inhibited ERK1/2 signalling, as judged by a reduction in phosphorylated ERK1/2 (Figure 6.13A and Figure 6.13B).

Knockdown of YOD1 or USP10, in combination with trametinib or GDC-0623, resulted in a statistically significant increase in the fraction of cells with sub-G1 DNA, compared to siLUC controls (Figure 6.14A). Knockdown of USP10 or YOD1 synergised with trametinib to induce cell death in HCT116 cells. In contrast, the effect observed with knockdown of USP10 or YOD1 and GDC-0623 appeared more additive. Indeed knockdown of USP10 resulted in a significant increase in the fraction of cells with sub-G1 DNA compared to siLUC transfection (Figure 6.14A). Western blot analysis of these experiments is discussed in section 6.2.9 (Figure 6.14B). Overall, the cell death response observed with PD901 was phenocopied with two further MEK1/2 inhibitors.

6.2.9. USP10 knockdown increases MCL1 protein expression but reduces BCL2 protein expression.

Western blot analysis of pro-survival and pro-apoptotic BCL2 proteins revealed that knockdown of USP10 resulted in an increase in MCL1 protein levels and a decrease in BCL2 protein levels, irrespective of MEK1/2 inhibition (Figure 6.11B and Figure 6.14B).

MCL1 is a key pro-survival BCL2 protein whose stability is regulated through post-translational modification, including ubiquitylation. The stability of MCL1 has been demonstrated to be regulated by two different DUBs, USP9x and USP13. USP9x binds to MCL1 resulting in the loss of K48-linked polyubiquitin and an increase in its stability. This has been linked to tumour cell survival and as such USP9x was deemed to be an oncogene (Schwickart *et al.*, 2010). However, in contrast to this, USP9x has also been shown to suppress tumour cell growth in a mouse model of pancreatic ductal adenocarcinoma (PDC), with loss of USP9x resulting in tumourgenesis (Perez-Mancera *et al.*, 2012). In addition to USP9x, USP13 regulates MCL1 stability in lung and ovarian tumour cells. Depletion of USP13 resulted in the reduction of MCL1 and suppression of tumour cell growth (Zhang *et al.*, 2018). Additionally, they identified USP10 as a candidate DUB for MCL1 in HEK293T cells; however, they demonstrated that knockdown of USP10 resulted in a decrease in MCL1 protein levels (Zhang *et al.*, 2018). Interestingly in HEK293T cells, knockdown of USP9x did not alter MCL1 protein levels. Together

Figure 6.13 Optimisation of alternative MEK1/2 inhibitors, trametinib and GDC-0623, in HCT116 cells.

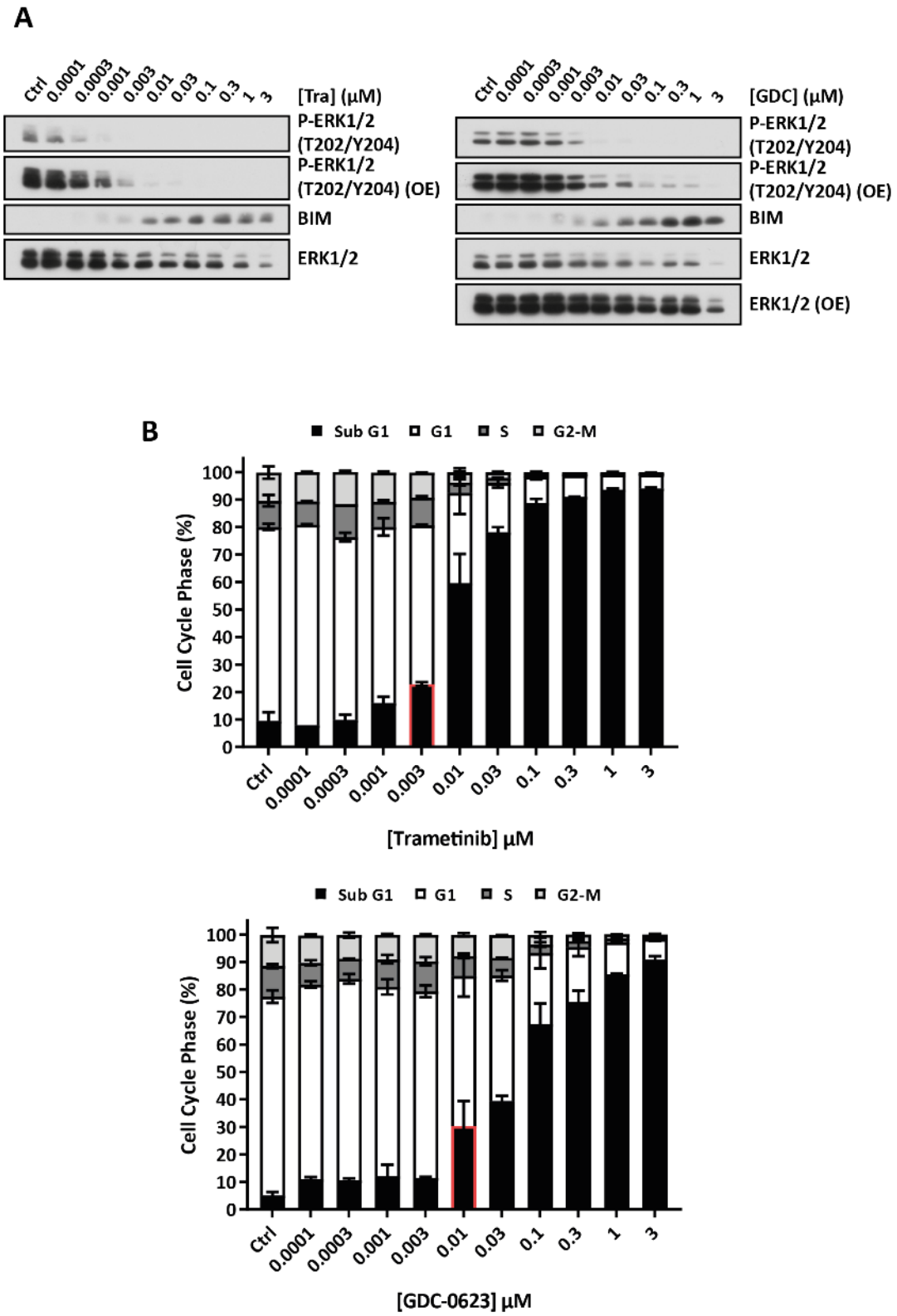

Figure 6.13 Optimisation of alternative MEK1/2 inhibitors, Trametinib and GDC-0623, in HCT116 cells. Cycling HCT116 cells were seeded and left to settle for 24 hrs, then treated with DMSO (Ctrl), increasing concentrations of Trametinib (Tra) or GDC-0623 (GDC) for 96 hrs after which **(A)** cells were lysed, fractionated by SDS-PAGE and subjected to western blotting with the antibodies indicated in the figure. This data is representative of one experiment, or **(B)** fixed and stained with propidium iodide and cell death (sub-G1 DNA) determined by flow cytometry. Results shown here are representative of the mean ± SD of 2 independent experiments, where each biological replicate is performed in technical triplicate.

Figure 6.14 The use of alternative MEK inhibitors phenocopy the affect seen previously with PD0325901.

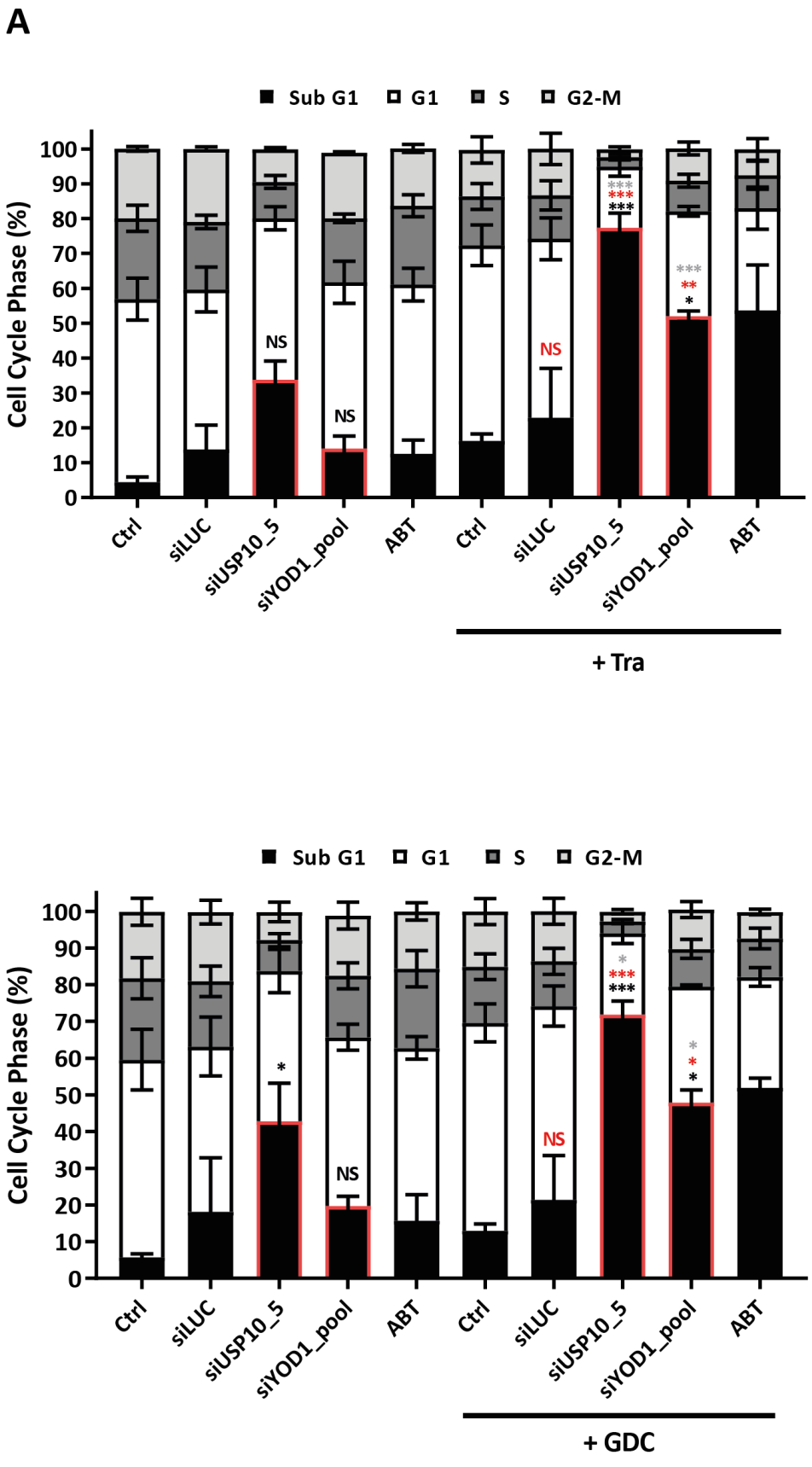

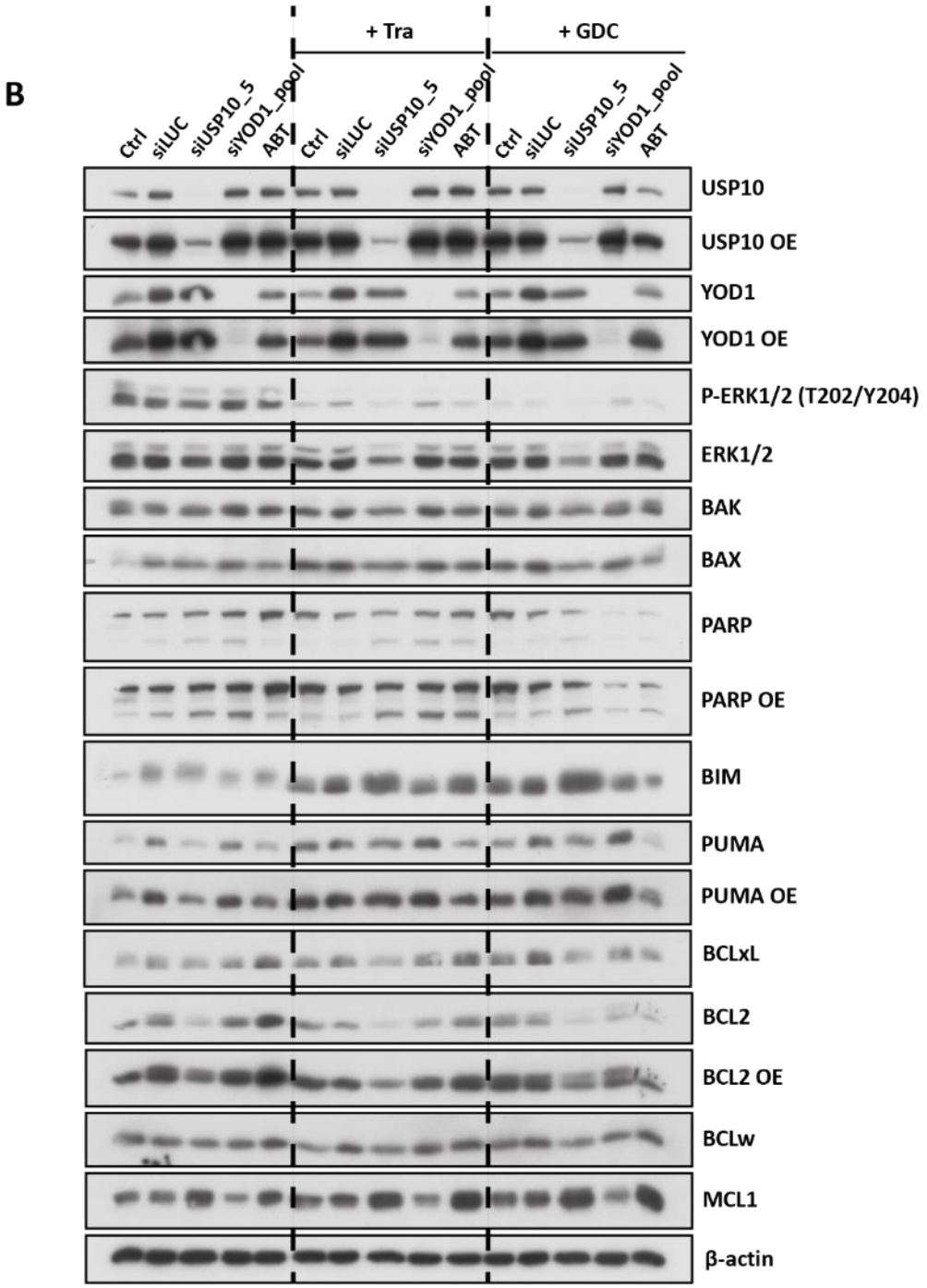

Figure 6.14 The use of alternative MEK inhibitors phenocopy the affect seen previously with PD0325901. Cycling HCT116 cells were left untransfected (Ctrl) or transfected with 10 nM of indictated siRNA. 24 hrs post-transfection cells were treated with DMSO, 0.003 μM Trametinib (Tra), 0.01 μM GDC-0623 (GDC) or 1 μM ABT-263 (ABT) for a further 96 hrs after which cells were **(A)** fixed and stained with propidium iodide and cell death (sub-G1 DNA) determined by flow cytometry. Results shown here are representative of the mean ± SD of three independent experiments, where each biological replicate is performed in technical triplicate, or **(B)** lysed, fractionated by SDS-PAGE and subjected to western blotting with the antibodies indicated in the figure. This data is representative of one experiment, of which two have been performed giving similar result. $P < 0.0001$ (***), $P < 0.001$ (**), $P < 0.01$ (*) or not significant (ns) for siLUC vs siUSP10/YOD1 or siLUC + MEKi vs siUSP10/YOD1 + MEKi (Black), Ctrl + MEKi vs siUSP10/YOD1 + MEKi or siLUC + MEKi (Red), siUSP10/YOD1 vs siUSP10/YOD1 + MEKi (grey), as determined by one-way ANOVA with Tukey post-hoc test. MEKi = MEK1/2 inhibitor.

these studies highlight that multiple DUBs can act on the same substrate, MCL1, in a context-dependent manner.

In contrast to that published with USP9x and USP13, knockdown of USP10, alone and in combination with a MEK1/2 inhibitor, resulted in an increase in MCL1 protein (Figure 6.11B and Figure 6.14B). Thus, one could speculate that USP10, rather than directly deubiquitylating MCL1, could act to deubiquitylate a negative regulator of MCL1. Therefore, knockdown of USP10 would result in the decreased stability or inactivation of the regulatory protein resulting in an increase in MCL1 protein levels. Of note, it would also be important to observe if knockdown of USP10 results in an increase in the mRNA levels of MCL1. This would provide indicate at what level USP10 affects MCL1 expression.

In contrast to that seen with MCL1, knockdown of USP10 resulted in a decrease in BCL2 protein in HCT116 cells (Figure 6.11B and Figure 6.14B). Aberrant expression of BCL2 is characteristic of many cancers, including colorectal cancer (Huang *et al.*, 2017a). BCL2 has been shown to be degraded by the proteasome in response to oxidative stress, and S-Nitroyslation of BCL2 inhibited this degradation (Azad *et al.*, 2006, Breitschopf *et al.*, 2000). In addition, Edison and colleagues demonstrated that ubiquitin-driven proteasomal degradation of BCL2 promotes apoptosis (Edison *et al.*, 2017). At the molecular level, as a result of apoptotic stimuli, ARTS (Sept4_i2) accumulates in the cytosol and binds to both XIAP (X-linked inhibitor of apoptosis), an E3 ligase, and BCL2, resulting in the polyubiquitylation and degradation of BCL2, as well as activation of caspases, promoting cell death (Bornstein *et al.*, 2011, Edison *et al.*, 2017, Edison *et al.*, 2012). Interesting, mono-ubiquitylation of BCL2, by Parkin, enhances the stability of BCL2 (Chen *et al.*, 2010). BCL2 interacts with Beclin1, inhibiting autophagy, under normal and starvation conditions, promoting cell survival (Chen *et al.*, 2010, Pattingre *et al.*, 2005). To date, there was no evidence of a DUB for BCL2 in the literature.

From the data presented here, knockdown of USP10 alone, or in combination with MEK1/2 inhibition, resulted in the loss of BCL2 protein (Figure 6.11B and Figure 6.14B). This suggests USP10 could be the DUB for BCL2, as knockdown of this DUB would prevent the deubiquitylation of BCL2, resulting in its increased degradation. Alternatively, a decrease in USP10 protein could prevent the deubiquitylation of an additional protein that is required to drive BCL2 expression. Therefore, knockdown of USP10 would result in the increased degradation of this regulatory protein and a decrease in BCL2 protein levels. In addition, knockdown of USP10 could act as an apoptotic stimulus, causing the XIAP-driven polyubiquitylation and degradation of BCL2.

Interestingly, knockdown of USP10, using siUSP10_1, appeared to alter the expression of MCL1 and BCL2 in a different manner to that seen with siUSP10_5 and siUSP10_69 (Figure 6.12B). Knockdown of USP10, using siUSP10_69, resulted in a marginal loss of BCL2 and an increase in MCL1 (Figure 6.14B),

thereby phenocopying that seen for knockdown of USP10 using siUSP10_5 (Figure 6.11B, Figure 6.12B and Figure 6.14B). Interestingly, this corroborates data presented in Figure 6.10, were both siRNAs (siUSP10_5 and siUSP10_69) produced a similar cell death response, with or without PD901. In contrast, knockdown of USP10, using siUSP10_1, resulted in a marginal increase in BCL2 and very little changes to MCL1 protein levels. Again, as previously described, siUSP10_1 could have off-target effects following transfection in HCT116 cells and this could account for the contradictory results.

6.2.10. Combined knockdown of USP10 and MCL1 inhibition did not result in an increase in cell death.

Since USP10 knockdown increased MCL1 protein levels it was speculated that this might protect cells from death. Therefore, the effect of inhibition of MCL1, in combination with USP10 siRNA, was investigated to see if it would result in a greater increase in cell death, than seen with PD901. For these experiments the potent and selective MCL1 inhibitor S63845 (S45) was used, which is currently in Phase I clinical trials for the treatment of patients with AML (Acute Myeloid Leukaemia) or MDS (Myelodysplastic Syndrome) (Kotschy *et al.*, 2016).

Treatment of HCT116 cells with increasing concentrations of the MCL1 inhibitor, S63845 (S45), resulted in a dose-dependent increase in MCL1 protein (Figure 6.15A), with minimal induction of cell death (Figure 6.15B). An increase in MCL1 protein following treatment with S45 has already been observed and was shown to be a consequence of an increased half-life of MCL1 (Kotschy *et al.*, 2016). Therefore, an increase in MCL1 protein was a good marker of S45 target engagement. Compared to the increase in cell death seen with the combined knockdown of USP10 and MEK1/2 inhibition, minimal cell death was observed with combined knockdown of USP10 and MCL1 inhibition (Figure 6.15C and Figure 6.15D). This suggests that the increase in MCL1 protein seen with USP10 knockdown was not hindering the cell death response in HCT116 cells.

6.2.11. Knockdown of YOD1 and USP10 in A375 cells did not combine with MEK1/2 inhibition to induce cell death.

A panel of colorectal carcinoma (CRC) and melanoma cell lines was screened to determine the endogenous protein levels of USP10 and YOD1. Western blot analysis revealed that the expression of these DUBs varied between the cell lines (Figure 6.16). Analysis revealed that YOD1 expression was generally higher in melanoma cell lines and expression of USP10 appeared to be highest in CRC cell lines that have an oncogenic KRas G13D mutation, such as HCT116 and LOVO cells. Analysis of the expression of pro-survival BCL2 proteins demonstrated that MCL1 expression was marginally lower in

CRC cell lines compared to melanoma cell lines, whilst expression of BCL2 was considerably higher in melanoma cell lines, compared to CRC cell lines, with the exception of the LOVO and SW48 cell lines. The melanoma cell line, A375, had comparable expression of USP10 and YOD1 to HCT116 cells and as such, the effect of knockdown of these DUBs in A375 cells was investigated, following MEK1/2 inhibition with PD901, and compared to the cell death response observed in HCT116 cells.

The concentration of PD901, required to inhibit MEK1/2 activity with minimal cell death, in A375 cells, for 5-days was demonstrated to be 0.01 μM (Figure 6.17A and Figure 6.17B). Neither knockdown of YOD1 nor USP10, in combination with PD901, resulted in a significant increase in cell death (Figure 6.17C). However, similar to that seen in HCT116 cells, knockdown of USP10, resulted in a marginal increase in MCL1 and a loss of BCL2 protein (Figure 6.17D). Additionally, knockdown of USP10, in A375 cells, resulted in an increase in PUMA and a loss of BCL-X_L protein. High basal expression of MCL1 in A375 cells could be the reason why only a marginal increase in MCL1 protein level was observed, as compared to that seen in HCT116 cells. Overall, this indicated that the increase in cell death seen in HCT116 with combined knockdown of YOD1 or USP10 with MEK1/2 inhibition was perhaps cell line dependent.

Figure 6.15 Inhibition of MCL1 and knockdown of USP10 did not result in an increase in the fraction of cells with sub-G1 DNA.

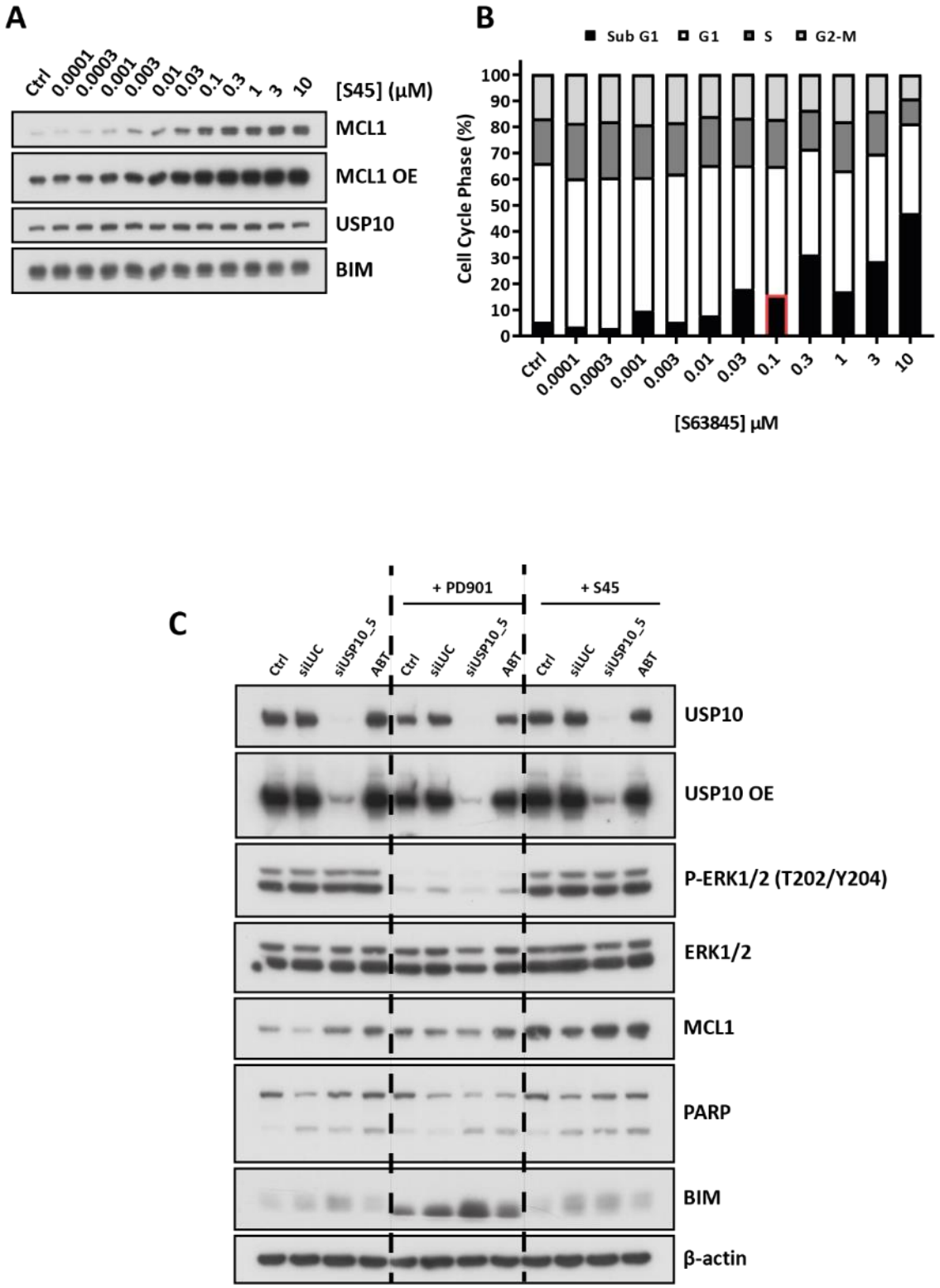

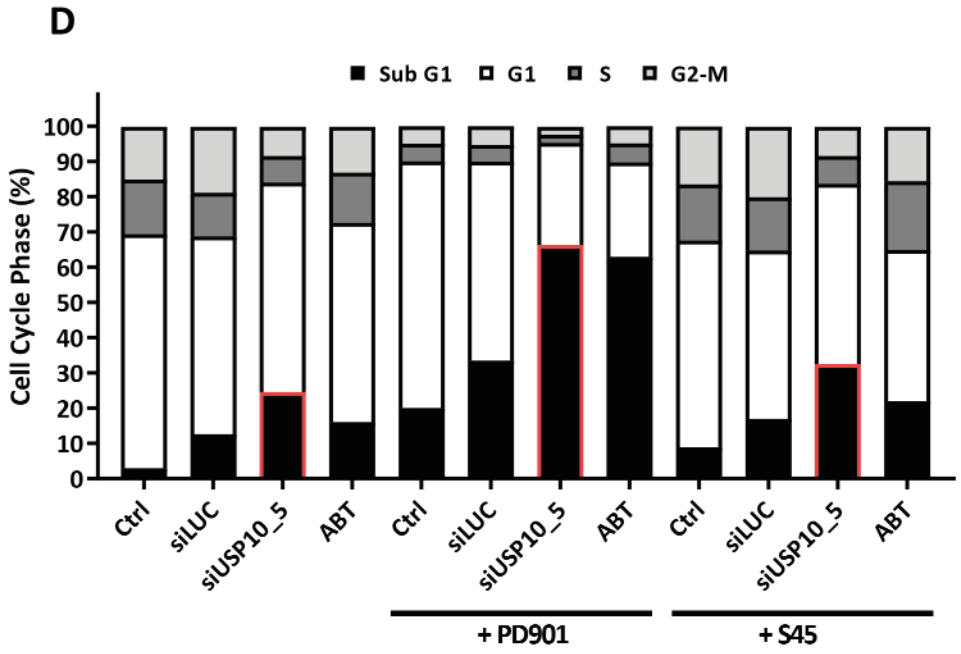

Figure 6.15 Inhibition of MCL1 and knockdown of USP10 did not result in an increase in the fraction of cells with sub-G1 DNA. (A + B) Cycling HCT116 cells were seeded and left to settle for 24 hrs, then treated with DMSO (Ctrl), increasing concentrations of S63845 (S45) for 96 hrs after which **(A)** cells were lysed, fractionated by SDS-PAGE and subjected to western blotting with the antibodies indicated in the figure. This data is representative of one experiment, or **(B)** fixed and stained with propidium iodide and cell death (sub-G1 DNA) determined by flow cytometry. Results shown here are representative of one experiment. **(C + D)** Cycling HCT116 cells were left untransfected (Ctrl) or transfected with 10 nM of indictated siRNA. 24 hrs post-transfection cells were treated with DMSO, 0.1 μM S63845 (S45) or 1 μM ABT-263 (ABT) for a further 96 hrs after which **(C)** cells were lysed, fractionated by SDS-PAGE and subjected to western blotting with the antibodies indicated in the figure. This data is representative of one experiment, or **(D)** fixed and stained with propidium iodide and cell death (sub-G1 DNA) determined by flow cytometry. Results shown here are representative of one experiment, where this biological replicate was performed in technical triplicate.

Figure 6.16 Screen of Colorectal carcinoma and Melanoma cell lines for expression of USP10 and YOD1.

		Driving mutation	
CRC	Colo205	BRAF	V600E
	HT29		
	DLD1	KRAS	G13D
	HCT116		
	LOVO		
	SW620	KRAS	G12V
	SW48	N/A	
Melanoma	A375	BRAF	V600E
	SK-MEL-28		
	WM266.4	BRAF	V600D
	MelJuso	HRAS	G13D
		NRAS	Q61R
	SK-MEL-30	NRAS	Q61K
	SK-MEL-2	NRAS	Q61R
	SK-MEL-31	N/A	

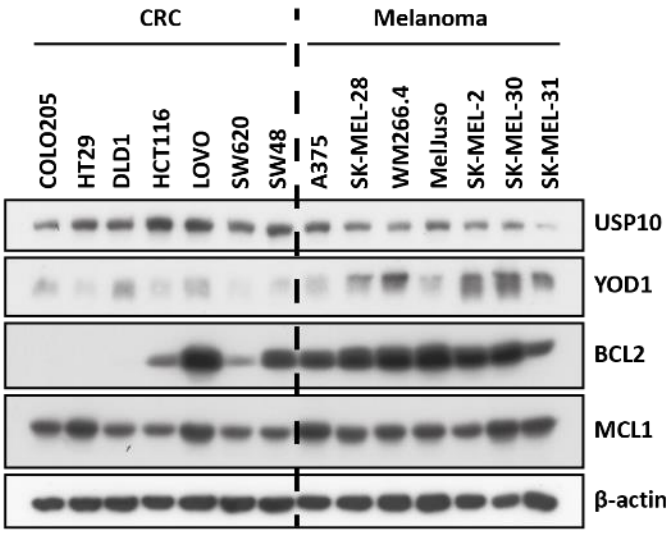

Figure 6.16 Screen of Colorectal carcinoma and Melanoma cell lines for expression of USP10 and YOD1. (A) A table showing oncogenic driving mutations of Colorectal carcinoma (CRC) and Melanoma cell lines. **(B)** SDS-PAGE analysis of seven CRC and Melanoma cell lines looking at the basal protein expression of USP10, YOD1 and VCIP135. This data is representative of one experiment, of which two have been performed giving similar results.

Figure 6.17 Despite no increase in cell death, knockdown of USP10 in A375 cells resulted in an decrease in BCL2 and an increase in MCL1 protein.

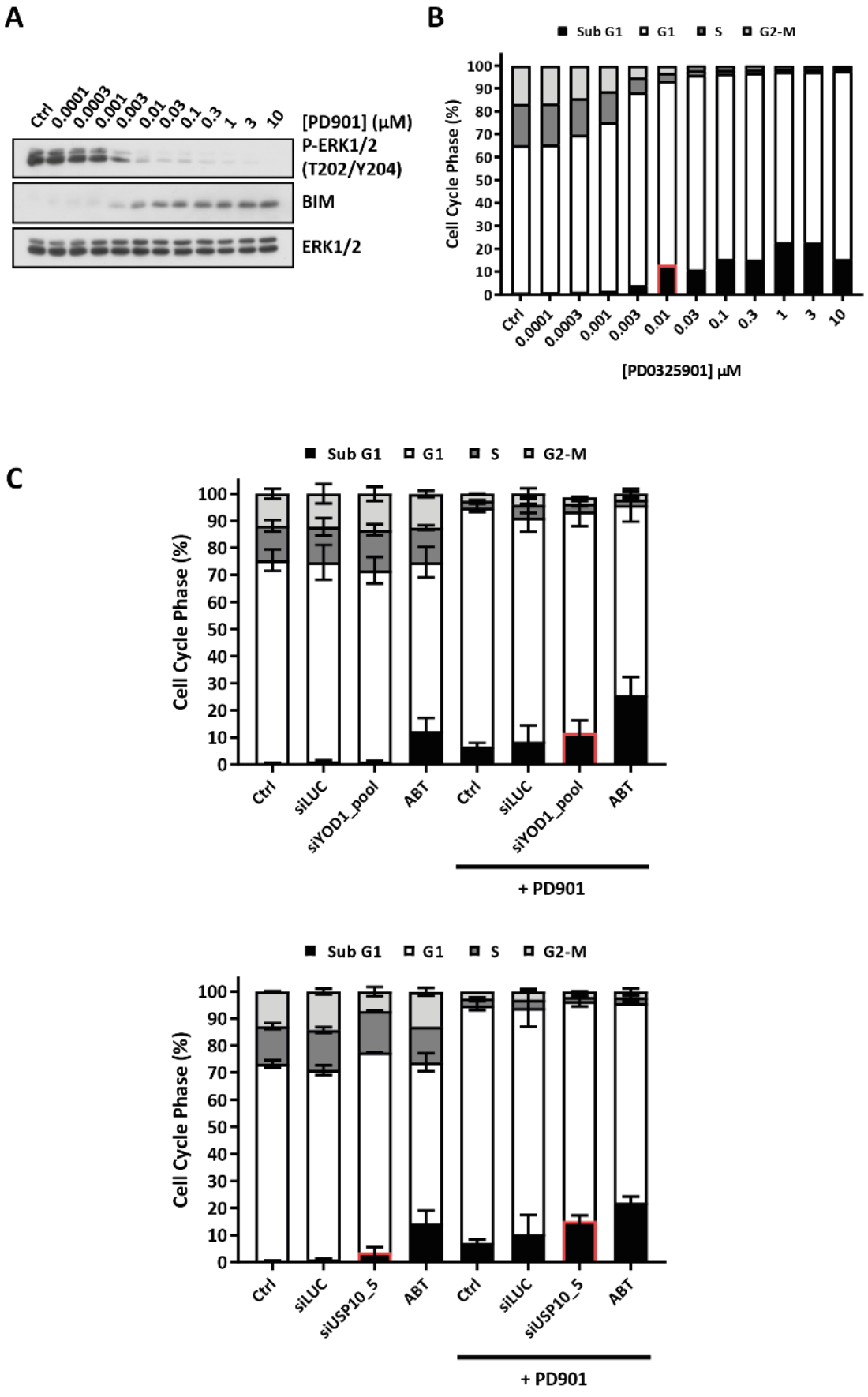

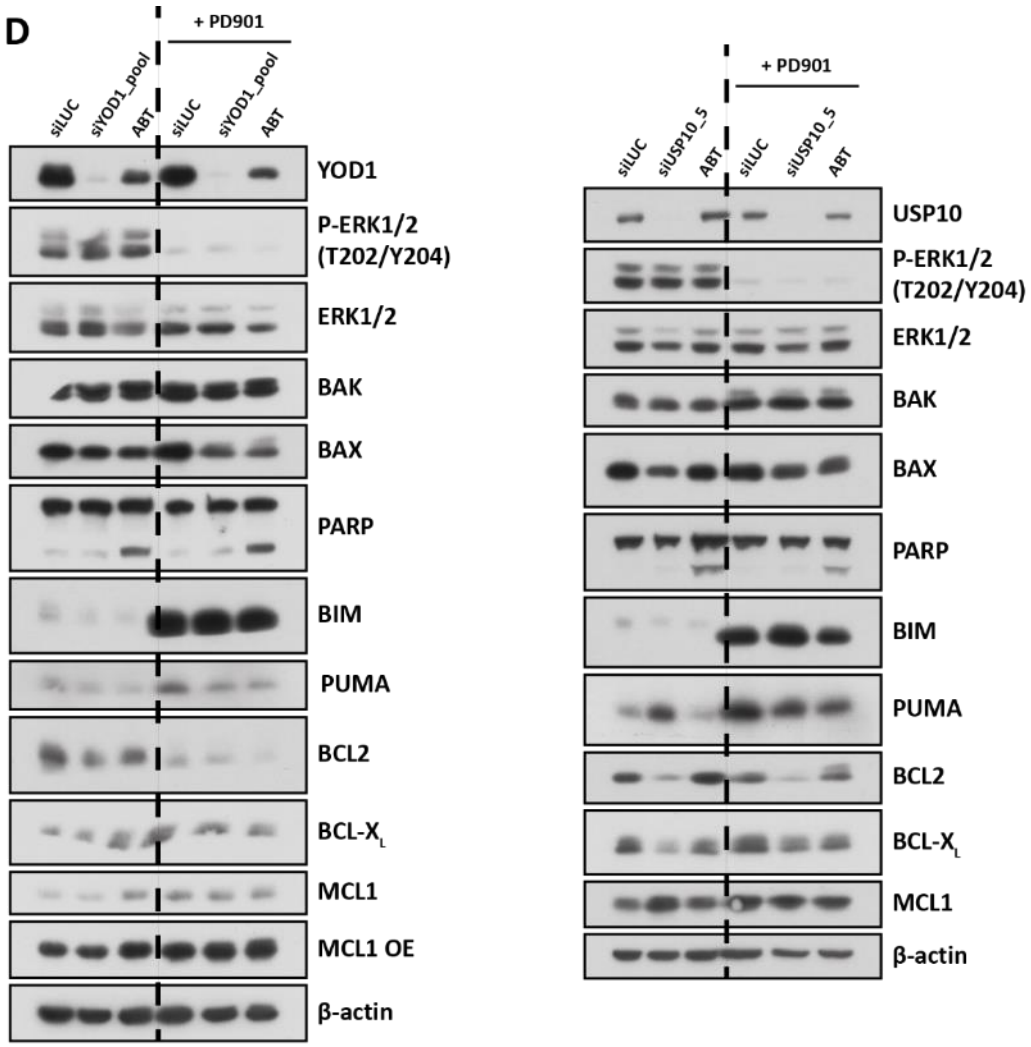

Figure 6.17 Despite no increase in cell death, knockdown of USP10 in A375 cells resulted in an decrease in BCL2 and an increase in MCL1 protein. (A + B) Cycling A375 cells were seeded and left to settle for 24 hrs, then treated with DMSO (Ctrl), increasing concentrations of PD0325901 (PD901) for 96 hrs after which **(A)** cells were lysed, fractionated by SDS-PAGE and subjected to western blotting with the antibodies indicated in the figure. This data is representative of one experiment, or **(B)** fixed and stained with propidium iodide and cell death (sub-G1 DNA) determined by flow cytometry. Results shown here are representative of one experiment. **(C + D)** Cycling A375 cells were left untransfected (Ctrl) or transfected with 10 nM of indictated siRNA. 24 hrs post-transfection cells were treated with DMSO, 0.01 μM PD0325901 (PD901) or 1 μM ABT-263 (ABT) for a further 96 hrs after which **(C)** cells were fixed and stained with propidium iodide and cell death (sub-G1 DNA) determined by flow cytometry. Results shown here are representative of the mean ± SD of two independent experiments, where each biological replicate is performed in technical triplicate, or **(D)** lysed, fractionated by SDS-PAGE and subjected to western blotting with the antibodies indicated in the figure. This data is representative of one experiment, of which two have been performed giving similar results

6.3. Discussion

Tumour cells addicted to ERK1/2 signalling can adapt to monotherapy with MEK1/2 inhibitors (Caunt *et al.*, 2015). Thus, additional treatments that synergise with MEK1/2 inhibition to induce cell death are of therapeutic benefit. Based on RNAi screening, Chapter 5, and further validation, Chapter 6, several DUBs, USP10, YOD1 and VCIP135, were identified that combine and even synergise with MEK1/2 inhibition to induce apoptosis of HCT116 cells. Of note, this effect was observed to be context dependent and may differ depending upon the driving oncogene.

6.3.1. Limitations and shortcomings of RNAi screens.

RNAi screens are widely used to interrogate gene function, typically utilising siRNA or shRNA to silence target gene expression, and are a powerful tool for analysing loss-of-function phenotypes in mammalian cells. However, one of the major limitations of RNAi screens is the off-target effects of siRNA (Jackson *et al.*, 2003, Jackson and Linsley, 2010). siRNA have the ability to bind to several mRNA, in addition to their intended target mRNA, with partial complementarity. In the majority of cases, partial sequence complementarity occurs between the 5' end (seed sequence) of the siRNA, and the 3'UTR of the off-target mRNA (Jackson *et al.*, 2003). Thus careful consideration needs to be made when designing siRNA, particularly within the seed sequence. Interestingly, some studies identified that the number of off-target genes silenced was proportional to the concentration of siRNA transfected into cells (Persengiev *et al.*, 2004). Therefore, it is advantageous to test multiple concentrations of siRNA and to choose the minimum required for knockdown of your target gene. The technology used to deliver the siRNA can also trigger off-target effects and induce a non-specific innate inflammatory response (Bridge *et al.*, 2003). Additionally transfection of siRNA can overwhelm the endogenous RNAi machinery, which might result in alterations to the processing of endogenous miRNA, known to regulate a wide variety of processes within the cell (Khan *et al.*, 2009). Ultimately, this can lead to unexpected phenotypes and complicates the interpretation of RNAi screen data. One off-target phenotype caused as a result of transfection of select siRNAs is a reduction in cell growth. This often correlates with the inability of this siRNA to target its intended mRNA (Jackson *et al.*, 2006). This off-target effect is relevant for this study as cell viability was used as an end point assay.

During initial experiments to validate 'hits' identified from the 5-day RNAi screen, three different siRNAs, with distinct sequences, were chosen to knockdown USP16 and USP10. Interestingly, the three different siRNAs targeting USP16 and USP10 generated different phenotypes. A large increase in the fraction of cells with sub-G1 DNA was observed with siUSP10_1 and siUSP16_O3D, alone, compared to the other siRNAs tested. As the two additional siRNAs generated comparable phenotypes to each

other one could conclude that the observed effect with siUSP10_1 and siUSP16_O3D was due to off-target effects of these siRNA. Indeed, observing the same phenotype using several siRNA with distinct sequences, particularly at the 5' end of the siRNA, targeting the same gene, increases confidence that the observed phenotype was as a consequence of silencing the intended target gene (Cullen, 2006, Echeverri *et al.*, 2006). Additional siRNAs or further validation of the phenotype may be required to confirm the cell death response observed with the remaining siRNAs.

There are multiple strategies to reduce off-target effects of siRNA. Chemical modification of the siRNA, such as 2'-O-methyl modification, within the 5' end of the siRNA has been shown to mitigate off-target effects of siRNA (Jackson *et al.*, 2006). Pooling of siRNA has been demonstrated to reduce off-target effects as a consequence of competition between the siRNA for knockdown of the target mRNA, providing a selective reduction of off-target events. In addition, if overexpression of a resistant form of the targeted mRNA 'rescues' cells from the observed phenotype this would confirm that this phenotype was not due to off-target gene silencing (Whither., 2003). Genome editing technologies, such as the CRISPR-cas9 system, could also be used to validate the observed phenotype. However, these technologies are not without caveats themselves.

In addition to off-target effects, siRNA transfection with the same siRNA, did not reproducibly generate the same statistically significant or synergistic effect when combined with MEK1/2 inhibition. For this study, a synergistic effect is one in which knockdown of a DUB and MEK1/2 inhibition combine to cause a greater increase in cell death than the sum of the cell death responses from these separate 'treatments', at the same doses. In contrast, an additive effect is one in which the effect of the two 'treatments' combined is the same as the sum of the cell death response from the 'treatments' separately, at the same doses. A synergistic effect is a more favourable outcome to combinatorial treatments as it would imply that knockdown of a DUB or MEK1/2 inhibition causes minimal cell death but combined to generate a significant, and therapeutically beneficial, increase in cell death.

During this study it was observed that knockdown of VCIP135/YOD1/USP10 combined with MEK1/2 inhibition with PD901 to promote BAK/BAX-dependent apoptosis of HCT116 cells. Unfortunately, the synergistic effect observed with knockdown of USP10 or YOD1, in combination with MEK1/2 inhibition, was not always reproducible and cell death observed following combination treatment was not always consistent or significant. In the case of USP10, the irreproducibility of the data was often as a result of an increase in cell death following knockdown of USP10 alone. For both USP10 and YOD1, variations in cell death observed following transfection of siLUC and PD901 treatment, aided in the inconsistency of the significance of data produced. Numerous factors could account for the observed effects, including culturing drift causing epigenetic changes, rendering cells more or less susceptible to siRNA

transfection as well as treatment with PD901. The age of the cells and therefore the proliferative state of the cells could also account for the different phenotypes observed, in addition to the health of the cells at the time of transfection. Batch-to-batch variability of any of the reagents, including PD901, used during these experiments could cause variable and inconsistent results.

6.3.2. Identification of key 'hits' from the DUB RNAi screen, in combination with MEK1/2 inhibition.

Of the 'hits' identified from the 5-day RNAi screen, the most promising were USP10, YOD1 and VCIP135. These three 'hits' are discussed in more detail below. Of note, knockdown of USP10 and YOD1 combined with three different MEK1/2 inhibitors to induce cell death, aiding in the validation of the initial results obtained using PD901.

6.3.2.1. VCIP135.

Transfection of siRNA against VCIP135 alone did not induce cell death of HCT116 cells. This therefore suggests that VCIP135 is functionally redundant, meaning an additional protein can play the role of VCIP135 in these cells, or that its function is not essential for viability. Alternatively, the siRNA knockdown of VCIP135 may not be sufficient to completely abolish VCIP135 activity. To assess if knockdown of VCIP135, in this system, was sufficient to impair function Golgi fragmentation could be assessed by examining the length of the Golgi cisternae, by electron microscopy, which should significantly reduce following VCIP135 depletion (Zhang *et al.*, 2014).

siVCIP135 combined with MEK1/2 inhibition to induce a significant increase in apoptosis. However, the underlying mechanism behind this combinatorial effect was not deduced. As previously described treatment of HCT116 cells with MEK1/2 inhibitors failed to cause a cytotoxic response, despite an induction of pro-apoptotic proteins due, in part, to residual pro-survival activity. Consequently it required inhibition of these pro-survival proteins to induce cell death (Sale and Cook, 2013). Knockdown of VCIP135 could result in the disruption of membrane fusion and defective distribution of pro-survival proteins. Thus, loss of VCIP135 could result in the inability of the 'inhibitory' pro-survival proteins to interact with pro-apoptotic proteins. Therefore, MEK1/2 inhibition, inducing pro-apoptotic proteins, and knockdown of VCIP135 would combine to induce cell death, comparable to that seen with MEK1/2 inhibition and BH3 mimetic treatment.

Additionally, as previously described both VCIP135 and ERK1/2 signalling regulate organelle morphology therefore one could speculate that the observed cell death, as a consequence of

knockdown of VCIP135 and MEK1/2 inhibition could be due to incomplete membrane fusion of multiple organelles resulting in detrimental changes to global organelle morphology. However further work needs to be done in order to decipher the mechanism underlying the cell death seen with combined knockdown of VCIP135 and PD901 treatment.

6.3.2.2. YOD1.

From the literature, YOD1 acts as a negative regulator of the Hippo signalling pathway; a pathway known to restrict cell proliferation and organ size (Kim *et al.*, 2017, Yu *et al.*, 2015, Zhao *et al.*, 2011). At the molecular level, YOD1 acts, via ITCH, to drive the degradation of LATS1/2, a negative regulator of the transcription co-activators YAP/TAZ. This results in the nuclear accumulation of YAP/TAZ, which interacts with TEAD/TEF transcription factors, to turn on transcription of cell cycle-promoting genes, thereby inducing cell proliferation (Kim and Jho, 2017, Kim *et al.*, 2017). In contrast to this down-regulation of YOD1, via miR-21, resulted in a decrease in ITCH, an increase in LATS1, overall significantly reducing YAP/TAZ transcriptional activity (Kim *et al.*, 2017). Therefore, it was speculated that knockdown of YOD1 would result in loss of YAP protein. Despite this, in HCT116 cells, knockdown of YOD1 resulted in a marginal increase in YAP protein compared to controls. In addition, a marginal increase in phosphorylated YAP (S127) was observed, following loss of YOD1, indicative of LATS1/2 – driven phosphorylation and inactivation of YAP. This suggests that knockdown of YOD1 could cause the cytoplasmic accumulation of inactive YAP which would fit with the idea that loss of YOD1 results in the reduction of YAP/TAZ transcriptional activity (Kim *et al.*, 2017).

Analysis of the expression of alternative proteins regulated by YOD1 may be required to confirm that knockdown of YOD1 in these experiments sufficiently impaired its function. To confirm that YAP/TAZ activity was reduced following knockdown of YOD1 the activity of the Hippo signalling pathway could be analysed using a reporter assay in which a luciferase gene is under the control of TEAD responsive elements. Under these conditions, one would expect that knockdown of YOD1 would result in nuclear export of YAP, loss of YAP-dependent gene transcription, and therefore a reduction in expression of the TEAD luciferase reporter, compared to basal conditions. This would also confirm if the observed increase in YAP resulted in an increase in activity.

Interestingly, ITCH has been demonstrated to be involved in multiple signalling pathways, including Notch signalling (Qiu *et al.*, 2000, Rossi *et al.*, 2006). Therefore, in addition to Hippo signalling, and its role independent of ITCH, in the regulation of the ER-associated protein degradation (Ernst *et al.*, 2009), YOD1 could control a much larger set of cellular processes and so knockdown of YOD1 could have a much wider impact on cell signalling pathways in addition to activation of Hippo signalling.

In HCT116 cells, knockdown of YOD1 combined with MEK1/2 inhibition, to induce BAK/BAX-dependent cell death. As previously stated both YOD1 and ERK1/2 signalling regulate components of the Hippo signalling pathway. Indeed, the deubiquitylating activity of YOD1 acts to activate YAP/TAZ signalling, inhibiting Hippo signalling and therefore inducing cell proliferation (Kim *et al.*, 2017) and ERK1/2 inhibition resulted in the reduction of YAP protein levels (You *et al.*, 2015). Data presented here demonstrated, in HCT116 cells, that knockdown of YOD1, in combination with PD901, resulted in the reduction of YAP protein. One could speculate that MEK1/2 inhibition has a dominant effect over YOD1 knockdown for the regulation of YAP expression, as knockdown of YOD1 alone was unable to reduce YAP protein.

However, why this combination induces a cell death response rather than a severe reduction in cell proliferation is not known. This could be as, in addition to its role in Hippo signalling, YAP has been shown to regulate apoptosis. Contrary to that already described, YAP can promote the transcription of pro-apoptotic proteins, including BAX, via binding to p73. Phosphorylation of YAP was required to disrupt this interaction and reduce the expression of apoptotic proteins (Basu *et al.*, 2003, Levy *et al.*, 2008). Interestingly, phosphorylation of YAP, by LATS1/2, has been shown to enhance the binding of p73 and resulted in apoptosis (Kawahara *et al.*, 2008, Strano and Blandino, 2007). As knockdown of YOD1 should alleviate inhibition of LATS1/2, LATS1/2, in this system, could phosphorylate YAP, suggested from Figure 6.8B, which could interact with p73 and induce the expression of pro-apoptotic proteins including BAX. Interestingly a marginal increase in BAX was observed following knockdown of YOD1. Therefore, it could be suggested that loss of YOD1 combined with inhibition of MEK1/2 to further drive the induction of apoptotic proteins and tip the balance towards cell death.

In contrast, inhibition of YAP, in ECA-109 cells, induced apoptosis and this correlated with a reduction in the BCL2/BCL-X_L protein ratio and phosphorylated ERK1/2 and an increase in p53 and caspase 3 levels (Cui and Li., 2017). Thus, they concluded that YAP was an oncogene in this cellular context. Interestingly, loss of BCL2 protein or phosphorylated ERK1/2 was not observed following knockdown of YOD1. However, similar to that previously described, one could conclude that combined knockdown of YOD1 and inhibition of MEK1/2 is required to reduce ERK1/2 phosphorylation and reduce YAP protein to drive apoptosis.

6.3.2.3. USP10.

Knockdown of USP10, in HCT116 cells (Figure 6.11) resulted in the loss of the G3BP2 protein, suggesting that the observed knockdown of USP10 was sufficient to impair a known function of USP10 (Takayama *et al.*, 2018). In addition to this, loss of p53 and PUMA protein was observed following knockdown of

USP10. However, the effect of knocking down USP10 on the p53 pathway needs to be further validated.

As previously described, under certain conditions, USP10 can act as an inhibitor of p53 signalling by increasing the expression of G3BP2, ultimately stimulating cell proliferation (Takayama *et al.*, 2018). In contrast, knockdown of USP10 enhanced the degradation of G3BP2, inhibiting G3BP2-driven nuclear export of stabilised p53 and p53 activity. This resulted in an increase in BAX protein and reduced cellular proliferation in part due to p53. Therefore, overall one could predict that loss of USP10 would cause the polyubiquitin-driven degradation of G3BP2 resulting in enhanced p53 signalling, reduced proliferation and apoptosis. Indeed, in some cases loss of USP10 resulted in the induction of cell death, which could have been caused by the observed loss of G3BP2.

Unlike that expected from above, knockdown of USP10 resulted in a loss of p53. Oi *et al.*demonstrated that G3BP1, an additional member of the G3BP family, interacts with USP10 and disrupts the interaction between USP10 and p53, thereby inhibiting the ubiquitin-driven degradation of p53 (Oi *et al.*, 2015). This could provide an explanation for the observed decrease in p53 following USP10 knockdown, as loss of USP10 would be similar to inhibition of its activity which would drive the polyubiquitylation and degradation of p53. This would also be consistent with the loss of PUMA observed following knockdown of USP10 (Figure 6.11B). However, contrary to that observed in this study, Oi *et al.*observed that knockdown of G3BP1 results in an accumulation p53. Overall, the underlying reason why loss of G3BP2 and/or p53 would synergise with PD901 to induce cell is unknown and requires further investigation.

Inhibition or downregulation of G3BP have been demonstrated to induce apoptosis (Zhang *et al.*, 2012). G3BP are involved in numerous signalling pathways required for tumourigenesis, including Ras signalling, via interaction between G3BP and RasGAP (Barnes *et al.*, 2002, Bos *et al.*, 2007). Downregulation of G3BP has been demonstrated to cause a reduction in RasGTP, impairing Ras signalling pathways, including ERK1/2 and PI3K signalling (Zhang *et al.*, 2012). Additionally, downregulation of G3BP sensitised cells to CDDP (cisplatin) treatment and resulted in a reduction in BCL2 protein, an increase in activated caspases and an increase in the fraction of cells with sub-G1 DNA, ultimately inducing apoptosis (Zhang *et al.*, 2012). Therefore, knockdown of USP10, via loss of G3BP2, has the potential to inhibit several Ras signalling pathways including PI3K signalling in addition to signalling via RAF. Thus, together with inhibition of ERK1/2 signalling, through MEK1/2 inhibition, the two treatments combined could act to significantly reduce Ras signalling and potentially overcome redundancy observed with either two alone to induce apoptosis.

Alternatively, the deubiquitylating activity of USP10 on G3BP2 and p53 may be unrelated and USP10 could act to stabilise additional oncogenic proteins whose loss would have a dominant effect and combine with MEK1/2 inhibition to drive apoptosis. Screening to identify USP10-binding partners would aid in fully understanding the effects of USP10 knockdown in HCT116 cells.

Interestingly, in A375 cells, knockdown of USP10 resulted in an accumulation of PUMA. This increase would support some of literature previously described, as loss of USP10 would result in enhanced degradation of G3BP2, inducing p53 activity and therefore expression of PUMA (Ashikari *et al.*, 2017, Takayama *et al.*, 2018). One could predict this would drive apoptosis, however, an increase in the fraction of cells with sub-G1 DNA following loss of USP10, or in combination with MEK1/2 inhibition was not observed.

Interrogation of the p53 status of HCT116 and A375 cells revealed that both are wild-type for p53, therefore the variation in cellular responses was not due to variation of p53 background. Instead, an additional protein, under the control of USP10, could be differentially expressed in these cells. Increased expression of an oncogenic protein, under the control of USP10, in HCT116 cells, compared to A375 cells, could mean that HCT116 cells have a higher dependency on this protein for proliferation/survival. Therefore, loss of USP10, alone or in combination with MEK1/2 inhibition, could affect the stability of this protein and would cause different effects on cell proliferation in these two cell lines.

In addition to loss of G3BP2, p53 and PUMA, knockdown of USP10 resulted in an increase in MCL1 protein in HCT116 cells. To investigate the effect of MCL1 protein levels on HCT116 cells, following USP10 knockdown, USP10 siRNA was combined with an MCL1 inhibitor. This combination failed to significantly enhance the cytoxicity of USP10 knockdown. Thus, unlike that seen by Wang *et al.*, 2014, where the increase in stability of MCL1 contributed to resistance to ABT-263, MCL1 upregulation was not the limiting factor for the induction of cell death.

Along with alteration in MCL1 protein levels, there was a decrease in BCL2 protein levels following USP10 knockdown. Knockdown of USP10 sensitised HCT116 cells to MEK1/2 inhibition and combined to induce apoptosis. Sale and Cook, revealed that the shift from a cytostatic to a cytotoxic response, seen with MEK1/2 inhibitor treatment followed by treatment with BH3 mimetics, was reliant upon the removal of pro-survival BCL2 protein activity (Sale and Cook, 2013). This is consistent with the theory that cell death seen with MEK1/2 inhibition and USP10 knockdown is reliant upon the combined increase of pro-apoptotic protein levels, as a consequence of MEK1/2 inhibition, and a decrease in the pro-survival protein, BCL2, seen with USP10 knockdown.

Overall, knockdown of several DUBs, such as VCIP135, YOD1 and USP10, have been identified that combine with MEK1/2 inhibition to induce apoptosis of HCT116 cells. More work needs to be done to identify the molecular mechanisms that underlie the observed cell death. This study would benefit from inhibitors that specifically target USP10, YOD1 and VCIP135. In addition, it would be worthwhile profiling additional cell lines that harbour KRas or NRas mutations in order to determine whether combined MEK1/2 inhibition and knockdown of these select DUBs induces cell death.

Chapter 7: Final discussion

7. Final Discussion

Regulated cell death (RCD) plays a major role in development, tissue homeostasis, inflammation, immunity and multiple pathophysiological conditions. There a multiple modes of RCD, which are activated and propagated through various molecular mechanisms. These include necroptosis, ferroptosis, immunogenic cell death (ICD), autophagy-dependent cell death (ADCD) and as discussed further apoptosis. In disease, RCD can cause irreversible loss of post-mitotic tissues, associated with myocardial infarction and neurodegeneration, and defects in RCD are associated with pathologies predominantly characterised by uncontrollable cell proliferation, including cancer (Galluzzi *et al.*, 2018).

Over the last 20 years there has been a huge effort to develop cytoprotective strategies aimed at targeting and disrupting RCD, however none have to date been approved for clinical trials. In contrast, inhibitors targeting pro-survival proteins to induce death, including BCL2 and MCL1, are clinically approved for the treatment of CLL patients (Ashkenazi *et al.*, 2017, Kotschy *et al.*, 2016). Targeted activation of RCD is suggested to be a much simpler clinical approach in part due to the emerging evidence that multiple RCD pathways are connected by key signalling molecules (Ashkenazi and Salvesen, 2014, Green and Llambi, 2015, Lalaoui *et al.*, 2015), thereby inhibitors may have to target multiple pathways simultaneously to reduce RCD.

Apoptosis is a mode of RCD, historically suggested to be a form of programmed cell death (PCD), characterised by morphological changes including nuclear fragmentation and membrane blebbing. This process is regulated through the action of the BCL2 protein family, grouped into pro-survival and pro-apoptotic proteins, which regulate MOMP and cell death. The discovery of interactions between pro-survival and pro-apoptotic proteins had major therapeutic implications and as such led to the development of BH3 mimetics which exploit this interaction and inhibit pro-survival proteins to drive apoptosis (Baell and Huang, 2002, Lessene *et al.*, 2008).

Recently, the historical view that apoptosis was a non-immunogenic response has been challenged. Instead, apoptotic cancer cell death, due to treatment with chemotherapeutic agents, including oxaplatin and cisplatin, and oncolytic viruses, was demonstrated to be immunogenic, due in part to release of danger-associated molecular patterns (DAMPs) (Inoue and Tani, 2014). As such, our understanding of apoptosis and the downstream cellular responses it causes appears to be evolving and therefore continued evaluation of how RCD, including apoptosis, is controlled is essential for understanding how RCD pathways can be targeted for therapeutic benefit.

7.1. Regulation of apoptosis by the Ras-RAF-MEK1/2-ERK1/2 signalling pathway

The Ras-regulated RAF-MEK1/2-ERK1/2 (ERK1/2) pathway regulates several components of the apoptotic signalling pathway. Predominantly, activation of ERK1/2 signalling results in the downregulation or inhibition of pro-apoptotic proteins and the upregulation of pro-survival proteins, thereby ultimately promoting cell survival (Cook *et al.*, 2017). Given this, tumour cells can develop numerous mechanisms to activate and maintain ERK1/2 signalling, thus evading apoptosis, to sustain cell proliferation and tumourigenesis. In contrast, inhibition of ERK1/2 signalling in these tumour cells has been demonstrated to drive the accumulation of pro-apoptotic proteins including BIM (Sale and Cook, 2013). Therefore, information regarding the regulation of BIM may play a role in oncogene-targeted cancer therapies (Gillings *et al.*, 2009).

7.1.1. ERK1/2-dependent regulation of BIM_{EL} – is there a role for RSK?

The phosphorylation status of BIM influences its pro-apoptotic function and stability. Multiple kinases have been shown to phosphorylate BIM_{EL} including p38 MAPK, JNK and ERK1/2. Whilst phosphorylation of BIM_{EL} by JNK has been demonstrated to potentiate its pro-apoptotic activity, ERK1/2-driven phosphorylation of BIM_{EL} induces its degradation (Ley *et al.*, 2003, Putcha *et al.*, 2003).

ERK1/2 phosphorylates BIM_{EL} on at least three Ser/Pro residues, including S69, resulting in its K48-linked polyubiquitylation and degradation (Hubner *et al.*, 2008, Ley *et al.*, 2003, Luciano *et al.*, 2003, Wiggins *et al.*, 2011). Results presented in Chapter 3 confirm these findings, using both mutagenesis studies and pharmacological inhibitors of MEK1/2 and ERK1/2. More recently, RSK1/2 has been proposed to regulate the interaction between BIM_{EL} and the E3 ligase $SCF^{\beta TrCP}$, thereby targeting BIM_{EL} for degradation (Dehan *et al.*, 2009); it was suggested that ERK1/2 cooperates with RSK1/2 to phosphorylate the BIM_{EL} degron, enabling the binding of βTrCP, thus driving the degradation of BIM_{EL}. Contrary to this, work presented in Chapter 3 conclusively demonstrated that RSK is not required to regulate the degradation of BIM_{EL} in HR1 cells, in addition to ERK1/2-addicted tumour cells. Mutagenesis of the serine residues within the BIM_{EL} degron did appear to increase the stability of BIM_{EL}, abolish its interaction with βTrCP and reduce its polyubiquitination. However, further analysis revealed that there was overlap between the ERK1/2 docking domain and the BIM_{EL} degron, therefore mutagenesis of the BIM_{EL} degron could stabilise BIM_{EL} by decreasing the ability of ERK1/2 to interact with BIM_{EL}. Indeed, the RSK1/2 phosphorylation site mutant was confirmed to impact the ability of ERK1/2 to bind to BIM_{EL} (Chapter Figure 3.5G and Figure 3.5H), thereby bringing into question the reliance on mutagenesis to assess the role of RSK in the degradation of BIM_{EL}. Conclusions drawn from

Chapter 3 were based on the use of three RSK inhibitors, all of which showed no role for RSK in the regulation of BIM_{EL}. As a whole, these results argue firmly against a role for RSK in the regulation of BIM_{EL} stability and further highlights the requirement of ERK1/2-dependent phosphorylation of BIM_{EL} to enable its interaction with βTrCP, thereby driving its degradation.

7.1.2. Is there an alternative kinase that cooperates with ERK1/2 to regulate the degradation of BIM_{EL}?

The main questions arising as a consequence of the findings from Chapter 3 are: Is an alternative kinase required for phosphorylation of BIM_{EL} within the BIM_{EL} degron, and therefore responsible for regulating the stability and degradation of BIM_{EL}, or is ERK1/2 sufficient, alone, to drive the degradation of BIM_{EL}.

Multiple proteins are polyubiquitylated and degraded as a consequence of βTrCP binding to a defined phospho-degron motif, DSGX(n)S, where X represents any amino acid. In the majority of cases, phosphorylation of serine residues within this degron is prerequisite to βTrCP binding. Additionally, the stability of multiple proteins has been demonstrated to be regulated by the cooperative action of two kinases. A classic example of this is the regulation of β-Catenin, which, as a consequence of phosphorylation by CK1α, is also phosphorylated by GSK3 within the described βTrCP binding motif, resulting it its targeted degradation. As ERK1/2 is a proline-directed Ser/Thr kinase it is unlikely to be able to phosphorylate BIM_{EL} at the suggested βTrCP binding motif (BIM_{EL}: SSGYFS); therefore an alternative kinase could phosphorylate BIM_{EL} within the described degron to cooperate with ERK1/2 to drive BIM_{EL} degradation. Several candidate kinases were considered that could be able to phosphorylate BIM_{EL} within the degron; however, inhibitors against these kinases failed to increase the stability of BIM_{EL} or abolish its interaction with βTrCP. Therefore, identifying alternative kinases for BIM_{EL} may require a large-scale approach, including treating HR1 cells with broad-spectrum inhibitors at high concentrations to see if any alter the interaction between βTrCP and BIM_{EL} and therefore regulate the stability of BIM_{EL}. An alternative approach might be to extract BIM_{EL} from cells by affinity purification and then employ mass spectrometry to identify interacting partners. Co-immunoprecipitation experiments would be required to confirm that the identified kinase(s) interacts with BIM_{EL}.

Alternatively, phosphorylation at the βTrCP binding motif may not be required for interaction between BIM_{EL} and βTrCP. Indeed, Kanemori *et al.* demonstrated that βTrCP can interact with CDC25A and CDC25B independent of phosphorylation within their βTrCP binding motifs (Kanemori *et al.*, 2005). Therefore, this presents the possibility that βTrCP could bind and polyubiquitylate BIM_{EL}, independent

of phosphorylation at the degron, and that ERK1/2 activity alone could regulate the stability of BIM_{EL}. Interestingly, Ewings *et al.* provided an alternative theory, which could corroborate the idea that phosphorylation at the BIM_{EL} degron is not required for βTrCP binding. Instead, ERK1/2-dependent phosphorylation of BIM_{EL} drives its dissociation from pro-survival proteins, BCL-X_L and MCL1, which renders BIM_{EL} susceptible for degradation (Ewings *et al.*, 2007). As such, the ability of βTrCP to interact with BIM_{EL} might not be dependent on phosphorylation per se, but instead rely upon phosphorylation for dissociation from pro-survival proteins to reveal the βTrCP binding motif. This is supported by findings by Ewings *et al.*, where mutation of the BH3 domain of BIM_{EL} drives its dissociation from pro-survival proteins and accelerates its degradation, suggesting that dissociation is a prerequisite for degradation (Ewings *et al.*, 2007). In addition, mutation of proline-directed Ser/Thr residues, known to be targeted by ERK1/2, stabilised BIM_{EL}, as demonstrated in Chapter 3, and have previously been shown to prevent the dissociation of BIM_{EL} from pro-survival proteins following ERK1/2 activation (Ewings *et al.*, 2007). This provides some evidence supporting the theory of dissociation-driven degradation. Given this, several questions still remain unanswered, including how phosphorylation drives dissociation from pro-survival proteins and does phosphorylation induce conformational changes that induce this dissociation and aid in revealing the βTrCP binding site of BIM_{EL}.

7.2. Regulation of apoptosis by ubiquitylation

Post-translational modifications regulate all aspects of a protein's existence, including its activity and stability. Ubiquitylation predominantly results in the degradation of a protein, however non-degradative roles for ubiquitylation have also emerged. Ubiquitylation is regulated by E1, E2 and E3 ligases; the latter catalyses the final enzymatic reaction required for ubiquitin (Ub) attachment. Ubiquitylation is opposed by deubiquitylating enzymes (DUBs), which remove Ub from its substrate.

Established in 1990 by Schwartz *et al.* there is now conclusive evidence linking ubiquitylation to apoptosis (Jesenberger and Jentsch, 2002, Orlowski, 1999, Schwartz *et al.*, 1990, Wojcik, 1999). Several substrates of the ubiquitin-proteasome system (UPS) are key regulators of apoptosis including, BCL2 proteins, IAPs and p53, thereby highlighting the critical role the UPS plays in the execution of apoptosis. In addition, ubiquitylation can play a non-degradative role in regulating apoptosis; for example, the K63-polyubiquitylation of RIP1 is required to recruit additional complexes resulting in the activation of TNFα-mediated NF-κB signalling and cell survival (Wertz *et al.*, 2004).

Studying the role of ubiquitylation in the regulation of apoptosis is important for establishing the signalling networks that balance life and death. In addition, dysregulation of apoptosis has been linked to multiple diseases including Alzheimer's disease, Parkinson's disease, cancer and autoimmune

diseases. As such unravelling the link between apoptosis and ubiquitylation could be of therapeutic benefit.

7.2.1. DUBs as therapeutic targets

The importance of Ub-targeted degradation was first highlighted following a Nobel Prize being awarded for the discovery of the ubiquitin-proteasome system (UPS) (Ciechanover *et al.*, 1980, Hershko *et al.*, 1980). This resulted in the development of proteasome inhibitors, which, in the majority of cases, induced apoptosis (Drexler, 1997, Shinohara *et al.*, 1996) and identified the potential therapeutic benefit of targeting ubiquitylation machinery. To date, inhibitors are being or have been developed that target several components of the ubiquitin system including DUBs (Cohen and Tcherpakov, 2010, Harrigan *et al.*, 2017).

Recognition that the dysregulation of DUBs contributes to multiple diseases including cancer and neurodegenerative diseases highlighted the possibility that DUBs could be a therapeutic target. However, it is not until recently that first generation DUB inhibitors have reached clinical trials.

The development of selective DUB inhibitors has been hindered by insufficient understanding of DUB biology and also the lack of tools to screen and assay DUB activity and inhibition. DUB activity-based probes (ABPs), such as the HA-UbVME probe described in Chapter 4, has enabled researchers to monitor DUB activity and inhibition of DUBs by small molecules, thereby assisting in characterising the selectivity of a DUB inhibitor (Hewings *et al.*, 2017). Indeed, ABPs have aided in identifying the selectivity of the USP7 inhibitor, P22077, and have been used to demonstrate that HBX19818 is selective for USP7, against a panel of DUBs (Altun *et al.*, 2011, Reverdy *et al.*, 2012).

Recently, Liang *et al.* suggested that the DUB USP30 regulates BAK/BAK-dependent apoptosis in cancer cells (Liang *et al.*, 2015). They demonstrated that knocking down USP30 sensitised cancer cells to BH3 mimetics and the combination resulted in cell death. Thus, inhibitors against USP30 have the potential to be used, in combination, to treat cancer. Inhibition of USP30, using the USP30 inhibitors MTX32 and MTX48, provided by Mission Therapeutics, together with the BH3 mimetic ABT-263, yielded varying results. Using the ABP, HA-Ub-VME, both inhibitors were found to rapidly and irreversibly inhibit USP30. Whilst MTX32 combined with ABT-263 to induce apoptosis of HCT116 cells, MTX48 did not. Further examination of the general inhibitor profiles of MTX32 and MTX48, using the ABP, highlighted the off-target nature of MTX32, thus indicating that apoptosis, induced as a consequence of combined treatment with MTX32 and the BH3 mimetic, was due to MTX32 inhibiting multiple, potentially essential, DUBs. Data generated in Chapter 4 highlights the need for tools such as ABPs to evaluate the

selectivity of DUBs. However, these technologies still have limitations, including the number of DUBs that can be labelled, as such further advancements in probe design and assay technologies would aid in driving the development of clinically relevant DUB inhibitors.

7.2.2. Identifying DUBs that regulate cell death driven by MEK1/2 inhibitors

The emergence of resistance to new cancer therapies, including MEK1/2 inhibitor monotherapy, necessitates the development of alternative strategies to delay and/or prevent its onset. As a consequence of the ERK1/2 pathway being closely integrated with ubiquitin signalling, it was hypothesised that knockdown of one or more DUBs could combine with MEK1/2 inhibition to drive tumour cell death. Therefore, inhibition of this DUB could be used in combination with MEK1/2 inhibitors for targeted treatment of ERK1/2 addicted tumour cells.

Given this, a DUB focused RNAi screen was undertaken to identify DUBs which, when knocked down, transformed MEK1/2 inhibition from a cytostatic to a cytotoxic response. With the shorter 3-day screen, very few DUBs were identified that robustly combined, when knocked down, with MEK1/2 inhibition to drive loss of cell viability and/or cell death. The two 3-day screens performed were valid as all controls, both negative and positive, for siRNA and inhibitors, generated raw data from multiple end-point analyses that matched the expected trend. Therefore, this could suggest that the original hypothesis may not be correct, and that despite the screen being valid, that knockdown of DUBs do not combine with MEK1/2 inhibition to drive tumour cell death. However, it could suggest that the method used to analyse the screen, sensitivity index (SI) analysis, may not have been the best method to test the hypothesis. Alternative analyses should be performed to clarify if the chosen analysis method was the limiting factor preventing the identification of 'hits' and if additional 'hits' would be obtained using an alternative method. Interestingly, Ye *et al.* concluded that RNAi screening is capable of identifying novel drug targets that can sensitise cancer cells to treatment however, if an inappropriate statistical method or model was applied to the screen data it could decrease the ability to detect 'true' hits and will increase false positive and negative results (Ye *et al.*, 2012). An example of an alternative method of analysis includes the use of a linear model, which describes both the effect of siRNA and drug individually, as well as the combined effect, and is thought to overcome problems associated with SI analysis including cross-plate variation, which is averaged during SI calculations (Ye *et al.*, 2012).

In addition, an RNAi screen may not be the best method to address the suggested hypothesis. Alternative approaches include a CRISPR-cas9 screen, which would knockout DUBs of interest, rather than knock them down, and would eliminate the risk that residual DUB activity could mask the

phenotype. Interestingly, information generated by DepMap (DepMap, 2019) suggests that there is limited overlap between the phenotype observed from siRNA knockdown and CRISPR knockout of the same gene in the same cancer cell line. In addition, small molecule DUB inhibitors may cause a similar effect to siRNA knockdown of a DUB as both rarely completely abolish the activity of their targets. Thus, siRNA may be more biologically relevant than CRISPR-cas9 for assessing the phenotype associated with loss of DUB activity.

Overall, it could be suggested that in order to observe a 'hit' for the designed DUB RNAi screen, irrespective of end-point assay analysis, statistical analysis and differences caused by experimental variability, the DUB must regulate, or be, the key gene driving tumour cell growth. Therefore, its knockdown would combine with MEK1/2 inhibition to drive a robust cell death phenotype. In addition, there might be functional redundancy between DUBs, therefore in order to observe a desired phenotype multiple DUBs may need to be targeted simultaneously.

7.2.3. Knockdown of USP10, YOD1 or VCIP135 combines with MEK1/2 inhibition to induce apoptosis of HCT116 cells

Data generated from the 5-day screen identified USP10, YOD1 and VCIP135 as 'hits'. Further analysis revealed that these DUBs repeatedly, when knocked down, combined with MEK1/2 inhibition, to drive cell death, in a BAK/BAX-dependent manner. However, combined knockdown of USP10 or YOD1 with MEK1/2 inhibition failed to cause cell death in A375 melanoma cells, therefore suggesting a cell line-specific phenotype. It would be interesting to see if knockdown of these DUBs combined with inhibitors that target different components of the ERK1/2 signalling pathway including RAF or ERK1/2 to induce apoptosis of HCT116 cells.

The exact molecular mechanism underlying how these DUBs aid in regulating apoptosis is unknown and requires further examination. The use of DUB-specific inhibitors in future work would be invaluable and would help reduce variability in phenotype caused as a consequence of transfection. In addition, CRISPR-cas9 USP10, YOD1 and VCIP135 knockout cells would be a useful tool to help elucidate the role these DUBs play in the regulation of apoptosis. In terms of large-scale future experiments, it would be interesting to perform affinity proteomics to identify substrates or binding partners of USP10, YOD1 and VCIP135. Proximity-dependent biotin identification (BioID) should enable the identification of proteins that interact with these DUBs in living cells. USP10, YOD1 or VCIP135 would be fused in-frame to an *E. coli* biotin conjugating mutant (BirA*) and expressed in cells. The enzyme would biotinylate proximal interacting proteins of these DUBs, which could then be affinity purified using streptavidin and identified using mass spectrometry. As this method does not require

protein-protein interactions to be maintained post-lysis, weak or transient interactors may be identified. It would be interesting to compare the interacting partners identified for catalytically active and catalytically inactive mutants of the DUBs, as some catalytically inactive mutants can 'trap substrates' analogous to the technique used to identify targets of protein-tyrosine phosphatases (PTPs) and 'ligase trapping' used to identify substrates of the E3 ligase SCF (Saf1) (Blanchetot *et al.*, 2005, Mark *et al.*, 2016, Mark *et al.*, 2014). Again, this may aid in identifying substrates that may bind transiently or weakly to catalytically active DUBs.

Of note, USP10 was found to regulate BCL2 protein stability. It would be interesting to evaluate how USP10 regulates the stability of BCL2, either directly or indirectly, whether knockdown of USP10 also resulted in loss of *BCL2* mRNA and conversely whether overexpression of USP10 promotes the stability of BCL2. The regulation of BCL2 by USP10 does provide one explanation as why combined knockdown of USP10 and MEK1/2 inhibition resulted in tumour cell death; loss of BCL2, as a consequence of USP10 knockdown, would lower the pro-survival response and combine with MEK1/2 inhibitors, known to induce pro-apoptotic proteins, to drive apoptosis (Sale and Cook, 2013).

7.3. Conclusions

Since the definition of apoptosis by Kerr in 1972, a vast body of work has established that apoptosis is a critical process required for cell death and as such is subject to tight regulation. Therapeutic manipulation of pathways regulating apoptosis has the potential to drive cell death, including cancer cell death. This study focused on the regulation of a key pro-apoptotic protein BIM_{EL} and established that RSK is not required to regulate the stability of BIM_{EL}. However further work will be required to confirm if ERK1/2 alone is required to regulate BIM_{EL} turnover.

The ubiquitin-proteasome system plays a pivotal role in the regulation of apoptosis. Given this, understanding the role that ubiquitin system components, including DUBs, play in the regulation of apoptosis could be exploited therapeutically to drive cell death. Recent advances in the development of DUB inhibitors will likely prove invaluable in the treatment of multiple diseases. Work performed in this thesis highlights that technologies aimed at assessing the selectivity of DUB inhibitors are critical and advances, aimed at improving assays and screens to identify and confirm the selectivity of DUBs, will be critical for DUB drug discovery and development. Finally this study identified several DUBs that, when knocked down, combine with MEK1/2 inhibition to enhance tumour cell death. Dependent on further evaluation, these DUBs could be targeted for therapeutic benefit to overcome resistance to MEK1/2 inhibitor monotherapy and drive tumour cell death.

Supplementary Information

Supplementary Information:

BRCC3

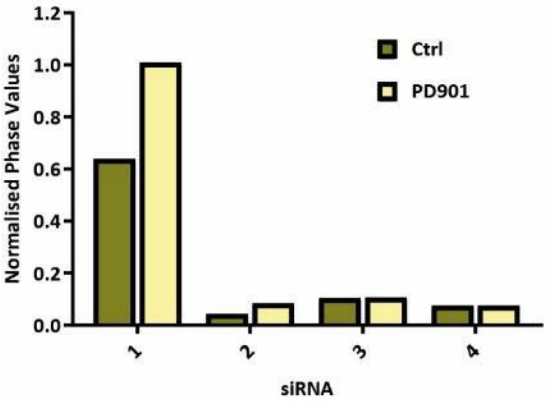

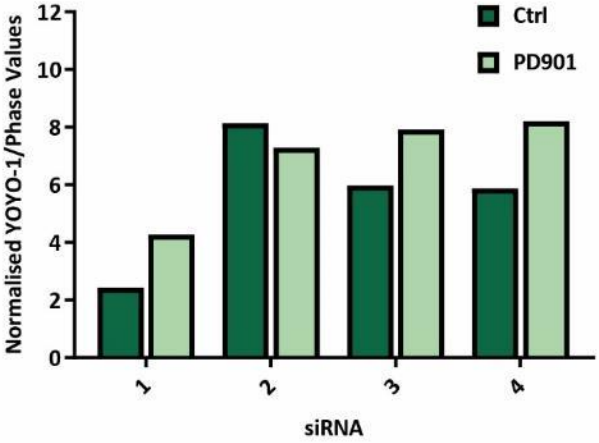

EIF3F

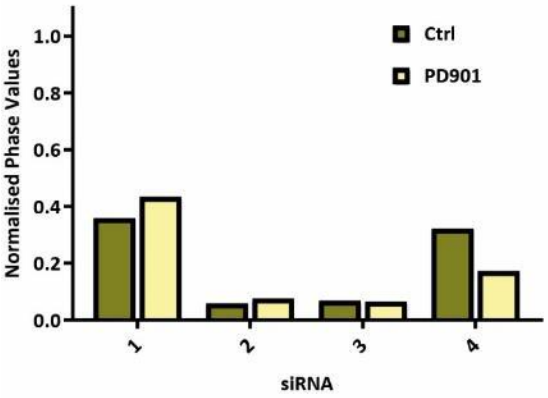

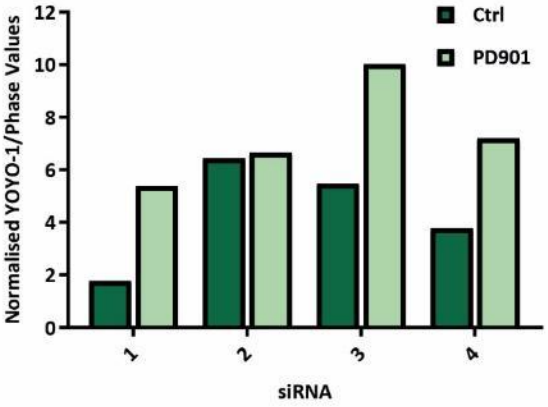

PSMD14

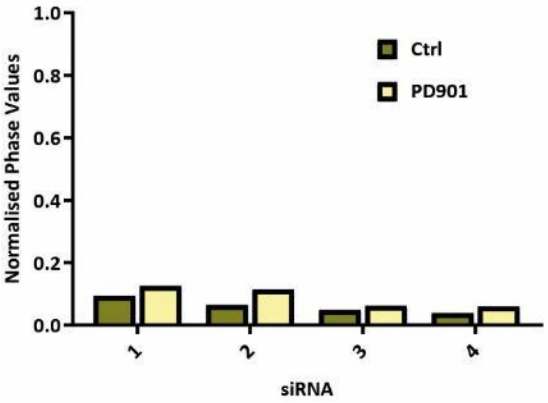

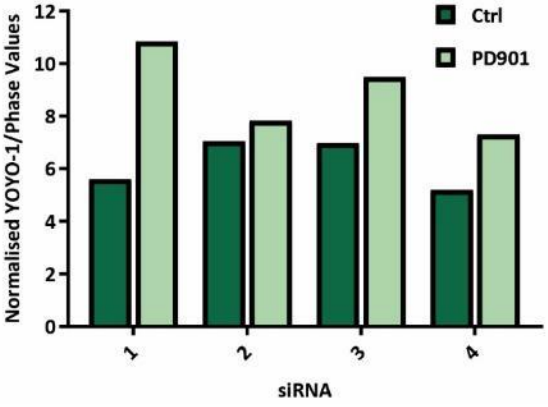

SENP5

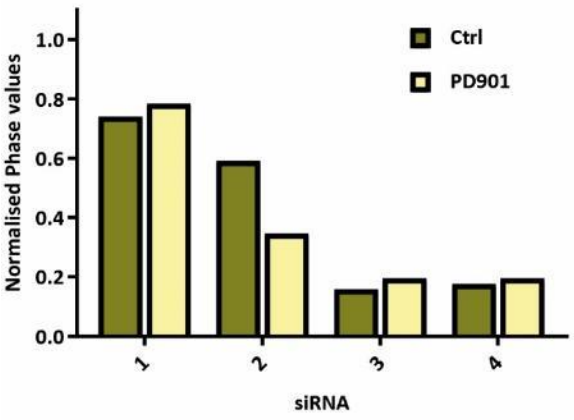

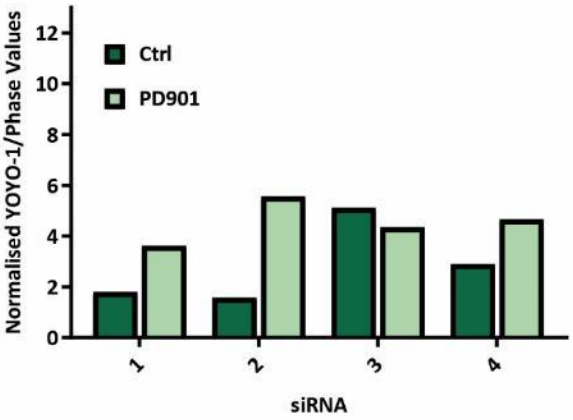

UCHL1

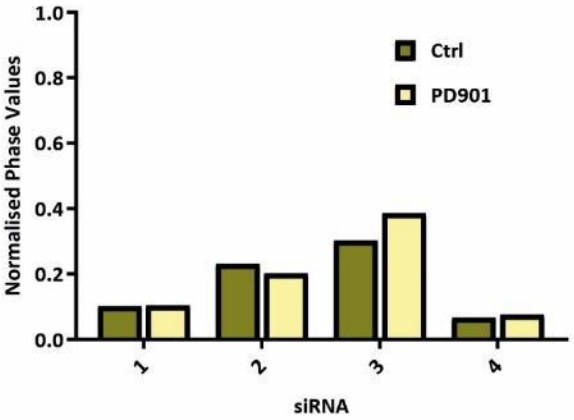

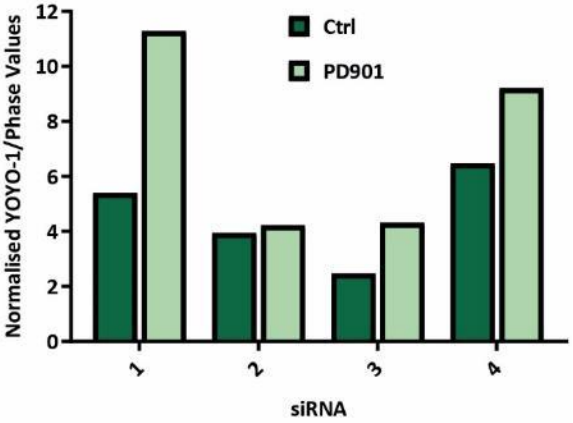

USP20

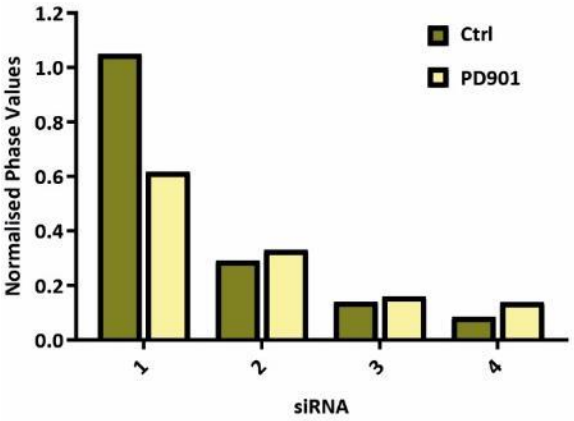

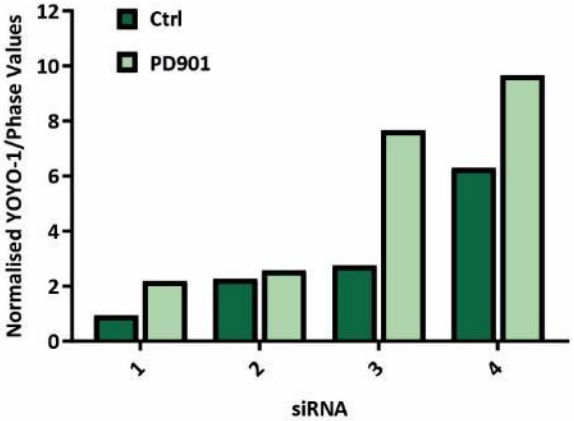

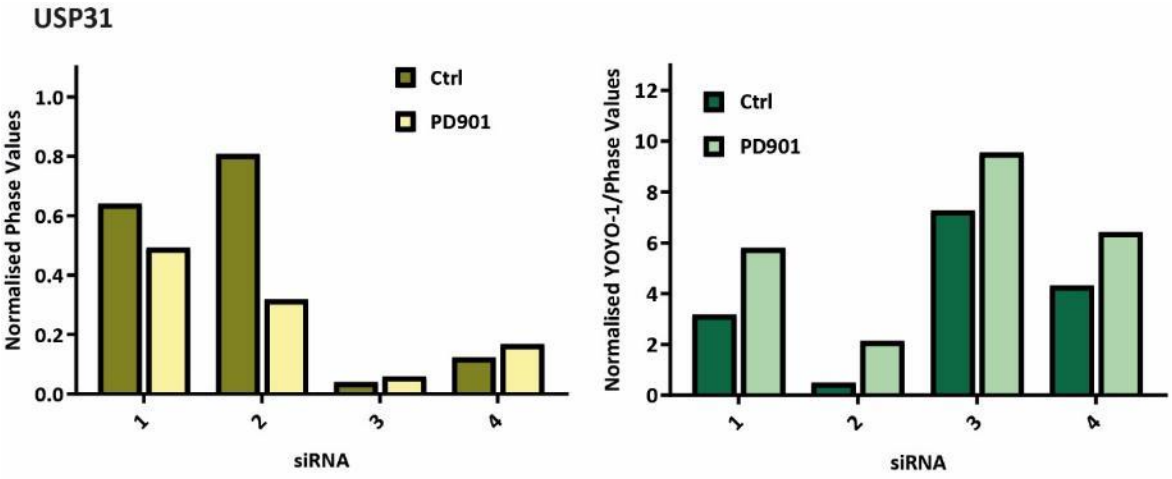
USP31
Ctrl
PD901
Normalised Phase Values
1.0
0.8
0.6
0.4
0.2
0.0
1
2
3
4
siRNA
Ctrl
PD901
Normalised YOYO-1/Phase Values
12
10
8
6
4
2
0
1
2
3
4
siRNA

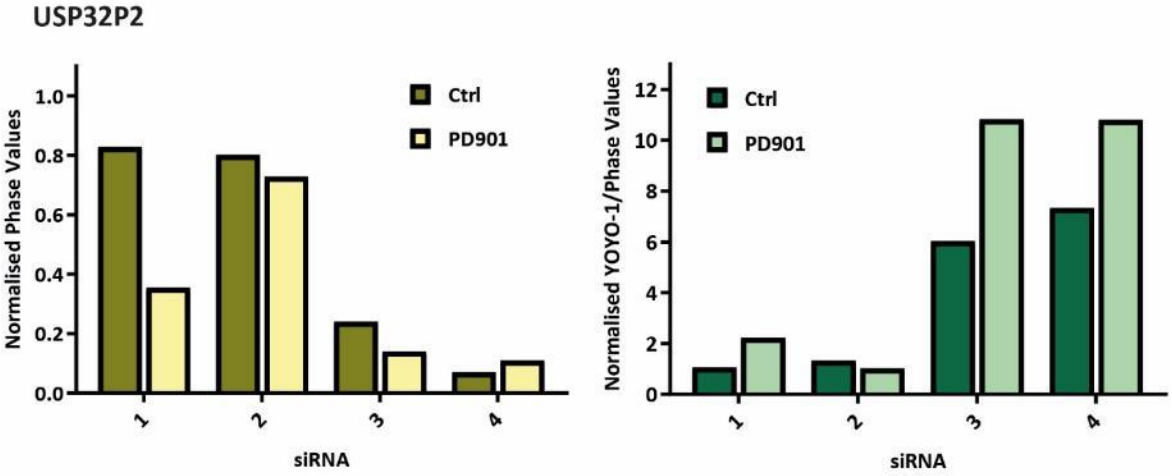
USP32P2
Ctrl
PD901
Normalised Phase Values
1.0
0.8
0.6
0.4
0.2
0.0
1
2
3
4
siRNA
Ctrl
PD901
Normalised YOYO-1/Phase Values
12
10
8
6
4
2
0
1
2
3
4
siRNA

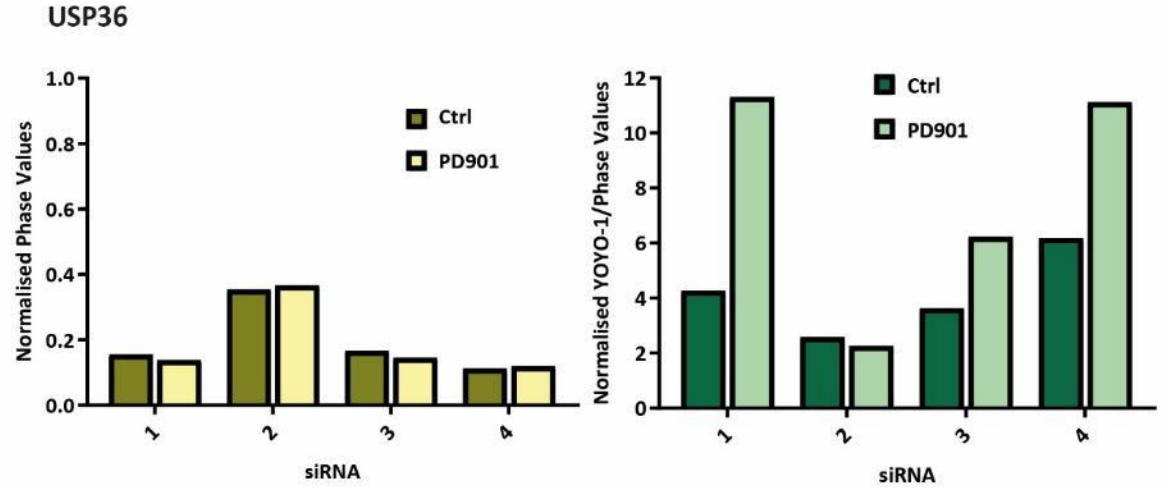
USP36
Ctrl
PD901
Normalised Phase Values
1.0
0.8
0.6
0.4
0.2
0.0
1
2
3
4
siRNA
Ctrl
PD901
Normalised YOYO-1/Phase Values
12
10
8
6
4
2
0
1
2
3
4
siRNA

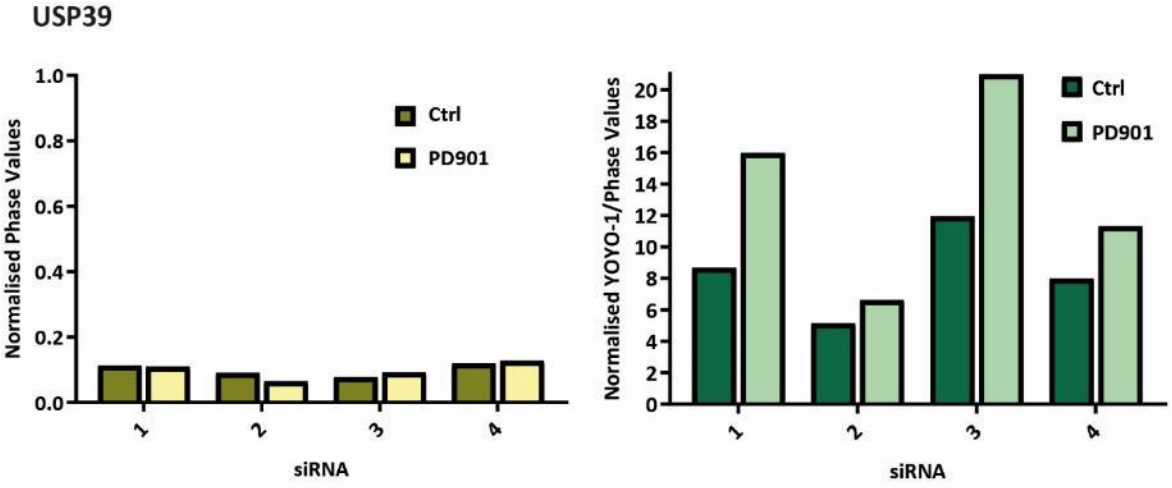
USP39
Normalised Phase Values
1.0
0.8
0.6
0.4
0.2
0.0
Ctrl
PD901
1
2
3
4
siRNA
Normalised YOYO-1/Phase Values
20
18
16
14
12
10
8
6
4
2
0
Ctrl
PD901
1
2
3
4
siRNA

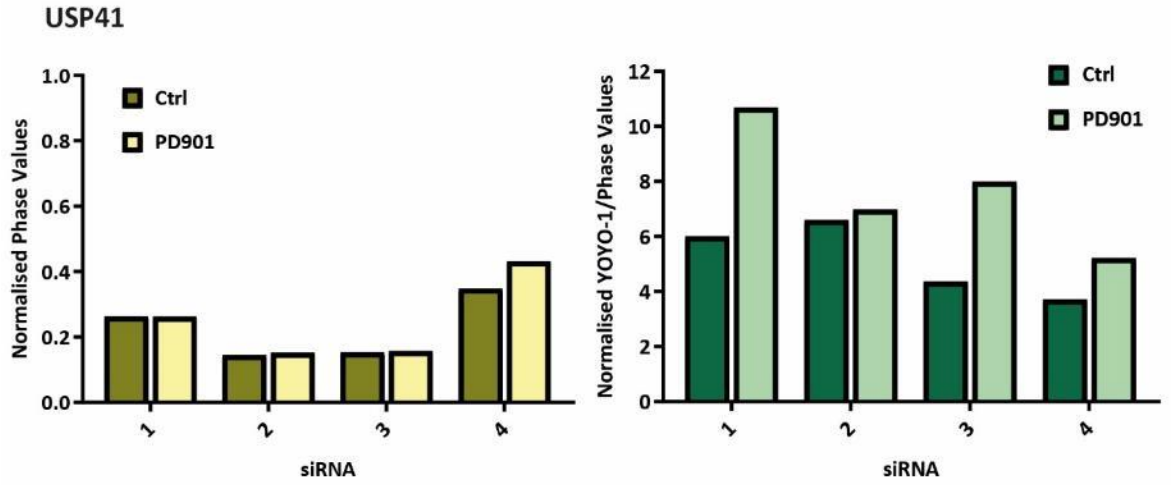
USP41
Normalised Phase Values
1.0
0.8
0.6
0.4
0.2
0.0
Ctrl
PD901
1
2
3
4
siRNA
Normalised YOYO-1/Phase Values
12
10
8
6
4
2
0
Ctrl
PD901
1
2
3
4
siRNA

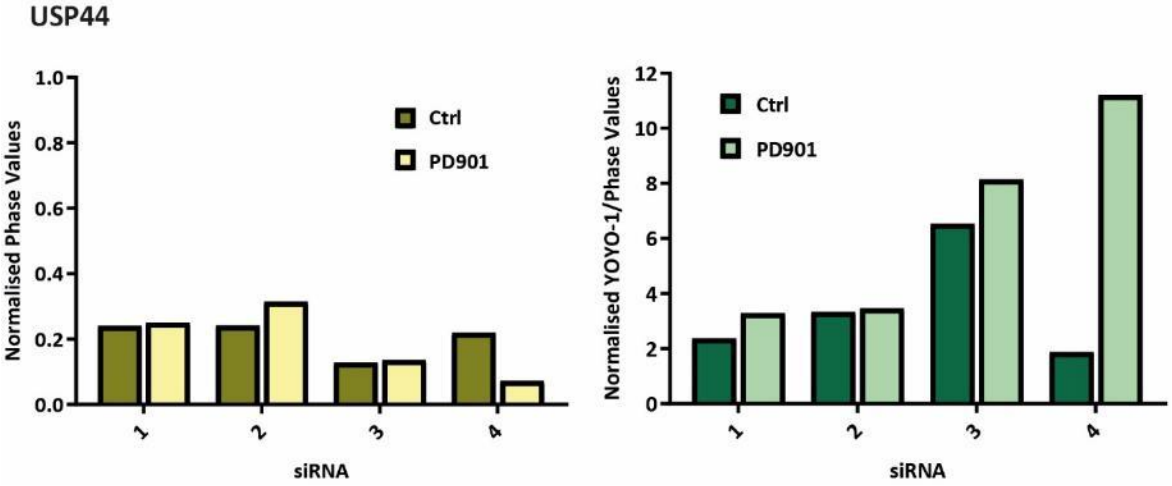
USP44
Normalised Phase Values
1.0
0.8
0.6
0.4
0.2
0.0
Ctrl
PD901
1
2
3
4
siRNA
Normalised YOYO-1/Phase Values
12
10
8
6
4
2
0
Ctrl
PD901
1
2
3
4
siRNA

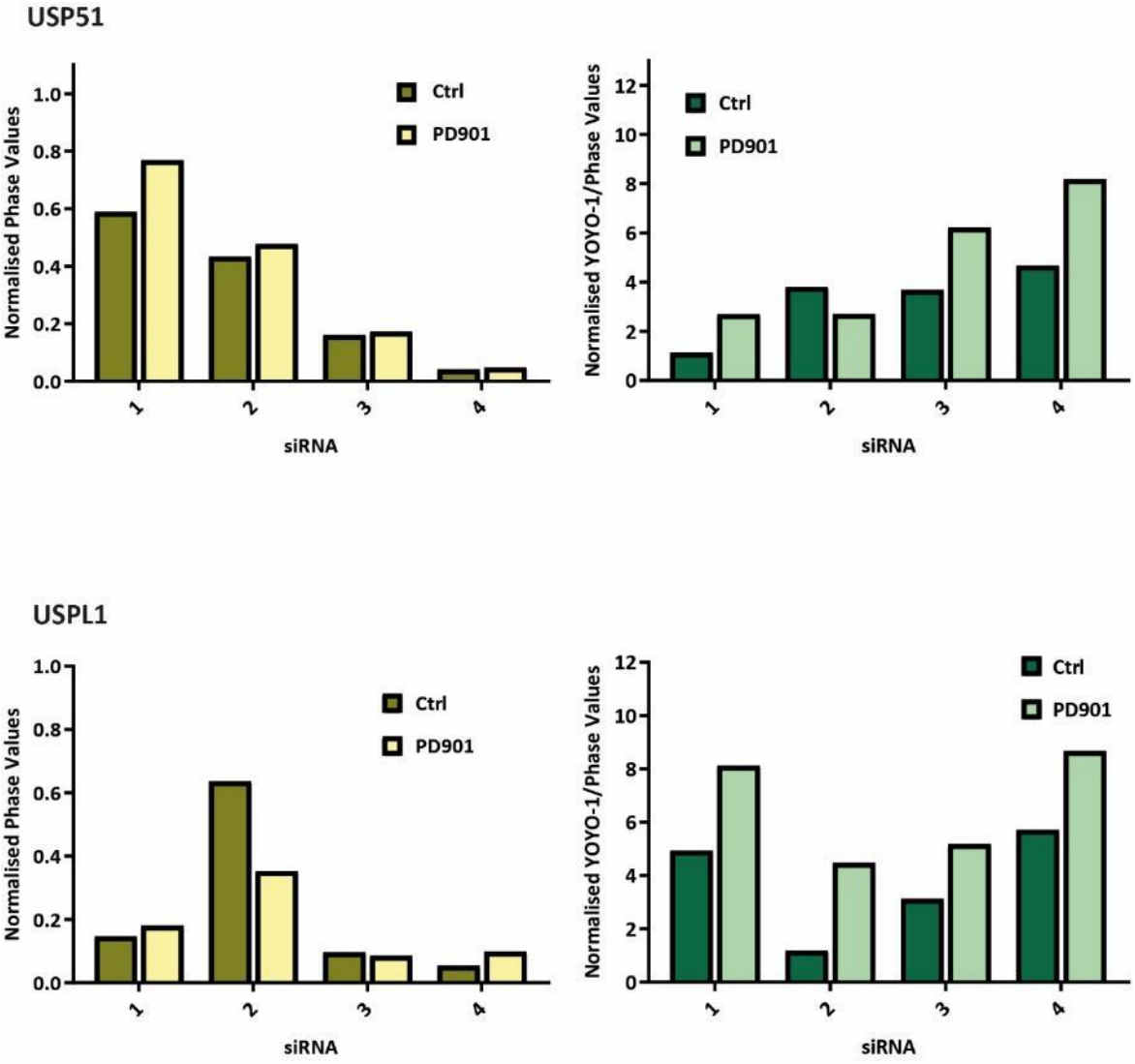

Additional bar graphs representative of normalised phase data and YOYO-1/Phase data for each 'hit' DUB. All data was taken from a single screen.
Ctrl = siRNA knockdown of select DUB
PD901 = siRNA knockdown of select DUB + PD901

References

ABDUL REHMAN, S. A., KRISTARIYANTO, Y. A., CHOI, S. Y., NKOSI, P. J., WEIDLICH, S., LABIB, K., HOFMANN, K. & KULATHU, Y. 2016. MINDY-1 Is a Member of an Evolutionarily Conserved and Structurally Distinct New Family of Deubiquitinating Enzymes. *Mol Cell,* 63**,** 146-55.

ADACHI, M., ZHAO, X. & IMAI, K. 2005. Nomenclature of dynein light chain-linked BH3-only protein Bim isoforms. *Cell Death Differ,* 12**,** 192-3.

ADAMS, J. M. & CORY, S. 2017. The BCL-2 arbiters of apoptosis and their growing role as cancer targets. *Cell Death Differ,* 25**,** 27.

ADARI, H., LOWY, D. R., WILLUMSEN, B. M., DER, C. J. & MCCORMICK, F. 1988. Guanosine triphosphatase activating protein (GAP) interacts with the p21 ras effector binding domain. *Science,* 240**,** 518-21.

ADORNO, M., SIKANDAR, S., MITRA, S. S., KUO, A., NICOLIS DI ROBILANT, B., HARO-ACOSTA, V., OUADAH, Y., QUARTA, M., RODRIGUEZ, J., QIAN, D., REDDY, V. M., CHESHIER, S., GARNER, C. C. & CLARKE, M. F. 2013. Usp16 contributes to somatic stem-cell defects in Down's syndrome. *Nature,* 501**,** 380-4.

AEBERSOLD, D. M., SHAUL, Y. D., YUNG, Y., YAROM, N., YAO, Z., HANOCH, T. & SEGER, R. 2004. Extracellular signal-regulated kinase 1c (ERK1c), a novel 42-kilodalton ERK, demonstrates unique modes of regulation, localization, and function. *Mol Cell Biol,* 24**,** 10000-15.

AGRAWAL, S. G., LIU, F.-T., WISEMAN, C., SHIRALI, S., LIU, H., LILLINGTON, D., DU, M.-Q., SYNDERCOMBE-COURT, D., NEWLAND, A. C., GRIBBEN, J. G. & JIA, L. 2008. Increased proteasomal degradation of Bax is a common feature of poor prognosis chronic lymphocytic leukemia. *Blood,* 111**,** 2790-2796.

AHRONIAN, L. G., SENNOTT, E. M., VAN ALLEN, E. M., WAGLE, N., KWAK, E. L., FARIS, J. E., GODFREY, J. T., NISHIMURA, K., LYNCH, K. D., MERMEL, C. H., LOCKERMAN, E. L., KALSY, A., GURSKI, J. M., JR., BAHL, S., ANDERKA, K., GREEN, L. M., LENNON, N. J., HUYNH, T. G., MINO-KENUDSON, M., GETZ, G., DIAS-SANTAGATA, D., IAFRATE, A. J., ENGELMAN, J. A., GARRAWAY, L. A. & CORCORAN, R. B. 2015. Clinical Acquired Resistance to RAF Inhibitor Combinations in BRAF-Mutant Colorectal Cancer through MAPK Pathway Alterations. *Cancer Discov,* 5**,** 358-67.

AKIYAMA, T., BOUILLET, P., MIYAZAKI, T., KADONO, Y., CHIKUDA, H., CHUNG, U. I., FUKUDA, A., HIKITA, A., SETO, H., OKADA, T., INABA, T., SANJAY, A., BARON, R., KAWAGUCHI, H., ODA, H., NAKAMURA, K., STRASSER, A. & TANAKA, S. 2003. Regulation of osteoclast apoptosis by ubiquitylation of proapoptotic BH3-only Bcl-2 family member Bim. *Embo j,* 22**,** 6653-64.

ALSOP, A. E., FENNELL, S. C., BARTOLO, R. C., TAN, I. K. L., DEWSON, G. & KLUCK, R. M. 2015. Dissociation of Bak α1 helix from the core and latch domains is required for apoptosis. *Nature Communications,* 6**,** 6841.

ALTUN, M., KRAMER, H. B., WILLEMS, L. I., MCDERMOTT, J. L., LEACH, C. A., GOLDENBERG, S. J., KUMAR, K. G., KONIETZNY, R., FISCHER, R., KOGAN, E., MACKEEN, M. M., MCGOURAN, J., KHORONENKOVA, S. V., PARSONS, J. L., DIANOV, G. L., NICHOLSON, B. & KESSLER, B. M. 2011. Activity-based chemical proteomics accelerates inhibitor development for deubiquitylating enzymes. *Chem Biol,* 18**,** 1401-12.

ANDERSON, M. A., HUANG, D. & ROBERTS, A. 2014. Targeting BCL2 for the treatment of lymphoid malignancies. *Semin Hematol,* 51**,** 219-27.

ANDREOTTI, P. E., CREE, I. A., KURBACHER, C. M., HARTMANN, D. M., LINDER, D., HAREL, G., GLEIBERMAN, I., CARUSO, P. A., RICKS, S. H., UNTCH, M. & *ET AL.* 1995. Chemosensitivity testing of human tumors using a microplate adenosine triphosphate luminescence assay: clinical correlation for cisplatin resistance of ovarian carcinoma. *Cancer Res,* 55**,** 5276-82.

ANJUM, R. & BLENIS, J. 2008. The RSK family of kinases: emerging roles in cellular signalling. *Nat Rev Mol Cell Biol,* 9**,** 747-58.

ANNIS, M. G., SOUCIE, E. L., DLUGOSZ, P. J., CRUZ-AGUADO, J. A., PENN, L. Z., LEBER, B. & ANDREWS, D. W. 2005. Bax forms multispanning monomers that oligomerize to permeabilize membranes during apoptosis. *Embo j,* 24**,** 2096-103.

AOKI, K., YAMADA, M., KUNIDA, K., YASUDA, S. & MATSUDA, M. 2011. Processive phosphorylation of ERK MAP kinase in mammalian cells. *Proc Natl Acad Sci U S A,* 108**,** 12675-80.

ARCILA, M. E., DRILON, A., SYLVESTER, B. E., LOVLY, C. M., BORSU, L., REVA, B., KRIS, M. G., SOLIT, D. B. & LADANYI, M. 2015. MAP2K1 (MEK1) Mutations Define a Distinct Subset of Lung Adenocarcinoma Associated with Smoking. *Clin Cancer Res,* 21**,** 1935-43.

ARESSY, B., JULLIEN, D., CAZALES, M., MARCELLIN, M., BUGLER, B., BURLET-SCHILTZ, O. & DUCOMMUN, B. 2010. A screen for deubiquitinating enzymes involved in the G(2)/M checkpoint identifies USP50 as a regulator of HSP90-dependent Wee1 stability. *Cell Cycle,* 9**,** 3815-22.

ARONCHIK, I., APPLETON, B. A., BASHAM, S. E., CRAWFORD, K., DEL ROSARIO, M., DOYLE, L. V., ESTACIO, W. F., LAN, J., LINDVALL, M. K., LUU, C. A., ORNELAS, E., VENETSANAKOS, E., SHAFER, C. M. & JEFFERSON, A. B. 2014. Novel potent and selective inhibitors of p90 ribosomal S6 kinase reveal the heterogeneity of RSK function in MAPK-driven cancers. *Mol Cancer Res,* 12**,** 803-12.

ARTHUR, J. S. 2008. MSK activation and physiological roles. *Front Biosci,* 13**,** 5866-79.

ARVIND, R., SHIMAMOTO, H., MOMOSE, F., AMAGASA, T., OMURA, K. & TSUCHIDA, N. 2005. A mutation in the common docking domain of ERK2 in a human cancer cell line, which was associated with its constitutive phosphorylation. *Int J Oncol,* 27**,** 1499-504.

ASGHAR, U., WITKIEWICZ, A. K., TURNER, N. C. & KNUDSEN, E. S. 2015. The history and future of targeting cyclin-dependent kinases in cancer therapy. *Nat Rev Drug Discov,* 14**,** 130-46.

ASHFORD, A. L., OXLEY, D., KETTLE, J., HUDSON, K., GUICHARD, S., COOK, S. J. & LOCHHEAD, P. A. 2014. A novel DYRK1B inhibitor AZ191 demonstrates that DYRK1B acts independently of GSK3beta to phosphorylate cyclin D1 at Thr(286), not Thr(288). *Biochem J,* 457**,** 43-56.

ASHIKARI, D., TAKAYAMA, K., TANAKA, T., SUZUKI, Y., OBINATA, D., FUJIMURA, T., URANO, T., TAKAHASHI, S. & INOUE, S. 2017. Androgen induces G3BP2 and SUMO-mediated p53 nuclear export in prostate cancer. *Oncogene,* 36**,** 6272-6281.

ASHKENAZI, A., FAIRBROTHER, W. J., LEVERSON, J. D. & SOUERS, A. J. 2017. From basic apoptosis discoveries to advanced selective BCL-2 family inhibitors. *Nat Rev Drug Discov,* 16**,** 273-284.

ASHKENAZI, A. & SALVESEN, G. 2014. Regulated cell death: signaling and mechanisms. *Annu Rev Cell Dev Biol,* 30**,** 337-56.

AZAD, N., VALLYATHAN, V., WANG, L., TANTISHAIYAKUL, V., STEHLIK, C., LEONARD, S. S. & ROJANASAKUL, Y. 2006. S-nitrosylation of Bcl-2 inhibits its ubiquitin-proteasomal degradation. A novel antiapoptotic mechanism that suppresses apoptosis. *J Biol Chem,* 281**,** 34124-34.

BAELL, J. B. & HUANG, D. C. 2002. Prospects for targeting the Bcl-2 family of proteins to develop novel cytotoxic drugs. *Biochem Pharmacol,* 64**,** 851-63.

BAI, J., SUI, J., DEMIRJIAN, A., VOLLMER, C. M., MARASCO, W. & CALLERY, M. P. 2005. Predominant Bcl-XL Knockdown Disables Antiapoptotic Mechanisms: Tumor Necrosis Factor–Related Apoptosis-Inducing Ligand–Based Triple Chemotherapy Overcomes Chemoresistance in Pancreatic Cancer Cells In vitro. *Cancer Res,* 65**,** 2344-2352.

BALAKIREV, M. Y., TCHERNIUK, S. O., JAQUINOD, M. & CHROBOCZEK, J. 2003. Otubains: a new family of cysteine proteases in the ubiquitin pathway. *EMBO Rep,* 4**,** 517-22.

BALMANNO, K. & COOK, S. J. 2009. Tumour cell survival signalling by the ERK1/2 pathway. *Cell Death Differ,* 16**,** 368-77.

BANSAL, A., RAMIREZ, R. D. & MINNA, J. D. 1997. Mutation analysis of the coding sequences of MEK-1 and MEK-2 genes in human lung cancer cell lines. *Oncogene,* 14**,** 1231.

BARBACID, M. 1987. ras genes. *Annu Rev Biochem,* 56**,** 779-827.

BARDWELL, A. J., ABDOLLAHI, M. & BARDWELL, L. 2003. Docking sites on mitogen-activated protein kinase (MAPK) kinases, MAPK phosphatases and the Elk-1 transcription factor compete for MAPK binding and are crucial for enzymic activity. *Biochem J,* 370**,** 1077-85.

BARNES, C. J., LI, F., MANDAL, M., YANG, Z., SAHIN, A. A. & KUMAR, R. 2002. Heregulin induces expression, ATPase activity, and nuclear localization of G3BP, a Ras signaling component, in human breast tumors. *Cancer Res,* 62**,** 1251-5.

BASILE, K. J. & APLIN, A. E. 2012. Downregulation of Noxa by RAF/MEK inhibition counteracts cell death response in mutant B-RAF melanoma cells. *Am J Cancer Res,* 2**,** 726-35.

BASU, S., TOTTY, N. F., IRWIN, M. S., SUDOL, M. & DOWNWARD, J. 2003. Akt phosphorylates the Yes-associated protein, YAP, to induce interaction with 14-3-3 and attenuation of p73-mediated apoptosis. *Mol Cell,* 11**,** 11-23.

BEN-SAHRA, I., HOWELL, J. J., ASARA, J. M. & MANNING, B. D. 2013. Stimulation of de novo pyrimidine synthesis by growth signaling through mTOR and S6K1. *Science,* 339**,** 1323-8.

BENETATOS, C. A., MITSUUCHI, Y., BURNS, J. M., NEIMAN, E. M., CONDON, S. M., YU, G., SEIPEL, M. E., KAPOOR, G. S., LAPORTE, M. G., RIPPIN, S. R., DENG, Y., HENDI, M. S., TIRUNAHARI, P. K., LEE, Y. H., HAIMOWITZ, T., ALEXANDER, M. D., GRAHAM, M. A., WENG, D., SHI, Y., MCKINLAY, M. A. & CHUNDURU, S. K. 2014. Birinapant (TL32711), a bivalent SMAC mimetic, targets TRAF2-associated cIAPs, abrogates TNF-induced NF-kappaB activation, and is active in patient-derived xenograft models. *Mol Cancer Ther,* 13**,** 867-79.

BERNARDI, R., SCAGLIONI, P. P., BERGMANN, S., HORN, H. F., VOUSDEN, K. H. & PANDOLFI, P. P. 2004. PML regulates p53 stability by sequestering Mdm2 to the nucleolus. *Nat Cell Biol,* 6**,** 665-72.

BERNDSEN, C. E. & WOLBERGER, C. 2014. New insights into ubiquitin E3 ligase mechanism. 21**,** 301-7.

BERNS, K., HIJMANS, E. M., MULLENDERS, J., BRUMMELKAMP, T. R., VELDS, A., HEIMERIKX, M., KERKHOVEN, R. M., MADIREDJO, M., NIJKAMP, W., WEIGELT, B., AGAMI, R., GE, W., CAVET, G., LINSLEY, P. S., BEIJERSBERGEN, R. L. & BERNARDS, R. 2004. A large-scale RNAi screen in human cells identifies new components of the p53 pathway. *Nature,* 428**,** 431-7.

BERTRAND, M. J., MILUTINOVIC, S., DICKSON, K. M., HO, W. C., BOUDREAULT, A., DURKIN, J., GILLARD, J. W., JAQUITH, J. B., MORRIS, S. J. & BARKER, P. A. 2008. cIAP1 and cIAP2 facilitate cancer cell survival by functioning as E3 ligases that promote RIP1 ubiquitination. *Mol Cell,* 30**,** 689-700.

BHATTACHARYA, S. & GHOSH, M. K. 2014. Cell death and deubiquitinases: perspectives in cancer. 2014**,** 435197.

BIGNONE, P. A., LEE, K. Y., LIU, Y., EMILION, G., FINCH, J., SOOSAY, A. E., CHARNOCK, F. M., BECK, S., DUNHAM, I., MUNGALL, A. J. & GANESAN, T. S. 2007. RPS6KA2, a putative tumour suppressor gene at 6q27 in sporadic epithelial ovarian cancer. *Oncogene,* 26**,** 683-700.

BINGOL, B., TEA, J. S., PHU, L., REICHELT, M., BAKALARSKI, C. E., SONG, Q., FOREMAN, O., KIRKPATRICK, D. S. & SHENG, M. 2014. The mitochondrial deubiquitinase USP30 opposes parkin-mediated mitophagy. *Nature,* 510**,** 370-5.

BINGOL, B, CORN, J, ZHANG USP30 Inhibitors and Methods of Use - WO2014/041111 A1 (2014).

BLANCHETOT, C., CHAGNON, M., DUBE, N., HALLE, M. & TREMBLAY, M. L. 2005. Substrate-trapping techniques in the identification of cellular PTP targets. *Methods,* 35**,** 44-53.

BOATRIGHT, K. M., RENATUS, M., SCOTT, F. L., SPERANDIO, S., SHIN, H., PEDERSEN, I. M., RICCI, J. E., EDRIS, W. A., SUTHERLIN, D. P., GREEN, D. R. & SALVESEN, G. S. 2003. A unified model for apical caspase activation. *Mol Cell,* 11**,** 529-41.

BOLDIN, M. P., GONCHAROV, T. M., GOLTSEV, Y. V. & WALLACH, D. 1996. Involvement of MACH, a novel MORT1/FADD-interacting protease, in Fas/APO-1- and TNF receptor-induced cell death. *Cell,* 85**,** 803-15.

BONNI, A., BRUNET, A., WEST, A. E., DATTA, S. R., TAKASU, M. A. & GREENBERG, M. E. 1999. Cell survival promoted by the Ras-MAPK signaling pathway by transcription-dependent and -independent mechanisms. *Science,* 286**,** 1358-62.

BORNSTEIN, B., GOTTFRIED, Y., EDISON, N., SHEKHTMAN, A., LEV, T., GLASER, F. & LARISCH, S. 2011. ARTS binds to a distinct domain in XIAP-BIR3 and promotes apoptosis by a mechanism that is different from other IAP-antagonists. *Apoptosis,* 16**,** 869-81.

BORODOVSKY, A., KESSLER, B. M., CASAGRANDE, R., OVERKLEEFT, H. S., WILKINSON, K. D. & PLOEGH, H. L. 2001. A novel active site-directed probe specific for deubiquitylating enzymes reveals proteasome association of USP14. *Embo j,* 20**,** 5187-96.

BORODOVSKY, A., OVAA, H., KOLLI, N., GAN-ERDENE, T., WILKINSON, K. D., PLOEGH, H. L. & KESSLER, B. M. 2002. Chemistry-based functional proteomics reveals novel members of the deubiquitinating enzyme family. *Chem Biol,* 9**,** 1149-59.

BOS, J. L. 1989. ras oncogenes in human cancer: a review. *Cancer Res,* 49**,** 4682-9.

BOS, J. L., REHMANN, H. & WITTINGHOFER, A. 2007. GEFs and GAPs: critical elements in the control of small G proteins. *Cell,* 129**,** 865-77.

BOUCHER, M. J., MORISSET, J., VACHON, P. H., REED, J. C., LAINE, J. & RIVARD, N. 2000. MEK/ERK signaling pathway regulates the expression of Bcl-2, Bcl-X(L), and Mcl-1 and promotes survival of human pancreatic cancer cells. *J Cell Biochem,* 79**,** 355-69.

BOUILLET, P., ZHANG, L. C., HUANG, D. C., WEBB, G. C., BOTTEMA, C. D., SHORE, P., EYRE, H. J., SUTHERLAND, G. R. & ADAMS, J. M. 2001. Gene structure alternative splicing, and chromosomal localization of pro-apoptotic Bcl-2 relative Bim. *Mamm Genome,* 12**,** 163-8.

BOYD, S. D., TSAI, K. Y. & JACKS, T. 2000. An intact HDM2 RING-finger domain is required for nuclear exclusion of p53. *Nat Cell Biol,* 2**,** 563-8.

BRASS, A. L., DYKXHOORN, D. M., BENITA, Y., YAN, N., ENGELMAN, A., XAVIER, R. J., LIEBERMAN, J. & ELLEDGE, S. J. 2008. Identification of host proteins required for HIV infection through a functional genomic screen. *Science,* 319**,** 921-6.

BREITSCHOPF, K., HAENDELER, J., MALCHOW, P., ZEIHER, A. M. & DIMMELER, S. 2000. Posttranslational modification of Bcl-2 facilitates its proteasome-dependent degradation: molecular characterization of the involved signaling pathway. *Mol Cell Biol,* 20**,** 1886-96.

BRIDGE, A. J., PEBERNARD, S., DUCRAUX, A., NICOULAZ, A. L. & IGGO, R. 2003. Induction of an interferon response by RNAi vectors in mammalian cells. *Nat Genet,* 34**,** 263-4.

BROEMER, M. & MEIER, P. 2009. Ubiquitin-mediated regulation of apoptosis. *Trends Cell Biol,* 19**,** 130-40.

BROUWER, J. M., WESTPHAL, D., DEWSON, G., ROBIN, A. Y., UREN, R. T., BARTOLO, R., THOMPSON, G. V., COLMAN, P. M., KLUCK, R. M. & CZABOTAR, P. E. 2014. Bak core and latch domains separate during activation, and freed core domains form symmetric homodimers. *Mol Cell,* 55**,** 938-946.

BUCHHEIT, C. L., ANGAROLA, B. L., STEINER, A., WEIGEL, K. J. & SCHAFER, Z. T. 2014. Anoikis evasion in inflammatory breast cancer cells is mediated by Bim-EL sequestration. *Cell Death Differ,* 22**,** 1275-1286.

BUCKLEY, M. F., SWEENEY, K. J., HAMILTON, J. A., SINI, R. L., MANNING, D. L., NICHOLSON, R. I., DEFAZIO, A., WATTS, C. K., MUSGROVE, E. A. & SUTHERLAND, R. L. 1993. Expression and amplification of cyclin genes in human breast cancer. *Oncogene,* 8**,** 2127-33.

BUDHIDARMO, R., NAKATANI, Y. & DAY, C. L. 2012. RINGs hold the key to ubiquitin transfer. *Trends Biochem Sci,* 37**,** 58-65.

BURKHARD, K. A., CHEN, F. & SHAPIRO, P. 2011. Quantitative analysis of ERK2 interactions with substrate proteins: roles for kinase docking domains and activity in determining binding affinity. *J Biol Chem,* 286**,** 2477-85.

BUSINO, L., DONZELLI, M., CHIESA, M., GUARDAVACCARO, D., GANOTH, D., DORRELLO, N. V., HERSHKO, A., PAGANO, M. & DRAETTA, G. F. 2003. Degradation of Cdc25A by beta-TrCP during S phase and in response to DNA damage. *Nature,* 426**,** 87-91.

BUTCH, E. R. & GUAN, K. L. 1996. Characterization of ERK1 activation site mutants and the effect on recognition by MEK1 and MEK2. *J Biol Chem,* 271**,** 4230-5.

BUTTERWORTH, M., PETTITT, A., VARADARAJAN, S. & COHEN, G. M. 2016. BH3 profiling and a toolkit of BH3-mimetic drugs predict anti-apoptotic dependence of cancer cells. *Br J Cancer,* 114**,** 638-41.

BUTTICAZ, C., MICHIELIN, O., WYNIGER, J., TELENTI, A. & ROTHENBERGER, S. 2007. Silencing of both β-TrCP1 and HOS (β-TrCP2) Is Required To Suppress Human Immunodeficiency Virus Type 1 Vpu-Mediated CD4 Down-Modulation. *Journal of Virology,* 81**,** 1502-1505.

BYUN, S., LEE, S. Y., LEE, J., JEONG, C. H., FARRAND, L., LIM, S., REDDY, K., KIM, J. Y., LEE, M. H., LEE, H. J., BODE, A. M., WON LEE, K. & DONG, Z. 2013. USP8 is a novel target for overcoming gefitinib resistance in lung cancer. *Clin Cancer Res,* 19**,** 3894-904.

CABRITA, M. A. & CHRISTOFORI, G. 2008. Sprouty proteins, masterminds of receptor tyrosine kinase signaling. *Angiogenesis,* 11**,** 53-62.

CALVISI, D. F., PINNA, F., MELONI, F., LADU, S., PELLEGRINO, R., SINI, M., DAINO, L., SIMILE, M. M., DE MIGLIO, M. R., VIRDIS, P., FRAU, M., TOMASI, M. L., SEDDAIU, M. A., MURONI, M. R., FEO, F. & PASCALE, R. M. 2008. Dual-Specificity Phosphatase 1 Ubiquitination in Extracellular Signal-Regulated Kinase–Mediated Control of Growth in Human Hepatocellular Carcinoma. *Cancer Res,* 68**,** 4192-4200.

CAMARGO, F. D., GOKHALE, S., JOHNNIDIS, J. B., FU, D., BELL, G. W., JAENISCH, R. & BRUMMELKAMP, T. R. 2007. YAP1 increases organ size and expands undifferentiated progenitor cells. *Curr Biol,* 17**,** 2054-60.

CARGNELLO, M. & ROUX, P. P. 2011. Activation and function of the MAPKs and their substrates, the MAPK-activated protein kinases. *Microbiol Mol Biol Rev,* 75**,** 50-83.

CARRIERE, A., RAY, H., BLENIS, J. & ROUX, P. P. 2008. The RSK factors of activating the Ras/MAPK signaling cascade. *Front Biosci,* 13**,** 4258-75.
CASALVIERI, K. A., MATHESON, C. J., BACKOS, D. S. & REIGAN, P. 2017. Selective Targeting of RSK Isoforms in Cancer. *Trends Cancer,* 3**,** 302-312.
CASHMAN, R., COHEN, H., BEN-HAMO, R., ZILBERBERG, A. & EFRONI, S. 2014. SENP5 mediates breast cancer invasion via a TGFbetaRI SUMOylation cascade. *Oncotarget,* 5**,** 1071-82.
CAUNT, C. J., ARMSTRONG, S. P., RIVERS, C. A., NORMAN, M. R. & MCARDLE, C. A. 2008. Spatiotemporal regulation of ERK2 by dual specificity phosphatases. *J Biol Chem,* 283**,** 26612-23.
CAUNT, C. J. & KEYSE, S. M. 2013. Dual-specificity MAP kinase phosphatases (MKPs): shaping the outcome of MAP kinase signalling. *Febs j,* 280**,** 489-504.
CAUNT, C. J., SALE, M. J., SMITH, P. D. & COOK, S. J. 2015. MEK1 and MEK2 inhibitors and cancer therapy: the long and winding road. *Nat Rev Cancer,* 15**,** 577-92.
CERTO, M., DEL GAIZO MOORE, V., NISHINO, M., WEI, G., KORSMEYER, S., ARMSTRONG, S. A. & LETAI, A. 2006. Mitochondria primed by death signals determine cellular addiction to antiapoptotic BCL-2 family members. *Cancer Cell,* 9**,** 351-65.
CHAN, D. C. 2012. Fusion and fission: interlinked processes critical for mitochondrial health. *Annu Rev Genet,* 46**,** 265-87.
CHAN, N. C., SALAZAR, A. M., PHAM, A. H., SWEREDOSKI, M. J., KOLAWA, N. J., GRAHAM, R. L., HESS, S. & CHAN, D. C. 2011. Broad activation of the ubiquitin-proteasome system by Parkin is critical for mitophagy. *Hum Mol Genet,* 20**,** 1726-37.
CHANG, F., STEELMAN, L. S., LEE, J. T., SHELTON, J. G., NAVOLANIC, P. M., BLALOCK, W. L., FRANKLIN, R. A. & MCCUBREY, J. A. 2003. Signal transduction mediated by the Ras/Raf/MEK/ERK pathway from cytokine receptors to transcription factors: potential targeting for therapeutic intervention. *Leukemia,* 17**,** 1263-93.
CHAUHAN, D., TIAN, Z., NICHOLSON, B., KUMAR, K. G., ZHOU, B., CARRASCO, R., MCDERMOTT, J. L., LEACH, C. A., FULCINNITI, M., KODRASOV, M. P., WEINSTOCK, J., KINGSBURY, W. D., HIDESHIMA, T., SHAH, P. K., MINVIELLE, S., ALTUN, M., KESSLER, B. M., ORLOWSKI, R., RICHARDSON, P., MUNSHI, N. & ANDERSON, K. C. 2012. A small molecule inhibitor of ubiquitin-specific protease-7 induces apoptosis in multiple myeloma cells and overcomes bortezomib resistance. *Cancer Cell,* 22**,** 345-58.
CHEN, C., SONG, J., WANG, J., XU, C., CHEN, C., GU, W., SUN, H. & WEN, X. 2017. Synthesis and biological evaluation of thiazole derivatives as novel USP7 inhibitors. *Bioorg Med Chem Lett,* 27**,** 845-849.
CHEN, D., FREZZA, M., SCHMITT, S., KANWAR, J. & DOU, Q. P. 2011a. Bortezomib as the first proteasome inhibitor anticancer drug: current status and future perspectives. *Curr Cancer Drug Targets,* 11**,** 239-53.
CHEN, D., GAO, F., LI, B., WANG, H., XU, Y., ZHU, C. & WANG, G. 2010. Parkin mono-ubiquitinates Bcl-2 and regulates autophagy. *J Biol Chem,* 285**,** 38214-23.
CHEN, F., HANCOCK, C. N., MACIAS, A. T., JOH, J., STILL, K., ZHONG, S., MACKERELL, A. D., JR. & SHAPIRO, P. 2006. Characterization of ATP-independent ERK inhibitors identified through in silico analysis of the active ERK2 structure. *Bioorg Med Chem Lett,* 16**,** 6281-7.
CHEN, Y. B., AON, M. A., HSU, Y. T., SOANE, L., TENG, X., MCCAFFERY, J. M., CHENG, W. C., QI, B., LI, H., ALAVIAN, K. N., DAYHOFF-BRANNIGAN, M., ZOU, S., PINEDA, F. J., O'ROURKE, B., KO, Y. H., PEDERSEN, P. L., KACZMAREK, L. K., JONAS, E. A. & HARDWICK, J. M. 2011b. Bcl-xL regulates mitochondrial energetics by stabilizing the inner membrane potential. *J Cell Biol,* 195**,** 263-76.
CHEN, Z. J. & SUN, L. J. 2009. Nonproteolytic functions of ubiquitin in cell signaling. *Mol Cell,* 33**,** 275-86.
CHERFILS, J. & ZEGHOUF, M. 2013. Regulation of small GTPases by GEFs, GAPs, and GDIs. *Physiol Rev,* 93**,** 269-309.
CHIPUK, J. E., MOLDOVEANU, T., LLAMBI, F., PARSONS, M. J. & GREEN, D. R. 2010. The BCL-2 family reunion. *Mol Cell,* 37**,** 299-310.
CHOU, J. J., LI, H., SALVESEN, G. S., YUAN, J. & WAGNER, G. 1999. Solution structure of BID, an intracellular amplifier of apoptotic signaling. *Cell,* 96**,** 615-24.
CHRESTA, C. M., DAVIES, B. R., HICKSON, I., HARDING, T., COSULICH, S., CRITCHLOW, S. E., VINCENT, J. P., ELLSTON, R., JONES, D., SINI, P., JAMES, D., HOWARD, Z., DUDLEY, P., HUGHES, G., SMITH, L., MAGUIRE, S., HUMMERSONE, M., MALAGU, K., MENEAR, K., JENKINS, R., JACOBSEN, M., SMITH, G. C., GUICHARD, S. & PASS, M. 2010. AZD8055 is a potent, selective, and orally bioavailable ATP-competitive mammalian target of rapamycin kinase inhibitor with in vitro and in vivo antitumor activity. *Cancer Res,* 70**,** 288-98.
CIECHANOVER, A., HELLER, H., ELIAS, S., HAAS, A. L. & HERSHKO, A. 1980. ATP-dependent conjugation of reticulocyte proteins with the polypeptide required for protein degradation. *Proceedings of the National Academy of Sciences,* 77**,** 1365-1368.
CLAGUE, M. J., BARSUKOV, I., COULSON, J. M., LIU, H., RIGDEN, D. J. & URBE, S. 2013. Deubiquitylases from genes to organism. *Physiol Rev,* 93**,** 1289-315.
CLAGUE, M. J., COULSON, J. M. & URBE, S. 2012. Cellular functions of the DUBs. *J Cell Sci,* 125**,** 277-86.
CLAGUE, M. J., COULSON, J. M. & URBÉ, S. 2008. Deciphering histone 2A deubiquitination. *Genome Biol,* 9**,** 202-202.
CLAGUE, M. J. & URBE, S. 2017. Integration of cellular ubiquitin and membrane traffic systems: focus on deubiquitylases. *Febs j,* 284**,** 1753-1766.
COHEN, M. S., ZHANG, C., SHOKAT, K. M. & TAUNTON, J. 2005. Structural bioinformatics-based design of selective, irreversible kinase inhibitors. *Science,* 308**,** 1318-21.

COHEN, P. & TCHERPAKOV, M. 2010. Will the ubiquitin system furnish as many drug targets as protein kinases? *Cell,* 143**,** 686-93.

COHN, M. A., KEE, Y., HAAS, W., GYGI, S. P. & D'ANDREA, A. D. 2009. UAF1 is a subunit of multiple deubiquitinating enzyme complexes. *J Biol Chem,* 284**,** 5343-51.

COHN, M. A., KOWAL, P., YANG, K., HAAS, W., HUANG, T. T., GYGI, S. P. & D'ANDREA, A. D. 2007. A UAF1-containing multisubunit protein complex regulates the Fanconi anemia pathway. *Mol Cell,* 28**,** 786-97.

COLLAND, F., FORMSTECHER, E., JACQ, X., REVERDY, C., PLANQUETTE, C., CONRATH, S., TROUPLIN, V., BIANCHI, J., AUSHEV, V. N., CAMONIS, J., CALABRESE, A., BORG-CAPRA, C., SIPPL, W., COLLURA, V., BOISSY, G., RAIN, J. C., GUEDAT, P., DELANSORNE, R. & DAVIET, L. 2009. Small-molecule inhibitor of USP7/HAUSP ubiquitin protease stabilizes and activates p53 in cells. *Mol Cancer Ther,* 8**,** 2286-95.

COLOTTA, F., ALLAVENA, P., SICA, A., GARLANDA, C. & MANTOVANI, A. 2009. Cancer-related inflammation, the seventh hallmark of cancer: links to genetic instability. *Carcinogenesis,* 30**,** 1073-81.

COMPAGNO, M., LIM, W. K., GRUNN, A., NANDULA, S. V., BRAHMACHARY, M., SHEN, Q., BERTONI, F., PONZONI, M., SCANDURRA, M., CALIFANO, A., BHAGAT, G., CHADBURN, A., DALLA-FAVERA, R. & PASQUALUCCI, L. 2009. Mutations of multiple genes cause deregulation of NF-kappaB in diffuse large B-cell lymphoma. *Nature,* 459**,** 717-21.

CONCIATORI, F., CIUFFREDA, L., BAZZICHETTO, C., FALCONE, I., PILOTTO, S., BRIA, E., COGNETTI, F. & MILELLA, M. 2018. mTOR Cross-Talk in Cancer and Potential for Combination Therapy. *Cancers,* 10.

CONG, L., RAN, F. A., COX, D., LIN, S., BARRETTO, R., HABIB, N., HSU, P. D., WU, X., JIANG, W., MARRAFFINI, L. A. & ZHANG, F. 2013. Multiplex Genome Engineering Using CRISPR/Cas Systems. *Science,* 339**,** 819-823.

COOK, S. J., STUART, K., GILLEY, R. & SALE, M. J. 2017. Control of cell death and mitochondrial fission by ERK1/2 MAP kinase signalling. *Febs j,* 284**,** 4177-4195.

COPE, C. L., GILLEY, R., BALMANNO, K., SALE, M. J., HOWARTH, K. D., HAMPSON, M., SMITH, P. D., GUICHARD, S. M. & COOK, S. J. 2014. Adaptation to mTOR kinase inhibitors by amplification of eIF4E to maintain cap-dependent translation. *J Cell Sci,* 127**,** 788-800.

CORCORAN, R. B., CHENG, K. A., HATA, A. N., FABER, A. C., EBI, H., COFFEE, E. M., GRENINGER, P., BROWN, R. D., GODFREY, J. T., COHOON, T. J., SONG, Y., LIFSHITS, E., HUNG, K. E., SHIODA, T., DIAS-SANTAGATA, D., SINGH, A., SETTLEMAN, J., BENES, C. H., MINO-KENUDSON, M., WONG, K.-K. & ENGELMAN, J. A. 2013. Synthetic Lethal Interaction of Combined BCL-XL and MEK Inhibition Promotes Tumor Regressions in KRAS Mutant Cancer Models. *Cancer Cell,* 23**,** 121-128.

CORNELISSEN, T., HADDAD, D., WAUTERS, F., VAN HUMBEECK, C., MANDEMAKERS, W., KOENTJORO, B., SUE, C., GEVAERT, K., DE STROOPER, B., VERSTREKEN, P. & VANDENBERGHE, W. 2014. The deubiquitinase USP15 antagonizes Parkin-mediated mitochondrial ubiquitination and mitophagy. *Human Molecular Genetics,* 23**,** 5227-5242.

CORTI, O., LESAGE, S. & BRICE, A. 2011. What genetics tells us about the causes and mechanisms of Parkinson's disease. *Physiol Rev,* 91**,** 1161-218.

CORY, S. & ADAMS, J. M. 2002. The Bcl2 family: regulators of the cellular life-or-death switch. *Nat Rev Cancer,* 2**,** 647-56.

COYAUD, E., MIS, M., LAURENT, E. M., DUNHAM, W. H., COUZENS, A. L., ROBITAILLE, M., GINGRAS, A. C., ANGERS, S. & RAUGHT, B. 2015. BioID-based Identification of Skp Cullin F-box (SCF)beta-TrCP1/2 E3 Ligase Substrates. *Mol Cell Proteomics,* 14**,** 1781-95.

CREMONA, C. A., SANCHO, R., DIEFENBACHER, M. E. & BEHRENS, A. 2016. Fbw7 and its counteracting forces in stem cells and cancer: Oncoproteins in the balance. *Semin Cancer Biol,* 36**,** 52-61.

CROUCH, S. P., KOZLOWSKI, R., SLATER, K. J. & FLETCHER, J. 1993. The use of ATP bioluminescence as a measure of cell proliferation and cytotoxicity. *J Immunol Methods,* 160**,** 81-8.

CULLEN, B. R. 2006. Enhancing and confirming the specificity of RNAi experiments. *Nat Methods,* 3**,** 677-81.

CUMMINS, J. M. & VOGELSTEIN, B. 2004. HAUSP is required for p53 destabilization. *Cell Cycle,* 3**,** 689-92.

CUNNINGHAM, C. N., BAUGHMAN, J. M., PHU, L., TEA, J. S., YU, C., COONS, M., KIRKPATRICK, D. S., BINGOL, B. & CORN, J. E. 2015. USP30 and parkin homeostatically regulate atypical ubiquitin chains on mitochondria. *Nat Cell Biol,* 17**,** 160-9.

CZABOTAR, P. E., LEE, E. F., VAN DELFT, M. F., DAY, C. L., SMITH, B. J., HUANG, D. C., FAIRLIE, W. D., HINDS, M. G. & COLMAN, P. M. 2007. Structural insights into the degradation of Mcl-1 induced by BH3 domains. *Proc Natl Acad Sci U S A,* 104**,** 6217-22.

CZABOTAR, P. E., LESSENE, G., STRASSER, A. & ADAMS, J. M. 2014. Control of apoptosis by the BCL-2 protein family: implications for physiology and therapy. *Nat Rev Mol Cell Biol,* 15**,** 49-63.

CZABOTAR, P. E., WESTPHAL, D., DEWSON, G., MA, S., HOCKINGS, C., FAIRLIE, W. D., LEE, E. F., YAO, S., ROBIN, A. Y., SMITH, B. J., HUANG, D. C., KLUCK, R. M., ADAMS, J. M. & COLMAN, P. M. 2013. Bax crystal structures reveal how BH3 domains activate Bax and nucleate its oligomerization to induce apoptosis. *Cell,* 152**,** 519-31.

D'ARCY, P., BRNJIC, S., OLOFSSON, M. H., FRYKNAS, M., LINDSTEN, K., DE CESARE, M., PEREGO, P., SADEGHI, B., HASSAN, M., LARSSON, R. & LINDER, S. 2011. Inhibition of proteasome deubiquitinating activity as a new cancer therapy. *Nat Med,* 17**,** 1636-40.

DAI, H., SMITH, A., MENG, X. W., SCHNEIDER, P. A., PANG, Y. P. & KAUFMANN, S. H. 2011. Transient binding of an activator BH3 domain to the Bak BH3-binding groove initiates Bak oligomerization. *J Cell Biol,* 194**,** 39-48.

DALBY, K. N., MORRICE, N., CAUDWELL, F. B., AVRUCH, J. & COHEN, P. 1998. Identification of regulatory phosphorylation sites in mitogen-activated protein kinase (MAPK)-activated protein kinase-1a/p90rsk that are inducible by MAPK. *J Biol Chem,* 273**,** 1496-505.

DAS NEVES, R. P., JONES, N. S., ANDREU, L., GUPTA, R., ENVER, T. & IBORRA, F. J. 2010. Connecting Variability in Global Transcription Rate to Mitochondrial Variability. *PLoS Biology,* 8**,** e1000560.

DAS THAKUR, M., FENG, Y., JAGANNATHAN, R., SEPPA, M. J., SKEATH, J. B. & LONGMORE, G. D. 2010. Ajuba LIM proteins are negative regulators of the Hippo signaling pathway. *Curr Biol,* 20**,** 657-62.

DATTA, S. R., KATSOV, A., HU, L., PETROS, A., FESIK, S. W., YAFFE, M. B. & GREENBERG, M. E. 2000. 14-3-3 proteins and survival kinases cooperate to inactivate BAD by BH3 domain phosphorylation. *Mol Cell,* 6**,** 41-51.

DAVIES, H., BIGNELL, G. R., COX, C., STEPHENS, P., EDKINS, S., CLEGG, S., TEAGUE, J., WOFFENDIN, H., GARNETT, M. J., BOTTOMLEY, W., DAVIS, N., DICKS, E., EWING, R., FLOYD, Y., GRAY, K., HALL, S., HAWES, R., HUGHES, J., KOSMIDOU, V., MENZIES, A., MOULD, C., PARKER, A., STEVENS, C., WATT, S., HOOPER, S., WILSON, R., JAYATILAKE, H., GUSTERSON, B. A., COOPER, C., SHIPLEY, J., HARGRAVE, D., PRITCHARD-JONES, K., MAITLAND, N., CHENEVIX-TRENCH, G., RIGGINS, G. J., BIGNER, D. D., PALMIERI, G., COSSU, A., FLANAGAN, A., NICHOLSON, A., HO, J. W., LEUNG, S. Y., YUEN, S. T., WEBER, B. L., SEIGLER, H. F., DARROW, T. L., PATERSON, H., MARAIS, R., MARSHALL, C. J., WOOSTER, R., STRATTON, M. R. & FUTREAL, P. A. 2002. Mutations of the BRAF gene in human cancer. *Nature,* 417**,** 949-54.

DE BENEDETTI, A. & GRAFF, J. R. 2004. eIF-4E expression and its role in malignancies and metastases. *Oncogene,* 23**,** 3189-99.

DE RUITER, N. D., BURGERING, B. M. T. & BOS, J. L. 2001. Regulation of the Forkhead Transcription Factor AFX by Ral-Dependent Phosphorylation of Threonines 447 and 451. *Mol Cell Biol,* 21**,** 8225-8235.

DEAK, M., CLIFTON, A. D., LUCOCQ, L. M. & ALESSI, D. R. 1998. Mitogen- and stress-activated protein kinase-1 (MSK1) is directly activated by MAPK and SAPK2/p38, and may mediate activation of CREB. *Embo j,* 17**,** 4426-41.

DEHAN, E., BASSERMANN, F., GUARDAVACCARO, D., VASILIVER-SHAMIS, G., COHEN, M., LOWES, K. N., DUSTIN, M., HUANG, D. C., TAUNTON, J. & PAGANO, M. 2009. betaTrCP- and Rsk1/2-mediated degradation of BimEL inhibits apoptosis. *Mol Cell,* 33**,** 109-16.

DEL GAIZO MOORE, V., BROWN, J. R., CERTO, M., LOVE, T. M., NOVINA, C. D. & LETAI, A. 2007. Chronic lymphocytic leukemia requires BCL2 to sequester prodeath BIM, explaining sensitivity to BCL2 antagonist ABT-737. *J Clin Invest,* 117**,** 112-21.

DEL GAIZO MOORE, V. & LETAI, A. 2013. BH3 profiling--measuring integrated function of the mitochondrial apoptotic pathway to predict cell fate decisions. *Cancer Lett,* 332**,** 202-5.

DENG, T., YAN, G., ZHOU, Y., HU, X., LI, J., HU, J., ZHANG, H., FENG, P., SHENG, X., CHEN, J., MA, H., SUN, Y., WEI, D., HU, B., LIU, J., TAN, W. & YE, M. 2017. Deubiquitylation and stabilization of p21 by USP11 is critical for cell cycle progression and DNA damage responses. *bioRxiv*.

DENG, Y., SHIPPS, G. W., COOPER, A., ENGLISH, J. M., ANNIS, D. A., CARR, D., NAN, Y., WANG, T., ZHU, H. Y., CHUANG, C.-C., DAYANANTH, P., HRUZA, A. W., XIAO, L., JIN, W., KIRSCHMEIER, P., WINDSOR, W. T. & SAMATAR, A. A. 2014. Discovery of Novel, Dual Mechanism ERK Inhibitors by Affinity Selection Screening of an Inactive Kinase. *J Med Chem,* 57**,** 8817-8826.

DEPMAP, B. 2019. DepMap Achilles 19Q1 Public.

DESHAIES, R. J. & JOAZEIRO, C. A. 2009. RING domain E3 ubiquitin ligases. *Annu Rev Biochem,* 78**,** 399-434.

DEWSON, G., KRATINA, T., SIM, H. W., PUTHALAKATH, H., ADAMS, J. M., COLMAN, P. M. & KLUCK, R. M. 2008. To trigger apoptosis, Bak exposes its BH3 domain and homodimerizes via BH3:groove interactions. *Mol Cell,* 30**,** 369-80.

DEWSON, G., MA, S., FREDERICK, P., HOCKINGS, C., TAN, I., KRATINA, T. & KLUCK, R. M. 2012. Bax dimerizes via a symmetric BH3:groove interface during apoptosis. *Cell Death Differ,* 19**,** 661-70.

DI BACCO, A., OUYANG, J., LEE, H. Y., CATIC, A., PLOEGH, H. & GILL, G. 2006. The SUMO-specific protease SENP5 is required for cell division. *Mol Cell Biol,* 26**,** 4489-98.

DIJKERS, P. F., MEDEMA, R. H., LAMMERS, J. W., KOENDERMAN, L. & COFFER, P. J. 2000. Expression of the pro-apoptotic Bcl-2 family member Bim is regulated by the forkhead transcription factor FKHR-L1. *Curr Biol,* 10**,** 1201-4.

DIMMELER, S., BREITSCHOPF, K., HAENDELER, J. & ZEIHER, A. M. 1999. Dephosphorylation Targets Bcl-2 for Ubiquitin-dependent Degradation: A Link between the Apoptosome and the Proteasome Pathway. *The Journal of Experimental Medicine,* 189**,** 1815-1822.

DOMINA, A. M., VRANA, J. A., GREGORY, M. A., HANN, S. R. & CRAIG, R. W. 2004. MCL1 is phosphorylated in the PEST region and stabilized upon ERK activation in viable cells, and at additional sites with cytotoxic okadaic acid or taxol. *Oncogene,* 23**,** 5301-15.

DONG, J., FELDMANN, G., HUANG, J., WU, S., ZHANG, N., COMERFORD, S. A., GAYYED, M. F., ANDERS, R. A., MAITRA, A. & PAN, D. 2007. Elucidation of a universal size-control mechanism in Drosophila and mammals. *Cell,* 130**,** 1120-33.

DOUGHERTY, M. K., MULLER, J., RITT, D. A., ZHOU, M., ZHOU, X. Z., COPELAND, T. D., CONRADS, T. P., VEENSTRA, T. D., LU, K. P. & MORRISON, D. K. 2005. Regulation of Raf-1 by direct feedback phosphorylation. *Mol Cell,* 17**,** 215-24.

DOWLING, R. J., TOPISIROVIC, I., ALAIN, T., BIDINOSTI, M., FONSECA, B. D., PETROULAKIS, E., WANG, X., LARSSON, O., SELVARAJ, A., LIU, Y., KOZMA, S. C., THOMAS, G. & SONENBERG, N. 2010. mTORC1-mediated cell proliferation, but not cell growth, controlled by the 4E-BPs. *Science,* 328**,** 1172-6.

DOWNWARD, J. 2003. Targeting RAS signalling pathways in cancer therapy. *Nature Reviews Cancer,* 3**,** 11.

DREXLER, H. C. 1997. Activation of the cell death program by inhibition of proteasome function. *Proc Natl Acad Sci U S A,* 94**,** 855-60.

DU, H., WOLF, J., SCHAFER, B., MOLDOVEANU, T., CHIPUK, J. E. & KUWANA, T. 2011. BH3 domains other than Bim and Bid can directly activate Bax/Bak. *J Biol Chem,* 286**,** 491-501.

DURCAN, T. M. & FON, E. A. 2015. The three 'P's of mitophagy: PARKIN, PINK1, and post-translational modifications. *Genes Dev,* 29**,** 989-99.

DURCAN, T. M., TANG, M. Y., PERUSSE, J. R., DASHTI, E. A., AGUILETA, M. A., MCLELLAND, G. L., GROS, P., SHALER, T. A., FAUBERT, D., COULOMBE, B. & FON, E. A. 2014. USP8 regulates mitophagy by removing K6-linked ubiquitin conjugates from parkin. *Embo j,* 33**,** 2473-91.

DURONIO, V. 2008. The life of a cell: apoptosis regulation by the PI3K/PKB pathway. *Biochem J,* 415**,** 333-44.

EA, C. K., DENG, L., XIA, Z. P., PINEDA, G. & CHEN, Z. J. 2006. Activation of IKK by TNFalpha requires site-specific ubiquitination of RIP1 and polyubiquitin binding by NEMO. *Mol Cell,* 22**,** 245-57.

EBLEN, S. T., SLACK-DAVIS, J. K., TARCSAFALVI, A., PARSONS, J. T., WEBER, M. J. & CATLING, A. D. 2004. Mitogen-activated protein kinase feedback phosphorylation regulates MEK1 complex formation and activation during cellular adhesion. *Mol Cell Biol,* 24**,** 2308-17.

ECHEVERRI, C. J., BEACHY, P. A., BAUM, B., BOUTROS, M., BUCHHOLZ, F., CHANDA, S. K., DOWNWARD, J., ELLENBERG, J., FRASER, A. G., HACOHEN, N., HAHN, W. C., JACKSON, A. L., KIGER, A., LINSLEY, P. S., LUM, L., MA, Y., MATHEY-PREVOT, B., ROOT, D. E., SABATINI, D. M., TAIPALE, J., PERRIMON, N. & BERNARDS, R. 2006. Minimizing the risk of reporting false positives in large-scale RNAi screens. *Nat Methods,* 3**,** 777-9.

EDGAR, ALEXANDER J., TROST, M., WATTS, C. & ZARU, R. 2014. A combination of SILAC and nucleotide acyl phosphate labelling reveals unexpected targets of the Rsk inhibitor BI-D1870. *Bioscience Reports,* 34**,** e00091.

EDISON, N., CURTZ, Y., PALAND, N., MAMRIEV, D., CHORUBCZYK, N., HAVIV-REINGEWERTZ, T., KFIR, N., MORGENSTERN, D., KUPERVASER, M., KAGAN, J., KIM, H. T. & LARISCH, S. 2017. Degradation of Bcl-2 by XIAP and ARTS Promotes Apoptosis. *Cell Rep,* 21**,** 442-454.

EDISON, N., ZURI, D., MANIV, I., BORNSTEIN, B., LEV, T., GOTTFRIED, Y., KEMENY, S., GARCIA-FERNANDEZ, M., KAGAN, J. & LARISCH, S. 2012. The IAP-antagonist ARTS initiates caspase activation upstream of cytochrome C and SMAC/Diablo. *Cell Death Differ,* 19**,** 356-68.

EDLICH, F., BANERJEE, S., SUZUKI, M., CLELAND, M. M., ARNOULT, D., WANG, C., NEUTZNER, A., TJANDRA, N. & YOULE, R. J. 2011. Bcl-x(L) retrotranslocates Bax from the mitochondria into the cytosol. *Cell,* 145**,** 104-16.

EDWIN, F., ANDERSON, K. & PATEL, T. B. 2010. HECT Domain-containing E3 Ubiquitin Ligase Nedd4 Interacts with and Ubiquitinates Sprouty2. *J Biol Chem,* 285**,** 255-264.

EGAN, J. E., HALL, A. B., YATSULA, B. A. & BAR-SAGI, D. 2002. The bimodal regulation of epidermal growth factor signaling by human Sprouty proteins. *Proceedings of the National Academy of Sciences,* 99**,** 6041-6046.

EISENHABER, B., CHUMAK, N., EISENHABER, F. & HAUSER, M. T. 2007. The ring between ring fingers (RBR) protein family. *Genome Biol,* 8**,** 209.

EKEROT, M., STAVRIDIS, M. P., DELAVAINE, L., MITCHELL, M. P., STAPLES, C., OWENS, D. M., KEENAN, I. D., DICKINSON, R. J., STOREY, K. G. & KEYSE, S. M. 2008. Negative-feedback regulation of FGF signalling by DUSP6/MKP-3 is driven by ERK1/2 and mediated by Ets factor binding to a conserved site within the DUSP6/MKP-3 gene promoter. *Biochem J,* 412**,** 287-98.

EL CHAMI, N., IKHLEF, F., KASZAS, K., YAKOUB, S., TABONE, E., SIDDEEK, B., CUNHA, S., BEAUDOIN, C., MOREL, L., BENAHMED, M. & REGNIER, D. C. 2005. Androgen-dependent apoptosis in male germ cells is regulated through the proto-oncoprotein Cbl. *J Cell Biol,* 171**,** 651-61.

ELGENDY, M., SHERIDAN, C., BRUMATTI, G. & MARTIN, S. J. 2011. Oncogenic Ras-induced expression of Noxa and Beclin-1 promotes autophagic cell death and limits clonogenic survival. *Mol Cell,* 42**,** 23-35.

ELLIS, H. M. & HORVITZ, H. R. 1986. Genetic control of programmed cell death in the nematode C. elegans. *Cell,* 44**,** 817-29.

EMERY, C. M., VIJAYENDRAN, K. G., ZIPSER, M. C., SAWYER, A. M., NIU, L., KIM, J. J., HATTON, C., CHOPRA, R., OBERHOLZER, P. A., KARPOVA, M. B., MACCONAILL, L. E., ZHANG, J., GRAY, N. S., SELLERS, W. R., DUMMER, R. & GARRAWAY, L. A. 2009. MEK1 mutations confer resistance to MEK and B-RAF inhibition. *Proc Natl Acad Sci U S A,* 106**,** 20411-6.

ENESA, K., ITO, K., LUONG LE, A., THORBJORNSEN, I., PHUA, C., TO, Y., DEAN, J., HASKARD, D. O., BOYLE, J., ADCOCK, I. & EVANS, P. C. 2008. Hydrogen peroxide prolongs nuclear localization of NF-kappaB in activated cells by suppressing negative regulatory mechanisms. *J Biol Chem,* 283**,** 18582-90.

ERNST, R., MUELLER, B., PLOEGH, H. L. & SCHLIEKER, C. 2009. The otubain YOD1 is a deubiquitinating enzyme that associates with p97 to facilitate protein dislocation from the ER. *Mol Cell,* 36**,** 28-38.

ESTEP, A. L., PALMER, C., MCCORMICK, F. & RAUEN, K. A. 2007. Mutation analysis of BRAF, MEK1 and MEK2 in 15 ovarian cancer cell lines: implications for therapy. *PLoS One,* 2**,** 0001279.

EWINGS, K. E., HADFIELD-MOORHOUSE, K., WIGGINS, C. M., WICKENDEN, J. A., BALMANNO, K., GILLEY, R., DEGENHARDT, K., WHITE, E. & COOK, S. J. 2007. ERK1/2-dependent phosphorylation of BimEL promotes its rapid dissociation from Mcl-1 and Bcl-xL. *Embo j,* 26**,** 2856-67.

FABER, A. C., CORCORAN, R. B., EBI, H., SEQUIST, L. V., WALTMAN, B. A., CHUNG, E., INCIO, J., DIGUMARTHY, S. R., POLLACK, S. F., SONG, Y., MUZIKANSKY, A., LIFSHITS, E., ROBERGE, S., COFFMAN, E. J., BENES, C. H., GOMEZ, H. L., BASELGA, J., ARTEAGA, C. L., RIVERA, M. N., DIAS-SANTAGATA, D., JAIN, R. K. & ENGELMAN, J. A. 2011. BIM expression in treatment-naive cancers predicts responsiveness to kinase inhibitors. *Cancer Discov,* 1**,** 352-65.

FABER, A. C., FARAGO, A. F., COSTA, C., DASTUR, A., GOMEZ-CARABALLO, M., ROBBINS, R., WAGNER, B. L., RIDEOUT, W. M., JAKUBIK, C. T., HAM, J., EDELMAN, E. J., EBI, H., YEO, A. T., HATA, A. N., SONG, Y., PATEL, N. U., MARCH, R. J., TAM, A. T., MILANO, R. J., BOISVERT, J. L., HICKS, M. A., ELMILIGY, S., MALSTROM, S. E., RIVERA, M. N., HARADA, H.,

WINDLE, B. E., RAMASWAMY, S., BENES, C. H., JACKS, T. & ENGELMAN, J. A. 2015. Assessment of ABT-263 activity across a cancer cell line collection leads to a potent combination therapy for small-cell lung cancer. *Proceedings of the National Academy of Sciences,* 112**,** E1288-E1296.

FALSCHLEHNER, C., STEINBRINK, S., ERDMANN, G. & BOUTROS, M. 2010. High-throughput RNAi screening to dissect cellular pathways: a how-to guide. *Biotechnol J,* 5**,** 368-76.

FAN, Y. H., CHENG, J., VASUDEVAN, S. A., DOU, J., ZHANG, H., PATEL, R. H., MA, I. T., ROJAS, Y., ZHAO, Y., YU, Y., ZHANG, H., SHOHET, J. M., NUCHTERN, J. G., KIM, E. S. & YANG, J. 2013. USP7 inhibitor P22077 inhibits neuroblastoma growth via inducing p53-mediated apoptosis. *Cell Death Dis,* 17**,** 400.

FANG, X., YU, S., EDER, A., MAO, M., BAST, R. C., JR., BOYD, D. & MILLS, G. B. 1999. Regulation of BAD phosphorylation at serine 112 by the Ras-mitogen-activated protein kinase pathway. *Oncogene,* 18**,** 6635-40.

FANG, Y., FU, D. & SHEN, X. Z. 2010. The potential role of ubiquitin c-terminal hydrolases in oncogenesis. *Biochim Biophys Acta,* 1**,** 1-6.

FARRELL, A. S. & SEARS, R. C. 2014. MYC Degradation. *Cold Spring Harbor Perspectives in Medicine,* 4**,** a014365.

FARSHI, P., DESHMUKH, R. R., NWANKWO, J. O., ARKWRIGHT, R. T., CVEK, B., LIU, J. & DOU, Q. P. 2015. Deubiquitinases (DUBs) and DUB inhibitors: a patent review. *Expert opinion on therapeutic patents,* 25**,** 1191-1208.

FLIERMAN, D., VAN DER HEDEN VAN NOORT, G. J., EKKEBUS, R., GEURINK, P. P., MEVISSEN, T. E., HOSPENTHAL, M. K., KOMANDER, D. & OVAA, H. 2016. Non-hydrolyzable Diubiquitin Probes Reveal Linkage-Specific Reactivity of Deubiquitylating Enzymes Mediated by S2 Pockets. *Cell Chem Biol,* 23**,** 472-82.

FLINT, A. J., TIGANIS, T., BARFORD, D. & TONKS, N. K. 1997. Development of "substrate-trapping" mutants to identify physiological substrates of protein tyrosine phosphatases. *Proc Natl Acad Sci U S A,* 94**,** 1680-5.

FRAILE, J. M., MANCHADO, E., LUJAMBIO, A., QUESADA, V., CAMPOS-IGLESIAS, D., WEBB, T. R., LOWE, S. W., LÓPEZ-OTÍN, C. & FREIJE, J. M. P. 2017. USP39 Deubiquitinase Is Essential for KRAS Oncogene-driven Cancer. *J Biol Chem,* 292**,** 4164-4175.

FRAILE, J. M., QUESADA, V., RODRIGUEZ, D., FREIJE, J. M. & LOPEZ-OTIN, C. 2012. Deubiquitinases in cancer: new functions and therapeutic options. *Oncogene,* 31**,** 2373-88.

FRENCH, J., STIRLING, R., WALSH, M. & KENNEDY, H. D. 2002. The expression of Ras-GTPase activating protein SH3 domain-binding proteins, G3BPs, in human breast cancers. *Histochem J,* 34**,** 223-31.

FRESCAS, D. & PAGANO, M. 2008. Deregulated proteolysis by the F-box proteins SKP2 and beta-TrCP: tipping the scales of cancer. *Nat Rev Cancer,* 8**,** 438-49.

FRIDAY, B. B. & ADJEI, A. A. 2008. Advances in targeting the Ras/Raf/MEK/Erk mitogen-activated protein kinase cascade with MEK inhibitors for cancer therapy. *Clin Cancer Res,* 14**,** 342-6.

FU, N. Y., SUKUMARAN, S. K. & YU, V. C. 2007. Inhibition of ubiquitin-mediated degradation of MOAP-1 by apoptotic stimuli promotes Bax function in mitochondria. *Proceedings of the National Academy of Sciences,* 104**,** 10051-10056.

FUCHS, S. Y., SPIEGELMAN, V. S. & KUMAR, K. G. 2004. The many faces of beta-TrCP E3 ubiquitin ligases: reflections in the magic mirror of cancer. *Oncogene,* 23**,** 2028-36.

FUELLER, J., BECKER, M., SIENERTH, A. R., FISCHER, A., HOTZ, C. & GALMICHE, A. 2008. C-RAF activation promotes BAD poly-ubiquitylation and turn-over by the proteasome. *Biochem Biophys Res Commun,* 370**,** 552-6.

FUJII, M., TAKATA, K., CHUANG, S. S., MIYATA-TAKATA, T., ANDO, M., SATO, Y. & YOSHINO, T. 2018. A20 (TNFAIP3) Alterations in Primary Intestinal Diffuse Large B-cell Lymphoma. *Acta Med Okayama,* 72**,** 23-30.

FULDA, S. & VUCIC, D. 2012. Targeting IAP proteins for therapeutic intervention in cancer. *Nat Rev Drug Discov,* 11**,** 109-24.

GALLUZZI, L., VITALE, I., AARONSON, S. A., ABRAMS, J. M., ADAM, D., AGOSTINIS, P., ALNEMRI, E. S., ALTUCCI, L., AMELIO, I., ANDREWS, D. W., ANNICCHIARICO-PETRUZZELLI, M., ANTONOV, A. V., ARAMA, E., BAEHRECKE, E. H., BARLEV, N. A., BAZAN, N. G., BERNASSOLA, F., BERTRAND, M. J. M., BIANCHI, K., BLAGOSKLONNY, M. V., BLOMGREN, K., BORNER, C., BOYA, P., BRENNER, C., CAMPANELLA, M., CANDI, E., CARMONA-GUTIERREZ, D., CECCONI, F., CHAN, F. K., CHANDEL, N. S., CHENG, E. H., CHIPUK, J. E., CIDLOWSKI, J. A., CIECHANOVER, A., COHEN, G. M., CONRAD, M., CUBILLOS-RUIZ, J. R., CZABOTAR, P. E., D'ANGIOLELLA, V., DAWSON, T. M., DAWSON, V. L., DE LAURENZI, V., DE MARIA, R., DEBATIN, K. M., DEBERARDINIS, R. J., DESHMUKH, M., DI DANIELE, N., DI VIRGILIO, F., DIXIT, V. M., DIXON, S. J., DUCKETT, C. S., DYNLACHT, B. D., EL-DEIRY, W. S., ELROD, J. W., FIMIA, G. M., FULDA, S., GARCIA-SAEZ, A. J., GARG, A. D., GARRIDO, C., GAVATHIOTIS, E., GOLSTEIN, P., GOTTLIEB, E., GREEN, D. R., GREENE, L. A., GRONEMEYER, H., GROSS, A., HAJNOCZKY, G., HARDWICK, J. M., HARRIS, I. S., HENGARTNER, M. O., HETZ, C., ICHIJO, H., JAATTELA, M., JOSEPH, B., JOST, P. J., JUIN, P. P., KAISER, W. J., KARIN, M., KAUFMANN, T., KEPP, O., KIMCHI, A., KITSIS, R. N., KLIONSKY, D. J., KNIGHT, R. A., KUMAR, S., LEE, S. W., LEMASTERS, J. J., LEVINE, B., LINKERMANN, A., LIPTON, S. A., LOCKSHIN, R. A., LOPEZ-OTIN, C., LOWE, S. W., LUEDDE, T., LUGLI, E., MACFARLANE, M., MADEO, F., MALEWICZ, M., MALORNI, W., MANIC, G., *et al.* 2018. Molecular mechanisms of cell death: recommendations of the Nomenclature Committee on Cell Death 2018. *Cell Death Differ,* 25**,** 486-541.

GANLEY, I. G. 2018. Organelle Turnover: A USP30 Safety Catch Restrains the Trigger for Mitophagy and Pexophagy. *Curr Biol,* 28**,** R842-R845.

GARCIA, D. A., BAEK, C., ESTRADA, M. V., TYSL, T., BENNETT, E. J., YANG, J. & CHANG, J. T. 2018. USP11 Enhances TGFbeta-Induced Epithelial-Mesenchymal Plasticity and Human Breast Cancer Metastasis. *Mol Cancer Res,* 16**,** 1172-1184.

GAVATHIOTIS, E., REYNA, D. E., BELLAIRS, J. A., LESHCHINER, E. S. & WALENSKY, L. D. 2012. Direct and selective small-molecule activation of proapoptotic BAX. *Nat Chem Biol,* 8**,** 639-45.

GAVATHIOTIS, E., REYNA, D. E., DAVIS, M. L., BIRD, G. H. & WALENSKY, L. D. 2010. BH3-triggered structural reorganization drives the activation of proapoptotic BAX. *Mol Cell,* 40**,** 481-92.

GAVATHIOTIS, E., SUZUKI, M., DAVIS, M. L., PITTER, K., BIRD, G. H., KATZ, S. G., TU, H. C., KIM, H., CHENG, E. H., TJANDRA, N. & WALENSKY, L. D. 2008. BAX activation is initiated at a novel interaction site. *Nature,* 455**,** 1076-81.

GAVORY, G., O'DOWD, C. R., HELM, M. D., FLASZ, J., ARKOUDIS, E., DOSSANG, A., HUGHES, C., CASSIDY, E., MCCLELLAND, K., ODRZYWOL, E., PAGE, N., BARKER, O., MIEL, H. & HARRISON, T. 2018. Discovery and characterization of highly potent and selective allosteric USP7 inhibitors. *Nat Chem Biol,* 14**,** 118-125.

GERLINGER, M., ROWAN, A. J., HORSWELL, S., MATH, M., LARKIN, J., ENDESFELDER, D., GRONROOS, E., MARTINEZ, P., MATTHEWS, N., STEWART, A., TARPEY, P., VARELA, I., PHILLIMORE, B., BEGUM, S., MCDONALD, N. Q., BUTLER, A., JONES, D., RAINE, K., LATIMER, C., SANTOS, C. R., NOHADANI, M., EKLUND, A. C., SPENCER-DENE, B., CLARK, G., PICKERING, L., STAMP, G., GORE, M., SZALLASI, Z., DOWNWARD, J., FUTREAL, P. A. & SWANTON, C. 2012. Intratumor heterogeneity and branched evolution revealed by multiregion sequencing. *N Engl J Med,* 366**,** 883-892.

GERSCH, M., GLADKOVA, C., SCHUBERT, A. F., MICHEL, M. A., MASLEN, S. & KOMANDER, D. 2017. Mechanism and regulation of the Lys6-selective deubiquitinase USP30. *Nat Struct Mol Biol,* 24**,** 920-930.

GEYER, R. K., YU, Z. K. & MAKI, C. G. 2000. The MDM2 RING-finger domain is required to promote p53 nuclear export. *Nat Cell Biol,* 2**,** 569-73.

GHOSH, A. P., KLOCKE, B. J., BALLESTAS, M. E. & ROTH, K. A. 2012. CHOP potentially co-operates with FOXO3a in neuronal cells to regulate PUMA and BIM expression in response to ER stress. *PLoS One,* 7**,** e39586.

GILBERT, D. F., ERDMANN, G., ZHANG, X., FRITZSCHE, A., DEMIR, K., JAEDICKE, A., MUEHLENBERG, K., WANKER, E. E. & BOUTROS, M. 2011. A novel multiplex cell viability assay for high-throughput RNAi screening. *PLoS One,* 6**,** 5.

GILLEY, J., COFFER, P. J. & HAM, J. 2003. FOXO transcription factors directly activate bim gene expression and promote apoptosis in sympathetic neurons. *J Cell Biol,* 162**,** 613-22.

GILLEY, R., LOCHHEAD, P. A., BALMANNO, K., OXLEY, D., CLARK, J. & COOK, S. J. 2012. CDK1, not ERK1/2 or ERK5, is required for mitotic phosphorylation of BIMEL. *Cell Signal,* 24**,** 170-80.

GILLINGS, A. S., BALMANNO, K., WIGGINS, C. M., JOHNSON, M. & COOK, S. J. 2009. Apoptosis and autophagy: BIM as a mediator of tumour cell death in response to oncogene-targeted therapeutics. *Febs j,* 276**,** 6050-62.

GILMARTIN, A. G., BLEAM, M. R., GROY, A., MOSS, K. G., MINTHORN, E. A., KULKARNI, S. G., ROMINGER, C. M., ERSKINE, S., FISHER, K. E., YANG, J., ZAPPACOSTA, F., ANNAN, R., SUTTON, D. & LAQUERRE, S. G. 2011. GSK1120212 (JTP-74057) is an inhibitor of MEK activity and activation with favorable pharmacokinetic properties for sustained in vivo pathway inhibition. *Clin Cancer Res,* 17**,** 989-1000.

GISPERT, S., RICCIARDI, F., KURZ, A., AZIZOV, M., HOEPKEN, H. H., BECKER, D., VOOS, W., LEUNER, K., MULLER, W. E., KUDIN, A. P., KUNZ, W. S., ZIMMERMANN, A., ROEPER, J., WENZEL, D., JENDRACH, M., GARCIA-ARENCIBIA, M., FERNANDEZ-RUIZ, J., HUBER, L., ROHRER, H., BARRERA, M., REICHERT, A. S., RUB, U., CHEN, A., NUSSBAUM, R. L. & AUBURGER, G. 2009. Parkinson phenotype in aged PINK1-deficient mice is accompanied by progressive mitochondrial dysfunction in absence of neurodegeneration. *PLoS One,* 4**,** 0005777.

GLADKOVA, C., MASLEN, S. L., SKEHEL, J. M. & KOMANDER, D. 2018. Mechanism of parkin activation by PINK1. *Nature,* 559**,** 410-414.

GOETZ, E. M., GHANDI, M., TREACY, D. J., WAGLE, N. & GARRAWAY, L. A. 2014. ERK Mutations Confer Resistance to Mitogen-Activated Protein Kinase Pathway Inhibitors. *Cancer Res,* 74**,** 7079-7089.

GOLDBERG, M. S., FLEMING, S. M., PALACINO, J. J., CEPEDA, C., LAM, H. A., BHATNAGAR, A., MELONI, E. G., WU, N., ACKERSON, L. C., KLAPSTEIN, G. J., GAJENDIRAN, M., ROTH, B. L., CHESSELET, M. F., MAIDMENT, N. T., LEVINE, M. S. & SHEN, J. 2003. Parkin-deficient mice exhibit nigrostriatal deficits but not loss of dopaminergic neurons. *J Biol Chem,* 278**,** 43628-35.

GOMEZ-BOUGIE, P., MENORET, E., JUIN, P., DOUSSET, C., PELLAT-DECEUNYNCK, C. & AMIOT, M. 2011. Noxa controls Mule-dependent Mcl-1 ubiquitination through the regulation of the Mcl-1/USP9X interaction. *Biochem Biophys Res Commun,* 413**,** 460-4.

GOTTFRIED, Y., ROTEM, A., LOTAN, R., STELLER, H. & LARISCH, S. 2004. The mitochondrial ARTS protein promotes apoptosis through targeting XIAP. *Embo j,* 23**,** 1627-35.

GRAHAM, R. R., COTSAPAS, C., DAVIES, L., HACKETT, R., LESSARD, C. J., LEON, J. M., BURTT, N. P., GUIDUCCI, C., PARKIN, M., GATES, C., PLENGE, R. M., BEHRENS, T. W., WITHER, J. E., RIOUX, J. D., FORTIN, P. R., GRAHAM, D. C., WONG, A. K., VYSE, T. J., DALY, M. J., ALTSHULER, D., MOSER, K. L. & GAFFNEY, P. M. 2008. Genetic Variants Near TNFAIP3 on 6q23 are Associated with Systemic Lupus Erythematosus (SLE). *Nature genetics,* 40**,** 1059-1061.

GRANER, E., TANG, D., ROSSI, S., BARON, A., MIGITA, T., WEINSTEIN, L. J., LECHPAMMER, M., HUESKEN, D., ZIMMERMANN, J., SIGNORETTI, S. & LODA, M. 2004. The isopeptidase USP2a regulates the stability of fatty acid synthase in prostate cancer. *Cancer Cell,* 5**,** 253-61.

GREEN, D. R., FERGUSON, T., ZITVOGEL, L. & KROEMER, G. 2009. Immunogenic and tolerogenic cell death. *Nat Rev Immunol,* 9**,** 353-63.

GREEN, D. R., GALLUZZI, L. & KROEMER, G. 2014. Cell biology. Metabolic control of cell death. *Science,* 345**,** 1250256.

GREEN, D. R. & LLAMBI, F. 2015. Cell Death Signaling. *Cold Spring Harb Perspect Biol,* 7.

GREEN, D. R., OGUIN, T. H. & MARTINEZ, J. 2016. The clearance of dying cells: table for two. *Cell Death Differ,* 23**,** 915-26.

GROSSE, L., WURM, C. A., BRUSER, C., NEUMANN, D., JANS, D. C. & JAKOBS, S. 2016. Bax assembles into large ring-like structures remodeling the mitochondrial outer membrane in apoptosis. *Embo j,* 35**,** 402-13.

GRZMIL, M., KAULFUSS, S., THELEN, P., HEMMERLEIN, B., SCHWEYER, S., OBENAUER, S., KANG, T. W. & BURFEIND, P. 2006. Expression and functional analysis of Bax inhibitor-1 in human breast cancer cells. *J Pathol,* 208**,** 340-9.

GU, Y., JONES, A. E., YANG, W., LIU, S., DAI, Q., LIU, Y., SWINDLE, C. S., ZHOU, D., ZHANG, Z., RYAN, T. M., TOWNES, T. M., KLUG, C. A., CHEN, D. & WANG, H. 2016. The histone H2A deubiquitinase Usp16 regulates hematopoiesis and hematopoietic stem cell function. *Proc Natl Acad Sci U S A,* 113**,** 22.

GUICCIARDI, M. E. & GORES, G. J. 2009. Life and death by death receptors. *Faseb j,* 23**,** 1625-37.

GUO, L., XU, J., QI, J., ZHANG, L., WANG, J., LIANG, J., QIAN, N., ZHOU, H., WEI, L. & DENG, L. 2013. MicroRNA-17-92a upregulation by estrogen leads to Bim targeting and inhibition of osteoblast apoptosis. *J Cell Sci,* 126**,** 978-88.

GUO, Y., SCHOELL, M. C. & FREEMAN, R. S. 2009. The von Hippel-Lindau protein sensitizes renal carcinoma cells to apoptotic stimuli through stabilization of BIM(EL). *Oncogene,* 28**,** 1864-74.

GUPTA, I., SINGH, K., VARSHNEY, N. K. & KHAN, S. 2018. Delineating Crosstalk Mechanisms of the Ubiquitin Proteasome System That Regulate Apoptosis. *Front Cell Dev Biol,* 6.

GUPTA, N., BADEAUX, M., LIU, Y., NAXEROVA, K., SGROI, D., MUNN, L. L., JAIN, R. K. & GARKAVTSEV, I. 2017. Stress granule-associated protein G3BP2 regulates breast tumor initiation. *Proc Natl Acad Sci U S A,* 114**,** 1033-1038.

GYRD-HANSEN, M. & MEIER, P. 2010. IAPs: from caspase inhibitors to modulators of NF-kappaB, inflammation and cancer. *Nat Rev Cancer,* 10**,** 561-74.

HAAHR, P., BORGERMANN, N., GUO, X., TYPAS, D., ACHUTHANKUTTY, D., HOFFMANN, S., SHEARER, R., SIXMA, T. K. & MAILAND, N. 2018. ZUFSP Deubiquitylates K63-Linked Polyubiquitin Chains to Promote Genome Stability. *Mol Cell,* 70**,** 165-174.

HALL, A. B., JURA, N., DASILVA, J., JANG, Y. J., GONG, D. & BAR-SAGI, D. 2003. hSpry2 is targeted to the ubiquitin-dependent proteasome pathway by c-Cbl. *Curr Biol,* 13**,** 308-14.

HAMMER, G. E., TURER, E. E., TAYLOR, K. E., FANG, C. J., ADVINCULA, R., OSHIMA, S., BARRERA, J., HUANG, E. J., HOU, B., MALYNN, B. A., REIZIS, B., DEFRANCO, A., CRISWELL, L. A., NAKAMURA, M. C. & MA, A. 2011. Expression of A20 by dendritic cells preserves immune homeostasis and prevents colitis and spondyloarthritis. *Nat Immunol,* 12**,** 1184-93.

HANAHAN, D. & WEINBERG, R. A. 2000. The hallmarks of cancer. *Cell,* 100**,** 57-70.

HANAHAN, D. & WEINBERG, R. A. 2011. Hallmarks of cancer: the next generation. *Cell,* 144**,** 646-74.

HANCOCK, C. N., MACIAS, A., LEE, E. K., YU, S. Y., MACKERELL, A. D. & SHAPIRO, P. 2005. Identification of Novel Extracellular Signal-Regulated Kinase Docking Domain Inhibitors. *J Med Chem,* 48**,** 4586-4595.

HAO, Y., SEKINE, K., KAWABATA, A., NAKAMURA, H., ISHIOKA, T., OHATA, H., KATAYAMA, R., HASHIMOTO, C., ZHANG, X., NODA, T., TSURUO, T. & NAITO, M. 2004. Apollon ubiquitinates SMAC and caspase-9, and has an essential cytoprotection function. *Nat Cell Biol,* 6**,** 849-60.

HARPER, J. W., ORDUREAU, A. & HEO, J. M. 2018. Building and decoding ubiquitin chains for mitophagy. *Nat Rev Mol Cell Biol,* 19**,** 93-108.

HARRIGAN, J. A., JACQ, X., MARTIN, N. M. & JACKSON, S. P. 2017. Deubiquitylating enzymes and drug discovery: emerging opportunities. *Nature Reviews Drug Discovery,* 17**,** 57.

HART, M., CONCORDET, J. P., LASSOT, I., ALBERT, I., DEL LOS SANTOS, R., DURAND, H., PERRET, C., RUBINFELD, B., MARGOTTIN, F., BENAROUS, R. & POLAKIS, P. 1999. The F-box protein beta-TrCP associates with phosphorylated beta-catenin and regulates its activity in the cell. *Curr Biol,* 9**,** 207-10.

HART, T., CHANDRASHEKHAR, M., AREGGER, M., STEINHART, Z., BROWN, K. R., MACLEOD, G., MIS, M., ZIMMERMANN, M., FRADET-TURCOTTE, A., SUN, S., MERO, P., DIRKS, P., SIDHU, S., ROTH, F. P., RISSLAND, O. S., DUROCHER, D., ANGERS, S. & MOFFAT, J. 2015. High-Resolution CRISPR Screens Reveal Fitness Genes and Genotype-Specific Cancer Liabilities. *Cell,* 163**,** 1515-26.

HARTWELL, L. H., SZANKASI, P., ROBERTS, C. J., MURRAY, A. W. & FRIEND, S. H. 1997. Integrating genetic approaches into the discovery of anticancer drugs. *Science,* 278**,** 1064-8.

HATZIVASSILIOU, G., HALING, J. R., CHEN, H., SONG, K., PRICE, S., HEALD, R., HEWITT, J. F., ZAK, M., PECK, A., ORR, C., MERCHANT, M., HOEFLICH, K. P., CHAN, J., LUOH, S. M., ANDERSON, D. J., LUDLAM, M. J., WIESMANN, C., ULTSCH, M., FRIEDMAN, L. S., MALEK, S. & BELVIN, M. 2013. Mechanism of MEK inhibition determines efficacy in mutant KRAS- versus BRAF-driven cancers. *Nature,* 501**,** 232-6.

HAUPT, Y., MAYA, R., KAZAZ, A. & OREN, M. 1997. Mdm2 promotes the rapid degradation of p53. *Nature,* 387**,** 296-9.

HAUSER, D. N. & HASTINGS, T. G. 2013. Mitochondrial dysfunction and oxidative stress in Parkinson's disease and monogenic parkinsonism. *Neurobiol Dis,* 51**,** 35-42.

HAUSER, H. P., BARDROFF, M., PYROWOLAKIS, G. & JENTSCH, S. 1998. A giant ubiquitin-conjugating enzyme related to IAP apoptosis inhibitors. *J Cell Biol,* 141**,** 1415-22.

HAY, E. D. 1995. An overview of epithelio-mesenchymal transformation. *Cells Tissues Organs,* 154**,** 8-20.

HE, M., ZHOU, Z., WU, G., CHEN, Q. & WAN, Y. 2017. Emerging role of DUBs in tumor metastasis and apoptosis: Therapeutic implication. *Pharmacol Ther,* 177**,** 96-107.

HEIDEKER, J. & WERTZ, I. E. 2015. DUBs, the regulation of cell identity and disease. *Biochem J,* 465**,** 1-26.

HERMANNS, T., PICHLO, C., WOIWODE, I., KLOPFFLEISCH, K., WITTING, K. F., OVAA, H., BAUMANN, U. & HOFMANN, K. 2018. A family of unconventional deubiquitinases with modular chain specificity determinants. *Nat Commun,* 9**,** 018-03148.

HERSHKO, A. & CIECHANOVER, A. 1998. The ubiquitin system. *Annu Rev Biochem,* 67**,** 425-79.

HERSHKO, A., CIECHANOVER, A., HELLER, H., HAAS, A. L. & ROSE, I. A. 1980. Proposed role of ATP in protein breakdown: conjugation of protein with multiple chains of the polypeptide of ATP-dependent proteolysis. *Proceedings of the National Academy of Sciences,* 77**,** 1783-1786.

HEWINGS, D. S., FLYGARE, J. A., BOGYO, M. & WERTZ, I. E. 2017. Activity-based probes for the ubiquitin conjugation-deconjugation machinery: new chemistries, new tools, and new insights. *Febs j,* 284**,** 1555-1576.

HEWINGS, D. S., HEIDEKER, J., MA, T. P., AHYOUNG, A. P., EL OUALID, F., AMORE, A., COSTAKES, G. T., KIRCHHOFER, D., BRASHER, B., PILLOW, T., POPOVYCH, N., MAURER, T., SCHWERDTFEGER, C., FORREST, W. F., YU, K., FLYGARE, J., BOGYO, M. & WERTZ, I. E. 2018. Reactive-site-centric chemoproteomics identifies a distinct class of deubiquitinase enzymes. *Nat Commun,* 9**,** 018-03511.

HICKEY, C. M., WILSON, N. R. & HOCHSTRASSER, M. 2012. Function and regulation of SUMO proteases. *Nat Rev Mol Cell Biol,* 13**,** 755-66.

HOCKINGS, C., ANWARI, K., NINNIS, R. L., BROUWER, J., O'HELY, M., EVANGELISTA, M., HINDS, M. G., CZABOTAR, P. E., LEE, E. F., FAIRLIE, W. D., DEWSON, G. & KLUCK, R. M. 2015. Bid chimeras indicate that most BH3-only proteins can directly activate Bak and Bax, and show no preference for Bak versus Bax. *Cell Death Dis,* 6**,** e1735.

HOLDERFIELD, M., DEUKER, M. M., MCCORMICK, F. & MCMAHON, M. 2014. Targeting RAF kinases for cancer therapy: BRAF-mutated melanoma and beyond. *Nat Rev Cancer,* 14**,** 455-67.

HONG, S. K., WU, P. K. & PARK, J. I. 2018. A cellular threshold for active ERK1/2 levels determines Raf/MEK/ERK-mediated growth arrest versus death responses. *Cell Signal,* 42**,** 11-20.

HOPPE, T. 2005. Multiubiquitylation by E4 enzymes: 'one size' doesn't fit all. *Trends Biochem Sci,* 30**,** 183-7.

HOTCHKISS, R. S., STRASSER, A., MCDUNN, J. E. & SWANSON, P. E. 2009. Cell death. *N Engl J Med,* 361**,** 1570-83.

HOU, J., LAM, F., PROUD, C. & WANG, S. 2012. Targeting Mnks for cancer therapy. *Oncotarget,* 3**,** 118-31.

HOWIE, H. L., SHIFLETT, S. L. & SO, M. 2008. Extracellular Signal-Regulated Kinase Activation by Neisseria gonorrhoeae Downregulates Epithelial Cell Proapoptotic Proteins Bad and Bim. *Infection and Immunity,* 76**,** 2715-2721.

HSU, S. Y., LIN, P. & HSUEH, A. J. 1998. BOD (Bcl-2-related ovarian death gene) is an ovarian BH3 domain-containing proapoptotic Bcl-2 protein capable of dimerization with diverse antiapoptotic Bcl-2 members. *Mol Endocrinol,* 12**,** 1432-40.

HU-LIESKOVAN, S., MOK, S., HOMET MORENO, B., TSOI, J., ROBERT, L., GOEDERT, L., PINHEIRO, E. M., KOYA, R. C., GRAEBER, T. G., COMIN-ANDUIX, B. & RIBAS, A. 2015. Improved antitumor activity of immunotherapy with BRAF and MEK inhibitors in BRAF(V600E) melanoma. *Sci Transl Med,* 7.

HU, M., LI, P., LI, M., LI, W., YAO, T., WU, J. W., GU, W., COHEN, R. E. & SHI, Y. 2002. Crystal structure of a UBP-family deubiquitinating enzyme in isolation and in complex with ubiquitin aldehyde. *Cell,* 111**,** 1041-54.

HUANG, H., REGAN, K. M., WANG, F., WANG, D., SMITH, D. I., VAN DEURSEN, J. M. & TINDALL, D. J. 2005. Skp2 inhibits FOXO1 in tumor suppression through ubiquitin-mediated degradation. *Proc Natl Acad Sci U S A,* 102**,** 1649-54.

HUANG, L., KINNUCAN, E., WANG, G., BEAUDENON, S., HOWLEY, P. M., HUIBREGTSE, J. M. & PAVLETICH, N. P. 1999. Structure of an E6AP-UbcH7 complex: insights into ubiquitination by the E2-E3 enzyme cascade. *Science,* 286**,** 1321-6.

HUANG, N. J., ZHANG, L., TANG, W., CHEN, C., YANG, C. S. & KORNBLUTH, S. 2012a. The Trim39 ubiquitin ligase inhibits APC/CCdh1-mediated degradation of the Bax activator MOAP-1. *J Cell Biol,* 197**,** 361-7.

HUANG, Q., LI, S., CHENG, P., DENG, M., HE, X., WANG, Z., YANG, C.-H., ZHAO, X.-Y. & HUANG, J. 2017a. High expression of anti-apoptotic protein Bcl-2 is a good prognostic factor in colorectal cancer: Result of a meta-analysis. *World Journal of Gastroenterology,* 23**,** 5018-5033.

HUANG, R. Y., GUILFORD, P. & THIERY, J. P. 2012b. Early events in cell adhesion and polarity during epithelial-mesenchymal transition. *J Cell Sci,* 125**,** 4417-22.

HUANG, T., YIN, L., WU, J., GU, J. J., DING, K., ZHANG, N., DU, M. Y., QIAN, L. X., LU, Z. W. & HE, X. 2017b. TNFAIP3 inhibits migration and invasion in nasopharyngeal carcinoma by suppressing epithelial mesenchymal transition. *Neoplasma,* 64**,** 389-394.

HUANG, X., SUMMERS, M. K., PHAM, V., LILL, J. R., LIU, J., LEE, G., KIRKPATRICK, D. S., JACKSON, P. K., FANG, G. & DIXIT, V. M. 2011. Deubiquitinase USP37 is activated by CDK2 to antagonize APC(CDH1) and promote S phase entry. *Mol Cell,* 42**,** 511-23.

HUBNER, A., BARRETT, T., FLAVELL, R. A. & DAVIS, R. J. 2008. Multisite phosphorylation regulates Bim stability and apoptotic activity. *Mol Cell,* 30**,** 415-25.

HUSNJAK, K. & DIKIC, I. 2012. Ubiquitin-binding proteins: decoders of ubiquitin-mediated cellular functions. *Annu Rev Biochem,* 81**,** 291-322.

HUTTI, J. E., TURK, B. E., ASARA, J. M., MA, A., CANTLEY, L. C. & ABBOTT, D. W. 2007. IkappaB kinase beta phosphorylates the K63 deubiquitinase A20 to cause feedback inhibition of the NF-kappaB pathway. *Mol Cell Biol,* 27**,** 7451-61.

IGUCHI, M., KUJURO, Y., OKATSU, K., KOYANO, F., KOSAKO, H., KIMURA, M., SUZUKI, N., UCHIYAMA, S., TANAKA, K. & MATSUDA, N. 2013. Parkin-catalyzed ubiquitin-ester transfer is triggered by PINK1-dependent phosphorylation. *J Biol Chem,* 288**,** 22019-32.

IKEDA, F., DERIBE, Y. L., SKANLAND, S. S., STIEGLITZ, B., GRABBE, C., FRANZ-WACHTEL, M., VAN WIJK, S. J., GOSWAMI, P., NAGY, V., TERZIC, J., TOKUNAGA, F., ANDROULIDAKI, A., NAKAGAWA, T., PASPARAKIS, M., IWAI, K., SUNDBERG, J. P., SCHAEFER, L., RITTINGER, K., MACEK, B. & DIKIC, I. 2011. SHARPIN forms a linear ubiquitin ligase complex regulating NF-kappaB activity and apoptosis. *Nature,* 471**,** 637-41.

INOUE, H. & TANI, K. 2014. Multimodal immunogenic cancer cell death as a consequence of anticancer cytotoxic treatments. *Cell Death Differ,* 21**,** 39-49.

ISSAENKO, O. A. & AMERIK, A. Y. 2012. Chalcone-based small-molecule inhibitors attenuate malignant phenotype via targeting deubiquitinating enzymes. *Cell Cycle,* 11**,** 1804-1817.

JACKSON, A. L., BARTZ, S. R., SCHELTER, J., KOBAYASHI, S. V., BURCHARD, J., MAO, M., LI, B., CAVET, G. & LINSLEY, P. S. 2003. Expression profiling reveals off-target gene regulation by RNAi. *Nat Biotechnol,* 21**,** 635-7.

JACKSON, A. L., BURCHARD, J., LEAKE, D., REYNOLDS, A., SCHELTER, J., GUO, J., JOHNSON, J. M., LIM, L., KARPILOW, J., NICHOLS, K., MARSHALL, W., KHVOROVA, A. & LINSLEY, P. S. 2006. Position-specific chemical modification of siRNAs reduces "off-target" transcript silencing. *Rna,* 12**,** 1197-1205.

JACKSON, A. L. & LINSLEY, P. S. 2010. Recognizing and avoiding siRNA off-target effects for target identification and therapeutic application. *Nat Rev Drug Discov,* 9**,** 57-67.

JACKSON, S. P. & DUROCHER, D. 2013. Regulation of DNA damage responses by ubiquitin and SUMO. *Mol Cell,* 49**,** 795-807.

JACOBS, D., GLOSSIP, D., XING, H., MUSLIN, A. J. & KORNFELD, K. 1999. Multiple docking sites on substrate proteins form a modular system that mediates recognition by ERK MAP kinase. *Genes Dev,* 13**,** 163-75.

JACQ, X., KEMP, M., MARTIN, N. M. & JACKSON, S. P. 2013. Deubiquitylating enzymes and DNA damage response pathways. *Cell Biochem Biophys,* 67**,** 25-43.

JEFFREY, P. D., RUSSO, A. A., POLYAK, K., GIBBS, E., HURWITZ, J., MASSAGUE, J. & PAVLETICH, N. P. 1995. Mechanism of CDK activation revealed by the structure of a cyclinA-CDK2 complex. *Nature,* 376**,** 313-20.

JESENBERGER, V. & JENTSCH, S. 2002. Deadly encounter: ubiquitin meets apoptosis. *Nat Rev Mol Cell Biol,* 3**,** 112-21.

JIN, J., SHIROGANE, T., XU, L., NALEPA, G., QIN, J., ELLEDGE, S. J. & HARPER, J. W. 2003. SCFbeta-TRCP links Chk1 signaling to degradation of the Cdc25A protein phosphatase. *Genes Dev,* 17**,** 3062-74.

JOHANNESSEN, C. M., BOEHM, J. S., KIM, S. Y., THOMAS, S. R., WARDWELL, L., JOHNSON, L. A., EMERY, C. M., STRANSKY, N., COGDILL, A. P., BARRETINA, J., CAPONIGRO, G., HIERONYMUS, H., MURRAY, R. R., SALEHI-ASHTIANI, K., HILL, D. E., VIDAL, M., ZHAO, J. J., YANG, X., ALKAN, O., KIM, S., HARRIS, J. L., WILSON, C. J., MYER, V. E., FINAN, P. M., ROOT, D. E., ROBERTS, T. M., GOLUB, T., FLAHERTY, K. T., DUMMER, R., WEBER, B. L., SELLERS, W. R., SCHLEGEL, R., WARGO, J. A., HAHN, W. C. & GARRAWAY, L. A. 2010. COT drives resistance to RAF inhibition through MAP kinase pathway reactivation. *Nature,* 468**,** 968-72.

JONES, A., KEMP, M., STOCKLEY, M., GIBSON, K. R. & WHITLOCK, G.A. Cyano-pyrrolidine compounds as USP30 inhibitors. WO2016156816 (2016).

JOO, H. M., KIM, J. Y., JEONG, J. B., SEONG, K. M., NAM, S. Y., YANG, K. H., KIM, C. S., KIM, H. S., JEONG, M., AN, S. & JIN, Y. W. 2011. Ret finger protein 2 enhances ionizing radiation-induced apoptosis via degradation of AKT and MDM2. *Eur J Cell Biol,* 90**,** 420-31.

JOO, H. Y., ZHAI, L., YANG, C., NIE, S., ERDJUMENT-BROMAGE, H., TEMPST, P., CHANG, C. & WANG, H. 2007. Regulation of cell cycle progression and gene expression by H2A deubiquitination. *Nature,* 449**,** 1068-72.

JOSEPH, E. W., PRATILAS, C. A., POULIKAKOS, P. I., TADI, M., WANG, W., TAYLOR, B. S., HALILOVIC, E., PERSAUD, Y., XING, F., VIALE, A., TSAI, J., CHAPMAN, P. B., BOLLAG, G., SOLIT, D. B. & ROSEN, N. 2010. The RAF inhibitor PLX4032 inhibits ERK signaling and tumor cell proliferation in a V600E BRAF-selective manner. *Proceedings of the National Academy of Sciences,* 107**,** 14903-14908.

KALKAVAN, H. & GREEN, D. R. 2017. MOMP, cell suicide as a BCL-2 family business. *Cell Death Differ,* 25**,** 46.

KALLURI, R. 2009. EMT: when epithelial cells decide to become mesenchymal-like cells. *J Clin Invest,* 119**,** 1417-9.

KALLURI, R. & WEINBERG, R. A. 2009. The basics of epithelial-mesenchymal transition. *J Clin Invest,* 119**,** 1420-8.

KANE, L. A., LAZAROU, M., FOGEL, A. I., LI, Y., YAMANO, K., SARRAF, S. A., BANERJEE, S. & YOULE, R. J. 2014. PINK1 phosphorylates ubiquitin to activate Parkin E3 ubiquitin ligase activity. *J Cell Biol,* 205**,** 143-53.

KANEMORI, Y., UTO, K. & SAGATA, N. 2005. Beta-TrCP recognizes a previously undescribed nonphosphorylated destruction motif in Cdc25A and Cdc25B phosphatases. *Proc Natl Acad Sci U S A,* 102**,** 6279-84.

KANGAS, L., GRONROOS, M. & NIEMINEN, A. L. 1984. Bioluminescence of cellular ATP: a new method for evaluating cytotoxic agents in vitro. *Med Biol,* 62**,** 338-43.

KARIN, M. & BEN-NERIAH, Y. 2000. Phosphorylation meets ubiquitination: the control of NF-[kappa]B activity. *Annu Rev Immunol,* 18**,** 621-63.

KARNOUB, A. E. & WEINBERG, R. A. 2008. Ras oncogenes: split personalities. *Nat Rev Mol Cell Biol,* 9**,** 517-31.

KASHATUS, J. A., NASCIMENTO, A., MYERS, L. J., SHER, A., BYRNE, F. L., HOEHN, K. L., COUNTER, C. M. & KASHATUS, D. F. 2015. Erk2 phosphorylation of Drp1 promotes mitochondrial fission and MAPK-driven tumor growth. *Mol Cell,* 57**,** 537-551.

KASSI, E., SOURLINGAS, T. G., SPILIOTAKI, M., PAPOUTSI, Z., PRATSINIS, H., ALIGIANNIS, N. & MOUTSATSOU, P. 2009. Ursolic acid triggers apoptosis and Bcl-2 downregulation in MCF-7 breast cancer cells. *Cancer Invest,* 27**,** 723-33.

KATO, M., SANADA, M., KATO, I., SATO, Y., TAKITA, J., TAKEUCHI, K., NIWA, A., CHEN, Y., NAKAZAKI, K., NOMOTO, J., ASAKURA, Y., MUTO, S., TAMURA, A., IIO, M., AKATSUKA, Y., HAYASHI, Y., MORI, H., IGARASHI, T., KUROKAWA, M., CHIBA, S., MORI, S., ISHIKAWA, Y., OKAMOTO, K., TOBINAI, K., NAKAGAMA, H., NAKAHATA, T., YOSHINO, T., KOBAYASHI, Y. & OGAWA, S. 2009. Frequent inactivation of A20 in B-cell lymphomas. *Nature,* 459**,** 712-6.

KATSUNO, Y., LAMOUILLE, S. & DERYNCK, R. 2013. TGF-beta signaling and epithelial-mesenchymal transition in cancer progression. *Curr Opin Oncol,* 25**,** 76-84.

KAVSAK, P., RASMUSSEN, R. K., CAUSING, C. G., BONNI, S., ZHU, H., THOMSEN, G. H. & WRANA, J. L. 2000. Smad7 binds to Smurf2 to form an E3 ubiquitin ligase that targets the TGF beta receptor for degradation. *Mol Cell,* 6**,** 1365-75.

KAWAHARA, M., HORI, T., CHONABAYASHI, K., OKA, T., SUDOL, M. & UCHIYAMA, T. 2008. Kpm/Lats2 is linked to chemosensitivity of leukemic cells through the stabilization of p73. *Blood*.

KAZLAUSKAITE, A., KONDAPALLI, C., GOURLAY, R., CAMPBELL, D. G., RITORTO, M. S., HOFMANN, K., ALESSI, D. R., KNEBEL, A., TROST, M. & MUQIT, M. M. 2014. Parkin is activated by PINK1-dependent phosphorylation of ubiquitin at Ser65. *Biochem J,* 460**,** 127-39.

KE, N., GODZIK, A. & REED, J. C. 2001. Bcl-B, a novel Bcl-2 family member that differentially binds and regulates Bax and Bak. *J Biol Chem,* 276**,** 12481-4.

KEMP, M. 2016. Recent Advances in the Discovery of Deubiquitinating Enzyme Inhibitors. *Prog Med Chem,* 55**,** 149-92.

KEMP, M., STOCKLEY, M & JONES,A. Cyanopyrrolidines as DUB inhibitors for the treatment of cancers. WO2017009650 (2017).

KERR, J. F., WYLLIE, A. H. & CURRIE, A. R. 1972. Apoptosis: a basic biological phenomenon with wide-ranging implications in tissue kinetics. *Br J Cancer,* 26**,** 239-57.

KHAN, A. A., BETEL, D., MILLER, M. L., SANDER, C., LESLIE, C. S. & MARKS, D. S. 2009. Transfection of small RNAs globally perturbs gene regulation by endogenous microRNAs. *Nat Biotechnol,* 27**,** 549-55.

KIDGER, A. M. & KEYSE, S. M. 2016. The regulation of oncogenic Ras/ERK signalling by dual-specificity mitogen activated protein kinase phosphatases (MKPs). *Semin Cell Dev Biol,* 50**,** 125-32.

KIDGER, A. M., SIPTHORP, J. & COOK, S. J. 2018. ERK1/2 inhibitors: New weapons to inhibit the RAS-regulated RAF-MEK1/2-ERK1/2 pathway. *Pharmacol Ther,* 187**,** 45-60.

KIM, H., TU, H. C., REN, D., TAKEUCHI, O., JEFFERS, J. R., ZAMBETTI, G. P., HSIEH, J. J. & CHENG, E. H. 2009. Stepwise activation of BAX and BAK by tBID, BIM, and PUMA initiates mitochondrial apoptosis. *Mol Cell,* 36**,** 487-99.

KIM, J.-O., KIM, S.-R., LIM, K.-H., KIM, J.-H., AJJAPPALA, B., LEE, H.-J., CHOI, J.-I. & BAEK, K.-H. 2015. Deubiquitinating enzyme USP37 regulating oncogenic function of 14-3-3γ. *Oncotarget,* 6**,** 36551-36576.

KIM, J., KUNDU, M., VIOLLET, B. & GUAN, K. L. 2011a. AMPK and mTOR regulate autophagy through direct phosphorylation of Ulk1. *Nat Cell Biol,* 13**,** 132-41.

KIM, N.-G., KOH, E., CHEN, X. & GUMBINER, B. M. 2011b. E-cadherin mediates contact inhibition of proliferation through Hippo signaling-pathway components. *Proceedings of the National Academy of Sciences,* 108**,** 11930-11935.

KIM, Y. & JHO, E.-H. 2017. *Deubiquitinase YOD1: The Potent Activator of YAP in Hepatomegaly and Liver Cancer*.

KIM, Y., KIM, W., SONG, Y., KIM, J.-R., CHO, K., MOON, H., RO, S. W., SEO, E., RYU, Y.-M., MYUNG, S.-J. & JHO, E.-H. 2017. Deubiquitinase YOD1 potentiates YAP/TAZ activities through enhancing ITCH stability. *Proceedings of the National Academy of Sciences,* 114**,** 4691-4696.

KIMURA, Y. & TANAKA, K. 2010. Regulatory mechanisms involved in the control of ubiquitin homeostasis. *J Biochem,* 147**,** 793-8.

KIPROWSKA, M. J., STEPANOVA, A., TODARO, D. R., GALKIN, A., HAAS, A., WILSON, S. M. & FIGUEIREDO-PEREIRA, M. E. 2017. Neurotoxic mechanisms by which the USP14 inhibitor IU1 depletes ubiquitinated proteins and Tau in rat cerebral cortical neurons: Relevance to Alzheimer's disease. *Biochim Biophys Acta Mol Basis Dis,* 6**,** 1.

KITADA, T., ASAKAWA, S., HATTORI, N., MATSUMINE, H., YAMAMURA, Y., MINOSHIMA, S., YOKOCHI, M., MIZUNO, Y. & SHIMIZU, N. 1998. Mutations in the parkin gene cause autosomal recessive juvenile parkinsonism. *Nature,* 392**,** 605-8.

KLASA, R. J., GILLUM, A. M., KLEM, R. E. & FRANKEL, S. R. 2002. Oblimersen Bcl-2 antisense: facilitating apoptosis in anticancer treatment. *Antisense Nucleic Acid Drug Dev,* 12**,** 193-213.

KLUGE, A. F., LAGU, B. R., MAITI, P., JALEEL, M., WEBB, M., MALHOTRA, J., MALLAT, A., SRINIVAS, P. A. & THOMPSON, J. E. 2018. Novel highly selective inhibitors of ubiquitin specific protease 30 (USP30) accelerate mitophagy. *Bioorg Med Chem Lett,* 28**,** 2655-2659.

KOMANDER, D. 2009. The emerging complexity of protein ubiquitination. *Biochem Soc Trans,* 37**,** 937-53.

KOMANDER, D., CLAGUE, M. J. & URBE, S. 2009a. Breaking the chains: structure and function of the deubiquitinases. *Nat Rev Mol Cell Biol,* 10**,** 550-63.

KOMANDER, D. & RAPE, M. 2012. The ubiquitin code. *Annu Rev Biochem,* 81**,** 203-29.

KOMANDER, D., REYES-TURCU, F., LICCHESI, J. D., ODENWAELDER, P., WILKINSON, K. D. & BARFORD, D. 2009b. Molecular discrimination of structurally equivalent Lys 63-linked and linear polyubiquitin chains. *EMBO Rep,* 10**,** 466-73.

KONDAPALLI, C., KAZLAUSKAITE, A., ZHANG, N., WOODROOF, H. I., CAMPBELL, D. G., GOURLAY, R., BURCHELL, L., WALDEN, H., MACARTNEY, T. J., DEAK, M., KNEBEL, A., ALESSI, D. R. & MUQIT, M. M. 2012. PINK1 is activated by mitochondrial membrane potential depolarization and stimulates Parkin E3 ligase activity by phosphorylating Serine 65. *Open Biol,* 2**,** 120080.

KÖNIG, R., ZHOU, Y., ELLEDER, D., DIAMOND, T. L., BONAMY, G. M. C., IRELAN, J. T., CHIANG, C.-Y., TU, B. P., DE JESUS, P. D., LILLEY, C. E., SEIDEL, S., OPALUCH, A. M., CALDWELL, J. S., WEITZMAN, M. D., KUHEN, K. L., BANDYOPADHYAY, S., IDEKER, T., ORTH, A. P., MIRAGLIA, L. J., BUSHMAN, F. D., YOUNG, J. A. & CHANDA, S. K. 2008. Global analysis of host-pathogen interactions that regulate early stage HIV-1 replication. *Cell,* 135**,** 49-60.

KONOPLEVA, M., CONTRACTOR, R., TSAO, T., SAMUDIO, I., RUVOLO, P. P., KITADA, S., DENG, X., ZHAI, D., SHI, Y. X., SNEED, T., VERHAEGEN, M., SOENGAS, M., RUVOLO, V. R., MCQUEEN, T., SCHOBER, W. D., WATT, J. C., JIFFAR, T., LING, X., MARINI, F. C., HARRIS, D., DIETRICH, M., ESTROV, Z., MCCUBREY, J., MAY, W. S., REED, J. C. & ANDREEFF, M. 2006. Mechanisms of apoptosis sensitivity and resistance to the BH3 mimetic ABT-737 in acute myeloid leukemia. *Cancer Cell,* 10**,** 375-88.

KOONTZ, L. M., LIU-CHITTENDEN, Y., YIN, F., ZHENG, Y., YU, J., HUANG, B., CHEN, Q., WU, S. & PAN, D. 2013. The Hippo effector Yorkie controls normal tissue growth by antagonizing scalloped-mediated default repression. *Dev Cell,* 25**,** 388-401.

KOTSCHY, A., SZLAVIK, Z., MURRAY, J., DAVIDSON, J., MARAGNO, A. L., LE TOUMELIN-BRAIZAT, G., CHANRION, M., KELLY, G. L., GONG, J. N., MOUJALLED, D. M., BRUNO, A., CSEKEI, M., PACZAL, A., SZABO, Z. B., SIPOS, S., RADICS, G., PROSZENYAK, A., BALINT, B., ONDI, L., BLASKO, G., ROBERTSON, A., SURGENOR, A., DOKURNO, P., CHEN, I., MATASSOVA, N., SMITH, J., PEDDER, C., GRAHAM, C., STUDENY, A., LYSIAK-AUVITY, G., GIRARD, A. M., GRAVE, F., SEGAL, D., RIFFKIN, C. D., POMILIO, G., GALBRAITH, L. C., AUBREY, B. J., BRENNAN, M. S., HEROLD, M. J., CHANG, C., GUASCONI, G., CAUQUIL, N., MELCHIORE, F., GUIGAL-STEPHAN, N., LOCKHART, B., COLLAND, F., HICKMAN, J. A., ROBERTS, A. W., HUANG, D. C., WEI, A. H., STRASSER, A., LESSENE, G. & GENESTE, O. 2016. The MCL1 inhibitor S63845 is tolerable and effective in diverse cancer models. *Nature,* 538**,** 477-482.

KOUZARIDES, T. 2007. Chromatin modifications and their function. *Cell,* 128**,** 693-705.

KOYANO, F., OKATSU, K., KOSAKO, H., TAMURA, Y., GO, E., KIMURA, M., KIMURA, Y., TSUCHIYA, H., YOSHIHARA, H., HIROKAWA, T., ENDO, T., FON, E. A., TREMPE, J. F., SAEKI, Y., TANAKA, K. & MATSUDA, N. 2014. Ubiquitin is phosphorylated by PINK1 to activate parkin. *Nature,* 510**,** 162-6.

KRAJEWSKI, S., KRAJEWSKA, M., TURNER, B. C., PRATT, C., HOWARD, B., ZAPATA, J. M., FRENKEL, V., ROBERTSON, S., IONOV, Y., YAMAMOTO, H., PERUCHO, M., TAKAYAMA, S. & REED, J. C. 1999. Prognostic significance of apoptosis regulators in breast cancer. *Endocr Relat Cancer,* 6**,** 29-40.

KRAMER, H. B., NICHOLSON, B., KESSLER, B. M. & ALTUN, M. 2012. Detection of ubiquitin–proteasome enzymatic activities in cells: Application of activity-based probes to inhibitor development. *Biochimica et Biophysica Acta (BBA) - Molecular Cell Research,* 1823**,** 2029-2037.

KREUZ, S., SIEGMUND, D., SCHEURICH, P. & WAJANT, H. 2001. NF-kappaB inducers upregulate cFLIP, a cycloheximide-sensitive inhibitor of death receptor signaling. *Mol Cell Biol,* 21**,** 3964-73.

KROEMER, G. & POUYSSEGUR, J. 2008. Tumor cell metabolism: cancer's Achilles' heel. *Cancer Cell,* 13**,** 472-82.

KRUSE, J. P. & GU, W. 2009. Modes of p53 regulation. *Cell,* 137**,** 609-22.

KUBBUTAT, M. H., JONES, S. N. & VOUSDEN, K. H. 1997. Regulation of p53 stability by Mdm2. *Nature,* 387**,** 299-303.

KUCHARSKA, A., RUSHWORTH, L. K., STAPLES, C., MORRICE, N. A. & KEYSE, S. M. 2009. Regulation of the inducible nuclear dual-specificity phosphatase DUSP5 by ERK MAPK. *Cell Signal,* 21**,** 1794-805.

KULATHU, Y. & KOMANDER, D. 2012. Atypical ubiquitylation - the unexplored world of polyubiquitin beyond Lys48 and Lys63 linkages. *Nat Rev Mol Cell Biol,* 13**,** 508-23.

KUMAGAI, A. & DUNPHY, W. G. 1991. The cdc25 protein controls tyrosine dephosphorylation of the cdc2 protein in a cell-free system. *Cell,* 64**,** 903-14.

KUMAR, A., CHAUGULE, V. K., CONDOS, T. E. C., BARBER, K. R., JOHNSON, C., TOTH, R., SUNDARAMOORTHY, R., KNEBEL, A., SHAW, G. S. & WALDEN, H. 2017. Parkin-phosphoubiquitin complex reveals cryptic ubiquitin-binding site required for RBR ligase activity. *Nat Struct Mol Biol,* 24**,** 475-483.

KUWANA, T., BOUCHIER-HAYES, L., CHIPUK, J. E., BONZON, C., SULLIVAN, B. A., GREEN, D. R. & NEWMEYER, D. D. 2005. BH3 domains of BH3-only proteins differentially regulate Bax-mediated mitochondrial membrane permeabilization both directly and indirectly. *Mol Cell,* 17**,** 525-35.

KUWANA, T., OLSON, N. H., KIOSSES, W. B., PETERS, B. & NEWMEYER, D. D. 2016. Pro-apoptotic Bax molecules densely populate the edges of membrane pores. *Scientific Reports,* 6**,** 27299.

KVANSAKUL, M. & HINDS, M. G. 2015. The Bcl-2 family: structures, interactions and targets for drug discovery. *Apoptosis,* 20**,** 136-50.

KWASNA, D., ABDUL REHMAN, S. A., NATARAJAN, J., MATTHEWS, S., MADDEN, R., DE CESARE, V., WEIDLICH, S., VIRDEE, S., AHEL, I., GIBBS-SEYMOUR, I. & KULATHU, Y. 2018. Discovery and Characterization of ZUFSP/ZUP1, a Distinct Deubiquitinase Class Important for Genome Stability. *Mol Cell,* 70**,** 150-164.

LALAOUI, N., LINDQVIST, L. M., SANDOW, J. J. & EKERT, P. G. 2015. The molecular relationships between apoptosis, autophagy and necroptosis. *Semin Cell Dev Biol,* 39**,** 63-9.

LAMOUILLE, S., XU, J. & DERYNCK, R. 2014. Molecular mechanisms of epithelial-mesenchymal transition. *Nat Rev Mol Cell Biol,* 15**,** 178-96.

LANG, V., JANZEN, J., FISCHER, G. Z., SONEJI, Y., BEINKE, S., SALMERON, A., ALLEN, H., HAY, R. T., BEN-NERIAH, Y. & LEY, S. C. 2003. betaTrCP-mediated proteolysis of NF-kappaB1 p105 requires phosphorylation of p105 serines 927 and 932. *Mol Cell Biol,* 23**,** 402-13.

LAPLANTE, M. & SABATINI, D. M. 2012. mTOR signaling in growth control and disease. *Cell,* 149**,** 274-93.

LARUE, L. & BELLACOSA, A. 2005. Epithelial-mesenchymal transition in development and cancer: role of phosphatidylinositol 3' kinase/AKT pathways. *Oncogene,* 24**,** 7443-54.

LATRES, E., CHIAUR, D. S. & PAGANO, M. 1999. The human F box protein beta-Trcp associates with the Cul1/Skp1 complex and regulates the stability of beta-catenin. *Oncogene,* 18**,** 849-54.

LAWRENCE, M. S., STOJANOV, P., MERMEL, C. H., ROBINSON, J. T., GARRAWAY, L. A., GOLUB, T. R., MEYERSON, M., GABRIEL, S. B., LANDER, E. S. & GETZ, G. 2014. Discovery and saturation analysis of cancer genes across 21 tumour types. *Nature,* 505**,** 495.

LEE, B. H., LEE, M. J., PARK, S., OH, D. C., ELSASSER, S., CHEN, P. C., GARTNER, C., DIMOVA, N., HANNA, J., GYGI, S. P., WILSON, S. M., KING, R. W. & FINLEY, D. 2010. Enhancement of proteasome activity by a small-molecule inhibitor of USP14. *Nature,* 467**,** 179-84.

LEE, E. G., BOONE, D. L., CHAI, S., LIBBY, S. L., CHIEN, M., LODOLCE, J. P. & MA, A. 2000. Failure to regulate TNF-induced NF-kappaB and cell death responses in A20-deficient mice. *Science,* 289**,** 2350-4.

LEE, Y.-J., HWANG, I.-S., LEE, Y.-J., LEE, C.-H., KIM, S.-H., NAM, H.-S., CHOI, Y.-J. & LEE, S.-H. 2014. Knockdown of Bcl-xL Enhances Growth-Inhibiting and Apoptosis-Inducing Effects of Resveratrol and Clofarabine in Malignant Mesothelioma H-2452 Cells. *Journal of Korean Medical Science,* 29**,** 1464-1472.

LEFLOCH, R., POUYSSÉGUR, J. & LENORMAND, P. 2008. Single and Combined Silencing of ERK1 and ERK2 Reveals Their Positive Contribution to Growth Signaling Depending on Their Expression Levels. *Mol Cell Biol,* 28**,** 511-527.

LEI, K. & DAVIS, R. J. 2003. JNK phosphorylation of Bim-related members of the Bcl2 family induces Bax-dependent apoptosis. *Proc Natl Acad Sci U S A,* 100**,** 2432-7.

LEI, Q. Y., ZHANG, H., ZHAO, B., ZHA, Z. Y., BAI, F., PEI, X. H., ZHAO, S., XIONG, Y. & GUAN, K. L. 2008. TAZ promotes cell proliferation and epithelial-mesenchymal transition and is inhibited by the hippo pathway. *Mol Cell Biol,* 28**,** 2426-36.

LEICHT, D. T., BALAN, V., KAPLUN, A., SINGH-GUPTA, V., KAPLUN, L., DOBSON, M. & TZIVION, G. 2007. Raf kinases: function, regulation and role in human cancer. *Biochim Biophys Acta,* 1773**,** 1196-212.

LESSENE, G., CZABOTAR, P. E. & COLMAN, P. M. 2008. BCL-2 family antagonists for cancer therapy. *Nat Rev Drug Discov,* 7**,** 989-1000.

LESSENE, G., CZABOTAR, P. E., SLEEBS, B. E., ZOBEL, K., LOWES, K. N., ADAMS, J. M., BAELL, J. B., COLMAN, P. M., DESHAYES, K., FAIRBROTHER, W. J., FLYGARE, J. A., GIBBONS, P., KERSTEN, W. J. A., KULASEGARAM, S., MOSS, R. M., PARISOT, J. P., SMITH, B. J., STREET, I. P., YANG, H., HUANG, D. C. S. & WATSON, K. G. 2013. Structure-guided design of a selective BCL-XL inhibitor. *Nat Chem Biol,* 9**,** 390.

LETAI, A. 2017. Apoptosis and Cancer. *Annual Review of Cancer Biology,* 1**,** 275-294.

LETAI, A., BASSIK, M. C., WALENSKY, L. D., SORCINELLI, M. D., WEILER, S. & KORSMEYER, S. J. 2002. Distinct BH3 domains either sensitize or activate mitochondrial apoptosis, serving as prototype cancer therapeutics. *Cancer Cell,* 2**,** 183-92.

LEVERSON, J. D., ZHANG, H., CHEN, J., TAHIR, S. K., PHILLIPS, D. C., XUE, J., NIMMER, P., JIN, S., SMITH, M., XIAO, Y., KOVAR, P., TANAKA, A., BRUNCKO, M., SHEPPARD, G. S., WANG, L., GIERKE, S., KATEGAYA, L., ANDERSON, D. J., WONG, C., EASTHAM-ANDERSON, J., LUDLAM, M. J. C., SAMPATH, D., FAIRBROTHER, W. J., WERTZ, I., ROSENBERG, S. H., TSE, C., ELMORE, S. W. & SOUERS, A. J. 2015. Potent and selective small-molecule MCL-1 inhibitors demonstrate on-target cancer cell killing activity as single agents and in combination with ABT-263 (navitoclax). *Cell Death &Amp; Disease,* 6**,** e1590.

LEVY, D., ADAMOVICH, Y., REUVEN, N. & SHAUL, Y. 2008. Yap1 phosphorylation by c-Abl is a critical step in selective activation of proapoptotic genes in response to DNA damage. *Mol Cell,* 29**,** 350-61.

LEY, R., BALMANNO, K., HADFIELD, K., WESTON, C. & COOK, S. J. 2003. Activation of the ERK1/2 signaling pathway promotes phosphorylation and proteasome-dependent degradation of the BH3-only protein, Bim. *J Biol Chem,* 278**,** 18811-6.

LEY, R., EWINGS, K. E., HADFIELD, K., HOWES, E., BALMANNO, K. & COOK, S. J. 2004. Extracellular signal-regulated kinases 1/2 are serum-stimulated "Bim(EL) kinases" that bind to the BH3-only protein Bim(EL) causing its phosphorylation and turnover. *J Biol Chem,* 279**,** 8837-47.

LEY, R., HADFIELD, K., HOWES, E. & COOK, S. J. 2005. Identification of a DEF-type docking domain for extracellular signal-regulated kinases 1/2 that directs phosphorylation and turnover of the BH3-only protein BimEL. *J Biol Chem,* 280**,** 17657-63.

LI, B. & DOU, Q. P. 2000. Bax degradation by the ubiquitin/proteasome-dependent pathway: Involvement in tumor survival and progression. *Proceedings of the National Academy of Sciences,* 97**,** 3850-3855.

LI, L., WANG, J., ZHANG, Y., ZHANG, Y., MA, L., WENG, W., QIAO, Y., XIAO, W., WANG, H., YU, W., PAN, Q., HE, Y. & SUN, F. 2013. MEK1 promotes YAP and their interaction is critical for tumorigenesis in liver cancer. *FEBS Lett,* 587**,** 3921-3927.

LI, M., BROOKS, C. L., KON, N. & GU, W. 2004. A dynamic role of HAUSP in the p53-Mdm2 pathway. *Mol Cell,* 13**,** 879-86.

LI, M., CHEN, D., SHILOH, A., LUO, J., NIKOLAEV, A. Y., QIN, J. & GU, W. 2002. Deubiquitination of p53 by HAUSP is an important pathway for p53 stabilization. *Nature,* 416**,** 648-53.

LIAN, B. S. X., YEK, A. E. H., SHUVAS, H., ABDUL RAHMAN, S. F., MUNIANDY, K. & MOHANA-KUMARAN, N. 2018. Synergistic anti-proliferative effects of combination of ABT-263 and MCL-1 selective inhibitor A-1210477 on cervical cancer cell lines. *BMC Res Notes,* 11**,** 018-3302.

LIANG, J., SAAD, Y., LEI, T., WANG, J., QI, D., YANG, Q., KOLATTUKUDY, P. E. & FU, M. 2010. MCP-induced protein 1 deubiquitinates TRAF proteins and negatively regulates JNK and NF-κB signaling. *The Journal of Experimental Medicine,* 207**,** 2959-2973.

LIANG, J. R., MARTINEZ, A., LANE, J. D., MAYOR, U., CLAGUE, M. J. & URBE, S. 2015. USP30 deubiquitylates mitochondrial Parkin substrates and restricts apoptotic cell death. *EMBO Rep,* 16**,** 618-27.

LIM, J., KELLEY, E. H., METHOT, J. L., ZHOU, H., PETROCCHI, A., CHEN, H., HILL, S. E., HINTON, M. C., HRUZA, A., JUNG, J. O., MACLEAN, J. K. F., MANSUETO, M., NAUMOV, G. N., PHILIPPAR, U., RAUT, S., SPACCIAPOLI, P., SUN, D. & SILIPHAIVANH, P. 2016. Discovery of 1-(1H-Pyrazolo[4,3-c]pyridin-6-yl)urea Inhibitors of Extracellular Signal-Regulated Kinase (ERK) for the Treatment of Cancers. *J Med Chem,* 59**,** 6501-6511.

LIN, Y. W., CHUANG, S. M. & YANG, J. L. 2003. ERK1/2 achieves sustained activation by stimulating MAPK phosphatase-1 degradation via the ubiquitin-proteasome pathway. *J Biol Chem,* 278**,** 21534-41.

LIN, Y. W. & YANG, J. L. 2006. Cooperation of ERK and SCFSkp2 for MKP-1 destruction provides a positive feedback regulation of proliferating signaling. *J Biol Chem,* 281**,** 915-26.

LITO, P., SABOROWSKI, A., YUE, J., SOLOMON, M., JOSEPH, E., GADAL, S., SABOROWSKI, M., KASTENHUBER, E., FELLMANN, C., OHARA, K., MORIKAMI, K., MIURA, T., LUKACS, C., ISHII, N., LOWE, S. & ROSEN, N. 2014. Disruption of CRAF-mediated MEK activation is required for effective MEK inhibition in KRAS mutant tumors. *Cancer Cell,* 25**,** 697-710.

LITTLE, A. S., BALMANNO, K., SALE, M. J., NEWMAN, S., DRY, J. R., HAMPSON, M., EDWARDS, P. A., SMITH, P. D. & COOK, S. J. 2011. Amplification of the driving oncogene, KRAS or BRAF, underpins acquired resistance to MEK1/2 inhibitors in colorectal cancer cells. *Sci Signal,* 4**,** ra17.

LIU, C., LI, Y., SEMENOV, M., HAN, C., BAEG, G.-H., TAN, Y., ZHANG, Z., LIN, X. & HE, X. 2002. Control of β-Catenin Phosphorylation/Degradation by a Dual-Kinase Mechanism. *Cell,* 108**,** 837-847.

LIU, X., DAI, S., ZHU, Y., MARRACK, P. & KAPPLER, J. W. 2003. The structure of a Bcl-xL/Bim fragment complex: implications for Bim function. *Immunity,* 19**,** 341-52.

LIU, Y. L., LAI, F., WILMOTT, J. S., YAN, X. G., LIU, X. Y., LUAN, Q., GUO, S. T., JIANG, C. C., TSENG, H. Y., SCOLYER, R. A., JIN, L. & ZHANG, X. D. 2014. Noxa upregulation by oncogenic activation of MEK/ERK through CREB promotes autophagy in human melanoma cells. *Oncotarget,* 5**,** 11237-51.

LIU, Z., SUN, C., OLEJNICZAK, E. T., MEADOWS, R. P., BETZ, S. F., OOST, T., HERRMANN, J., WU, J. C. & FESIK, S. W. 2000. Structural basis for binding of Smac/DIABLO to the XIAP BIR3 domain. *Nature,* 408**,** 1004-8.

LLAMBI, F., WANG, Y. M., VICTOR, B., YANG, M., SCHNEIDER, D. M., GINGRAS, S., PARSONS, M. J., ZHENG, J. H., BROWN, S. A., PELLETIER, S., MOLDOVEANU, T., CHEN, T. & GREEN, D. R. 2016. BOK Is a Non-canonical BCL-2 Family Effector of Apoptosis Regulated by ER-Associated Degradation. *Cell,* 165**,** 421-33.

LOCK, P., I, S. T., STRAFFON, A. F., SCHIEB, H., HOVENS, C. M. & STYLLI, S. S. 2006. Spred-2 steady-state levels are regulated by phosphorylation and Cbl-mediated ubiquitination. *Biochem Biophys Res Commun,* 351**,** 1018-23.

LONG, G. V., STROYAKOVSKIY, D., GOGAS, H., LEVCHENKO, E., DE BRAUD, F., LARKIN, J., GARBE, C., JOUARY, T., HAUSCHILD, A., GROB, J. J., CHIARION SILENI, V., LEBBE, C., MANDALA, M., MILLWARD, M., ARANCE, A., BONDARENKO, I., HAANEN, J. B., HANSSON, J., UTIKAL, J., FERRARESI, V., KOVALENKO, N., MOHR, P., PROBACHAI, V., SCHADENDORF, D., NATHAN, P., ROBERT, C., RIBAS, A., DEMARINI, D. J., IRANI, J. G., CASEY, M., OUELLET, D., MARTIN, A. M., LE, N., PATEL, K. & FLAHERTY, K. 2014. Combined BRAF and MEK inhibition versus BRAF inhibition alone in melanoma. *N Engl J Med,* 371**,** 1877-88.

LOPEZ-VICENTE, L., ARMENGOL, G., PONS, B., COCH, L., ARGELAGUET, E., LLEONART, M., HERNANDEZ-LOSA, J., DE TORRES, I. & RAMON Y CAJAL, S. 2009. Regulation of replicative and stress-induced senescence by RSK4, which is down-regulated in human tumors. *Clin Cancer Res,* 15**,** 4546-53.

LOVELL, J. F., BILLEN, L. P., BINDNER, S., SHAMAS-DIN, A., FRADIN, C., LEBER, B. & ANDREWS, D. W. 2008. Membrane binding by tBid initiates an ordered series of events culminating in membrane permeabilization by Bax. *Cell,* 135**,** 1074-84.

LU, L., LI, Y., KIM, S. M., BOSSUYT, W., LIU, P., QIU, Q., WANG, Y., HALDER, G., FINEGOLD, M. J., LEE, J.-S. & JOHNSON, R. L. 2010. Hippo signaling is a potent in vivo growth and tumor suppressor pathway in the mammalian liver. *Proceedings of the National Academy of Sciences,* 107**,** 1437-1442.

LUCIANO, F., JACQUEL, A., COLOSETTI, P., HERRANT, M., CAGNOL, S., PAGES, G. & AUBERGER, P. 2003. Phosphorylation of Bim-EL by Erk1/2 on serine 69 promotes its degradation via the proteasome pathway and regulates its proapoptotic function. *Oncogene,* 22**,** 6785-93.

LUNDGREN, K., WALWORTH, N., BOOHER, R., DEMBSKI, M., KIRSCHNER, M. & BEACH, D. 1991. mik1 and wee1 cooperate in the inhibitory tyrosine phosphorylation of cdc2. *Cell,* 64**,** 1111-22.

LUO, J., SOLIMINI, N. L. & ELLEDGE, S. J. 2009. Principles of cancer therapy: oncogene and non-oncogene addiction. *Cell,* 136**,** 823-37.

LUO, S., GARCIA-ARENCIBIA, M., ZHAO, R., PURI, C., TOH, P. P., SADIQ, O. & RUBINSZTEIN, D. C. 2012. Bim inhibits autophagy by recruiting Beclin 1 to microtubules. *Mol Cell,* 47**,** 359-70.

MA, S., HOCKINGS, C., ANWARI, K., KRATINA, T., FENNELL, S., LAZAROU, M., RYAN, M. T., KLUCK, R. M. & DEWSON, G. 2013. Assembly of the Bak apoptotic pore: a critical role for the Bak protein alpha6 helix in the multimerization of homodimers during apoptosis. *J Biol Chem,* 288**,** 26027-38.

MACUREK, L., LINDQVIST, A., LIM, D., LAMPSON, M. A., KLOMPMAKER, R., FREIRE, R., CLOUIN, C., TAYLOR, S. S., YAFFE, M. B. & MEDEMA, R. H. 2008. Polo-like kinase-1 is activated by aurora A to promote checkpoint recovery. *Nature,* 455**,** 119-23.

MAEHAMA, T. & DIXON, J. E. 1998. The tumor suppressor, PTEN/MMAC1, dephosphorylates the lipid second messenger, phosphatidylinositol 3,4,5-trisphosphate. *J Biol Chem,* 273**,** 13375-8.

MALI, P., YANG, L., ESVELT, K. M., AACH, J., GUELL, M., DICARLO, J. E., NORVILLE, J. E. & CHURCH, G. M. 2013. RNA-guided human genome engineering via Cas9. *Science,* 339**,** 823-6.

MALUMBRES, M. & BARBACID, M. 2001. To cycle or not to cycle: a critical decision in cancer. *Nat Rev Cancer,* 1**,** 222-31.

MARANI, M., HANCOCK, D., LOPES, R., TENEV, T., DOWNWARD, J. & LEMOINE, N. R. 2004. Role of Bim in the survival pathway induced by Raf in epithelial cells. *Oncogene,* 23**,** 2431-41.

MARCASSA, E., KALLINOS, A., JARDINE, J., RUSILOWICZ-JONES, E. V., MARTINEZ, A., KUEHL, S., ISLINGER, M., CLAGUE, M. J. & URBE, S. 2018. Dual role of USP30 in controlling basal pexophagy and mitophagy. *EMBO Rep,* 19**,** 12 .

MARK, K. G., LOVELESS, T. B. & TOCZYSKI, D. P. 2016. Isolation of ubiquitinated substrates by tandem affinity purification of E3 ligase-polyubiquitin-binding domain fusions (ligase traps). *Nat Protoc,* 11**,** 291-301.

MARK, K. G., SIMONETTA, M., MAIOLICA, A., SELLER, C. A. & TOCZYSKI, D. P. 2014. Ubiquitin ligase trapping identifies an SCF(Saf1) pathway targeting unprocessed vacuolar/lysosomal proteins. *Mol Cell,* 53**,** 148-61.

MARKS, J. L., GONG, Y., CHITALE, D., GOLAS, B., MCLELLAN, M. D., KASAI, Y., DING, L., MARDIS, E. R., WILSON, R. K., SOLIT, D., LEVINE, R., MICHEL, K., THOMAS, R. K., RUSCH, V. W., LADANYI, M. & PAO, W. 2008. Novel MEK1 mutation identified by mutational analysis of epidermal growth factor receptor signaling pathway genes in lung adenocarcinoma. *Cancer Res,* 68**,** 5524-8.

MARTENS-DE KEMP, S. R., NAGEL, R., STIGTER-VAN WALSUM, M., VAN DER MEULEN, I. H., VAN BEUSECHEM, V. W., BRAAKHUIS, B. J. & BRAKENHOFF, R. H. 2013. Functional genetic screens identify genes essential for tumor cell survival in head and neck and lung cancer. *Clin Cancer Res,* 19**,** 1994-2003.

MARTIN, Y., CABRERA, E., AMOEDO, H., HERNANDEZ-PEREZ, S., DOMINGUEZ-KELLY, R. & FREIRE, R. 2015. USP29 controls the stability of checkpoint adaptor Claspin by deubiquitination. *Oncogene,* 34**,** 1058-63.

MASOUMI-MOGHADDAM, S., AMINI, A. & MORRIS, D. L. 2014. The developing story of Sprouty and cancer. *Cancer Metastasis Rev,* 33**,** 695-720.

MATSUDA, N., SATO, S., SHIBA, K., OKATSU, K., SAISHO, K., GAUTIER, C. A., SOU, Y.-S., SAIKI, S., KAWAJIRI, S., SATO, F., KIMURA, M., KOMATSU, M., HATTORI, N. & TANAKA, K. 2010. PINK1 stabilized by mitochondrial depolarization recruits Parkin to damaged mitochondria and activates latent Parkin for mitophagy. *J Cell Biol,* 189**,** 211-221.

MATSUURA, K., HUANG, N. J., COCCE, K., ZHANG, L. & KORNBLUTH, S. 2016. Downregulation of the proapoptotic protein MOAP-1 by the UBR5 ubiquitin ligase and its role in ovarian cancer resistance to cisplatin. *Oncogene,* 36**,** 1698.

MAURER, U., CHARVET, C., WAGMAN, A. S., DEJARDIN, E. & GREEN, D. R. 2006. Glycogen synthase kinase-3 regulates mitochondrial outer membrane permeabilization and apoptosis by destabilization of MCL-1. *Mol Cell,* 21**,** 749-60.

MCCULLOUGH, J., CLAGUE, M. J. & URBE, S. 2004. AMSH is an endosome-associated ubiquitin isopeptidase. *J Cell Biol,* 166**,** 487-92.

MCCULLOUGH, J., ROW, P. E., LORENZO, O., DOHERTY, M., BEYNON, R., CLAGUE, M. J. & URBE, S. 2006. Activation of the endosome-associated ubiquitin isopeptidase AMSH by STAM, a component of the multivesicular body-sorting machinery. *Curr Biol,* 16**,** 160-5.

MCDONNELL, J. M., FUSHMAN, D., MILLIMAN, C. L., KORSMEYER, S. J. & COWBURN, D. 1999. Solution structure of the proapoptotic molecule BID: a structural basis for apoptotic agonists and antagonists. *Cell,* 96**,** 625-34.

MCGOURAN, J. F., KRAMER, H. B., MACKEEN, M. M., DI GLERIA, K., ALTUN, M. & KESSLER, B. M. 2012. Fluorescence-based active site probes for profiling deubiquitinating enzymes. *Org Biomol Chem,* 10**,** 3379-83.

MCILWAIN, D. R., BERGER, T. & MAK, T. W. 2013. Caspase functions in cell death and disease. *Cold Spring Harb Perspect Biol,* 5**,** a008656.

MEBRATU, Y. & TESFAIGZI, Y. 2009. How ERK1/2 Activation Controls Cell Proliferation and Cell Death Is Subcellular Localization the Answer? *Cell Cycle,* 8**,** 1168-1175.

MEI, Y., DU, W., YANG, Y. & WU, M. 2005. Puma*Mcl-1 interaction is not sufficient to prevent rapid degradation of Mcl-1. *Oncogene,* 24**,** 7224.

MENG, W., SAWASDIKOSOL, S., BURAKOFF, S. J. & ECK, M. J. 1999. Structure of the amino-terminal domain of Cbl complexed to its binding site on ZAP-70 kinase. *Nature,* 398**,** 84-90.

MENG, Z., MOROISHI, T. & GUAN, K.-L. 2016. Mechanisms of Hippo pathway regulation. *Genes Dev,* 30**,** 1-17.

MENON, S. & MANNING, B. D. 2008. Common corruption of the mTOR signaling network in human tumors. *Oncogene,* 27**,** 352.

MERINO, D., WHITTLE, J. R., VAILLANT, F., SERRANO, A., GONG, J.-N., GINER, G., MARAGNO, A. L., CHANRION, M., SCHNEIDER, E., PAL, B., LI, X., DEWSON, G., GRÄSEL, J., LIU, K., LALAOUI, N., SEGAL, D., HEROLD, M. J., HUANG, D. C. S., SMYTH, G. K., GENESTE, O., LESSENE, G., VISVADER, J. E. & LINDEMAN, G. J. 2017. Synergistic action of the MCL-1 inhibitor S63845 with current therapies in preclinical models of triple-negative and HER2-amplified breast cancer. *Science Translational Medicine,* 9.

METZGER, M. B., HRISTOVA, V. A. & WEISSMAN, A. M. 2012. HECT and RING finger families of E3 ubiquitin ligases at a glance. *J Cell Sci,* 125**,** 531-7.

MEVISSEN, T. E., HOSPENTHAL, M. K., GEURINK, P. P., ELLIOTT, P. R., AKUTSU, M., ARNAUDO, N., EKKEBUS, R., KULATHU, Y., WAUER, T., EL OUALID, F., FREUND, S. M., OVAA, H. & KOMANDER, D. 2013. OTU deubiquitinases reveal mechanisms of linkage specificity and enable ubiquitin chain restriction analysis. *Cell,* 154**,** 169-84.

MEVISSEN, T. E. T. & KOMANDER, D. 2017. Mechanisms of Deubiquitinase Specificity and Regulation. *Annu Rev Biochem,* 86**,** 159-192.

MIYOSHI, Y., NAKAYAMA, S., TORIKOSHI, Y., TANAKA, S., ISHIHARA, H., TAGUCHI, T., TAMAKI, Y. & NOGUCHI, S. 2006. High expression of ubiquitin carboxy-terminal hydrolase-L1 and -L3 mRNA predicts early recurrence in patients with invasive breast cancer. *Cancer Sci,* 97**,** 523-9.

MIZUNO, E., IURA, T., MUKAI, A., YOSHIMORI, T., KITAMURA, N. & KOMADA, M. 2005. Regulation of epidermal growth factor receptor down-regulation by UBPY-mediated deubiquitination at endosomes. *Mol Biol Cell,* 16**,** 5163-74.

MIZUNO, E., KITAMURA, N. & KOMADA, M. 2007. 14-3-3-dependent inhibition of the deubiquitinating activity of UBPY and its cancellation in the M phase. *Exp Cell Res,* 313**,** 3624-3634.

MOJSA, B., LASSOT, I. & DESAGHER, S. 2014. Mcl-1 Ubiquitination: Unique Regulation of an Essential Survival Protein. *Cells,* 3**,** 418-437.

MOLDOVEANU, T., GRACE, C. R., LLAMBI, F., NOURSE, A., FITZGERALD, P., GEHRING, K., KRIWACKI, R. W. & GREEN, D. R. 2013. BID-induced structural changes in BAK promote apoptosis. *Nat Struct Mol Biol,* 20**,** 589-97.

MONTAGUT, C., SHARMA, S. V., SHIODA, T., MCDERMOTT, U., ULMAN, M., ULKUS, L. E., DIAS-SANTAGATA, D., STUBBS, H., LEE, D. Y., SINGH, A., DREW, L., HABER, D. A. & SETTLEMAN, J. 2008. Elevated CRAF as a potential mechanism of acquired resistance to BRAF inhibition in melanoma. *Cancer Res,* 68**,** 4853-61.

MONTERO, J. & LETAI, A. 2017. Why do BCL-2 inhibitors work and where should we use them in the clinic? *Cell Death Differ,* 25**,** 56.

MORGAN, M. T., HAJ-YAHYA, M., RINGEL, A. E., BANDI, P., BRIK, A. & WOLBERGER, C. 2016. Structural basis for histone H2B deubiquitination by the SAGA DUB module. *Science,* 351**,** 725-8.

MORISHIMA, Y., WANG, A. M., YU, Z., PRATT, W. B., OSAWA, Y. & LIEBERMAN, A. P. 2008. CHIP deletion reveals functional redundancy of E3 ligases in promoting degradation of both signaling proteins and expanded glutamine proteins. *Human Molecular Genetics,* 17**,** 3942-3952.

MORIZANE, Y., HONDA, R., FUKAMI, K. & YASUDA, H. 2005. X-linked inhibitor of apoptosis functions as ubiquitin ligase toward mature caspase-9 and cytosolic Smac/DIABLO. *J Biochem,* 137**,** 125-32.

MORRIS, E. J., JHA, S., RESTAINO, C. R., DAYANANTH, P., ZHU, H., COOPER, A., CARR, D., DENG, Y., JIN, W., BLACK, S., LONG, B., LIU, J., DINUNZIO, E., WINDSOR, W., ZHANG, R., ZHAO, S., ANGAGAW, M. H., PINHEIRO, E. M., DESAI, J., XIAO, L., SHIPPS, G., HRUZA, A., WANG, J., KELLY, J., PALIWAL, S., GAO, X., BABU, B. S., ZHU, L., DAUBLAIN, P., ZHANG, L., LUTTERBACH, B. A., PELLETIER, M. R., PHILIPPAR, U., SILIPHAIVANH, P., WITTER, D., KIRSCHMEIER, P., BISHOP, W. R., HICKLIN, D., GILLILAND, D. G., JAYARAMAN, L., ZAWEL, L., FAWELL, S. & SAMATAR, A. A. 2013. Discovery of a Novel ERK Inhibitor with Activity in Models of Acquired Resistance to BRAF and MEK Inhibitors. *Cancer Discov,* 3**,** 742-750.

MOUSTAFA-KAMAL, M., GAMACHE, I., LU, Y., LI, S. & TEODORO, J. G. 2013. BimEL is phosphorylated at mitosis by Aurora A and targeted for degradation by betaTrCP1. *Cell Death Differ,* 20**,** 1393-403.

MURALI, R., WIESNER, T. & SCOLYER, R. A. 2013. Tumours associated with BAP1 mutations. *Pathology,* 45**,** 116-26.

MUSONE, S. L., TAYLOR, K. E., LU, T. T., NITITHAM, J., FERREIRA, R. C., ORTMANN, W., SHIFRIN, N., PETRI, M. A., KAMBOH, M. I., MANZI, S., SELDIN, M. F., GREGERSEN, P. K., BEHRENS, T. W., MA, A., KWOK, P. Y. & CRISWELL, L. A. 2008. Multiple polymorphisms in the TNFAIP3 region are independently associated with systemic lupus erythematosus. *Nat Genet,* 40**,** 1062-4.

NADEAU, R. J., TOHER, J. L., YANG, X., KOVALENKO, D. & FRIESEL, R. 2007. Regulation of Sprouty2 stability by mammalian Seven-in-Absentia homolog 2. *J Cell Biochem,* 100**,** 151-60.

NAKAGAWA, T., ARAKI, T., NAKAGAWA, M., HIRAO, A., UNNO, M. & NAKAYAMA, K. 2015. S6 Kinase- and β-TrCP2-Dependent Degradation of p19(Arf) Is Required for Cell Proliferation. *Mol Cell Biol,* 35**,** 3517-3527.

NAKAJIMA, W. & TANAKA, N. 2007. Synergistic induction of apoptosis by p53-inducible Bcl-2 family proteins Noxa and Puma. *J Nippon Med Sch,* 74**,** 148-57.

NAKAMURA, N. & HIROSE, S. 2008. Regulation of mitochondrial morphology by USP30, a deubiquitinating enzyme present in the mitochondrial outer membrane. *Mol Biol Cell,* 19**,** 1903-11.

NARENDRA, D., TANAKA, A., SUEN, D. F. & YOULE, R. J. 2008. Parkin is recruited selectively to impaired mitochondria and promotes their autophagy. *J Cell Biol,* 183**,** 795-803.

NARENDRA, D. P. & YOULE, R. J. 2011. Targeting mitochondrial dysfunction: role for PINK1 and Parkin in mitochondrial quality control. *Antioxid Redox Signal,* 14**,** 1929-38.

NAZARIAN, R., SHI, H., WANG, Q., KONG, X., KOYA, R. C., LEE, H., CHEN, Z., LEE, M. K., ATTAR, N., SAZEGAR, H., CHODON, T., NELSON, S. F., MCARTHUR, G., SOSMAN, J. A., RIBAS, A. & LO, R. S. 2010. Melanomas acquire resistance to B-RAF(V600E) inhibition by RTK or N-RAS upregulation. *Nature,* 468**,** 973-7.

NEGRINI, S., GORGOULIS, V. G. & HALAZONETIS, T. D. 2010. Genomic instability--an evolving hallmark of cancer. *Nat Rev Mol Cell Biol,* 11**,** 220-8.

NICKLAS, S., HILLJE, A.-L., OKAWA, S., RUDOLPH, I.-M., COLLMANN, F. M., VAN WUELLEN, T., DEL SOL, A. & SCHWAMBORN, J. C. 2018. A complex of the ubiquitin ligase TRIM32 and the deubiquitinase USP7 balances the level of c-Myc ubiquitination and thereby determines neural stem cell fate specification. *Cell Death & Differentiation,* 26**,** 728-740.

NIENDORF, S., OKSCHE, A., KISSER, A., LOHLER, J., PRINZ, M., SCHORLE, H., FELLER, S., LEWITZKY, M., HORAK, I. & KNOBELOCH, K. P. 2007. Essential role of ubiquitin-specific protease 8 for receptor tyrosine kinase stability and endocytic trafficking in vivo. *Mol Cell Biol,* 27**,** 5029-39.

NIJMAN, S. M., LUNA-VARGAS, M. P., VELDS, A., BRUMMELKAMP, T. R., DIRAC, A. M., SIXMA, T. K. & BERNARDS, R. 2005. A genomic and functional inventory of deubiquitinating enzymes. *Cell,* 123**,** 773-86.

NIKOLAEV, S. I., RIMOLDI, D., ISELI, C., VALSESIA, A., ROBYR, D., GEHRIG, C., HARSHMAN, K., GUIPPONI, M., BUKACH, O., ZOETE, V., MICHIELIN, O., MUEHLETHALER, K., SPEISER, D., BECKMANN, J. S., XENARIOS, I., HALAZONETIS, T. D., JONGENEEL, C. V., STEVENSON, B. J. & ANTONARAKIS, S. E. 2011. Exome sequencing identifies recurrent somatic MAP2K1 and MAP2K2 mutations in melanoma. *Nat Genet,* 44**,** 133-9.

NIPHAKIS, M. J. & CRAVATT, B. F. 2014. Enzyme inhibitor discovery by activity-based protein profiling. *Annu Rev Biochem,* 83**,** 341-77.

NIU, X., BRAHMBHATT, H., MERGENTHALER, P., ZHANG, Z., SANG, J., DAUDE, M., EHLERT, F. G. R., DIEDERICH, W. E., WONG, E., ZHU, W., POGMORE, J., NANDY, J. P., SATYANARAYANA, M., JIMMIDI, R. K., ARYA, P., LEBER, B., LIN, J., CULMSEE, C., YI, J. & ANDREWS, D. W. 2017. A Small-Molecule Inhibitor of Bax and Bak Oligomerization Prevents Genotoxic Cell Death and Promotes Neuroprotection. *Cell Chem Biol,* 24**,** 493-506.

NUNNARI, J. & SUOMALAINEN, A. 2012. Mitochondria: in sickness and in health. *Cell,* 148**,** 1145-59.

NURSE, P. 1990. Universal control mechanism regulating onset of M-phase. *Nature,* 344**,** 503-8.

O'BRIEN, S., MOORE, J. O., BOYD, T. E., LARRATT, L. M., SKOTNICKI, A. B., KOZINER, B., CHANAN-KHAN, A. A., SEYMOUR, J. F., GRIBBEN, J., ITRI, L. M. & RAI, K. R. 2009. 5-year survival in patients with relapsed or refractory chronic lymphocytic leukemia in a randomized, phase III trial of fludarabine plus cyclophosphamide with or without oblimersen. *J Clin Oncol,* 27**,** 5208-12.

O'CONNOR, L., STRASSER, A., O'REILLY, L. A., HAUSMANN, G., ADAMS, J. M., CORY, S. & HUANG, D. C. 1998. Bim: a novel member of the Bcl-2 family that promotes apoptosis. *Embo j,* 17**,** 384-95.

O'NEILL, K. L., HUANG, K., ZHANG, J., CHEN, Y. & LUO, X. 2016. Inactivation of prosurvival Bcl-2 proteins activates Bax/Bak through the outer mitochondrial membrane. *Genes Dev,* 30**,** 973-88.

O, B., E, E., L.L, P., J, K. & DIEHL, J. A. 2009. Lysine 269 is essential for cyclin D1 ubiquitylation by the SCF(Fbx4/αB-crystallin) ligase and subsequent proteasome-dependent degradation. *Oncogene,* 28**,** 4317-4325.

OBEROI-KHANUJA, T. K., MURALI, A. & RAJALINGAM, K. 2013. IAPs on the move: role of inhibitors of apoptosis proteins in cell migration. *Cell Death Dis,* 5**,** 311.

OBERST, A., POP, C., TREMBLAY, A. G., BLAIS, V., DENAULT, J. B., SALVESEN, G. S. & GREEN, D. R. 2010. Inducible dimerization and inducible cleavage reveal a requirement for both processes in caspase-8 activation. *J Biol Chem,* 285**,** 16632-42.

OH, K. H., YANG, S. W., PARK, J. M., SEOL, J. H., IEMURA, S., NATSUME, T., MURATA, S., TANAKA, K., JEON, Y. J. & CHUNG, C. H. 2011. Control of AIF-mediated cell death by antagonistic functions of CHIP ubiquitin E3 ligase and USP2 deubiquitinating enzyme. *Cell Death Differ,* 18**,** 1326-36.

OH, K. J., SINGH, P., LEE, K., FOSS, K., LEE, S., PARK, M., LEE, S., ALUVILA, S., PARK, M., SINGH, P., KIM, R. S., SYMERSKY, J. & WALTERS, D. E. 2010. Conformational changes in BAK, a pore-forming proapoptotic Bcl-2 family member, upon membrane insertion and direct evidence for the existence of BH3-BH3 contact interface in BAK homo-oligomers. *J Biol Chem,* 285**,** 28924-37.

OHTAKE, F., TSUCHIYA, H., SAEKI, Y. & TANAKA, K. 2018. K63 ubiquitylation triggers proteasomal degradation by seeding branched ubiquitin chains. *Proceedings of the National Academy of Sciences,* 115**,** 1401-1408.

OI, N., YUAN, J., MALAKHOVA, M., LUO, K., LI, Y., RYU, J., ZHANG, L., BODE, A. M., XU, Z., LI, Y., LOU, Z. & DONG, Z. 2015. Resveratrol induces apoptosis by directly targeting Ras-GTPase-activating protein SH3 domain-binding protein 1. *Oncogene,* 34**,** 2660-71.

OJESINA, A. I., LICHTENSTEIN, L., FREEMAN, S. S., PEDAMALLU, C. S., IMAZ-ROSSHANDLER, I., PUGH, T. J., CHERNIACK, A. D., AMBROGIO, L., CIBULSKIS, K., BERTELSEN, B., ROMERO-CORDOBA, S., TREVIÑO, V., VAZQUEZ-SANTILLAN, K., GUADARRAMA, A. S., WRIGHT, A. A., ROSENBERG, M. W., DUKE, F., KAPLAN, B., WANG, R., NICKERSON, E., WALLINE, H. M., LAWRENCE, M. S., STEWART, C., CARTER, S. L., MCKENNA, A., RODRIGUEZ-SANCHEZ, I. P., ESPINOSA-CASTILLA, M., WOIE, K., BJORGE, L., WIK, E., HALLE, M. K., HOIVIK, E. A., KRAKSTAD, C., GABIÑO, N. B., GÓMEZ-MACÍAS, G. S., VALDEZ-CHAPA, L. D., GARZA-RODRÍGUEZ, M. L., MAYTORENA, G., VAZQUEZ, J., RODEA, C., CRAVIOTO, A., CORTES, M. L., GREULICH, H., CRUM, C. P., NEUBERG, D. S., HIDALGO-MIRANDA, A., ESCARENO, C. R., AKSLEN, L. A., CAREY, T. E., VINTERMYR, O. K., GABRIEL, S. B., BARRERA-SALDAÑA, H. A., MELENDEZ-ZAJGLA, J., GETZ, G., SALVESEN, H. B. & MEYERSON, M. 2013. Landscape of genomic alterations in cervical carcinomas. *Nature,* 506**,** 371.

OKAMOTO, T., ZOBEL, K., FEDOROVA, A., QUAN, C., YANG, H., FAIRBROTHER, W. J., HUANG, D. C., SMITH, B. J., DESHAYES, K. & CZABOTAR, P. E. 2013. Stabilizing the pro-apoptotic BimBH3 helix (BimSAHB) does not necessarily enhance affinity or biological activity. *ACS Chem Biol,* 8**,** 297-302.

OKUDA, M., HORN, H. F., TARAPORE, P., TOKUYAMA, Y., SMULIAN, A. G., CHAN, P. K., KNUDSEN, E. S., HOFMANN, I. A., SNYDER, J. D., BOVE, K. E. & FUKASAWA, K. 2000. Nucleophosmin/B23 is a target of CDK2/cyclin E in centrosome duplication. *Cell,* 103**,** 127-40.

OLTERSDORF, T., ELMORE, S. W., SHOEMAKER, A. R., ARMSTRONG, R. C., AUGERI, D. J., BELLI, B. A., BRUNCKO, M., DECKWERTH, T. L., DINGES, J., HAJDUK, P. J., JOSEPH, M. K., KITADA, S., KORSMEYER, S. J., KUNZER, A. R., LETAI, A., LI, C., MITTEN, M. J., NETTESHEIM, D. G., NG, S., NIMMER, P. M., O'CONNOR, J. M., OLEKSIJEW, A., PETROS, A. M., REED, J. C., SHEN, W., TAHIR, S. K., THOMPSON, C. B., TOMASELLI, K. J., WANG, B., WENDT, M. D., ZHANG, H., FESIK, S. W. & ROSENBERG, S. H. 2005. An inhibitor of Bcl-2 family proteins induces regression of solid tumours. *Nature,* 435**,** 677-81.

ORIAN, A., GONEN, H., BERCOVICH, B., FAJERMAN, I., EYTAN, E., ISRAEL, A., MERCURIO, F., IWAI, K., SCHWARTZ, A. L. & CIECHANOVER, A. 2000. SCF(beta)(-TrCP) ubiquitin ligase-mediated processing of NF-kappaB p105 requires phosphorylation of its C-terminus by IkappaB kinase. *Embo j,* 19**,** 2580-91.

ORLOWSKI, R. Z. 1999. The role of the ubiquitin-proteasome pathway in apoptosis. *Cell Death Differ,* 6**,** 303-13.

ORMANDY, C. J., MUSGROVE, E. A., HUI, R., DALY, R. J. & SUTHERLAND, R. L. 2003. Cyclin D1, EMS1 and 11q13 amplification in breast cancer. *Breast Cancer Res Treat,* 78**,** 323-35.

ORTHWEIN, A., NOORDERMEER, S. M., WILSON, M. D., LANDRY, S., ENCHEV, R. I., SHERKER, A., MUNRO, M., PINDER, J., SALSMAN, J., DELLAIRE, G., XIA, B., PETER, M. & DUROCHER, D. 2015. A mechanism for the suppression of homologous recombination in G1 cells. *Nature,* 528**,** 422-6.

OUCHIDA, A. T., KACAL, M., ZHENG, A., AMBROISE, G., ZHANG, B., NORBERG, E. & VAKIFAHMETOGLU-NORBERG, H. 2018. USP10 regulates the stability of the EMT-transcription factor Slug/SNAI2. *Biochem Biophys Res Commun,* 502**,** 429-434.

OZAKI, K., KADOMOTO, R., ASATO, K., TANIMURA, S., ITOH, N. & KOHNO, M. 2001. ERK pathway positively regulates the expression of Sprouty genes. *Biochem Biophys Res Commun,* 285**,** 1084-8.

PAN, D. 2010. The Hippo Signaling Pathway in Development and Cancer. *Dev Cell,* 19**,** 491-505.
PAN, R., RUVOLO, V. R., WEI, J., KONOPLEVA, M., REED, J. C., PELLECCHIA, M., ANDREEFF, M. & RUVOLO, P. P. 2015. Inhibition of Mcl-1 with the pan-Bcl-2 family inhibitor (-)BI97D6 overcomes ABT-737 resistance in acute myeloid leukemia. *Blood,* 126**,** 363-372.
PARRISH, A. B., FREEL, C. D. & KORNBLUTH, S. 2013. Cellular mechanisms controlling caspase activation and function. *Cold Spring Harb Perspect Biol,* 5**,** 1-24.
PATTINGRE, S., TASSA, A., QU, X., GARUTI, R., LIANG, X. H., MIZUSHIMA, N., PACKER, M., SCHNEIDER, M. D. & LEVINE, B. 2005. Bcl-2 antiapoptotic proteins inhibit Beclin 1-dependent autophagy. *Cell,* 122**,** 927-39.
PAU, G., WALTER, T., NEUMANN, B., HÉRICHÉ, J.-K., ELLENBERG, J. & HUBER, W. 2013. Dynamical modelling of phenotypes in a genome-wide RNAi live-cell imaging assay. *BMC Bioinformatics,* 14**,** 308-308.
PENG, J., SCHWARTZ, D., ELIAS, J. E., THOREEN, C. C., CHENG, D., MARSISCHKY, G., ROELOFS, J., FINLEY, D. & GYGI, S. P. 2003. A proteomics approach to understanding protein ubiquitination. *Nat Biotechnol,* 21**,** 921-6.
PENG, R., TONG, J. S., LI, H., YUE, B., ZOU, F., YU, J. & ZHANG, L. 2013. Targeting Bax interaction sites reveals that only homo-oligomerization sites are essential for its activation. *Cell Death Differ,* 20**,** 744-54.
PEREZ-MANCERA, P. A., RUST, A. G., VAN DER WEYDEN, L., KRISTIANSEN, G., LI, A., SARVER, A. L., SILVERSTEIN, K. A., GRUTZMANN, R., AUST, D., RUMMELE, P., KNOSEL, T., HERD, C., STEMPLE, D. L., KETTLEBOROUGH, R., BROSNAN, J. A., LI, A., MORGAN, R., KNIGHT, S., YU, J., STEGEMAN, S., COLLIER, L. S., TEN HOEVE, J. J., DE RIDDER, J., KLEIN, A. P., GOGGINS, M., HRUBAN, R. H., CHANG, D. K., BIANKIN, A. V., GRIMMOND, S. M., WESSELS, L. F., WOOD, S. A., IACOBUZIO-DONAHUE, C. A., PILARSKY, C., LARGAESPADA, D. A., ADAMS, D. J. & TUVESON, D. A. 2012. The deubiquitinase USP9X suppresses pancreatic ductal adenocarcinoma. *Nature,* 486**,** 266-70.
PERIMENIS, P., GALARIS, A., VOULGARI, A., PRASSA, M. & PINTZAS, A. 2016. IAP antagonists Birinapant and AT-406 efficiently synergise with either TRAIL, BRAF, or BCL-2 inhibitors to sensitise BRAFV600E colorectal tumour cells to apoptosis. *BMC Cancer,* 16**,** 016-2606.
PERSENGIEV, S. P., ZHU, X. & GREEN, M. R. 2004. Nonspecific, concentration-dependent stimulation and repression of mammalian gene expression by small interfering RNAs (siRNAs). *Rna,* 10**,** 12-8.
PESCHARD, P. & PARK, M. 2003. Escape from Cbl-mediated downregulation: a recurrent theme for oncogenic deregulation of receptor tyrosine kinases. *Cancer Cell,* 3**,** 519-23.
PICKART, C. M. 2001. Mechanisms underlying ubiquitination. *Annu Rev Biochem,* 70**,** 503-33.
PIHAN, P., CARRERAS-SUREDA, A. & HETZ, C. 2017. BCL-2 family: integrating stress responses at the ER to control cell demise. *Cell Death Differ,* 24**,** 1478-1487.
PLANAS-SILVA, M. D. & WEINBERG, R. A. 1997. The restriction point and control of cell proliferation. *Curr Opin Cell Biol,* 9**,** 768-72.
PLENGE, R. M., COTSAPAS, C., DAVIES, L., PRICE, A. L., DE BAKKER, P. I., MALLER, J., PE'ER, I., BURTT, N. P., BLUMENSTIEL, B., DEFELICE, M., PARKIN, M., BARRY, R., WINSLOW, W., HEALY, C., GRAHAM, R. R., NEALE, B. M., IZMAILOVA, E., ROUBENOFF, R., PARKER, A. N., GLASS, R., KARLSON, E. W., MAHER, N., HAFLER, D. A., LEE, D. M., SELDIN, M. F., REMMERS, E. F., LEE, A. T., PADYUKOV, L., ALFREDSSON, L., COBLYN, J., WEINBLATT, M. E., GABRIEL, S. B., PURCELL, S., KLARESKOG, L., GREGERSEN, P. K., SHADICK, N. A., DALY, M. J. & ALTSHULER, D. 2007. Two independent alleles at 6q23 associated with risk of rheumatoid arthritis. *Nat Genet,* 39**,** 1477-82.
POLYAK, K. & WEINBERG, R. A. 2009. Transitions between epithelial and mesenchymal states: acquisition of malignant and stem cell traits. *Nat Rev Cancer,* 9**,** 265-73.
POPOV, N., WANZEL, M., MADIREDJO, M., ZHANG, D., BEIJERSBERGEN, R., BERNARDS, R., MOLL, R., ELLEDGE, S. J. & EILERS, M. 2007. The ubiquitin-specific protease USP28 is required for MYC stability. *Nat Cell Biol,* 9**,** 765-74.
POULIKAKOS, P. I., PERSAUD, Y., JANAKIRAMAN, M., KONG, X., NG, C., MORICEAU, G., SHI, H., ATEFI, M., TITZ, B., GABAY, M. T., SALTON, M., DAHLMAN, K. B., TADI, M., WARGO, J. A., FLAHERTY, K. T., KELLEY, M. C., MISTELI, T., CHAPMAN, P. B., SOSMAN, J. A., GRAEBER, T. G., RIBAS, A., LO, R. S., ROSEN, N. & SOLIT, D. B. 2011. RAF inhibitor resistance is mediated by dimerization of aberrantly spliced BRAF(V600E). *Nature,* 480**,** 387-90.
POURDEHNAD, M., TRUITT, M. L., SIDDIQI, I. N., DUCKER, G. S., SHOKAT, K. M. & RUGGERO, D. 2013. Myc and mTOR converge on a common node in protein synthesis control that confers synthetic lethality in Myc-driven cancers. *Proc Natl Acad Sci U S A,* 110**,** 11988-93.
PRATILAS, C. A., TAYLOR, B. S., YE, Q., VIALE, A., SANDER, C., SOLIT, D. B. & ROSEN, N. 2009. (V600E)BRAF is associated with disabled feedback inhibition of RAF-MEK signaling and elevated transcriptional output of the pathway. *Proc Natl Acad Sci U S A,* 106**,** 4519-24.
PRIETO, J., LEÓN, M., PONSODA, X., SENDRA, R., BORT, R., FERRER-LORENTE, R., RAYA, A., LÓPEZ-GARCÍA, C. & TORRES, J. 2016. Early ERK1/2 activation promotes DRP1-dependent mitochondrial fission necessary for cell reprogramming. *Nature Communications,* 7**,** 11124.
PUISIEUX, A., BRABLETZ, T. & CARAMEL, J. 2014. Oncogenic roles of EMT-inducing transcription factors. *Nat Cell Biol,* 16**,** 488-94.
PUTCHA, G. V., LE, S., FRANK, S., BESIRLI, C. G., CLARK, K., CHU, B., ALIX, S., YOULE, R. J., LAMARCHE, A., MARONEY, A. C. & JOHNSON, E. M., JR. 2003. JNK-mediated BIM phosphorylation potentiates BAX-dependent apoptosis. *Neuron,* 38**,** 899-914.
PUTCHA, G. V., MOULDER, K. L., GOLDEN, J. P., BOUILLET, P., ADAMS, J. A., STRASSER, A. & JOHNSON, E. M. 2001. Induction of BIM, a proapoptotic BH3-only BCL-2 family member, is critical for neuronal apoptosis. *Neuron,* 29**,** 615-28.

PUTHALAKATH, H., HUANG, D. C., O'REILLY, L. A., KING, S. M. & STRASSER, A. 1999. The proapoptotic activity of the Bcl-2 family member Bim is regulated by interaction with the dynein motor complex. *Mol Cell,* 3**,** 287-96.

PUTHALAKATH, H., O'REILLY, L. A., GUNN, P., LEE, L., KELLY, P. N., HUNTINGTON, N. D., HUGHES, P. D., MICHALAK, E. M., MCKIMM-BRESCHKIN, J., MOTOYAMA, N., GOTOH, T., AKIRA, S., BOUILLET, P. & STRASSER, A. 2007. ER stress triggers apoptosis by activating BH3-only protein Bim. *Cell,* 129**,** 1337-49.

QIU, L., JOAZEIRO, C., FANG, N., WANG, H. Y., ELLY, C., ALTMAN, Y., FANG, D., HUNTER, T. & LIU, Y. C. 2000. Recognition and ubiquitination of Notch by Itch, a hect-type E3 ubiquitin ligase. *J Biol Chem,* 275**,** 35734-7.

QIU, X.-B. & GOLDBERG, A. L. 2002. Nrdp1/FLRF is a ubiquitin ligase promoting ubiquitination and degradation of the epidermal growth factor receptor family member, ErbB3. *Proceedings of the National Academy of Sciences,* 99**,** 14843-14848.

QIU, X. B. & GOLDBERG, A. L. 2005. The membrane-associated inhibitor of apoptosis protein, BRUCE/Apollon, antagonizes both the precursor and mature forms of Smac and caspase-9. *J Biol Chem,* 280**,** 174-82.

QIU, X. B., MARKANT, S. L., YUAN, J. & GOLDBERG, A. L. 2004. Nrdp1-mediated degradation of the gigantic IAP, BRUCE, is a novel pathway for triggering apoptosis. *Embo j,* 23**,** 800-10.

RAHIGHI, S., IKEDA, F., KAWASAKI, M., AKUTSU, M., SUZUKI, N., KATO, R., KENSCHE, T., UEJIMA, T., BLOOR, S., KOMANDER, D., RANDOW, F., WAKATSUKI, S. & DIKIC, I. 2009. Specific recognition of linear ubiquitin chains by NEMO is important for NF-kappaB activation. *Cell,* 136**,** 1098-109.

RAKOVIC, A., GRUNEWALD, A., KOTTWITZ, J., BRUGGEMANN, N., PRAMSTALLER, P. P., LOHMANN, K. & KLEIN, C. 2011. Mutations in PINK1 and Parkin impair ubiquitination of Mitofusins in human fibroblasts. *PLoS One,* 6**,** 0016746.

RAMAKRISHNA, S., SURESH, B. & BAEK, K. H. 2011. The role of deubiquitinating enzymes in apoptosis. *Cell Mol Life Sci,* 68**,** 15-26.

RANGANATHAN, A., PEARSON, G. W., CHRESTENSEN, C. A., STURGILL, T. W. & COBB, M. H. 2006. The MAP kinase ERK5 binds to and phosphorylates p90 RSK. *Arch Biochem Biophys,* 449**,** 8-16.

REDMAN, K. L. & RECHSTEINER, M. 1989. Identification of the long ubiquitin extension as ribosomal protein S27a. *Nature,* 338**,** 438-40.

REEVE, A. K., GRADY, J. P., COSGRAVE, E. M., BENNISON, E., CHEN, C., HEPPLEWHITE, P. D. & MORRIS, C. M. 2018. Mitochondrial dysfunction within the synapses of substantia nigra neurons in Parkinson's disease. *npj Parkinson's Disease,* 4**,** 9.

RENA, G., BAIN, J., ELLIOTT, M. & COHEN, P. 2004. D4476, a cell-permeant inhibitor of CK1, suppresses the site-specific phosphorylation and nuclear exclusion of FOXO1a. *EMBO Rep,* 5**,** 60-5.

RENA, G., WOODS, Y. L., PRESCOTT, A. R., PEGGIE, M., UNTERMAN, T. G., WILLIAMS, M. R. & COHEN, P. 2002. Two novel phosphorylation sites on FKHR that are critical for its nuclear exclusion. *Embo j,* 21**,** 2263-71.

REVERDY, C., CONRATH, S., LOPEZ, R., PLANQUETTE, C., ATMANENE, C., COLLURA, V., HARPON, J., BATTAGLIA, V., VIVAT, V., SIPPL, W. & COLLAND, F. 2012. Discovery of specific inhibitors of human USP7/HAUSP deubiquitinating enzyme. *Chem Biol,* 19**,** 467-77.

REYES-TURCU, F. E., VENTII, K. H. & WILKINSON, K. D. 2009. Regulation and cellular roles of ubiquitin-specific deubiquitinating enzymes. *Annu Rev Biochem,* 78**,** 363-97.

REYSKENS, K. M. S. E. & ARTHUR, J. S. C. 2016. Emerging Roles of the Mitogen and Stress Activated Kinases MSK1 and MSK2. *Frontiers in Cell and Developmental Biology,* 4**,** 56.

RICHARDSON, P. G., HIDESHIMA, T. & ANDERSON, K. C. 2003. Bortezomib (PS-341): a novel, first-in-class proteasome inhibitor for the treatment of multiple myeloma and other cancers. *Cancer Control,* 10**,** 361-9.

RIEDL, S. J. & SALVESEN, G. S. 2007. The apoptosome: signalling platform of cell death. *Nat Rev Mol Cell Biol,* 8**,** 405-13.

RIEDL, S. J. & SHI, Y. 2004. Molecular mechanisms of caspase regulation during apoptosis. *Nat Rev Mol Cell Biol,* 5**,** 897-907.

RINEHART, J., ADJEI, A. A., LORUSSO, P. M., WATERHOUSE, D., HECHT, J. R., NATALE, R. B., HAMID, O., VARTERASIAN, M., ASBURY, P., KALDJIAN, E. P., GULYAS, S., MITCHELL, D. Y., HERRERA, R., SEBOLT-LEOPOLD, J. S. & MEYER, M. B. 2004. Multicenter phase II study of the oral MEK inhibitor, CI-1040, in patients with advanced non-small-cell lung, breast, colon, and pancreatic cancer. *J Clin Oncol,* 22**,** 4456-62.

RISTIC, G., TSOU, W. L. & TODI, S. V. 2014. An optimal ubiquitin-proteasome pathway in the nervous system: the role of deubiquitinating enzymes. *Front Mol Neurosci,* 7**,** 72.

RITORTO, M. S., EWAN, R., PEREZ-OLIVA, A. B., KNEBEL, A., BUHRLAGE, S. J., WIGHTMAN, M., KELLY, S. M., WOOD, N. T., VIRDEE, S., GRAY, N. S., MORRICE, N. A., ALESSI, D. R. & TROST, M. 2014. Screening of DUB activity and specificity by MALDI-TOF mass spectrometry. *Nature Communications,* 5**,** 4763.

RITT, D. A., MONSON, D. M., SPECHT, S. I. & MORRISON, D. K. 2010. Impact of feedback phosphorylation and Raf heterodimerization on normal and mutant B-Raf signaling. *Mol Cell Biol,* 30**,** 806-19.

ROBERTS, A. W., SEYMOUR, J. F., BROWN, J. R., WIERDA, W. G., KIPPS, T. J., KHAW, S. L., CARNEY, D. A., HE, S. Z., HUANG, D. C., XIONG, H., CUI, Y., BUSMAN, T. A., MCKEEGAN, E. M., KRIVOSHIK, A. P., ENSCHEDE, S. H. & HUMERICKHOUSE, R. 2012. Substantial susceptibility of chronic lymphocytic leukemia to BCL2 inhibition: results of a phase I study of navitoclax in patients with relapsed or refractory disease. *J Clin Oncol,* 30**,** 488-96.

ROBIN, A. Y., KRISHNA KUMAR, K., WESTPHAL, D., WARDAK, A. Z., THOMPSON, G. V., DEWSON, G., COLMAN, P. M. & CZABOTAR, P. E. 2015. Crystal structure of Bax bound to the BH3 peptide of Bim identifies important contacts for interaction. *Cell Death Dis,* 9**,** 141.

ROBINSON, K. S., CLEMENTS, A., WILLIAMS, A. C., BERGER, C. N. & FRANKEL, G. 2011. Bax inhibitor 1 in apoptosis and disease. *Oncogene,* 30**,** 2391-400.

ROFFE, M., LUPINACCI, F. C., SOARES, L. C., HAJJ, G. N. & MARTINS, V. R. 2015. Two widely used RSK inhibitors, BI-D1870 and SL0101, alter mTORC1 signaling in a RSK-independent manner. *Cell Signal,* 27**,** 1630-42.

ROLEN, U., KOBZEVA, V., GASPARJAN, N., OVAA, H., WINBERG, G., KISSELJOV, F. & MASUCCI, M. G. 2006. Activity profiling of deubiquitinating enzymes in cervical carcinoma biopsies and cell lines. *Mol Carcinog,* 45**,** 260-9.

ROMANO, G., ACUNZO, M., GAROFALO, M., DI LEVA, G., CASCIONE, L., ZANCA, C., BOLON, B., CONDORELLI, G. & CROCE, C. M. 2012. MiR-494 is regulated by ERK1/2 and modulates TRAIL-induced apoptosis in non-small-cell lung cancer through BIM down-regulation. *Proc Natl Acad Sci U S A,* 109**,** 16570-5.

ROMEO, Y., ZHANG, X. & ROUX, P. P. 2012. Regulation and function of the RSK family of protein kinases. *Biochem J,* 441**,** 553-69.

RONG, Y. & DISTELHORST, C. W. 2008. Bcl-2 protein family members: versatile regulators of calcium signaling in cell survival and apoptosis. *Annu Rev Physiol,* 70**,** 73-91.

ROSENWALD, I. B., KASPAR, R., ROUSSEAU, D., GEHRKE, L., LEBOULCH, P., CHEN, J. J., SCHMIDT, E. V., SONENBERG, N. & LONDON, I. M. 1995. Eukaryotic translation initiation factor 4E regulates expression of cyclin D1 at transcriptional and post-transcriptional levels. *J Biol Chem,* 270**,** 21176-80.

ROSKOSKI, R., JR. 2012. MEK1/2 dual-specificity protein kinases: structure and regulation. *Biochem Biophys Res Commun,* 417**,** 5-10.

ROSS, J. M., OLSON, L. & COPPOTELLI, G. 2015. Mitochondrial and Ubiquitin Proteasome System Dysfunction in Ageing and Disease: Two Sides of the Same Coin? *Int J Mol Sci,* 16**,** 19458-76.

ROSSI, M., AQEILAN, R. I., NEALE, M., CANDI, E., SALOMONI, P., KNIGHT, R. A., CROCE, C. M. & MELINO, G. 2006. The E3 ubiquitin ligase Itch controls the protein stability of p63. *Proceedings of the National Academy of Sciences,* 103**,** 12753-12758.

ROUX, P. P., RICHARDS, S. A. & BLENIS, J. 2003. Phosphorylation of p90 ribosomal S6 kinase (RSK) regulates extracellular signal-regulated kinase docking and RSK activity. *Mol Cell Biol,* 23**,** 4796-804.

RUBIN, C., LITVAK, V., MEDVEDOVSKY, H., ZWANG, Y., LEV, S. & YARDEN, Y. 2003. Sprouty fine-tunes EGF signaling through interlinked positive and negative feedback loops. *Curr Biol,* 13**,** 297-307.

RUDIN, C. M., HANN, C. L., GARON, E. B., RIBEIRO DE OLIVEIRA, M., BONOMI, P. D., CAMIDGE, D. R., CHU, Q., GIACCONE, G., KHAIRA, D., RAMALINGAM, S. S., RANSON, M. R., DIVE, C., MCKEEGAN, E. M., CHYLA, B. J., DOWELL, B. L., CHAKRAVARTTY, A., NOLAN, C. E., RUDERSDORF, N., BUSMAN, T. A., MABRY, M. H., KRIVOSHIK, A. P., HUMERICKHOUSE, R. A., SHAPIRO, G. I. & GANDHI, L. 2012. Phase II study of single-agent navitoclax (ABT-263) and biomarker correlates in patients with relapsed small cell lung cancer. *Clin Cancer Res,* 18**,** 3163-9.

RUSHWORTH, L. K., HINDLEY, A. D., O'NEILL, E. & KOLCH, W. 2006. Regulation and role of Raf-1/B-Raf heterodimerization. *Mol Cell Biol,* 26**,** 2262-72.

RUSSO, A. A., JEFFREY, P. D. & PAVLETICH, N. P. 1996. Structural basis of cyclin-dependent kinase activation by phosphorylation. *Nat Struct Biol,* 3**,** 696-700.

RYAN, K. M., PHILLIPS, A. C. & VOUSDEN, K. H. 2001. Regulation and function of the p53 tumor suppressor protein. *Curr Opin Cell Biol,* 13**,** 332-7.

SACCO, J. J., COULSON, J. M., CLAGUE, M. J. & URBE, S. 2010. Emerging roles of deubiquitinases in cancer-associated pathways. *IUBMB Life,* 62**,** 140-57.

SAEI, A. A., SABATIER, P., TOKAT, U. G., CHERNOBROVKIN, A., PIRMORADIAN, M. & ZUBAREV, R. A. 2018. Comparative Proteomics of Dying and Surviving Cancer Cells Improves the Identification of Drug Targets and Sheds Light on Cell Life/Death Decisions. *Mol Cell Proteomics,* 17**,** 1144-1155.

SAHTOE, D. D., VAN DIJK, W. J., EKKEBUS, R., OVAA, H. & SIXMA, T. K. 2016. BAP1/ASXL1 recruitment and activation for H2A deubiquitination. *Nature Communications,* 7**,** 10292.

SALAH, Z., MELINO, G. & AQEILAN, R. I. 2011. Negative regulation of the Hippo pathway by E3 ubiquitin ligase ITCH is sufficient to promote tumorigenicity. *Cancer Res,* 71**,** 2010-20.

SALE, M. J. & COOK, S. J. 2013. The BH3 mimetic ABT-263 synergizes with the MEK1/2 inhibitor selumetinib/AZD6244 to promote BIM-dependent tumour cell death and inhibit acquired resistance. *Biochem J,* 450**,** 285-94.

SALE, M. J. & COOK, S. J. 2014. The increase in BIK expression following ERK1/2 pathway inhibition is a consequence of G(1) cell-cycle arrest and not a direct effect on BIK protein stability. *Biochem J,* 459**,** 513-24.

SALVADOR-GALLEGO, R., MUND, M., COSENTINO, K., SCHNEIDER, J., UNSAY, J., SCHRAERMEYER, U., ENGELHARDT, J., RIES, J. & GARCIA-SAEZ, A. J. 2016. Bax assembly into rings and arcs in apoptotic mitochondria is linked to membrane pores. *Embo j,* 35**,** 389-401.

SAPKOTA, GOPAL P., CUMMINGS, L., NEWELL, FELICITY S., ARMSTRONG, C., BAIN, J., FRODIN, M., GRAUERT, M., HOFFMANN, M., SCHNAPP, G., STEEGMAIER, M., COHEN, P. & ALESSI, DARIO R. 2007. BI-D1870 is a specific inhibitor of the p90 RSK (ribosomal S6 kinase) isoforms in vitro and in vivo. *Biochemical Journal,* 401**,** 29-38.

SARRAF, S. A., RAMAN, M., GUARANI-PEREIRA, V., SOWA, M. E., HUTTLIN, E. L., GYGI, S. P. & HARPER, J. W. 2013. Landscape of the PARKIN-dependent ubiquitylome in response to mitochondrial depolarization. *Nature,* 496**,** 372-6.

SATO, Y., YOSHIKAWA, A., YAMAGATA, A., MIMURA, H., YAMASHITA, M., OOKATA, K., NUREKI, O., IWAI, K., KOMADA, M. & FUKAI, S. 2008. Structural basis for specific cleavage of Lys 63-linked polyubiquitin chains. *Nature,* 455**,** 358-62.

SATTLER, M., LIANG, H., NETTESHEIM, D., MEADOWS, R. P., HARLAN, J. E., EBERSTADT, M., YOON, H. S., SHUKER, S. B., CHANG, B. S., MINN, A. J., THOMPSON, C. B. & FESIK, S. W. 1997. Structure of Bcl-xL-Bak peptide complex: recognition between regulators of apoptosis. *Science,* 275**,** 983-6.

SAXTON, R. A. & SABATINI, D. M. 2017. mTOR Signaling in Growth, Metabolism, and Disease. *Cell,* 168**,** 960-976.

SCHEFFZEK, K., AHMADIAN, M. R., KABSCH, W., WIESMÜLLER, L., LAUTWEIN, A., SCHMITZ, F. & WITTINGHOFER, A. 1997. The Ras-RasGAP Complex: Structural Basis for GTPase Activation and Its Loss in Oncogenic Ras Mutants. *Science,* 277**,** 333-339.

SCHEID, M. P., SCHUBERT, K. M. & DURONIO, V. 1999. Regulation of bad phosphorylation and association with Bcl-x(L) by the MAPK/Erk kinase. *J Biol Chem,* 274**,** 31108-13.

SCHILE, A. J., GARCIA-FERNANDEZ, M. & STELLER, H. 2008. Regulation of apoptosis by XIAP ubiquitin-ligase activity. *Genes Dev,* 22**,** 2256-66.

SCHOENFELD, A. R., APGAR, S., DOLIOS, G., WANG, R. & AARONSON, S. A. 2004a. BRCA2 is ubiquitinated in vivo and interacts with USP11, a deubiquitinating enzyme that exhibits prosurvival function in the cellular response to DNA damage. *Mol Cell Biol,* 24.

SCHOENFELD, A. R., APGAR, S., DOLIOS, G., WANG, R. & AARONSON, S. A. 2004b. BRCA2 is ubiquitinated in vivo and interacts with USP11, a deubiquitinating enzyme that exhibits prosurvival function in the cellular response to DNA damage. *Mol Cell Biol,* 24**,** 7444-55.

SCHULER, M., BOSSY-WETZEL, E., GOLDSTEIN, J. C., FITZGERALD, P. & GREEN, D. R. 2000. p53 induces apoptosis by caspase activation through mitochondrial cytochrome c release. *J Biol Chem,* 275**,** 7337-42.

SCHWARTZ, L. M., MYER, A., KOSZ, L., ENGELSTEIN, M. & MAIER, C. 1990. Activation of polyubiquitin gene expression during developmentally programmed cell death. *Neuron,* 5**,** 411-9.

SCHWICKART, M., HUANG, X., LILL, J. R., LIU, J., FERRANDO, R., FRENCH, D. M., MAECKER, H., O'ROURKE, K., BAZAN, F., EASTHAM-ANDERSON, J., YUE, P., DORNAN, D., HUANG, D. C. & DIXIT, V. M. 2010. Deubiquitinase USP9X stabilizes MCL1 and promotes tumour cell survival. *Nature,* 463**,** 103-7.

SCORRANO, L., OAKES, S. A., OPFERMAN, J. T., CHENG, E. H., SORCINELLI, M. D., POZZAN, T. & KORSMEYER, S. J. 2003. BAX and BAK regulation of endoplasmic reticulum Ca2+: a control point for apoptosis. *Science,* 300**,** 135-9.

SEBOLT-LEOPOLD, J. S., DUDLEY, D. T., HERRERA, R., VAN BECELAERE, K., WILAND, A., GOWAN, R. C., TECLE, H., BARRETT, S. D., BRIDGES, A., PRZYBRANOWSKI, S., LEOPOLD, W. R. & SALTIEL, A. R. 1999. Blockade of the MAP kinase pathway suppresses growth of colon tumors in vivo. *Nat Med,* 5**,** 810-6.

SEKI, A., COPPINGER, J. A., JANG, C. Y., YATES, J. R. & FANG, G. 2008. Bora and the kinase Aurora a cooperatively activate the kinase Plk1 and control mitotic entry. *Science,* 320**,** 1655-8.

SHALINI, S., DORSTYN, L., DAWAR, S. & KUMAR, S. 2015. Old, new and emerging functions of caspases. *Cell Death Differ,* 22**,** 526-39.

SHAO, Y. & APLIN, A. E. 2012. ERK2 phosphorylation of serine 77 regulates Bmf pro-apoptotic activity. *Cell Death Dis,* 3**,** e253.

SHE, Q. B., MA, W. Y., ZHONG, S. & DONG, Z. 2002. Activation of JNK1, RSK2, and MSK1 is involved in serine 112 phosphorylation of Bad by ultraviolet B radiation. *J Biol Chem,* 277**,** 24039-48.

SHEMBADE, N., MA, A. & HARHAJ, E. W. 2010. Inhibition of NF-κB Signaling by A20 Through Disruption of Ubiquitin Enzyme Complexes. *Science,* 327**,** 1135-1139.

SHERR, C. J. & MCCORMICK, F. 2002. The RB and p53 pathways in cancer. *Cancer Cell,* 2**,** 103-12.

SHERR, C. J. & ROBERTS, J. M. 1999. CDK inhibitors: positive and negative regulators of G1-phase progression. *Genes Dev,* 13**,** 1501-12.

SHI, D., POP, M. S., KULIKOV, R., LOVE, I. M., KUNG, A. L. & GROSSMAN, S. R. 2009. CBP and p300 are cytoplasmic E4 polyubiquitin ligases for p53. *Proc Natl Acad Sci U S A,* 106**,** 16275-80.

SHIBA-FUKUSHIMA, K., IMAI, Y., YOSHIDA, S., ISHIHAMA, Y., KANAO, T., SATO, S. & HATTORI, N. 2012. PINK1-mediated phosphorylation of the Parkin ubiquitin-like domain primes mitochondrial translocation of Parkin and regulates mitophagy. *Sci Rep,* 2**,** 19.

SHIMAMURA, A., BALLIF, B. A., RICHARDS, S. A. & BLENIS, J. 2000. Rsk1 mediates a MEK-MAP kinase cell survival signal. *Curr Biol,* 10**,** 127-35.

SHIMANE, K., KOCHI, Y., HORITA, T., IKARI, K., AMANO, H., HIRAKATA, M., OKAMOTO, A., YAMADA, R., MYOUZEN, K., SUZUKI, A., KUBO, M., ATSUMI, T., KOIKE, T., TAKASAKI, Y., MOMOHARA, S., YAMANAKA, H., NAKAMURA, Y. & YAMAMOTO, K. 2010. The association of a nonsynonymous single-nucleotide polymorphism in TNFAIP3 with systemic lupus erythematosus and rheumatoid arthritis in the Japanese population. *Arthritis Rheum,* 62**,** 574-9.

SHIMIZU, K., FUKUSHIMA, H., OGURA, K., LIEN, E. C., NIHIRA, N. T., ZHANG, J., NORTH, B. J., GUO, A., NAGASHIMA, K., NAKAGAWA, T., HOSHIKAWA, S., WATAHIKI, A., OKABE, K., YAMADA, A., TOKER, A., ASARA, J. M., FUKUMOTO, S., NAKAYAMA, K. I., NAKAYAMA, K., INUZUKA, H. & WEI, W. 2017. The SCF^{β-TRCP} E3 ubiquitin ligase complex targets Lipin1 for ubiquitination and degradation to promote hepatic lipogenesis. *Sci Signal,* 10.

SHIN, E. J., SHIN, H. M., NAM, E., KIM, W. S., KIM, J. H., OH, B. H. & YUN, Y. 2012. DeSUMOylating isopeptidase: a second class of SUMO protease. *EMBO Rep,* 13**,** 339-46.

SHINOHARA, K., TOMIOKA, M., NAKANO, H., TONE, S., ITO, H. & KAWASHIMA, S. 1996. Apoptosis induction resulting from proteasome inhibition. *Biochem J,* 317**,** 385-8.

SKAUG, B., CHEN, J., DU, F., HE, J., MA, A. & CHEN, Z. J. 2011. Direct, noncatalytic mechanism of IKK inhibition by A20. *Mol Cell,* 44**,** 559-71.

SKOWYRA, D., CRAIG, K. L., TYERS, M., ELLEDGE, S. J. & HARPER, J. W. 1997. F-box proteins are receptors that recruit phosphorylated substrates to the SCF ubiquitin-ligase complex. *Cell,* 91**,** 209-19.

SONG, H., MAK, K. K., TOPOL, L., YUN, K., HU, J., GARRETT, L., CHEN, Y., PARK, O., CHANG, J., SIMPSON, R. M., WANG, C.-Y., GAO, B., JIANG, J. & YANG, Y. 2010. Mammalian Mst1 and Mst2 kinases play essential roles in organ size control and tumor suppression. *Proceedings of the National Academy of Sciences,* 107**,** 1431-1436.

SOUERS, A. J., LEVERSON, J. D., BOGHAERT, E. R., ACKLER, S. L., CATRON, N. D., CHEN, J., DAYTON, B. D., DING, H., ENSCHEDE, S. H., FAIRBROTHER, W. J., HUANG, D. C., HYMOWITZ, S. G., JIN, S., KHAW, S. L., KOVAR, P. J., LAM, L. T., LEE, J., MAECKER, H. L., MARSH, K. C., MASON, K. D., MITTEN, M. J., NIMMER, P. M., OLEKSIJEW, A., PARK, C. H., PARK, C. M., PHILLIPS, D. C., ROBERTS, A. W., SAMPATH, D., SEYMOUR, J. F., SMITH, M. L., SULLIVAN, G. M., TAHIR, S. K., TSE, C., WENDT, M. D., XIAO, Y., XUE, J. C., ZHANG, H., HUMERICKHOUSE, R. A., ROSENBERG, S. H. & ELMORE, S. W. 2013. ABT-199, a potent and selective BCL-2 inhibitor, achieves antitumor activity while sparing platelets. *Nat Med,* 19**,** 202-8.

SOWA, M. E., BENNETT, E. J., GYGI, S. P. & HARPER, J. W. 2009. Defining the human deubiquitinating enzyme interaction landscape. *Cell,* 138**,** 389-403.

SPRATT, D. E., WALDEN, H. & SHAW, G. S. 2014. RBR E3 ubiquitin ligases: new structures, new insights, new questions. *Biochem J,* 458**,** 421-37.

STEVAUX, O. & DYSON, N. J. 2002. A revised picture of the E2F transcriptional network and RB function. *Curr Opin Cell Biol,* 14**,** 684-91.

STORER, A. C. & MENARD, R. 1994. Catalytic mechanism in papain family of cysteine peptidases. *Methods Enzymol,* 244**,** 486-500.

STRANO, S. & BLANDINO, G. 2007. YAP1 meets tumor suppression. *Mol Cell,* 27**,** 863-4.

STRASSER, A., CORY, S. & ADAMS, J. M. 2011. Deciphering the rules of programmed cell death to improve therapy of cancer and other diseases. *Embo j,* 30**,** 3667-83.

STRASSER, A., JOST, P. J. & NAGATA, S. 2009. The many roles of FAS receptor signaling in the immune system. *Immunity,* 30**,** 180-92.

STRAUB, C. S. 2011. Targeting IAPs as an approach to anti-cancer therapy. *Curr Top Med Chem,* 11**,** 291-316.

STRAUSFELD, U., LABBE, J. C., FESQUET, D., CAVADORE, J. C., PICARD, A., SADHU, K., RUSSELL, P. & DOREE, M. 1991. Dephosphorylation and activation of a p34cdc2/cyclin B complex in vitro by human CDC25 protein. *Nature,* 351**,** 242-5.

SUN, J., LI, T., ZHAO, Y., HUANG, L., SUN, H., WU, H. & JIANG, X. 2018. USP10 inhibits lung cancer cell growth and invasion by upregulating PTEN. *Mol Cell Biochem,* 441**,** 1-7.

SUN, W., TAN, X., SHI, Y., XU, G., MAO, R., GU, X., FAN, Y., YU, Y., BURLINGAME, S., ZHANG, H., REDNAM, S. P., LU, X., ZHANG, T., FU, S., CAO, G., QIN, J. & YANG, J. 2010. USP11 negatively regulates TNFalpha-induced NF-kappaB activation by targeting on IkappaBalpha. *Cell Signal,* 22**,** 386-94.

SUZUKI, M., YOULE, R. J. & TJANDRA, N. 2000. Structure of Bax: coregulation of dimer formation and intracellular localization. *Cell,* 103**,** 645-54.

SUZUKI, Y., NAKABAYASHI, Y. & TAKAHASHI, R. 2001. Ubiquitin-protein ligase activity of X-linked inhibitor of apoptosis protein promotes proteasomal degradation of caspase-3 and enhances its anti-apoptotic effect in Fas-induced cell death. *Proc Natl Acad Sci U S A,* 98**,** 8662-7.

SWATEK, K. N. & KOMANDER, D. 2016. Ubiquitin modifications. *Cell Res,* 26**,** 399-422.

TAIT, S. W. & GREEN, D. R. 2010. Mitochondria and cell death: outer membrane permeabilization and beyond. *Nat Rev Mol Cell Biol,* 11**,** 621-32.

TAIT, S. W. G., DE VRIES, E., MAAS, C., KELLER, A. M., D'SANTOS, C. S. & BORST, J. 2007. Apoptosis induction by Bid requires unconventional ubiquitination and degradation of its N-terminal fragment. *J Cell Biol,* 179**,** 1453-1466.

TAKAHASHI, H., CHEN, M. C., PHAM, H., MATSUO, Y., ISHIGURO, H., REBER, H. A., TAKEYAMA, H., HINES, O. J. & EIBL, G. 2013. Simultaneous knock-down of Bcl-xL and Mcl-1 induces apoptosis through Bax activation in pancreatic cancer cells. *Biochim Biophys Acta,* 12**,** 14.

TAKAI, Y., SASAKI, T. & MATOZAKI, T. 2001. Small GTP-binding proteins. *Physiol Rev,* 81**,** 153-208.

TAKAYAMA, K. I., SUZUKI, T., FUJIMURA, T., TAKAHASHI, S. & INOUE, S. 2018. Association of USP10 with G3BP2 Inhibits p53 Signaling and Contributes to Poor Outcome in Prostate Cancer. *Mol Cancer Res,* 16**,** 846-856.

TAYLOR, W. R. & STARK, G. R. 2001. Regulation of the G2/M transition by p53. *Oncogene,* 20**,** 1803-15.

THIERY, J. P., ACLOQUE, H., HUANG, R. Y. & NIETO, M. A. 2009. Epithelial-mesenchymal transitions in development and disease. *Cell,* 139**,** 871-90.

THOMPSON, S., PEARSON, A. N., ASHLEY, M. D., JESSICK, V., MURPHY, B. M., GAFKEN, P., HENSHALL, D. C., MORRIS, K. T., SIMON, R. P. & MELLER, R. 2011. Identification of a novel Bcl-2-interacting mediator of cell death (Bim) E3 ligase, tripartite motif-containing protein 2 (TRIM2), and its role in rapid ischemic tolerance-induced neuroprotection. *J Biol Chem,* 286**,** 19331-9.

THOMSON, W., BARTON, A., KE, X., EYRE, S., HINKS, A., BOWES, J., DONN, R., SYMMONS, D., HIDER, S., BRUCE, I. N., WILSON, A. G., MARINOU, I., MORGAN, A., EMERY, P., CARTER, A., STEER, S., HOCKING, L., REID, D. M., WORDSWORTH, P., HARRISON, P., STRACHAN, D. & WORTHINGTON, J. 2007. Rheumatoid arthritis association at 6q23. *Nat Genet,* 39**,** 1431-3.

TIACCI, E., PARK, J. H., DE CAROLIS, L., CHUNG, S. S., BROCCOLI, A., SCOTT, S., ZAJA, F., DEVLIN, S., PULSONI, A., CHUNG, Y. R., CIMMINIELLO, M., KIM, E., ROSSI, D., STONE, R. M., MOTTA, G., SAVEN, A., VARETTONI, M., ALTMAN, J. K., ANASTASIA, A., GREVER, M. R., AMBROSETTI, A., RAI, K. R., FRATICELLI, V., LACOUTURE, M. E., CARELLA, A. M., LEVINE, R. L., LEONI, P., RAMBALDI, A., FALZETTI, F., ASCANI, S., CAPPONI, M., MARTELLI, M. P., PARK, C. Y., PILERI, S. A., ROSEN, N., FOA, R., BERGER, M. F., ZINZANI, P. L., ABDEL-WAHAB, O., FALINI, B. & TALLMAN, M. S. 2015. Targeting Mutant BRAF in Relapsed or Refractory Hairy-Cell Leukemia. *N Engl J Med,* 373**,** 1733-47.

TIAN, X., ISAMIDDINOVA, N. S., PEROUTKA, R. J., GOLDENBERG, S. J., MATTERN, M. R., NICHOLSON, B. & LEACH, C. 2011. Characterization of selective ubiquitin and ubiquitin-like protease inhibitors using a fluorescence-based multiplex assay format. *Assay Drug Dev Technol,* 9**,** 165-73.

TOKUNAGA, F., NAKAGAWA, T., NAKAHARA, M., SAEKI, Y., TANIGUCHI, M., SAKATA, S., TANAKA, K., NAKANO, H. & IWAI, K. 2011. SHARPIN is a component of the NF-kappaB-activating linear ubiquitin chain assembly complex. *Nature,* 471**,** 633-6.

TOKUNAGA, F., SAKATA, S.-I., SAEKI, Y., SATOMI, Y., KIRISAKO, T., KAMEI, K., NAKAGAWA, T., KATO, M., MURATA, S., YAMAOKA, S., YAMAMOTO, M., AKIRA, S., TAKAO, T., TANAKA, K. & IWAI, K. 2009. Involvement of linear polyubiquitylation of NEMO in NF-κB activation. *Nat Cell Biol,* 11**,** 123.

TOTSUKAWA, G., KANEKO, Y., UCHIYAMA, K., TOH, H., TAMURA, K. & KONDO, H. 2011. VCIP135 deubiquitinase and its binding protein, WAC, in p97ATPase-mediated membrane fusion. *Embo j,* 30**,** 3581-93.

TOUZEAU, C., RYAN, J., GUERRIERO, J., MOREAU, P., CHONGHAILE, T. N., LE GOUILL, S., RICHARDSON, P., ANDERSON, K., AMIOT, M. & LETAI, A. 2016. *BH3 profiling identifies heterogeneous dependency on Bcl-2 family members in multiple myeloma and predicts sensitivity to BH3 mimetics*, Leukemia. 2016 Mar;30(3):761-4. doi: 10.1038/leu.2015.184. Epub 2015 Jul 15.

TRAHEY, M. & MCCORMICK, F. 1987. A cytoplasmic protein stimulates normal N-ras p21 GTPase, but does not affect oncogenic mutants. *Science,* 238**,** 542-5.

TRAN, N. H., WU, X. & FROST, J. A. 2005. B-Raf and Raf-1 are regulated by distinct autoregulatory mechanisms. *J Biol Chem,* 280**,** 16244-53.

TRIPATHI, K. & GARG, M. 2018. Mechanistic regulation of epithelial-to-mesenchymal transition through RAS signaling pathway and therapeutic implications in human cancer. *J Cell Commun Signal,* 12**,** 513-527.

TSE, C., SHOEMAKER, A. R., ADICKES, J., ANDERSON, M. G., CHEN, J., JIN, S., JOHNSON, E. F., MARSH, K. C., MITTEN, M. J., NIMMER, P., ROBERTS, L., TAHIR, S. K., XIAO, Y., YANG, X., ZHANG, H., FESIK, S., ROSENBERG, S. H. & ELMORE, S. W. 2008. ABT-263: a potent and orally bioavailable Bcl-2 family inhibitor. *Cancer Res,* 68**,** 3421-8.

TSUJIMOTO, Y., YUNIS, J., ONORATO-SHOWE, L., ERIKSON, J., NOWELL, P. C. & CROCE, C. M. 1984. Molecular cloning of the chromosomal breakpoint of B-cell lymphomas and leukemias with the t(11;14) chromosome translocation. *Science,* 224**,** 1403-6.

TURNBULL, A. P., IOANNIDIS, S., KRAJEWSKI, W. W., PINTO-FERNANDEZ, A., HERIDE, C., MARTIN, A. C. L., TONKIN, L. M., TOWNSEND, E. C., BUKER, S. M., LANCIA, D. R., CARAVELLA, J. A., TOMS, A. V., CHARLTON, T. M., LAHDENRANTA, J., WILKER, E., FOLLOWS, B. C., EVANS, N. J., STEAD, L., ALLI, C., ZARAYSKIY, V. V., TALBOT, A. C., BUCKMELTER, A. J., WANG, M., MCKINNON, C. L., SAAB, F., MCGOURAN, J. F., CENTURY, H., GERSCH, M., PITTMAN, M. S., MARSHALL, C. G., RAYNHAM, T. M., SIMCOX, M., STEWART, L. M. D., MCLOUGHLIN, S. B., ESCOBEDO, J. A., BAIR, K. W., DINSMORE, C. J., HAMMONDS, T. R., KIM, S., URBÉ, S., CLAGUE, M. J., KESSLER, B. M. & KOMANDER, D. 2017. Molecular basis of USP7 inhibition by selective small-molecule inhibitors. *Nature,* 550**,** 481.

UCHIYAMA, K., JOKITALO, E., KANO, F., MURATA, M., ZHANG, X., CANAS, B., NEWMAN, R., RABOUILLE, C., PAPPIN, D., FREEMONT, P. & KONDO, H. 2002. VCIP135, a novel essential factor for p97/p47-mediated membrane fusion, is required for Golgi and ER assembly in vivo. *J Cell Biol,* 159**,** 855-66.

UCHIYAMA, K., TOTSUKAWA, G., PUHKA, M., KANEKO, Y., JOKITALO, E., DREVENY, I., BEURON, F., ZHANG, X., FREEMONT, P. & KONDO, H. 2006. p37 is a p97 adaptor required for Golgi and ER biogenesis in interphase and at the end of mitosis. *Dev Cell,* 11**,** 803-16.

UNNIYAMPURATH, U., PILANKATTA, R. & KRISHNAN, M. N. 2016. RNA Interference in the Age of CRISPR: Will CRISPR Interfere with RNAi? *International Journal of Molecular Sciences,* 17**,** 291.

URBE, S., LIU, H., HAYES, S. D., HERIDE, C., RIGDEN, D. J. & CLAGUE, M. J. 2012. Systematic survey of deubiquitinase localization identifies USP21 as a regulator of centrosome- and microtubule-associated functions. *Mol Biol Cell,* 23**,** 1095-103.

UREN, R. T., O'HELY, M., IYER, S., BARTOLO, R., SHI, M. X., BROUWER, J. M., ALSOP, A. E., DEWSON, G. & KLUCK, R. M. 2017. Disordered clusters of Bak dimers rupture mitochondria during apoptosis. *Elife,* 6**,** 19944.

VALENTE, E. M., ABOU-SLEIMAN, P. M., CAPUTO, V., MUQIT, M. M., HARVEY, K., GISPERT, S., ALI, Z., DEL TURCO, D., BENTIVOGLIO, A. R., HEALY, D. G., ALBANESE, A., NUSSBAUM, R., GONZALEZ-MALDONADO, R., DELLER, T., SALVI, S., CORTELLI, P., GILKS, W. P., LATCHMAN, D. S., HARVEY, R. J., DALLAPICCOLA, B., AUBURGER, G. & WOOD, N. W. 2004. Hereditary early-onset Parkinson's disease caused by mutations in PINK1. *Science,* 304**,** 1158-60.

VAN DELFT, M. F., WEI, A. H., MASON, K. D., VANDENBERG, C. J., CHEN, L., CZABOTAR, P. E., WILLIS, S. N., SCOTT, C. L., DAY, C. L., CORY, S., ADAMS, J. M., ROBERTS, A. W. & HUANG, D. C. 2006. The BH3 mimetic ABT-737 targets selective Bcl-2 proteins and efficiently induces apoptosis via Bak/Bax if Mcl-1 is neutralized. *Cancer Cell,* 10**,** 389-99.

VANBROCKLIN, M. W., VERHAEGEN, M., SOENGAS, M. S. & HOLMEN, S. L. 2009. Mitogen-activated protein kinase inhibition induces translocation of Bmf to promote apoptosis in melanoma. *Cancer Res,* 69**,** 1985-94.

VANDENBERG, C. J. & CORY, S. 2013. ABT-199, a new Bcl-2-specific BH3 mimetic, has in vivo efficacy against aggressive Myc-driven mouse lymphomas without provoking thrombocytopenia. *Blood,* 121**,** 2285-8.

VAUX, D. L., CORY, S. & ADAMS, J. M. 1988. Bcl-2 gene promotes haemopoietic cell survival and cooperates with c-myc to immortalize pre-B cells. *Nature,* 335**,** 440-2.

VAUX, D. L. & SILKE, J. 2005. IAPs, RINGs and ubiquitylation. *Nat Rev Mol Cell Biol,* 6**,** 287-97.

VENNE, A. S., KOLLIPARA, L. & ZAHEDI, R. P. 2014. The next level of complexity: crosstalk of posttranslational modifications. *Proteomics,* 14**,** 513-24.

VENTII, K. H. & WILKINSON, K. D. 2008. Protein partners of deubiquitinating enzymes. *Biochem J,* 414**,** 161-75.

VINAS-CASTELLS, R., BELTRAN, M., VALLS, G., GOMEZ, I., GARCIA, J. M., MONTSERRAT-SENTIS, B., BAULIDA, J., BONILLA, F., DE HERREROS, A. G. & DIAZ, V. M. 2010. The hypoxia-controlled FBXL14 ubiquitin ligase targets SNAIL1 for proteasome degradation. *J Biol Chem,* 285**,** 3794-805.

VITALE, I., MANIC, G., DE MARIA, R., KROEMER, G. & GALLUZZI, L. 2017. DNA Damage in Stem Cells. *Mol Cell,* 66**,** 306-319.

VIVES-BAUZA, C., ZHOU, C., HUANG, Y., CUI, M., DE VRIES, R. L., KIM, J., MAY, J., TOCILESCU, M. A., LIU, W., KO, H. S., MAGRANE, J., MOORE, D. J., DAWSON, V. L., GRAILHE, R., DAWSON, T. M., LI, C., TIEU, K. & PRZEDBORSKI, S. 2010. PINK1-dependent recruitment of Parkin to mitochondria in mitophagy. *Proc Natl Acad Sci U S A,* 107**,** 378-83.

VLASSCHAERT, C., COOK, D., XIA, X. & GRAY, D. A. 2017. The Evolution and Functional Diversification of the Deubiquitinating Enzyme Superfamily. *Genome Biology and Evolution,* 9**,** 558-573.

VLASSCHAERT, C., XIA, X., COULOMBE, J. & GRAY, D. A. 2015. Evolution of the highly networked deubiquitinating enzymes USP4, USP15, and USP11. *BMC Evolutionary Biology,* 15**,** 230.

VOUSDEN, K. H. & LU, X. 2002. Live or let die: the cell's response to p53. *Nat Rev Cancer,* 2**,** 594-604.

VUCIC, D., DIXIT, V. M. & WERTZ, I. E. 2011. Ubiquitylation in apoptosis: a post-translational modification at the edge of life and death. *Nat Rev Mol Cell Biol,* 12**,** 439-52.

WAGLE, N., EMERY, C., BERGER, M. F., DAVIS, M. J., SAWYER, A., POCHANARD, P., KEHOE, S. M., JOHANNESSEN, C. M., MACCONAILL, L. E., HAHN, W. C., MEYERSON, M. & GARRAWAY, L. A. 2011. Dissecting therapeutic resistance to RAF inhibition in melanoma by tumor genomic profiling. *J Clin Oncol,* 29**,** 3085-96.

WAKIOKA, T., SASAKI, A., KATO, R., SHOUDA, T., MATSUMOTO, A., MIYOSHI, K., TSUNEOKA, M., KOMIYA, S., BARON, R. & YOSHIMURA, A. 2001. Spred is a Sprouty-related suppressor of Ras signalling. *Nature,* 412**,** 647-51.

WAN, L., TAN, M., YANG, J., INUZUKA, H., DAI, X., WU, T., LIU, J., SHAIK, S., CHEN, G., DENG, J., MALUMBRES, M., LETAI, A., KIRSCHNER, M. W., SUN, Y. & WEI, W. 2014. APC(Cdc20) suppresses apoptosis through targeting Bim for ubiquitination and destruction. *Dev Cell,* 29**,** 377-91.

WAN, P. T., GARNETT, M. J., ROE, S. M., LEE, S., NICULESCU-DUVAZ, D., GOOD, V. M., JONES, C. M., MARSHALL, C. J., SPRINGER, C. J., BARFORD, D. & MARAIS, R. 2004. Mechanism of activation of the RAF-ERK signaling pathway by oncogenic mutations of B-RAF. *Cell,* 116**,** 855-67.

WANG, B., NI, Z., DAI, X., QIN, L., LI, X., XU, L., LIAN, J. & HE, F. 2014. The Bcl-2/xL inhibitor ABT-263 increases the stability of Mcl-1 mRNA and protein in hepatocellular carcinoma cells. *Mol Cancer,* 13**,** 1476-4598.

WANG, C., GAO, D., GUO, K., KANG, X., JIANG, K., SUN, C., LI, Y., SUN, L., SHU, H., JIN, G., SUN, H., WU, W. & LIU, Y. 2012. Novel synergistic antitumor effects of rapamycin with bortezomib on hepatocellular carcinoma cells and orthotopic tumor model. *BMC Cancer,* 12**,** 166-166.

WANG, C. Y., MAYO, M. W., KORNELUK, R. G., GOEDDEL, D. V. & BALDWIN, A. S., JR. 1998. NF-kappaB antiapoptosis: induction of TRAF1 and TRAF2 and c-IAP1 and c-IAP2 to suppress caspase-8 activation. *Science,* 281**,** 1680-3.

WANG, E., KAWAOKA, S., ROE, J. S., SHI, J., HOHMANN, A. F., XU, Y., BHAGWAT, A. S., SUZUKI, Y., KINNEY, J. B. & VAKOC, C. R. 2015a. The transcriptional cofactor TRIM33 prevents apoptosis in B lymphoblastic leukemia by deactivating a single enhancer. *Elife,* 28**,** 06377.

WANG, K. & ZHANG, X. C. 2014. Inhibition of SENP5 suppresses cell growth and promotes apoptosis in osteosarcoma cells. *Exp Ther Med,* 7**,** 1691-1695.

WANG, L., CHANVORACHOTE, P., TOLEDO, D., STEHLIK, C., MERCER, R. R., CASTRANOVA, V. & ROJANASAKUL, Y. 2008. Peroxide is a key mediator of Bcl-2 down-regulation and apoptosis induction by cisplatin in human lung cancer cells. *Mol Pharmacol,* 73**,** 119-27.

WANG, X., D'ARCY, P., CAULFIELD, T. R., PAULUS, A., CHITTA, K., MOHANTY, C., GULLBO, J., CHANAN-KHAN, A. & LINDER, S. 2015b. Synthesis and evaluation of derivatives of the proteasome deubiquitinase inhibitor b-AP15. *Chem Biol Drug Des,* 86**,** 1036-48.

WANG, X., MAZURKIEWICZ, M., HILLERT, E. K., OLOFSSON, M. H., PIERROU, S., HILLERTZ, P., GULLBO, J., SELVARAJU, K., PAULUS, A., AKHTAR, S., BOSSLER, F., KHAN, A. C., LINDER, S. & D'ARCY, P. 2016. The proteasome deubiquitinase inhibitor VLX1570 shows selectivity for ubiquitin-specific protease-14 and induces apoptosis of multiple myeloma cells. *Sci Rep,* 6.

WANG, Y., SATOH, A., WARREN, G. & MEYER, H. H. 2004. VCIP135 acts as a deubiquitinating enzyme during p97-p47-mediated reassembly of mitotic Golgi fragments. *J Cell Biol,* 164**,** 973-8.

WARR, M. R., MILLS, J. R., NGUYEN, M., LEMAIRE-EWING, S., BAARDSNES, J., SUN, K. L., MALINA, A., YOUNG, J. C., JEYARAJU, D. V., O'CONNOR-MCCOURT, M., PELLEGRINI, L., PELLETIER, J. & SHORE, G. C. 2011. Mitochondrion-dependent N-terminal processing of outer membrane Mcl-1 protein removes an essential Mule/Lasu1 protein-binding site. *J Biol Chem,* 286**,** 25098-107.

WAUER, T., SIMICEK, M., SCHUBERT, A. & KOMANDER, D. 2015a. Mechanism of phospho-ubiquitin-induced PARKIN activation. *Nature,* 524**,** 370-4.

WAUER, T., SWATEK, K. N., WAGSTAFF, J. L., GLADKOVA, C., PRUNEDA, J. N., MICHEL, M. A., GERSCH, M., JOHNSON, C. M., FREUND, S. M. & KOMANDER, D. 2015b. Ubiquitin Ser65 phosphorylation affects ubiquitin structure, chain assembly and hydrolysis. *Embo j,* 34**,** 307-25.

WEBER, A., HEINLEIN, M., DENGJEL, J., ALBER, C., SINGH, P. K. & HACKER, G. 2016. The deubiquitinase Usp27x stabilizes the BH3-only protein Bim and enhances apoptosis. *EMBO Rep,* 17**,** 724-38.

WEBER, C. K., SLUPSKY, J. R., KALMES, H. A. & RAPP, U. R. 2001. Active Ras Induces Heterodimerization of cRaf and BRaf. *Cancer Res,* 61**,** 3595-3598.

WEE, Y., LIU, Y., LU, J., LI, X. & ZHAO, M. 2018. *Identification of novel prognosis-related genes associated with cancer using integrative network analysis*.

WEI, M. C., ZONG, W. X., CHENG, E. H., LINDSTEN, T., PANOUTSAKOPOULOU, V., ROSS, A. J., ROTH, K. A., MACGREGOR, G. R., THOMPSON, C. B. & KORSMEYER, S. J. 2001. Proapoptotic BAX and BAK: a requisite gateway to mitochondrial dysfunction and death. *Science,* 292**,** 727-30.

WEINSTEIN, I. B. & JOE, A. 2008. Oncogene addiction. *Cancer Res,* 68**,** 3077-80.

WEINSTOCK, J., WU, J., CAO, P., KINGSBURY, W. D., MCDERMOTT, J. L., KODRASOV, M. P., MCKELVEY, D. M., SURESH KUMAR, K. G., GOLDENBERG, S. J., MATTERN, M. R. & NICHOLSON, B. 2012. Selective Dual Inhibitors of the Cancer-Related Deubiquitylating Proteases USP7 and USP47. *ACS Med Chem Lett,* 3**,** 789-92.

WEISS, M. B., ABEL, E. V., MAYBERRY, M. M., BASILE, K. J., BERGER, A. C. & APLIN, A. E. 2012. TWIST1 is an ERK1/2 effector that promotes invasion and regulates MMP-1 expression in human melanoma cells. *Cancer Res,* 72**,** 6382-92.

WEN, Y. Y., YANG, Z. Q., SONG, M., LI, B. L., YAO, X. H., CHEN, X. L., ZHAO, J., LU, Y. Y., ZHU, J. J. & WANG, E. H. 2010. The expression of SIAH1 is downregulated and associated with Bim and apoptosis in human breast cancer tissues and cells. *Mol Carcinog,* 49**,** 440-9.

WERTZ, I. E., O'ROURKE, K. M., ZHOU, H., EBY, M., ARAVIND, L., SESHAGIRI, S., WU, P., WIESMANN, C., BAKER, R., BOONE, D. L., MA, A., KOONIN, E. V. & DIXIT, V. M. 2004. De-ubiquitination and ubiquitin ligase domains of A20 downregulate NF-kappaB signalling. *Nature,* 430**,** 694-9.

WESTON, C. R., BALMANNO, K., CHALMERS, C., HADFIELD, K., MOLTON, S. A., LEY, R., WAGNER, E. F. & COOK, S. J. 2003. Activation of ERK1/2 by deltaRaf-1:ER* represses Bim expression independently of the JNK or PI3K pathways. *Oncogene,* 22**,** 1281-93.

WESTPHAL, D., DEWSON, G., MENARD, M., FREDERICK, P., IYER, S., BARTOLO, R., GIBSON, L., CZABOTAR, P. E., SMITH, B. J., ADAMS, J. M. & KLUCK, R. M. 2014a. Apoptotic pore formation is associated with in-plane insertion of Bak or Bax central helices into the mitochondrial outer membrane. *Proc Natl Acad Sci U S A,* 111**,** E4076-85.

WESTPHAL, D., KLUCK, R. M. & DEWSON, G. 2014b. Building blocks of the apoptotic pore: how Bax and Bak are activated and oligomerize during apoptosis. *Cell Death Differ,* 21**,** 196-205.

WHITFIELD, J., NEAME, S. J., PAQUET, L., BERNARD, O. & HAM, J. 2001. Dominant-negative c-Jun promotes neuronal survival by reducing BIM expression and inhibiting mitochondrial cytochrome c release. *Neuron,* 29**,** 629-43.

WICKENDEN, J. A., JIN, H., JOHNSON, M., GILLINGS, A. S., NEWSON, C., AUSTIN, M., CHELL, S. D., BALMANNO, K., PRITCHARD, C. A. & COOK, S. J. 2008. Colorectal cancer cells with the BRAF(V600E) mutation are addicted to the ERK1/2 pathway for growth factor-independent survival and repression of BIM. *Oncogene,* 27**,** 7150-61.

WIGGINS, C. M., BAND, H. & COOK, S. J. 2007. c-Cbl is not required for ERK1/2-dependent degradation of BimEL. *Cell Signal,* 19**,** 2605-11.

WIGGINS, C. M., TSVETKOV, P., JOHNSON, M., JOYCE, C. L., LAMB, C. A., BRYANT, N. J., KOMANDER, D., SHAUL, Y. & COOK, S. J. 2011. BIM(EL), an intrinsically disordered protein, is degraded by 20S proteasomes in the absence of poly-ubiquitylation. *J Cell Sci,* 124**,** 969-77.

WILFLING, F., WEBER, A., POTTHOFF, S., VOGTLE, F. N., MEISINGER, C., PASCHEN, S. A. & HACKER, G. 2012. BH3-only proteins are tail-anchored in the outer mitochondrial membrane and can initiate the activation of Bax. *Cell Death Differ,* 19**,** 1328-36.

WILLIS, S. N., CHEN, L., DEWSON, G., WEI, A., NAIK, E., FLETCHER, J. I., ADAMS, J. M. & HUANG, D. C. 2005. Proapoptotic Bak is sequestered by Mcl-1 and Bcl-xL, but not Bcl-2, until displaced by BH3-only proteins. *Genes Dev,* 19**,** 1294-305.

WILLIS, S. N., FLETCHER, J. I., KAUFMANN, T., VAN DELFT, M. F., CHEN, L., CZABOTAR, P. E., IERINO, H., LEE, E. F., FAIRLIE, W. D., BOUILLET, P., STRASSER, A., KLUCK, R. M., ADAMS, J. M. & HUANG, D. C. 2007. Apoptosis initiated when BH3 ligands engage multiple Bcl-2 homologs, not Bax or Bak. *Science,* 315**,** 856-9.

WILSON, B. E., MOCHON, E. & BOXER, L. M. 1996. Induction of bcl-2 expression by phosphorylated CREB proteins during B-cell activation and rescue from apoptosis. *Mol Cell Biol,* 16**,** 5546-56.

WILTSHIRE, T. D., LOVEJOY, C. A., WANG, T., XIA, F., O'CONNOR, M. J. & CORTEZ, D. 2010. Sensitivity to poly(ADP-ribose) polymerase (PARP) inhibition identifies ubiquitin-specific peptidase 11 (USP11) as a regulator of DNA double-strand break repair. *J Biol Chem,* 285**,** 14565-71.

WINKLHOFER, K. F. & HAASS, C. 2010. Mitochondrial dysfunction in Parkinson's disease. *Biochim Biophys Acta,* 1**,** 29-44.

WINSTON, J. T., STRACK, P., BEER-ROMERO, P., CHU, C. Y., ELLEDGE, S. J. & HARPER, J. W. 1999. The SCFbeta-TRCP-ubiquitin ligase complex associates specifically with phosphorylated destruction motifs in IkappaBalpha and beta-catenin and stimulates IkappaBalpha ubiquitination in vitro. *Genes Dev,* 13**,** 270-83.

WOJCIK, C. 1999. Proteasomes in apoptosis: villains or guardians? *Cell Mol Life Sci,* 56**,** 908-17.

WOLFEL, T., HAUER, M., SCHNEIDER, J., SERRANO, M., WOLFEL, C., KLEHMANN-HIEB, E., DE PLAEN, E., HANKELN, T., MEYER ZUM BUSCHENFELDE, K. H. & BEACH, D. 1995. A p16INK4a-insensitive CDK4 mutant targeted by cytolytic T lymphocytes in a human melanoma. *Science,* 269**,** 1281-4.

WROBLEWSKI, D., MIJATOV, B., MOHANA-KUMARAN, N., LAI, F., GALLAGHER, S. J., HAASS, N. K., ZHANG, X. D. & HERSEY, P. 2013. The BH3-mimetic ABT-737 sensitizes human melanoma cells to apoptosis induced by selective BRAF inhibitors but does not reverse acquired resistance. *Carcinogenesis,* 34**,** 237-247.

WU, G., XU, G., SCHULMAN, B. A., JEFFREY, P. D., HARPER, J. W. & PAVLETICH, N. P. 2003. Structure of a beta-TrCP1-Skp1-beta-catenin complex: destruction motif binding and lysine specificity of the SCF(beta-TrCP1) ubiquitin ligase. *Mol Cell,* 11**,** 1445-56.

WU, H.-C., LIN, Y.-C., LIU, C.-H., CHUNG, H.-C., WANG, Y.-T. & LIN, Y.-W. 2014. USP11 regulates PML stability to control Notch-induced malignancy in brain tumours. *Nat Commun,* 5.

XIAO, Y., NIMMER, P., SHEPPARD, G. S., BRUNCKO, M., HESSLER, P., LU, X., ROBERTS-RAPP, L., PAPPANO, W. N., ELMORE, S. W., SOUERS, A. J., LEVERSON, J. D. & PHILLIPS, D. C. 2015. MCL-1 Is a Key Determinant of Breast Cancer Cell Survival: Validation of MCL-1 Dependency Utilizing a Highly Selective Small Molecule Inhibitor. *Mol Cancer Ther,* 14**,** 1837-47.

XU, M., TAKANASHI, M., OIKAWA, K., TANAKA, M., NISHI, H., ISAKA, K., KUDO, M. & KURODA, M. 2009. USP15 plays an essential role for caspase-3 activation during Paclitaxel-induced apoptosis. *Biochem Biophys Res Commun,* 388**,** 366-71.

XU, Q. & REED, J. C. 1998. Bax inhibitor-1, a mammalian apoptosis suppressor identified by functional screening in yeast. *Mol Cell,* 1**,** 337-46.

XU, Y., LEE, S. H., KIM, H. S., KIM, N. H., PIAO, S., PARK, S. H., JUNG, Y. S., YOOK, J. I., PARK, B. J. & HA, N. C. 2010. Role of CK1 in GSK3beta-mediated phosphorylation and degradation of snail. *Oncogene,* 29**,** 3124-33.

YAMAGUCHI, N., OYAMA, M., KOZUKA-HATA, H. & INOUE, J. 2013. Involvement of A20 in the molecular switch that activates the non-canonical NF-small ka, CyrillicB pathway. *Sci Rep,* 3.

YANG, J. & WEINBERG, R. A. 2008. Epithelial-mesenchymal transition: at the crossroads of development and tumor metastasis. *Dev Cell,* 14**,** 818-29.

YANG, J. Y., ZONG, C. S., XIA, W., YAMAGUCHI, H., DING, Q., XIE, X., LANG, J. Y., LAI, C. C., CHANG, C. J., HUANG, W. C., HUANG, H., KUO, H. P., LEE, D. F., LI, L. Y., LIEN, H. C., CHENG, X., CHANG, K. J., HSIAO, C. D., TSAI, F. J., TSAI, C. H., SAHIN, A. A., MULLER, W. J., MILLS, G. B., YU, D., HORTOBAGYI, G. N. & HUNG, M. C. 2008. ERK promotes tumorigenesis by inhibiting FOXO3a via MDM2-mediated degradation. *Nat Cell Biol,* 10**,** 138-48.

YANG, W., LEE, Y. H., JONES, A. E., WOOLNOUGH, J. L., ZHOU, D., DAI, Q., WU, Q., GILES, K. E., TOWNES, T. M. & WANG, H. 2014. The histone H2A deubiquitinase Usp16 regulates embryonic stem cell gene expression and lineage commitment. *Nat Commun,* 5.

YANG, Y., FANG, S., JENSEN, J. P., WEISSMAN, A. M. & ASHWELL, J. D. 2000. Ubiquitin protein ligase activity of IAPs and their degradation in proteasomes in response to apoptotic stimuli. *Science,* 288**,** 874-7.

YANO, T., ITO, K., FUKAMACHI, H., CHI, X. Z., WEE, H. J., INOUE, K., IDA, H., BOUILLET, P., STRASSER, A., BAE, S. C. & ITO, Y. 2006. The RUNX3 tumor suppressor upregulates Bim in gastric epithelial cells undergoing transforming growth factor beta-induced apoptosis. *Mol Cell Biol,* 26**,** 4474-88.

YAO, Y., ZHANG, Y., SHI, M., SUN, Y., CHEN, C., NIU, M., ZHANG, Q., ZENG, L., YAO, R., LI, H., YANG, J., LI, Z. & XU, K. 2018. Blockade of deubiquitinase USP7 overcomes bortezomib resistance by suppressing NF-kappaB signaling pathway in multiple myeloma. *J Leukoc Biol,* 19**,** 2A1017-420RR.

YATIM, N., CULLEN, S. & ALBERT, M. L. 2017. Dying cells actively regulate adaptive immune responses. *Nat Rev Immunol,* 17**,** 262-275.

YAU, R. & RAPE, M. 2016. The increasing complexity of the ubiquitin code. *Nat Cell Biol,* 18**,** 579-86.

YE, F., BAUER, J. A., PIETENPOL, J. A. & SHYR, Y. 2012. Analysis of high-throughput RNAi screening data in identifying genes mediating sensitivity to chemotherapeutic drugs: statistical approaches and perspectives. *BMC Genomics,* 13**,** 1471-2164.

YECIES, D., CARLSON, N. E., DENG, J. & LETAI, A. 2010. Acquired resistance to ABT-737 in lymphoma cells that up-regulate MCL-1 and BFL-1. *Blood,* 115**,** 3304-13.

YILMAZ, M. & CHRISTOFORI, G. 2009. EMT, the cytoskeleton, and cancer cell invasion. *Cancer Metastasis Rev,* 28**,** 15-33.

YOON, S. & SEGER, R. 2006. The extracellular signal-regulated kinase: multiple substrates regulate diverse cellular functions. *Growth Factors,* 24**,** 21-44.

YOST, C., TORRES, M., MILLER, J. R., HUANG, E., KIMELMAN, D. & MOON, R. T. 1996. The axis-inducing activity, stability, and subcellular distribution of beta-catenin is regulated in Xenopus embryos by glycogen synthase kinase 3. *Genes Dev,* 10**,** 1443-54.

YOU, B., YANG, Y.-L., XU, Z., DAI, Y., LIU, S., MAO, J.-H., TETSU, O., LI, H., JABLONS, D. M. & YOU, L. 2015. Inhibition of ERK1/2 down-regulates the Hippo/YAP signaling pathway in human NSCLC cells. *Oncotarget,* 6**,** 4357-4368.

YOULE, R. J. & STRASSER, A. 2008. The BCL-2 protein family: opposing activities that mediate cell death. *Nat Rev Mol Cell Biol,* 9**,** 47-59.

YU, F. X., ZHAO, B. & GUAN, K. L. 2015. Hippo Pathway in Organ Size Control, Tissue Homeostasis, and Cancer. *Cell,* 163**,** 811-28.

YU, M., LIU, K., MAO, Z., LUO, J., GU, W. & ZHAO, W. 2016. USP11 Is a Negative Regulator to gammaH2AX Ubiquitylation by RNF8/RNF168. *J Biol Chem,* 291**,** 959-67.

YUAN, J., LUO, K., ZHANG, L., CHEVILLE, J. C. & LOU, Z. 2010. USP10 regulates p53 localization and stability by deubiquitinating p53. *Cell,* 140**,** 384-96.

YUE, W., CHEN, Z., LIU, H., YAN, C., CHEN, M., FENG, D., YAN, C., WU, H., DU, L., WANG, Y., LIU, J., HUANG, X., XIA, L., LIU, L., WANG, X., JIN, H., WANG, J., SONG, Z., HAO, X. & CHEN, Q. 2014. A small natural molecule promotes mitochondrial fusion through inhibition of the deubiquitinase USP30. *Cell Res,* 24**,** 482-96.

ZARU, R., RONKINA, N., GAESTEL, M., ARTHUR, J. S. & WATTS, C. 2007. The MAPK-activated kinase Rsk controls an acute Toll-like receptor signaling response in dendritic cells and is activated through two distinct pathways. *Nat Immunol,* 8**,** 1227-35.

ZHA, J., HARADA, H., YANG, E., JOCKEL, J. & KORSMEYER, S. J. 1996. Serine phosphorylation of death agonist BAD in response to survival factor results in binding to 14-3-3 not BCL-X(L). *Cell,* 87**,** 619-28.

ZHAI, D., KE, N., ZHANG, H., LADROR, U., JOSEPH, M., EICHINGER, A., GODZIK, A., NG, S. C. & REED, J. C. 2003. Characterization of the anti-apoptotic mechanism of Bcl-B. *Biochem J,* 376**,** 229-36.

ZHANG, H., GUTTIKONDA, S., ROBERTS, L., UZIEL, T., SEMIZAROV, D., ELMORE, S. W., LEVERSON, J. D. & LAM, L. T. 2011. Mcl-1 is critical for survival in a subgroup of non-small-cell lung cancer cell lines. *Oncogene,* 30**,** 1963-8.

ZHANG, H., ZHANG, S., HE, H., ZHAO, W., CHEN, J. & SHAO, R. G. 2012. GAP161 targets and downregulates G3BP to suppress cell growth and potentiate cisplaitin-mediated cytotoxicity to colon carcinoma HCT116 cells. *Cancer Sci,* 103**,** 1848-56.

ZHANG, S., ZHANG, M., JING, Y., YIN, X., MA, P., ZHANG, Z., WANG, X., DI, W. & ZHUANG, G. 2018. Deubiquitinase USP13 dictates MCL1 stability and sensitivity to BH3 mimetic inhibitors. *Nature Communications,* 9**,** 215.

ZHANG, W., CHENG, G. Z., GONG, J., HERMANTO, U., ZONG, C. S., CHAN, J., CHENG, J. Q. & WANG, L. H. 2008. RACK1 and CIS mediate the degradation of BimEL in cancer cells. *J Biol Chem,* 283**,** 16416-26.

ZHANG, X. & WANG, Y. 2015. Cell cycle regulation of VCIP135 deubiquitinase activity and function in p97/p47-mediated Golgi reassembly. *Mol Biol Cell,* 26**,** 2242-51.

ZHANG, X., ZHANG, H. & WANG, Y. 2014. Phosphorylation regulates VCIP135 function in Golgi membrane fusion during the cell cycle. *J Cell Sci,* 127**,** 172-81.

ZHANG, Y., XIONG, Y. & YARBROUGH, W. G. 1998. ARF promotes MDM2 degradation and stabilizes p53: ARF-INK4a locus deletion impairs both the Rb and p53 tumor suppression pathways. *Cell,* 92**,** 725-34.

ZHANG, Z., ZHU, W., LAPOLLA, S. M., MIAO, Y., SHAO, Y., FALCONE, M., BOREHAM, D., MCFARLANE, N., DING, J., JOHNSON, A. E., ZHANG, X. C., ANDREWS, D. W. & LIN, J. 2010. Bax forms an oligomer via separate, yet interdependent, surfaces. *J Biol Chem,* 285**,** 17614-27.

ZHAO, B., LI, L. & GUAN, K.-L. 2010a. Hippo signaling at a glance. *J Cell Sci,* 123**,** 4001-4006.

ZHAO, B., LI, L., TUMANENG, K., WANG, C. Y. & GUAN, K. L. 2010b. A coordinated phosphorylation by Lats and CK1 regulates YAP stability through SCF(beta-TRCP). *Genes Dev,* 24**,** 72-85.

ZHAO, B., TUMANENG, K. & GUAN, K. L. 2011. The Hippo pathway in organ size control, tissue regeneration and stem cell self-renewal. *Nat Cell Biol,* 13**,** 877-83.

ZHAO, B., WEI, X., LI, W., UDAN, R. S., YANG, Q., KIM, J., XIE, J., IKENOUE, T., YU, J., LI, L., ZHENG, P., YE, K., CHINNAIYAN, A., HALDER, G., LAI, Z.-C. & GUAN, K.-L. 2007. Inactivation of YAP oncoprotein by the Hippo pathway is involved in cell contact inhibition and tissue growth control. *Genes Dev,* 21**,** 2747-2761.

ZHAO, G., ZHU, Y., ENO, C. O., LIU, Y., DELEEUW, L., BURLISON, J. A., CHAIRES, J. B., TRENT, J. O. & LI, C. 2014. Activation of the proapoptotic Bcl-2 protein Bax by a small molecule induces tumor cell apoptosis. *Mol Cell Biol,* 34**,** 1198-207.

ZHAO, J., ZHAI, B., GYGI, S. P. & GOLDBERG, A. L. 2015. mTOR inhibition activates overall protein degradation by the ubiquitin proteasome system as well as by autophagy. *Proc Natl Acad Sci U S A,* 112**,** 15790-7.

ZHONG, Q., GAO, W., DU, F. & WANG, X. 2005. Mule/ARF-BP1, a BH3-only E3 ubiquitin ligase, catalyzes the polyubiquitination of Mcl-1 and regulates apoptosis. *Cell,* 121**,** 1085-95.

ZHOU, D., CONRAD, C., XIA, F., PARK, J.-S., PAYER, B., YIN, Y., LAUWERS, G. Y., THASLER, W., LEE, J. T., AVRUCH, J. & BARDEESY, N. 2009. Mst1 and Mst2 maintain hepatocyte quiescence and suppress the development of hepatocellular carcinoma through inactivation of the Yap1 oncogene. *Cancer Cell,* 16**,** 425-438.

ZHOU, H., XU, M., HUANG, Q., GATES, A. T., ZHANG, X. D., CASTLE, J. C., STEC, E., FERRER, M., STRULOVICI, B., HAZUDA, D. J. & ESPESETH, A. S. 2008. Genome-scale RNAi screen for host factors required for HIV replication. *Cell Host Microbe,* 4**,** 495-504.

ZHOU, Y., TOZZI, F., CHEN, J., FAN, F., XIA, L., WANG, J., GAO, G., ZHANG, A., XIA, X., BRASHER, H., WIDGER, W., ELLIS, L. M. & WEIHUA, Z. 2012. Intracellular ATP levels are a pivotal determinant of chemoresistance in colon cancer cells. *Cancer Res,* 72**,** 304-14.

ZHOU, Z., LUO, A., SHRIVASTAVA, I., HE, M., HUANG, Y., BAHAR, I., LIU, Z. & WAN, Y. 2017. Regulation of XIAP Turnover Reveals a Role for USP11 in Promotion of Tumorigenesis. *EBioMedicine,* 15**,** 48-61.

ZHU, H. Y., DESAI, J., DENG, Y., COOPER, A., WANG, J., SHIPPS, J., SAMATAR, A., CARR, D. & WINDSOR, W. 2015. Discovery of hydroxyaniline amides as selective Extracellular Regulated Kinase (Erk) inhibitors. *Bioorg Med Chem Lett,* 25**,** 1627-9.

ZHUO, X., GUO, X., ZHANG, X., JING, G., WANG, Y., CHEN, Q., JIANG, Q., LIU, J. & ZHANG, C. 2015. Usp16 regulates kinetochore localization of Plk1 to promote proper chromosome alignment in mitosis. *J Cell Biol,* 210**,** 727-35.

ZONG, W. X., EDELSTEIN, L. C., CHEN, C., BASH, J. & GELINAS, C. 1999. The prosurvival Bcl-2 homolog Bfl-1/A1 is a direct transcriptional target of NF-kappaB that blocks TNFalpha-induced apoptosis. *Genes Dev,* 13**,** 382-7.

ZOTTI, T., UVA, A., FERRAVANTE, A., VESSICHELLI, M., SCUDIERO, I., CECCARELLI, M., VITO, P. & STILO, R. 2011. TRAF7 protein promotes Lys-29-linked polyubiquitination of IkappaB kinase (IKKgamma)/NF-kappaB essential modulator (NEMO) and p65/RelA protein and represses NF-kappaB activation. *J Biol Chem,* 286**,** 22924-33.

ZUNINO, R., SCHAUSS, A., RIPPSTEIN, P., ANDRADE-NAVARRO, M. & MCBRIDE, H. M. 2007. The SUMO protease SENP5 is required to maintain mitochondrial morphology and function. *J Cell Sci,* 120**,** 1178-88.